

THESIS FOR THE DEGREE OF DOCTOR OF PHILOSOPHY

# **Pressure-Based Leakage Characterisation of Bulk Pipelines**



**Prepared by:**

**Rene Nsanzubuhoro**

**Supervised by:**

**Professor Kobus van Zyl**

Thesis submitted in fulfilment of the requirements for the degree of

“Doctor of Philosophy”

Department of Civil Engineering

University of Cape Town, South Africa

February 2019

The copyright of this thesis vests in the author. No quotation from it or information derived from it is to be published without full acknowledgement of the source. The thesis is to be used for private study or non-commercial research purposes only.

Published by the University of Cape Town (UCT) in terms of the non-exclusive license granted to UCT by the author.

## Declaration

I, Rene Nsanzubuhoro, know the meaning of plagiarism and declare that all the work in this document, save for that which is properly acknowledged, is my own.

Signed:

Signed by candidate

Date: 09-02-2019

## Acknowledgements

My thanks are due to many people who have helped directly and indirectly in the production of this thesis:

- My supervisor, Prof Kobus van Zyl, who was always willing to motivate, guide and advise me throughout the thesis. I will always be grateful for his help and support.
- I would also like to thank all the members of the Water Distribution Systems Research Group at the University of Cape Town for their friendship and assistance throughout my studies. Asaph and Malunga deserve special mention in this regard.
- I would like to express my gratitude to Shaun Osler of ABB for donating some of the equipment used for this research, and for all his guidance and advise.
- Berno Wellman deserves a special mention for his support in assembling the device developed in this study.
- I am also indebted to the bulk water suppliers: the City of Cape Town, Overberg Municipality and the City of Tshwane, as well as consulting engineers Resolve who all took part in the study.
- Mr Charles Nichols, Nooredien Hassen and Mr Tahir Mukkadam for their technical expertise and guidance in the laboratory.
- The Water Research Council and the Postgraduate Funding Office at the University of Cape Town who funded my studies.
- The staff of the Department of Civil Engineering at the University of Cape Town deserve a special mention for their support and assistance.
- I would like to express my gratitude to my father and mother, Emmanuel and Martha, my twin sisters, Consolata and Christa, and my brother Remy Nsanzubuhoro for their love and support.
- Finally, I would like to thank my wife, Xochiwe, and daughter, Bella for their unfailing love and support throughout my studies.

## List of Abbreviations

AC	Asbestos Cement
AWWA	American Water Work Association
AZP	Average Zone Point
BABE	Burst and Background Estimates
CARL	Current Annual Real Losses
DMA	District Metered Area
EIF	Economic Intervention Frequency
EPA	Environmental Protection Agency
FAVAD	Fixed and Variable Area discharge
FCM	Federation of Canadian Municipalities
GRP	Glass Reinforced Pipes
HDPE	High density polyethylene
ILI	Infrastructure Leakage Index
ITA	Inverse Transient Analysis
IWA	International Water Association
LDPE	Low density polyethylene
MDPE	Medium density polyethylene
MNF	Minimum Night Flow
NRC	National Research Council
NRW	Non-Revenue Water
OWB	Overberg Water Board
PI	Performance indicator
PVC	Polyvinyl Chloride
PCAE	Pipe Condition Assessment Equipment
RC	Reinforced Concrete
SCG	Stress crack growth
SEM	Scanning electron microscopy
SIV	System Input Volume
SCC	Stress corrosion cracking
UARL	Unavoidable Annual Real Losses
WHO	World Health Organisation
WRC	Water Research Council

## List of Symbols

$\sigma_l$	Longitudinal stress
$\sigma_c$	Circumferential stress
$\varepsilon_{circ}$	Circumferential strain
$\varepsilon_{long}$	Longitudinal strain
$Q$	Flow rate ( $m^3/s$ )
$t$	Time (s)
$b$	Pipe wall thickness
$\gamma$	Specific weight of water ( $N/m^3$ )
$\rho$	Density of water ( $kg/m^3$ )
$g$	Gravitational constant ( $m/s^2$ )
$E$	Modulus of elasticity
$E_R$	Relaxation modulus (MPa)
$F$	Shape factor of soil
$f$	Friction factor
$\nu$	Poisson's ratio of the material
$\mathcal{V}$	Kinematic viscosity ( $m^2/s$ )
$\beta$	Demand Elasticity
$C_d$	Discharge Coefficient
$C_E$	Emitter coefficient ( $m^{5/2}/s$ )
$\zeta$	Orifice resistance coefficient
$d$	Pipe diameter ( $m$ )
$s$	Pipe wall thickness ( $m$ )
$h_s$	Static head ( $m$ )
$h_d$	Demand head ( $m$ )
$h_f$	Frictional head loss ( $m$ )
$h_l$	Leakage fraction ( $m$ )
$\delta h$	Differential pressure head ( $m$ )
$h$	Total leak discharge pressure head ( $m$ )
$V_o$	Velocity of outgoing flow ( $m/s$ )
$V_i$	Velocity of incoming flow ( $m/s$ )
$\delta P$	Differential pressure (Pa)

$A$	Leak area ( $m^2$ )
$A'$	Effective leak area ( $m^2$ )
$A_o$	Initial leak area ( $mm^2$ )
$A_i$	Cross-sectional area of pipe or flow source (incoming flow) ( $m^2$ )
$A_e$	Elastic and reversible change in leak area ( $m^2$ )
$A_v$	Visco-elastic component of leak area ( $m^2$ )
$\alpha$	Emitter exponent ( <i>usually 0.5</i> )
$x$	Fractional location ( $m$ )
$N_c$	Kinetic energy coefficient of vena contracta of leak flow ( $J$ )
$A_c$	Area of vena contracta of leak flow ( $m^2$ )
$V$	Velocity ( $m/s$ )
$\forall$	Volume of water ( $m^3$ )
$m$	Head-area slope of leak ( $mm^2/m$ )
$m'$	Effective head area slope ( $mm^2/m$ )
$m_e$	Head-area slope for elastic material ( $m^{-1}$ )
$k$	Coefficient of permeability
$L_c$	Length of crack ( $m$ )
$P_w$	Wetted perimeter of flow ( $m$ )
$\sigma_l$	Longitudinal stress along pipe ( $N/m^2$ )
$\tau_\sigma$	Relaxation time of strain during constant load (s)
$C$	Leakage coefficient
$N1$	Leakage exponent
$L_N$	Leakage number
$Re$	Reynold's number
$\forall_{out}$	Volume of water leaking out
$R_s$	Reliability of the pump system,
$R_p$	Reliability of the pump,
$R_m$	Reliability of the motor,
$R_c$	Reliability of the control unit,
$R_{pt}$	Reliability of the power station, and
$R_v$	Reliability of the valves

## Abstract

Water losses in distribution systems are a huge problem internationally and also in South Africa where more than a third of the water entering the water supply networks is lost through pipe leaks. With water demand increasing due to population growth and urbanisation, water resources are under greater stress and water supply failures are becoming more common.

A great deal of work has been done over the past two decades on managing water losses in distribution systems. The Water Loss Task Force of the International Water Association (IWA) played a leading role in this effort, with the “IWA water balance” now widely used as a basis in municipal water loss programs.

One of the areas that have received relatively little attention is leakage on bulk pipeline systems. Bulk pipelines connect water treatment plants to bulk reservoirs and distribute water from reservoirs to different towns or water supply zones. Bulk pipes may be operated using pumps or gravity, and generally do not supply consumers directly.

It is difficult to determine what the water losses in a bulk pipeline are, as the high flow rates make it impractical or prohibitively expensive to measure flow rates at both ends of these pipelines. Cheaper solutions, such as clamp-on ultrasonic flow meters or reservoir drop tests, are prone to problems and do not have the required accuracy.

Due to the lack of reliable and effective methods, water losses on bulk pipes are often assumed to be 2 or 3 %. However, these losses may, in fact, be much greater, and due to the large flow of water transported by bulk pipelines, even small fractions of losses represent large volumes of water.

The aim of this project was to develop a method for identifying the size and type of leak present in real bulk water pipelines with minimal disturbance to the operation of the infrastructure. This was achieved by developing a mobile device called the pipe condition assessment equipment (PCAE), which uses pressure testing in combination with the latest models on the behaviour of leaks areas with pressure to assess the condition of the bulk pipeline.

To verify the efficacy of the PCAE, the device was first tested on three uPVC pipes with known leakage characteristics in the laboratory (a 12mm round hole, 100mm by 1mm circumferential crack and a 100mm by 1mm longitudinal crack). As expected, the round hole had very small head-area slopes which are negligible, whilst the circumferential crack showed a negative head-



area slope and the longitudinal crack portrayed a large positive head-area slope. These results were consistent with previous laboratory experiments that investigated the behaviour of round holes and longitudinal and circumferential cracks.

Bulk water suppliers and municipalities were then approached to take part in the study. Several bulk pipelines were tested using the PCAE. The results of the field test are discussed in terms of the pre-testing procedures to prepare for the tests, their repeatability and the effectiveness of the device to detect, quantify and characterise leakage on the pipeline.

For pipelines with undetectable leakage, a non-intrusive technique that uses a dynamic pressure drop signature from an isolated pipe, to detect and quantify undetectable leakage, was developed. The leakage characteristics of the isolated pipe were estimated from the pressure vs time data. In summary, if the pressure remained constant the pipe was without a leak. If the pressure dropped, a novel mathematical model was fitted to the pressure vs time curve, using the known pipe properties, to determine the characteristics of the leak or leaks present in the pipe.

Overall, the PCAE was capable of assessing the extent of leakage on a range of pipe materials, diameters and lengths. It was found that out of the eleven bulk pipelines tested in this study, three could not be tested due to dysfunctional isolation valves and failed connection points. The other eight pipelines that were successfully tested were found to be leaking. The effective initial leak areas for the tested pipelines ranged from  $4.88\text{mm}^2$  to  $137.66\text{mm}^2$ , whilst the effective head-area slope ranged from  $0.0032\text{ mm}^2/\text{m}$  to  $3.14\text{ mm}^2/\text{m}$  and the N1 leakage exponents were found to range from 0.56 up to 1.09.

Finally, since there are no well-founded performance indicators for bulk systems, this study also described the findings from analyses of several potential performance indicators using the data from the bulk pipelines tested using the PCAE. The challenges in comparing water losses of different bulk pipelines are highlighted. Based on this, it was found that because every bulk pipeline has its unique characteristic regarding structural parameters such as diameter, pipe material, type of couplings, and operating pressure, the preferred performance indicator for assessing water losses in bulk systems mainly depends on the purpose of the analysis.

# Table of Contents

<b>Declaration.....</b>	<b>i</b>
<b>Acknowledgements .....</b>	<b>ii</b>
<b>List of Abbreviations .....</b>	<b>iii</b>
<b>List of Symbols .....</b>	<b>iv</b>
<b>Abstract.....</b>	<b>vi</b>
<b>Table of Contents .....</b>	<b>viii</b>
<b>List of Figures.....</b>	<b>xv</b>
<b>List of Tables .....</b>	<b>xxvi</b>
<b>1 Introduction .....</b>	<b>1-1</b>
<b>1.1 Background.....</b>	<b>1-1</b>
<b>1.2 Problem statement.....</b>	<b>1-3</b>
<b>1.3 Goal and Objectives of the research.....</b>	<b>1-3</b>
1.1.1 Developing a pipe condition assessment equipment .....	1-4
1.1.2 Testing real bulk pipelines using PCAE .....	1-5
1.1.3 A dynamic pressure test approach for leakage characterisation .....	1-5
1.1.4 Evaluating potential new performance indicators for bulk pipelines .....	1-6
<b>1.4 Scope and limitations .....</b>	<b>1-6</b>
<b>1.5 Layout of the thesis .....</b>	<b>1-7</b>
<b>2 Literature Review .....</b>	<b>2-9</b>
<b>2.1 Introduction .....</b>	<b>2-9</b>
<b>2.2 Water loss and leakage .....</b>	<b>2-10</b>
2.2.1 Definitions and terminology of water loss and leakage.....	2-10
2.2.2 Factors influencing leakage .....	2-12
2.2.3 Impact of leakage.....	2-13
2.2.4 Present status of water losses in South Africa .....	2-15
<b>2.3 Water loss management.....</b>	<b>2-17</b>
2.3.1 Introduction.....	2-17
2.3.2 Implementing successful water loss management programmes .....	2-17
2.3.3 Measures taken to manage water losses in South Africa.....	2-20

<b>2.4</b>	<b>Sources of leakage in pipe systems .....</b>	<b>2-21</b>
2.4.1	Introduction.....	2-21
2.4.2	Factors that influence pipe failures .....	2-21
2.4.3	Failure mechanisms .....	2-21
<b>2.5</b>	<b>Leak detection methods for water pipelines .....</b>	<b>2-25</b>
2.5.1	Introduction.....	2-25
2.5.2	Leakage control strategies.....	2-25
2.5.3	Factors that influence leakage control strategies .....	2-26
2.5.4	Current leak detection methods .....	2-27
<b>2.6</b>	<b>Leakage modelling for water pipe systems .....</b>	<b>2-35</b>
2.6.1	Introduction.....	2-35
2.6.2	Orifice equation .....	2-35
2.6.3	Power equation.....	2-37
2.6.4	Modified orifice equation .....	2-48
2.6.5	Relationship between the modified orifice equation and the power equation	2-59
<b>2.7</b>	<b>Components of bulk water pipelines .....</b>	<b>2-64</b>
2.7.1	Introduction.....	2-64
2.7.2	Pipelines.....	2-64
2.7.3	Pump stations .....	2-66
2.7.4	Pipeline valves .....	2-67
<b>2.8</b>	<b>Pipe materials used for bulk water pipelines.....</b>	<b>2-68</b>
2.8.1	Introduction.....	2-68
2.8.2	Metallic pipelines.....	2-68
2.8.3	Non-metallic pipes .....	2-77
<b>2.9</b>	<b>Existing knowledge about leakage on bulk pipelines.....</b>	<b>2-86</b>
2.9.1	Unreported leak frequency variation by geographic region .....	2-86
2.9.2	Unreported leak frequency variations by pipe material and diameter .....	2-87
2.9.3	Unreported leak frequency related to the age of mains .....	2-88
2.9.4	Variations in the leak flow rates of bulk pipelines .....	2-89
<b>2.10</b>	<b>Conclusion.....</b>	<b>2-91</b>
<b>3</b>	<b>Design of the test equipment.....</b>	<b>3-92</b>
<b>3.1</b>	<b>Introduction .....</b>	<b>3-92</b>
<b>3.2</b>	<b>Prototype status .....</b>	<b>3-92</b>

3.2.1	Introduction.....	3-92
3.2.2	Existing device for distribution systems .....	3-93
3.2.3	Modification of the current device for bulk systems .....	3-96
<b>3.3</b>	<b>Concept design for bulk pipeline test equipment .....</b>	<b>3-97</b>
3.3.1	Introduction.....	3-97
3.3.2	Prototype design.....	3-97
<b>3.4</b>	<b>Constructing the pipe condition assessment equipment (PCAE) .....</b>	<b>3-111</b>
<b>3.5</b>	<b>Final prototype of the pipe condition assessment equipment (PCAE) for bulk pipelines.....</b>	<b>3-111</b>
<b>4</b>	<b>Experimental Verification Tests.....</b>	<b>4-114</b>
<b>4.1</b>	<b>Introduction .....</b>	<b>4-114</b>
<b>4.2</b>	<b>Available equipment and environment .....</b>	<b>4-114</b>
<b>4.3</b>	<b>Experimental setup .....</b>	<b>4-116</b>
<b>4.4</b>	<b>Experimental procedure, data collection and analysis methodology .....</b>	<b>4-118</b>
4.4.1	Experiment procedure .....	4-118
4.4.2	Data collection .....	4-121
4.4.3	Data analysis procedure .....	4-122
<b>4.5</b>	<b>Laboratory results and discussion .....</b>	<b>4-127</b>
4.5.1	Results for round holes .....	4-128
4.5.2	Results for longitudinal cracks.....	4-135
4.5.3	Results for the circumferential crack .....	4-142
<b>4.6</b>	<b>Summary of results .....</b>	<b>4-149</b>
<b>4.7</b>	<b>Conclusion.....</b>	<b>4-151</b>
<b>5</b>	<b>Field Tests.....</b>	<b>5-153</b>
<b>5.1</b>	<b>Introduction .....</b>	<b>5-153</b>
<b>5.2</b>	<b>Field test procedure.....</b>	<b>5-154</b>
<b>5.3</b>	<b>Lynnwood Road to Koedoesnek reservoir pipeline .....</b>	<b>5-155</b>
5.3.1	Introduction.....	5-155
5.3.2	Leak test procedure .....	5-158
5.3.3	Leak test results.....	5-159
<b>5.4</b>	<b>Simon Vermooten to Murrayfield Reservoir Pipeline.....</b>	<b>5-167</b>
5.4.1	Introduction.....	5-167
5.4.2	Leak Test Procedure .....	5-169

5.4.3	Leak Test Results .....	5-170
<b>5.5</b>	<b>Garsfontein to Parkmore High Level reservoir pipeline.....</b>	<b>5-171</b>
5.5.1	Introduction.....	5-171
5.5.2	Leak test procedure .....	5-174
5.5.3	Leak test results for the GP pipeline .....	5-181
<b>5.6</b>	<b>Brickfields and Constantia Reservoir pipeline.....</b>	<b>5-188</b>
5.6.1	Introduction.....	5-188
5.6.2	Leak test procedure .....	5-189
5.6.3	Leak test results for the BC pipeline.....	5-190
<b>5.7</b>	<b>Fort Klapperkop reservoirs to Carina pipeline.....</b>	<b>5-190</b>
5.7.1	Introduction.....	5-190
5.7.2	Leak Test Procedure .....	5-193
5.7.3	Leak test data analysis and results .....	5-197
<b>5.8</b>	<b>BS 8 Pipeline - Test 1.....</b>	<b>5-205</b>
5.8.1	Introduction.....	5-205
5.8.2	Leak test procedure .....	5-208
5.8.3	Leak test data analysis and results .....	5-211
5.8.4	Comparing the leak test results with field condition .....	5-222
<b>5.9</b>	<b>BS 8 Pipeline - Test 2.....</b>	<b>5-223</b>
5.9.1	Introduction.....	5-223
5.9.2	Leak test procedure .....	5-224
5.9.3	Leak test results.....	5-227
5.9.4	Comparison of BS8-pipeline Test 1 and Test 2 .....	5-232
<b>5.10</b>	<b>Wingfield Pipeline – Test 1.....</b>	<b>5-233</b>
5.10.1	Introduction.....	5-233
5.10.2	Leak test procedure .....	5-235
5.10.3	Leak test results.....	5-237
<b>5.11</b>	<b>Wingfield Pipeline – Test 2.....</b>	<b>5-244</b>
5.11.1	Introduction.....	5-244
5.11.2	Leak test procedure .....	5-245
<b>5.12</b>	<b>Wingfield Pipeline – Test 3.....</b>	<b>5-246</b>
5.12.1	Introduction.....	5-246
5.12.2	Leak Test Procedure .....	5-248
5.12.3	Leak Test Results .....	5-249

5.13	<b>Conclusions .....</b>	<b>5-250</b>
<b>6</b>	<b>Dynamic Pressure Tests .....</b>	<b>6-253</b>
6.1	<b>Introduction .....</b>	<b>6-253</b>
6.2	<b>Derivation methodology.....</b>	<b>6-253</b>
6.3	<b>The derivation of an analytical solution for the dynamic pressure .....</b>	<b>6-254</b>
6.3.1	Conservation of mass .....	6-254
6.3.2	Total change in volume.....	6-255
6.3.3	Change in volume due to compressibility.....	6-259
6.3.4	Change in volume due to leakage .....	6-259
6.3.5	Pressure and time relationship .....	6-260
6.4	<b>Discontinuities in the analytical solution.....</b>	<b>6-262</b>
6.4.1	Case 1: negative head-area slope and positive initial leak area .....	6-262
6.4.2	Case 2: positive head-area slopes and negative initial leak area .....	6-263
6.4.3	Case 3: negative head-area slopes and negative initial leak area.....	6-264
6.5	<b>Optimisation process to determine the true leakage parameters .....</b>	<b>6-266</b>
6.6	<b>Numerical approximation for verifying the analytical solution .....</b>	<b>6-266</b>
6.6.1	Introduction.....	6-266
6.6.2	Developing the numerical model .....	6-266
6.6.3	Comparing the numerical and analytical solutions .....	6-269
6.6.4	Analysis procedure.....	6-270
6.6.5	Results.....	6-271
6.7	<b>Laboratory tests: pressure drop tests.....</b>	<b>6-274</b>
6.7.1	Introduction.....	6-274
6.7.2	Experimental setup.....	6-275
6.7.3	Test pipe samples .....	6-276
6.7.4	Experimental procedure .....	6-277
6.7.5	Experimental test data analysis procedure .....	6-278
6.7.6	Results of the pressure drop experiment .....	6-282
6.8	<b>Field application of the pressure drop test.....</b>	<b>6-292</b>
6.8.1	Introduction.....	6-292
6.8.2	Leak test procedure .....	6-293
6.8.3	Pressure drop test data .....	6-294
6.8.4	Analysis of the pressure drop data .....	6-296

6.8.5	Leakage characterisation.....	6-303
<b>6.9</b>	<b>Conclusion.....</b>	<b>6-303</b>
<b>7</b>	<b>Assessing water losses in bulk pipelines .....</b>	<b>7-305</b>
<b>7.1</b>	<b>Introduction .....</b>	<b>7-305</b>
<b>7.2</b>	<b>Characteristics of non-revenue water (NRW) .....</b>	<b>7-305</b>
7.2.1	Introduction.....	7-305
7.2.2	Water balance.....	7-306
7.2.3	Challenges in bulk water systems .....	7-307
<b>7.3</b>	<b>Performance indicators for transmission mains .....</b>	<b>7-308</b>
7.3.1	Introduction.....	7-308
7.3.2	Total real losses in bulk pipelines.....	7-309
7.3.3	Real losses per mains length .....	7-309
7.3.4	Real losses per lateral surface .....	7-310
7.3.5	Effective initial leakage area per lateral surface .....	7-311
<b>7.4</b>	<b>Results of data analyses from performance indicators.....</b>	<b>7-312</b>
7.4.1	Introduction.....	7-312
7.4.2	Total real losses.....	7-313
7.4.3	Real losses per mains length .....	7-314
7.4.4	Real losses per lateral surface .....	7-316
7.4.5	Effective initial leak area per lateral surface.....	7-318
<b>7.5</b>	<b>Conclusion.....</b>	<b>7-321</b>
<b>8</b>	<b>Conclusions.....</b>	<b>8-323</b>
<b>8.1</b>	<b>Summary of this study .....</b>	<b>8-323</b>
8.1.1	The pipe condition assessment equipment (PCAЕ).....	8-323
8.1.2	Bulk pipeline field tests using the device .....	8-324
8.1.3	Dynamic pressure test for modelling and characterising small leaks .....	8-325
8.1.4	Performance indicators for assessing water losses in bulk pipelines.....	8-327
<b>8.2</b>	<b>Contributions to the field.....</b>	<b>8-327</b>
8.2.1	Technology for leak detection and characterisation .....	8-327
8.2.2	Leakage modelling.....	8-328
8.2.3	Performance indicators for bulk systems .....	8-329
<b>8.3</b>	<b>Recommendation for further work .....</b>	<b>8-329</b>
8.3.1	Pipe condition assessment device .....	8-329

8.3.2	Dynamic pressure test .....	8-330
<b>9</b>	<b>References.....</b>	<b>9-332</b>
<b>10</b>	<b>Appendix.....</b>	<b>10-1</b>
<b>10.1</b>	<b>Calibration certificates for instrumentations .....</b>	<b>10-1</b>
<b>10.2</b>	<b>Spreadsheet design for analysing PCAE data .....</b>	<b>10-3</b>



# List of Figures

Figure 2-1: Typical relationship between leakage rate ( $Q$ ) and runtime ( $t$ ) of leaks (Ziegler et al., 2009)	2-12
Figure 2-2: Road damage caused by underground undetected leak in Tanjong Bungah, Penang (Ying, 2015).....	2-14
Figure 2-3: International % non-revenue water (Mckenzie, Siqalaba & Wegelin, 2012) ...	2-16
Figure 2-4: Illustrating mechanisms that generate failures in buried pipes (Mora-Rodríguez et al., 2013) .....	2-22
Figure 2-5: Illustrating failure modes for pipelines (FCM & NRC, 2003).....	2-24
Figure 2-6: Bathtub curve of pipe performance with age (Najafi & Gokhale, 2005).....	2-24
Figure 2-7: Schematic of tethered inline leak location technology (Pure Technologies, 2015) .....	2-28
Figure 2-8: Schematic of sensors placed on bulk pipeline (Ecologics, 2017) .....	2-29
Figure 2-9: Apparatus used by Ledochowski to estimate burst elevation (Ledochowski, 1956) .....	2-31
Figure 2-10: Two examples showing the comparison of transient pressure waves for the intact system and leaking system after the downstream valve is closed (Ostapkowicz, 2016). 2-34	
Figure 2-11: Geometry for the orifice equation (Wolmarans, 2015).....	2-35
Figure 2-12: Discharge coefficients for orifice shape (Wolmarans, 2015).....	2-37
Figure 2-13: The general relationship between pressure and leakage rates using the power equation (Lambert, 2002).....	2-40
Figure 2-14: The maximum laminar and transitional flow rates for different leak openings (Clayton & van Zyl, 2007).....	2-42
Figure 2-15: How viscoelastic behaviour affects the N1 (Ssozi, Reddy & van Zyl, 2015). 2-44	
Figure 2-16: Fluidisation zone from vertical water leak jet (Ma, 2011).....	2-45

Figure 2-17: The initial orifice condition (left) and visual inspection after 100 hours of exposure to scouring (right) (Pike, 2015).....	2-46
Figure 2-18: The areas of 60mm long cracks in a class 6 uPVC pipe as a function (Cassa, van Zyl & Laubscher, 2010).....	2-48
Figure 2-19: Fixed and variable leak areas (Schwaller & van Zyl, 2014).....	2-49
Figure 2-20: The stress distribution around a longitudinal crack (a) deformed and (b) scaled up view of deformation.....	2-50
Figure 2-21: The stress distribution around a spiral crack (a) deformed and (b) scaled up view of deformation.....	2-51
Figure 2-22: The stress distribution around a circumferential crack (a) deformed and (b) scaled up view of deformation.....	2-51
Figure 2-23: The stress distribution around a circular hole .....	2-51
Figure 2-24: Data showing test of HDPE pipe (Ferrante, 2012) .....	2-52
Figure 2-25: Flow against pressure (Ferrante, 2012).....	2-53
Figure 2-26: Comparison of results of system FAVAD leak area $A_{0s}$ and the sum of individual areas (Schwaller, van Zyl & Kabaasha, 2015).....	2-57
Figure 2-27: Results of the comparison between system FAVAD head-area slope ( $m_s$ ) and the sum of individual leak head-area slopes ( $\Sigma m$ ) (Schwaller, van Zyl & Kabaasha, 2015) 2-58	
Figure 2-28: The plot of the power equation and the leakage number for various $m/A_0$ (Cassa & van Zyl, 2011).....	2-61
Figure 2-29: The relationship between the leakage exponent $N_1$ and the leakage number $L_N$ (Deyi, van Zyl & Shepherd, 2014).....	2-62
Figure 2-30: System initial area $A_{0s}$ vs leakage number $L_N$ (Deyi, van Zyl & Shepherd, 2014) .....	2-63
Figure 2-31: A failed cast iron pipe (The National Academies of Science and Engineering, 2011) .....	2-70
Figure 2-32: Cast iron rust tubercles (Huifang et al., 2014) .....	2-70

Figure 2-33: (a) Bell and spigot joint of cast iron pipes, (b) ground movement mechanics, (c) change in joint alignment due to ground movement (Rajani & Ahmed, 2013).....	2-71
Figure 2-34: Cross section of a ductile iron pipe showing graphitisation, City of Ottawa (De Rose & Parkinson, 1985) .....	2-72
Figure 2-35: External corrosion of ductile iron pipe .....	2-73
Figure 2-36: Ductile iron pipes used for drinking water: (a) the various components (AVA, 2010) and (b) commercially available ductile iron pipes (Robor Suppliers, 2015).....	2-73
Figure 2-2-377: Dent and hole in ductile pipe created by third party damage (Makar, Desnoyers & McDonald, 2001) .....	2-74
Figure 2-38: Formation of a seamless pipe (Liu, 2003).....	2-75
Figure 2-39: The different types of welding for seamed steel pipes (Liu, 2003) .....	2-75
Figure 2-40: Photograph of a failed weldment in a steel pipe (Lee et al., 2013).....	2-76
Figure 2-41: Histogram of failure rate based on failure mode of steel pipes (Rajeev et al., n.d.) .....	2-77
Figure 2-42: Polymerisation process .....	2-78
Figure 2-43: PVC pipe failure (Dueck, 2010) .....	2-79
Figure 2-44: Events leading to a blown-out section (Burn et al., 2004).....	2-80
Figure 2-45: Failure modes of PE pipes (O'Connor & Denton, 2012).....	2-81
Figure 2-46: Ductile failure mode of a PE pipe under pressure(O'Connor & Denton, 2012). 2-82	
Figure 2-47: Creep rupture curve (O'Connor & Denton, 2012).....	2-82
Figure 2-48: Brittle failure of a PE pipe - slit type fractures (O'Connor & Denton, 2012)	2-83
Figure 2-49: A GRP pipe being slewed into position (GRANT, 2016).....	2-83
Figure 2-50: GRP pipe failure (Australia, 2003) .....	2-84
Figure 2-51: Failure mode of an AC pipe: longitudinal split.....	2-84

Figure 2-52: Measure frequency of unreported leaks compared with the estimated pipe age (Laven & Lambert, 2012) .....	2-88
Figure 2-53: Histogram showing the distribution of number of leaks among the five flow rate classifications (Laven & Lambert, 2012).....	2-89
Figure 2-54: Histogram showing the contribution of each leak size to the total leakage rate (Laven & Lambert, 2012) .....	2-90
Figure 3-1 Process and component design of the system .....	3-93
Figure 3-2 Isometric view of the main components .....	3-94
Figure 3-3: Screen shots of various displays of the app .....	3-96
Figure 3-4: Process and component design of the system .....	3-98
Figure 3-5: Rototank dimensions (Roto Tank, 2016) .....	3-99
Figure 3-6: Euroflow horizontal multistage stainless-steel centrifugal pump(Euroflow. 2016) .....	3-100
Figure 3-7: Pump performance curves of different pump models (Euroflow, 2016) .....	3-100
Figure 3-8:Constant pressure inverter (DAB Water Technology, 2016).....	3-102
Figure 3-9: ABB Process Master FEX500 electromagnetic flow meter (ABB, 2017).....	3-103
Figure 3-10: PVC flange that connects to the electromagnetic flow meter.....	3-104
Figure 3-11: ABB 266 HART pressure transmitter.(ABB, 2018a) .....	3-105
Figure 3-12: ABB field-mount paperless recorder SM500F (ABB, 2018b) .....	3-106
Figure 3-13: (a) schematic view of the electrical connections (b) the actual connection..	3-107
Figure 3-14: Generator to be used for the bulk system device .....	3-108
Figure 3-15: 50mm compact PVC ball valve .....	3-110
Figure 3-16: 2" Kinetic air release valve .....	3-110
Figure 3-17: Pipe condition assessment equipment (PCAЕ) with component labels.....	3-112
Figure 3-18: Isometric views of the main components.....	3-112

Figure 3-19: The test equipment mounted onto a trailer (side view).....	3-113
Figure 3-20: Constructed pipe condition assessment equipment (Pcae) outside the laboratory at the University of Cape Town .....	3-113
Figure 4-1: Picture of the hydraulic section of the Civil Engineering Laboratory at the University of Cape Town (Malde & van Zyl, 2015) .....	4-115
Figure 4-2: Setup of the Pcae in the laboratory.....	4-115
Figure 4-3: Test pipes (a) round hole, (b) longitudinal crack, and (c) circumferential crack..	4-116
Figure 4-4: Test rig developed by van Zyl and Malde (2017).....	4-117
Figure 4-5: Experimental setup showing the connection point .....	4-117
Figure 4-6: Device setup: (A) supply pipe from underground reservoir, (B) 200 litre water tank, (C) tank to device connection, (D) Pcae, and (E) device to test rig connection .....	4-118
Figure 4-7: Inverter showing a set point pressure of 1 bar .....	4-119
Figure 4-8: Electromagnetic flow meter display panel.....	4-120
Figure 4-9: Graphic illustration of leak test algorithm .....	4-120
Figure 4-10: Data Manager Pro chart view (ABB, 2018b).....	4-121
Figure 4-11: Flow and pressure raw data for the 12mm round hole.....	4-128
Figure 4-12: Flow against head graph with power function fitted for the 12mm round hole..	4-130
Figure 4-13: Effective leak area against pressure head for the 12mm round hole .....	4-132
Figure 4-14: Leak area against pressure head for the 12mm round hole.....	4-133
Figure 4-15: Comparison of the power equation and the modified orifice equation with the experimental data .....	4-135
Figure 4-16: Flow and pressure raw data for the longitudinal crack .....	4-136
Figure 4-17: Flow against adjusted pressure for the longitudinal cracks .....	4-137
Figure 4-18: Effective area against pressure head for the longitudinal crack.....	4-139

Figure 4-19: Leak area against pressure head for the longitudinal crack .....	4-140
Figure 4-20: Flow against pressure head for the longitudinal crack.....	4-142
Figure 4-21: Flow and pressure raw data for the circumferential crack .....	4-143
Figure 4-22: Flow against adjusted pressure head graph with power function fitted for the circumferential crack .....	4-145
Figure 4-23: Effective leak area against adjusted pressure head for the circumferential crack4-146	
Figure 4-24: Leak area against adjusted pressure head for the circumferential crack.....	4-147
Figure 4-25: Comparison of the power equation and the modified orifice equation to the experimental data .....	4-149
Figure 5-1: Layout of the LK pipeline with the location of the valves.....	5-156
Figure 5-2: Google earth image of the location of chamber housing valve AV1 and the Koedoesnek reservoir.....	5-157
Figure 5-3: Google earth image of reservoir configuration .....	5-157
Figure 5-4: Connection of testing equipment .....	5-158
Figure 5-5: PCAE setup with trailer in loading bay .....	5-158
Figure 5-6: Elevation profile of the LK pipeline .....	5-160
Figure 5-7: Elevation profile with nodes for the LK pipeline .....	5-161
Figure 5-8: Flow and pressure raw data for the LK pipeline.....	5-162
Figure 5-9: Flow against adjusted pressure head graph with power function fitted for the circumferential crack for node 2, 3 and4 .....	5-164
Figure 5-10: Effective leak area against pressure for node 2, 3 and 4 on the LK pipeline	5-165
Figure 5-11: Layout of the SVM pipeline with the location of the valves. ....	5-168
Figure 5-12: Google earth image of Murrayfield reservoir configuration.....	5-168
Figure 5-13: Constant flow observed after valve AV1 was closed .....	5-169
Figure 5-14: Constant flow observed after both valve AV1 and V2 were closed .....	5-170

Figure 5-15: Map showing GP pipeline route starting at AV1 (5bar+) and ending at V2 (5 bar+)	5-171
Figure 5-16: Google earth image of Garsfontein reservoir setup	5-172
Figure 5-17: Google earth image of High Level reservoir configuration	5-173
Figure 5-18: Chamber housing valve V2, Valve V3, valve V4 and other apparatus installed on the GP pipeline	5-173
Figure 5-19: Connection of testing equipment	5-174
Figure 5-20: Flow and pressure raw data for the GP pipeline -first attempt	5-175
Figure 5-21: Flow and pressure raw data for the GP pipeline-second attempt	5-176
Figure 5-22: Flow and pressure raw data for the GP pipeline-third attempt	5-177
Figure 5-23: Showing air pocket collecting at a high point in a pipe	5-178
Figure 5-24: Alternative connection point – in red	5-179
Figure 5-25: Alternative connection point	5-179
Figure 5-26: Flow and pressure raw data for the GP pipeline-fourth attempt	5-180
Figure 5-27: Elevation profile of the GP pipeline	5-181
Figure 5-28: Elevation profile with nodes for the GP pipeline	5-182
Figure 5-29: Flow and Pressure raw data showing the stabilised data range selected for the GP pipeline	5-183
Figure 5-30: Flow against pressure data with power equation fitted for ode2, node 3 and node 4	5-185
Figure 5-31: Effective leak area against pressure for node2,3 and 4 on the GP pipeline	5-187
Figure 5-32: Layout of BC pipeline route starting at AV1 and ending at V2	5-189
Figure 5-33: Map showing FC pipeline route starting at AV1 (5bar+) and ending at V2 0.3 bar+)	5-191
Figure 5-34: Google earth image of configuration at Carina street where isolation V2 was housed and the PCAE was connected	5-191

Figure 5-35: Carina street inside chamber housing isolation valve V2.....	5-192
Figure 5-36: Image of Fort Klapperkop reservoir setup. ....	5-192
Figure 5-37: PRV's that were closed to isolate the FC pipeline.....	5-193
Figure 5-38: PCAE connection point on the PRV .....	5-194
Figure 5-39: Flow and pressure raw data for the FC pipeline- attempt 1 .....	5-195
Figure 5-40: Flow and pressure raw data for the FC pipeline- attempt 2 .....	5-196
Figure 5-41: Elevation profile of the FC pipeline.....	5-197
Figure 5-42: Flow and pressure raw data showing the stabilised data range selected.....	5-199
Figure 5-43: Flow against pressure with power equation fitted for node 2, node3 and node 4 on the FC pipeline.....	5-201
Figure 5-44: Effective leakage area against pressure head for node2 node 3 and node 4 on the FC pipeline.....	5-203
Figure 5-45: Part of the Overberg water network that shows the BS 8 pipeline spanning from V1 to V2.....	5-206
Figure 5-46: BS 8 pipeline layout with locations of the components used for the leak test....	5-207
Figure 5-47: Showing the Overberg test pipeline elevation profile.....	5-208
Figure 5-48: Air valve concrete chamber .....	5-208
Figure 5-49: (a) Air valve (b) BS 8 Pipeline stop valve connection.....	5-209
Figure 5-50: PCAE connected to the BS 8 pipeline .....	5-209
Figure 5-51: Showing the colour of water during the flushing process of the BS8 pipeline test 1 pipeline.....	5-210
Figure 5-52: PCAE water tank being filled Up at AV2.....	5-211
Figure 5-53: Elevation profile showing the different points analysed (top, centre and bottom) on the BS 8 pipeline.....	5-212



Figure 5-54: Elevation profile of the BS 8 pipeline with various nodes depicting change in pipe material and diameter.....	5-213
Figure 5-55: Showing the pressure and flow data for the BS8 pipeline test 1.....	5-215
Figure 5-56: Flow Rate against Pressure for the Three Scenarios.....	5-217
Figure 5-57: Showing the Modified Orifice Equation Leakage Parameters.....	5-219
Figure 5-58: Shows the comparison of the power equation and the modified orifice equation to the data.....	5-221
Figure 5-59: Location of the Jongensklip reservoir.....	5-224
Figure 5-60: Jongensklip Reservoir.....	5-225
Figure 5-61: Filling the PCAE Water Tank using a Hosepipe Connected to the Tap Reservoir.....	5-225
Figure 5-62: AV1 the Topmost Air Valve where the PCAE was Connected for the.....	5-226
Figure 5-63: BS8 pipeline elevation profile with nodes from 0-8 showing its various pipe material and diameters.....	5-227
Figure 5-64: Flow and Pressure Profile.....	5-229
Figure 5-65: Flow and Pressure data with a power equation fitted for node 1, 2 and i.....	5-230
Figure 5-66: Effective area against the pressure head for node 1, node 2 and node i.....	5-232
Figure 5-67: Wingfield pipeline layout.....	5-233
Figure 5-68: Elevation profile from valve V2 to valve V4.....	5-234
Figure 5-69: Shows the PCAE 50mm hosepipe being connected to the fire hydrant.....	5-235
Figure 5-70: Showing the colour of water during flushing.....	5-235
Figure 5-71: Shows the clear water after flushing.....	5-236
Figure 5-72: Shows the flow against pressure raw data for the Wingfield test pipe.....	5-237
Figure 5-73: Flow and pressure head for the varying pump speeds.....	5-239
Figure 5-74: Flow against pressure data.....	5-240

Figure 5-75: The nett result of flow against pressure curves.....	5-240
Figure 5-76: Effective area against pressure Head for the Wingfield Test 1.....	5-242
Figure 5-77: Effective Area against pressure for the Wingfield pipeline.....	5-243
Figure 5-78: The nett result of the effective area against pressure for the Wingfield pipeline. .....	5-243
Figure 5-79: Typical failure mechanisms in AC pipes ( Greyvenstein & van Zyl, 2005).	5-244
Figure 5-80: Wingfield pipeline layout.....	5-245
Figure 5-81: Fire hydrant connection .....	5-245
Figure 5-82: Failed fire hydrant pipe .....	5-246
Figure 5-83: Replaced fire hydrant pipe and head.....	5-247
Figure 5-84: Wingfield pipeline layout.....	5-247
Figure 5-85: Covered fire hydrant .....	5-248
Figure 5-86: Installed fire hydrant head with the PCAE Connected .....	5-249
Figure 5-87: Flow and pressure raw data for Wingfield test 3 .....	5-250
Figure 6-1: Isolated pipeline with leakage Q.....	6-255
Figure 6-2: Analytical pressure head against time.....	6-272
Figure 6-3: Numerical pressure head plotted against time for various time intervals .....	6-273
Figure 6-4: Schematic layout of the main components (Taylor, 2018).....	6-275
Figure 6-5: Photograph showing experimental setup .....	6-276
Figure 6-6: Pipe01 with round hole leak.....	6-276
Figure 6-7: Measured pressure head against time.....	6-283
Figure 6-8: Cumulative mass measured in the bucket against time.....	6-284
Figure 6-9: Measured leakage flow rate against time .....	6-285
Figure 6-10: Measured flow rate against pressure .....	6-286
Figure 6-11: Effective leakage area against pressure head.....	6-287

Figure 6-12: Plot of measured flow rate against pressure head .....	6-289
Figure 6-13: Measured cumulative volume against pressure head readings .....	6-290
Figure 6-14: Correlation between $m_{\text{measured}}$ and $m_{\text{numerical}}$ against pressure head .....	6-291
Figure 6-15: Comparison of $h_{\text{numerical}}$ and $h_{\text{measured}}$ .....	6-292
Figure 6-16: The pipeline layout at the University of Cape Town .....	6-293
Figure 6-17: The underground fire hydrant connection.....	6-294
Figure 6-18: The raw data output from the UCT pipeline test .....	6-295
Figure 6-19: Pressure against time data for the UCT pipeline test .....	6-296
Figure 6-20: Measured pressure and calculated pressure from guessed leakage parameters ..	6-298
Figure 6-21: Measured pressure head and pressure calculated from the simulated leakage parameters .....	6-299
Figure 6-22: Plot of calculated pressure and measured pressured against time .....	6-301
Figure 6-23: Calculated pressure head against time and measured pressure head against time .....	6-302
Figure 7-1: Illustrating a typical transmission main network .....	7-308
Figure 7-2: Real losses per annum for the tested pipelines .....	7-314
Figure 7-3: Real losses per mains length .....	7-316
Figure 7-4: Real losses per lateral surface .....	7-318
Figure 7-5: Results of the effective initial leak area for each pipeline. ....	7-320
Figure 7-6: Effective initial leak area per lateral surface.....	7-321

## List of Tables

Table 2-1: IWA standard water balance with terminology.....	2-10
Table 2-2: South Africa's national water balance 2009/10 (Mckenzie, Siquelaba & Wegelin, 2012).....	2-15
Table 2-3: Illustrating pipe failure mechanisms (American Water Works Service Company Inc. 2002).....	2-23
Table 2-4: Failure rate versus failure mechanisms .....	2-25
Table 2-5: Summary of N1 values reported in various studies.....	2-38
Table 2-6: The values of N1 for different flow regimes (Clayton & van Zyl, 2007) .....	2-41
Table 2-7: The leakage exponents for various pipe materials (Greyvenstein & van Zyl, 2005) .....	2-43
Table 2-8: Value assets of the Rand Water Board (Rand Water, 2007).....	2-64
Table 2-9: The design life of bulk water distribution assets (Rand Water, 2006).....	2-66
Table 2-10: PVC pipes to BS 3505.....	2-79
Table 2-11: Types of concrete pipes and their applications (Liu, 2003) .....	2-85
Table 2-12: A summary of the Observed Reinforced Concrete failure modes from Pratt et al., (2011) study .....	2-86
Table 2-13: Measured frequencies of unreported leaks on bulk pipelines in different geographical regions (Laven & Lambert, 2012).....	2-87
Table 2-14: Measured frequencies of unreported leaks on bulk pipelines in different materials(Laven & Lambert, 2012).....	2-87
Table 2-15: Measure frequencies of unreported leaks on bulk pipelines with different diameters .....	2-88
Table 2-16: Qualitative size classifications for leak flow rates in the UK (Bond et al. (2007)2-89	
Table 3-1: Details of the system components .....	3-95

Table 3-2: Performance table of the pump (Euroflow, 2016).....	3-101
Table 3-3: Cross-sections, flow velocities, pipe lengths and friction losses for various pipe diameters .....	3-109
Table 4-1: Parameters used to calculate the friction head loss for each step.....	4-124
Table 4-2: Hydraulic components and their minor loss coefficients .....	4-124
Table 4-3: Average flow, pressure and adjusted pressure for the 12mm round hole .....	4-129
Table 4-4: N1 values obtained by other researchers for the round holes in uPVC pipes ..	4-130
Table 4-5: Summary of the modified orifice equation results .....	4-131
Table 4-6: Summary of leakage parameters for the round hole leak.....	4-134
Table 4-7: Average measured flow, pressure and adjusted pressure for the longitudinal crack .....	4-136
Table 4-8: Summary of the modified orifice equation results .....	4-138
Table 4-9: Summary of leakage parameters for the longitudinal crack.....	4-141
Table 4-10: Average flow, pressure and adjusted pressure for the circumferential crack.	4-144
Table 4-11: Summary of modified orifice equation results for the circumferential crack	4-146
Table 4-12: Summary of leakage parameters for the circumferential crack.....	4-148
Table 4-13: Summary of the leakage parameters obtained for various types of leaks .....	4-150
Table 4-14: Comparison of results with van Zyl & Malde's (2017)study.....	4-151
Table 5-1: Summary of the tested pipelines and their respective locations in South Africa ...	5-153
Table 5-2: The averaged stabilised flow and pressure data for each node .....	5-163
Table 5-3: Summary of power equation leakage parameters for node 2, node 3 and node 4..	5-164
Table 5-4: Summary of modified orifice equation leakage parameters for the LK pipeline ...	5-166
Table 5-5: Pipe properties for each node .....	5-182

Table 5-6: Flow and adjusted pressure for each node on the GP pipeline.....	5-184
Table 5-7: Summary of power equation leakage parameters for node 2, 3 and 4 on the GP pipeline.....	5-185
Table 5-8: Effective leak area and adjusted pressure for node2, 3 and 4 on the GP pipeline .	5-186
Table 5-9: Summary of the modified orifice equation leakage parameters for node 2,3 and 4 on the GP pipeline.....	5-187
Table 5-10: Summary of pipe properties between nodes.....	5-198
Table 5-11: Summary of the flow and adjusted pressures for each node on the FC pipeline .	5-200
Table 5-12: Summary of the power equation leakage parameters for node 2, 3 and 4 on the FC pipeline.....	5-201
Table 5-13: Summary of effective leak area and pressure for each node on the FC pipeline .	5-202
Table 5-14: Summary of the modified orifice equation leakage parameters for node 2, 3 and 4 on the FC pipeline.....	5-204
Table 5-15: Summary of the various pipe sections properties of the BS8 pipeline used for analysis.....	5-214
Table 5-16: Averaged flow and pressure values for the BS 8 pipeline at the top centre and bottom. ....	5-216
Table 5-17: Showing the N1 Leakage Parameters Results.....	5-217
Table 5-18: The Effective Area against pressure for the Three Scenarios .....	5-218
Table 5-19: Shows a Summary of the Modified Orifice Equation Leakage Parameter Results .....	5-220
Table 5-20: Power equation and modified orifice equations for the three case scenarios.	5-221
Table 5-21: Characteristics of the leakage detected on the steel section of the BS 8 Pipeline	5-223

Table 5-22: Node elevations .....	5-228
Table 5-23: The averaged flow and pressure at Node 1, 2, and i .....	5-230
Table 5-24: Summary of the N1 leakage parameters found for BS8 pipeline Test 2.....	5-231
Table 5-25: Comparison of results from test 1 and test 2 of the BS8-Pipeline .....	5-233
Table 5-26: Shows the averaged stabilised flow and pressure for Each Step Test.....	5-238
Table 5-27: Summary of the N1 leakage parameters.....	5-241
Table 5-28: Summary of successful tests.....	5-252
Table 6-1: Pipe, fluid and leak properties .....	6-270
Table 6-2: Measured properties of the test pipes .....	6-274
Table 6-3: Constant properties taken from literature.....	6-274
Table 6-4: Leakage parameters for the power equation.....	6-286
Table 6-5: Results of the leakage parameters for the modified orifice equation.....	6-288
Table 6-6: Table of constants.....	6-297
Table 6-7: Leakage parameters .....	6-299
Table 6-8: Results of the leakage parameters for the analytical solution .....	6-301
Table 7-1: IWA water balance (Farley, 2001) .....	7-306
Table 7-2: Results of real losses calculated from the modified orifice equation.....	7-313
Table 7-3: Water loss reference values .....	7-315
Table 7-4: Results of the real losses per mains length.....	7-315
Table 7-5: Results of real losses per lateral surface.....	7-317
Table 7-6: Results of effective initial leak area per lateral surface indicator .....	7-319

# 1 Introduction

## 1.1 Background

A common trait amongst all water pipes is that their condition deteriorates over time (Kleiner & Rajani, 2001). There are various causes of water pipe deterioration, including corrosive environments, soil movement, poor construction standards, fluctuation of water pressure and excessive vibrations (Hunaidi et al., 2004). Deteriorating water pipes inevitably lead to the formation of cracks and holes, causing leakage to occur.

Leakage through deteriorating pipe systems is one of the components contributing to water loss and comprises the real (physical) losses from pipes, joints, fittings, and overflows from service reservoirs (Farley, 2001). Leakage is most frequently defined as the amount of water that escapes from the pipe system by means other than through controlled action (Puust et al., 2010).

Leakage in pipe systems is classified into two categories, namely: background and burst-related leakage. Background leakage typically comprises of small leaks that drip and seep water from leaky joints, valves or fittings. Burst-related leakage, on the other hand, comprises of large individual leaks often resulting from a sudden rupture of a joint or other major structural pipe failure (Puust, et al., 2010). Commonly used flow rate boundary between background leakage and burst leakage is 250 l/hr.

Even though burst-related leakage is more catastrophic in failure, background leakage still contributes the largest share of real water losses. This is because background leaks typically occur more frequently and have much longer runtimes than burst-related leaks (D. Ziegler et al., 2009). The long run-time is due to the nature of background leaks, which are typically difficult and sometimes impossible to detect without costly and invasive efforts such as excavating the pipe.

A great deal of work has been done on managing background and burst-related leakage in distribution pipe systems that supply water to consumers. This is evident from literature sources such as the International Water Association (IWA) (Lambert & Hirner, 2000) and American Water Works Association (AWWA) guidelines, which provide state of the art guidelines to water auditing and reduction of water losses in distribution systems (Thornton & Lambert, 2005).



One area that has received very little attention, however, is leakage in bulk pipe systems. Koelbl & Zipperer (2018) indicate that for bulk systems, so far there are no suitable water loss assessment methods and performance indicators available.

Unlike distribution pipe systems, bulk pipe materials and diameters are rather homogeneous and have limited number of connections (off-takes). Bulk pipelines typically connect water treatment plants to bulk reservoirs and distribute water from reservoirs to different towns or water supply zones, and thus transport large volumes of water. Consequently, there is a need to investigate improved methods for assessing water losses in bulk pipelines. In this study, the term “bulk pipelines” is used interchangeably with “transmission mains” and both terms are defined as any pipelines that do not supply directly to consumers.

One of the important tasks that the IWA Water Loss Specialist Group has been carrying out is to investigate why leakage flow rates in pipe systems are significantly more sensitive to pressure than predicted by the orifice equation (Lambert, 2000). Consequently, pipe leaks are typically modelled using a power equation, both in leakage management practice and hydraulic modelling studies (Lambert, 2000; Schwaller & van Zyl, 2014).

Although hydraulic theory predicts that the power equation exponent (known as the leakage exponent and commonly denoted with symbols  $\alpha$  or  $N1$ ) has to be 0.5, field tests from various countries have reported leakage exponents ranging from 0.36 to 2.79 (Thornton & Lambert, 2007). It has been demonstrated in numerous individual leakage studies that varying leakage areas may be the cause of the wide range of  $N1$  values, and this is widely accepted as the main reason for the observed variability in  $N1$  (van Zyl et al., 2017).

Significant progress in understanding the behavior of leaks areas in pipes has been made in the last decade. Laboratory experiments (Malde & van Zyl, 2015) and several studies that used finite element simulations (Cassa & van Zyl, 2013; Ssozi, Reddy & van Zyl, 2015; Nsanzubuhoro, van Zyl & Zingoni, 2016) have shown that leakage areas vary linearly with pressure, irrespective of the leak type, loading conditions or pipe material and section properties.

Based on the extensive research into pipe leakage behaviour, the distribution systems research group at the University of Cape Town, under the guidance of Prof JE van Zyl, developed a pipe condition assessment system for assessing the condition of pipes and valves in distribution systems. This system, however, was designed and limited to distribution systems pipes i.e.

pipes with a diameter less or equal to 110mm and is not capable of testing bulk pipelines - which typically comprise of pipelines with diameters greater than 110mm.

## **1.2 Problem statement**

It is often difficult to determine water losses in a bulk pipe system because of the high flow rates and pressures. The high flow rates make it impractical or prohibitively expensive to measure flow rates at both ends of bulk pipelines (Burstall, 1997). Consequently, water audits have long been challenging due to the lack of reliable methods for assessing leakage in bulk pipelines (Laven & Lambert, 2012).

A more serious challenge experienced in developing countries such as South Africa, is skills shortages at various levels, coupled with inadequate transfer of skills and experience (Webb, Mergelas & Laven, 2009).

Furthermore, any efforts to carry out bulk water pipeline condition assessments are limited to very poor keeping of pipeline records, inaccurate and non-existing “as-built” drawings and limited maintenance programs that make any inspection challenging. This has forced the use of educated guesses and assumptions, which can be misleading. For example, leakage is often assumed to be 2 or 3% of the total inflow for bulk pipeline systems (Burstall, 1997). However, due to the large flows of water conveyed by bulk pipelines, even 2 or 3% losses represent large volumes of water lost.

To date, very little is known about the extent of leakage on bulk pipelines in South Africa and internationally. Therefore, there is a great need to develop a simple, low-cost pipe condition assessment technique that can survey large sections of pipe infrastructure in short periods of time with minimal disturbance to the operation of the infrastructure.

## **1.3 Goal and Objectives of the research**

The primary goal of this research is develop a technique for assessing the condition of bulk water pipelines with minimal disturbance to the operation of the infrastructure. The technique is based on earlier research into pipe leakage behaviour and is applied to bulk pipelines. The technique uses a pressure testing method in combination with the latest theoretical models of the behaviour of leaks areas with pressure to determine the characteristics and extent of leaks

in the bulk pipelines, thus providing an application of assessing bulk pipelines – an application for which this approach has not yet been explored.

Pressure testing is an established technique to test the water tightness of new bulk pipelines before they are commissioned. The proposed technique can be viewed as a modification of this method and entails measuring leakage flow and pressure in an isolated section of the pipe. The results are used to determine the characteristics and extent of water losses in the isolated pipe section. The test can be performed in a short space of time to minimize disruption to the system operation.

Developing a standard way to assess the condition of bulk pipelines has numerous benefits, one of which is to provide a standardized dataset on the true condition of bulk pipelines from different countries, which currently does not exist. This dataset can be used to develop suitable empirical performance indicators – like the Unavoidable Annual Real Losses (UARL) for distribution pipelines.

The goal of developing an effective technique for assessing the condition of bulk pipelines was achieved in this study through developing and verifying a device for leak detection and characterization and thereafter testing various bulk pipelines in the field. The following are the main objectives and the novelty of this study:

### **1.1.1 Developing a pipe condition assessment equipment**

It has already been mentioned that the assessment of leakage in bulk pipelines is challenging due to the lack of reliable methods that currently exist. Although numerous new leak detection devices have been developed and deployed, questions about their efficiency, effectiveness and economic viability have impeded their wide scale deployment for bulk pipes.

A novel condition assessment device, called the PCAE, was designed and constructed for leak detection and characterisation. The device consists of a water storage tank, power supply, variable speed pump, electromagnetic water meter, pressure sensor, data recorder and various valves.

The device is connected to an existing access point on a bulk pipeline, such as a blank flange, fire hydrant or air valve. The device then performs a pressure test on an isolated bulk pipeline. The test data is stored on an SD card housed by the data recorder and analysed further with relevant software to (a) detect leakage, (b) quantify leakage and (c) identify the leakage

characteristics. This device has the potential to identify much smaller leaks than is currently possible through other devices.

### **1.1.2 Testing real bulk pipelines using PCAE**

The PCAE was first tested in the laboratory on a pipe with known leakage characteristics, before it was taken to the field for trials on real pipelines. Once the efficacy of the device was verified through the experimental tests, bulk water suppliers and municipalities were approached to take part in the study.

To test a real bulk pipeline, a section of the pipe was isolated, and the PCAE was connected to an access point. Once initial checks have been performed to ensure that the section was isolated and no air was present in the pipe, the variable speed pump of the device was used to induce a sequence of different pressures in the pipe. At each pressure, the flow rate into the pipe, which represented the leakage rate, was measured. The data was then being analysed to determine the pipe's initial leak area and head-area slope.

Unlike in acceptance testing for new pipes, the proposed method does not require the working pressure of the pipe to be exceeded, and thus the risk of damaging the pipe or isolating valves through the test is negligible. In addition, the test can be performed in a short space of time to minimize disruption to the system operation.

### **1.1.3 A dynamic pressure test approach for leakage characterisation**

When a pressurised pipe without any leakage is isolated from the rest of the pipe network, its pressure will remain constant at the pre-isolation level. However, if the isolated pipe has a leak, the pressure in the pipe will drop due to the water leaving the pipe.

The PCAE was installed on the test pipe section via a convenient connection point to record the pressure in the pipe. The test pipe was then isolated from the rest of the pipe network by closing valves, and the pressure readings were recorded.

The leakage characteristics of the test pipe were estimated from the recorded pressure against time data. Generally, if the pressure remained constant, then the pipe was without a leak. However, if the pressure dropped with time, then this would indicate a leak in the pipe.

A novel mathematical model was developed to describe the pressure drop behaviour for pipelines. The derived mathematical model uses the known properties of the pipe to estimate

the size of the leak and the type of leak (round holes, corrosion leaks, longitudinal or circumferential cracks) present in the pipe.

#### **1.1.4 Evaluating potential new performance indicators for bulk pipelines**

Performance indicators are useful tools to monitor or assess a water utility's performance and analyse performance trends. Various performance indicators have been developed for assessing water losses in water distribution systems. These indicators consider relevant structural network parameters that are intrinsic to distribution systems networks. However, thus far, for bulk pipelines no such performance indicators and assessment schemes exist.

Various performance indicators were used to compare the different bulk pipelines that were tested, using the PCAE. A novel performance indicator suitable for technical purposes was also introduced and then applied to assess the bulk pipelines that were tested with the device. This novel indicator uses the estimated leak area size and the calculated total lateral surface of pipe, and thus gives an indication of the size of the leak relative to the surface of the pipe.

### **1.4 Scope and limitations**

The scope and limitations for the research are as follows:

- The laboratory tests carried out in this study were limited to pipe samples with an outer diameter of 110mm and a length 800mm. The restriction on 110mm was due to the Viking Johnson (VJ) couplings that clamp the pipe in the laboratory, which can only fit a sample of that diameter
- In the laboratory, leaks were artificially induced, and these leaks were limited to round holes, circumferential cracks and longitudinal cracks. The laboratory tests used to verify the PCAE were limited to the following leaks: 12mm round hole, the longitudinal and circumferential cracks were limited to a 100mm by 1mm slit. Whilst, the laboratory test used to verify the dynamic pressure test were limited to a 1mm round hole.
- For the field tests, information about the tested pipelines were sourced from site visits and useful resources provided by the pipeline owner (e.g. as built drawings, GIS and Google Earth data files).

- For the theoretical model developed to describe the dynamic pressure of isolated sections of pipe with leaks, it was assumed that the pipeline deforms only elastically when evaluating the variation of the internal pipe volume with changes in pressure due to pipe wall strain.
- The number of pipelines tested in the field was dependent on the availability of the pipe owners.

## 1.5 Layout of the thesis

This thesis is divided into eight chapters including this introductory chapter. The first part of the thesis (i.e. Chapter 2) contains background information and reviews of existing literature on water losses, leakage modelling, components of bulk pipeline networks and leakage detection technologies.

The second part of this thesis (Chapters 3 to 7) presents the application of a novel approach to characterise leakage on a range of bulk pipe materials, diameters and length. The design and construction of a novel device for leakage characterisation is first described, this is followed by experimental tests carried out to verify the efficacy of the device, thereafter field tests are carried out and finally various performance indicators are evaluated to compare the bulk pipelines tested in the field.

The main conclusions and some recommendations for further work are presented in Chapter 8. A summary of the contributions to the field of leakage modelling and characterisation in bulk pipelines are also provided in chapter 8.

A more detailed outline of the six core chapters is presented next:

**Chapter 2** introduces a literature review of the latest research on the relationship between pressure, leakage and leakage area. Several direct and indirect leakage detection and condition monitoring techniques are also reviewed.

**Chapter 3** deals with the conceptualisation, design and construction process followed to assemble the PCAE. The pipe condition assessment prototype and the leakage test algorithm are described, highlighting the device's capabilities and limitations.

**Chapter 4** explains the experimental methodology, describing the development of a suitable experimental procedure in the laboratory to test pipes with known leakage characteristics, using the PCAE. Three leak types were tested, namely: round hole, longitudinal crack and circumferential crack.

**Chapter 5** introduces the field tests carried out using the PCAE. Several bulk pipelines at different South African bulk water suppliers and municipalities were tested to determine the extent of leakage on a range of pipe materials, diameters and ages. The latest models on the behaviour of leaks area with pressure, discussed in Chapter 2, are used to characterise and determine the extent of water losses on the tested bulk pipelines.

**Chapter 6** proposes a new mathematical model that uses pressure and time data of an isolated pipe section to identify and characterise leakage. The mathematical model considers the following: the variation of the internal pipe volume with changes in pressure due to pipe wall strain, the compressibility of the fluid inside the pipe, orifice hydraulics and the variation in the leak area as a function of pressure. An experimental setup was used to verify the mathematical model. Thereafter, a real pipeline was tested using this approach.

**Chapter 7** applies some suitable bulk pipeline performance indicators for assessing water losses on the pipes tested as described in Chapter 5. For each indicator the pipelines are ordered from the pipeline found to have the largest water losses to the pipe with the lowest water losses. An investigation was carried out to verify whether the order of the pipelines changed depending on the indicator used.

## 2 Literature Review

### 2.1 Introduction

This literature review focusses primarily on the broad field of water losses, and in particular on water losses due to water leakage and the mitigation of such leakage. The literature review begins with an overview of water losses and leakage, highlighting the main factors that influence leakage, and the impact thereof.

Attention is then drawn to the means of interventions required to manage water losses, which include the development of a sound and effective leakage mitigation strategy. This is followed by an overview of a number of direct and indirect leakage detection and condition monitoring techniques.

The literature review then explores various leakage modelling techniques, mainly the orifice equation, the power equation and the modified orifice equation. In this study, emphasis is placed on the modified orifice equation model because this model has been proposed to provide a more realistic model of leakage behaviour (van Zyl et al., 2017). Furthermore, the modified orifice equation can be used to characterise individual leaks as well as multiple leaks in water distribution systems. It is, therefore, recommended in the literature that the modified orifice equation should be tested for application in identifying and characterising leakage on bulk pipelines, as this approach has not yet been explored.

The focus of the literature study then shifts to bulk pipeline systems, which are explored in some detail and the various components of a bulk pipeline system outlined. The typical pipe materials used for bulk pipelines are also discussed.

Finally, an overview of what we currently know about leakage on bulk pipelines is given. The need for a simple, low-cost pipe condition assessment technique that can survey bulk pipeline infrastructure in short periods of time with minimal disturbance to the operation of the infrastructure is then highlighted.



## 2.2 Water loss and leakage

### 2.2.1 Definitions and terminology of water loss and leakage

Rogers (2014) simply defines water loss as the difference between the total production of water and the total consumed or billed. However, there is much more to it than this. In 2000, the International Water Association (IWA) task force published an international best practice water balance approach to calculate water losses. Table 2-1 illustrates the components of the IWA standard water balance.

Table 2-1: IWA standard water balance with terminology

System input volume (corrected for known errors)	Authorised consumption	Billed authorised consumption	Billed metered consumption (including water exported)	Revenue water
			Billed unmetered consumption	
		Unbilled authorised consumption	Unbilled metered consumption	Non-revenue water (NRW)
			Unbilled unmetered consumption	
	Water losses	Apparent losses	Unauthorised consumption	
			Customer metering inaccuracies	
		Real losses	Leakage on transmission and/or distribution mains	
			Leakage and overflows at utility's storage tanks	
Leakage on service connections up to point of customer metering				

As can be seen from Table 2-1, water loss is the difference between *System input volume* and *Authorised consumption* and consists of two main components: *Apparent losses* and *Real losses*, which ultimately contribute to *Non-Revenue Water* (NRW) and require significant resources to mitigate effectively. The third component, *Unbilled Authorised Consumption*, can be controlled fairly well without much resource. It is therefore imperative to understand the *Real losses* and *Apparent losses* components of water losses in order to make meaningful achievements towards reducing water loss and subsequently *Non-Revenue Water*.

#### 2.2.1.1 Apparent losses

Apparent losses are losses that are not due to physical leaks in the infrastructure but are caused by other factors. These factors can be unauthorised consumption (typically theft or illegal use),

meter inaccuracies and data handling errors. This component of the water balance is usually systematically estimated based on local knowledge of the systems (Lambert, 2002).

In summary, apparent losses are comprised of all water that is successfully delivered to the customer but is not metered or recorded accurately which results in an error in the actual customer consumption.

### **2.2.1.2 Real losses**

Real losses are the actual water volumes that are lost through all types of leaks, bursts and overflows up to the point of customer metering (Farley, 2003). Ziegler et al., (2009) further explain that real losses can be classified according to their (a) location, and (b) their size and runtime.

#### *(a) Location*

- ***Leakage on transmission and distribution mains:*** may occur at the pipes (bursts due to extraneous causes or corrosion), joints (disconnection, damaged gaskets) and valves (operational or maintenance failure) and, typically, have medium to high flow rates and short to medium runtimes.
- ***Leakage and overflows at utility's storage tanks:*** largely caused by deficient or damaged level controls. In addition, seepage may occur from masonry or concrete walls that are not water tight. Water losses that occur from tanks are often underestimated and, though easy to detect, repair is usually elaborate and expensive.
- ***Leakage from service connections:*** service connections are usually referred to as the weak points of water supply networks, because their joints and fittings exhibit high failure rates. Leaks on service connections are usually difficult to detect due to their comparatively low flow rates.

#### *(b) Size and runtime*

***Reported or visible leaks:*** these usually come from bursts or ruptures of joints in pipe systems. The leaking water will appear at the surface quickly, depending on the water pressure, leak size, as well as on the soil and surface characteristics. These are often obvious and no special equipment is required to locate such leaks see Figure 2-1.

- ***Unreported or hidden leaks:*** Farley (2001) reports these leaks to have flow rates greater than 250 l/h at 50 m pressure, but because of unfavourable conditions they do not appear at the surface.

- Background leakage:** these leaks have flow rates less than 250 l/hour at 50 m pressure and do not appear at the surface. These are very small leaks and cannot be detected using acoustic leak detection methods. It is often assumed that many background leaks are never detected and repaired but leak until the effective part is replaced. As can be seen in Figure 2-1, background leaks have the longest run-times and thus often contribute a major share in real water losses. While apparent losses can nearly be eliminated completely, a certain level of real losses will always remain in any water supply. This amount is called the Unavoidable Annual Real Losses (UARL). The difference between the Current Annual Real Losses (CARL) and the UARL is considered to be potentially recoverable real losses (Farley, 2001). The ratio between the CARL and UARL gives the Infrastructure Leakage Level (ILL).

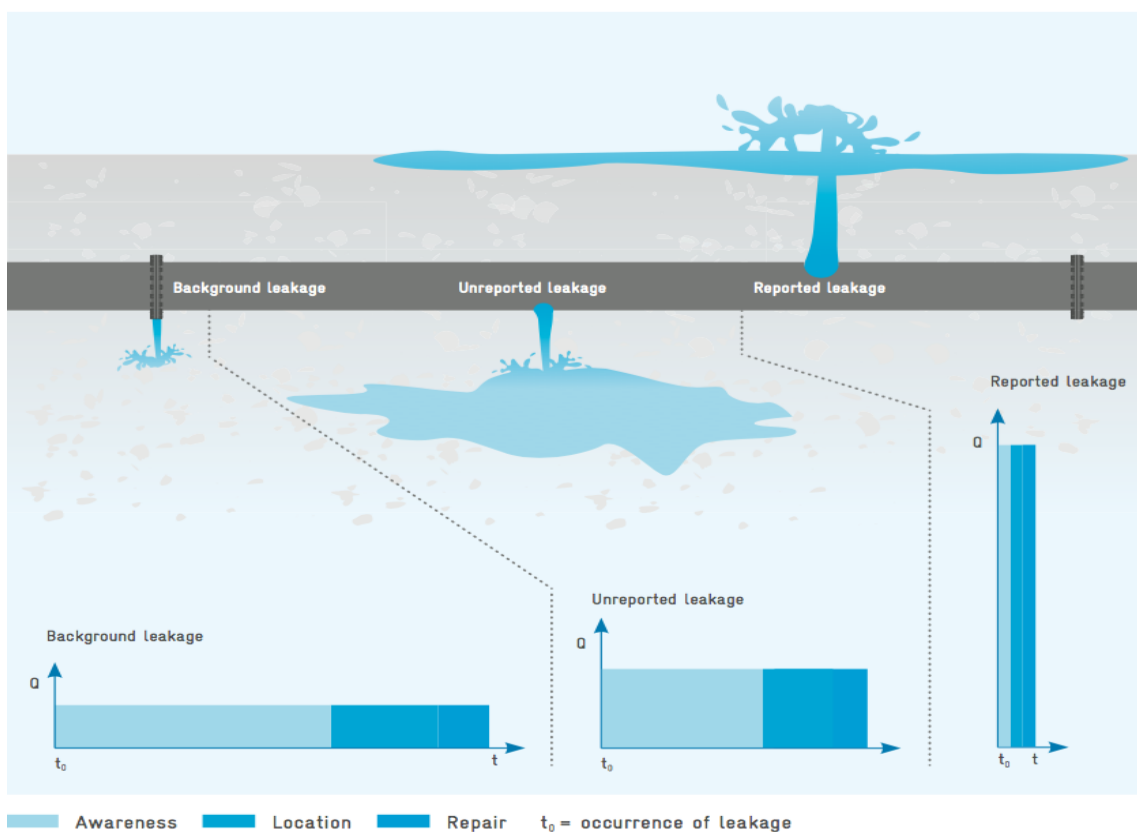


Figure 2-1: Typical relationship between leakage rate ( $Q$ ) and runtime ( $t$ ) of leaks (Ziegler et al., 2009)

## 2.2.2 Factors influencing leakage

It has been accepted that real losses cannot be entirely eliminated, due to economic and technical reasons. Nonetheless, by understanding the factors that influence leakage, it is

possible to manage them within economic limits. Farley (2001) identified four key factors that influence leakage within a pipe network:

- **Resources:** availability of water, finances and personnel
- **Infrastructure conditions:** regarding pipe materials, operating system pressures and renewal of rehabilitation policy
- **Institutional attitude:** institutional structures, regulation and politics
- **Leakage control policy:** activity, perception and technical expertise.

Water loss reduction requires a holistic approach where all these four key factors are taken into account. It is no good, for example, having increased leak detection activities with deteriorating infrastructure conditions because the overall outcome will not yield any positive results with regards to curbing water loss. Furthermore, even if the financial means are available, without the correct policies and institutional structures there will not be any positive effect.

### **2.2.3 Impact of leakage**

Leakage impairs all aspects of the sustainability of operating water supply systems, of both bulk and distribution systems. In many cases leakage presents the biggest barrier to the primary objectives of water supply systems, namely to supply adequate quality and quantity of water to consumers (Ziegler et al., 2011). Additionally, Ziegler et al. (2011) listed four areas of negative impact of leakage: (a) economic impact, (b) technical impact, (c) social impact, and (d) environmental impact.

#### *(a) Economic impact*

Portable water is treated and transported to the end user. There are obvious costs associated with this process. Water companies/utilities hope to recover these costs by billing consumers. Water that is lost along the way to the consumer translates to a loss of revenue for the water utilities. Furthermore, bursts that result in high flow rate leaks often results in expensive repair work. Also, those leaks that remain undetected for long periods of time often cause damage to surrounding infrastructure such as roads and buildings, as illustrated in Figure 2-2.



*Figure 2-2: Road damage caused by underground undetected leak in Tanjung Bungah, Penang (Ying, 2015)*

*(b) Technical impact*

Leakage will increase the loads on wastewater and stormwater systems. These increased loads result in increased treatment costs due to the additional water being received by the wastewater treatment plants. Leaks may also cause air to enter into the pipes which can result in water hammers, damage to water meters, increased susceptibility to corrosion and measurement errors for water utilities. Water quality issues may arise as a result of leaks in a pipe that allow the infiltration of pollutants from pipe surroundings.

*(c) Social impact*

The social issues related to leakage is the mistrust that develops between water utilities and consumers. This mistrust surfaces when municipalities/water utilities are unable to satisfy consumer demand because of leakages and various forms of water losses. This dissatisfaction by the consumer often negatively affects their willingness to pay water bills (Ziegler et al., 2009).

*(d) Environmental impact*

Water is a finite resource and in some regions, particularly in sub-Saharan Africa, it is a scarce resource (Webb, Mergelas & Laven, 2009). It is therefore imperative to handle water economically. However, leakage does not allow the sustainable use of this resource, primarily

because it places further stress on the environment due to the need for additional extraction. As noted by Colombo & Karney (2002), leakages also cause inefficient energy distribution through the network and are thus wasting the energy that is used for pumping the water.

### 2.2.4 Present status of water losses in South Africa

In a study done by Mckenzie, Siqalaba & Wegelin (2012), the state of South Africa’s water losses was probed from data collected from 132 municipalities. This data represented over 75% of the total municipal water supply. Table 2-2 shows the results of the data analysis presented in the form of an IWA water balance. According to the data, the national non-revenue water figure is estimated to be 36.8%. Of the 36.8%, 25.4% was estimated to be *real losses* through leakage.

Table 2-2: South Africa's national water balance 2009/10 (Mckenzie, Siqalaba & Wegelin, 2012)

<b>System Input Volume</b> 100.0%	<b>Authorised Consumption</b> 68.2%	<b>Billed Authorised</b> 63.2%	<b>Revenue Water</b> 63.2%
	<b>Water Losses</b> 31.8%	<b>Unbilled Authorised</b> 5.0%	<b>Non-revenue Water</b> 36.8%
		<b>Commercial Losses</b> 6.4%	
		<b>Real or Physical Losses</b> 25.4%	

South Africa’s non-revenue water figures (36.8%) are similar to the international average (~37%) as indicated in Figure 2-3. Mckenzie, Siqalaba & Wegelin (2012) maintain that while South Africa compares well to the international average, it does not compare well to other developed water-scarce countries such as Australia, whose non-revenue water levels are less than 10%. The study by Mckenzie, Siqalaba & Wegelin (2012) also estimates the national ILI to be at 6.8, which is on par with the world average. Despite the finding that South Africa’s

water losses are on par with the international norms, there is still a lot of scope for improving this status. Also, considering that South Africa is a water-scarce country, it cannot afford to waste much water.

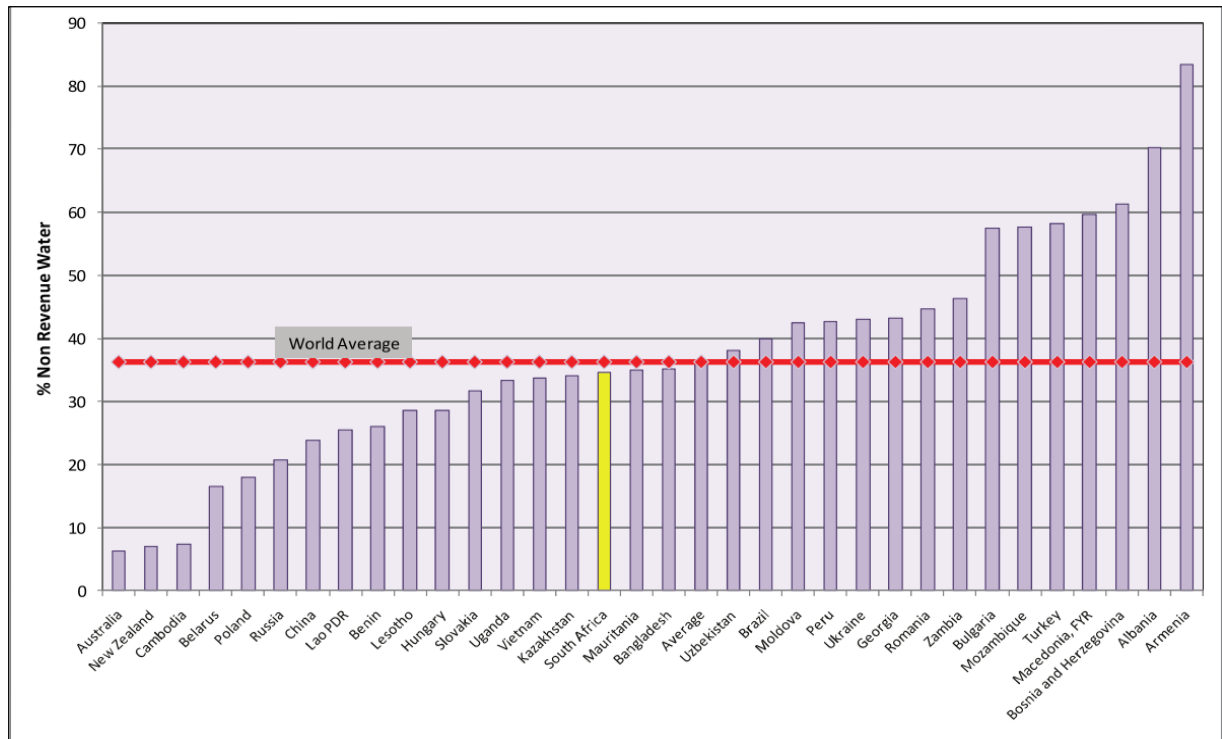


Figure 2-3: International % non-revenue water (Mckenzie, Siqalaba & Wegelin, 2012)

Another concern in South Africa is the high per capita water use of around 235 l/c/d. This is an indication that the average citizen still does not understand the scarcity of this resource. In addition, the current national volume of non-revenue water is about 1 580 million m<sup>3</sup> of water per annum. According to Mckenzie & Seago (2005) this volume of non-revenue water is equivalent to the water supply of Rand Water (Africa’s largest water utility). At the nominal production rate for the various municipal categories, the current South African non-revenue water represents about R7,2 billion per annum.

Mckenzie, Siqalaba & Wegelin (2012) also highlight concerns regarding the lack of responses, poor quality data and fabrication of results from municipalities. About 45% of municipalities could not report on the water volumes entering and leaving their networks, and this could be attributed to poor record keeping, indicating that no water demand management was taking place at these municipalities. More recently, figures from the Department of Water and Sanitation, quoted by van Vuuren (2014), reveal that only 52% of municipalities participated in a later study, indicating a further drop in participation from 75% in the previous study.

## **2.3 Water loss management**

### **2.3.1 Introduction**

It is essential that water utilities manage water losses in their water network systems as this leads to an improved economic efficiency of the whole system as well as to improved services to clients. However, before designing a strategy for managing water losses, decision makers should be aware of the importance of providing financial and personnel resources towards initiatives for reducing water losses.

Ziegler et al. (2009) list some reasons that may justify increased expenditure on managing water losses for decision makers:

- *Operating cost efficiency:* a well-maintained pipe system will require fewer repairs, lower production costs and prevent costs associated with damage due to bursts or excessive water losses.
- *Improved metering and billing:* improved water supply with minimal leaks and intrusion has a positive impact on apparent losses because air inside the system can lead to metering errors.
- *Reduced health risks:* sewage and other pollutants can infiltrate the pipe system through leaks and trigger water-borne diseases in low pressure systems or in the case of intermittent supply.
- *Reduced loads on sewers:* water lost filtrates to sewer systems and increases the load on sewer pipes and wastewater treatment plants.

### **2.3.2 Implementing successful water loss management programmes**

In order to achieve effective water management, a strategy must be developed and implemented. Farley (2003) presented the following central questions to be answered when developing a strategy:

- How much water is being lost?
- Where is it being lost?
- Why is it being lost?
- What strategies can be introduced to reduce losses?
- How can the strategy be maintained?



These questions are explored further in the next sections.

### ***2.3.2.1 How much water is being lost?***

Firstly, the development of a suitable strategy requires a detailed assessment of the water entering and exiting the system. Not all pipes, however, have flow meters at both ends of the pipe system, and the flow meters, especially for large diameter pipelines, are often not accurate enough to detect substantial leakage. Surveys and comprehensive assessments of pipe infrastructure are therefore required in the initial stages of developing a water strategy to accurately determine leakage and pipe condition (Prinsloo, Wrigglesworth & Webb, 2011).

As stated by Lambert (2000), the most important part of determining how much water is being lost in a system is to accurately quantify the volume of water which is entering the system. This view is supported by Rogers (2014) who states that an immediate and precise way of quantifying leakage is needed which is not subject to measurement errors. Rogers suggests that in distribution networks the minimum night flow approach was developed for this precise reason.

The results of a network assessment can be summarised in form of the IWA water balance. The IWA water balance presents the different components of NRW and provides guidance on how much water is lost through real losses, such as leaks, and how much water is lost through apparent losses. It clearly indicates how the water entering the system is allocated. Based on a study by the Environmental Protection Agency [EPA], 2010 on leakage management technologies in the UK, it was suggested that before any pipe testing strategy is developed, the approximate water balance must first be determined with available equipment such as flow meters.

### ***2.3.2.2 Where is water being lost?***

For the water management strategy to be most effective, it is important that the most critical pipelines, those that leak the most, are identified and rehabilitated in priority sequence (Bennis et al., 2011). When the state of leakage of all the pipe systems is known, an engineering evaluation must then be conducted to identify and prioritise pipes and pipe sections in need of urgent repair or replacement (Prinsloo, Wrigglesworth & Webb, 2011).

### ***2.3.2.3 Why is water being lost?***

The evaluation process must not only ascertain the amount of leakage but also include an assessment of the physical condition of the pipe asset to understand why water is being lost.

The type of deterioration mechanisms present, the existing and potential failure modes as well as the expected frequencies of the failures are all valuable data through which the risk of the asset can be determined (Liu et al., 2012).

#### ***2.3.2.4 What strategies can be introduced to reduce water losses?***

Decisions such as whether to undertake leakage reduction work and what level of leakage is acceptable are ultimately economically motivated. The cost of treating and pumping the water that never reaches the customer is an economic loss. An economic investment that increases exponentially as the allowable leakage is lowered, is needed to recover it. An optimum balance therefore exists between savings and investment; this is specific to each network (Rogers, 2014).

It is therefore advisable that the economic level of leakage for every pipe system is known before a decision is made on the leakage strategy for that pipe system (Farley, 2003). The economic level of leakage is the level below which the cost of identifying and repairing the leaks will be higher than the value of water lost. The total elimination of all leaks will never be economically, nor physically, feasible and thus the economic level of leakage can be used as a guideline to determine whether a leakage reduction strategy is justifiable or not (Fantozzi & Lambert cited in Bennis et al., 2011).

Once the water leakage strategies for reducing pipeline losses have been implemented successfully, the remaining question is how the strategy can be maintained (Farley, 2003).

#### ***2.3.2.5 How can the strategy be maintained?***

One way of maintaining a functioning system is by implementing monitoring programmes that track the deterioration of the system (Prinsloo, Wrigglesworth & Webb, 2011). With such a strategy, continuous monitoring or regular testing of the infrastructure must be carried out. The advantage of this strategy is that intervention is only carried out on pipe systems that are in need of attention, while the disadvantage is the cost of continuous condition monitoring.

Another method calls for planned intervention at suitable intervals. The Economic Intervention Frequency (EIF) (Lambert & Lalonde (2005) cited in Laven, (2012) is the frequency at which the cost of an intervention equals the value of the water lost through leaks since the previous intervention. Determining EIF for all pipe systems would be the best first step in determining the ideal intervals between interventions. A suitable frequency can also be determined by statistical modelling of historic failure rates or by modelling and forecasting of deterioration

based on measured deterioration (Liu et al., 2012). For both these methods, however, accurate and detailed historic data, obtained from pipe inspections, is required.

With water leakage strategies in place for the pipe systems, funds, tools and available technologies can be pro-actively allocated to where they are most needed (Prinsloo, Wrigglesworth & Webb, 2011). It should be clear that all the above steps to developing and implementing a sound water strategy strongly depend on information available on the condition of the pipe system. According to Prinsloo, Wrigglesworth & Webb (2011) this information should form the basis of such a strategy. Therefore, in cases where the condition of the pipe infrastructure is not known, an effective water management strategy is strongly dependant on an efficient and preferably low-cost pipe condition monitoring technique.

### **2.3.3 Measures taken to manage water losses in South Africa**

In order to combat water loss in South Africa, municipalities have to manage their networks better. A recent development by South Africa called the “No Drop” certification has been designed to assist municipalities to assess and improve their water use efficiencies. This certification programme will be used to assess, verify and validate a municipality’s efficiency against set criteria (Herbst & Raletjena, 2015).

The “No Drop” certification will entail a yearly assessment and a score of all the water supply systems within the various municipalities. The results of these assessments will be used to acknowledge and award municipalities for good practice. On the reverse side, the “No Drop” score also directs the necessary regulatory assistance and support interventions to resolve non-compliance in municipalities with a low “No Drop” score.

Another initiative by the South African government to curb water losses is the commencement of the “War on Leaks” which is a training programme that aims to empower the South African youth to play a role in the fight against water leaks.

According to Mckenzie, Siqalaba & Wegelin (2012), 25% non-revenue water is a realistic target for South Africa and is achievable over a period of 10 years, if R2 billion is invested annually. This is a justifiable expense considering that water is becoming increasingly scarce and valuable. Another source puts the required investment at 2% of the value of South Africa’s current water infrastructure (van Vuuren, 2014).

## 2.4 Sources of leakage in pipe systems

### 2.4.1 Introduction

As water infrastructure ages and deteriorates over time, engineers continuously need an understanding of the state of the infrastructure to make informed decisions on whether to replace or repair. Pipelines in particular are the major assets of water systems, and pipeline failures will most likely impact on the level of service provided by the water provider.

This section gives an overview of the various sources of leakage. Sources of leakage can vary significantly depending on the type of pipe failure. Pipe failures are influenced by numerous factors that will also be discussed here.

### 2.4.2 Factors that influence pipe failures

Pipe failures can take any shape or form, hence there are so many modes of pipeline failures. A report by the Federation of Canadian Municipalities & the National Research Council (2002) describe numerous factors that can affect the rate of deterioration of water distribution pipelines that may lead to their failure. These factors are categorised as follows:

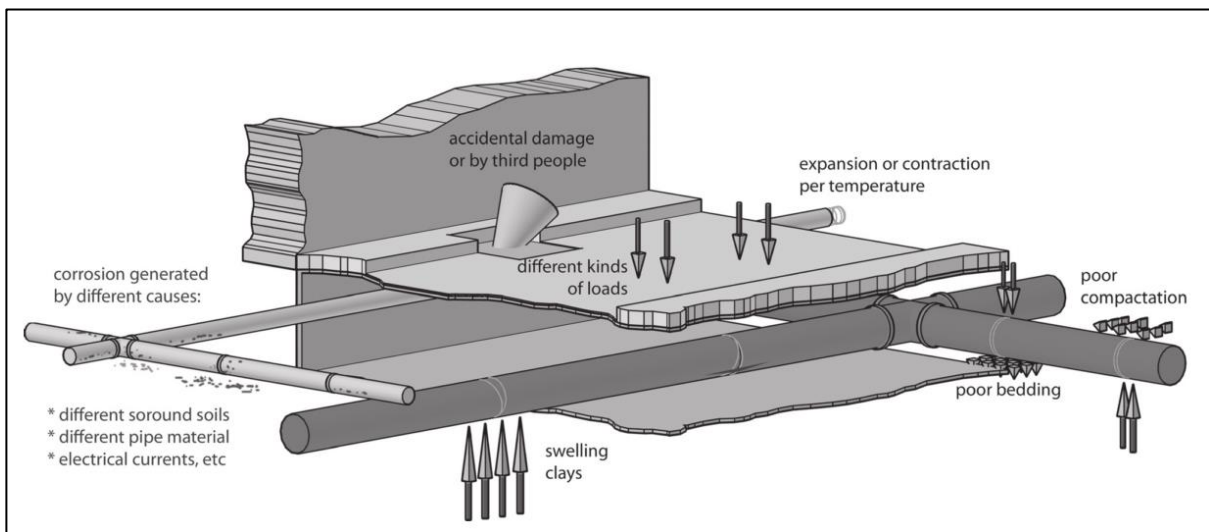
- **Physical factors:** these include pipe material, the pipe wall thickness, pipe age, pipe vintage (pipes made at a particular time and place), pipe diameter, type of joints, thrust restraints (inadequate thrusts and restraints can increase longitudinal stress), pipe lining and coating, dissimilar metals (susceptible to galvanic corrosion), pipe installations, pipe manufacturer.
- **Environmental factors:** pipe bedding, trench backfill, soil type, ground water, climate, pipe location, disturbances, stray electrical currents, seismic activity.
- **Operational factors:** internal water pressure, transient pressure (changes in internal pressure change the stress conditions acting on the pipe), leakage, water quality (some water is aggressive and promotes corrosion), flow velocity (rate of internal corrosion is greater in unlined dead-ended mains), backflow potential (cross connections with systems that do not contain potable water can contaminate the system), operation and maintenance practices.

### 2.4.3 Failure mechanisms

Kleiner & Rajani (2001) have suggested three main aspects of mechanisms that generate pipe failures. These aspects somewhat overlap with the factors reported by the Federation of

Canadian Municipalities & the National Research Council. 2003. They are listed here and illustrated in Figure 2-4:

- structural properties of pipes, pipe material, interaction between soil and pipe, and facility quality
- internal loads due to operation pressure and external loads, and accidental or intentional damage
- material deterioration due to internal and external chemical environments.



*Figure 2-4: Illustrating mechanisms that generate failures in buried pipes (Mora-Rodríguez et al., 2013)*

According to Kleiner & Rajani (2001), pipe deterioration can be classified into two categories: structural deterioration and inner surface deterioration. During structural deterioration, the pipe's structural resistance and ability to support loads diminishes. During inner surface deterioration, the pipe's hydraulic capacity diminishes with water quality issues arising, and structural resistance reduction occurs in the case of severe corrosion.

The American Water Works Service Company Inc. (2002) also reckons that in order to minimise pipeline failures and maximise the life of assets, it is important to understand the failure mechanisms of pipes. These failure mechanisms, which are a result of structural deterioration or inner surface deterioration, are listed in Table 2-3.

Table 2-3: Illustrating pipe failure mechanisms (American Water Works Service Company Inc. 2002)

Operational/physical/Environmental	Applies to	Chemical	Applies to
Manufacturing defects	M,P,C	Internal corrosion	M,C
Improper design/installation	M,P,C	External corrosion - soil	M,C
Geologic instability	M,P,C	External corrosion - other	M,C
Higher operating pressure	M,P,C	Leadite corrosion	M
Hydraulic transients	M,P,C	Leadite expansion	M
Change in water temperature	M	Material incompatibilities	M
Excessive external loads	M,P,C	Gasket deterioration	M,P,C
Damage from digging	M,P,C	Material fatigue	P

M Metallic (ductile or cast iron)

P Plastic (PVC or HDPE)

C Concrete (Reinforced or pre-stressed)

Leadite, a sulphur based joint sealing compound used in the 1940's and 1950's to seal the joints of metallic pipes.

Kleiner & Rajani (2001) have published models of different types of breaks in pipe walls that are caused by three different factors:

- circumferential breaks caused by longitudinal tension  
longitudinal breaks caused by circumferential tension, also known as cross-section stresses or hoop stresses, and
- cracks in union caused by a cross-sectional tension in the pipe union.

Figure 2-5 below summarises the different types of structural failure modes and provides the cause of each. It is worth noting that there are other failure modes that do not fit into any of the classes prescribed below in Figure 2-5.

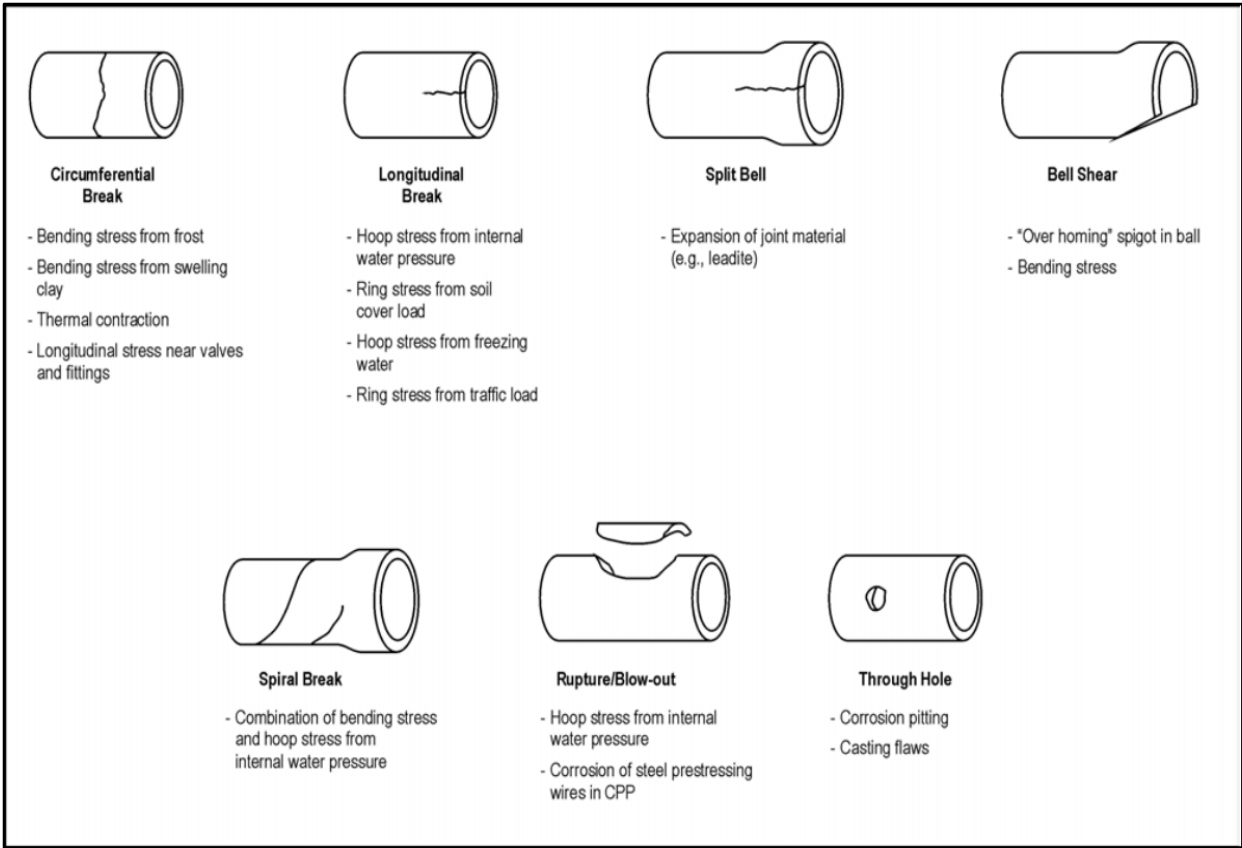


Figure 2-5: Illustrating failure modes for pipelines (FCM & NRC, 2003)

Finally, the pipe’s age is another important indicator of pipe failure. As is shown in Figure 2-6, when the pipe is first installed it has a high probability of experiencing failure as a result of construction defects. During the pipe’s mid-life, this probability of pipe failure decreases. However, as the pipe approaches the end of its design life, the probability of failure starts to increase again until the pipe eventually has no more useful life.

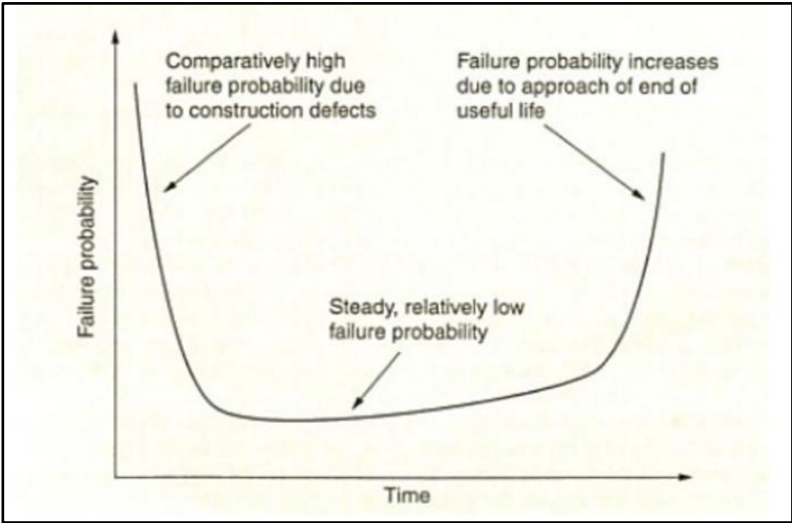


Figure 2-6: Bathtub curve of pipe performance with age (Najafi & Gokhale, 2005)

Muhlbauer (2004) describes some failure mechanisms as time dependant, whilst others are random, see Table 2-4. Time-dependant failure mechanisms are associated with aging effects and thus with time the failure tendency increases. Random failure mechanisms that only change with a changing environment are usually associated with constant failure.

*Table 2-4: Failure rate versus failure mechanisms*

<b>Failure mechanisms</b>	<b>Nature of mechanisms</b>	<b>Failure rate tendency</b>
Corrosion	Time dependant	Increase
Cracking	Time dependant	Increase
Third party damage	Random	Constant
Laminations/blistering	Random	Constant
Earth movements	Random (except for slow-acting instabilities)	Constant
Material degradation	Time dependant	Increase
Material defects	Random	Constant

## **2.5 Leak detection methods for water pipelines**

### **2.5.1 Introduction**

Water distribution is generally done through underground pipes. Monitoring the underground water pipelines is more difficult than monitoring those located on the ground in open spaces. Permanent water loss occurs if there is a disturbance in pipelines such as leakage. Leaks in pipes can be caused by several factors, such as the pipe's age, improper installation, and natural disasters. Therefore, a solution is required to detect and control the damage when there is a leak.

This section aims to give an overview of the current leak detection methods for water pipelines. The methods are described, and their limitations are also outlined.

### **2.5.2 Leakage control strategies**

According to Farley (2003), two different types of leakage control strategies exist, namely passive control and active control. These will be discussed in the following sections.



### ***2.5.2.1 Passive leakage control***

Passive control is a reactive approach whereby the operation team attends to leaks that are reported to them or that they come across by coincidence. Only leaks with significant effect on the functioning of the system and visible leaks are attended to with this strategy.

When it comes to passive leakage control strategies, the need for rehabilitation and replacement of pipes is decided on criteria such as the number of recent failures, age, material and risk.

### ***2.5.2.2 Active leakage control***

Active leakage control, on the other hand, is a pro-active approach that involves the deployment of operators to investigate systems and detect leaks that have not been reported. This approach includes regular surveys and monitoring of leakage and pipe condition.

For active leakage control, a number of distress indicators exist for water pipes that, if detected, can give the operator a good indication on the condition and risk of failure of the pipe system. The distress indicators that are most commonly detected include pipe leakage, corrosion, pipe wall defects and lining defects.

Significant cost savings can result from active detection approaches, because they allow the water utility to maintain their pipelines and identify only specific sections in need of replacement, instead of replacing the entire pipeline (Prinsloo, Wrigglesworth & Webb, 2011).

## **2.5.3 Factors that influence leakage control strategies**

In order for the most suitable leakage control strategy for a network to be deployed, the following factors must be considered (Farley, 2003) and are discussed here in some detail.

### ***2.5.3.1 Financial constraints on equipment and labour***

Due to the high cost associated with the equipment and labour required for active leakage control, this strategy appears to be expensive. In many cases, funds available for such strategies are constrained as the monetary benefits are not realised. Passive strategies, however, often result in late identification of failures. The consequences of these failures as well as the increased effort required to rectify them require considerably more funding than would be needed if active strategies were implemented.

### ***2.5.3.2 Risk and consequences of failure***

The consequences of unexpected downtime due to pipe failure also affect the leakage control strategy. If, for instance, the pipe system supplies important consumers such as power stations

that are solely dependent on the supply, consequences can be detrimental and extremely expensive. Active control would be an absolute necessity in such cases.

### ***2.5.3.3 Pipe accessibility and geological conditions***

In some cases, active control can be difficult and expensive to implement because access to the pipe may be restricted. This can be due to the pipe passing through rough terrain or through restricted areas. Passive control in turn may be ineffective in rural areas where pipe bursts can remain unnoticed for long periods of time.

Geological conditions, such as the soil type and moisture content, also play a role in determining the most suitable strategy. In pipe environments where bursts do not show on the ground surface, passive control methods may be ineffective. The applicability and effectiveness of certain active control methods are also influenced by ground conditions.

### ***2.5.3.4 Scarcity and value of water***

Passive control strategies can be justified in water abundant environments and in cases where little production energy has been transferred to the water. In water scarce countries, however, a high level of activity and investment in leakage monitoring is justifiable.

Unfortunately, in most developing countries passive leakage control is the most common strategy, even though active strategies would be more suitable in many conditions. Reasons for this include funding constraints, poor management and a lack of knowledge of active assessment technologies.

## **2.5.4 Current leak detection methods**

Methods used for active condition monitoring of pipes are generally one of two types, either direct or indirect. Direct condition assessments involve the direct assessment and identification of the pipe condition and defects, as well as the interpretation of signals emitted from these defects. Indirect condition assessments involve the analytical interpretation of data obtained from conditions induced onto the pipe systems.

In this section, direct and indirect condition assessment methods that are commercially available are discussed. The limitation of each method is also highlighted.

### ***2.5.4.1 Inline leak detection approach***

The Sahara system is an in-line detection technique and is shown schematically in Figure 2-7. This technique uses acoustic sensors in combination with a CCTV camera to simultaneously

identify leak locations and inspect the internal condition of the pipe. The location of leaks and rough estimates of the leak sizes are identified from the distinct noises detected by the parachute apparatus (Webb, Mergelas & Laven, 2009).

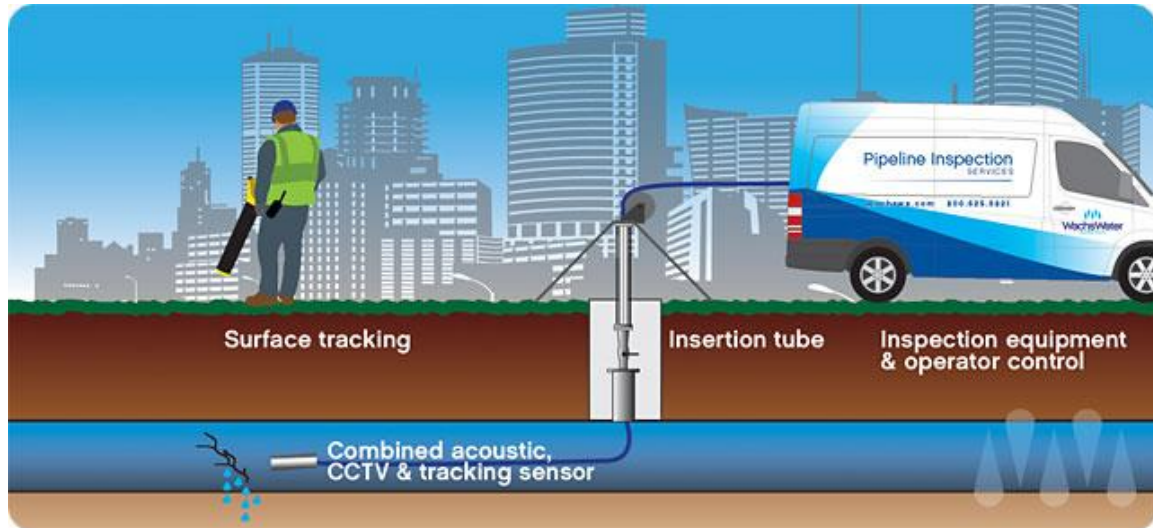


Figure 2-7: Schematic of tethered inline leak location technology (Pure Technologies, 2015)

The technique makes use of a tethered device that is fitted with a parachute which uses the flow of the pipeline to pull the system through the entire length of the pipe. By 2008, tethered inline leak detection was in active use across the United Kingdom, continental Europe and North America (Webb, Mergelas & Laven, 2009). One of the main advantages of the system is its compact size when the parachute is in a collapsed position, enabling the device to travel through obstacles in the pipeline, as well allowing for the device to be easily introduced into the pipe through small pipe openings.

#### 2.5.4.1.1 Limitations of the Sahara system

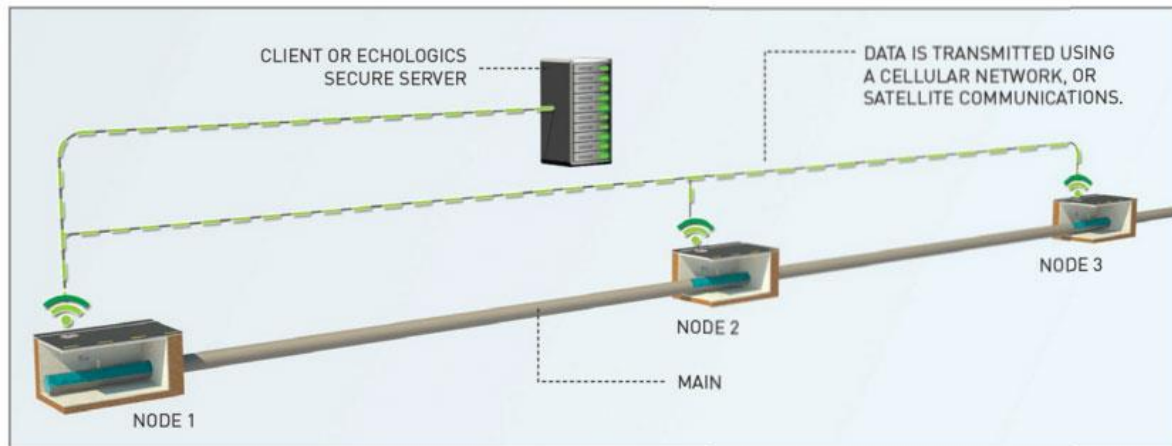
A limitation of this approach is the presence of complex interconnected networks which present operational challenges and risks that make inline technologies completely impractical. The inline approach is best suited for very long point-to-point pipelines.

Furthermore, in comparison to other in-line inspection methods it is quite expensive (typically around R325 000 per km) and requires highly skilled operators to trace the device on the ground surface as it travels through the pipe.

#### 2.5.4.2 Correlators

This approach involves the use of sophisticated transmission main correlators. These correlators are developed to have sensors with acoustic filters and signal processing algorithms.

As can be seen in Figure 2-8, the nodes placed on the pipeline are sensors that collect data about pressure, flow and leak detection and use wireless transmission to send that data to a central server.



*Figure 2-8: Schematic of sensors placed on bulk pipeline (Ecologics, 2017)*

The time delay between the two measurements is measured by correlation. With the propagation noise velocity known and the distance between the two sensors, the location of the leak can be detected (Hunaidi & Chu, 1999).

#### **2.5.4.2.1 Limitation of correlators**

The performance of this technology can be compromised by high environmental acoustic noise that can hide sounds emitted from leaks, especially for low pressures. A further drawback of this approach is that the effectiveness is dependent on a number of factors that influence the amount of noise created by leaks. For instance, higher pressure pipe leaks generate more noise than low pressure leaks (Hunaidi & Chu, 1999).

Pipe material also has a significant effect, with a large amount of attenuation experienced in plastic pipes, while signals travel furthest in metal pipes. Rigid pipe materials also lead to higher predominant frequencies that are usually less susceptible to low frequency interference. It is thus clear that this method is not effective for all types of pipe systems. Large, low pressure pipe leaks in plastic pipes, for example, are harder to detect than small, high pressure pinhole leaks in steel pipes.

Finally, this approach requires highly skilled operators that are able to identify and distinguish between leakage signals and acoustic noises (Hunaidi & Chu, 1999).

### ***2.5.4.3 Detection techniques by conservation of mass***

#### **2.5.4.3.1 General description**

Conservation of mass techniques require the measurement of flow into and out of the pipeline, with mass flow appearing to be the easiest and most common of these techniques (Ostapkowicz, 2016). The mass flow technique can accurately determine the existence of leaks as well as the combined intensity of all the leaks. It, however, lacks the ability to locate the leaks (Ostapkowicz, 2016).

The most primitive application of the mass flow technique is achieved by simply installing flow meters at the beginning and at the end of the pipeline under inspection. The difference in the flow entering and leaving the pipe indicates the amount of leakage from the system, with accuracy solely dependent on the flow meters used. Flow conditions other than steady state conditions negatively influence the accuracy of this method, partially due to the delay in the pipe inlet and outlet flows in respect to the pressure changes (Ostapkowicz, 2016; Turkowski & Bratek, 2007).

An adaption of this technique exists for water distribution networks and allows for identifying the approximate location of leaking pipe sections. It is known as the District Meter Area (DMA) technique. With this approach, a network is divided into a number of sections known as District Meter Areas (DMAs). The inflow to each DMA is measured and monitored. Leakage can then be pinpointed by progressively isolating the DMAs and the pipes within the DMA networks (Rogers, 2014).

#### **2.5.4.3.2 Conservation of mass to pinpoint pipe burst elevation**

Ledochowski (1956) suggested another method to narrow down the location of a leak, if it is known that only a single leak exists. This method assumes that the leakage flow can be categorised by the common orifice equation, with a constant orifice coefficient of 0.5.

With the pipeline pressure known at a reference level, and the flow rate known before and after adding a certain amount of pressure, the head or the flow coefficient can easily be calculated by solving the following two equations simultaneously:

$$Q_1 = Ch^{0.5}$$

*Equation 2-1*

$$Q_2 = C(h + p)^{0.5}$$

The elevation of the leak is then determined from this head. With the leak elevation known, the potential leak site can be obtained from the pipeline profile. Tests were carried out by isolating a section of the pipe and applying a test pump to a convenient connection point on the pipe. The following apparatus was used:

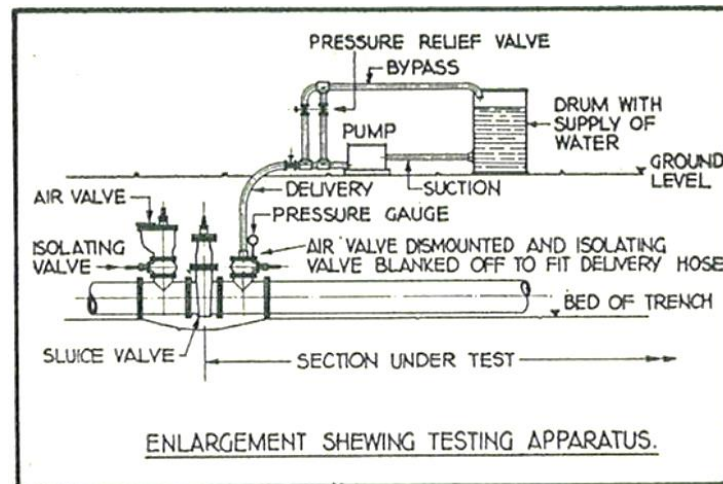


Figure 2-9: Apparatus used by Ledochowski to estimate burst elevation (Ledochowski, 1956)

A pump transfers water from a supply drum into the pipe. Shortly before the feeder pipe enters the pipe section under test, a bypass splits from the feeder pipe and returns the water supplied by the pump back into the supply drum. Two control valves, one on the feeder branch and the other on the bypass branch, can be adjusted to control the flow into the pipe section and to maintain the desired pressure. A pressure relief valve, which is fitted just after the pump and also feeds into the bypass, is set to a maximum allowable pipe pressure to protect the pipeline from becoming over-pressurised. A pressure gauge indicates the current system pressure.

A desired pressure in the pipe is then maintained and the leakage or flow rate at this pressure is determined by measuring the drop in water level in the supply drum.

Unfortunately, the author encountered difficulties in maintaining a desired pressure and making accurate readings while the pump was running, due to the vibrations of the pump. The author therefore altered the method slightly. With the alternative method, the pump is switched on until the desired pressure in the pipe is achieved. The pump is then switched off and the amount of water that flows back into the supply drum is measured in conjunction with the resulting pressure drop. This test was carried out over a short period of time in order to limit the effect of the leakage from the pipeline. A relation between water lost and drop in pressure was

obtained in this way. Thereafter, the pipe was pressured again. This time, the valves were closed, so that no water could exit the pressured pipe except through the leak. Time and pressure readings were then observed, and a time-pressure relation was obtained. With these two relations, the relationship between pressure and leakage rate could be plotted, from which the leak elevation could be obtained by solving the above two orifice equations.

This system proved advantageous in identifying the elevation of large leaks and thereby assisting in locating those leaks on systems with considerable slopes. This method is, however, only suitable for estimating the leak location if only one leak exists on the pipe section under test.

#### ***2.5.4.4 Negative pressure wave and gradient methods***

##### **2.5.4.4.1 Description**

These methods are indirect condition monitoring techniques than can detect abrupt new leaks such as pipe bursts. In steady state conditions, when a burst occurs in a pipe, it will generate negative pressure waves into both the upstream and downstream direction of the pipeline. With the negative pressure wave method, the waves can be detected with sensitive sensors at either end or, preferably, at multiple locations on the pipeline. The leak location can then be calculated using the measured time of flight of the upstream and downstream wave in conjunction with the pipe wave speed. The gradient method requires multiple sensors on the pipeline which detect the degree of attenuation of the pressure waves created by the leak. The degree of wave attenuation over distance can be graphed as straight lines that intersect at the leak location (Ostapkowicz, 2016)

##### **2.5.4.4.2 Limitations**

These methods can only be used to detect and locate large leaks and cannot be used to detect existing or slowly increasing leaks (Ostapkowicz, 2016).

#### ***2.5.4.5 Inverse transient method***

##### **2.5.4.5.1 Description**

Inverse transient analysis (ITA) was formally introduced in 1994 by James A. Liggett and Li-Chung Chen. Since the introduction of ITA, experimental studies by Vitkovsky et al., (2001) as well as field studies by Stephens et al., (2005) have shown that the ITA is a promising leak detection technique.

ITA involves injecting hydraulic transients with known intensity at a given location in a network (e.g. a controlled opening/closing of a fire hydrant). The transient signals are then recorded at various predetermined locations throughout the system. In parallel, a computer model of the network is coded into a transient analysis software program in which identical transient events are presented. The model is run for numerous sets of system parameters, a process facilitated by optimization routines such as genetic algorithms, where the objective function seeks to minimise the sum of squared differences between measured and computed pressure responses, until the best match obtained.

Discrepancies between response signatures (pressure traces at certain locations) can indicate the presence of leaks, assuming that accurate information regarding system condition and demand is available.

The inverse transient method and frequency domain techniques obtain leak information from transients with the inverse method. That is, instead of using system characteristics to determine the system's state, the known system state is used to identify system characteristics such as leaks. Leaks, for instance, generally cause a sudden drop in pressure due to the absorption of energy by the leak, and can be identified by analysing the time of flight of the wave and the characteristic wave speed of the pipeline.

#### **2.5.4.5.2 Limitations**

A known limitation of the ITA method is its reliance on the availability of an accurate transient model of the network. For instance, it can become very complex and time consuming to mathematically model a long pipe section with all its components, and the resulting models often depend on a number of assumptions for pipe parameters such as pipe wall friction (Karney, Khani & Halfawy, 2008).

Another limitation of using the ITA is the challenge of distinguishing leak signals from signals caused by other system features. Air cavities in the pipelines, for instance, cause discrepancies between the actual and modelled results, often raising false alarms (Ostapkowicz, 2016).

#### **2.5.4.6 *Frequency domain technique***

##### **2.5.4.6.1 Description**

The frequency domain technique is an alternative approach to the ITA method that does not solely rely on the accuracy of the systems parameters. With this method, steady oscillatory flow is induced in the pipeline by operating a valve downstream of the pipe to a set pattern.



The frequency response of the network is then measured and analysed at the downstream valve for a range of frequencies.

The response of the network is then compared to a modelled frequency response for the pipe without leaks, which is numerically calculated from the known pipe characteristics (Colombo, Lee & Karney, 2009). Obtaining the expected frequency response at the closing valve is much simpler and requires much less computational input in comparison to the inverse transient method. The leaks and leak magnitudes are then identified from the amplitudes of the measured frequency response, as shown in Figure 2-10.

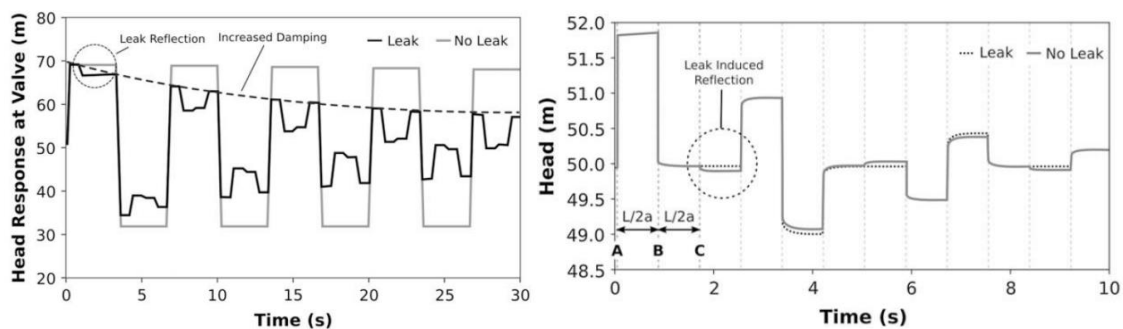


Figure 2-10: Two examples showing the comparison of transient pressure waves for the intact system and leaking system after the downstream valve is closed (Ostapkowicz, 2016)

#### 2.5.4.6.2 Limitations

An advantage of the transient analysis approach is that the methods only cause a disruption in the operation of the pipe for a short period of time. The frequency response method has the additional advantage that all actions and measurements are taken at one location on the pipeline (Lee et al., 2005). A drawback of this method is that transient states must be created through the opening and closing of valves, abnormal to the normal operation of the plant. This leads to an increased risk of failure of the pipeline and may require the operating conditions to be constrained (Lee et al., 2005). Furthermore, this technique requires highly qualified staff due to its current complexity (Ostapkowicz, 2016).

A number of field tests have been carried out and are reported on in the literature (Colombo et al., 2009). Although these tests prove that the above methods can be successful in identifying and pinpointing leakage, this technique remains too complicated and error prone for successful commercial implementation. Significant work is still needed to develop this approach into a practical leak detection method (Colombo et al., 2009).

## 2.6 Leakage modelling for water pipe systems

### 2.6.1 Introduction

This section gives an overview of the state-of-the-art methodologies for leakage modelling. Given that leakage has a variety sources as was explored in the previous section, and that pipe failures can take on any form or shape, a discussion on techniques for modelling leakage is now provided.

The following three leakage models will be discussed: the orifice equation, the power equation and the modified orifice equation.

### 2.6.2 Orifice equation

#### 2.6.2.1 Description of the orifice equation

An orifice is an opening (usually circular) in the side or base of a tank or reservoir through which fluid is discharged in the form of a jet, usually into the atmosphere. The volume of flow discharged through an orifice will depend on the head (height) of the fluid above the level of the orifice and it can therefore be used as a means of flow measurement. The term 'small' is applied to an orifice with a diameter or vertical dimension which is small compared to the head producing the flow. This means that it can be assumed that this head does not vary appreciably from point to point (Finnemore & Franzini, 2009).

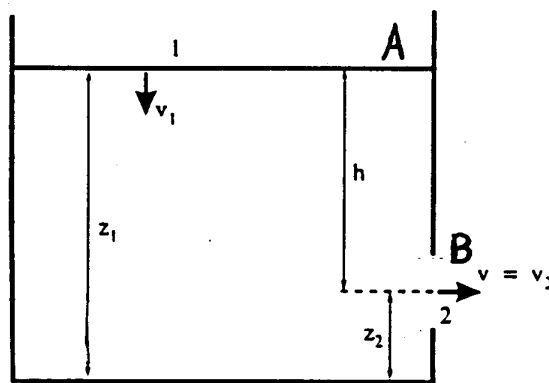


Figure 2-11: Geometry for the orifice equation (Wolmarans, 2015)

Figure 2-11 shows a small orifice in the side of a tank containing liquid with a free surface open to the atmosphere. At a point 1 on the free surface, the pressure  $p_1$  is atmospheric and, if the tank is large, the velocity  $AV_1$  will be negligible. In the region of the orifice, conditions are rather uncertain, but at some point 2 in the jet, just outside the orifice, the pressure  $p_2$  will again be atmospheric and the velocity  $v_2$  will be that of the jet  $v$ . When the datum for potential

energy at the centre of the orifice is taken and Bernoulli's equation applied at 1 and 2, assuming that there is no loss of energy, where the total energy is the sum of the kinetic, pressure and potential energy, the following equation results:

$$\frac{v_1^2}{2g} + \frac{P_1}{\rho g} + z_1 = \frac{v_2^2}{2g} + \frac{P_2}{\rho g} + z_2$$

$$0 + 0 + h = \frac{v_2^2}{2g}$$

$$v_2 = \sqrt{2gh}$$

*Equation 2-3*

This is a statement of *Torricelli's theorem* (Savić, Casey, & Kapelan, 2011), namely that the velocity of the issuing jet is proportional to the square root of the head-producing flow. This equation applies to any fluid, with  $h$  being expressed as a head of the fluid flowing through the orifice. Theoretically, if  $A$  is the cross-sectional area of the orifice, the following equation applies:

$$Q = A \times v_2 = A\sqrt{2gh}$$

*Equation 2-4*

It should be noted that this equation indicates that for a circular orifice, discharge will be proportional to the square root of the pressure head. In practice, the actual discharge is considerably less than the theoretical discharge given by the above equation, which must be modified by introducing a *coefficient of discharge*  $C_d$ , so that

$$Q_{actual} = C_d \times Q = C_d A \sqrt{2gh}$$

*Equation 2-5*

The main reason for this is that the shape of the orifice influences the shape and size of the jet, so that the cross-sectional area of the jet is not necessarily the same as that of the orifice. Additionally, the viscosity of the liquid will strongly influence the flow rate. Typical values of  $C_d$  for water are given in Figure 2-12.

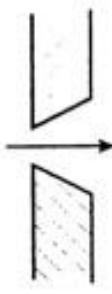
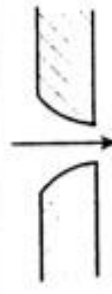

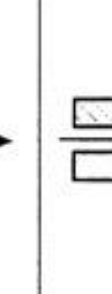
Shape:	Sharp Edged	Rounded	Tube or Nozzle	Borda Mouthpiece
$C_d$	0,61	0,98	0,82	0,51
diagram				

Figure 2-12: Discharge coefficients for orifice shape (Wolmarans, 2015)

A leak in a pipe can be considered an orifice for which the leakage flow rate  $Q$  can be described as a function of the orifice area  $A$  and pressure head  $h$  by the orifice equation, and thus expressed as follows:

$$Q = C_d A \sqrt{2gh}$$

Equation 2-6

### 2.6.2.2 Limitation of the orifice equation

After the realization that leaks are expected to behave like orifices, utility practitioners used this equation to implement pressure management schemes, which entailed releasing excess pressure from a distributions system in order to reduce leakage.

In theory, utility practitioners and researchers expected the pressure head exponent to be 0.5 as suggested by the orifice equation. However, as the orifice equation was being used for pressure management, it was quite evident that the leakage exponent is not fixed to 0.5 but can vary.

While the orifice equation predicts leakage to be proportional to the square root of the pressure head, field tests have shown that this equation does not provide a satisfactory model for the behaviour of pipe system leakage with pressure.

## 2.6.3 Power equation

### 2.6.3.1 Description of the Power equation

The limitations of the orifice equation prompted practitioners to find other ways to improve leakage modelling and to satisfactorily model leakage in pipe systems under pressure. In

particular, the objective was to develop a model that incorporates the varying pressure head exponents into pressure management. An empirical equation that relates leakage flow rate and pressure was developed and called the power equation; it is expressed as follows:

$$Q = Ch^{N1}$$

*Equation 2-7*

Where  $Q$  is the leakage flow rate ( $m^3/s$ ),  $C$  ( $m^{3-N1}/s$ ) is the leakage coefficient,  $h$  (m) is the pressure head, and  $N1$  is the leakage exponent. The  $N1$  value is a more important parameter than the  $C$  value because of its position as an exponent. It therefore has a greater influence on the leak flow than the  $C$  value (Clayton & van Zyl, 2007).

A number of field studies on systems with numerous leaks have shown that  $N1$  can range significantly from 0.5 to 2.8 with a median of 1.15. There are also studies that have reported  $N1$  values less than 0.5, which relates to a decrease in the leak area (Greyvenstein & van Zyl 2005). These variations in  $N1$  values confirm that leakage in water distribution systems is more sensitive to pressure than conventionally assumed by the use of the orifice flow equation (Clayton & van Zyl, 2007). A summary of the  $N1$  values found in the literature are shown in Table 2-5.

*Table 2-5: Summary of N1 values reported in various studies*

<b>Author</b>	<b>N1 Values</b>	<b>Conditions</b>
Ogura, (1979) in Schwaller & van Zyl, 2014.	1.39-1.72	Slits
Malde & van Zyl (2015)	0.500 0.501 0.496 0.499	mPVC round hole (12 mm diameter) HDPE round hole (12 mm diameter) Steel round hole (12 mm diameter) uPVC round hole (12 mm diameter)
Hiki, (1981)	0.5	Drilled holes
May (1994)	0.5 1.5 2.5	Fixed area Size = f (pressure) Longitudinal
Lambert (2000)	0.52-2.79 0.5 1.5	Literature UK metal pipes UK plastic pipes

Lambert (1997)	0.36-2.79	Literature
Farley & Throw (2003)	0.70-1.68 0.63-2.12 0.52-2.79	UK (1977) Japan (1979) Brazil (1999)
Lambert et. al. (2013)	0.5-1.6 0.5 0.5-1.0 >1.0  0.5- 2.0 0.8-1.0	Function of ILI, based on literature Circular holes, Re > 4 000 Small circular leaks in general Corrosion clusters Longitudinal cracks: Length to Width Ratio L/W = low L/W = high (for PVC pipes) AC pipes
Walski et al. (2009)	0.66-0.76	Drilled holes
Walski et al. (2009)	0.47-0.74** Mean = 0.58 Median = 0.54	Slits and holes of various lengths and sizes for a number of pipe diameters in PVC pipe
Greyvenstein & van Zyl (2005)	0.52 1.38-1.85 0.79-1.04 0.41-0.53 0.67-2.3	Round hole Longitudinal PVC Longitudinal AC Circumferential Corrosion steel
Noack & Ullanicki (2007)	0.5-1.2	f (soil permeability)
Malde & van Zyl (2015)	0.4328 0.1850 0.4991 0.4578	mPVC spiral (50mm x 1mm) HDPE spiral (50mm x 1mm) Steel spiral (50mm x 1mm) uPVC spiral (50mm x 1mm)
Ashcroft & Taylor, cited in Lambert (2000)	1.39-1.72 1.23-1.97 1.52	10 mm slit in plastic pipe 20 mm slit in plastic pipe Average under varying pressure
Ogura (1979)	1.15	Average in steel distribution systems in Japan
Deyi, van Zyl & Shepherd (2014)	0.18-3.33	Mainly plastic distribution systems in South Africa

(Charalambous, 2005)	0.64-2.83 Average = 1.47	Field study on 15 DMAs in Cyprus for mixed AC, PVC and MDPE pipes
Malde & van Zyl (2015)	0.9887 0.5002 0.8691	mPVC longitudinal (50 mm x 1mm) Steel longitudinal (50 mm x 1mm) uPVC longitudinal (50 mm x 1mm)

The ranges of exponents listed in Table 2-5 suggest that there are substantial differences in the impact of pressure on the rate of leakage. Figure 2-13 shows a convenient way of demonstrating the effect of the leakage exponent  $NI$  on the pressure-leakage relationship. The general relationship between the ratio of pressure ( $P_1/P_0$ ) and the ratio of the leakage flow rate ( $L_1/L_0$ ) for different values of  $NI$  is shown. Figure 2-13 also shows that as the  $NI$  increases, the sensitivity of leakage to changes in pressure also increases.

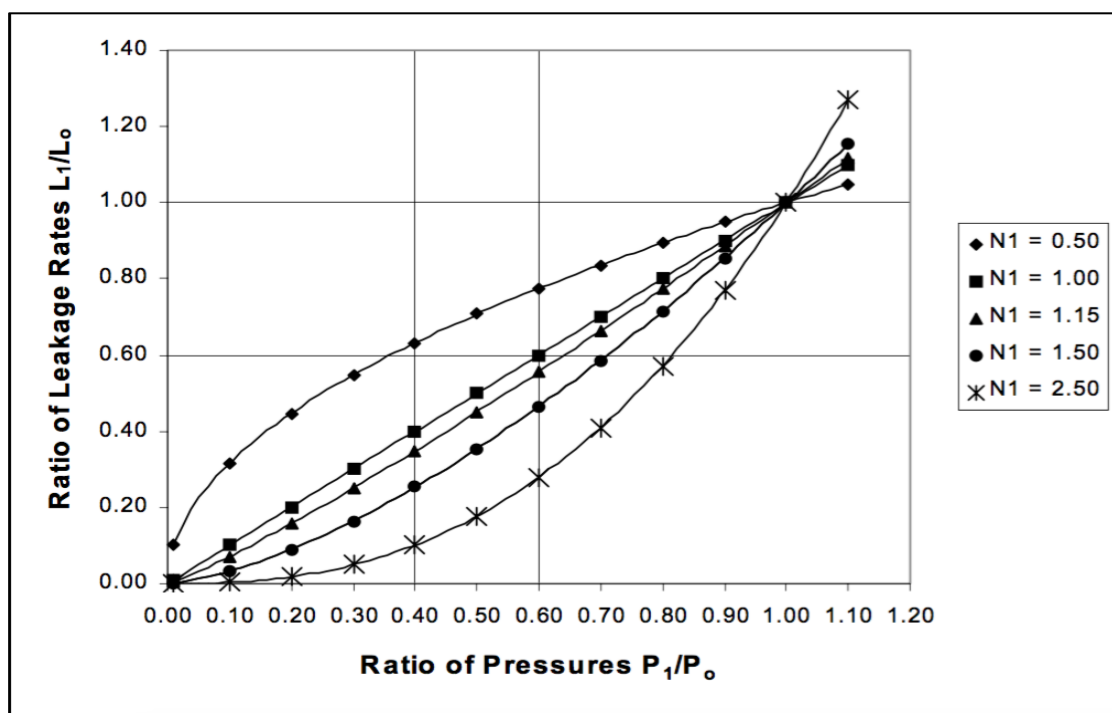


Figure 2-13: The general relationship between pressure and leakage rates using the power equation (Lambert, 2002)

Figure 2-13 indicates that a 40% reduction in pressure (i.e.  $P_1/P_0 = 0.6$ ) will result in a leakage reduction of approximately 20%. Leakage exponents ( $NI$ ) values of 0.5, 1.00, 1.15, 1.50 and 2.50 lead to a respective 40%, 45%, 55% and 70% leakage reduction. This indicates that the leakage exponent has a great influence in understanding the status quo of water pipelines and

estimating the potential impact of pressure management. It is therefore essential to understand the mechanisms responsible for the observed leakage exponents.

### 2.6.3.2 Factors influencing the leakage exponent $N1$

Various mechanism can be responsible for the observed  $N1$  values. Clayton and van Zyl (2007) investigated four factors that may be responsible for the range of leakage exponents that have been observed in the field and in experimental studies, namely (a) leak hydraulics, (b) pipe material behaviour, (c) soil hydraulics, and (d) water demand. These factors will be discussed here in some detail.

**(a) Leak hydraulics:** The hydraulic behaviour of orifices has been studied extensively and can be predicted with a great degree of certainty. It has been accepted that the leakage exponent of a fixed leak can be assumed to be 0.5 and that the discharge coefficient is often not constant but expressed in terms of the Reynolds number. It is therefore feasible to assume that a certain type of leak can be modelled using a fixed discharge coefficient, but with varying leakage exponents (i.e. higher or lower than the theoretical 0.5).

Another aspect of leak hydraulics that can affect the leakage exponent  $N1$  is the flow regime, whether it is turbulent or laminar. Experiments have shown the typical values of  $N1$  for laminar, turbulent and transitional flow conditions:

Table 2-6: The values of  $N1$  for different flow regimes (Clayton & van Zyl, 2007)

Flow regime	Re	N1
Laminar flow	< 10	1
Transitional flow		0.5 - 1
Fully turbulent flow	>4000-5000	0.5

If the Reynolds number is written as a function of discharge through the leak, the formula is as follows:

$$Re = \frac{4vA}{kP}$$

Equation 2-8

Where  $v$  is the velocity (m/s),  $P$  is the wetted perimeter (m),  $Re$  is the Reynolds number, and  $k$  = Kinematic viscosity (m<sup>2</sup>/s). Two expressions can be developed to estimate the maximum laminar and transitional flow rates that are possible in a typical water distribution system:



$$q = \frac{\pi v^2 R_e^2}{4C_d \sqrt{2gh}}$$

Equation 2-9

$$q = \frac{(n+1)k^2 R_e^2}{4C_d n \sqrt{2gh}}$$

Equation 2-10

Where  $h$  is the pressure head ( $m$ ),  $g$  is the acceleration due to gravity ( $m/s^2$ ),  $n$  is the aspect ratio of a rectangle, and  $C_d$  is the discharge coefficient. Using equations 2-6 and 2-7, Clayton & van Zyl (2007) plotted leak flow rate ( $l/h$ ) against typical pressure range ( $m$ ) for different types of leak openings. Figure 2-14 shows the results of this plot. The maximum laminar and transitional flow rates for the different leak types are illustrated.

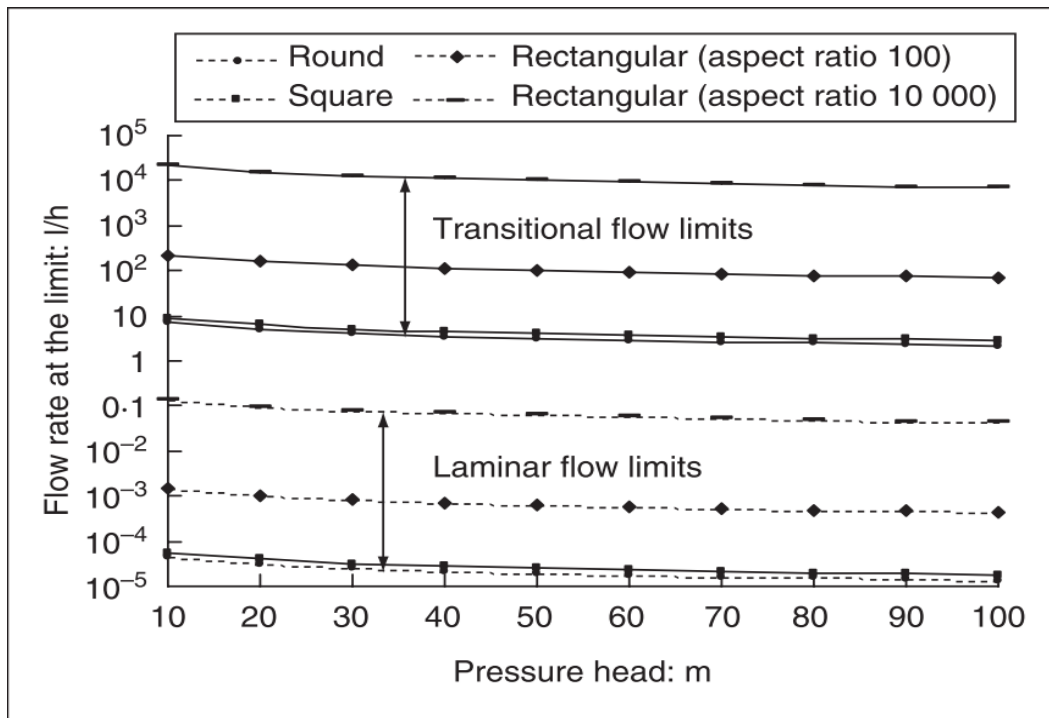


Figure 2-14: The maximum laminar and transitional flow rates for different leak openings (Clayton & van Zyl, 2007)

Figure 2-14 shows that certain types of leak openings (namely rectangular) have higher laminar and transitional flow rates than round holes and square holes. This is due to their much larger wetted perimeters.

**(b) Pipe material behaviour:** The material behaviour of pipes is thought to play the most significant role in affecting the pressure-leakage relationship and thus the  $NI$ . Understanding the failure behaviour and the associated leakage exponents will assist in leakage modelling and

in understanding the complexity. It has become more apparent that leak areas are not fixed but expand, to varying degrees, with increasing pressure. Some leak areas also remain closed at low pressures but open when the pressure is increased high enough.

Buckley, (2005) carried out theoretical work at the University of Johannesburg's Water Research Group of which he developed the following basic model for the flow rate through a round hole in an elastic pipe taking into account the effect of pipe material expansion on the leakage rate. The developed model was expressed as follows:

$$Q = C_d \frac{\pi d_0^2}{4} \sqrt{2g} \left( H^{0.5} + \frac{2c\rho g D}{3tE} H^{1.5} + \frac{c^2 \rho^2 g^2 D^2}{9t^2 E^2} H^{2.5} \right)$$

Equation 2-11

Where  $d_0$  is the Original Leak Hole Diameter,  $D$  is the Pipe Diameter,  $E$  is the Elastic Modulus,  $t$  is the Pipe Thickness and  $c$  is a Constant. From Equation 2-8, it is interesting to note that the leakage exponents vary from 0.5 to 2.5; this corresponds to the  $NI$  values observed in the field and in experimental tests (Clayton & van Zyl, 2007). This relationship also shows that the leak area expansion is much more complex than the power equation indicates.

When leakage was calculated using equation 2-8, it was found that the terms with the exponents of 1.5 and 2.5 contribute very little to the leakage rate under normal pressure conditions for round holes. Hikki (1981) supports this phenomenon that the leakage through round holes can be characterised by a leakage exponent of 0.5.

Another aspect of pipe material that can affect the  $NI$  is the material property, because pipes fail in different characteristic ways depending on the type of pipe, as shown in .

Table 2-7. This table indicates that the leakage exponents ( $NI$ ) varies for different materials and different failure types.

Table 2-7: The leakage exponents for various pipe materials (Greyvenstein & van Zyl, 2005)

Failure type	Leakage exponent		
	uPVC	Asbestos cement	Mild steel
Round hole	0.52	-	0.52
Longitudinal crack	1.38 – 1.85	0.79 – 1.04	-
Circumferential crack	0.41 – 0.53	-	-
Corrosion cluster	-	-	0.67-2.30

There are some key insights that can be drawn from Table 2-7. Firstly, the highest leakage exponents were found to occur in corroded steel pipes. Secondly, it was found that round holes generally have leakage exponents close to the theoretical 0.5, and that this is true regardless of the pipe material. Thirdly, besides the high exponents resulting from corrosion failure, longitudinal cracks were found to also have high leakage exponents. Finally, the leakage exponent of the circumferential crack was found to be less than 0.5, implying that the crack could be closing up as the internal pressure increases.

Clayton and van Zyl's (2007) study also confirmed these findings and discussed the fact the different materials fail in different characteristic ways. They also mention that longitudinal cracks are common in asbestos cement, while metallic pipes such as steel and cast-iron pipes often leak through holes formed by corrosion. Small cast iron pipes were found to fail in bending, resulting in circumferential cracks. Due to the high coefficient of thermal expansion these cracks open and close depending on the temperature in small cast-iron pipes.

Ssozi, Reddy and van Zyl (2015) carried out a finite element study in which they investigated the viscoelastic behaviour of pipe materials. The study found that materials that undergo viscoelastic behaviour generally have higher  $N1$  exponent values as shown in Figure 2-15 below.

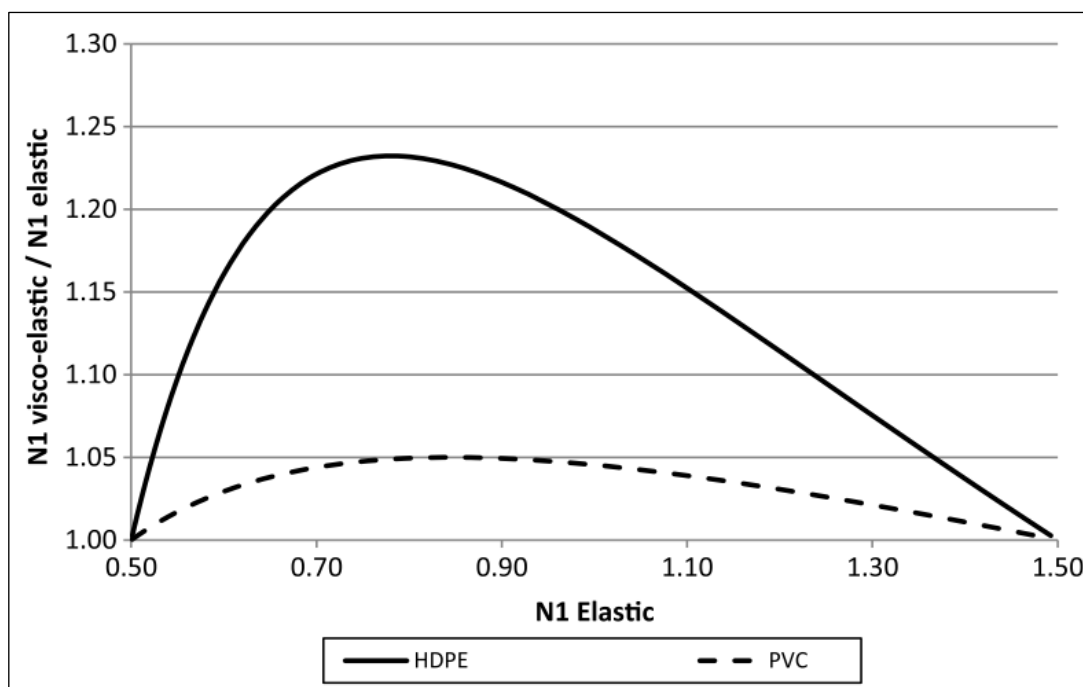


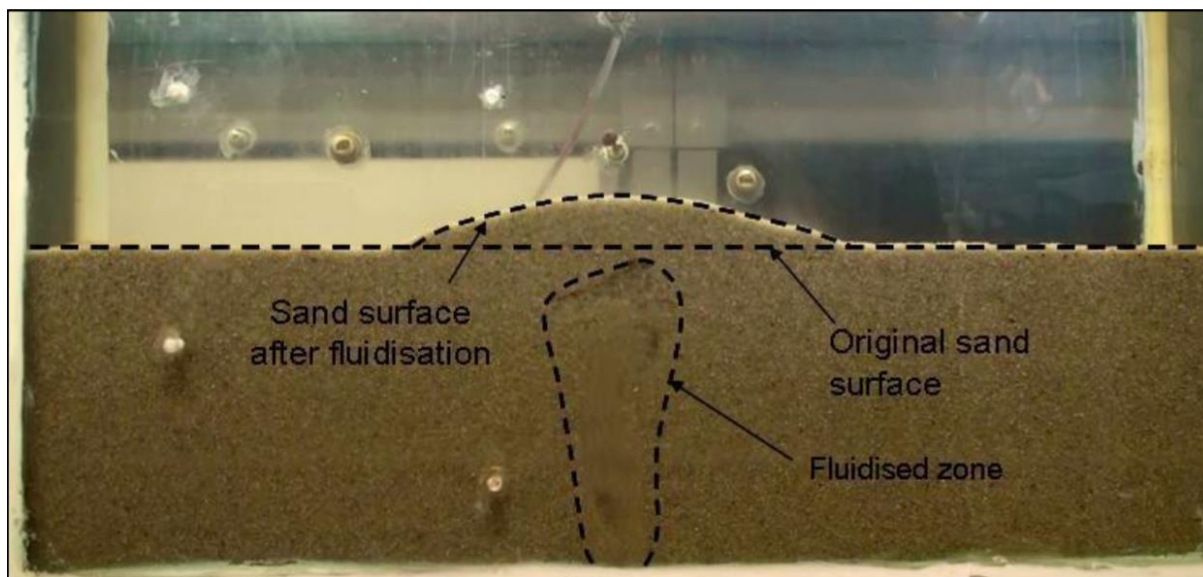
Figure 2-15: How viscoelastic behaviour affects the  $N1$  (Ssozi, Reddy & van Zyl, 2015)

(c) **Soil hydraulics:** Another factor that plays a part in the pressure-leakage relationships, observed in the field and in laboratory experiments, is the effect of soil around a leaking pipe. Water that leaks from the pipe travels through the surrounding soil. Following a simplistic model of geotechnical seepage theory, the leakage flow rate should be linearly proportional to the pressure head of the water in the pipe. This is also known as Darcy's Law and is expressed as follows:

$$Q = F k h$$

*Equation 2-12*

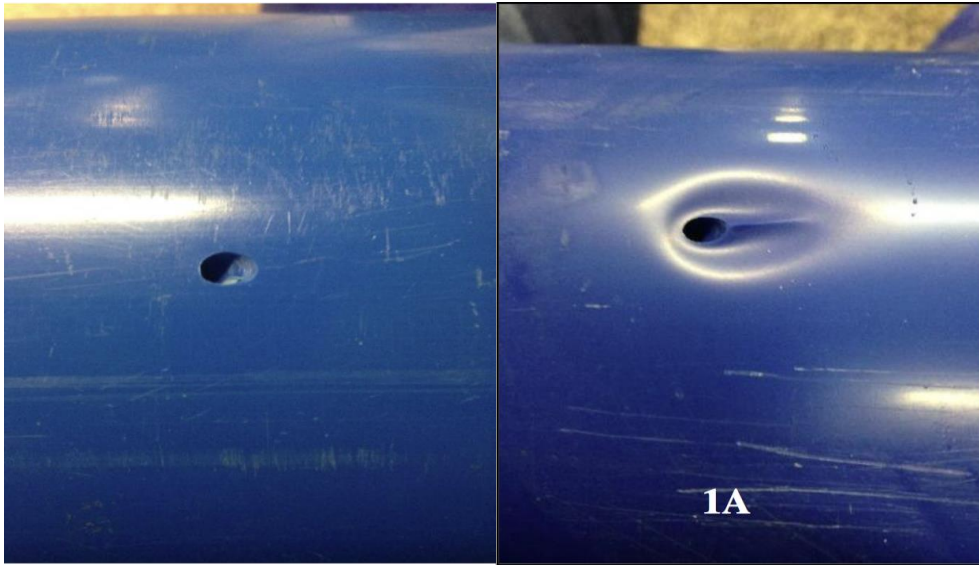
Where  $q$  is leakage flow rate from the pipe,  $F$  is the shape factor for the soil,  $k$  is the coefficient of permeability of the soil and  $h$  is the pressure head. Clayton and van Zyl (2007) mention the fact that the assumptions that underpin equation 2-9 do not necessarily apply to leaking pipes. One of the reasons for this is that the interaction between the surrounding soil and leaking pipe is a complex phenomenon as shown in Figure 2-16. It can be seen from the figure that a fluidised zone develops when the water jet interacts with the soil particles.



*Figure 2-16: Fluidisation zone from vertical water leak jet (Ma, 2011)*

This phenomenon was investigated further by Pike (2015) in an experimental study

. In his study it was demonstrated that due to the scouring process that occurs at the pipe wall, small leaks have the potential to develop into large leaks over time, as shown in Figure 2-17. This process was found to be highly influenced, mainly by the orientation of the leak but also by the size of the soil grains and high flow rates.



*Figure 2-17: The initial orifice condition (left) and visual inspection after 100 hours of exposure to scouring (right) (Pike, 2015)*

As a result of the interaction between the soil mass and water jet from the leaking pipe, the relationship between head loss and flow is unlikely to be linear. In addition, the turbulent flow regime, the changing geometry of the unconfined flow regime, hydraulic fracturing and piping all contribute towards a complex interaction between the soil particles and the flow rate from the leak (Clayton & van Zyl, 2007).

**(d) Water demand:** The aspect of water demand is also thought to play an influential role in the pressure-leakage relationship observed in the field and in experimental tests. During field tests it is often impossible to distinguish between legitimate water consumption and system leakage. For this reason it is pivotal to understand the relationship between pressure and legitimate water consumption. Clayton and van Zyl (2007) express the effect of pressure on water demand as follows:

$$Q_{demand} = Ch^{\beta}$$

*Equation 2-13*

Where  $Q_{demand}$  is the legitimate water demand,  $C$  is a constant coefficient and  $\beta$  is the demand elasticity to pressure. It is quite clear that equation 2-10 resembles the  $NI$  leakage equation. The demand elasticity takes into account human behaviour change, e.g. with increased water pressure through taps as is illustrated below.

Bartlett, (2004) conducted a study on the water consumption at a student village at the University of Johannesburg. In his study, Bartlett (2004) varied the system pressure of the

village and monitored the associated water demand. He found that the demand elasticity for indoor usage was approximately 0.2. The outdoor water demand elasticity was found to be 0.5. Outdoor consumption was found to be time based rather than volume based, indicating that higher exponents are expected for outdoor water demand.

In large systems it is inevitable to include legitimate water consumption in the minimum measured night flows. Since the combined leakage exponent can be found to be less than 0.5, Clayton and van Zyl (2007) claim that there is a possibility that system leakage exponents are underestimated if they are measured in systems that contain demand.

### ***2.6.3.3 Disadvantages of the power equation***

Despite the wide use of the power equation, Schwaller, van Zyl & Kabaasha (2015) point out a number of disadvantages in using it:

- The power equation is an empirical equation and is not underpinned by fundamental fluid mechanics theory. The form of the equation replicates that of the Torricelli equation, however, the two constants ( $C$  and  $NI$ ) are determined experimentally.
- The values of the constants ( $C$  and  $NI$ ) are not constant but are functions of pressures at which the  $NI$  test is done.
- The equation is difficult to interpret because the units of  $C$  include the variable  $NI$ , making it difficult to distinguish between the factors affecting the  $NI$  and the constant  $C$ .

Furthermore, the constants  $C$  and  $NI$  exponents do not provide any informative characteristics of a leak. Ferrante et al. (2014) investigated the application of the power equation to a system with several leaks. In this study, a simulation of 100 districts with 100 leaks each was carried out. When the  $NI$  was used it was found that the system leakage exponent ( $NI$ ) was often higher than the mean local leak exponent.

Using artificially induced leaks in thick and thin steel pipes and polyethylene pipes, Ferrante et al. (2011) also demonstrated that the power equation does not accurately characterise the leaks, as the variation of the leak area with pressure head is not accurately captured.

Finally, the  $NI$  parameter does not give an indication of how sensitive the leak is to pressure variation. In essence, according to Ferrante et al. (2011), the power equation fails to accurately model a true representation of the direct relationship between pressure and leakage.

## 2.6.4 Modified orifice equation

### 2.6.4.1 Description of the modified orifice equation

The modified orifice equation (known in leakage practice as the fixed and variable area discharge, or FAVAD, equation) was introduced by May in 1994. This theory was later confirmed by Cassa, van Zyl & Laubscher (2010 using finite element analysis to test three 60mm long leaks in a 110mm class 6 uPVC pipe. The cracks were oriented in longitudinal, circumferential and spiral directions. The leak areas were determined at different pressures and plotted against the pressure head as shown in Figure 2-18.

As indicated by Figure 2-18, the intercept of the line with the area axis shows the initial area  $A_0$ , and the slope of the line indicates the head-area slope of each crack. Preliminary observations show that longitudinal cracks have the highest head-area slopes, followed by the spiral crack and finally the circumferential crack, with head-area slopes of  $1.195 \times 10^{-3} \text{mm}$ ,  $0.2446 \times 10^{-3} \text{mm}$  and  $0.8801 \times 10^{-3} \text{mm}$ , respectively.

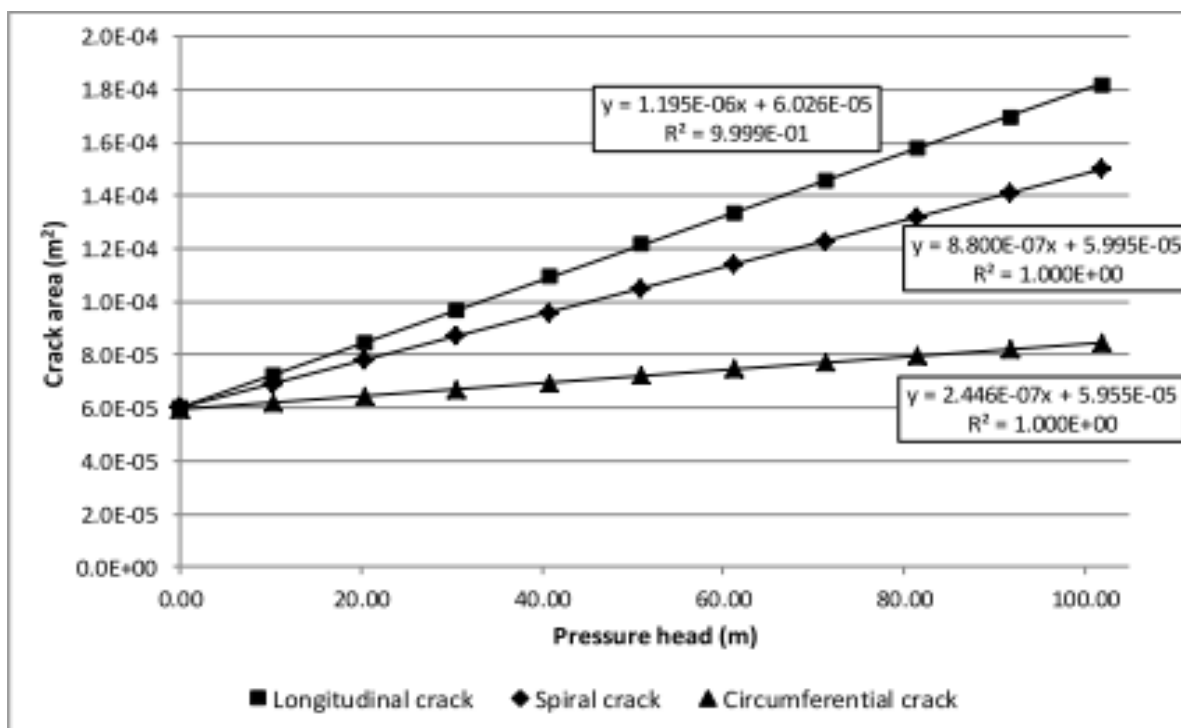


Figure 2-18: The areas of 60mm long cracks in a class 6 uPVC pipe as a function (Cassa, van Zyl & Laubscher, 2010)

The study concluded that the leak area (whether a circular, longitudinal or circumferential crack) is a linear function of pressure, regardless of the pipe material, as long as the pipe material behaves elastically. The pressure response of a leak can thus be characterised by an initial area

(under zero pressure conditions)  $A_0$  and the head-area slope (gradient of the linear line)  $m$ . The general expression for the leak area as a function of pressure head is therefore given as:

$$A = A_0 + mh$$

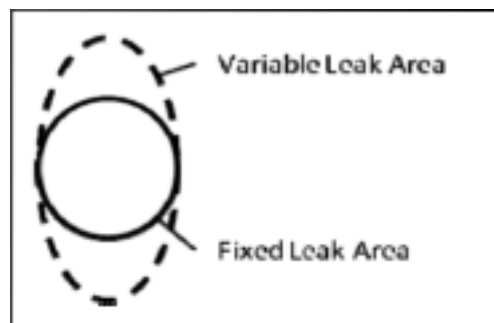
*Equation 2-14*

When equation 2-11 is replaced into the Torricelli equation, this results in the proposed modified orifice equation which is expressed as follows:

$$Q = C_d\sqrt{2g}(A_0h^{0.5} + mh^{1.5})$$

*Equation 2-15*

Where  $A_0$  is the fixed leak area ( $m^2$ ) and  $m$  is the head-area slope (m). While this modified orifice equation is identical to the FAVAD equation proposed by May (1994), it is interpreted differently. Indeed, a leak is made up of a fixed and a variable area as shown in Figure 2-19; however, instead of interpreting leaks as either fixed or variable, all leaks in a system can be considered to have variable areas. In other words, all leaks will increase in area when the pressure is increased.



*Figure 2-19: Fixed and variable leak areas (Schwaller & van Zyl, 2014)*

Based on the modified orifice equation, the discharge of one single leak is therefore a result of:

- the discharge through the fixed initial area of the leak:  $Q_0 = C_d\sqrt{2g}(A_0h^{0.5})$
- and the discharge through the area increasing with pressure:  $Q_1 = C_d\sqrt{2g}(mh^{1.5})$

This means that for leaks with small head-area slopes,  $Q_0$  is likely to be dominant, resulting in an effective leakage exponent of 0.5. Conversely, for flexible leaks with high head-area slopes,  $Q_1$  is likely to be dominant, resulting in a leakage exponent of 1.5. It is clear that under elastic conditions, the pressure response of a leak can be fully characterised by knowing its initial area  $A_0$  and the head-area slope  $m$ .



### 2.6.4.2 Pipe material behaviour and the modified orifice equation

Pipe material behaviour plays a pivotal role in how leaks behave in a pressurised pipe. Due to material property variations, different material failures show different failure mechanisms (Clayton & van Zyl, 2007). The various pipe materials and their associated failure modes are discussed in detail in Section 2.8.

Using finite element modelling, Cassa, van Zyl & Laubscher (2010) investigated the behaviour of various leak openings in pressurised pipes. Three failure mechanisms were investigated, namely circular holes, longitudinal and circumferential cracks. The pipe materials included were uPVC, steel, cast iron and asbestos cement. Linear elastic behaviour was assumed for all pipe material deformation. The main findings of this study were as follows:

- The type of leak opening has a significant effect of the local stress distribution. In other words, high stress concentrations around the leak were found in certain regions of the leak opening. For instance, all cracks had their highest stresses at crack tips, as shown in Figure 2-20 to Figure 2-22, whereas round holes had their highest stresses at the inner lip of the round hole, as can be seen in Figure 2-23.

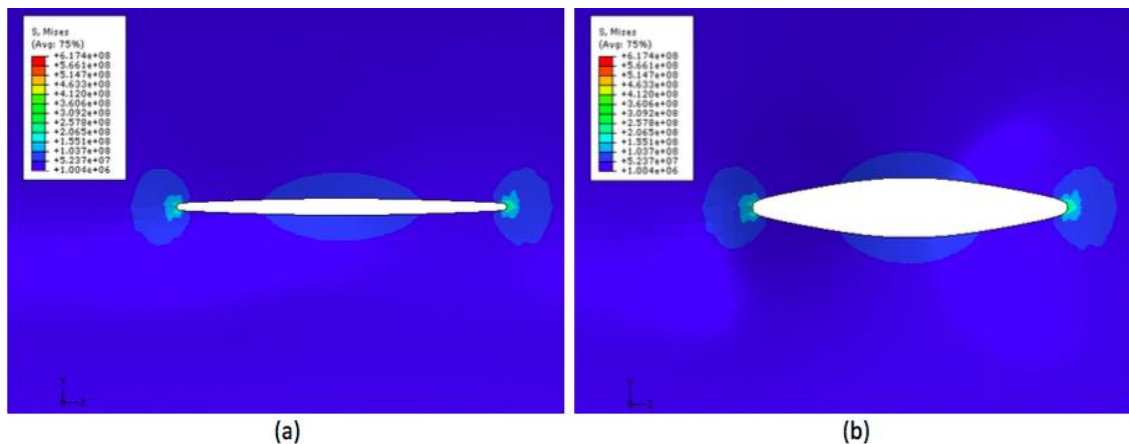


Figure 2-20: The stress distribution around a longitudinal crack (a) deformed and (b) scaled up view of deformation

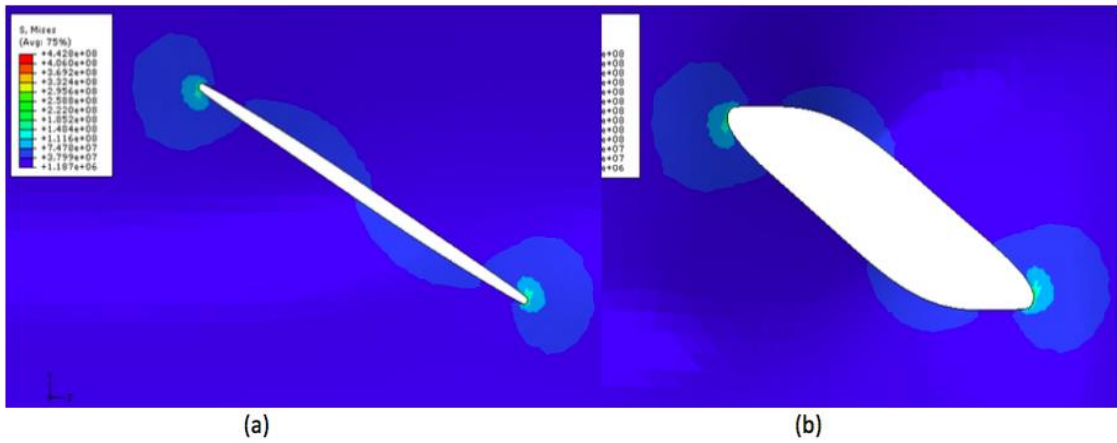


Figure 2-21: The stress distribution around a spiral crack (a) deformed and (b) scaled up view of deformation

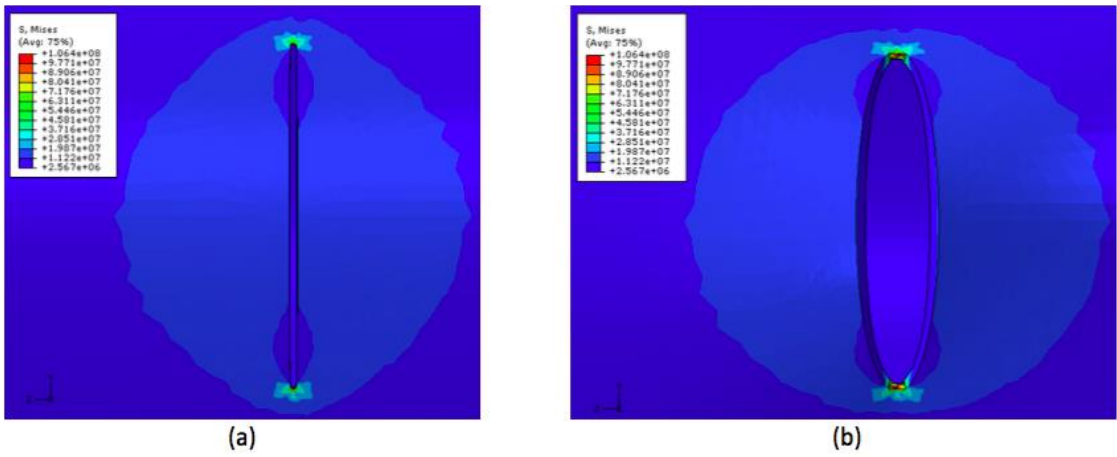


Figure 2-22: The stress distribution around a circumferential crack (a) deformed and (b) scaled up view of deformation

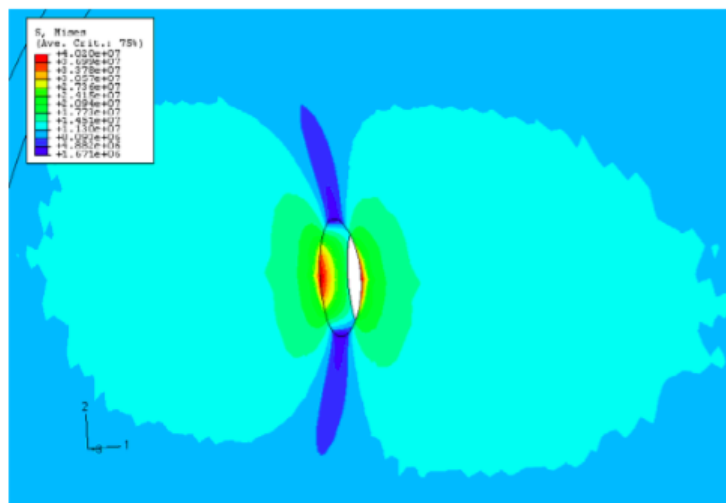
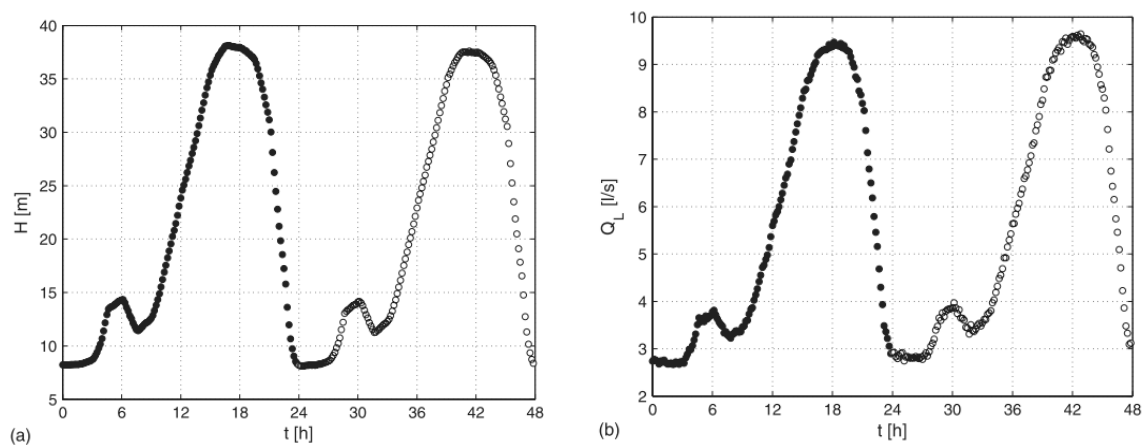


Figure 2-23: The stress distribution around a circular hole

- The areas of all three leak types were found to increase linearly with pressure in all the materials investigated. The modified orifice equation therefore gives a better description of the behaviour of leaks. These results were also experimentally confirmed by Ferrante (2012) and Malde & van Zyl (2015).

In certain cases the elastic limit is exceeded and other material behaviour, such as viscoelastic and plastic deformation, are introduced. Ferrante's (2012) experimental study showed that the viscoelastic behaviour of the pipe material, elastic and elastoplastic, influence the pressure head-discharge relationship differently.

It has been shown that pipe materials that undergo viscoelastic behaviour are synonymous to hysteretic behaviour. An experimental test of a high-density polyethylene (HDPE) pipe was carried out. The variation of time ( $t$ ), with pressure head ( $H$ ) and leak flow ( $Q$ ) for this experiment are shown in Figure 2-24. The test allowed for two peaks every 24 hours, which would be representative of the typical cycle of real-world pipe systems. The black circles represent the data point of the first 24 hours of the profile and the empty circles represent the data points on the second day (Ferrante, 2012).



*Figure 2-24: Data showing test of HDPE pipe (Ferrante, 2012)*

Figure 2-24(a) shows that the two local maxima of the pressure head (at about  $t=17$  and 41 hours) decreases with time, i.e  $h=38$  m and  $h=36$  m at  $t=17$  hrs and  $t=41$  hrs, respectively. In contrast, Figure 2-24(b) indicates that the local maxima of the leak flow rate increase with time. The data points of the experimental test are plotted on the flow against pressure domain as illustrated in Figure 2-25.

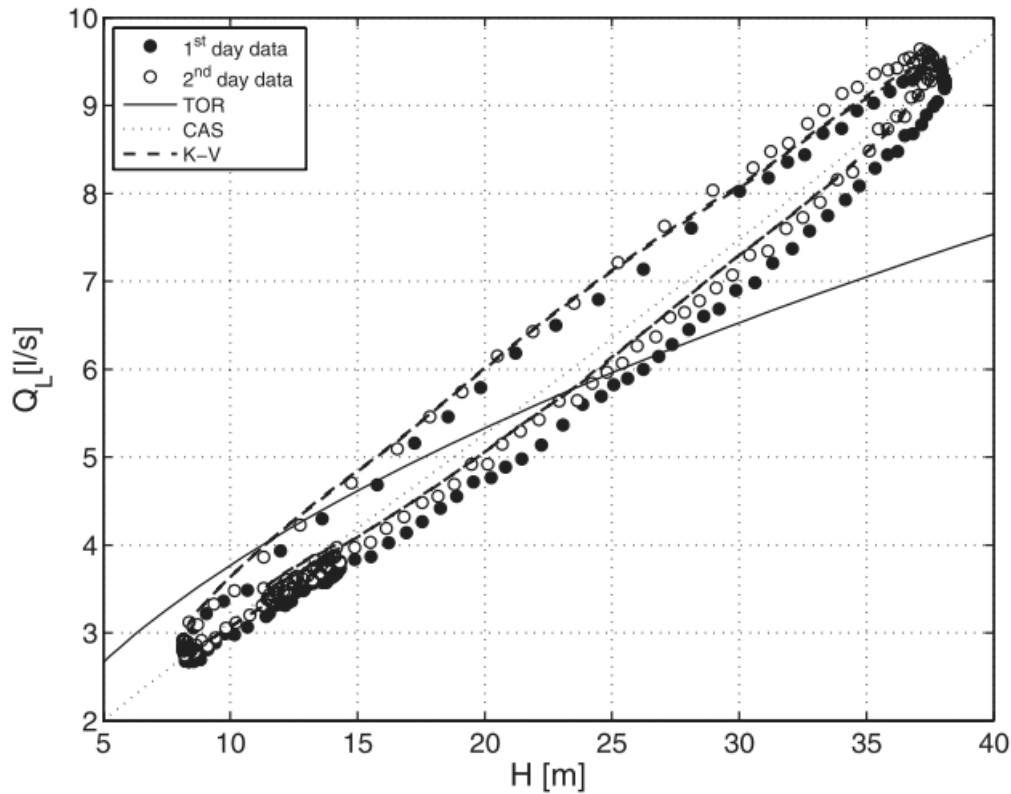


Figure 2-25: Flow against pressure (Ferrante, 2012)

Figure 2-25 shows the data from the 1<sup>st</sup> day and the 2<sup>nd</sup> day. It also shows the modified orifice equation (CAS in Figure 2-25) by Cassa, van Zyl & Laubscher (2010), the Torricelli equation (TOR in Figure 2-25) and the classical viscoelastic model by Kelvin-Voigt (K-V in Figure 2-25). Hysterical behaviour of the HDPE pipe is quite evident with a single value of head (H) associated with two distinct values of Flow (Q). Figure 2-25 clearly shows that the Torricelli equation does not explain the hysterical behaviour shown by the data.

According to Ferrante (2012), the modified equation proposed by Cassa, van Zyl & Laubscher (2010) also does not correctly interpret the hysteric behaviour, simply because it is defined by a bijective function. For this reason, Ssozi, Reddy & van Zyl (2015) proposed another equation that takes into account hysteric behaviour, where the total leak area can be described as:

$$A(t) = A_0 + \Delta A_e + \Delta A_v$$

Equation 2-16

Where  $\Delta A_e$  represents the elastic change in area, which can be predicted with a linear relationship, and  $\Delta A_v$  representing the viscoelastic change in area, which is time dependant.

### 2.6.4.3 Characterising individual leaks with the modified orifice equation

It has now been established that all leaks will expand with increasing pressure, however, the rate of expansion that is described through the head-area slope ( $m$ ) differs for each type of leak. The head-area slope can also be expressed as a function of the pipe parameters (Schwaller, 2012).

A study by Cassa & van Zyl (2014) investigated the sensitivity of the head-area slope  $m$  to different materials, sections and crack properties. A realistic range of values were determined for each parameter. The investigation was carried out for longitudinal, circumferential and spiral cracks.

In their study they concluded that longitudinal cracks produced the highest head-area slopes, followed by spiral cracks and then circumferential cracks. The parameters that were found to have the greatest impact on the head-area slope  $m$  was the crack length, followed by the wall thickness, elastic modulus, internal diameter and longitudinal stress. It was found that the crack width and Poisson's ratio effect on the head-area slope is small enough to be negligible. Cassa & van Zyl (2014) then developed three empirical equations that can be used to predict the head-area slopes for the individual crack types. The equations are presented here:

$$m_{long} = \frac{2.93157 \times d^{0.3379} \times L_c^{4.80} \times 10^{0.5997(\log L_c)^2} \times \rho \times g}{E \times b^{1.746}}$$

Equation 2-17

$$m_{spiral} = \frac{3.7714 \times d^{0.178569} \times L_c^{6.051} \times \sigma_l^{0.0928} \times 10^{1.05(L_c)^2} \times \rho \times g}{E \times b^{1.6795}}$$

Equation 2-18

$$m_{circ} = \frac{1.64802 \times 10^{-5} \times L_c^{4.87992662} \times \sigma_l^{1.09182555} \times 10^{0.82763163(\log L_c)^2} \times \rho \times g}{E \times b^{0.33824224} \times d^{0.186376316}}$$

Equation 2-19

Where  $m$  is the head-area slope,  $d$  is the internal diameter,  $E$  is the elastic modulus,  $\sigma_l$  is the longitudinal stress,  $\rho$  is the fluid density,  $g$  is the acceleration due to gravity,  $b$  is the pipe wall thickness, and  $L_c$  is the crack length.

Nsanzubuhoro, van Zyl and Zingoni (2016) carried out a study on round holes. They investigated the sensitivity of the head-area slope  $m$  of round holes to different materials, sections and round hole properties. The following equation was derived to predict the head-area slope of round holes:

$$m_{holes} = 8 \left[ \left( \frac{A_0 K \rho g r}{b E} \right) (\alpha - \nu + 1 - \nu \alpha) \right] - (8 \times 10^{-9})$$

*Equation 2-20*

Where  $A_0$  is the initial hole area,  $K$  is the stress intensity,  $\rho$  is the fluid density,  $g$  is the acceleration due to gravity,  $b$  is the pipe wall thickness,  $E$  is the elastic modulus,  $\nu$  is the Poisson's ratio,  $\alpha$  is the ratio of longitudinal stress to circumferential stress, and  $r$  is the internal pipe radius.

In the round hole study, it was concluded that the head-area slope of round holes is generally much smaller than those of longitudinal, circumferential and spiral cracks. The head-area slopes of round hole leaks can generally be assumed to be zero. An exception may be corrosion holes in metal pipes where the wall thickness surrounding the hole has been reduced substantially. It must be noted that these equations are all subject to the assumption of linear elastic behaviour and thus may not be valid for cracks where plastic deformation or hysteresis may occur.

De Miranda et al. (2014) presented another method to evaluate leakage through a longitudinal crack in a pressurised pipe using a physically-based analytical model. The model, adopted by the authors, considers the longitudinal crack as a classical elastic beam with tangential constraints. For this case, the head-area slope was found to take the following form:

$$m_{long} = \frac{12 \rho g L R^4 \pi (1 - \nu^2)}{a E s^3}$$

*Equation 2-21*

This formula was validated through comparison with published work, such as finite element studies by Cassa and van Zyl (2013) and experimental studies by Greyvenstein & van Zyl (2005). In all cases good correlations were achieved.

#### 2.6.4.4 Analysing pipe systems with the modified orifice equation

Thus far, the discussion about the modified orifice equation has focused on individual leaks. The study by Ferrante et al. (2014) showed that the modified orifice equation has the same functional dependence on a local scale (individual leaks) as on a global scale (multiple leaks).

Schwaller (2012) showed that the modified orifice equation can be used to determine the initial leak area ( $A_0$ ) and the head-area slope ( $m$ ) of a pipe system. Estimates of the average zone pressure (AZP) and the leakage flow rate ( $Q$ ), before and after pressure reduction, can be used to determine the  $A_{0s}$  and  $m_s$  of the system. To do this the modified orifice equation is written in the form:

$$Q = C_{ds}\sqrt{2g}(A_{0s}h^{0.5} + m_s h^{1.5})$$

Equation 2-22

Where  $A_{0s}$  is the initial leak area of the system,  $m_s$  is the head-area slope of the systems, and  $C_{ds}$  is the discharge coefficient of the system. From this the following equations were developed to estimate the two system parameters, i.e. system head-area slope and initial leak area:

$$m_{sys} = \frac{h_2^{0.5}Q_1 - h_1^{0.5}Q_2}{C_{ds}\sqrt{2g}(h_1^{1.5}h_2^{0.5} - h_2^{1.5}h_1^{0.5})}$$

Equation 2-23

$$A_{0s} = \frac{Q_1}{C_{ds}\sqrt{2gh_1}} - m_s h_1$$

Equation 2-24

Where the  $h_1$  and  $h_2$  are the AZP before and after pressure reduction, and  $Q_1$  and  $Q_2$  are the corresponding leakage rates before and after pressure reduction.  $g$  is the acceleration due to gravity, and  $C_{ds}$  is the system discharge coefficient.

The system modified orifice equation parameters values ( $m_{system}$  and  $A_{o\ system}$ ) were compared to the sum of individual leak parameters (i.e.  $\sum m_i$ . And  $\sum A_{oi}$ ). In order to do this, a spreadsheet model which consisted of different numbers of leaks at different random positions with random parameters was used to estimate leakage rate at two different pressure points. Specialist input and assumption were required to make reasonable guestimates on various leak properties and parameters. The following assumptions were considered for the different leak parameters (Schwaller & van Zyl, 2014):

- the discharge coefficient  $C_d$  was modelled using a normal distribution
- the initial leak area  $A_0$  was modelled using different normal distributions for background leaks and bursts
- the head area slope was modelled as a power equation of the leak area, according to a study by Cassa & van Zyl (2011)
- the pressure was also modelled using a uniform distribution with a known mean and a stipulated range.

As can be seen from Figure 2-26 and Figure 2-27, good correlations were found between the systems and individual leakage parameters:

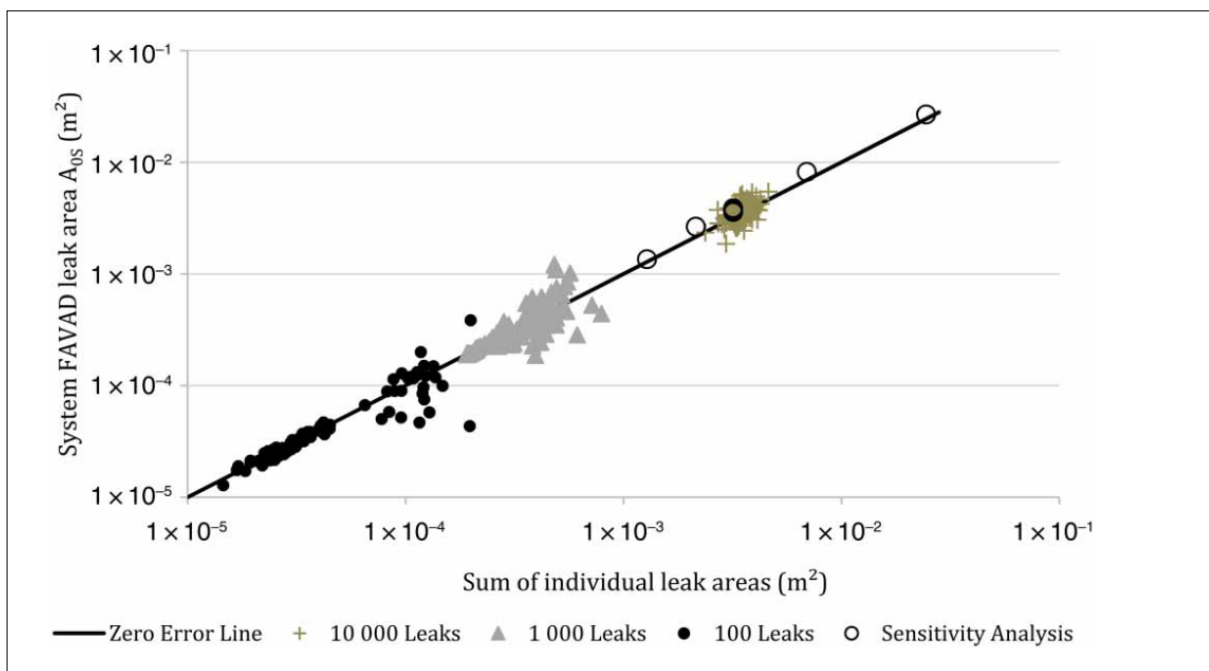


Figure 2-26: Comparison of results of system FAVAD leak area  $A_{0s}$  and the sum of individual areas (Schwaller, van Zyl & Kabaasha, 2015)



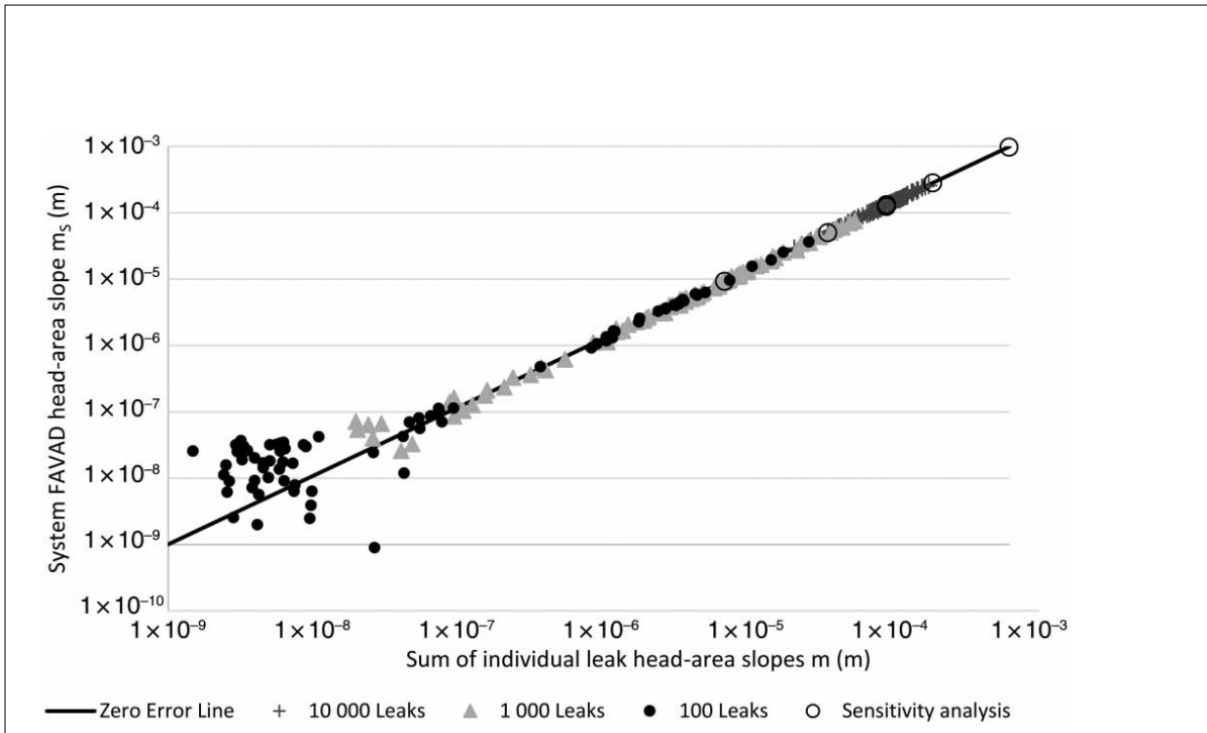


Figure 2-27: Results of the comparison between system FAVAD head-area slope ( $m_s$ ) and the sum of individual leak head-area slopes ( $\Sigma m$ ) (Schwaller, van Zyl & Kabaasha, 2015)

The implications of the findings of Figure 2-26 and Figure 2-27 are as follows:

- the sum of all individual initial leak areas in a pipe system is approximately equal to the systems initial leakage
- the sum of all individual leak head-area slopes in a pipe system is approximately equal to the system head-area slope.

A concern that was observed in the study by Schwaller, van Zyl & Kabaasha (2015) was the sensitivity of the modified orifice equation parameters to the varying elevation of the system which led to a high number of errors. It was observed that systems on horizontal or constant terrain will have the lowest number of errors. However, even for large terrain variations, the estimation of the error will remain small when compared to the order of magnitude the parameter values can potentially adopt. For this reason, the modified orifice equation still provides a good estimate of the state of a pipe system.

In another study by Ferrante, Meniconi & Brunone (2014), the modified orifice equation parameters were randomly varied to understand the extent to which the mean values closely characterise the pipe system. In this study, the pipe systems were assumed to be horizontal and the FAVAD equation for a system is given as:

$$Q = n\bar{Q} = \bar{c}h^{0.5} + \bar{d}h^{1.5}$$

*Equation 2-25*

By randomly varying either the parameter  $c$  or  $d$  for individual leaks, Ferrante, Meniconi & Brunone (2014) showed that for multiple leaks in a pipe system that could vary by these two parameters, in a horizontal pipe system the parameters are closely characterised by the mean values of  $\bar{c}$  or  $\bar{d}$ . Even the effects of  $h$  perturbation were found to be negligible. In conclusion, it is clear that the modified orifice equation has been repeatedly proven to provide a good estimate of the leak characteristics of a system.

### **2.6.5 Relationship between the modified orifice equation and the power equation**

Although the two equations are mutually exclusive in terms of their underpinning assumptions, Cassa & van Zyl (2011) derived a relationship that links the power equation and the modified orifice equation. This relationship is particularly useful because it allows for leakage practitioners and researchers to convert between the conventional power equation and the parameters of the modified orifice equation.

#### **2.6.5.1 Analytical exploration of the relationship**

In order to find a way to relate the two equations, Cassa & van Zyl (2011) carried out an analytical exploration that started by equating the power equation and the modified orifice equation as follows:

$$Ch^{N1} = C_d\sqrt{2g}(A_0h^{0.5} + mh^{1.5})$$

*Equation 2-26*

Dividing the left hand side and the right hand side by  $C_dA_0\sqrt{2gh}$  results in:

$$C'h^{N1-0.5} = 1 + \frac{mh}{A_0}$$

*Equation 2-27*

Where  $C' = \frac{C}{C_d\sqrt{2gA_0}}$

The term  $mh/A_0$  in Equation 2-27 represents the ratio between the expanding area ( $mh$ ) and the fixed area ( $A_0$ ) of the leak area and is defined as the leakage number  $L_N$ , as follows:

$$L_N = \frac{mh}{A_0}$$

Equation 2-28

Properties of the  $L_N$ :

- when  $L_N = 1$ , fixed area and expanding areas contributes equal flows
- when  $L_N < 1$ , fixed area contributes more flow than expanding area
- when  $L_N > 1$ , expanding area contributes more flow than fixed area
- $L_N = 0$  at  $h = 0$
- $L_N \rightarrow \infty$  as  $A_0 \rightarrow 0$

With further manipulation of Equation 2-27, Cassa & van Zyl (2011) found an expression for  $NI$  in the form:

$$NI = \frac{\ln(L_N + 1) - \ln(C')}{\ln(h)} + \frac{1}{2}$$

Equation 2-29

Equation 2-29 confirms that the  $NI$  exponent is a function of pressure head  $h$ , but it is also not a satisfactory expression since  $C'$  is also a function of pressure head  $h$ . However, after exploring the limits of this equation (i.e. the limits as  $h$  approaches zero, and the limit as  $h$  approaches infinity), Cassa & van Zyl (2011) produced the following useful results:

- As  $h$  approaches zero,  $NI$  becomes equal to 0.5 and the leakage coefficient (in Equation 2-27) becomes  $C = C_d A_0 \sqrt{2g}$ . Therefore, at a pressure of zero the leak behaviour can be described by the orifice equation. These leaks can also be described as fixed leaks.
- As  $h$  approaches infinity,  $NI$  becomes equal to 1.5 and the leakage coefficient (in Equation 2-27) becomes  $C = C_d m \sqrt{2g}$ . Therefore, if the pressure is sufficiently high the leakage behaviour can be described by the variable part of the modified orifice equation, indicating the extent of leak area variation.

### 2.6.5.2 Significance of leakage number

Cassa & van Zyl (2011) plotted the leakage exponent ( $NI$ ) against the leakage number ( $L_N$ ), shown in Figure 2-28. It was found that when the leakage number  $L_N$  is calculated for different values of head-area slopes  $m$  and initial areas  $A_0$ , and pressures  $h$ , the relationship between the  $L_N$  and the  $NI$  are plotted on the same curve, as is shown in Figure 2-28.

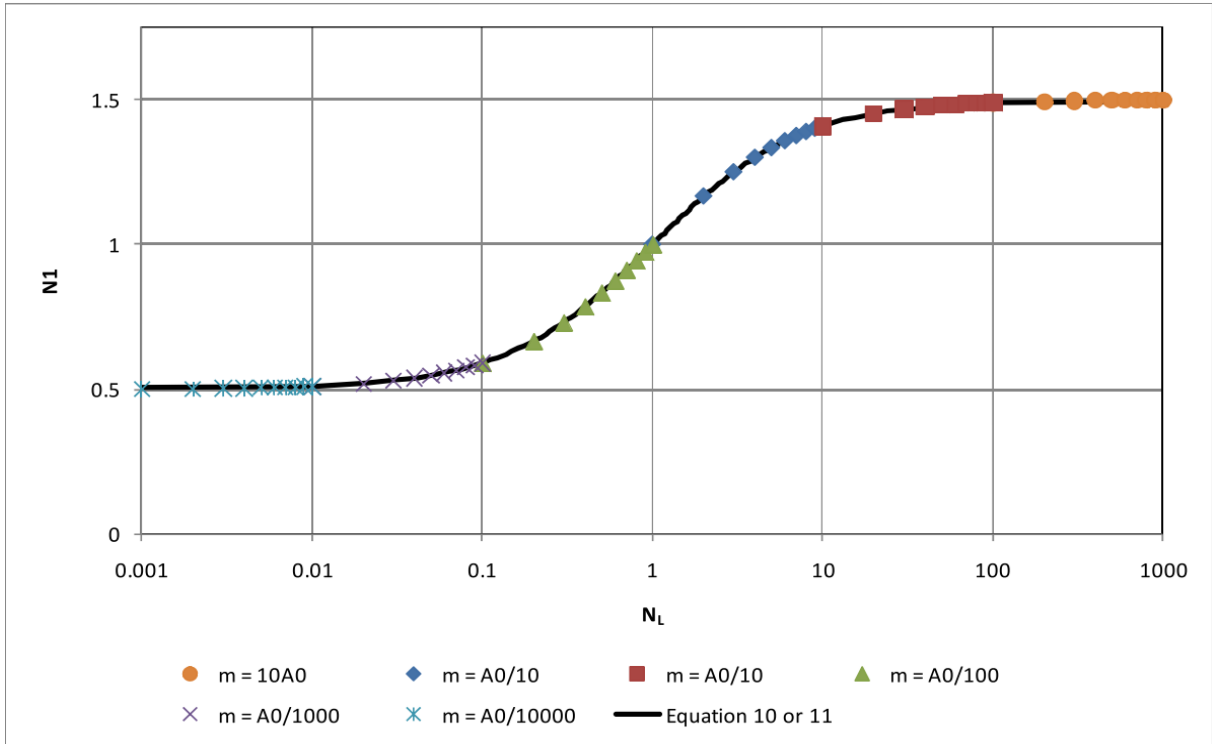


Figure 2-28: The plot of the power equation and the leakage number for various  $m/A_0$  (Cassa & van Zyl, 2011)

Figure 2-28 shows that the curve has an upper boundary of 1.5 and a lower boundary of 0.5. These are the same boundaries given by the modified orifice equation. This observed relationship also shows the following characteristics:

- $N_1 = 1$  when  $L_N = 1$
- $N_1 > 1$  when  $L_N > 1$
- $N_1 < 1$  when  $L_N < 1$
- $N_1$  is virtually 0.5 for all  $L_N < 0.01$
- $N_1$  is virtually 1.5 for all  $L_N < 100$

Furthermore, the following relationship can be drawn from Figure 2-28 and the above characteristics between the leakage exponent ( $N_1$ ) and the leakage number ( $L_N$ ):

$$L_N = \frac{N_1 - 0.5}{1.5 - N_1}$$

Equation 2-30

$$N_1 = \frac{1.5L_N + 0.5}{L_N + 1}$$

Equation 2-31

This finding was tested in a field study by Deyi, van Zyl & Shepherd (2014). In their study, the power and modified orifice equation parameters were obtained for a selected number of pressure management zones in the KwaDabeka Township water distribution system, in eThekweni. The results of this study showed that the  $NI$  values obtained have a large variation ranging from 0.18 to 3.33. The modified orifice equation was used to estimate the system head-area slope,  $m_s$ , and the system initial area  $A_{0s}$ . From these parameters the leakage number ( $L_N$ ) was calculated using Equation 2-30. The  $NI$  values obtained were plotted against the leakage number as shown in Figure 2-29.

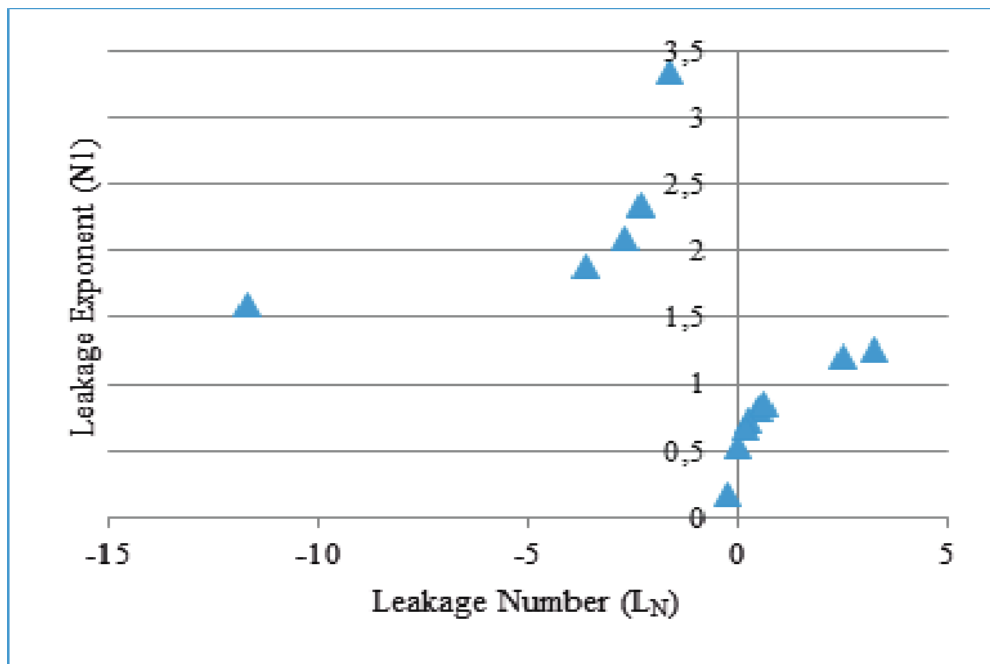


Figure 2-29: The relationship between the leakage exponent  $NI$  and the leakage number  $L_N$  (Deyi, van Zyl & Shepherd, 2014)

From Figure 2-29 it was noted that the  $NI$  values below 1.5 plotted in the same quadrant as the plot shown by van Zyl and Cassa (2011) in Figure 2-28. However,  $NI$  values greater than 1.5 plotted on a completely different quadrant, having negative leakage numbers.

Upon further investigation of the findings illustrated in Figure 2-29, Deyi, van Zyl & Shepherd (2014) plotted the system initial leak area ( $A_{0s}$ ) against the leakage number ( $L_N$ ), as shown in Figure 2-30. It was found that all the  $NI$  values greater than 1.5 had system leak areas  $A_{0s}$  below zero which in reality is not possible.

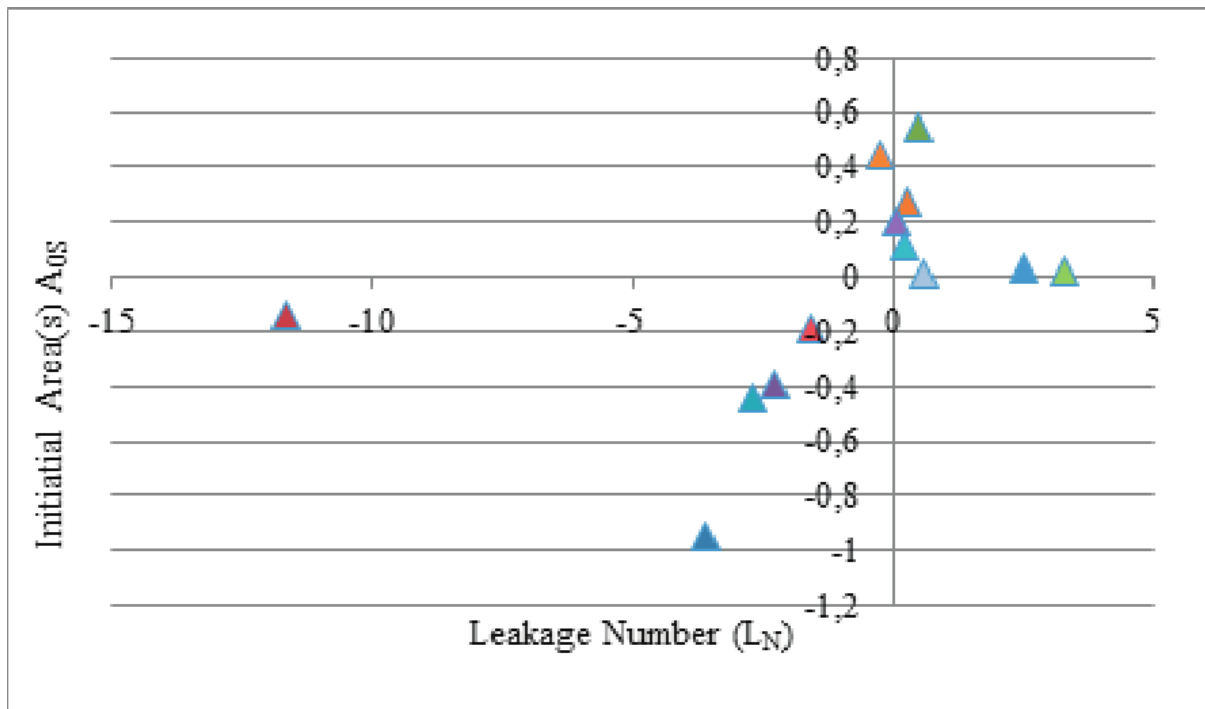


Figure 2-30: System initial area  $A_{0s}$  vs leakage number  $L_N$  (Deyi, van Zyl & Shepherd, 2014)

Deyi, van Zyl & Shepherd (2014) suggested some reasons for these anomalies:

- measurement errors
- plastic deformation playing a role in the behaviour of the leaks, and
- leaking zone boundary valves.

## 2.7 Components of bulk water pipelines

### 2.7.1 Introduction

In this section, components of bulk water distribution systems are discussed. A good understanding of the entire system and its components is absolutely critical in order to develop a strategy of how best to implement condition assessment interventions, such as the one to be carried out in this study.

Bulk water distribution systems generally require large capital investments. Table 2-8 presents data, from an annual report (Rand Water, 2007) published by a South African bulk water supplier - Rand Water, of the capital requirements of their various asset categories. Rand water supplies potable water to the Gauteng province and other areas of South Africa and is the largest water utility in Africa.

*Table 2-8: Value assets of the Rand Water Board (Rand Water, 2007)*

<b>Asset Categories</b>	<b>Value (R'000)</b>	<b>% of total value</b>
Land and buildings	246 042	5.6
Plants and reservoirs	1 720 065	39.3
Bulk water distribution pipelines	2 292 794	52.3
Vehicles	121 961	2.8
<b>Total</b>	<b>4 380 863</b>	<b>100</b>

From the data in Table 2-8 it can be seen that the pipeline assets constitute the largest percentage of the total capital requirements, at 52.3%. Furthermore, the annual report also explains that bulk pipelines are critical from an operational point of view because they are used to distribute water to the end users, and any pipeline failure will impact on the level of service experienced by the affected end users. This re-emphasises why it is critical for bulk pipelines to be well maintained, and that leaks are detected and repaired when they occur.

In this study, the following components were identified as critical when it comes to understanding bulk water distribution systems: the pipelines used to convey the water, the pump stations, the valves isolating the pipeline, and the storage tanks.

### 2.7.2 Pipelines

Bulk water distribution pipelines are critical from an operational point of view, as they are used to convey large amounts of water from one point to another. The range of pipe diameters can

vary from system to system. In this study bulk pipelines are not classified based on their diameter, but rather the pipe function; in other words pipelines that, for example, transfer water from a reservoir to another reservoir or from a treatment plant to a reservoir; such a pipe will be considered a bulk pipeline. However, any pipeline directly servicing a consumer is not considered a bulk pipeline.

The American Lifeline Alliance (2005) report on guidelines for water pipelines states that general pipeline design approach entails designing a system to safely accommodate internal pressures, vertical earth load, surface live load, pipe deformation, fatigue and fluid transients.

Pipelines are made of a range of different materials, each material with its own unique characteristics. These pipe materials are mainly classified as either metallic or non-metallic. Pipe materials are discussed in detail in Section 2.8. The failure of a pipeline can have a wide-ranging impact on an economic, environmental and social level (Agrawal & Sinha, 2015).

Pipelines may fail due to age-related material failure, considering the fact that pipelines have a limited design life. Table 2-9 presents the design lifespan associated with commonly encountered assets of Rand Water. The table shows that the design lifespan of pipelines can vary significantly, with some pipelines lasting as long as 75 years whereas others lasting only up to 20 years.

Age, however, is not the only reason why pipelines can fail. External factors such as environmental conditions around the pipe can also play a role. Knowledge and information about these two factors are critical to predict the pipeline failure (Nel, 2009).



Table 2-9: The design life of bulk water distribution assets (Rand Water, 2006)

Asset	Design lifespan (Years)
<b>Storage facilities</b>	
Reservoir and storage tank	80
<b>Pipelines</b>	
Pipeline – Steel shell	75
Pipeline – Steel with cement mortar lining	50
Pipeline – Steel with epoxy lining	50
Pipeline – Steel with HDPE lining	50
Pipeline – Steel with Bitumen lining	25
Pipeline – Steel with Bitumen coating	50
Pipeline – Steel with Bituguard coating	75
Pipeline – Steel with Sintercoat coating	50
Pipeline – Steel with cathodic protection	20
Pipeline – Pre-stressed concrete	30
Pipeline - HDPE	25
Pipeline - GRP	30

### 2.7.3 Pump stations

Pump stations consist of a number of sub-systems that form the pump system. These sub-systems consist of pumps, motors, controls, power transmission and valves. The reliability of a pump and its electrical power supply is important within the bulk water distribution environment, when pumping is required (Cullinane, 1985).

The reliability of the whole pump system is a critical aspect of bulk water distribution. Cullinane (1985) indicated that the reliability of a particular pump system, consisting of a series of systems, can be calculated by using equation 2-29:

$$R_S = R_P \times R_M \times R_C \times R_{PT} \times (R_V)^2$$

*Equation 2-32*

Where  $R_S$  is the reliability of the pump system,  $R_P$  is the reliability of the pump,  $R_m$  is the reliability of the motor,  $R_c$  is the reliability of the control unit,  $R_{pt}$  is the reliability of the power station, and  $R_v$  is the reliability of the valves (1 intake and 1 delivery valve).

This equation suggests that sub-system failures are all independent of each another. In other words, the failure of one sub-system component is neither influenced by, nor does it influence, the failure of another component of the sub-system. Reliable electrical power supply is important within the bulk water distribution, especially when pumping is required.

## 2.7.4 Pipeline valves

Valves in bulk water pipeline systems control the flow of water and are used to isolate a section of the distribution pipeline to facilitate repair. Large valves are usually housed in valve chambers providing easy access for maintenance or future replacement.

The following types of pipeline valves are used (Burstall, 1997):

- Line valves: their function is to section the pipeline into manageable lengths. This is useful when work is carried out on a section of the pipe.
- Bypass valves: these are typically fitted on main valves. Their function is to provide a slow charging rate across the main shut valve. This avoids surging and allows the air in the section of pipeline being charged to escape by way of the air valves.
- Branch valves: their function is to isolate a branch line from the main pipeline. They are fitted as close as possible to the main pipeline.
- Air valves: their function is threefold: first, to allow air to escape when the pipeline is charged; second, to allow air to enter the pipeline when water is being discharged from the pipeline; and third, to allow dissolved air to escape at minor high points.
- Scour valves: these need to work when they are needed. They are vital to the emergency operation of a pipeline, e.g. shutdowns.
- Non-return valves: these valves allow flow in one direction only. Typically, they are found on scour valve outlet pipes, fitted to prevent backflow into the main pipe.

## **2.8 Pipe materials used for bulk water pipelines**

### **2.8.1 Introduction**

An inline leak detection survey carried out on bulk pipelines across South Africa showed that pipe materials used for these pipelines varies quite significantly (Webb, Mergelas & Laven, 2009). The materials used for bulk water pipelines that were surveyed include: uPVC, steel, pre-stressed concrete, asbestos cement, and HDPE, including slip-lined pipelines, all ranging from 300 mm in diameter to over 2 m in diameter.

Pipe material options, e.g. cast iron, steel, ductile iron, pre-stressed concrete, asbestos cement (AC) and many more, cannot simply be equated. Various aspects such as material properties, costs, environmental conditions and other factors may guide the selection of a particular pipe material. Pipeline engineers therefore need a thorough understanding of the characteristics of the various types of pipes that are commercially available (Liu, 2003).

In this section, two broad classifications of pipeline material will be used, namely metallic and non-metallic pipelines. The properties of each pipe and their associated failure mechanisms will be discussed in some details. The author has also tried to show the strengths and weaknesses of each pipe material discussed.

### **2.8.2 Metallic pipelines**

The majority of metal pipes are strong and not easily breakable, but they are more affected by heat and electricity and less resistant to corrosion than non-metallic pipes. Metallic pipe materials used in bulk pipelines that are discussed in this section include: ductile iron, cast iron and steel.

#### ***2.8.2.1 Cast iron pipe***

Ordinary cast iron pipes are made of iron containing 3% to 4% of carbon in the form of graphite flakes. They are classified into two types: “Pit Cast Grey Iron” and “Centrifugal Cast Grey Iron” pipes (Liu, 2003). Cast iron pipes are typically brittle and therefore behave like all brittle materials, i.e. catastrophic failures are common.

Pit cast iron pipes were the first manufactured cast iron pipes, and they are made by pouring molten iron into a sand mould which was kept on end and lodged in a pit - similar to pouring concrete. The pipe was designed with greater wall thickness than required for the internal and external loading, resulting in inconsistencies in the wall thickness. It was well received in

industry in spite of not having any kind of internal or external corrosion protection (Liu et al., 2012).

In 1920, “spun” or “centrifugally” cast iron pipe was introduced, which was manufactured by centrifugally casting pipe in a sand mould. The tensile strength of the pipe was improved due to the alteration of molecular composition of the metal because of the centrifugal forces experienced by the molten iron. The walls were also made thinner, reducing the inconsistencies in the wall thickness. This resulted in greater strength, and cement was also used for interior lining to prevent interior corrosion (Liu et al., 2012).

Cast iron pipe failures are more diverse and complex than is usually appreciated by water utilities (Makar, Desnoyers & McDonald, 2001). The failure modes vary depending on the diameter of the pipe. Smaller diameter pipes have lower water pressure but also smaller moments of inertia, which makes them more susceptible to longitudinal bending failures that result in circumferential cracks. Larger pipes, on the other hand, have higher pressures and higher moments of inertia, and thus have a tendency for longitudinal cracking and shearing at the bell (Makar, Desnoyers & McDonald, 2001).

Most cast iron failures are associated with corrosion. The predominant deterioration mechanism of the exterior of cast iron pipes is electrochemical corrosion which produces damages in the form of holes (Mora-Rodríguez et al., 2013). Corrosion-induced failures are common to all pipe diameters. Two types of corrosion processes are observed in a cast iron pipe (Makar, Desnoyers & McDonald, 2001):

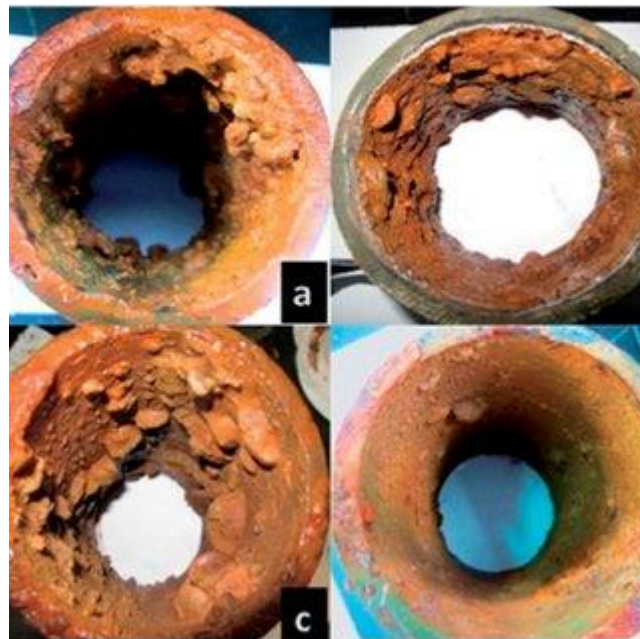
- simple corrosion pitting, and
- graphitization: here some of the iron is removed, leaving behind a matrix of graphite flakes that are held together by iron oxide.

Damage in cast iron pipes typically appears as graphitization graphite flakes (Figure 2-31) that appears in the iron part of a pipe affected by corrosion (Mora-Rodríguez et al., 2013).



*Figure 2-31: A failed cast iron pipe (The National Academies of Science and Engineering, 2011)*

Cast iron pipe interiors can sometimes be exposed to incrustations (Makar, Desnoyers & McDonald, 2001). Erosion and cracks by corrosion reduce the inner diameter and allow rust tubercles to form inside the pipe as is shown in Figure 2-32. Severe internal corrosion can also lead to structural deterioration of the pipe and poor water quality. An economic solution to extend the asset life of a cast iron pipe is to deploy in-situ cement mortar lining or other methods of lining. These lining solutions also improve the flow and water quality for approximately one third to one quarter of the cost of a new main. Chemical cleaning of unlined pipes is an alternative to relining (Burstall, 1997).



*Figure 2-32: Cast iron rust tubercles (Huifang et al., 2014)*

Other failures of cast iron pipes can be attributed to rapid pressure variations, e.g. surges, due to their brittle nature. Control valves which open or close too quickly and malfunctioning air valves are also reasons for cast iron pipes failing catastrophically. Manually operated line valves should not cause problems if carried out under the proper waterworks procedure (Burstall, 1997).

Finally, cast iron pipes also experience joint failures. As a result of the deterioration of joints over a period of time, leaks caused by pipe breaks are often observed near the joints. Figure 2-33 (a) represents a bell and spigot joint which is the most common type of joint in cast iron pipes. Reed, Smart & Robinson (2006) conducted a survey among a number of utilities in order to obtain information about potential failure modes and causes of failure for the most common joint types in cast iron pipes. It was found that the failure of sealing used in lead joints is the most problematic failure. Rajani & Abdel-Akher (2013) also suggest that ground movements, shown by Figure 2-33 (b), can lead to a change in joint alignment, as can be seen in Figure 2-33 (c). A large change to the joint alignment can lead to leakage and ultimately joint failure.

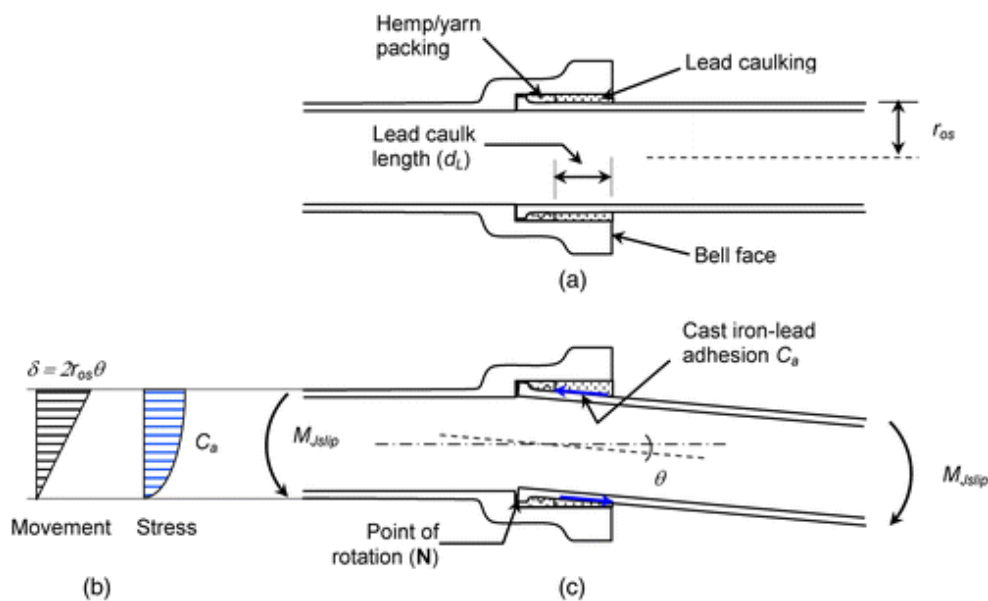


Figure 2-33: (a) Bell and spigot joint of cast iron pipes, (b) ground movement mechanics, (c) change in joint alignment due to ground movement (Rajani & Ahmed, 2013)

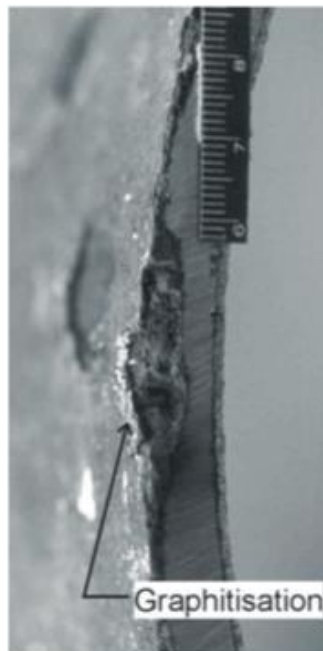
### 2.8.2.2 Ductile iron

Ductile iron pipes are made of iron containing approximately 3.5% carbon in spheroidal or nodular form and a magnesium alloy. Ductile iron is a material that is supple and does not rupture easily (Liu, 2003). Both ductile iron and cast iron contain iron as a common element, but there is a difference between them based on their compositions. The differences in

composition lead to other variances in their material properties, and they can therefore be used in different applications.

Rajani & Kleiner (2003) mention that when ductile iron pipes were introduced in North America in the late 1950s, ductile iron had more advanced properties than cast iron. The key difference between ductile iron and cast iron is that ductile iron is more flexible, durable and stronger.

Unlike cast iron, ductile iron does not have a matrix of cast iron flakes. Instead, during its manufacturing process, fine carbon spheres are produced in the metal. As a result, there is a lack of connection between the graphite spheres in the material, and hence it is assumed that graphitisation does not occur (Makar, Desnoyers & McDonald, 2001). However, a report by the British Water Research Centre (De Rose & Parkinson, 1985) that presents both forms of grey cast iron pipe and compares them to ductile iron pipe, reports examples of observed graphitisation in ductile iron (Figure 2-34). Even though graphitisation is less common in ductile iron pipes than cast iron pipes, it is still clearly a possibility.



*Figure 2-34: Cross section of a ductile iron pipe showing graphitisation, City of Ottawa (De Rose & Parkinson, 1985)*

Ductile iron pipes were initially laid and used with minimal or no corrosion protection because ductile iron corrodes much slower than cast iron (Rajani & Kleiner, 2003). Within a few years it became apparent that unprotected ductile pipes placed in aggressive soils also tend to corrode,

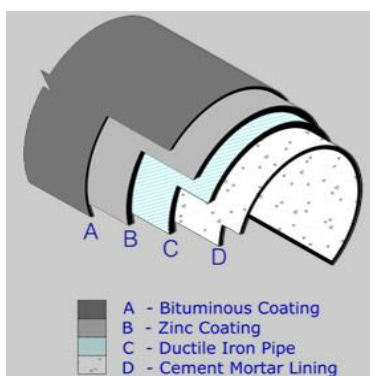
as is shown in Figure 2-35. The predominant deterioration mechanism of ductile iron exterior is electrochemical corrosion.



*Figure 2-35: External corrosion of ductile iron pipe*

Currently, many methods and techniques to protect ductile iron pipes from corrosion have been developed or adopted. These methods typically include polyethylene encasement, stray current control and cathodic protection (Kroon et al., 2005). Rajani and Kleiner (2003) explain that these protection methods perform well under some circumstances and poorly under others. It is often difficult to tell whether a reported success or failure can be attributed to the quality of implementing a method or whether it is inherent in the method's ability to perform under a given set of conditions.

Figure 2-36 (a) shows an example of how some ductile iron pipes are protected. Figure 2-36 (a) shows an internal centrifugally-applied cement mortar lining inside the ductile iron pipe. On the outside, the pipe has a zinc coating that forms a stable protective layer of insoluble zinc salts as well as a layer of bituminous coating which further enhances the corrosion resistance of the pipe. Figure 2-36 (b) shows what the finished protected ductile iron product looks like.



(a)

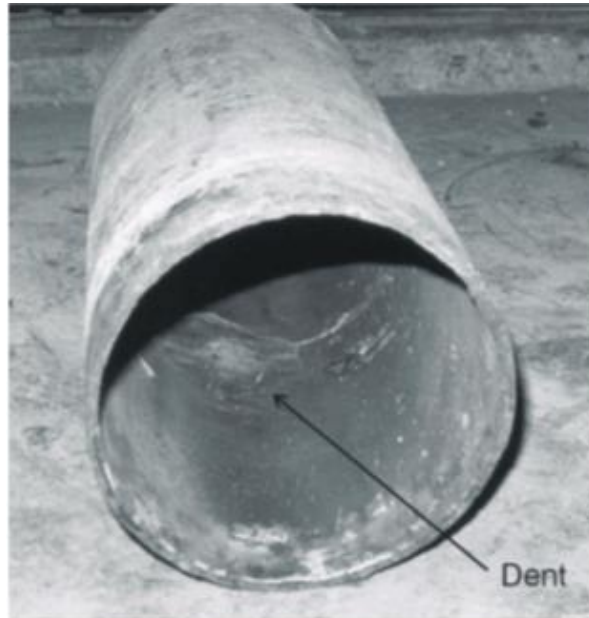


(b)

*Figure 2-36: Ductile iron pipes used for drinking water: (a) the various components (AVA, 2010) and (b) commercially available ductile iron pipes (Robor Suppliers, 2015)*



Human error can also contribute to ductile iron pipeline failures. A common source of failure is third party damage, for example when excavations are made on or near pipelines without accurate knowledge of their location. This frequently causes pipeline damage or failure, as is shown in Figure 2-2-377. These sort of failures are common to all buried infrastructure.

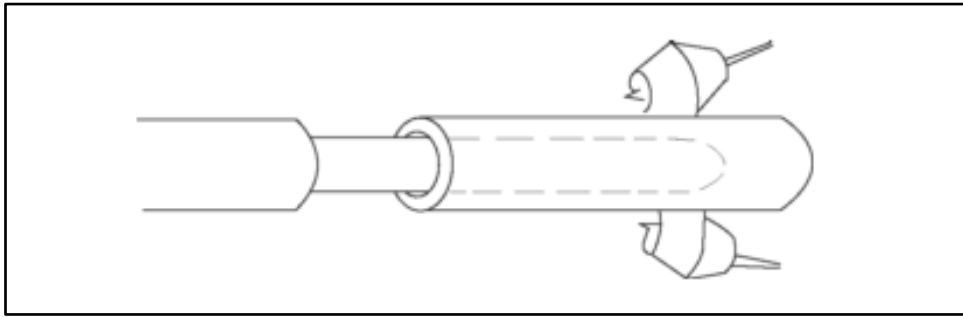


*Figure 2-2-377: Dent and hole in ductile pipe created by third party damage (Makar, Desnoyers & McDonald, 2001)*

### **2.8.2.3 Steel pipe**

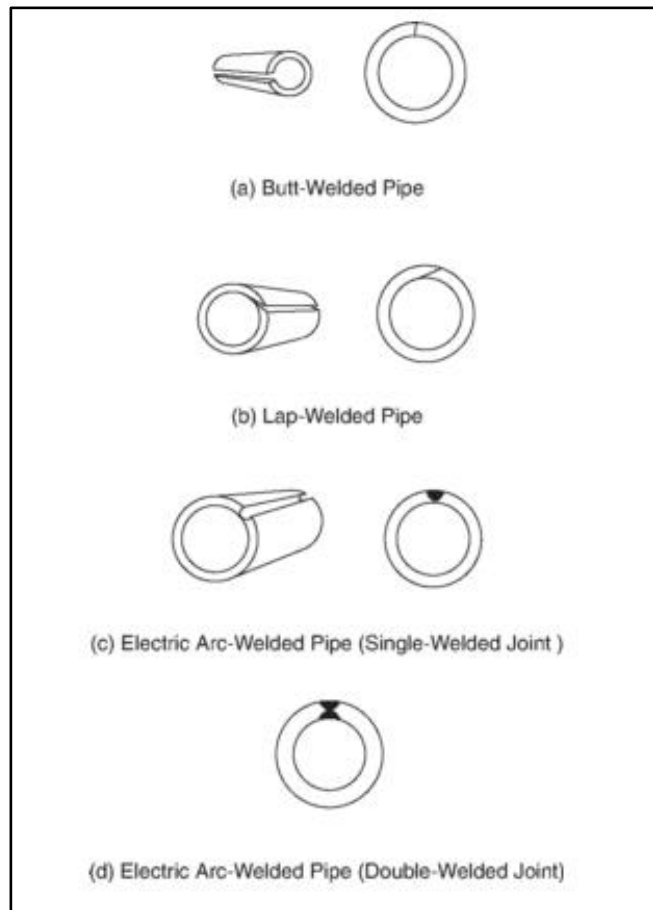
Ordinary steel pipes are made of carbon steel. They are either seamless or seamed (welded). Steel that is used in water pipelines is inherently strong, yet ductile, and does not fracture easily. However, if no preventive measures are taken against both external corrosion and internal corrosion, steel pipes can severely corrode (Burstall, 1997).

A seamless steel pipe is made from a solid rod (billet) of steel, which is pierced by a cold rod to form a hollow round section as shown in Figure 2-38. The two rollers in the figure grip and turn the rod, causing the rod to rotate and advance towards the piercing point, forming a hole through the length of the rod (Liu, 2003).



*Figure 2-38: Formation of a seamless pipe (Liu, 2003)*

The seamed steel pipelines are made of steel sheets or steel plates that are rolled or press formed into circular shape, with the edge (seam) of each pipe closed by welding. Liu (2003) describes four possible types of weld as shown in Figure 2-39: (a) butt weld which is a double-welded joint, (b) lap weld, (c) electric arc weld which is a single-welded joint, and (d) electric arc weld which is also a double-welded joint.



*Figure 2-39: The different types of welding for seamed steel pipes (Liu, 2003)*

The first two examples are furnace welded and are typically only deployed for small pipes; the last two weld techniques are mostly for large pipes used for bulk systems. One of the problems

encountered with seamed steel pipes is the corrosion mechanism in the weldments that results in longitudinal cracks, as is illustrated by Figure 2-40 (Lee et al., 2013). Experimental procedures that involved macroscopic inspections, metallographic observations, scanning electron microscopy (SEM) and energy dispersive X-ray revealed that seamed steel pipes can be susceptible to stress corrosion cracking (SCC), which is a corrosion mechanism induced by residual stress in the welding seam (Lee et al., 2013).



*Figure 2-40: Photograph of a failed weldment in a steel pipe (Lee et al., 2013)*

Steel pipes undergo various other forms of failure such as circumferential splits, longitudinal splits, blown out pieces and pipe wall rupture or tear. The most common type of failure in steel pipes, however, is blow-out holes. This type of failure occurs due to pitting and perforation of the pipe wall. The Water Association of Australia (2003) further states that whenever extensive wall thinning has occurred, ductile rupture and tearing of the wall are always a possibility.

Rajeev et al. (n.d.) presented statistical analyses of pipe failure data on large diameter steel water mains collected from five Australian water utilities. The analyses identified the factors that lead to failures of various pipes including steel. From the failure inspection reports provided by the Australian water utilities, data on the mode of failure, causes of failure, and corrosion and pit characteristics, was obtained.

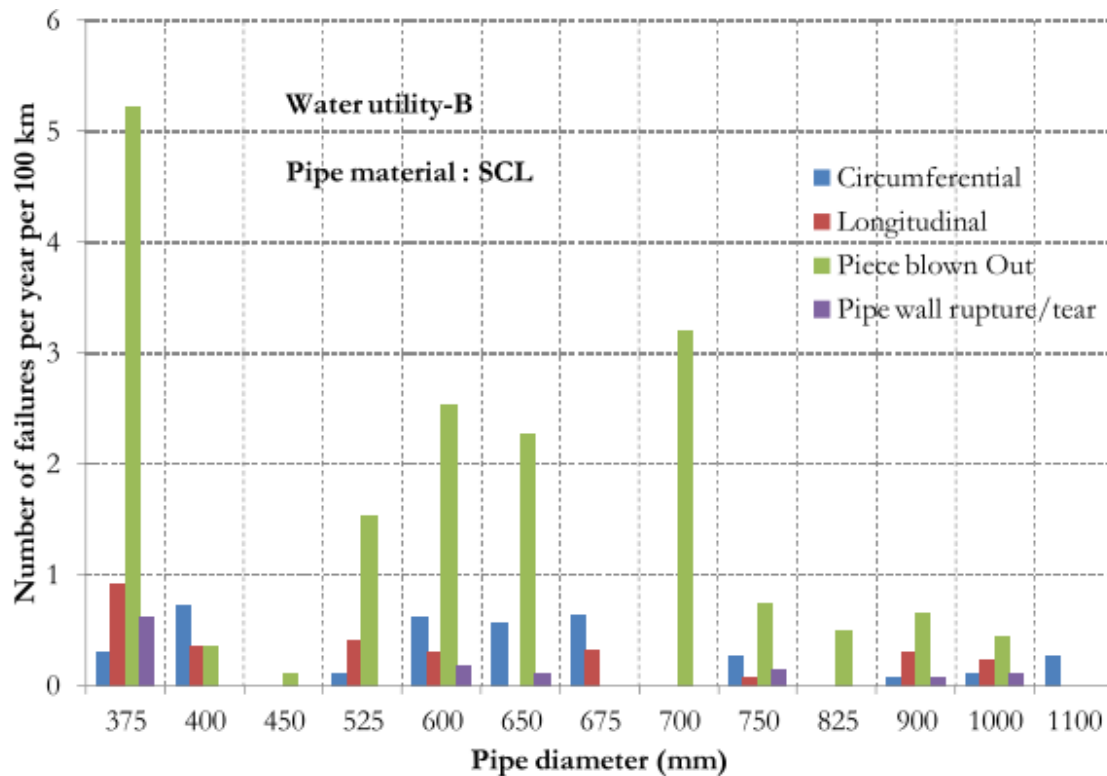


Figure 2-41: Histogram of failure rate based on failure mode of steel pipes (Rajeev et al., n.d.)

Figure 2-41 shows that the failure mode with the highest frequency across the entire diameter range in steel pipes was the blown-out pieces. Longitudinal and circumferential failures were observed across the whole diameter range. A general evaluation of the data highlighted corrosion as the main cause of failure across all diameters.

The primary driving factors of failure mode for blown-out pieces are internal pressure and corrosion. Longitudinal splits also occur as a result of internal pressure and corrosion (SSC), whilst circumferential splits are due to external loadings and ground movements. Rajeev et al. (n.d.) point out that it was not clear how ground movements could affect large diameter pipes, because they generally have higher moments of inertia and higher rigidity against bending. Pipe wall rupture is simply a result of the pipe wall thinning due to excessive corrosion.

### 2.8.3 Non-metallic pipes

Although non-metallic pipes may not be structurally as strong as metallic pipes, they are usually lighter in weight, more economical, and have certain advantages such as being more corrosion resistant. A brief discussion about various non-metallic pipes is provided in this section.

### 2.8.3.1 Plastic pipes

In recent years the use of plastics in the manufacturing of pipes has increased. Composition of the pipe depends on the type and these typically come in various forms. Plastic pipes are well known to withstand attacks from acids and alkalis as well as bacterial attack. Some of the common plastics used are polyvinyl chloride (PVC), polyethylene (PE), polypropylene (PP) and acrylonitrile butadiene-styrene(ABC) (Farshad, 2006). The first two will be discussed here because of their frequent use in bulk water pipeline systems.

#### 2.8.3.1.1 Polyvinyl chloride

Polyvinyl chloride is made from the vinyl chloride monomer which undergoes a polymerisation process (Farshad, 2006), which is a form of linking together as shown in Figure 2-42.

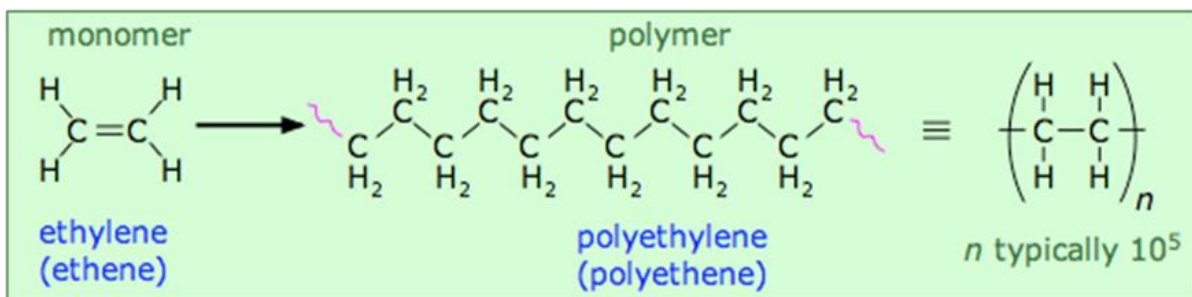


Figure 2-42: Polymerisation process

The monomer can be obtained from petroleum. When PVC pipes are manufactured, other ingredients are added to the polymer. The ingredients are mixed in a high-speed mixer at approximately  $120^{\circ}\text{C}$  before being cooled to about  $50^{\circ}\text{C}$ , and then finally undergo an extrusion process. There are two types of PVC:

- rigid PVC (or un-plasticised PVC – uPVC)
- plasticised PVC: this usually has plasticisers added during the manufacturing process which make it safe and more flexible than uPVC.

PVC pipes are sometimes graded as B, C, D and E as illustrated in Table 2-10. These categories differ only by the thickness of the pipe wall.

Table 2-10: PVC pipes to BS 3505

Nominal diameter	Outside diameter to nearest mm	Inside diameter to the nearest mm			
		B	C	D	E
		60 m head	90m head	120m head	150m head
100	114	107	105	102	99
150	168	159	155	151	146
225	244	232	226	220	214
300	324	308	301	294	286
450	457	434	424	412	-
600	609	580	566	-	-

PVC pipes are known to be brittle and therefore the common associated failures are catastrophic and typically occur in the form of cracks along their walls, see Figure 2-43. PVC pipes can also easily be damaged if struck by tools during the installation process (Carroll, 1985).



Figure 2-43: PVC pipe failure (Dueck, 2010)

PVC can also be damaged during the manufacturing process because the material is made in a gelation process by which it is melted and then allowed to reform several times to strengthen

individual crystallites into a strong polymer (Burn et al., 2004). Interruptions in this process can result in an increase in the material's brittleness, thereby making it more prone to cracks.

PVC pipes also experience blown-out sections, starting with a longitudinal split as is shown in Figure 2-44.

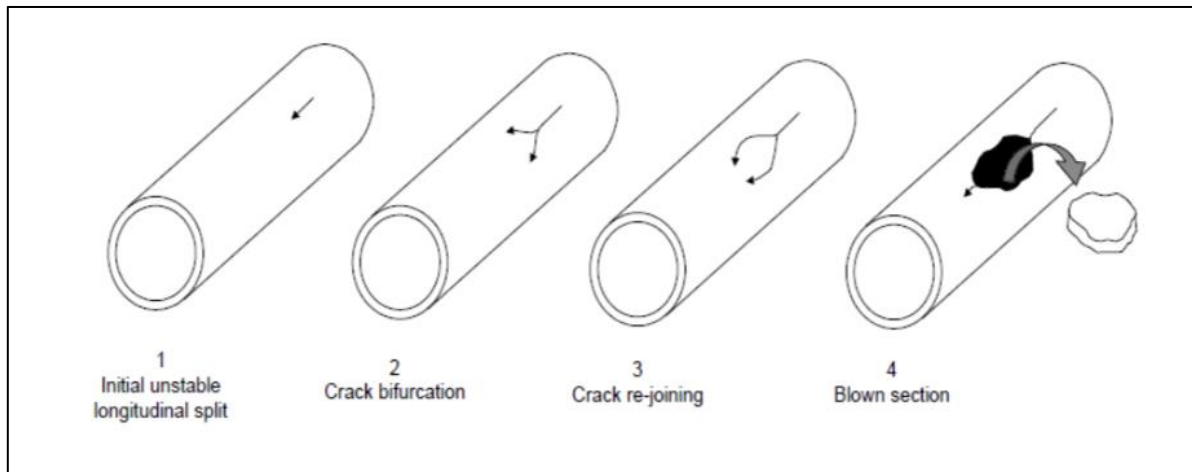


Figure 2-44: Events leading to a blown-out section (Burn et al., 2004)

Another failure mode that is associated with PVC is leaking joints. These failures occur because PVC pipelines are joined with non-elastomeric seal joints and the lead compounds are likely to result in joint leaks.

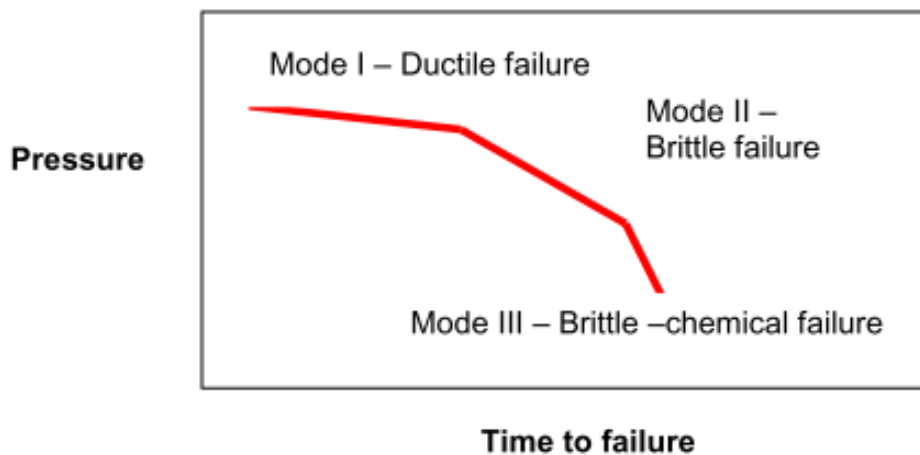
### 2.8.3.1.2 Polyethylene

Polyethylene (PE) was discovered in 1933. It is basically a by-product of crude oil. Its usage in the water industry has increased significantly as a result of continuous development of polyethylene materials. A variety of materials are now available; these include high density polyethylene (HDPE) which is produced through a low pressure process, and medium density polyethylene (MDPE) and low density polyethylene (LDPE) which are manufactured through a relatively high pressure technique (Farshad, 2006).

HDPE pipes are most commonly used in bulk water pipelines (O'Connor & Denton, 2012). They are known to have a non-corrosive nature, chemical inertness and a long-term durability offering. They have, in many ways, solved leakage though corrosion issues of traditional iron, steel and concrete pipes. However, global operators of HDPE pipelines, or any PE pipeline for that matter, have reported that the major threat to the integrity of these pipelines, other than third party damage, is poor fusion jointing. Joints are usually the weak point of HDPE systems. Axial loads or bending stresses that are caused by thermal expansion or contraction, or even

ground movement, increase the risk of failure of substandard joints (O'Connor & Denton, 2012). There are three main types of fusion joint geometry for PE pipelines, namely: butt weld, socket joint and saddle joint.

Another failure mechanism of polyethylene pipes, according to O'Connor and Denton (2012), is the stress crack growth (SCG). This is a phenomenon in PE materials whereby slow growing cracks can emerge due to the presence of stress in the material. This failure can also occur in PE joints. Early research of HDPE pipes established that SCGs in the material was one of three major failure modes of PE pipelines, as is illustrated in Figure 2-45.



*Figure 2-45: Failure modes of PE pipes (O'Connor & Denton, 2012)*

Ductile failure, mode I in Figure 2-45, typically occurs as a result of yielding and reflects the propensity of a material to undergo large scale irreversible plastic deformation when under stress. Localised expansion of the wall and eventually a rupture of the deformed zone occur as shown in Figure 2-46.



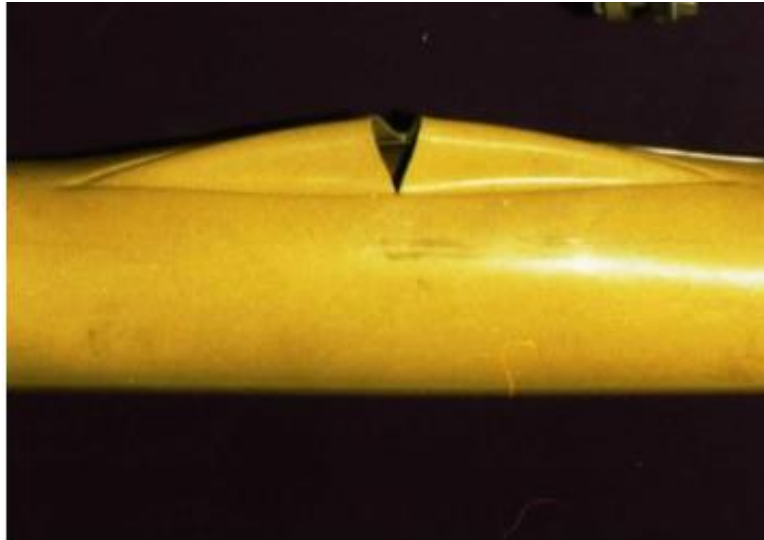


Figure 2-46: Ductile failure mode of a PE pipe under pressure(O'Connor & Denton, 2012)

Failure mode II is associated with creep, creep rupture and SCG. Creep is a time-dependant phenomenon and is non-reversible when the material is exposed to constant stress (O'Connor & Denton, 2012). Figure 2-47 shows the creep rupture curve.

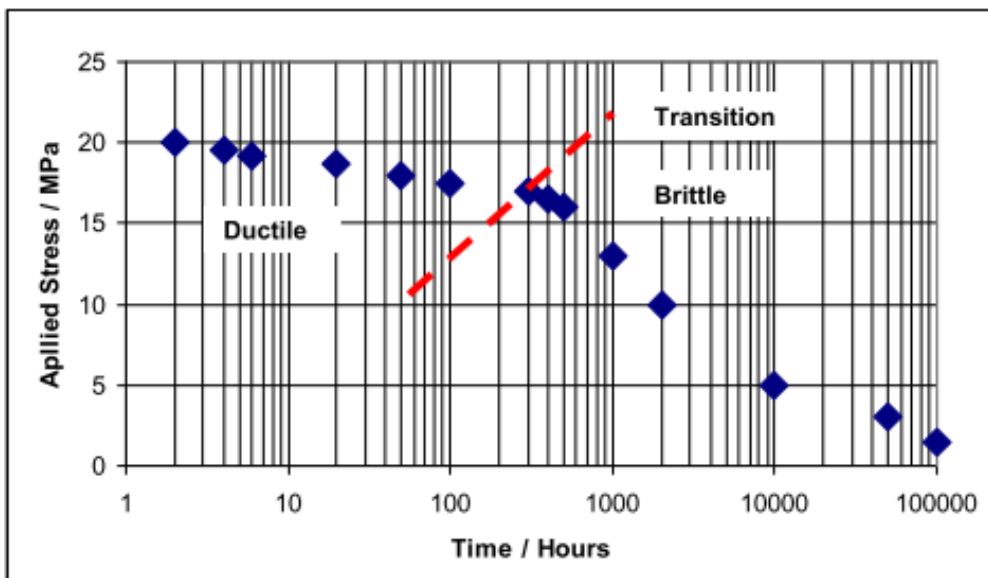
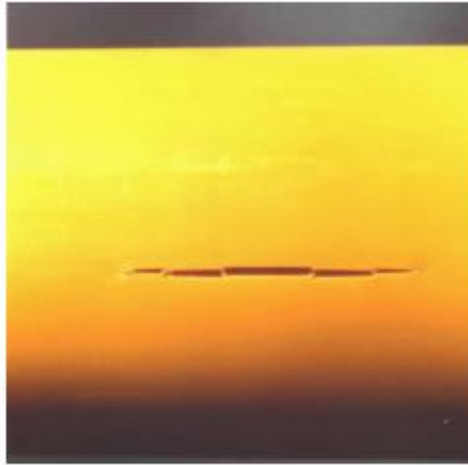


Figure 2-47: Creep rupture curve (O'Connor & Denton, 2012)

The brittle regime exhibits failures that are slit type fractures which lie parallel to the pipe's extrusion direction as is shown in Figure 2-48. The driving force of this type of failure is the circumferential hoop stress in the pipe material.



*Figure 2-48: Brittle failure of a PE pipe - slit type fractures (O'Connor & Denton, 2012)*

### **2.8.3.2 Glass reinforced pipes (GRPs)**

Glass reinforced pipes (GRPs) are commonly known as fibre glass pipes. They were first introduced in the United States in 1950. The fibre glass composites used to make these pipes are made from fibre reinforcements, thermosetting resins and other additives such as fillers, catalysts, hardeners and accelerators. The use of GRPs in large diameter water pipe application is growing rapidly (Najafi & Gokhale, 2005).



*Figure 2-49: A GRP pipe being slewed into position (GRANT, 2016)*

GRP material is not affected by corrosion but usually fails through pipe rapture where the material tears and creates an opening in the pipe wall, as shown in Figure 2-50. This is often associated with damage that is caused to the pipe during construction.



*Figure 2-50: GRP pipe failure (Australia, 2003)*

### **2.8.3.3 Asbestos cement (AC)**

Asbestos cement (AC) is made of several layers of asbestos fibres soaked in cement. Asbestos is a naturally occurring mineral. It was thought that AC was unable to be affected by corrosion, especially electrolytic corrosion (Burstall, 1997). However, a field report by Mordak & Wheeler (1988) showed that AC pipes degrade over time, internally by contact with the water and externally by the soil environment. AC is a brittle material and therefore cast or ductile iron is used for bends and fittings.

Because AC pipes are brittle, they typically undergo catastrophic failures. The most common failure is a longitudinal split, shown in Figure 2-51, which is associated with general pipe deterioration and broken backs (Burstall, 1997). In some places, the use of asbestos cement has been discontinued.



*Figure 2-51: Failure mode of an AC pipe: longitudinal split*

### 2.8.3.4 Concrete

Concrete pipes can be divided into low-pressure and high-pressure types. The low-pressure pipes are normally made of plain concrete. These are normally used in applications that do not operate under high or even moderate internal pressure, for example for sewers or culverts. Plain concrete pipes can easily withstand high external pressure imposed on them by earth and traffic above, because of their high compressive strength (Liu, 2003).

The high-pressure pipes are made up of pre-stressed concrete. Conceptually, these types of concrete pipes are similar to ductile iron systems. One factor concerning pre-stressed concrete pipes is the corrosion of the steel components. However, cathodic protection can easily mitigate this (Burstall, 1997).

A summary of the types of concrete pipes, their pressure ratings, and typical applications are shown in Table 2-11.

*Table 2-11: Types of concrete pipes and their applications (Liu, 2003)*

<b>Type</b>	<b>Maximum Pressure allowed (MPa)</b>	<b>Typical Application</b>
Plain concrete pipe (PCP)	Practically 0	Gravity flow or non-pressure flow, as for certain sewers and culverts
Reinforced concrete non-cylinder pipe (RCNCP)	0.4	Sewers, storm drain, irrigation pipes
Reinforced concrete cylinder pipe (RCCP)	1.7	Sewers, water mains
Pre-stressed concrete cylinder pipe (PSCCP)	2.8	High-pressure water and sewer lines
Pre-tensioned concrete cylinder (PTCCP)	2.8	Same as for PSCCP

Due to the sheer hefty weight of concrete pipes, they often come in short lengths. As a result, more joints are usually needed for concrete than for other pipes. These joints are often the weakest points of concrete pipes (Gerges, Issa & Fawaz, 2016).

An investigation was conducted by Pratt et al., (2011) into the deterioration and failure of pipeline assets in the Perth metropolitan region, Australia, with a focus on reinforced concrete and cast iron pipes. The main objective of this study was to improve the knowledge base of the underground infrastructure for asset management purposes. The study was done by implementing a sample collection and analysis procedure, and then by analysing relationships between pipe failures and their environment. For the reinforced concrete 37 samples were analysed. It was found that at least 28 of the pipe samples tested failed as a result of joint failures, as is shown in Table 2-12. The authors of the study also observed that internal corrosion was more aggressive than external corrosion in all the analysed samples.

*Table 2-12: A summary of the Observed Reinforced Concrete failure modes from Pratt et al., (2011) study*

<b>Failure Mode</b>	<b>Number of Samples</b>
Joint Failure	28
Crack	2
Internal corrosion	5
No observed failure	2

## **2.9 Existing knowledge about leakage on bulk pipelines**

A study on the frequency of unreported leaks on bulk pipelines across the world was carried out by Laven and Lambert (2012) with the use of the Sahara system. A repository of data containing the results of 3 000 km of international inline leak survey data was made available to the authors. The data was provided by two companies namely: Pure Technologies Ltd, and WRc Plc.

Inline surveys were preferred because they have higher sensitivities to small leaks. It is reported that inline technologies have the capacity for finding even tiny leaks, down to 0.02 litres/minute (Laven & Lambert, 2012). Laven and Lambert (2012) therefore concluded that inline survey data would provide a sound picture of the frequency of detectable unreported leaks on transmission lines.

### **2.9.1 Unreported leak frequency variation by geographic region**

The data collected by the authors was first analysed by geographic region to understand the variations of unreported leaks on bulk pipelines across different regions. In the 3 221 km of

bulk pipelines surveyed, the authors indicated an average frequency of 92 unreported leaks/100 km. Table 2-13 illustrates the variation of the measured frequencies of unreported leaks in different geographical regions.

*Table 2-13: Measured frequencies of unreported leaks on bulk pipelines in different geographical regions (Laven & Lambert, 2012)*

<b>Region</b>	<b>Distance (km)</b>	<b>Leaks</b>	<b>Leaks/100km</b>
Worldwide	3221	2966	92
North America	711	496	70
Latin America	186	40	22
Europe	1583	2023	128
Africa	383	244	64
Asia & South Pacific	298	150	50
Middle East	60	13	22

Table 2-13 shows that the variations ranged from 22 to 128 leaks/100 km.

### **2.9.2 Unreported leak frequency variations by pipe material and diameter**

Table 2-14 shows the pipe material records of 2 500 km of bulk pipeline data (Laven & Lambert, 2012). There is a wide variation in the unreported leaks frequencies by material. Cast iron has the highest leak frequency, followed by ductile iron, steel, and lastly concrete with the lowest leak frequency.

*Table 2-14: Measured frequencies of unreported leaks on bulk pipelines in different materials(Laven & Lambert, 2012)*

<b>Material</b>	<b>Distance (km)</b>	<b>Leaks</b>	<b>Leaks / 100 km</b>
Cast iron	1127	1871	166
Ductile iron	199	142	71
Steel	296	87	29
Concrete	961	417	43

For a smaller sample of 1 116 km of bulk pipeline, a breakdown of unreported leak frequencies by pipe diameter is shown in Table 2-15. There is a clear trend that larger bulk pipelines have a smaller frequency of unreported leaks.

Table 2-15: Measure frequencies of unreported leaks on bulk pipelines with different diameters

Material	Distance (km)	Leaks	Leaks / 100 km
< 600 mm	47	31	66
600 to 900	302	267	88
1050 to 1500	399	141	35
> 1500 mm	368	52	14

### 2.9.3 Unreported leak frequency related to the age of mains

With regards to unreported leaks and the age of bulk pipelines, it was found that the number of unreported leaks per km of pipe increases with age. Pipes of about 1 500 km, of which the age could be estimated, were grouped and a plot of leakage rate against age is shown Figure 2-52.

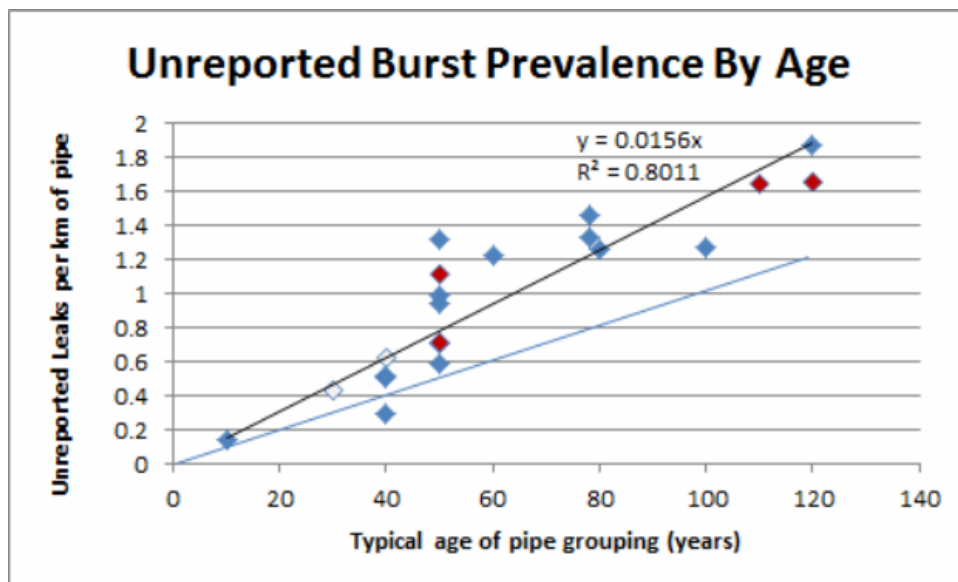


Figure 2-52: Measure frequency of unreported leaks compared with the estimated pipe age (Laven & Lambert, 2012)

Figure 2-52 shows that there is a positive correlation between unreported leaks and pipe age. According to Lambert and Laven (2012), this correlation indicates the possibility that unreported leaks in the bulk pipelines that were surveyed are forming at a pace of around 1.56 leaks per 100 km per year. These leaks then accumulate as a backlog over time rather than being reported and reach a steady state frequency.

### 2.9.4 Variations in the leak flow rates of bulk pipelines

In the survey done by Laven & Lambert, (2012) a consistent methodology for classifying leak flow rates based on the use of inline survey data was employed. The inline surveys come with data of flow rates detected upon inspection. The leak data is grouped in five qualitative size bands, generally described as “very small” through to “very large”. A UK study by Bond et al. (2007), and also cited by Lambert and Laven (2012), was undertaken to excavate and measure roughly 400 leaks to confirm the approximate minimum and maximum flow rates for each grouping. Table 2-16 provides a summary of the categories of leaks.

Table 2-16: Qualitative size classifications for leak flow rates in the UK (Bond et al. (2007))

	Size 1	Size 2	Size 3	Size 4	Size 5
	m <sup>3</sup> /hr	m <sup>3</sup> /hr	m <sup>3</sup> /hr	m <sup>3</sup> /hr	m <sup>3</sup> /hr
<b>Min</b>	0.23	1.6	6.7	11.8	16.9
<b>Median</b>	0.93	4.2	9.3	14.4	25.5
<b>Max</b>	1.6	6.7	11.8	16.9	34.0

A useful way to illustrate how the leaks in the five size categories contribute to the total real losses from unreported leaks is through histograms, as is shown in Figure 2-53 and Figure 2-54.

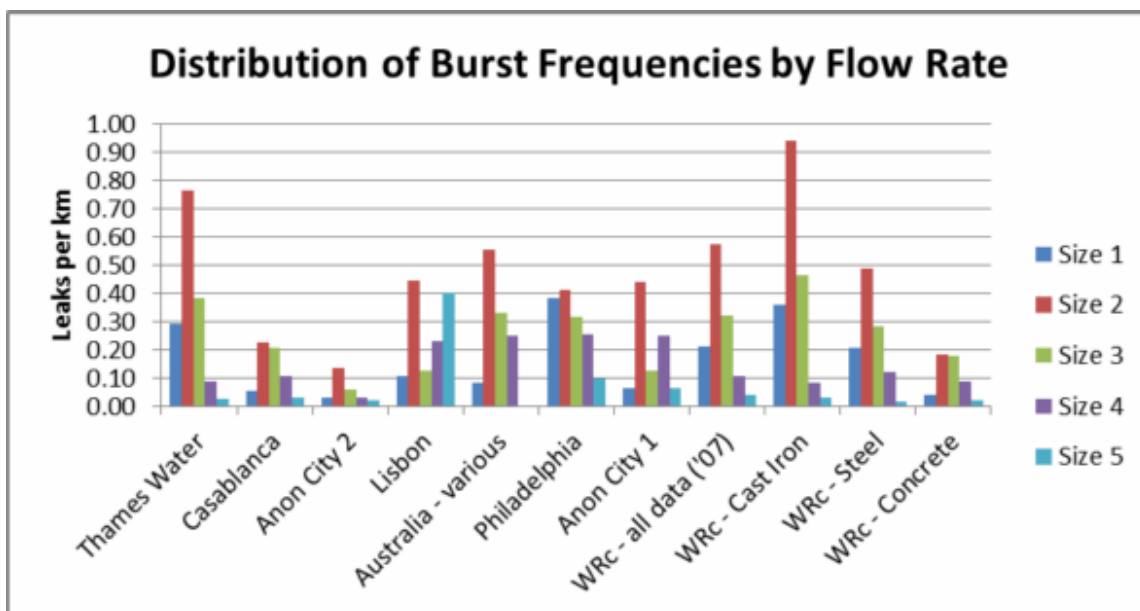


Figure 2-53: Histogram showing the distribution of number of leaks among the five flow rate classifications (Laven & Lambert, 2012)



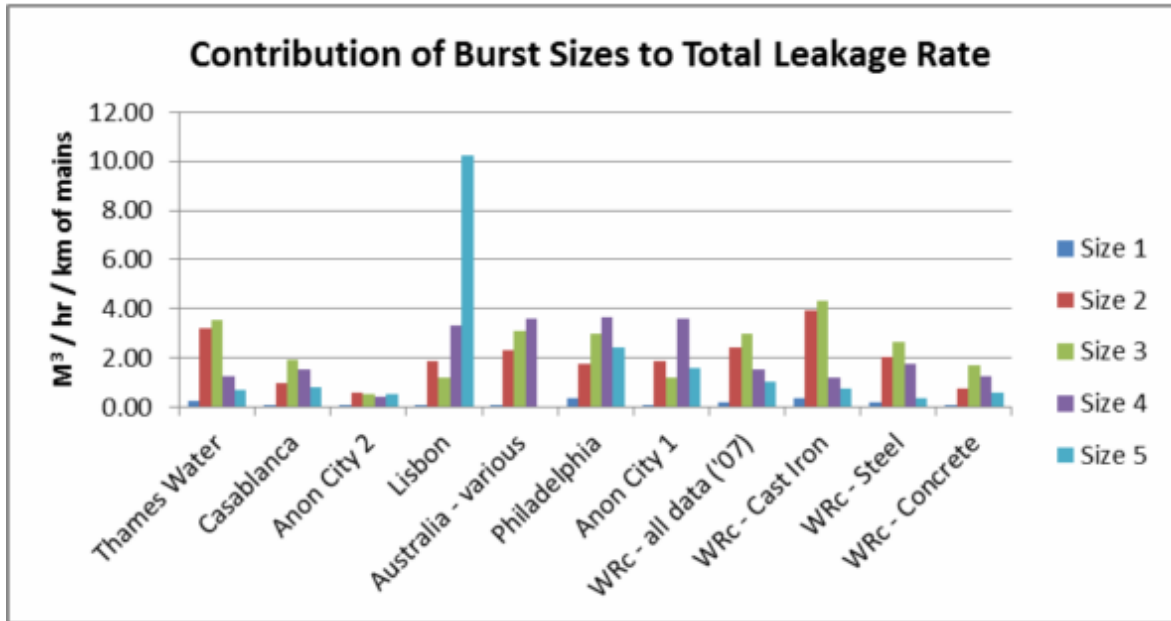


Figure 2-54: Histogram showing the contribution of each leak size to the total leakage rate (Laven & Lambert, 2012)

According to Figure 2-533 and Figure 2-54, the smaller leaks make up the majority of leaks per km, and the less frequent larger leaks contribute more to the water loss.

## 2.10 Conclusion

Field and laboratory studies have shown that leakage from water distribution systems is substantially more sensitive to changes in pressure than conventionally believed. It has now been established that the major reason for this behaviour is that the areas of holes and cracks in pipes are not static, but change with variations in pressure.

An unacceptable amount of water is lost unnecessarily through leakage. Large potential therefore exists for countering this trend by reducing these losses. One of the main contributors to these losses is pipeline leakage, and by monitoring the condition and leakage of distribution and bulk pipelines, effective intervention can be implemented to reduce these losses.

A lot of research focuses on reducing leakage from water distribution networks. The leakage from bulk transfer systems must, however, not be overseen, as large amounts of pumped water may be lost through these systems without water utilities realising it.

A large number of leak detection and pipe condition monitoring techniques exist, as presented in this chapter of the study, all come with one or more of the following important limitations:

- The testing equipment is highly specialised and expensive, resulting in high operating costs for the duration of the test.
- The assessment method is dependent on highly skilled labour which is scarce and expensive.
- The method is labour intensive and time consuming, making assessments of long lengths of pipe expensive.
- The method requires the pipeline to be taken out of operation and/or emptied, which results in water loss and supply interruptions.

It is therefore clear that further research and development on improved leak detection and condition assessment techniques is warranted, as all the techniques discussed have one or more important limitations.

## **3 Design of the test equipment**

### **3.1 Introduction**

The pipe condition assessment equipment (Pcae) proposed in this study will help to address the water leakage problems in several ways. The primary function of the device is to assess the condition of individual pipes in a system. This assessment includes determining the size and types of leaks present on the pipe, the effectiveness of the system valves and identifying any anomalies such as illegal connections and unrecorded network elements. The results of the test are collected through a recorder with a built-in SD external memory, and the data is analysed to provide information for prioritising leak repairs and maintenance interventions for pipeline systems.

The device will also create opportunities for job creation and thereby addressing the lack of technical staff. The provision of this service can be outsourced to independent community contractors or to established contractors employing local people. The operators will be trained to operate the device, identify potential system problems and perform simple maintenance functions.

To date a pipe condition device has been designed for the typical diameters of pipes found in water distribution systems (also referred to as the small device). However, the current device cannot be used for bulk pipelines. This chapter describes the modification made to the existing device which resulted in a prototype that can test larger pipes such as those found in bulk supply systems.

### **3.2 Prototype status**

#### **3.2.1 Introduction**

This section will discuss the status of the pipe condition assessment system that was developed at the University of Cape Town to assess the condition of pipes and valves in distribution systems. The section will also highlight some of the key differences between the pipe condition assessment system that was designed for distribution systems and the pipe condition assessment equipment developed in this study for bulk pipelines.

### 3.2.2 Existing device for distribution systems

The existing device was designed to assess the condition of individual pipes in a distribution system only. The device consists of various hydraulic and control components that are typically used to conduct a series of tests on pipeline systems. Two further elements were developed to support the device proficiencies, namely an Android app and a cloud-based management system.

The main device consists of a water tank, a pump, valves, flow meters, pressure transducer, a generator and a GPS unit linked to a central processing and communication unit. For the small device, all these components are installed on a hand-drawn trolley, allowing it to be easily moved from one location to another.

The latest process and component design of the device is shown schematically in Figure 3-1 and in isometric view in Figure 3-2. Details of the various components that were used are given in Table 3-1.

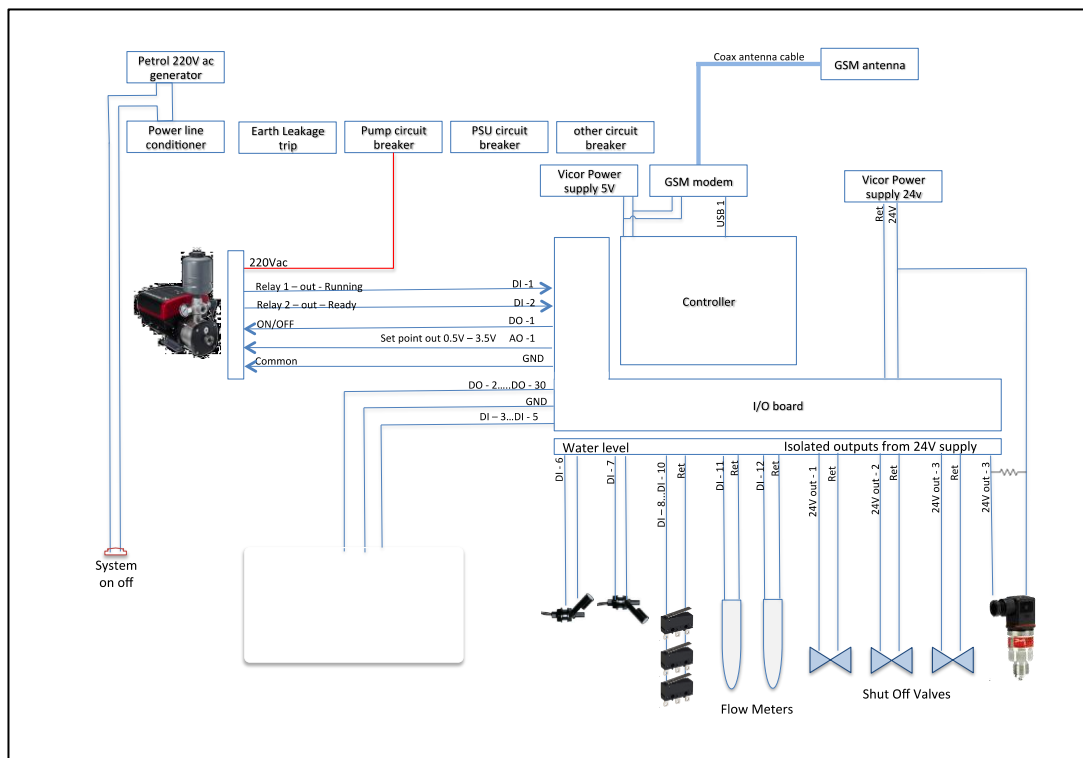
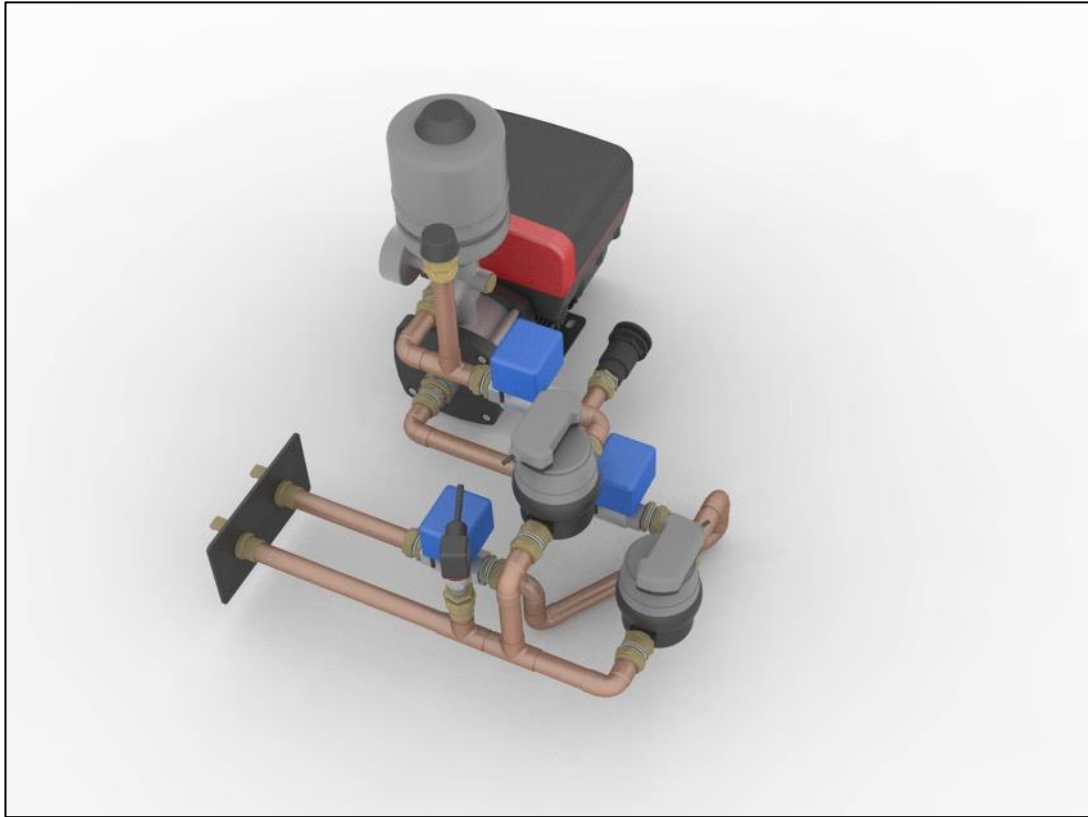


Figure 3-1 Process and component design of the system

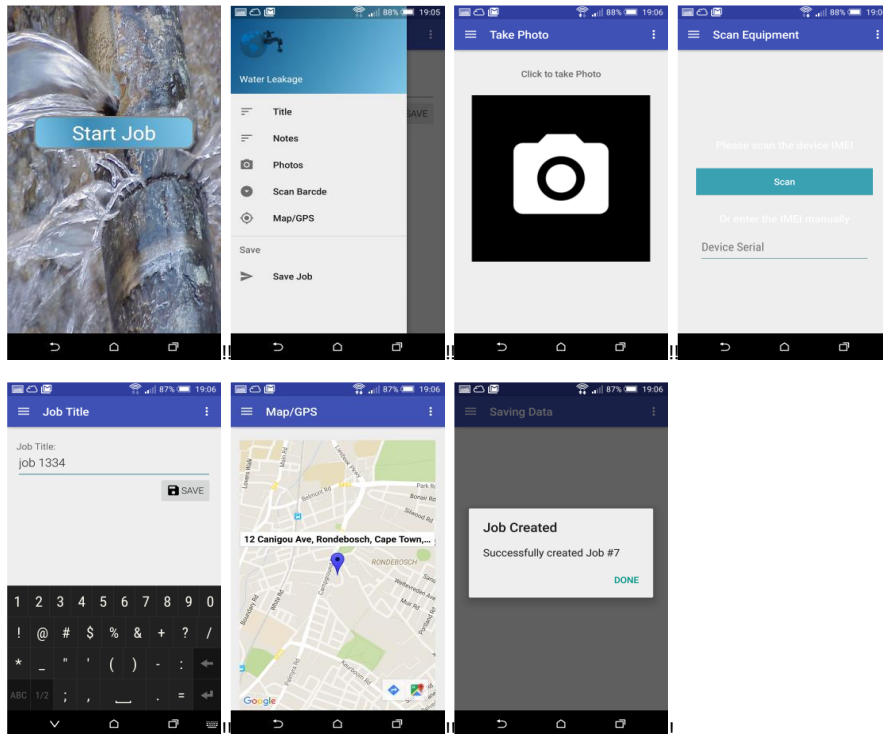


*Figure 3-2 Isometric view of the main components*

*Table 3-1: Details of the system components*

Item	Qty	Model	Price (Excl VAT) per unit	supplier
Pump	1	Grundfos CMBE 1-44 I-U-A-D-D-A AVBE	R13,135.00	Tricom Africa 021 948 8636
Pressure sensor	1	Included in above	-	Tricom Africa 021 948 8636
Solenoid valve	3	US-20 24VDC	R,1203.00	ACDC
Flow meter	2	Aquadis		ltron
Level sensor	2	LS-103-3	R263.00	ACDC
Power supply	1	VI-RU022-CYXX	R7,509.00	Future electronics Inc (Vicor)
GSM modem	1	Sierra Wireless GL6100	R1100.00	Avnet Copp
Antenna	1	Wireshark	R125.00	Poynting Antennas
Controller	1	TBD		
IO board	1/2	TBD		
Generator	1	TBD		
IP67 Panel Mount LED Indicator	28	906-3164 (pack of 50)	R15.46	RS components
Buttons (process) RED	2	AF3	R94.00	ACDC
Buttons (process) Green	1	AF4	R94.00	ACDC
System power switch	1	AK-3PA	R317.00	ACDC
Contact block for power switch	2	S11 + S12	R323.00	ACDC
Emergency stop switch	1	ECX1131	R169.00	ACDC
Circuit breaker PSU	1	NB1-3	R47.00	ACDC
Circuit Breaker pump	1	NB1-6	R43.00	ACDC
Earth leakage	1	NL2-25	R320.00	ACDC
Mains line filter	1	DL-10D1	R269.00	ACDC
DB board	1	GW40026	R205.00	ACDC
Running hour meter	1	SQ48R 230VAC	R237.00	ACDC
Panel voltmeter	1	SQ48-300VAC	R236.00	ACDC
Panel pressure gauge	1	GGE10R	R49.00	ACDC
Flexible hose 60cm	1	FH60	R198.00	ACDC

The additional element of the device which incorporates an Android app runs on a compatible smartphone or tablet. The purpose of the app is to guide the operators to the next pipe for testing. It then assists the operator to identify the distribution system components (i.e. valves, hydrants etc.). Using the GPS and GIS functionality, the operator is able to locate and identify which valves to close and which house connections to isolate to successfully carry out the test. Furthermore, the app takes the operators through the different steps of the pipe test and allows them to take pictures and add some comments about the problems observed in the field. Figure 4 gives a screen shot of the interface of the app.



*Figure 3-3: Screen shots of various displays of the app*

The final element, the cloud-based management system that schedules the next pipe to be tested, links the app to the GIS data, manages the tests conducted, and collects and analyses the test data. The management system may be linked to various other databases and systems to analyse the test data, incorporate other system data and schedule pipe repair or replacement actions.

### **3.2.3 Modification of the current device for bulk systems**

The modification of the existing device is twofold. Firstly, the operating system of the device is modified: the existing device is fully automated, while the device developed for bulk pipelines will be manually operated. Secondly, unlike the current prototype that uses GSM functionality together with a cloud-based management system to store the data, the modified device for bulk pipelines will be fitted with a data recorder which archives data via an external SD card.

In addition, the existing device is limited to testing only distribution pipelines, i.e. pipes with a diameter less or equal to 110mm. The modified device proposed in this study, which will predominantly be used to test bulk pipelines, will be designed to test any size pipe.

## **3.3 Concept design for bulk pipeline test equipment**

### **3.3.1 Introduction**

The modified pipe condition assessment equipment (PCAE) was designed under the guidance of Prof J.E van Zyl at the University of Cape Town. The design process was an iterative process involving multiple interim designs before the final design was decided upon. This process was intended to ultimately improve the quality and functionality of the PCAE design. Further consultations were done with relevant parties from industry to ensure that the final design complied with various standards. The calibration certificates for all instrumentation were provided and are attached in Appendix 10.1

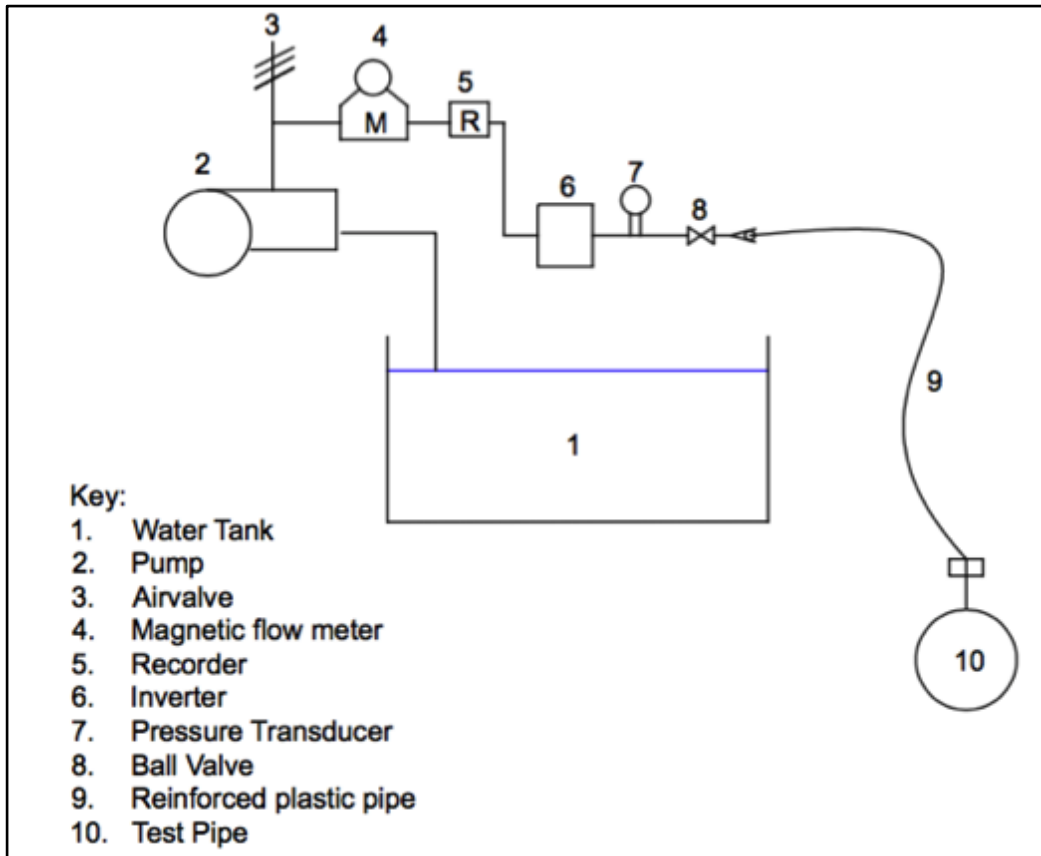
### **3.3.2 Prototype design**

The following considerations informed the design of the equipment:

- It must be suitable for testing both bulk and distribution system pipelines.
- It must consist of materials that can withstand up to 12 bars of pressure.
- It must be capable of measuring and accurately logging both flow rates and pressure.
- The water metering solution must be able to measure the minimum possible flow rates (i.e. flow rates < 250l/hr) and possess the capabilities of transmitting the data.
- The pressure sensor should have the capability of transmitting pressure data at a frequency of at least 100ms.
- It must ensure that any excess air is removed from the pipe work prior to testing.
- It must be mobile and robust enough to handle field environments.

Several apparatuses were incorporated into the PCAE to satisfy these considerations. Figure 3-4 shows the process and component design of the PCAE which contains: a water tank, a series of valves, a magnetic flow meter, an inverter, a pump, uPVC pipes and a plastic reinforced hose adaptor.





*Figure 3-4: Process and component design of the system*

The detailed technical description of the individual components used to construct the PCAE are discussed in the next section.

### **3.3.2.1 Storage tank**

Due to the large volumes of water that are conveyed by bulk systems, a water source bigger than the 200l water tank, installed in the distribution system device, will be required. The proposed water source, for the bulk pipeline device, is a horizontal water tank called a RotoTank shown in Figure 3-5, with a five times more capacity than the distribution system device, i.e 1000l.

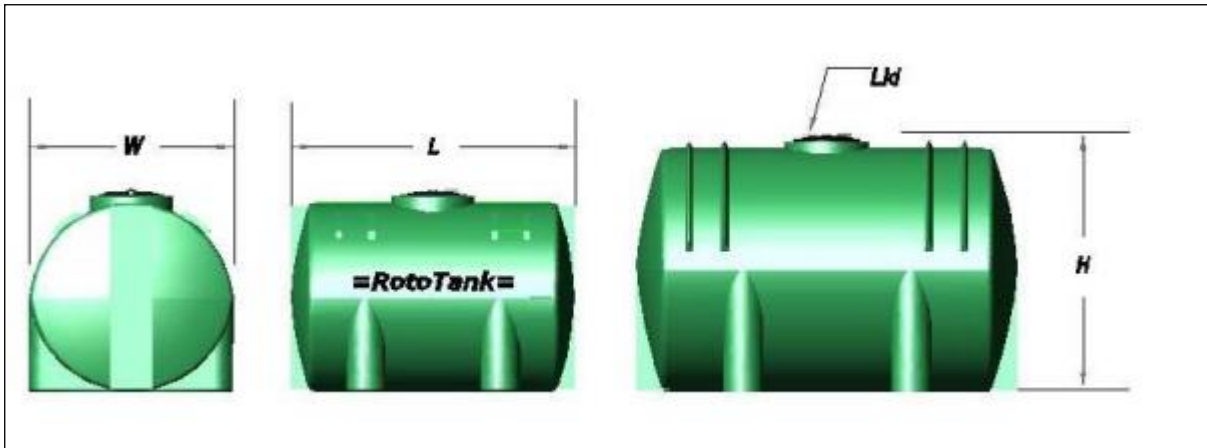


Figure 3-5: Rototank dimensions (Roto Tank, 2016)

### 3.3.2.2 Pump

The following criteria was used to select a pump for the PCAE:

- The pump should be designed for conveying water.
- The pump construction materials should be compatible with water, i.e. they must be rust resistant.
- The pump inlet conditions must be such that the system net positive suction head (NPSH) is marginally greater than the NPSH required to prevent cavitation problems. In other words,  $NPSH_{available} > NPSH_{required}$ .
- The pump power source should be compatible with local power inlets.
- The pump should be a pressure-controlled variable speed pump to carry out the necessary pressure tests.
- The pump's maximum pressure should not exceed the maximum allowable pressure for the pipelines.
- The pump's environment is also an important factor because the pump will be used in the field as well as in the laboratory. It should therefore be robust and easy to transport.

The HS18-40N-1 horizontal multistage stainless-steel centrifugal pump was selected. This pump is suitable to convey water and its materials are compatible for this application. Figure

3-6 shows this pump and its installation sketch, where  $L = 440\text{mm}$ ,  $L_1 = 186\text{mm}$ ,  $L_2 = 168\text{mm}$ ,  $H = 255\text{mm}$  and  $D = 165\text{ mm}$ .

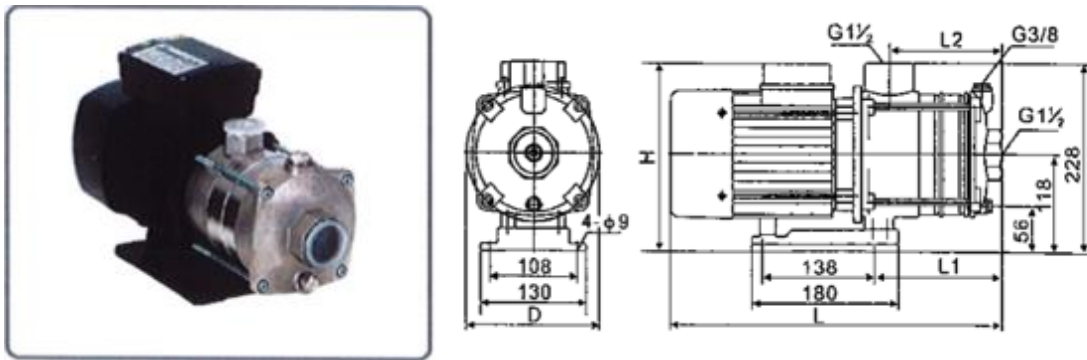


Figure 3-6: Euroflow horizontal multistage stainless-steel centrifugal pump (Euroflow, 2016)

In Figure 3-7, the performance curve of the selected pump is demonstrated by the 40N-1 pump curve. The 40N-1 pump curve shows that the maximum flow rate which this pump can deliver is  $16\text{m}^3/\text{hour}$ . The Net Positive Suction Head (NPSH) point for the pump is also shown in Figure 3-7, as the intercept between the 40N-1 curve and the NPSH curve.

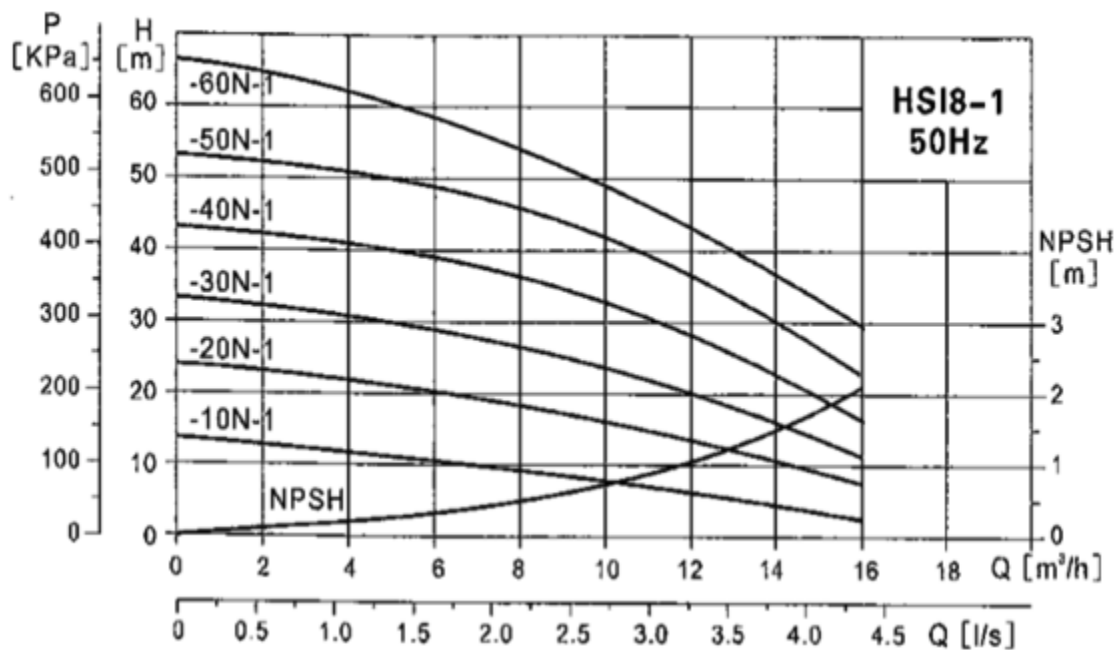


Figure 3-7: Pump performance curves of different pump models (Euroflow, 2016)

The NPSH required for the 40N-1 pump is about  $1.8\text{m}$ , as can be seen from Figure 3-7. The equipment's available NPSH can be calculated using Equation 3-1, and knowing the pump inlet pressure and liquid vapour pressure:

$$NPSH_{available} = \frac{P_{inlet}}{\rho g} + \frac{v_{inlet}^2}{2g} - \frac{P_{vapour}}{\rho g}$$

Equation 3-1

Where  $P_{inlet}$ , is the inlet pressure,  $\rho$  is the density of water,  $g$  is the acceleration,  $v_{inlet}$  is the inlet velocity and  $P_{vapour}$  is the vapour pressure of water at 20<sup>0</sup> C, which is the assumed temperature of water in pipe systems.

The inlet pressure head is 1,4m, which is obtained from the height difference between the suction inlet and the minimum water level in the tank, which is 10% of the tank height. The inlet velocity is 2,26 m/s, which was calculated using the pump maximum flow rate and the pipe cross sectional area, determined from the pipe diameter of 50mm. The vapour pressure of water is 2,34 KN/m<sup>2</sup>, obtained from Table A.1 of Finnemore & Franzini's book (2009:732) on fluid mechanics. Substituting these values into Equation 3-1, the NPSH available is calculated to be:

$$NPSH_{available} = 1,4 + \frac{2,26^2}{2 \times 9,8} - \frac{2,34 \times 10^3}{1000 \times 9,8} = 1,4m$$

The available NPSH of 1,4 m, is greater than the required NPSH of 1,2m. This indicates that no cavitation problems will occur.

Table 3-2 shows the performance table of the pump. According to the table, the HS18-40N-1 pump model requires 1.5 kW power to drive the motor. The minimum and maximum flow rates the pump can deliver are 4m<sup>3</sup>/h and 16m<sup>3</sup>/h, respectively. The minimum and maximum pressure heads are 17m and 41m.

Table 3-2: Performance table of the pump (Euroflow, 2016)

MODEL	Driving motor P2(kW)	Q (m <sup>3</sup> /h)	4.0	6.0	8.0	10	12	14	16
HS18-10N-1	0.55	H (m)	11	10	9	8	7	6	5
HS18-20N-1	0.75		22	20	19	18	13	11	8
HS18-30N-1	1.1		31	29	26	24	20	16	11
HS18-40N-1	1.5		41	39	37	33	28	23	17
HS18-50N-1	2.2		51	49	46.5	42	37	30	23
HS18-60N-1	3.0		62	58	52	48	42	36	30

### **3.3.2.3 Inverter**

The pump comes with a DAB active driver plus inverter, shown in Figure 3-8, that is used to control the variable speed pump. The inverter will also ensure that the pump uses the minimum power necessary to meet the pumping needs, avoiding unwanted waste and resulting in significant energy savings.



*Figure 3-8: Constant pressure inverter (DAB Water Technology, 2016)*

This inverter has an integrated electronic pressure transducer, flow sensor and an inbuilt non-return valve. This inverter has a 32mm male thread inlet connection and a 32mm female thread outlet connection. The inverter will be primarily used to set the test pressure for the PCAE.

### **3.3.2.4 Flow meter**

The metering solution is a critical component of the PCAE because the potential minimum leakage level that can be detected depends on the minimum level the flow meter can measure accurately. For this reason, electromagnetic flow meters were considered appropriate for the PCAE, due to their accuracies.

The selected electromagnetic flow meter must adhere to the following criteria:

- it must measure up to the pump's maximum operating flow rate of 16 cubic metres per hour
- it must have the lowest possible starting flow and the least possible uncertainty

- it must have logging capabilities that allow for the flow to be logged, and finally
- it must be robust, easily movable and not battery operated.

The ABB Process Master FEX500 electromagnetic water meter, shown in Figure 3-9, fits the above criteria and was therefore selected for the PCAE.



*Figure 3-9: ABB Process Master FEX500 electromagnetic flow meter (ABB, 2017)*

The Process Master FEX500 electromagnetic flow meter has a nominal diameter of 25mm and weighs 6.4kg. It can measure flows ranging from 0.4m<sup>3</sup>/hr to 24m<sup>3</sup>/hr and detect and cut off low flows that are 1% of the maximum flow rate.

The ABB electromagnetic flow meter comes with calibration certificates and thus does not require any calibration. It must, however, always be level during operations. For this reason, a level will be mounted on the device to ensure that the meter is level during the tests.

To connect the electromagnetic flow meter to the PCAE, a PVC flange, shown in Figure 3-10, will be connected to the outer flange of the meter using a suitable bolt and nut connection. The PVC flange will then have an adapter piece that can easily be connected to the rest of the pipe work.



*Figure 3-10: PVC flange that connects to the electromagnetic flow meter*

### **3.3.2.5 Pressure transmitter**

A pressure transmitter is required to log the pressure readings of the PCAE during tests. A pressure transmitter converts pressure into an analogue electrical signal which outputs a pressure reading at a specific point. The required transmitter must adhere to the following criteria:

- it must be robust and easily mountable
- it must be water proof
- it must signal pressures at 0.001Hz
- it must have logging capabilities which allow for the pressure readings to be logged.

The ABB 2600T series analogue pressure transmitter was selected because it fits these criteria. Moreover, it is capable of logging pressures at 10ms.



*Figure 3-11: ABB 266 HART pressure transmitter.(ABB, 2018a)*

### ***3.3.2.6 Data logging solution***

A logging solution was required to log the data from the electromagnetic flow meter and the pressure transducer. There are different types of loggers that have various levels of sophistication and interactivity. The most basic logger is a portable device that can connect to the flow meter or the pressure transducer to keep track of the data. For this study, a more advanced data logger was required and had to meet the following criteria:

- it must be capable of displaying pressure and flow profiles of the PCAE during tests
- it must have the capability of logging and storing data that can be accessed and analysed, using appropriate analysis software.

The ABB field-mount paperless recorder SM500F, shown in Figure 3-12, was selected as a suitable logging solution. This recorder has important capabilities such as live display of the data, logging data on an SD card and also the possibility of accessing and analysing the data using software.





*Figure 3-12: ABB field-mount paperless recorder SM500F (ABB, 2018b)*

The recorder shown in Figure 3-12 has multiple electrical connections, as shown in Figure 3-13 (a). The recorder itself is powered through the power supply connection, shown as G in Figure 3-13 (a), containing the live, neutral and earth connection. The electromagnetic flow meter and the pressure transmitter are connected to the recorder as digital inputs.

The electromagnetic flow meter has a positive (red) and a negative (blue) wire which come from the meter and connect to the recorder at B3 and B4, respectively. The connection B3 and B4 are shown in Figure 3-14 (a).

The pressure transmitter, on the other hand, has three connections, namely a positive (red), a negative (blue) and a terminal (black). The positive and negative wires from the transmitter connect to the recorder at D3 and A3, and the terminal connection is a single black wire from A4 to D4, as shown in Figure 3-13 (a). Figure 3-13 (b) is a picture of the actual connections.

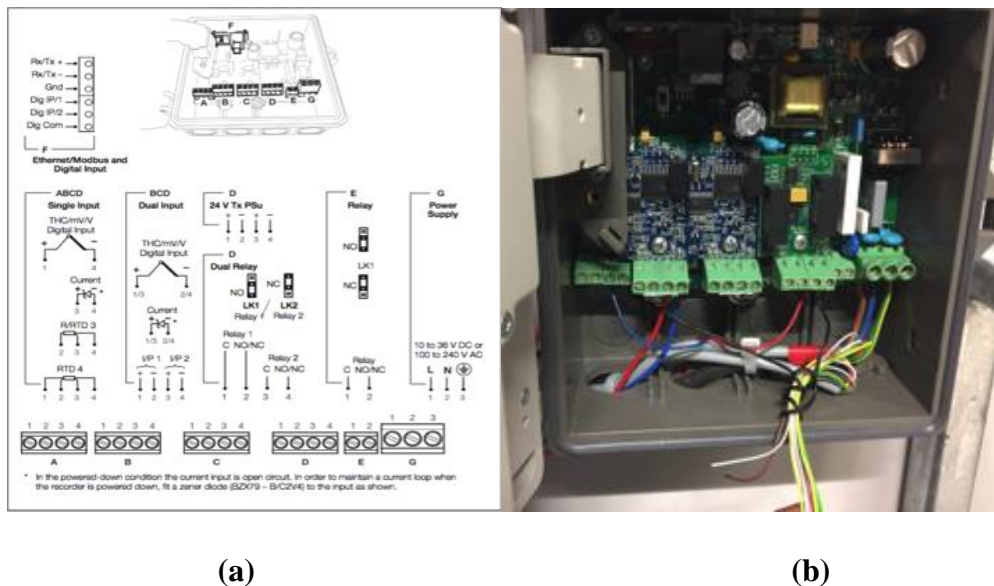


Figure 3-13: (a) schematic view of the electrical connections (b) the actual connection

The flow and pressure profile of the PCAE are displayed on a chart output, as shown on the screen of the recorder in Figure 3-12. At the same time, the data is stored on a SD card. The SD card can be placed in the SD slot of a computer and the data can be accessed and analysed using the Data Manager Pro software.

### 3.3.2.7 Generator

The generator will be used mainly during the field testing where a power source might not be available. To determine the size of the generator needed, the total wattage of the maximum number of items to be run simultaneously was calculated. This was done to ensure that the required wattage to operate the PCAE never exceeds the maximum run rating of the generator.

The PCAE items identified to require electric power input are the pump, inverter, magnetic flow meter, recorder, and the pressure transducer. The total wattage of these items was calculated to be 2.4kW. Therefore, the Ryobi RG-2700 generator, fitted with an overload protection switch, was selected (see Figure 3-14).



*Figure 3-14: Generator to be used for the bulk system device*

The selected generator has a power output of 2.7kW and is air cooled. The maximum run rating, which is the maximum allowable total wattage, is 2.5kW and can run the PCAE. The generator comes with a 4-stroke engine. The fuel tank is 12 litres and uses unleaded petrol. The generator has a minimum run time of 10 hours. Given that each field test can take approximately 1 hour, a full tank allows for at least 9 tests. The dimensions of the generator are 44(w) x 53(l) x 46(h) cm and its nett weight is 41,50kg.

### **3.3.2.8 Pipes**

The PCAE was assembled using class 12 uPVC pipes. These pipes were selected because they are rigid, readily available and can sustain the maximum pump pressures of 41m (see pump curve in Figure 3-7). To maintain material compatibility, all the connection pieces, fittings and bends are also uPVC. The pipes will not have any thread finishing and therefore all connections to the pipes will be solvent; however, connections to various other equipment may have thread and therefore will have to suit those instrumentation's connections.

Class 12 uPVC pipes were chosen because they are rigid enough and can withstand the high pressures required to run the bulk system tests. To determine the appropriate size of the class 12 pipes, it is necessary to calculate the following parameters: (a) the cross-sectional area of the pipe using Equation 3-2, (b) the flow velocity for various cross-sectional areas using Equation 3-3, and (c) the pipe's friction head losses using Equation 3-4.

$$A = \frac{\pi D^2}{4}$$

*Equation 3-2*

$$v = \frac{Q}{A}$$

Equation 3-3

$$h_f = \frac{fLv^2}{2Dg}$$

Equation 3-4

Given that the PCAE's maximum flow rate will be 16m<sup>3</sup>/h, obtained from the maximum flow rate delivered by the pump, the equivalent cross-sections (A), flow velocities (v), and friction head losses (h<sub>f</sub>) can be calculated for various pipe diameter sizes (D) and lengths (L) as shown in Table 3-3.

Table 3-3: Cross-sections, flow velocities, pipe lengths and friction losses for various pipe diameters

Pipe diameter (mm)	Area (m <sup>2</sup> )	Velocity (m/s)	h <sub>f</sub> (m)
20	3.1 x 10 <sup>-4</sup>	14.5	26.93
30	7.1 x 10 <sup>-4</sup>	6.29	3.55
40	1.3 x 10 <sup>-3</sup>	3.54	0.84
50	2.0 x 10 <sup>-3</sup>	2.26	0.28
60	2.8 x 10 <sup>-3</sup>	1.57	0.11
70	3.8 x 10 <sup>-3</sup>	1.15	0.05

From Table 3-3 the 50 mm pipe diameter was chosen because it gives a reasonable flow velocity of 2.26 m/s and a frictional head loss of 0.28 m, which were considered reasonable by the author.

### 3.3.2.9 Ball valves

Hand operated ball valves will be used for the PCAE to control the flow. Figure 3-15 shows the PVC ball valve that was chosen. The valve will have a solvent connection to the pipes. The reason for choosing this ball valve is the easy visual confirmation of the valve's status, i.e. the handle will lie parallel in alignment with the flow when opened, and perpendicular to it when closed.



*Figure 3-15: 50mm compact PVC ball valve*

### **3.3.2.10 Air release valves**

The air release valve will be used to release any air pockets in the PCAE. The air will result in bubble formation which normally gathers at localised high points along the pipe profile. Positioning of the air valve is important. In this case, it will be placed at the first highest point in the pipeline profile to prevent air entering components that are air sensitive, e.g. the magnetic flow meter. Figure 3-16 shows the air release valve that will be used to release any free air in the PCAE.



*Figure 3-16: 2" Kinetic air release valve*

### **3.4 Constructing the pipe condition assessment equipment (PCAЕ)**

After the final design concept was approved, the next phase of the process was the construction of the PCAЕ. The first step before construction was the purchase of all required apparatus that was listed. Manufacturers were contacted and approached to assist with acquiring the necessary components.

Due to the iterative nature of the design, it was often difficult to pre-empt the challenges that would arise with the actual construction of the PCAЕ. It was often necessary to solve problems as they were encountered. One such example was having to design a frame that would adequately support the weight of the electromagnetic flow meter and the recorder. This required sourcing personnel who could mould the steel frame to the necessary specifications.

Another unforeseen challenge was the difficulty presented by the presence of pieces of apparatus with varying pipe inlet/outlet diameters. This resulted in the need for several adaptors that would either increase or reduce the pipe diameter to make it fit accordingly. Additional adaptors would make the device longer than anticipated. This problem was dealt with by simply reducing the length of the 50mm uPVC pipes to maintain a reasonable size that was portable.

### **3.5 Final prototype of the pipe condition assessment equipment (PCAЕ) for bulk pipelines**

Figure 3-17 shows the prototype of the PCAЕ design with all the components assembled and labelled. Figure 3-18 shows three isometric views of the PCAЕ with all its components, before it is mounted to a trailer.

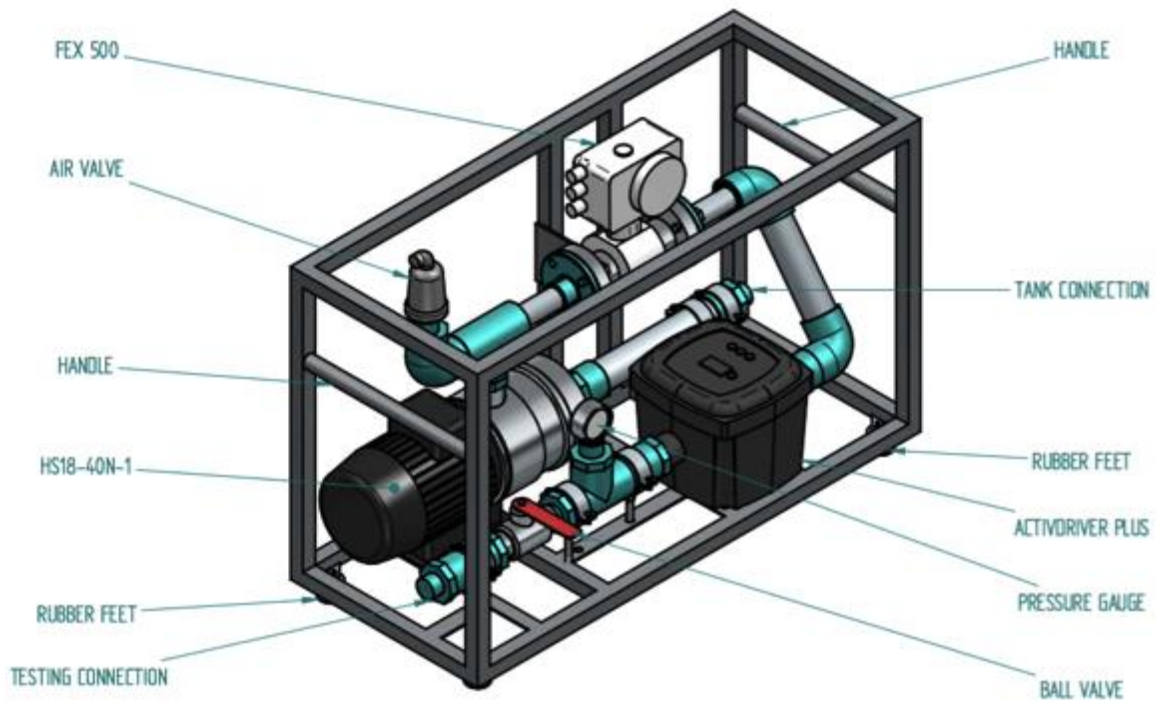


Figure 3-17: Pipe condition assessment equipment (PCAE) with component labels

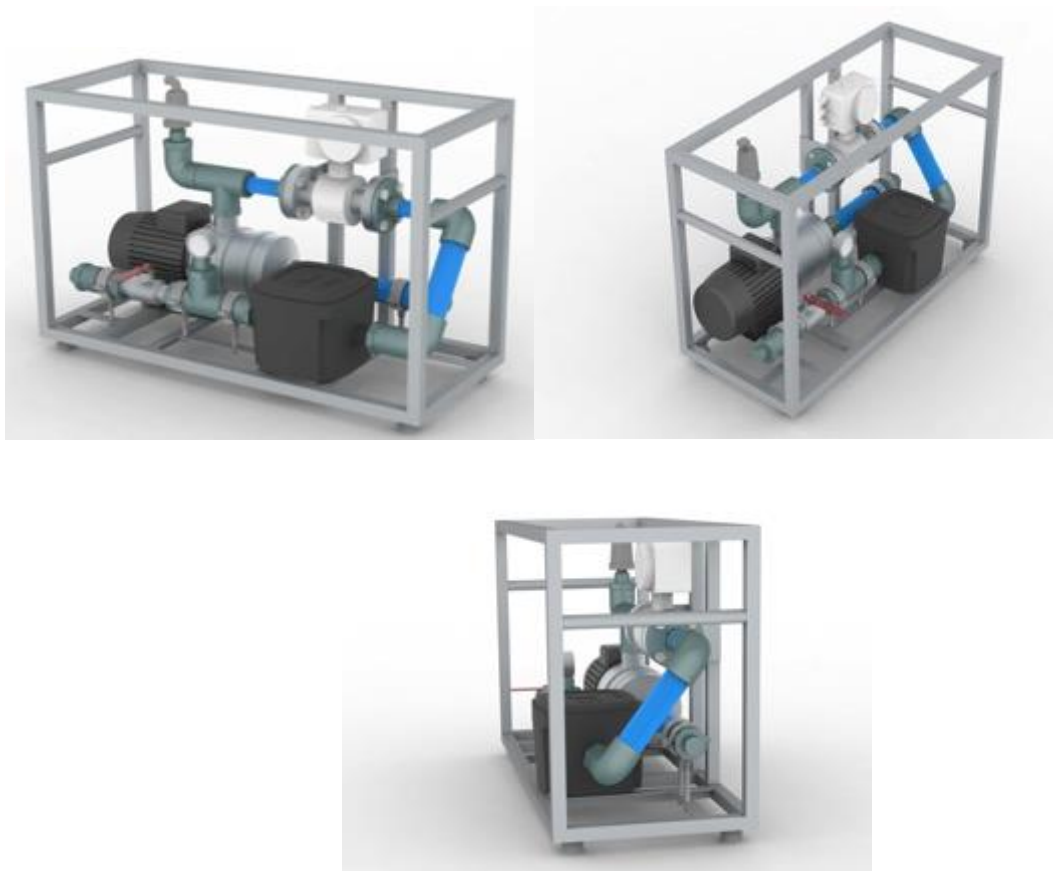


Figure 3-18: Isometric views of the main components

After the components were assembled, the water tightness of all the joints was tested. The device was then mounted onto the trailer as shown in Figure 3-19. Figure 3-20 shows the actual constructed PCAE prototype just outside the laboratory, at the University of Cape Town.



*Figure 3-19: The test equipment mounted onto a trailer (side view)*



*Figure 3-20: Constructed pipe condition assessment equipment (PCAE) outside the laboratory at the University of Cape Town*



# 4 Experimental Verification Tests

## 4.1 Introduction

This chapter reports how the PCAE described in Chapter 3 was tested in the laboratory. A standard experimental and analytical procedure was developed to verify the equipment. Firstly, a description of the available resources in terms of equipment and environment is given. Thereafter, the experimental setup is described, followed by the experimental procedure, data collection and data analysis methodology.

Three pipes with known leakage characteristics were tested, namely a 12mm round hole, a 100mm by 1mm longitudinal crack, and a 100mm by 1mm circumferential crack. The leakage parameters for the power equation and the modified orifice equation were evaluated for each leak type. The results obtained were compared to the experimental leakage parameter results reported for similar leak types from the study by van Zyl and Malde (2017).

## 4.2 Available equipment and environment

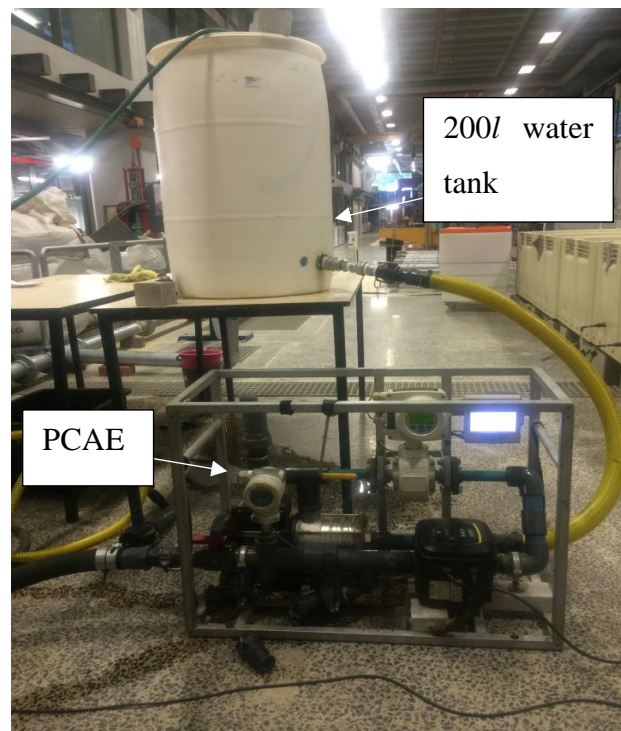
The experiments were carried out at the University of Cape Town's Civil Engineering Laboratory. The laboratory contains a hydraulic engineering section which is made up of a drainage floor, an underground reservoir and a wall unit pipe network with two magnetic flow meters and a pump.

The drainage floor in the laboratory is rectangular with an approximate length of 8 meters and a width of 5.5 meters. The floor is surrounded by a drainage trench which directs water into an underground reservoir, as illustrated in Figure 4-1.



*Figure 4-1: Picture of the hydraulic section of the Civil Engineering Laboratory at the University of Cape Town (Malde & van Zyl, 2015)*

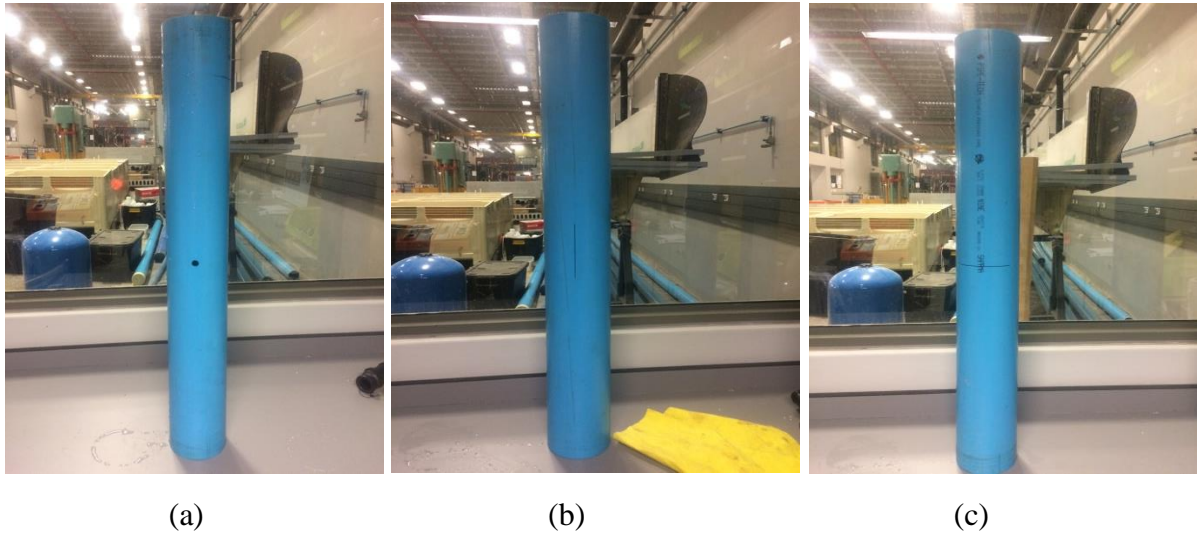
Due to limited space, the trailer with the 1000-litre water tank did not fit into the laboratory. Instead, a 200-litre water tank was used. The 200l-litre tank was placed on a table and filled with recycled water sourced from the underground reservoir in the laboratory. Figure 4-2 shows the 200-litre water tank on the table and the PCAE on the ground.



*Figure 4-2: Setup of the PCAE in the laboratory*

In this experimental study, pipes with known leakage characteristics were tested. The test pipes consisted of three 800mm long, 110mm (outer diameter) class 9-uPVC pipes that had a

maximum working pressure of 9 bars. Figure 4-3 shows pictures of the three test pipes that were drilled and cut to create sources of leakage, namely: (a) a 12mm diameter round hole, (b) a 100mm by 1mm longitudinal crack and (c) a 100mm by 1mm circumferential crack.

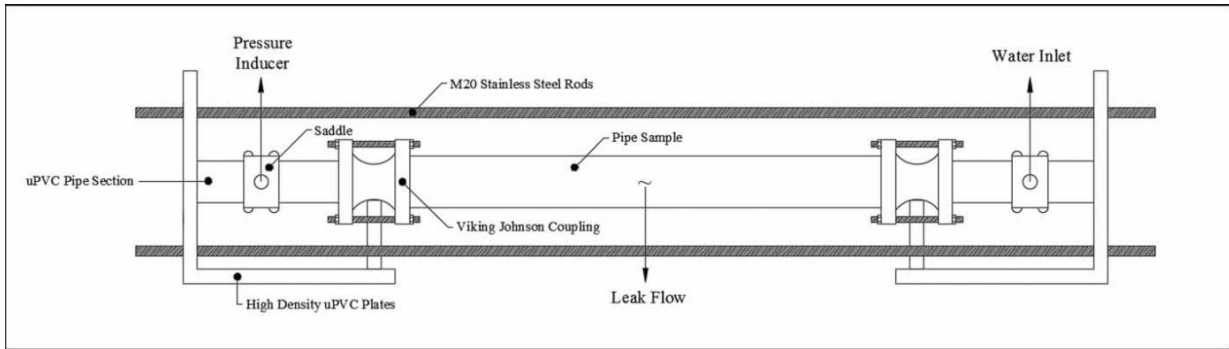


*Figure 4-3: Test pipes (a) round hole, (b) longitudinal crack, and (c) circumferential crack*

### **4.3 Experimental setup**

The experimental setup required constraining a pipe with a leak under high internal pressure so that both flow and pressure readings could be acquired using the PCAE. In order to achieve this, an experimental test rig, developed by van Zyl and Malde (2017) for testing the behaviour of various types of leaks, was used in the laboratory. Two minor modifications were made to this test rig, namely: (a) a convenient connection point was installed via which the PCAE could be connected, and (b) the pressure transducer was replaced with an air valve.

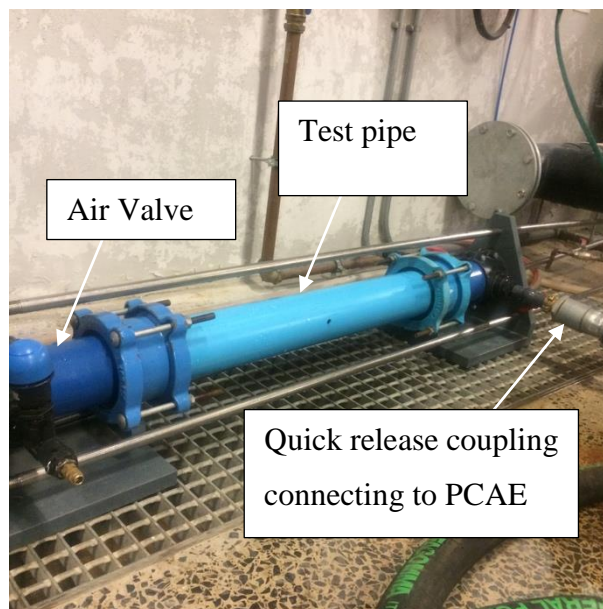
The test rig as developed by van Zyl and Malde (2017) has two end pieces. Each end piece was constructed using high density uPVC plates with a thickness of 25mm. A class 9, 110mm uPVC pipe section of 180mm length was then connected to the uPVC plates. The other end of the uPVC pipe was connected to a Viking Johnson (VJ) coupling which then connects to the pipe being tested. The uPVC pipe section of each end piece has a saddle with a hole drilled through to allow for an inlet flow in one end piece and a pressure transducer connection in the other end piece. The main components of the test rig are shown in Figure 4-4.



*Figure 4-4: Test rig developed by van Zyl and Malde (2017)*

A pipe sample was connected in between the two VJ couplings. Because the VJ couplings do not provide enough tension restraint to keep the pipe sample in place under high pressure, van Zyl and Malde (2017) installed three stainless steel rods that were used to provide sufficient restraint to the setup. The steel rods are tapped through the uPVC plates in the experimental setup.

Two modifications were made to the test rig shown in Figure 4-4. The first modification was replacing the water inlet connection with a quick release coupling which was used to conveniently connect the hose pipe that joins the test rig and the PCAE. The second modification was replacing the pressure transducer with an air valve that was used to get rid of any trapped air in the test rig. *Figure 4-5* shows a picture of the modified test rig.



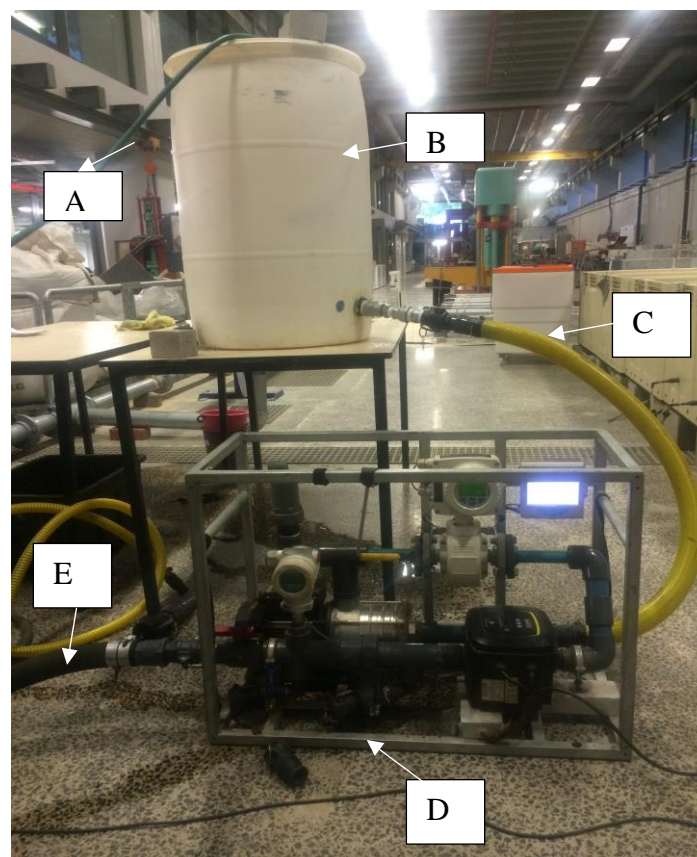
*Figure 4-5: Experimental setup showing the connection point*

The pressure and flow were measured by the PCAE upstream of the test rig.

## 4.4 Experimental procedure, data collection and analysis methodology

### 4.4.1 Experiment procedure

As described above in section 4.2 (see Figure 4-2), the PCAE was detached from the trailer with the 1000-litre water tank and placed on the drainage floor of the laboratory as shown in Figure 4-6. A 200-litre water tank was used as the main source of water. This was done in consideration of the fact that the 1000-litre water tank could not be transported into the laboratory.



*Figure 4-6: Device setup: (A) supply pipe from underground reservoir, (B) 200 litre water tank, (C) tank to device connection, (D) PCAE, and (E) device to test rig connection*

To avoid using clean municipal water, the tests were carried out using recyclable water collected and stored in the laboratory's underground reservoir. Using a submersible pump, the recycled water was pumped directly into the water tank, as shown in Figure 4-6. To avoid having the water in the tank run out, the water from the underground reservoir was continuously supplied to the 200-liter tank to keep it full during the tests.

Once the water tank was filled, the variable speed pump was switched on, and the inverter was used to set various pump speed to vary the pressures. Figure 4-7 shows the inverter displaying a set point pressure (SP) of 1 bar. The pressures were varied incrementally by changing the set point pressure (SP) of the inverter. This was done by simply using the “+” button to increase the pressure and the “-” button to decrease the pressure.



*Figure 4-7: Inverter showing a set point pressure of 1 bar*

The inverter has an inbuilt pressure transducer that displays the working pressure of the variable speed pump, and therefore the working pressure of the PCAE. The inverter was initially set to the highest pressure. Then pressures were increased and decreased in about five steps by varying the pump speed. Each step lasted about 30 seconds and was long enough to ensure that both flow and pressure readings stabilised.

At each set point pressure, the flow rate through the leak area was recorded by the electromagnetic flow meter. The flow rate reading was displayed on the electromagnetic flow meter display panel, as shown in Figure 4-8.

To investigate and characterise the behaviour of the leak in the pipe (the main operational function of the equipment), the set point pressure and the flow rate were recorded for analysis. Because of the flow rate fluctuation at each set point pressure, 10 flow rate readings were recorded and then averaged to obtain a single flow rate (l/hr) for each set point pressure.



Figure 4-8: Electromagnetic flow meter display panel

Figure 4-9 shows a graphical illustration of the leak test procedure that was carried out after the tank was filled with water.

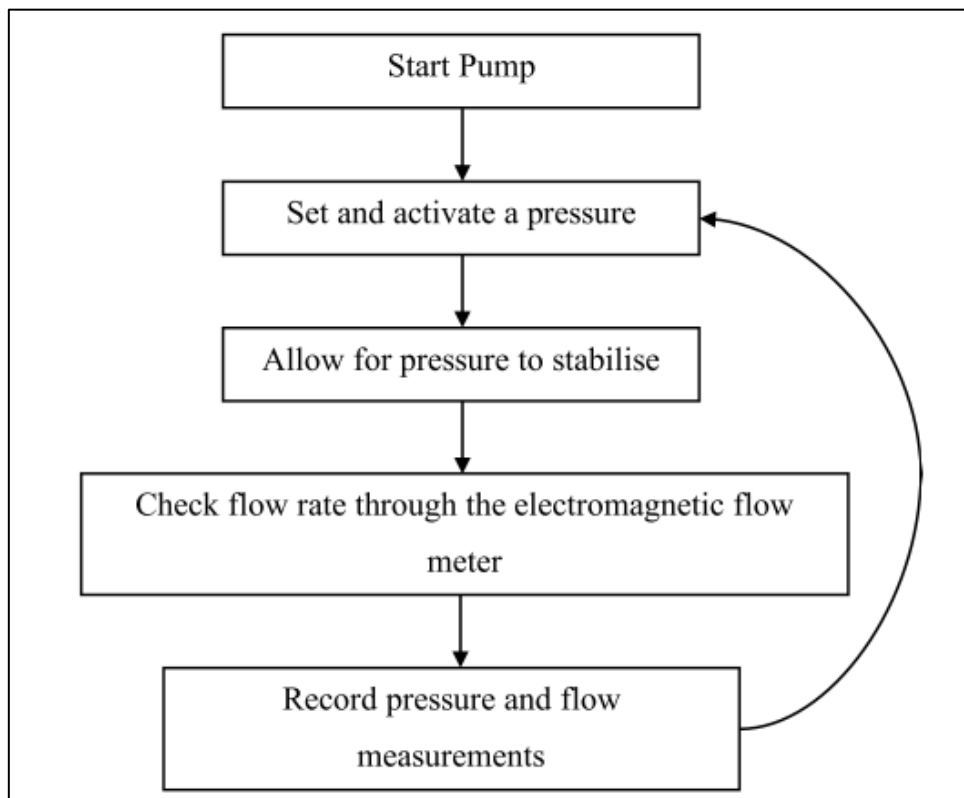


Figure 4-9: Graphic illustration of leak test algorithm

The pressure and flow data readings were recorded manually by simply logging the data into a laboratory note book. Once the data was recorded, it was then fed into Microsoft Excel for further analysis and characterisation of the leak behaviour.

The test ended by switching off the pump and closing the throttle valve on the suction side of the pump. The equipment was then disconnected from the test pipe. The next test pipe could then be connected and the test procedure was repeated.

#### 4.4.2 Data collection

The PCAE’s recorder output produces data files containing the pressure and flow rate readings. These data files can be downloaded from the recorder’s external storage media (SD card). The SD card can then be inserted in a computer and analysed with the Data Manager Pro v 1.7.3 application. This application was the most suitable because of its compatibility with the ABB products installed in the PCAE.

Data Manager Pro is a process data management and analysis application used to store and review data that is archived by the ABB Screen Master paperless recorder which is mounted onto the PCAE. Figure 4-10 shows the Data Manager Pro interface with its various features.

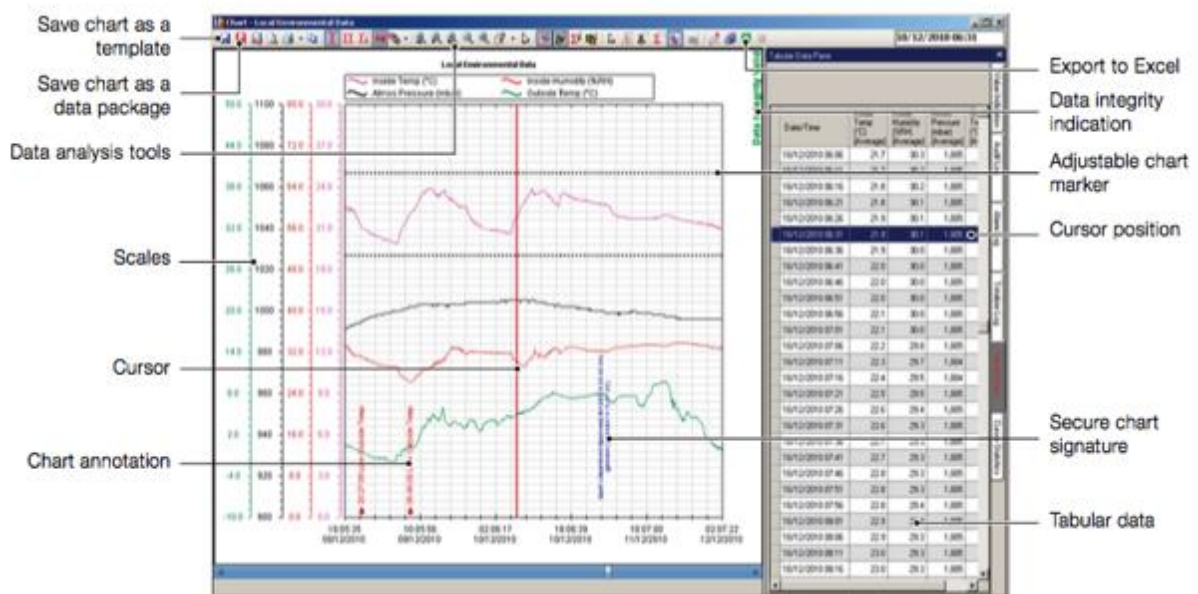


Figure 4-10: Data Manager Pro chart view (ABB, 2018b)

The archived data from the PCAE recorder was transferred to Data Manager Pro using an SD memory card. Once the SD card was inserted into the computer and the Data Manager Pro was open on the computer, the data could be imported via the “File Import” icon. Once the data



was imported, it could be viewed graphically, as shown in Figure 4-10, or exported to a Microsoft Excel compatible format, using the “Export to Excel” icon.

### **4.4.3 Data analysis procedure**

The raw pressure and flow data were entered onto a spreadsheet in Microsoft Excel and the following steps were performed on the data:

#### ***4.4.3.1 Step 1: interpretation of the data***

The raw flow and pressure data were plotted against time. Experimental data points were obtained by identifying stable sections of the flow and pressure graphs and then taking the average values over each of the ranges.

The flow and pressure data points were recorded in litres/min and bars, respectively. The units were then converted to SI units of  $m^3/s$  and  $m$  for the flow rate and pressure, respectively. The following conversions were used:

$$Q_{measured}(m^3/s) = Q_{measured}(l/min) \times 1/60000.$$

*Equation 4-1*

$$h_{measured}(m) = h_{measured}(bar) \times 10.1997$$

*Equation 4-2*

#### ***4.4.3.2 Step 2: determining the actual pressure in the test pipe***

Since the pressure sensor of the PCAE is not located at the leak, the measured pressure data point values had to be adjusted in order to estimate the true pressure at the leak. This adjustment was done by accounting for (a) the elevation difference between the pressure sensor and the leak, (b) head losses due to friction between the pressure sensor and the leak, and (c) minor losses due to the various hydraulic components between the pressure sensor and the leak.

The elevation correction was determined by measuring the height between the device’s pressure sensor and the leak. Since the device was on the floor (see Figure 4-6), the height from the floor to the pressure sensor of the device was measured first; thereafter the height from the floor to the leak was measured. The difference between them was 0.05 meters.

The friction losses were calculated to account for friction loss between the PCAE's pressure sensor and the entry point into the test rig. To do so, the first step was to calculate the Reynolds equation, given here,

$$R = \frac{4Q}{\pi Dv}$$

*Equation 4-3*

Where  $Q$  is the flow rate,  $D$  is the internal diameter, and  $v$  is the kinematic viscosity. All flow was observed to be turbulent. Using the parameters given in Table 4-1, the friction factor,  $f$ , was calculated for each data point using the Haaland equation for turbulent flow, given here as:

$$\frac{1}{\sqrt{f}} = -1.8 \log \left[ \left( \frac{e/D}{3.7} \right)^{1.11} + \frac{6.9}{R} \right]$$

*Equation 4-4*

Finally, to calculate the friction head loss,  $h_f$ , for each data point, the Darcy Weisbach equation was used:

$$h_f = \frac{fLv^2}{2Dg} = f \frac{L}{D} \frac{\left( \frac{Q}{\pi D^2 / 4} \right)^2}{2g}$$

*Equation 4-5*

Where  $h_f$  is the friction head loss (m),  $Q$  is the measured flow rate ( $\text{m}^3/\text{s}$ ),  $D$  is the internal diameter of the pipe (m),  $f$  is the friction coefficient,  $g$  is the acceleration due to gravity ( $\text{m}/\text{s}^2$ ) and  $L$  is the length pipe (m). The parameters used to calculate the friction head loss are given in Table 4-1.

Table 4-1: Parameters used to calculate the friction head loss for each step

Parameter	Value
Delivery line Internal diameter, $D$ (m)	0.0452
Length of delivery line, $L$ (m)	10
Acceleration due to gravity, $g$ (m/s <sup>2</sup> )	9.81
Rubber hose pipe Absolute roughness, $e$ (mm)	0.05
Kinematic viscosity, $\nu$ (m <sup>2</sup> /s)	$11.39 \times 10^{-7}$

The minor losses were calculated to take into account the effect of the various hydraulic components between the pressure sensor and the test rig. The hydraulic components are listed below in Table 4-2, with their respective minor loss coefficient obtained from Finnemore and Franzini (2009).

Table 4-2: Hydraulic components and their minor loss coefficients

Hydraulic components	Minor loss coefficient, K
Ball valve	0.1
Adapter (Sudden Contraction)	0.3
Adapter (Sudden Expansion)	0.75
Rubber hose pipe bends	0.5
Straight connectors	0.2

The minor loss coefficients in Table 4-2 were added up and the minor loss for each data point was calculated, using the minor head loss equation given here:

$$h_m = \sum K \frac{(4Q/\pi D^2)^2}{2g}$$

Equation 4-6

Finally, once the measured pressure ( $h_{measured}$ ) from the pressure transmitter is obtained. The adjusted pressure values were obtained by subtracting the elevation height,  $\Delta z$ , friction head loss,  $h_f$ , and the minor head loss,  $h_m$ , from the measured average pressure, and the pressure at the leak could thus be established using the following equation:

$$h_{adjusted} = h_{measured} - h_f - h_m - \Delta z$$

Equation 4-7

#### **4.4.3.3 Step 3: determining leakage parameters for the power equation**

The leakage parameters for the power equation were determined empirically. The flow rate ( $Q$ ) and adjusted pressure ( $h_{adjusted}$ ) values were plotted with a power equation fitted to the data. The power equation has a coefficient value, representing the leakage coefficient ( $C$ ) and an exponent value representing the leakage exponent ( $N1$ ), respectively. The  $N1$  equation is given here:

$$Q = C h^{N1}$$

*Equation 4-8*

In order to verify the power equation leakage parameters, Equation 4-8 is converted into an equivalent linear function by applying logs of base 10 on both sides of the equation. This results in the following linear expression:

$$\text{Log}_{10}Q = \text{Log}_{10}C + N1 \text{Log}_{10}h_{adjusted}$$

*Equation 4-9*

The slope and intercept of Equation 4-9 represents the  $N1$  leakage exponent and the log of the leakage coefficient, respectively. Using the Microsoft Excel function of Slope and Intercept and the flow and adjusted pressure data, the slopes and intercept of the linear function in Equation 4-9 can be obtained. The  $N1$  leakage exponent value is obtained directly from the slope of the linear equation; however, in order to obtain the leakage coefficient, the following formulation is required:

$$C = 10^{\text{Log}_{10}C}$$

*Equation 4-10*

#### **4.4.3.4 Step 4: calculating the effective leak area ( $C_dA$ )**

The effective leak area,  $C_dA$ , at each pressure step was calculated by re-arranging the orifice equation as follows:

$$C_dA = \frac{Q}{\sqrt{2 g h_{adjusted}}}$$

*Equation 4-11*

Where  $C_d$  is the discharge coefficient,  $Q$  is the measured flow rate ( $m^3/s$ ),  $h_{adjusted}$  is the test pipe pressure (m),  $g$  is the acceleration due to gravity ( $m/s^2$ ) and  $A$  is the equivalent leak area ( $m^2$ ).

If the total effective leak area of the system is estimated at different pressures, the effective leakage area can be plotted against pressure and a linear function fitted to the data points. The intercept of this line with the effective area axis gives the effective initial leak area ( $C_d A_0$  or  $A'$ ), and the slope of this line gives the effective head-area slope ( $C_d m$  or  $m'$ ).

#### ***4.4.3.5 Step 5: determining the leakage parameters for the modified orifice equation***

Since the leak sources are drilled into the pipe, the actual initial leak area can be physically measured and thus is known ( $A_{0,known}$ ). Consequently, the discharge coefficient ( $C_d$ ) can be estimated by dividing the obtained initial effective leak area ( $C_d A_0$ ), determined in step 4, by the known initial leak area ( $A_{0,known}$ ) as follows:

$$C_d = \frac{C_d A_0}{A_{0,known}}$$

*Equation 4-12*

#### ***4.4.3.6 Step 6: estimating the leakage flow rate***

The leakage flow rates were estimated using the power equation and the modified orifice equation models. The leakage parameters for the power equation ( $N1, C$ ) were substituted into the power equation, and the leakage parameters for the modified orifice equation ( $C_d A_0, C_d m$ ) were substituted in the modified orifice equation. The leakage equations models are given as follows:

Power Equation:

$$Q = C h^{N1}$$

*Equation 4-13*

Modified Orifice Equation:

$$Q = \sqrt{2g}[(C_d A_0)h^{0.5} + (C_d m)h^{1.5}]$$

*Equation 4-14*

Once the leakage parameters are substituted into their respective leakage equation models, the flow rates,  $Q$ , can be obtained and plotted for a range of pressure heads, i.e.  $h = 0, 15, 20, 25, 30, 35m$ . The leakage flow rates,  $Q$ , obtained using the leakage equation models are plotted against pressure as continuous lines. The measured experimental flow rate data points are plotted against the measured pressure as discrete data points on the same flow vs pressure graphs. This is done to determine whether the measured flow and pressure data points correlate with the power equation and modified orifice equation flow rate models.

#### **4.4.3.7 Step 7: determining the leakage number**

Finally, a dimensionless leakage number ( $LN$ ) is calculated for the leak. The leakage number ( $LN$ ) represents the ratio between the expanding leakage area and the fixed leak area, and is expressed as follows:

$$L_N = \frac{mh}{A_0}$$

*Equation 4-15*

A simple equation was proposed by Cassa and van Zyl (2010) to convert between the leakage number ( $LN$ ) and the leakage exponent ( $N1$ ):

$$L_N = \frac{N1 - 0.5}{1.5 - N1}$$

*Equation 4-16*

$$N1 = \frac{1.5 L_N - 0.5}{L_N + 1}$$

*Equation 4-17*

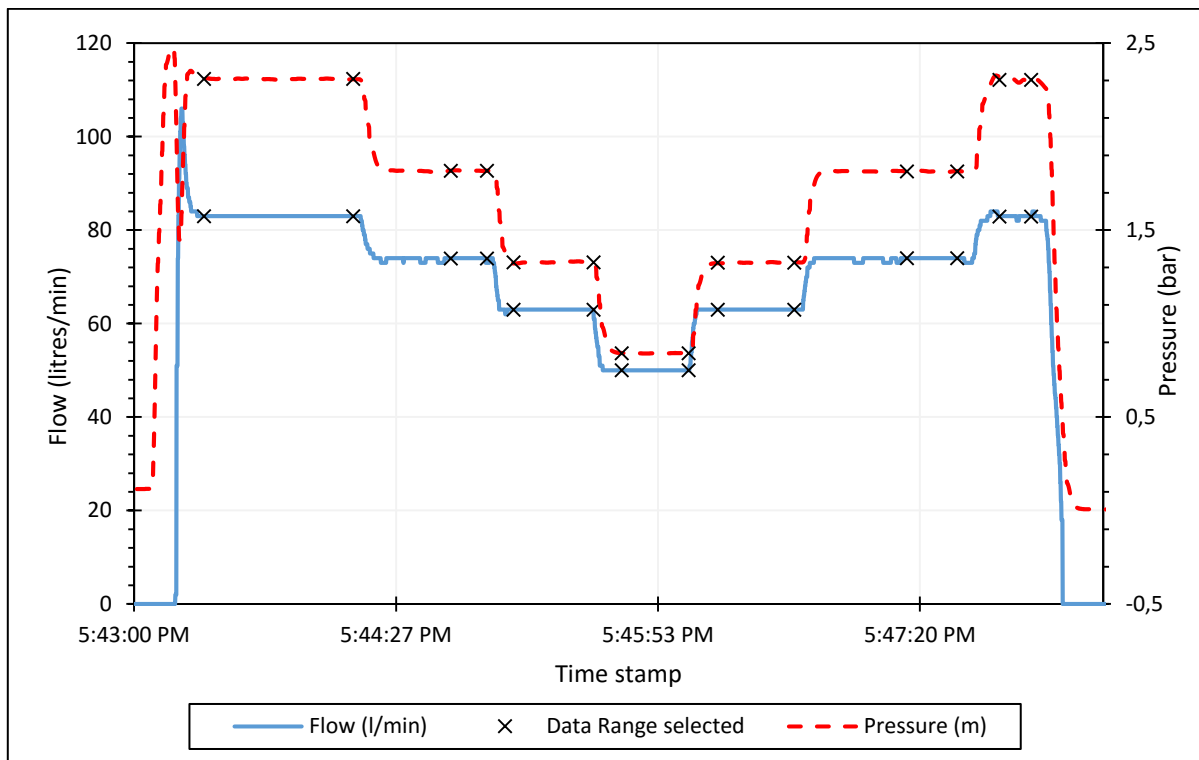
## **4.5 Laboratory results and discussion**

This section details the experimental test results obtained. Experimental raw data containing flow and pressure was collected for three leak tests, namely for a round hole, a longitudinal crack, and a circumferential crack. The raw data for each test was analysed using the analysis procedure discussed in Section 4.4.3.

### 4.5.1 Results for round holes

This test was used to assess the behaviour of round holes in pressurised pipes. For this experiment, a 12mm round hole was tested and the PCAE was used to investigate the leak's behaviour. The pressure head and flow rate data were recorded from the PCAE.

The raw flow and pressure data for the 12mm round hole leak were plotted against time, shown in Figure 4-11. The stable sections of the flow and pressure steps are indicated by the star markers. Each step was held long enough until both flow and pressure stabilised.



*Figure 4-11: Flow and pressure raw data for the 12mm round hole*

The average values over each of the stabilised ranges were calculated. Table 4-3 below shows the averaged flow and pressure data points. The table also shows the following for each data point: the calculated Reynolds number, friction factor, friction head loss, minor head loss values, and the final column shows the adjusted pressure head.

*Table 4-3: Average flow, pressure and adjusted pressure for the 12mm round hole*

Average Flow (l/min)	Average Flow (m <sup>3</sup> /s)	Average Pressure (bar)	Average Pressure (m)	Reynolds Number	Friction Factor	Friction Head Loss, h <sub>f</sub> (m)	Minor Loss, h <sub>m</sub> (m)	Adjusted Pressure Head, h <sub>adjusted</sub> (m)
83	1.38x10 <sup>-03</sup>	2.31	23.55	34212	0.451	3.78	0.081	19.59
73.96	1.23x10 <sup>-03</sup>	1.82	18.54	30485	0.451	3.00	0.072	15.37
62.99	1.05x10 <sup>-03</sup>	1.33	13.55	25965	0.451	2.18	0.062	11.21
50.00	8.33x10 <sup>-04</sup>	0.84	8.58	20609	0.451	1.37	0.049	7.06
63.00	1.05x10 <sup>-03</sup>	1.33	13.52	25968	0.451	2.18	0.062	11.18
74.00	1.23x10 <sup>-03</sup>	1.81	18.51	30502	0.451	3.00	0.072	15.33
82.92	1.38x10 <sup>-03</sup>	2.30	23.50	34180	0.451	3.77	0.081	19.55

#### ***4.5.1.1 Leakage parameters for the power equation***

The average flow and adjusted pressure head values, given in Table 4-3, were plotted on a graph and fitted with a power function. Figure 4-12 shows the flow against adjusted pressure head graph for the round hole leak. The power equation was used to determine the leakage coefficient (*C*) and leakage exponent (*N1*) which are 3x10<sup>-04</sup> and 0.50, respectively.



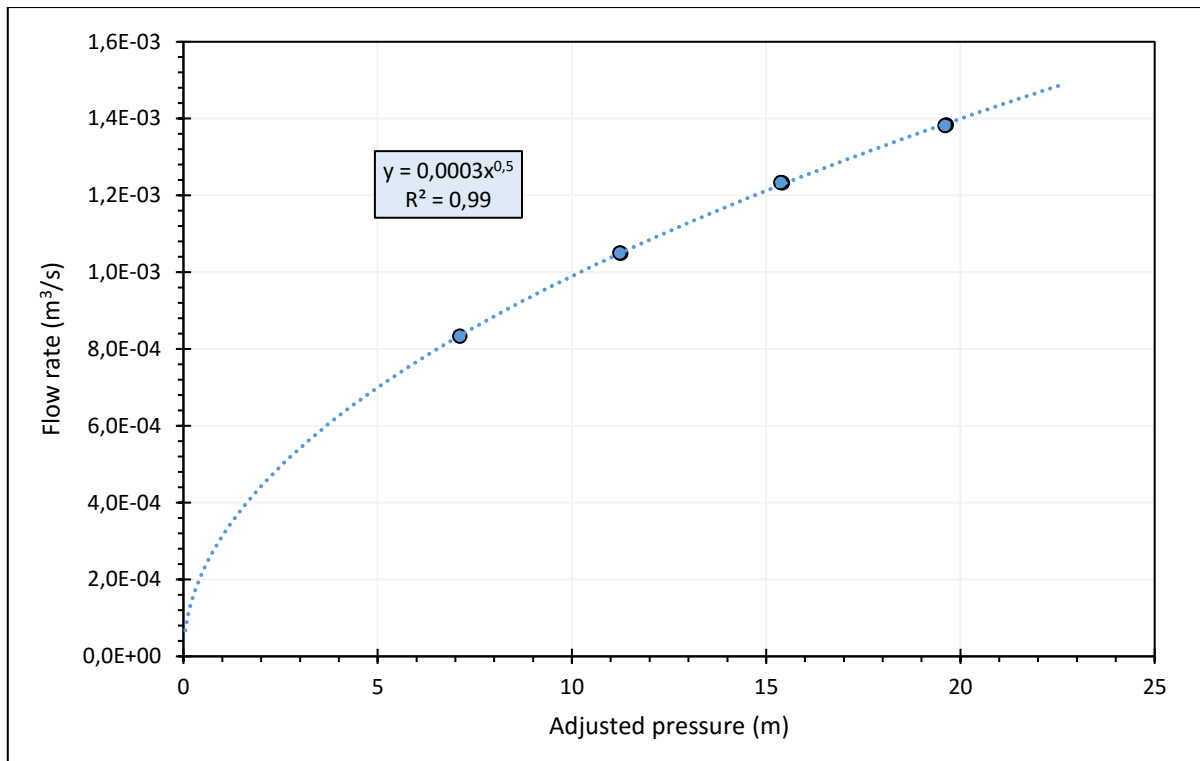


Figure 4-12: Flow against head graph with power function fitted for the 12mm round hole

The leakage parameter results for the power equation, shown in Figure 4-12, were compared, in Table 4-4, to the results obtained for uPVC round holes by van Zyl and Malde (2017), Greyvenstein & van Zyl (2005) and Thornton & Lambert (2005).

Table 4-4:  $N1$  values obtained by other researchers for the round holes in uPVC pipes

Author	$N1$ Value for uPVC round hole	% Difference with $N1$ value obtained
Malde & van Zyl (2015)	0.49	2
Greyvenstein & van Zyl (2005)	0.52	4
Thornton and Lambert (2005)	0.50	0

Table 4-4 shows that the  $N1$  value of 0.50, obtained using the PCAE, compares relatively well with previous experimental  $N1$  leakage exponent values that were found by other researchers. A maximum percentage difference of 4% is obtained.

#### 4.5.1.2 Leakage parameters for the modified orifice equation

The effective leak area,  $A'$ , was calculated for each data point. In Table 4-5, column 3 shows the effective leak area calculated for each averaged pressure and flow data point for the 12 mm round hole leak.

Table 4-5: Summary of the modified orifice equation results

Measured Average Flow (l/min)	Adjusted pressure head, $h_{adjusted}$ (m)	Effective leak area, $A'$ (mm <sup>2</sup> )	Leak Area, $A$ (mm <sup>2</sup> )
$1.38 \times 10^{-3}$	19.59	70.56	112.8
$1.23 \times 10^{-3}$	15.37	70.97	113.4
$1.05 \times 10^{-3}$	11.21	70.79	113.2
$8.33 \times 10^{-4}$	7.06	70.78	113.2
$1.05 \times 10^{-3}$	11.18	70.88	113.3
$1.23 \times 10^{-3}$	15.33	71.11	113.7
$1.38 \times 10^{-3}$	19.55	70.56	112.8

The effective leak area and the adjusted pressure head from Table 4-5 were plotted and a linear function fitted to the sample points. Figure 4-13 shows the  $A'$  against head graph for the data set and a linear function fitted to the data points.

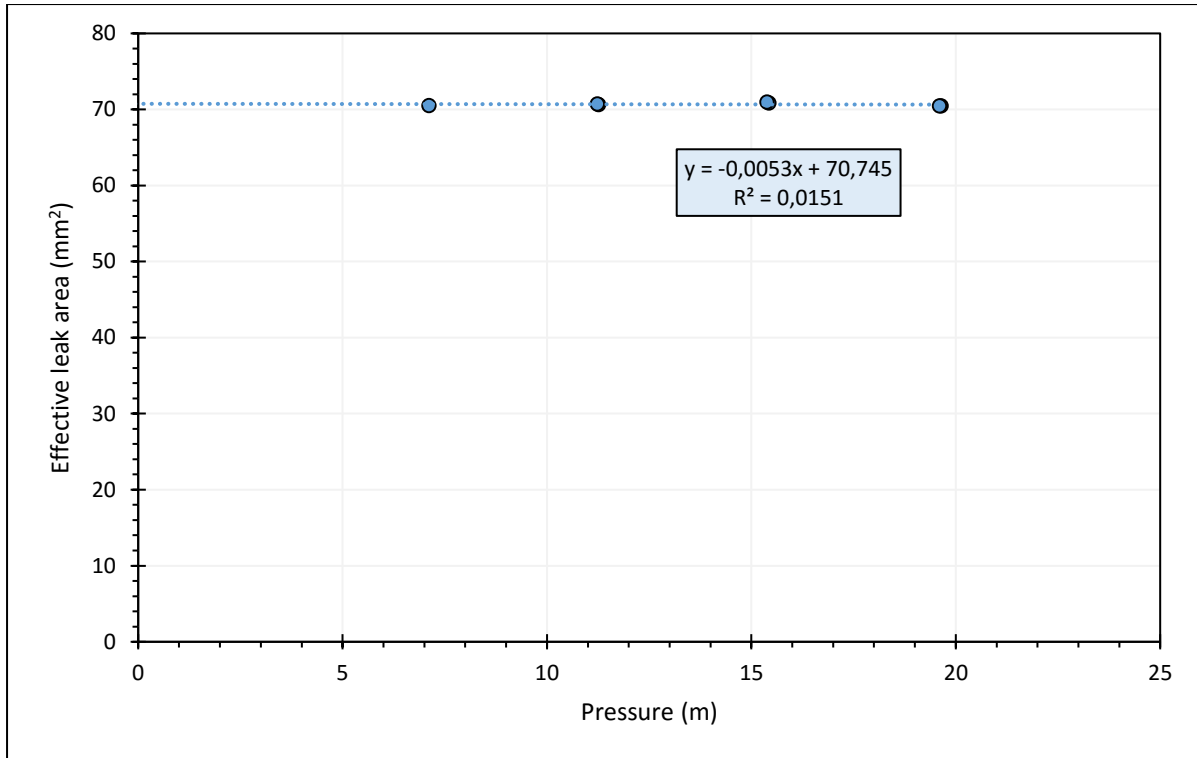
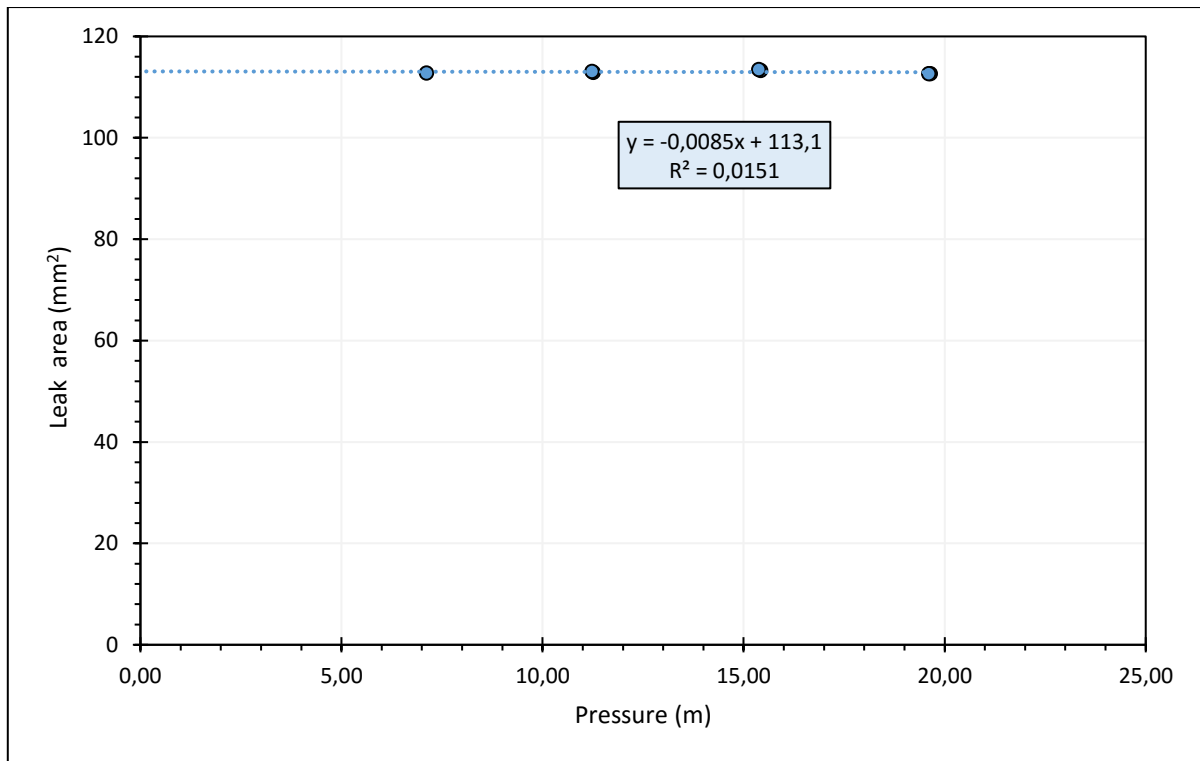


Figure 4-13: Effective leak area against pressure head for the 12mm round hole

In Figure 4-13, the intercept of the linear line with the effective leak area axis gives the effective initial leak area,  $A'_0$ , as  $70.7 \text{ mm}^2$ , and the slope of the line gives the effective head-area slope as  $-0.0053 \text{ mm}^2/\text{m}$ . Since  $A_0$  ( $113.09 \text{ mm}^2$ ) is known (calculated physically from the test pipe), the discharge coefficient ( $C_d$ ) can be determined directly as 0.63, using Equation 4-12.

The leak area ( $A$ ) values are determined by dividing the effective leak  $A'$  or  $C_d A$  values by  $C_d$ . The calculated leak areas, given in Table 4-5, are plotted against the adjusted head values to acquire the initial leak area, ( $A_0$ ) and head-area slope ( $m$ ). Figure 4-14 shows the leak area against adjusted pressure for the 12mm round hole uPVC class 9 pipe.



*Figure 4-14: Leak area against pressure head for the 12mm round hole*

The linear function fitted through the data points in Figure 4-14 shows that the intercept  $A_0$  is  $113.1 \text{ mm}^2$ , which is the same as the physically calculated value for a 12mm round hole area. The intercept  $A_0$  value is expected to be the same as the physically determined leak area for any leak shape and size. The head area slope was obtained as  $-0.009 \text{ mm}^2/\text{m}$ , which is the same as the head-area slope obtained in van Zyl and Malde's (2017) experimental study.

#### ***4.5.1.3 Estimating flow rates using the power equation and the modified orifice equation***

The process of estimating flow rates involves substituting the power equation leakage parameters and modified orifice equation leakage parameters in their respective flow rate equation models. Table 4-6 shows a summary of the power equation leakage parameters as well as the modified orifice equation leakage parameters.

Table 4-6: Summary of leakage parameters for the round hole leak

Leakage Parameter	Value
Leakage Exponent, N1	0.50
Leakage coefficient, C	0.00031
Effective head-area slope, $m'$ (mm <sup>2</sup> /m)	-0.009
Effective initial leak area, $A'_0$ (mm <sup>2</sup> )	113.1

Using the leakage parameters for the power equation ( $N1$  and  $C$ ) in Table 4-6, the power equation model can be expressed as follows:

$$Q = 0.00031 h^{0.50}$$

*Equation 4-18*

Using the leakage parameters for the modified orifice equation ( $m'$  and  $A'_0$ ) in Table 4-6, the modified orifice equation model can be expressed as follows:

$$Q = \sqrt{2g}(113.1 h^{0.5} - 0.009 h^{1.5}) \times 10^{-6}$$

*Equation 4-19*

In order to compare the equations to the experimental data, a series of flow rates were generated for various pressure heads. These were then plotted with the measured experimental data to see how well the equations fit the data. Figure 4-15 compares the power equation (Equation 4-18) and the modified orifice equation (Equation 4-19) to the experimental data measured during the 12mm round hole test.

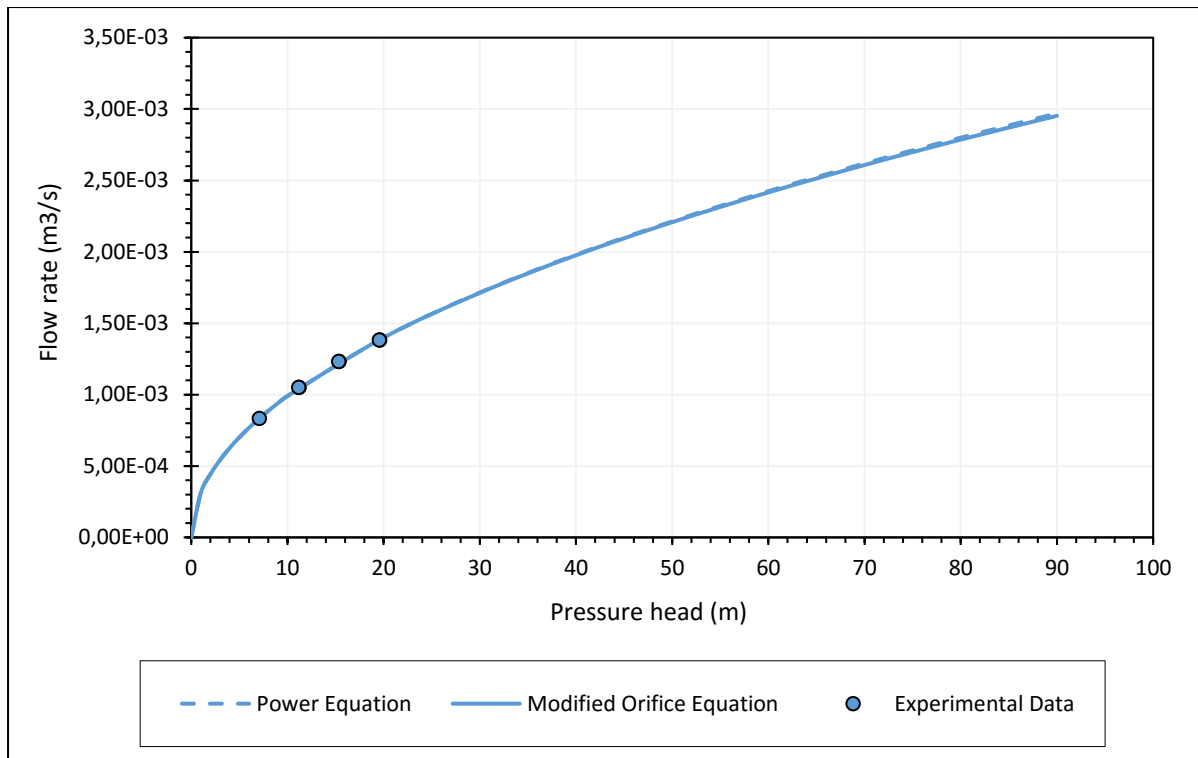


Figure 4-15: Comparison of the power equation and the modified orifice equation with the experimental data

Figure 4-15 shows that both the power equation and the modified orifice equation very closely matched the measured experimental data points. This result suggests that both the modified orifice equation and the power equation can be used for the round hole (Equation 4-18 and Equation 4-19 respectively) to estimate the leakage rate,  $Q$ , from the pipe at different pressures.

#### 4.5.2 Results for longitudinal cracks

This test was used to assess the behaviour of longitudinal cracks in pressurised pipes. For this experiment, a 50mm by 2mm longitudinal crack was tested. Using the condition assessment equipment, the behaviour of this leak was assessed. Pressure and flow data, obtained from the equipment, was used to investigate the leakage characteristics of the longitudinal crack. Thereafter, the results were compared with studies by other researchers and practitioners on the behaviour of longitudinal leaks.

The raw flow and pressure data for the longitudinal crack is plotted against time in Figure 4-11. Each step was held long enough for both flow and pressure to stabilise. The stabilised sections of the flow and pressure steps are indicated by the star markers.

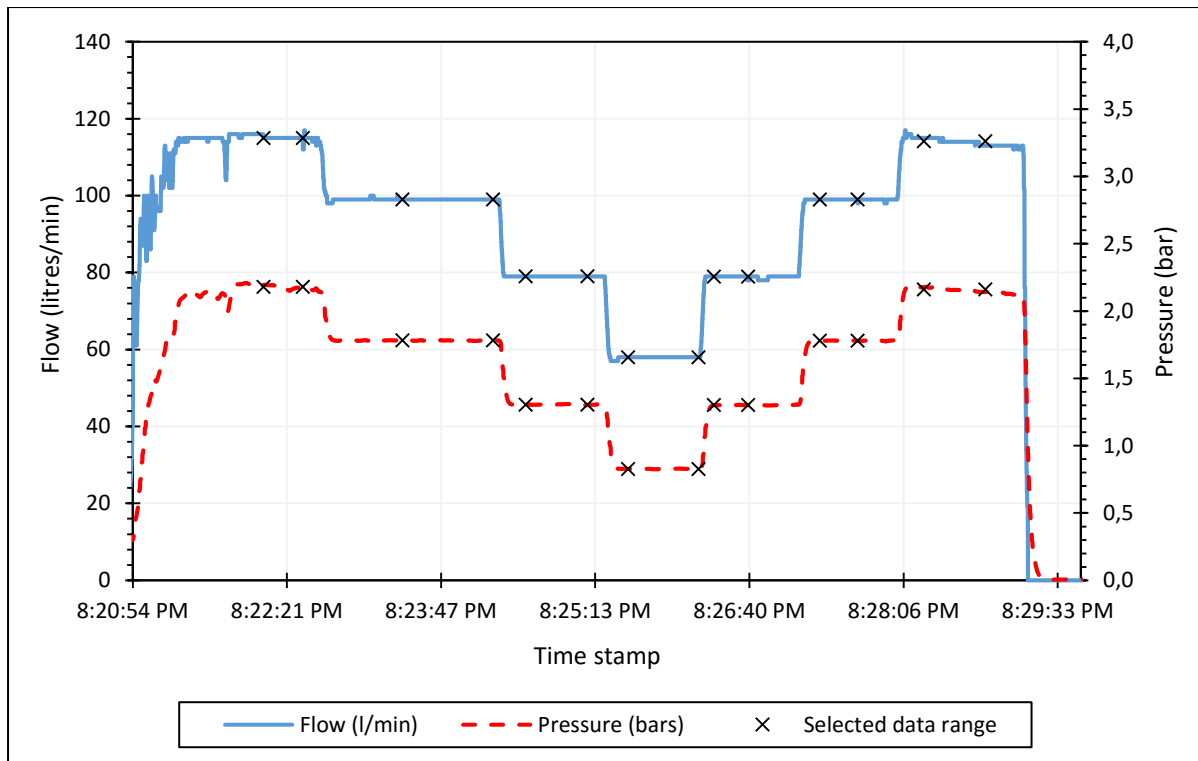


Figure 4-16: Flow and pressure raw data for the longitudinal crack

The average flow and pressure for each stabilised step is shown in Table 4-7. The stabilised pressures were adjusted by taking into account the elevation difference between the pressure sensor and the leak (0.05 m), the friction losses and the minor loss. In Table 4-7, the last column shows the adjusted pressure.

Table 4-7: Average measured flow, pressure and adjusted pressure for the longitudinal crack

Measured Average Flow (l/min)	Measured Average Flow ( $\text{m}^3/\text{s}$ )	Measured Average Pressure (bar)	Measured Average Pressure (m)	Reynolds Number, $R$	Friction Factor, $f$	Friction Head Loss, $h_f$ (m)	Minor Loss, $h_m$ (m)	Adjusted Pressure Head, $h_{\text{adjusted}}$ (m)
115.0	$1.92 \times 10^{-3}$	2.18	22.22	47396	0.36	5.92	0.113	16.14
99.0	$1.65 \times 10^{-3}$	1.78	18.17	40807	0.36	4.39	0.097	13.64
79.0	$1.32 \times 10^{-3}$	1.31	13.32	32563	0.36	2.79	0.077	10.39
58.0	$0.97 \times 10^{-3}$	0.83	8.44	23907	0.36	1.51	0.057	6.83
79.0	$1.32 \times 10^{-3}$	1.30	13.28	32552	0.36	2.79	0.077	10.36
99.0	$1.65 \times 10^{-3}$	1.78	18.16	40805	0.36	4.39	0.097	13.62
114.2	$1.90 \times 10^{-3}$	2.16	22.03	47058	0.36	5.84	0.112	16.03

#### 4.5.2.1 Leakage parameters for the power equation

The flow rate against pressure head for the longitudinal crack is plotted in Figure 4-17. A power equation was fitted to the data, and it is evident that the equation fits the data very well, given that the  $R^2$  value is 0.998. The power equation is used to determine the leakage coefficient ( $C$ ) and leakage exponent ( $N1$ ) which are 0.0002 and 0.80, respectively. Overall, higher pressures produce higher flow rates as expected.

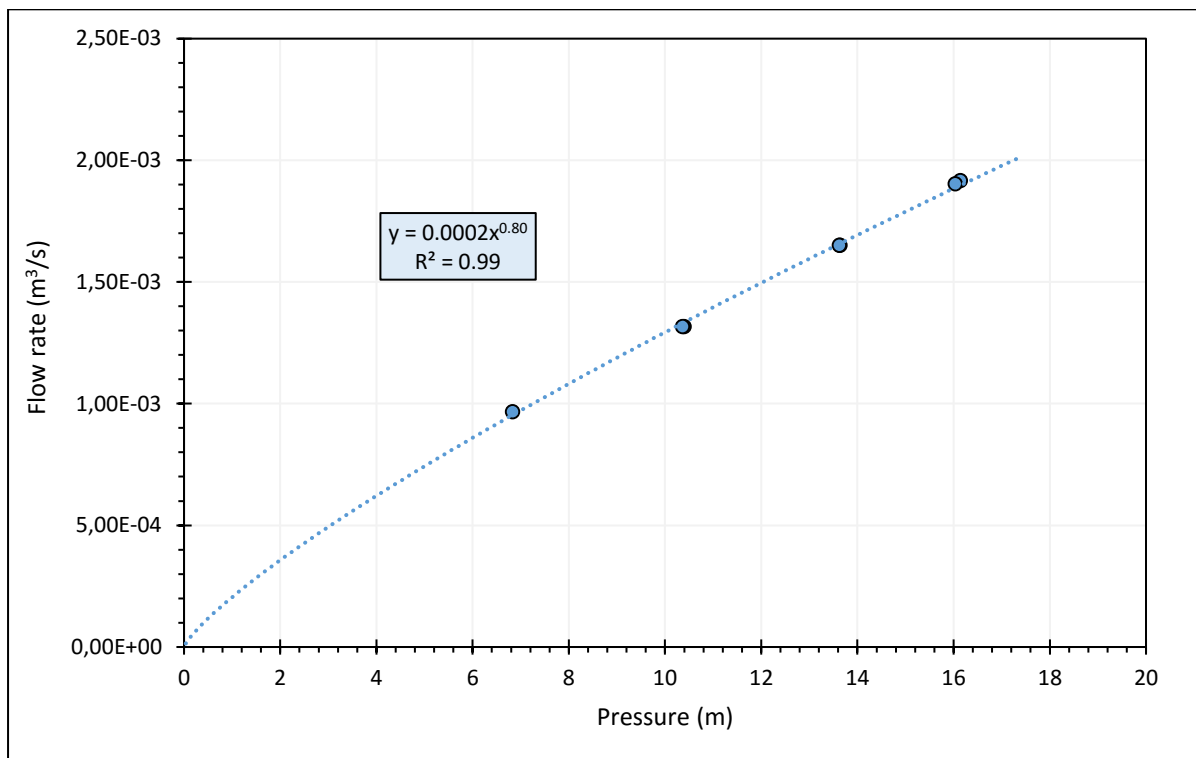


Figure 4-17: Flow against adjusted pressure for the longitudinal cracks

The leakage parameter results for the power equation, shown in Figure 4-17, were compared to the results obtained for the same uPVC longitudinal crack tested in van Zyl and Malde's (2017) experimental study. It was observed that the leakage exponent of 0.8, obtained using the PCAE, is slightly lower than the expected value of 1.01 obtained by van Zyl and Malde (2017) for a longitudinal crack. This difference between the results could be due to the fact that the pressure sensor location differed for the respective experimental setups. For the device, the pressure sensor measured the pressure upstream of the leak, whilst the pressure sensor in van Zyl and Malde's (2017) study was located downstream of the leak.



#### 4.5.2.2 Leakage parameters for the modified orifice equation

The effective leak area ( $C_dA$  or  $A'$ ) for each measured average flow and adjusted pressure head was calculated using Equation 4-11, and the results are given in the third column of Table 4-8.

Table 4-8: Summary of the modified orifice equation results

Measured Average Flow ( $m^3/s$ )	Adjusted Pressure Head , $h_{adjusted}(m)$	Effective Leak Area, $A'$ ( $mm^2$ )	Leak Area, $A$ ( $mm^2$ )
$1.92 \times 10^{-03}$	16.14	107.70	164.72
$1.65 \times 10^{-03}$	13.64	100.88	154.28
$1.32 \times 10^{-03}$	10.39	92.20	141.01
$9.67 \times 10^{-04}$	6.83	83.51	127.73
$1.32 \times 10^{-03}$	10.36	92.31	141.17
$1.65 \times 10^{-03}$	13.62	100.93	154.36
$1.90 \times 10^{-03}$	16.03	107.29	164.09

The effective leak areas,  $A'$ , are plotted against the adjusted pressure head in Figure 4-18, and a linear line is fitted to the data points. The intercept and slope of the linear line gives the effective initial leak area and the effective head-area slope respectively.

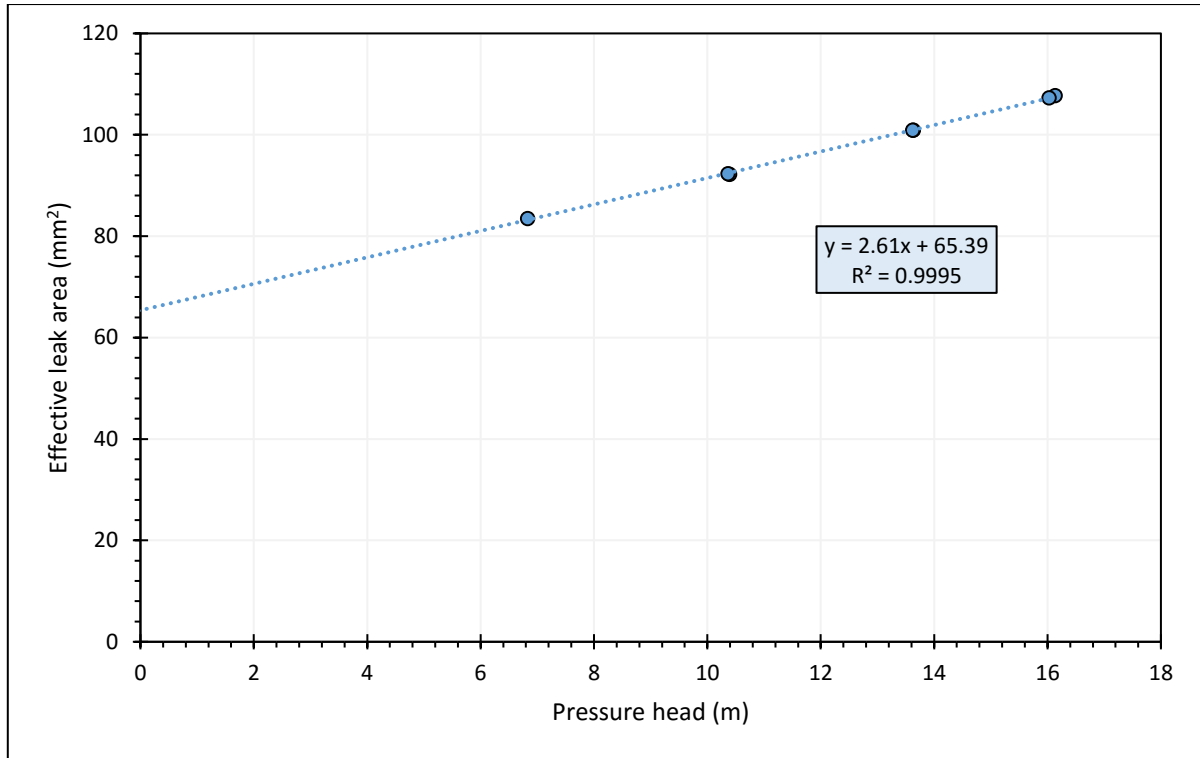
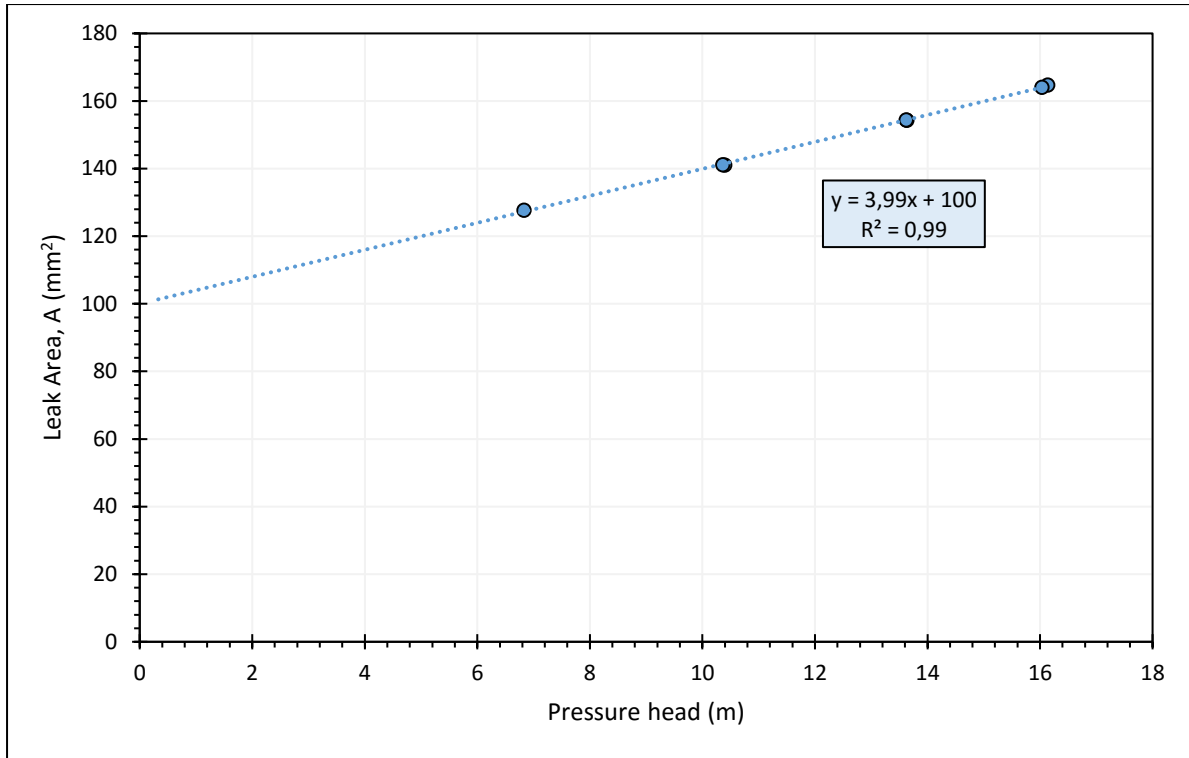


Figure 4-18: Effective area against pressure head for the longitudinal crack

Figure 4-18 shows that the intercept of the linear function was  $A'_0 = 65.39 \text{ mm}^2$ , and the slope of the linear function was  $m' = 2.61 \text{ mm}^2/\text{m}$ . The obtained effective leak area was 3.98% higher than the head-area slope obtained for the 100mm longitudinal crack in van Zyl and Malde's (2017) experimental study, which was  $2.51 \text{ mm}^2/\text{m}$ . This 3.98% difference could be due to the position of the pressure sensor. For example, in van Zyl & Malde's (2017) study the pressure sensor was located downstream of the leak, while in this study, the pressure sensor mounted on the PCAE was connected upstream of the leak. The main difference between the two positions is the local influence the leak might have on the pressure; this may affect the pressure reading of the downstream sensor, as was the case in van Zyl and Malde's (2017) study.

The leak Area ( $A$ ) values are determined by dividing the effective leak areas ( $A'$  or  $C_d A$ ) values by  $C_d$ . Since the initial leak area,  $A_0$  ( $100 \text{ mm}^2$ ), is known (calculated physically from the test pipe), the discharge coefficient ( $C_d$ ) can be determined directly as 0.65, using Equation 4-12. The leak areas are obtained, as provided in the fourth column of Table 4-8. The leak areas,  $A$ , are plotted against the adjusted pressure head values to acquire the initial leak area ( $A_0$ ) and head-area slope ( $m$ ). Figure 4-19 shows the leak area against adjusted pressure for the uPVC class 9 longitudinal crack (100mm by 1mm).



*Figure 4-19: Leak area against pressure head for the longitudinal crack*

The linear function fitted through the data points in Figure 4-19 shows that the intercept  $A_0$  is  $100 \text{ mm}^2$ , which is the same as the physically calculated value for a  $100\text{mm}$  by  $1\text{mm}$  longitudinal crack area. The head area slope was obtained as  $3.99 \text{ mm}^2/\text{m}$ .

#### ***4.5.2.3 Estimating the flow rate***

The process of estimating flow rates involves substituting the leakage parameters for both the power equation and the modified orifice equation in their respective flow rate equation models. Table 4-9 shows a summary of the leakage parameters for both equations as obtained for the tested longitudinal crack.

Table 4-9: Summary of leakage parameters for the longitudinal crack

Leakage Parameter	Value
Leakage Exponent, N1	0.80
Leakage coefficient, C	$2.05 \times 10^{-4}$
Effective Head-area slope, $m'$ (mm <sup>2</sup> /m)	2.61
Effective Initial leak area, $A'_0$ (mm <sup>2</sup> )	65.38

Using the leakage parameters for the power equation (N1 and C) in Table 4-9, the power equation model can be expressed as follows:

$$Q = 2.05 \times 10^{-4} h^{0.80}$$

Equation 4-20

Using the leakage parameters for the modified orifice equation (  $m'$  and  $A'_0$  ) in Table 4-9, the modified orifice equation model can be expressed as follows:

$$Q = \sqrt{2g}(65.38 h^{0.5} + 2.61 h^{1.5}) \times 10^{-6}$$

Equation 4-21

In order to compare the equations to the experimental data, a series of flow rates were generated for various pressure heads. These were then plotted with the measured data to see how well the equations fitted the data. Figure 4-20 compares the power equation (Equation 4-20) and the modified orifice equation (Equation 4-21) obtained for longitudinal cracks, to the experimental measured data for the longitudinal crack.

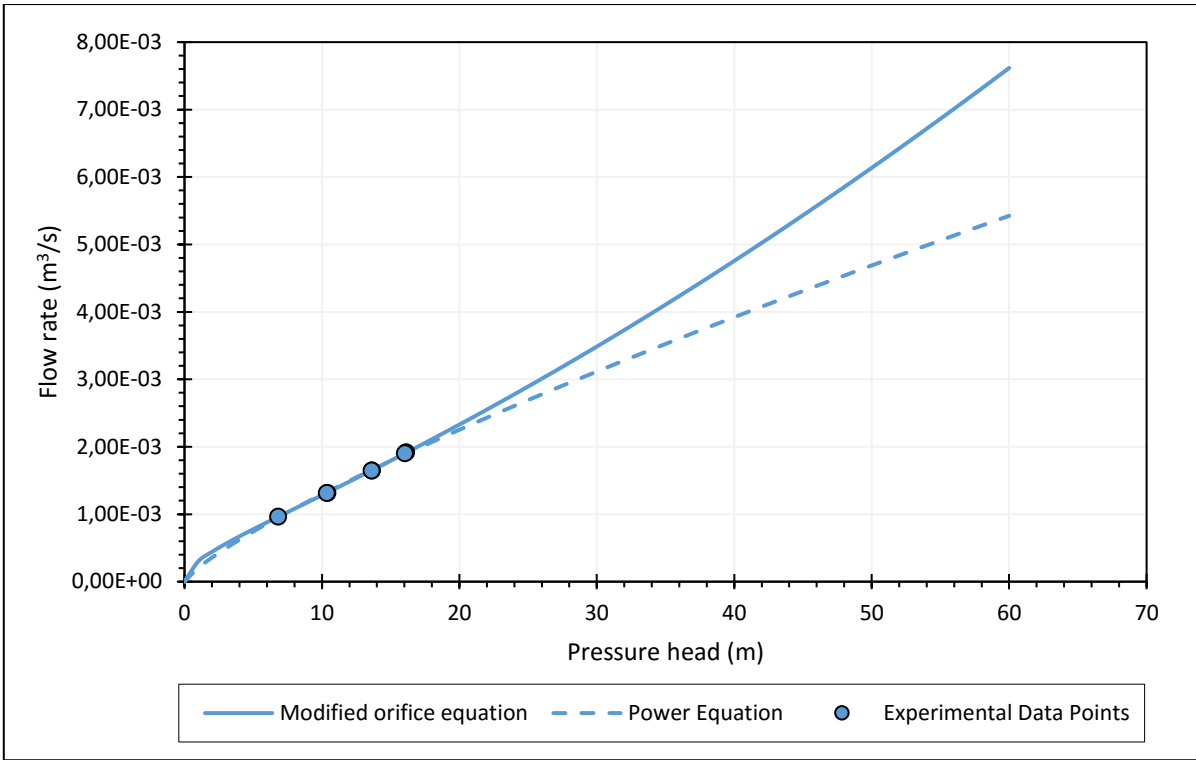


Figure 4-20: Flow against pressure head for the longitudinal crack

Figure 4-20 shows that the power equation and the modified orifice equation are closer together at the experimental pressure heads range. However, at pressure heads above and below the experimental pressure head range the modified orifice equation predicts higher leakage flow rates compared to the leakage flow rates predicted by power equation. The higher flow rates shown on the modified orifice equation graph can be attributed to the large head-area slope associated with the longitudinal crack pipe leakage behaviour. The large head-area slope increases the leakage through the expanding part of the leak in the modified orifice equation,  $C_d m h^{1.5}$  (see Equation 4-14).

### 4.5.3 Results for the circumferential crack

This test was used to assess the behaviour of circumferential cracks in pressurised pipes. For this test, a 100mm by 1mm circumferential crack was investigated. Once the pressure and flow data were obtained, the circumferential leak behaviour was characterised, as stipulated for the previous tests.

The raw flow and pressure data for the circumferential crack were plotted against time in Figure 4-21, and the stable sections of the flow and pressure steps are indicated by the star markers. Each step was held long enough for both flow and pressure to stabilise.

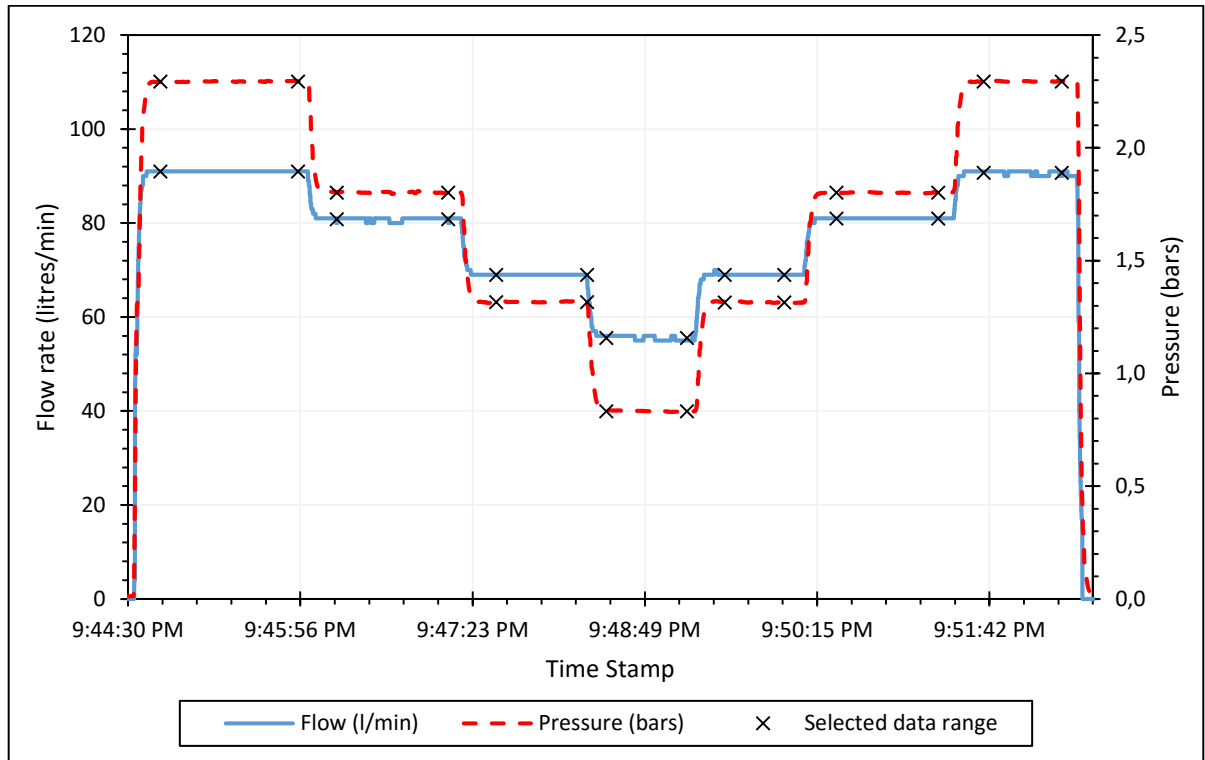


Figure 4-21: Flow and pressure raw data for the circumferential crack

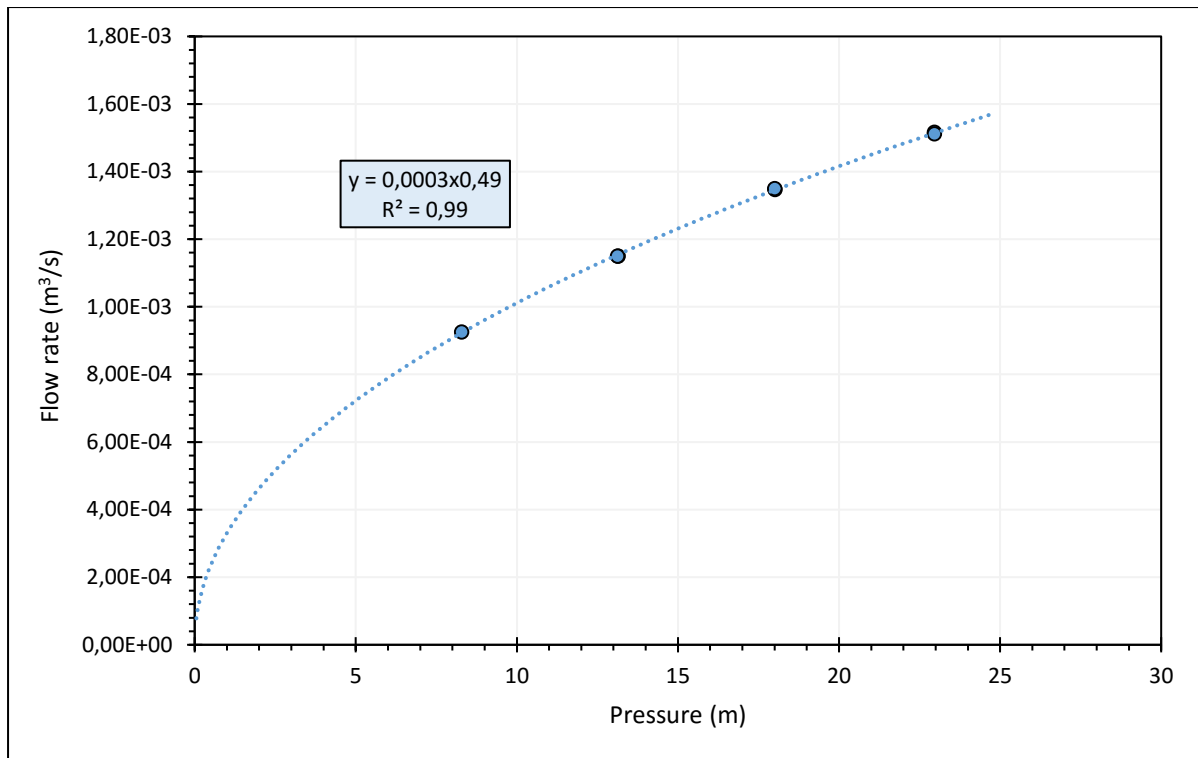
The average values for each of the stabilised flow and pressure ranges were calculated. Table 4-3 below shows the averaged flow and pressure data points. The table also shows the following for each data point: the calculated Reynolds number, friction factor, friction head loss, minor head loss values, and the final column shows the adjusted pressure head, after taking into account the  $h_r =$  eight difference of 0.005m.

*Table 4-10: Average flow, pressure and adjusted pressure for the circumferential crack*

Measured Average Flow (l/min)	Measured Average Flow (m <sup>3</sup> /s)	Measured Average Pressure (bar)	Measured Average Pressure (m)	Reynolds Number	Friction Factor	Friction Head Loss, h <sub>f</sub> (m)	Minor Loss, h <sub>m</sub> (m)	Adjusted Pressure Head, h <sub>adjusted</sub> (m)
91.00	1.52x10 <sup>-03</sup>	2.29	23.40	37509	0.4504	0.30	0.089	22.96
80.83	1.35x10 <sup>-03</sup>	1.80	18.39	33317	0.4505	0.24	0.079	18.02
68.99	1.15x10 <sup>-03</sup>	1.32	13.43	28438	0.4506	0.17	0.068	13.14
55.54	9.26x10 <sup>-04</sup>	0.83	8.50	22895	0.4508	0.11	0.054	8.28
69.00	1.15x10 <sup>-03</sup>	1.32	13.42	28441	0.4506	0.17	0.068	13.13
81.00	1.35x10 <sup>-03</sup>	1.80	18.37	33387	0.4505	0.24	0.079	18.01
90.71	1.51x10 <sup>-03</sup>	2.29	23.40	37391	0.4504	0.30	0.089	22.96

#### ***4.5.3.1 Leakage parameters for the power equation***

The average flow and adjusted pressure head values, given in Table 4-10, are plotted on a graph and fitted with a power function. Figure 4-22 shows the flow against adjusted pressure head graph for the circumferential crack. The power equation is used to determine the leakage coefficient ( $C$ ) and leakage exponent ( $N1$ ) for the circumferential crack, which are  $3.00 \times 10^{-04}$  and 0.48 respectively.



*Figure 4-22: Flow against adjusted pressure head graph with power function fitted for the circumferential crack*

The leakage parameter results for the power equation of the circumferential crack, shown in Figure 4-22, were compared to the results obtained for the same uPVC 100mm<sup>2</sup> circumferential crack tested in van Zyl and Malde's (2017) experimental study. It was observed that the leakage exponent of 0.48, obtained in Figure 4-22, is higher than the value of 0.33 obtained by van Zyl and Malde (2017) for the circumferential crack. The difference between the results could be due to the fact that the pressure sensor location which differed for the respective experimental setup. When using the PCAE, the pressure sensor measured the pressure upstream of the leak, while in van Zyl and Malde's (2017) experimental setup the pressure sensor was located downstream of the leak.

#### ***4.5.3.2 Leakage parameters for the modified orifice equation***

The effective leak area,  $A'$ , for the circumferential crack was calculated for each data point. In Table 4-11, column 3 shows the effective leak area calculated for each pressure and flow data point.



Table 4-11: Summary of modified orifice equation results for the circumferential crack

Measured Average Flow (m <sup>3</sup> /s)	Adjusted Pressure Head, h adjusted (m)	Effective Leak Area, A' (mm <sup>2</sup> )	Leak Area, A (mm <sup>2</sup> )
1.52x10 <sup>-03</sup>	22.96	71.45	98.13
1.35x10 <sup>-03</sup>	18.02	71.65	98.40
1.15x10 <sup>-03</sup>	13.14	71.62	98.35
9.26x10 <sup>-04</sup>	8.28	72.62	99.74
1.15x10 <sup>-03</sup>	13.13	71.65	98.40
1.35x10 <sup>-03</sup>	18.01	71.82	98.64
1.51x10 <sup>-03</sup>	22.96	71.23	97.82

The effective leak area,  $A'$ , and the adjusted pressure head,  $h_{adjusted}$ , from Table 4-11, are plotted and a linear function fitted to the sample data points, as illustrated by Figure 4-23.

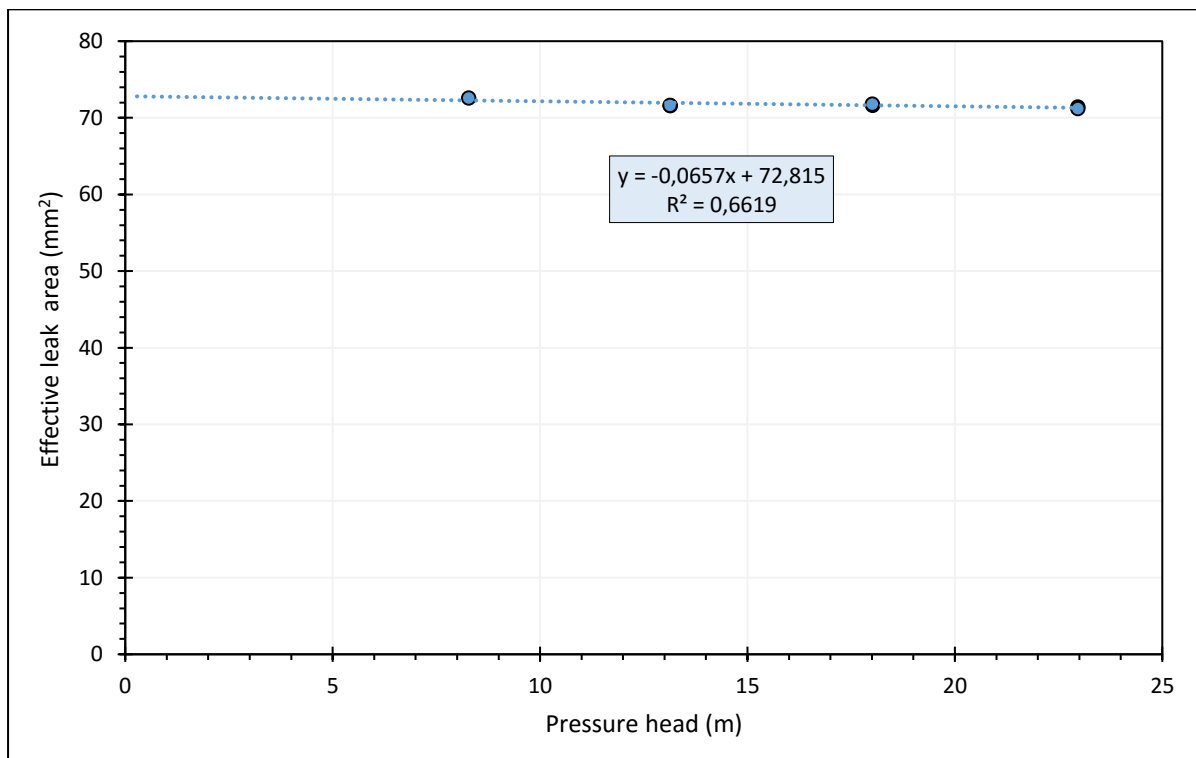


Figure 4-23: Effective leak area against adjusted pressure head for the circumferential crack

Figure 4-23 shows that the intercept of the linear function, which gives the effective initial leak area, was  $A'_0 = 72.82 \text{ mm}^2$ , and the slope of the linear function, which gives the effective head-area slope, was  $m' = -0.066 \text{ mm}^2/\text{m}$ . The negative effective head-area slope suggests that the circumferential leak area reduces as pressure increases.

Given that the initial leak area ( $A_0$ ) of the leak was known (calculated physically from the test pipe), the discharge coefficient  $C_d$  could be calculated directly as 0.73, using Equation 4-12. Using the obtained  $C_d$ , the leak areas are calculated and given in the fourth column of Table 4-11. The leak areas,  $A$ , are plotted against the adjusted pressure head,  $h_{adjusted}$  values. Figure 4-24 shows the leak area against adjusted pressure for the circumferential crack (100mm by 1mm).

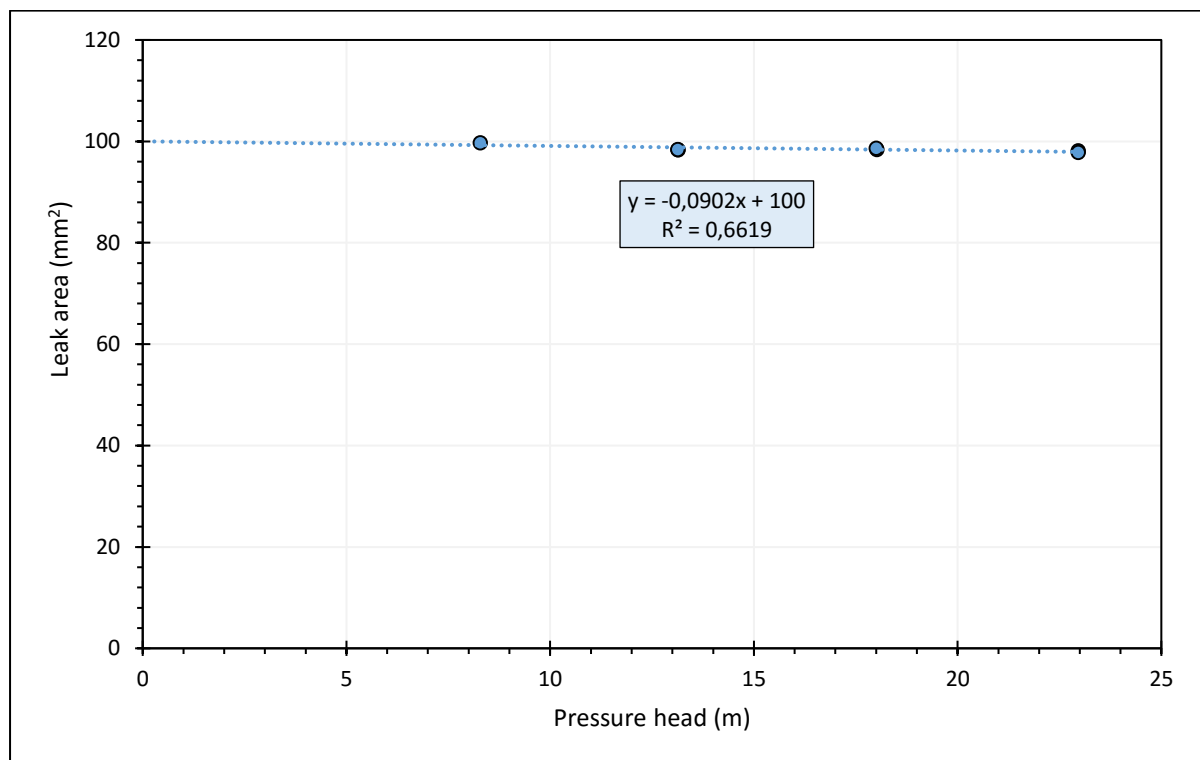


Figure 4-24: Leak area against adjusted pressure head for the circumferential crack

The linear function fitted through the data points in Figure 4-24 shows that the intercept  $A_0$  is  $100 \text{ mm}^2$ , which is consistent with the physically calculated area for the 100mm by 1mm circumferential crack area. The head-area slope was obtained as  $-0.0902 \text{ mm}^2/\text{m}$ , suggesting that the leak reduces by  $0.0902 \text{ mm}^2$  per meter of internal pressure applied to the test pipe.

### 4.5.3.3 Estimating the flow rate

Table 4-12 shows a summary of the leakage parameters for the circumferential crack. The leakage parameters are substituted into their respective flow rate equation models, and the equations can be used to determine the leakage rate from the pipe at different pressures.

*Table 4-12: Summary of leakage parameters for the circumferential crack*

Leakage Parameters	Values
Leakage Exponent, N1	0.486
Leakage Coefficient, C	$3.31 \times 10^{-4}$
Effective initial leak area, $A_0'$ (mm <sup>2</sup> )	72.82
Effective head area slope, $m'$ (mm <sup>2</sup> /m)	-0.066

Using the leakage parameters for the power equation ( $N1$  and  $C$ ) in Table 4-12, the power equation model can be expressed as follows:

$$Q = 3.31 \times 10^{-4} h^{0.486}$$

*Equation 4-22*

Using the leakage parameters for the modified orifice equation ( $m'$  and  $A_0'$ ) in Table 4-12, the modified orifice equation model can be expressed as follows:

$$Q = \sqrt{2g}(72.82 h^{0.5} - 0.066 h^{1.5}) \times 10^{-6}$$

*Equation 4-23*

Figure 4-25 shows the leakage rate from the pipe at different pressures for the power equation (Equation 4-20) and for the modified orifice equation (Equation 4-23). The experimental data points are also plotted in Figure 4-25, to compare the equations to the experimental data.

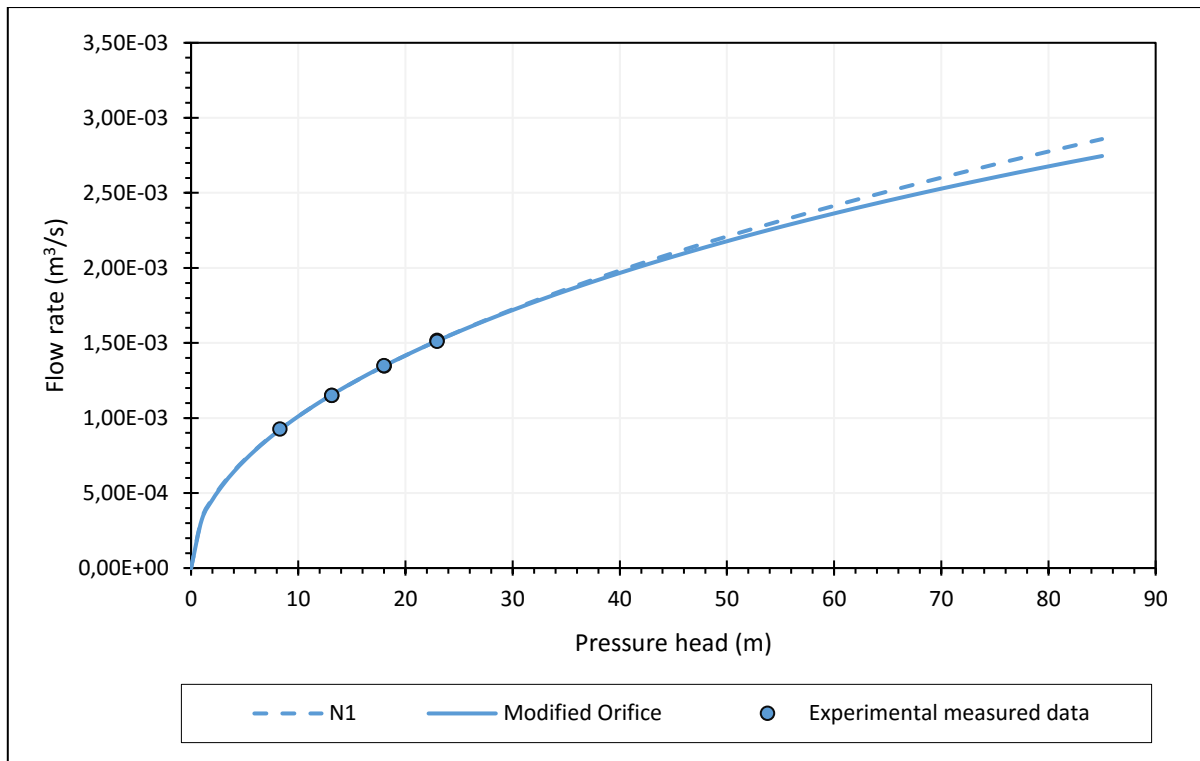


Figure 4-25: Comparison of the power equation and the modified orifice equation to the experimental data

Figure 4-25 shows that at lower pressures the power equation and the modified orifice equation start closer together; however as the pressure increases, the power equation has slightly higher leakage flow rates. It can also be seen that both the power and modified orifice equations very closely matched the measured data.

## 4.6 Summary of results

Table 4-13 presents a summary of the various leakage parameter results for the three leak types tested in the experimental verification tests. The table shows that the longitudinal crack displayed the highest leakage exponent; this was expected as longitudinal cracks are more sensitive to pressure compared to the round hole and circumferential crack. Furthermore, the effective head-area slope for the round hole and circumferential crack were negative, indicating that these leak areas reduced with increasing pressure. However, the longitudinal crack portrayed a large positive effective head-area, suggesting that the longitudinal leak area increases with increasing pressure head.

Table 4-13: Summary of the leakage parameters obtained for various types of leaks

Leak Type	N1	C	$A'_0$ (mm <sup>2</sup> )	$m'$ (mm <sup>2</sup> /m)	$C_d$
12 mm round hole	0.50	$3.13 \times 10^{-04}$	70.745	-0.0053	0.63
100 mm longitudinal crack	0.80	$2.05 \times 10^{-04}$	65.39	2.61	0.65
100 mm circumferential crack	0.48	$3.31 \times 10^{-04}$	72.81	-0.0657	0.73

The results obtained were compared with those in van Zyl and Malde's (2017) study, and the summary of the comparison is given in Table 4-14. In the table, the 2<sup>nd</sup> column represents the results obtained by van Zyl & Malde (2017), and the 3<sup>rd</sup> column represents the results obtained when using the PCAE.

Table 4-14: Comparison of results with van Zyl & Malde's (2017) study

12mm Round Hole	(van Zyl & Malde, 2017)	PCAE Results
N1	0.496	0.500
C	3.09E-04	3.13E-04
$m'$ (mm <sup>2</sup> /m)	-0.009	-0.009
$A'_0$ (mm <sup>2</sup> )	113.1	113.1
$C_d$	0.61	0.63
100mm Longitudinal	(van Zyl & Malde, 2017)	PCAE Results
N1	0.959	0.80
C	1.26E-04	2.05E-04
$m'$ (mm <sup>2</sup> /m)	2.40	2.61
$A'_0$ (mm <sup>2</sup> )	64.55	65.38
$C_d$	0.64	0.65
100mm Circumferential	(van Zyl & Malde, 2017)	PCAE Results
N1	0.429	0.485
C	3.96E-04	3.31E-04
$m'$ (mm <sup>2</sup> /m)	-0.104	-0.066
$A'_0$ (mm <sup>2</sup> /m)	73.164	72.82
$C_d$	0.73	0.73

Table 4-14 shows that for all three types of leaks, the results obtained using the PCAE are comparable to the results obtained in van Zyl and Malde's (2017) experimental study. This shows that the device is capable of characterising leakage.

## 4.7 Conclusion

This chapter reported on experimental tests that were carried out to verify the efficacy of the PCAE which was designed and constructed. The PCAE was used to test various pipes with known leakage characteristics in the laboratory.

The experimental setup involved a test rig originally designed by van Zyl and Malde (2017) to determine the leakage parameters of a pipe with an individual leak. The PCAE was connected

to the test rig to test three pipes with the following sources of leakage: a 12mm round hole, a 100mm by 1mm longitudinal crack, and a 100mm by 1mm circumferential crack.

For each leak type the flow and pressure raw data were used to estimate the leakage parameters for the power equation and the modified orifice equation respectively. The results obtained are consistent with previous experimental work done by van Zyl and Malde (2017), i.e. the round hole leak displayed a very small head-area slope, the circumferential crack also had a small negative head-area slope, and the longitudinal crack was found to have the largest head-area slope.

# 5 Field Tests

## 5.1 Introduction

The main objective of the field test is to assess the condition of bulk pipelines at various sites. The data obtained from the condition assessment equipment is used to characterise the extent of leakage in the pipelines. In particular, the size, type and crack length of the leak will be estimated.

Before any field tests are carried out, some comprehensive planning is done in consultation with the pipeline asset manager and their teams. In most cases, the test pipelines are operational, and have to be temporarily decommissioned for the duration of the tests. This means that any potential interruptions to consumers have to be identified and the affected consumers must be informed accordingly before the tests are carried out.

The names and location of the various pipes that were tested in this study are given Table 5-1. The Pretoria tests were carried out with the assistance of a Masters student also carrying out research in the field of leakage, at the University of Cape Town. The Cape Town tests were carried out under the supervision of Prof Kobus van Zyl.

*Table 5-1: Summary of the tested pipelines and their respective locations in South Africa*

<b>Pipeline name</b>	<b>Location</b>
Simon Vermooten to Murrayfield Reservoir	Pretoria
Lynwood Road to Koedoesnek Reservoir	Pretoria
Garsfontein to Parkmore High Level	Pretoria
Brickfields and Constantia Reservoir	Pretoria
Fort Klapperkop Reservoirs to Carine	Pretoria
BS 8 Pipeline- Test 1	Cape Town
BS 8 Pipeline- Test 2	Cape Town
Wingfield Test 1	Cape Town
Wingfield Test 2	Cape Town
Wingfield Test 3	Cape Town
UCT pipeline	Cape Town



## 5.2 Field test procedure

The field tests always start with a site inspection prior to testing the pipeline. The site inspection entails a survey of the pipeline network to be tested. As-built drawings of the pipeline network are requested before the survey is carried out. The as-built drawings are used to map and locate various pipeline infrastructure accessories that are critical to successfully carry out the tests. Notably, these pipeline accessories, for the most part, include: isolation valves, fire hydrants and any alternative ideal points of connection to the pipeline.

Any discrepancies between the as built drawings and the pipeline on site are noted. Once the pipeline network is satisfactorily surveyed, a suitable pipeline in the network is identified for testing. The selected test pipeline ought to adhere to the following criteria:

- Have existing and functional isolation valves along the pipeline to isolate the pipe during the tests.
- Have a point of connection above or below ground, that links to the pipeline and is located between the two isolation valves, e.g. a fire hydrant
- Pipeline must have the least interruptions to supply when decommissioned for the tests.
- Pipeline should be accessible by the PCAE

Each criterion listed above is important in order to carry out the test successfully. In particular, the pipeline connection point and the capability of isolating the pipeline are paramount, because these capabilities are critical components of the test procedure carried out when using the PCAE.

The site inspections also provides the opportunity to ensure that all equipment necessary is available. Specifically, it is important to ensure that any connection apparatus required to connect the PCAE to the pipeline access point should be arranged.

The connection points can differ from one pipeline to another. For example, along a potential stretch of pipeline, the connection may include amongst others, fire hydrants, scour valves, air valves, or in some cases a combination of these. Regardless of the connection found on site, it is important to ensure prior the tests, a suitable adaptor is organized, that can conveniently

connect the PCAE to the pipeline connection point. In cases where multiple above ground pipeline connection options are available, it is best to opt for the most convenient.

With the assistance and consultation of the pipeline asset managers, information pertaining to the selected test pipe is gathered. This information consists of three aspects.

- Firstly, some details about the pipelines historic structural integrity.
- Secondly, information regarding guidelines and specifications about how the pipeline isolation valves and access points are operated on site.
- Finally, information regarding all stakeholders who are potentially affected when the test pipe is decommissioned during the test, and sending out letters of notice to inform all affected stakeholders.

A Microsoft Excel spreadsheet was designed to analyse the PCAE data obtained from each test. The spreadsheet consists of multiple workbooks with the following details: the equipment information, test site information, test pipeline elevation profile, leak test pressure and flow data, head loss analysis and the leakage parameters. Appendix 10.2 illustrates the spreadsheet for one of the pipelines.

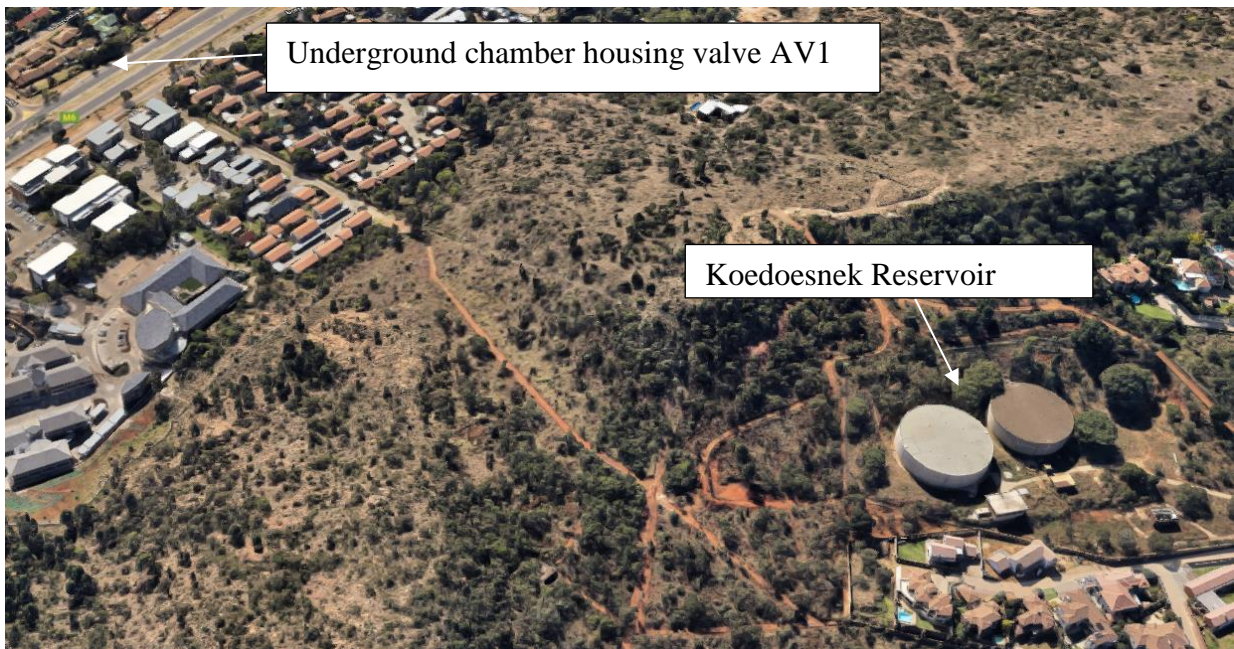
## **5.3 Lynnwood Road to Koedoesnek reservoir pipeline**

### **5.3.1 Introduction**

The examined steel bulk pipeline- hereafter referred to as the Lynnwood to Koedoesnek pipeline (LK pipeline) - connected the main pipe on Lynwood road to the Koedoesnek Reservoir. The reservoir then supplies a section of the City of Tshwane. The main characteristics of the FS pipeline were: Length = 707m, and the diameter of the pipes = 500mm.

The LK pipeline layout is shown in Figure 5-1, starting at the isolation valve (AV1), which was pressurised by gravity to a pressure of at least 10 bars, then the pipeline consistently rises to the final isolation valve (V2) just before the Koedoesnek reservoir which is on a hill. The elevation difference between valve AV1 and V2 was of approximately 50 meters. The PCAE was in the chamber that housed valve V2.





*Figure 5-2: Google earth image of the location of chamber housing valve AV1 and the Koedoesnek reservoir*

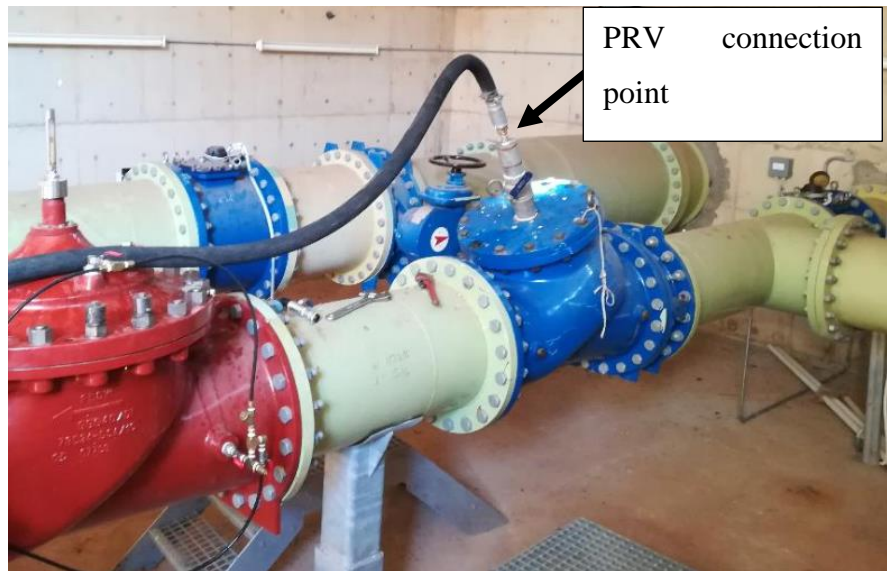
Figure 5-3 shows a google earth close up configuration of the Koedoesnek Reservoirs and the chamber with the PRV's and isolation valve V2. The chamber had three pressure regulating valves (PRV's), and the isolation valve V2 was just downstream of the PRV's (and upstream of the reservoir).



*Figure 5-3: Google earth image of reservoir configuration*

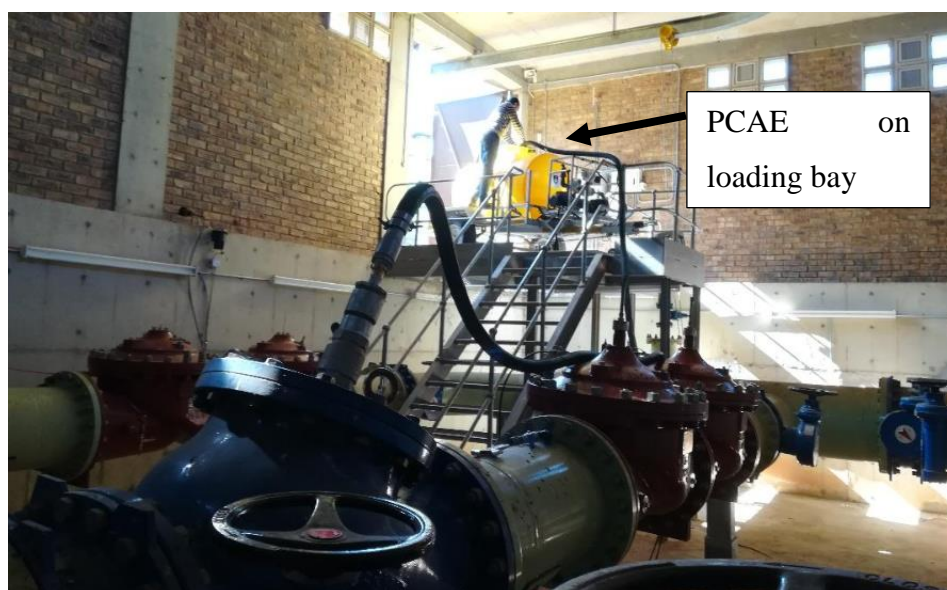
### 5.3.2 Leak test procedure

The PCAE was connected to one of the PRV's at the Koedoesneck reservoir chamber. The PRV had a connection stop valve point, as shown in Figure 5-4.



*Figure 5-4: Connection of testing equipment*

The PCAE trailer was pushed into the loading bay of the chamber in order for the PCAE hosepipe to reach the water tank, as illustrated in Figure 5-5.



*Figure 5-5: PCAE setup with trailer in loading bay*

The tank was filled by opening the stop valve at the connection point. The flow into the tank was observed to be strong and unobstructed. Once the tank was full, the stop valve was closed and the next step was to isolate the LK pipeline by closing valve AV1 and V2, shown in Figure 5-1.

The first valve to be isolated was valve AV1 that was housed in a concrete chamber. Upon arrival at the chamber, it was noticed that valve AV1 was submerged in water because the chamber was flooded. A team from the Tshwane Metropolitan Municipality was arranged to pump the water out of the chamber, using a petrol pump. This process took about an hour. After the chamber was emptied, valve AV1 was then closed. A leak on a coupling was identified to be responsible for the flooded chamber. The leak was however, on the supply side of the isolation valve and not on the LK pipeline that was tested. The isolation valve AV1 appeared to seal effectively. The next valve to isolate was valve AV1, which also appeared to seal effectively.

It was evident that the LK pipeline was already depressurising after isolating the pipeline. A slight suction of air into the rubber hose, which was still connected to the LK pipeline, was observed suggesting that the pipeline was isolated.

The hosepipe was then connected to the PCAE and the pump was activated at maximum pressure. The pressure was then dropped at increments of 0.5 bars up to 1.5 bar, and the flow was allowed to stabilise for each pressure step. Thereafter, the pressure was increased at increments of 0.5 bar.

### **5.3.3 Leak test results**

#### ***5.3.3.1 Data analysis procedure***

The LK pipeline was analysed as a pipeline rising from the bottom isolation valve AV1, on the delivery line, to the reservoir, as shown in Figure 5-7. The maximum vertical difference between the bottom and top of the pipeline was 90 meters and the horizontal distance from the bottom isolation to the top of the pipe was evaluated to be 706m.

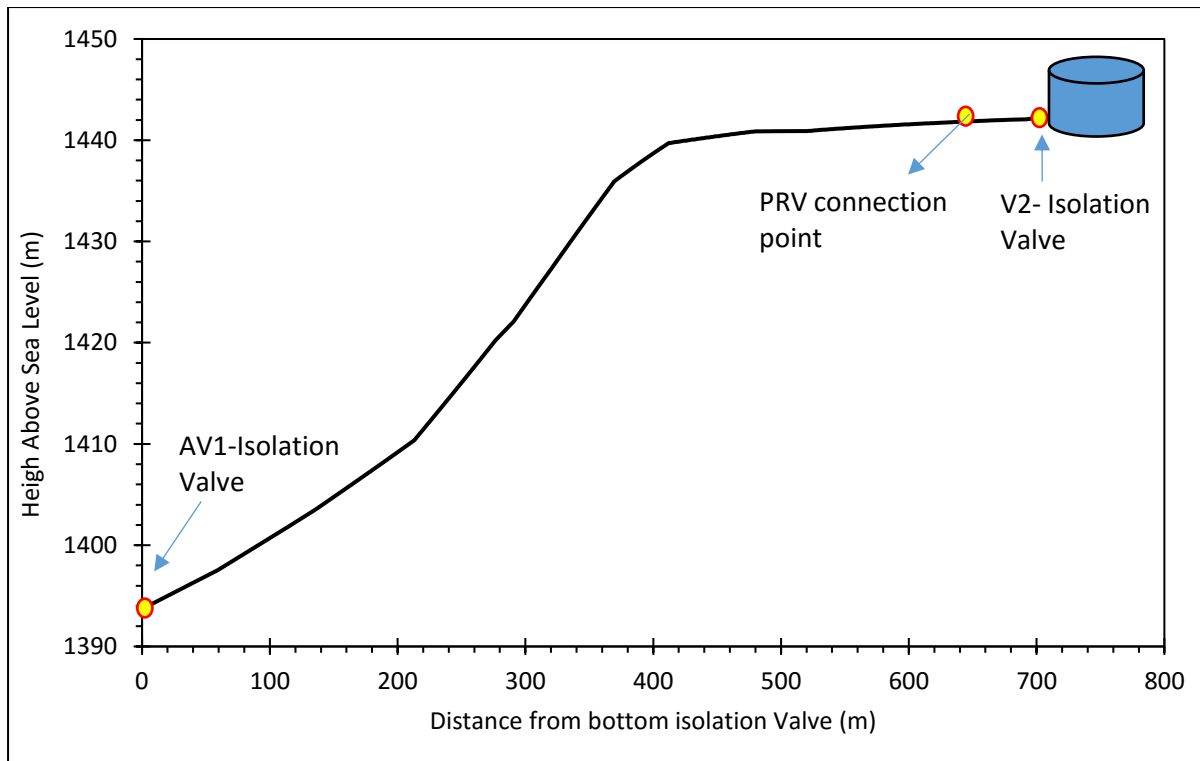
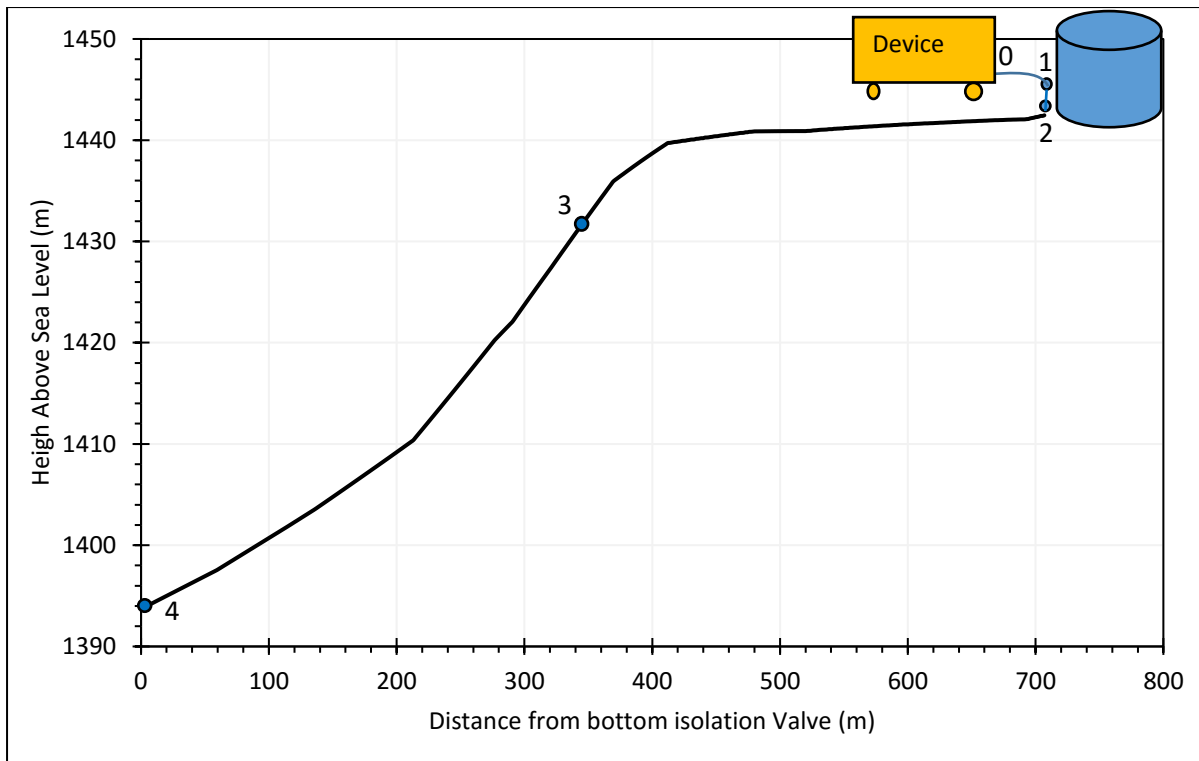


Figure 5-6: Elevation profile of the LK pipeline

Nodes were assigned at various points along the pipeline as shown in Figure 5-7. Node 0 to node 1, represented the hosepipe connecting the PCAE to the LK pipeline. Node 1- 2 represented the stop valve on the PRV onto which the PCAE hosepipe was connected to access the pipeline. Node 2-4 are points along the pipeline, of which node 2 represents the highest point, node 3, is an intermediate, and finally node 4 is a node at the bottom of the pipeline.

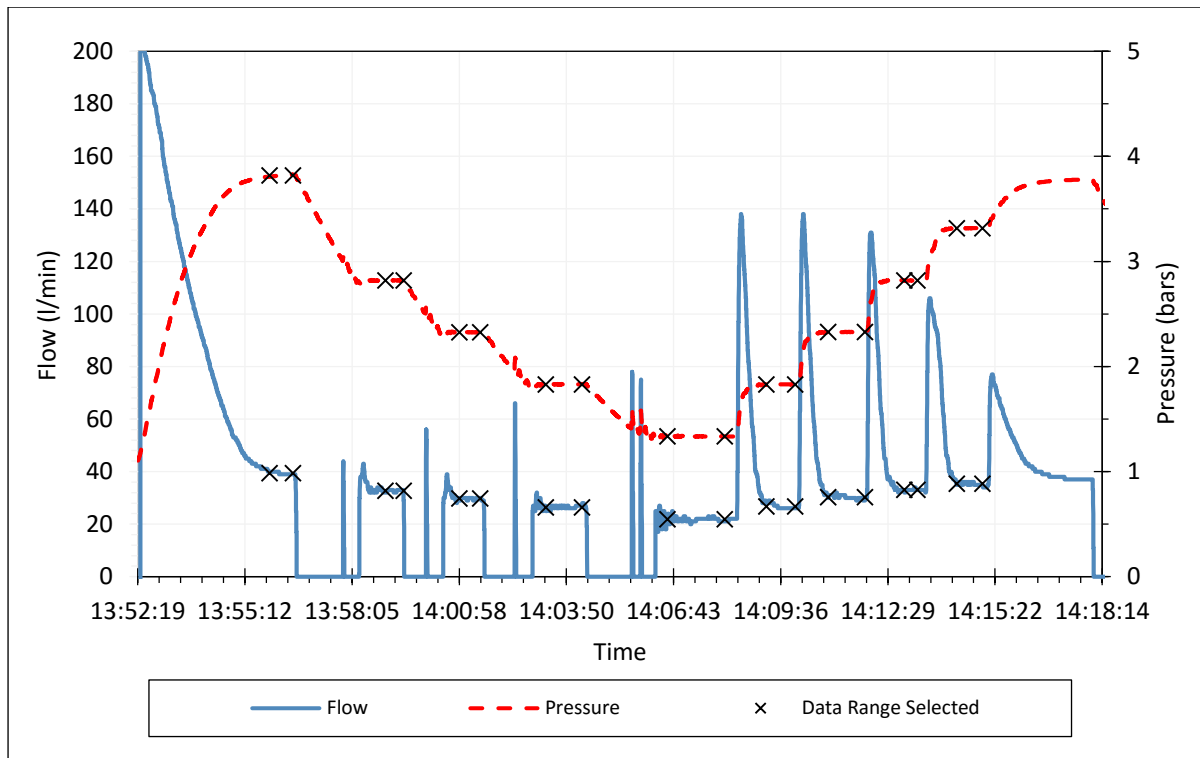


*Figure 5-7: Elevation profile with nodes for the LK pipeline*

### **5.3.3.2 Data interpretation**

The raw flow and pressure data obtained from the PCAE recorder is plotted against time in Figure 5-8. Considering that the pressure before the isolation valve AV1 on the delivery line was more than 10 bars, the fact that the pressure could be controlled demonstrates that the isolation valves sealed properly. As can be seen from the figure, the pressure was dropped at increments of 0.5 bars, and a flow rate was detected, suggesting that a leak exists in the pipeline. The leakage flow rate was then allowed to stabilise before another pressure increment was set.





*Figure 5-8: Flow and pressure raw data for the LK pipeline*

A clear relationship between the leakage flow rate and pressure was evident in the data. The graph clearly shows a step down and step up pattern repeated for both data sets. The stabilised data range of each step was used for further analysis. The selected stabilised range of the pressure and flow rate is shown by the cross markers.

The pressure and flow data in Figure 5-9 represents the data measured by the pressure sensor and magnetic flow meter of the device. Using Bernoulli's principal the pressure was adjusted for the various nodes in order to obtain the actual pressure at each node. The flow rate was presumed to be the same throughout the pipeline, because of the conservation of mass. Table 5-2 shows a summary of the adjusted pressures for each node.

*Table 5-2: The averaged stabilised flow and pressure data for each node*

Flow rate, Q	h at node 0	h at node 1	h at node 2	h at node 3	h at node 4
$1.01 \times 10^{-03}$	28.31	30.07	30.64	35.45	74.79
$9.35 \times 10^{-04}$	23.34	25.11	25.71	30.52	69.86
$8.50 \times 10^{-04}$	18.24	20.03	20.67	25.48	64.82
$7.71 \times 10^{-04}$	13.24	15.04	15.70	20.51	59.85
$8.51 \times 10^{-04}$	18.26	20.04	20.68	25.49	64.83
$9.34 \times 10^{-04}$	23.33	25.10	25.71	30.52	69.86
$1.01 \times 10^{-03}$	28.32	30.08	30.65	35.46	74.80
$1.09 \times 10^{-03}$	33.35	35.09	35.63	40.44	79.78

It can be seen from Table 5-2 that the highest pressures occurred at node 4, followed by node 3, then node 2, node 1, and the smallest pressure was at node 0. The highest pressure occurred at node 4 because this was the lowest node on the pipeline. The average pressure difference between the measured pressure and the pressure at node 4 was approximately 46m.

Since the objective of the analysis was to evaluate the leakage characteristics on the pipeline, only node 2, node 3 and node 4, that were located on the pipeline, were analysed further.

### ***5.3.3.3 Leakage parameters for the power equation***

Figure 5-9 shows the graph of flow rate plotted against pressure head for nodes 2, 3 and 4 on the LK pipeline. A power equation was fitted to the data for each node. It can be seen that the power equation fits all data well. The data was then used as a basis for calculating power equation leakage parameters.

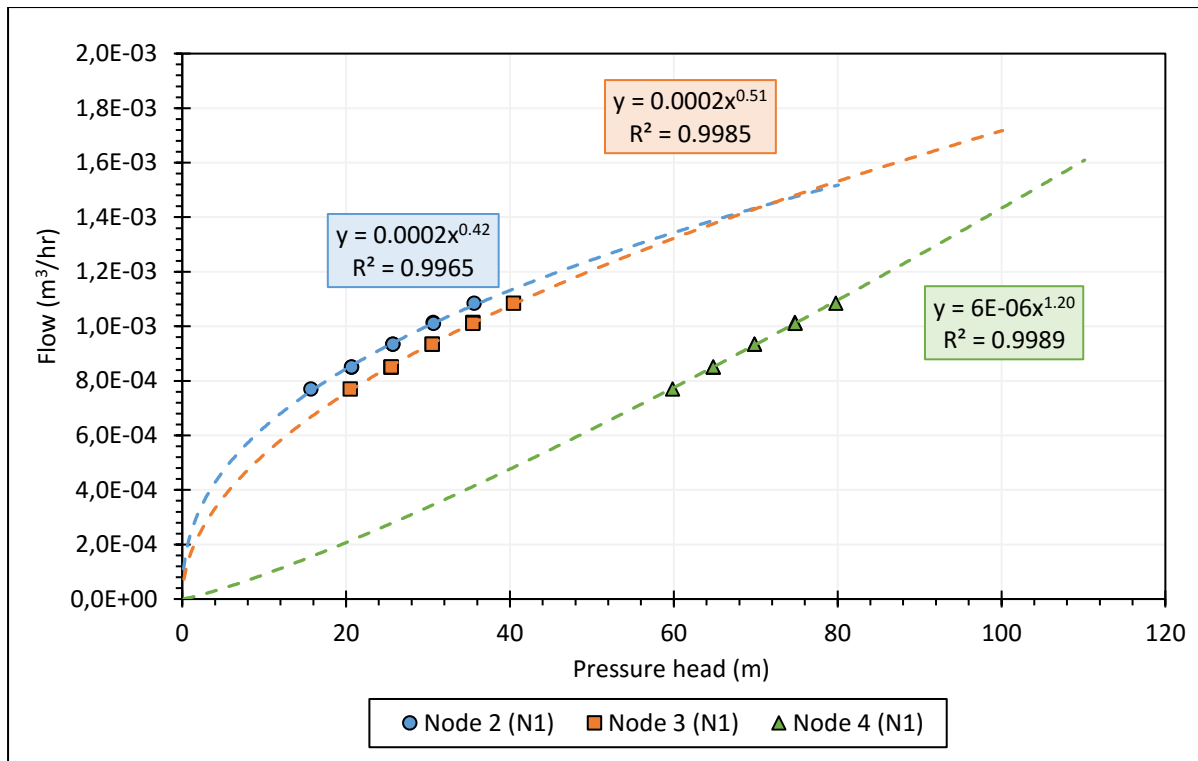


Figure 5-9: Flow against adjusted pressure head graph with power function fitted for the circumferential crack for node 2, 3 and 4

The results in Figure 5-9 shows some variation in the leakage exponent, with the leakage exponent generally increasing with decreasing elevation. It can be seen that Node 2, at the highest elevation, had the smallest leakage exponent of 0.42, whilst Node 4, at the bottom of the pipeline, had the highest leakage exponent of 1.20. Node 3, the intermediate node, was found to have a leakage exponent of 0.51, which lies between 0.42 and 1.20. The results of the N1 leakage parameters obtained from the power equation in Figure 5-9 for node 2, 3 and 4 are summarised in Table 5-3.

Table 5-3: Summary of power equation leakage parameters for node 2, node 3 and node 4

Node	Leakage Coefficient, C	Leakage Exponent, N1
2	$2 \times 10^{-4}$	0.42
3	$2 \times 10^{-4}$	0.51
4	$6 \times 10^{-6}$	1.20

In practice, rigid pipes, such as the steel that was tested, are typically assumed to have N1 values of 0.5, as illustrated by the result obtained for node 3. However rigid pipes with extensive corrosion may have greater N1 values, such as the result found at node 4, suggesting

that the pipeline could be experiencing some moderate to extensive corrosion damage at this node (Greyvenstein & van Zyl ,2005). On the other hand, the leakage exponent result substantially less than 0.5, found at node 2, is an unlikely result for a rigid pipe, and thus could be an indication that there is no leak at this node.

### 5.3.3.4 Leakage parameters for the modified orifice equation

The effective leak area ( $C_dA$ ) was plotted against pressure head as shown in Figure 5-10. A straight line was fitted to the data in order to obtain the effective head-area slope ( $C_d m$ ) and the effective initial leak area ( $C_d A_0$ ) from the gradient and intercept terms of the equation respectively. It can be seen that the linear equation fits the data points very well, with an  $R^2$  of 0.99.

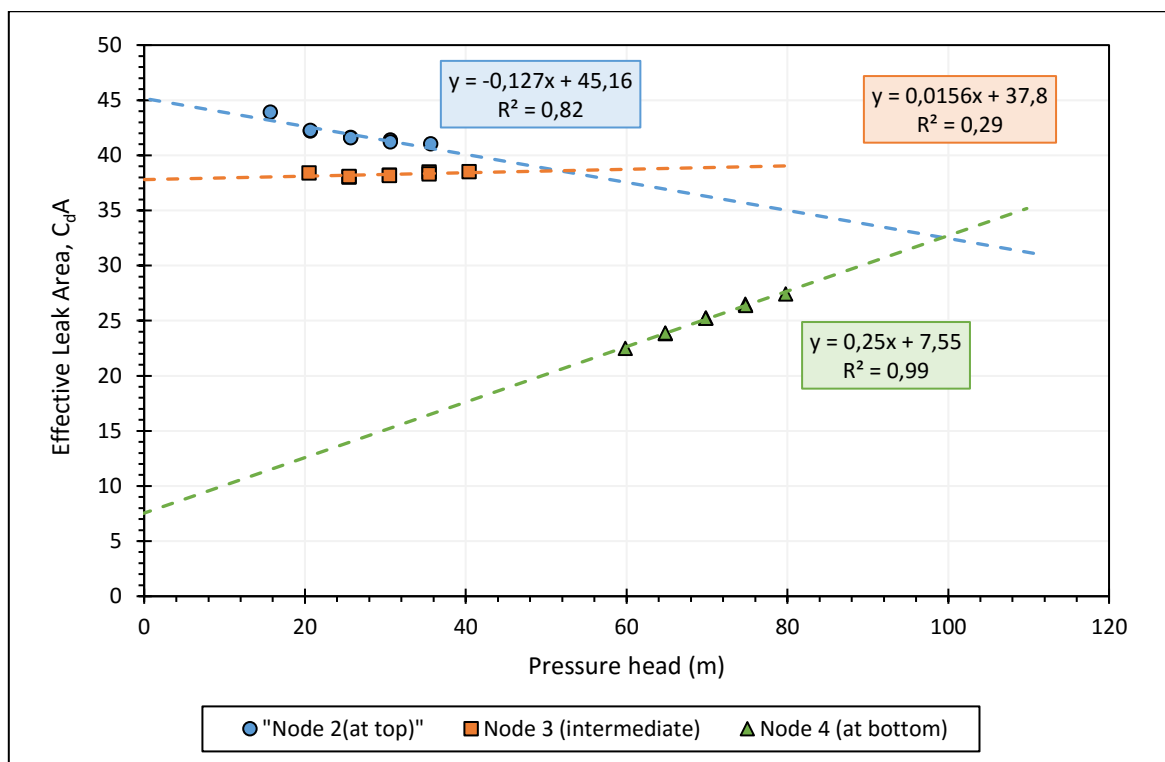


Figure 5-10: Effective leak area against pressure for node 2, 3 and 4 on the LK pipeline

The results in Figure 5-10 show that the modified orifice equation leakage parameters varied for the three nodes investigated. It can be seen that node 2 displayed a negative effective head-area slope, suggesting that the leak area decreased with increasing pressure. Nodes 3 and 4 both displayed a positive effective head-area slope, suggesting that the leak area increased with

increasing pressure. The modified orifice equation results for the pipeline are summarised in Table 5-4.

*Table 5-4: Summary of modified orifice equation leakage parameters for the LK pipeline*

Node	Effective Initial leakage area, $A'_0$ (mm <sup>2</sup> )	Effective head-area slope, $m'$ (mm <sup>2</sup> /m)	Leak Characteristic
2	45.2	-0.13	Circumferential crack
3	37.8	0.016	Round hole
4	7.55	0.25	Longitudinal crack

The results shown in Table 5-4, show that if all the leakage occurred at node 2, then the leak could be characterised as a circumferential crack with an effective initial crack area of 45.2 mm<sup>2</sup> that reduces by 0.13 mm<sup>2</sup> per meter of pressure subjected to the pipeline. This leak type is unlikely to occur on a steel pipeline, because typical failure modes for steel pipes have been found to be predominantly corrosion failure, and in some cases longitudinal cracks, but hardly circumferential cracks (Greyvenstein & van Zyl, 2005).

The results obtained for node 3, show that if the leakage occurred at node 3, then the leak could be characterised as a round hole leak, that may occur due to corrosion. This is mainly due to the small head-area slope of 0.016 mm<sup>2</sup> per meter of pressure subjected to the pipeline. The initial leak area of the round hole was estimated to be 37.8 mm<sup>2</sup>.

Finally, the results for node 4, shows that if the leakage occurred at node 4, then the leak type could be characterised as a longitudinal crack; with an initial crack area of 7.55 mm<sup>2</sup> which expands by 0.25 mm<sup>2</sup> per meter of pressure subjected to the pipe. This result is characteristic to a longitudinal crack because of the positive head-area slope that is greater than 0.1mm<sup>2</sup>/m (Malde & van Zyl, 2015)

The leakage flow rate,  $Q$ , from the pipe at each node, can be predicted for different pressures in the pipeline using the modified orifice equations developed using the results in Table 5-4, as follows:

For node 1:

$$Q_{at\ node\ 2} = \sqrt{2g}(45.2 h^{0.5} - 0.13 h^{1.5}) \times 10^{-6}$$

*Equation 5-1*

For node 2:

$$Q_{at\ node\ 3} = \sqrt{2g}(37.8 h^{0.5} + 0.016 h^{1.5}) \times 10^{-6}$$

*Equation 5-2*

And for node 3:

$$Q_{at\ node\ 4} = \sqrt{2g}(7.55h^{0.5} + 0.25 h^{1.5} ) \times 10^{-6}$$

*Equation 5-3*

## **5.4 Simon Vermooten to Murrayfield Reservoir Pipeline**

### **5.4.1 Introduction**

The examined steel bulk pipeline – hereafter referred to as the Simon Vermooten to Murray pipeline (SVM pipeline) - connects a main pipe on Simon Vermooten Road to the Murrayfield reservoir in Pretoria. The main characteristics of the pipeline are: Length = 1460m and pipe diameter = 500mm.

The SVM pipeline layout is shown in Figure 5-11 starting at isolation valve AV1, and then consistently rises, following the road, via an intermediate isolation valve (V2) to the final isolation valve (V3). The pipeline is pressurised by gravity to 17 bars downstream of isolation valve AV1. The elevation difference between valve AV1 and V3 is approximately 90 meters.

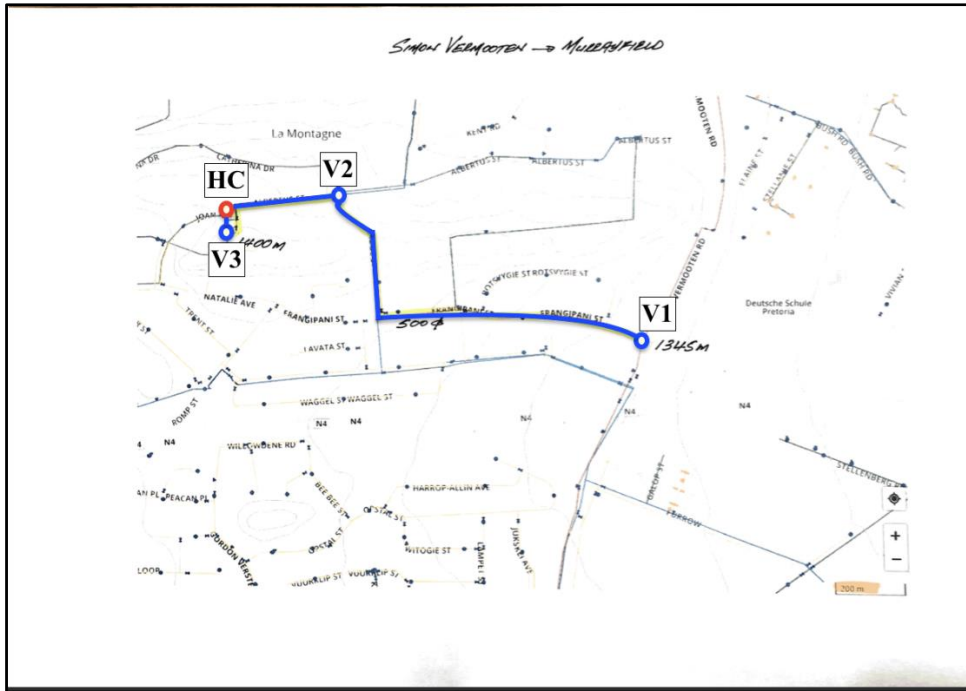


Figure 5-11: Layout of the SVM pipeline with the location of the valves.

A google earth image of the reservoir configuration, where isolation valve V3 and the connection point were located, is shown in Figure 5-12.

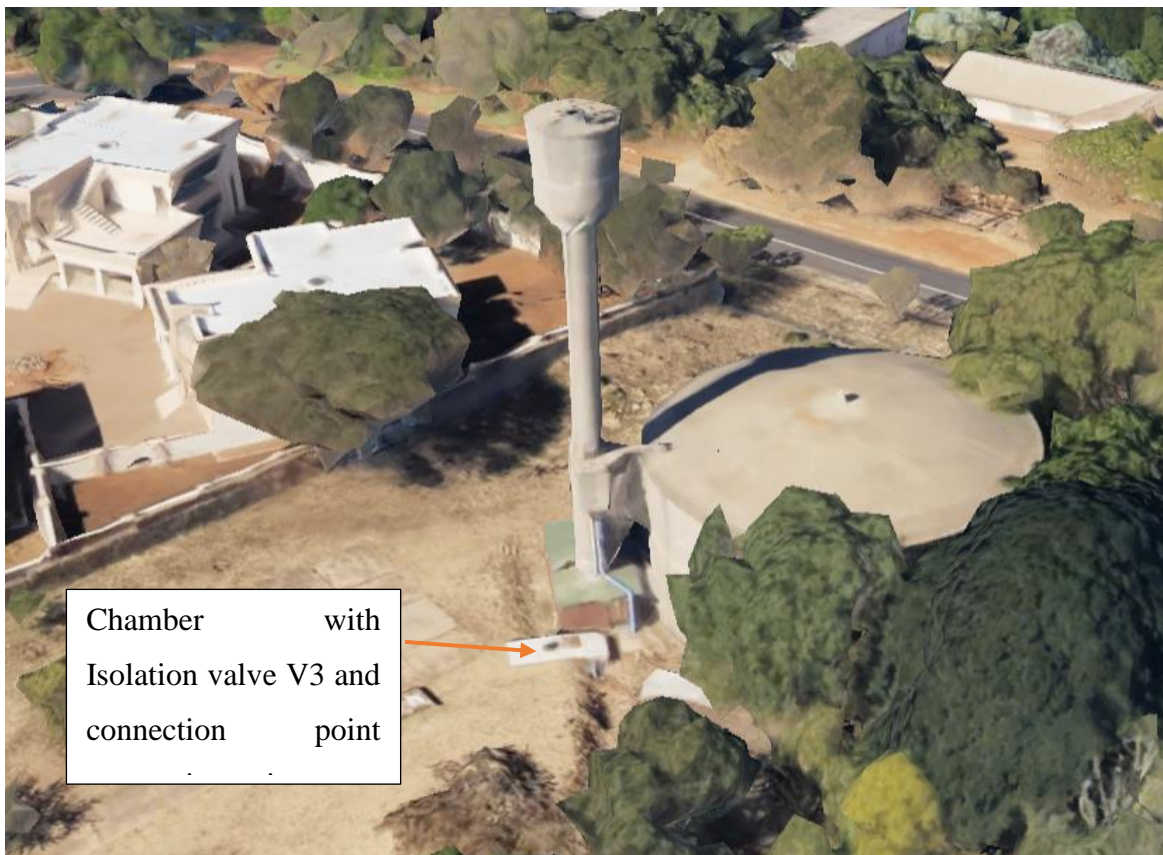


Figure 5-12: Google earth image of Murrayfield reservoir configuration

## 5.4.2 Leak Test Procedure

The operations team arrived on site after already having closed isolation valve 1. They were then instructed to open the valve again, so that the pipeline can operate as normal. This was important since the PCAE water tank was not yet filled.

After the valve, AV1, was opened, a suitable connection point to the pipeline was identified. The most suitable connection point turned out to be a 2.25-inch stop valve located in the chamber that housed isolation valve V3. Figure 5-12 shows the location of the concrete chamber. The PCAE water tank was then filled by means of a hosepipe that was connected to the 2.25-inch stop valve.

The pressure before isolating the SVM pipeline was measured to be around 7.7 bar. The operations team then closed valve V2, as well as valve V3. The SVM pipe was then connected to the testing equipment and a pressure of approximately 7.7 bars was again measured. This was an indication that the valve V2 was not isolating properly.

The operations team then opened valve V2 and closed valve AV1. In an attempt to depressurise the SVM pipeline, the PCWE hosepipe, which was connected to the connection point, was allowed to run freely to the atmosphere. The flow decreased up to a certain point, after which a constant flow was observed to continue flowing from the hose, as shown in Figure 5-13. This was a significant flow and was presumed to be because of the isolation valve AV1 not sealing properly.



*Figure 5-13: Constant flow observed after valve AV1 was closed*



The operations team then proceeded to close valve 2 as well. The flow from the hose pipe decreased further, but a significant flow still remained, presumably indicating that valve V2 was also not sealing properly.



*Figure 5-14: Constant flow observed after both valve AV1 and V2 were closed*

The hose pipe was then re-connected to the testing equipment and the pressure was measured. The measured pressure started at 3.5 bar and consistently increased to roughly eight bar, after which the pressure remained consistent. This was a similar pressure measured before the isolation valves were closed.

Because of the high pressure measured in the SVM pipeline, which exceeded the capacity of the testing equipment, the test could not be conducted.

### **5.4.3 Leak Test Results**

No results were obtained for this test. However, it was discovered that the SVM pipeline isolation valves to the supply line did not seal. Subsequently, the pressure in the pipeline equalised to the supply pressure after isolation.

In this case, even though the leak test was conducted on the highest point of the pipeline, the eight bars pressure measure at the highest point, still exceeded the capacity of the equipment, which was limited to 4.2 bars. Thus, the SVM pipeline could not be pressurised by the test equipment.

## 5.5 Garsfontein to Parkmore High Level reservoir pipeline

### 5.5.1 Introduction

The examined steel bulk pipeline- hereafter referred to as the Garsfontein to Parkmore High Level Reservoir pipeline (GP pipeline) – was pressurised by the national bulk water supplier, Rand Water to a pressure of at least 6 bars . The main characteristics of the pipeline were: Length = 2640m and the pipe diameter = 406mm.

The layout of the GP pipeline is shown in Figure 5-15, starting at the isolation valve AV1, located near the Garsfontein reservoir site. The pipeline then dips 60 meters down through a narrow valley and then rises to the Parkmore High Level reservoir. The final isolation valves, V2, V3 and V4 are located approximately 40 meters upstream of the Parkmore High Level reservoir. The pipeline is pressurised by a Rand Water line to a pressure of at least six bar.

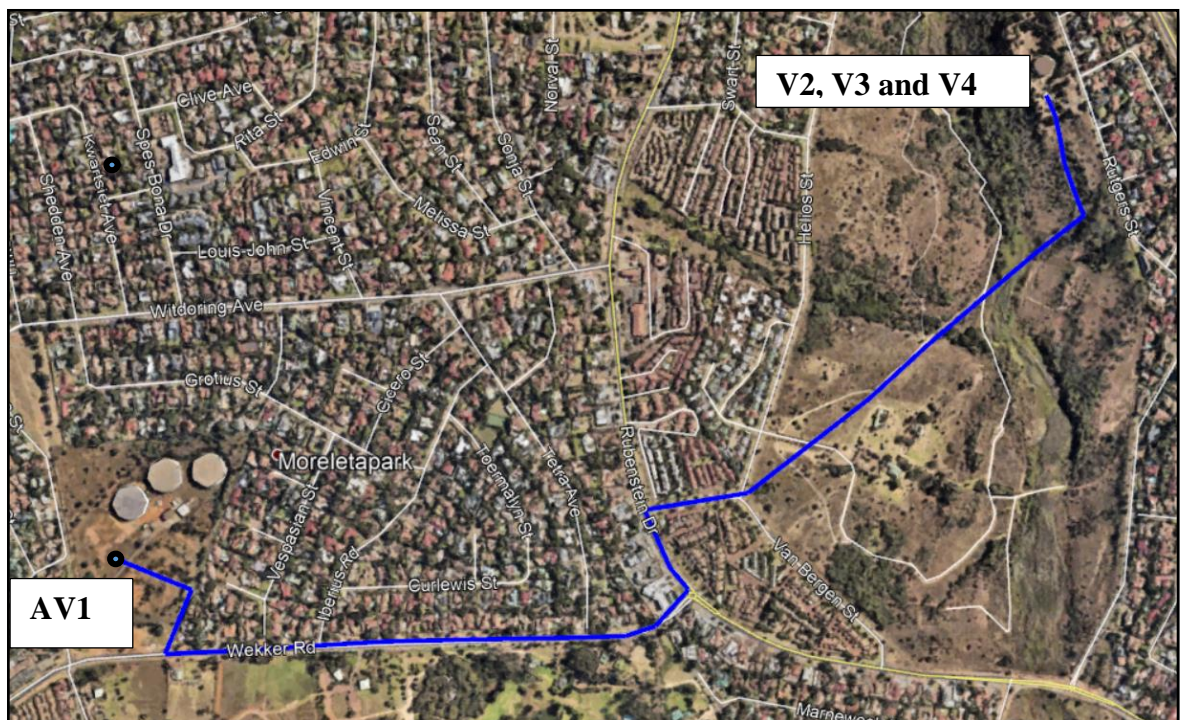


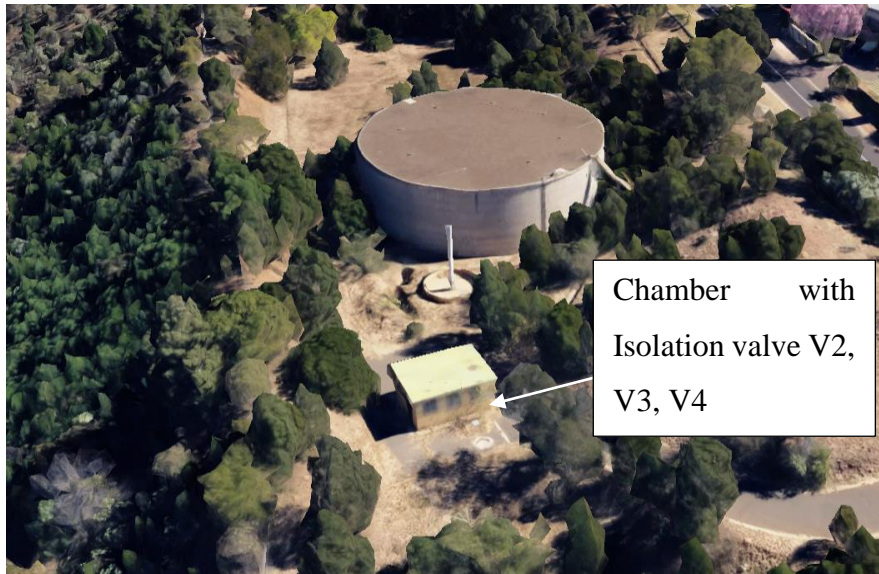
Figure 5-15: Map showing GP pipeline route starting at AV1 (5bar+) and ending at V2 (5 bar+)

A google earth image of the Garsfontein reservoir site configuration is shown in Figure 5-16, with the location of Isolation valve AV1, which was a PRV housed in an underground concrete chamber. By isolating this PRV, the pipeline was isolated from the main source supplying the pipeline.



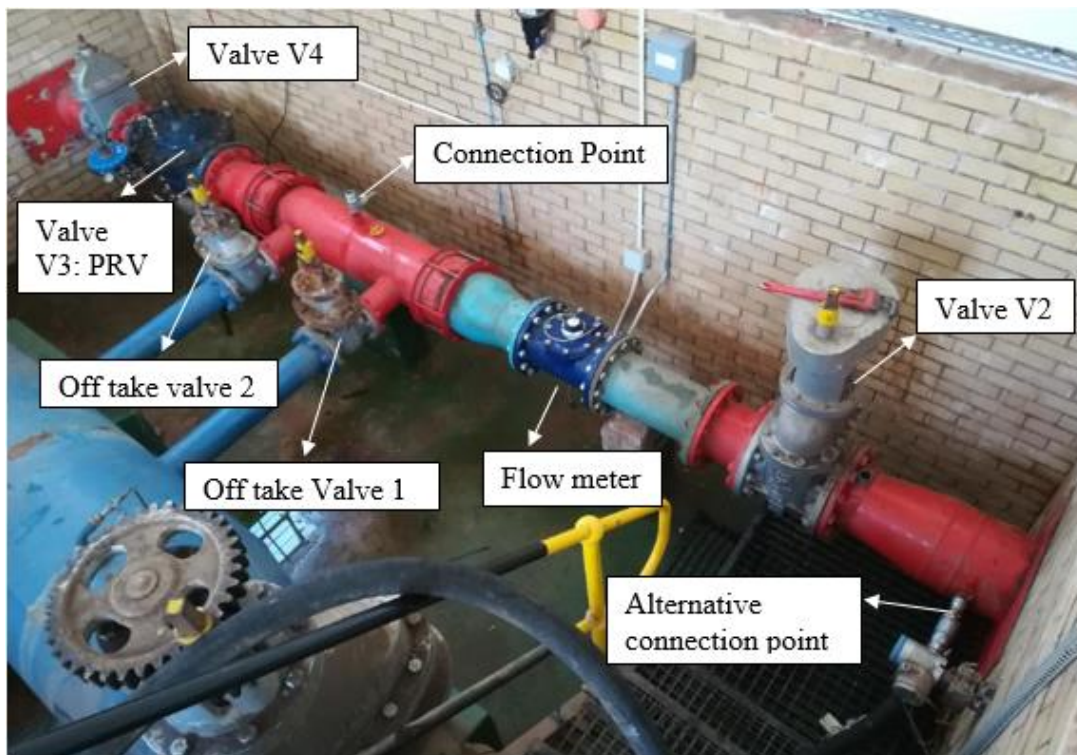
*Figure 5-16: Google earth image of Garsfontein reservoir setup*

Figure 5-17 shows the google earth image of the Parkmore High Level Reservoir, with the location of the chamber that housed isolation valve 2, isolation valve 3 and isolation V4. This chamber was also, where the device was connected.



*Figure 5-17: Google earth image of High Level reservoir configuration*

Figure 5-18 shows the setup in the chamber-housing valve V2, V3 and V4. From Figure 5-18, it can be seen that isolation valve V2 was a gate valve, V3 was a PRV and V4 was another gate valve. There were some apparatus installed on the pipeline, and these included; a flow meter, as well as, two off-takes supplying to a distribution network from the reservoir.

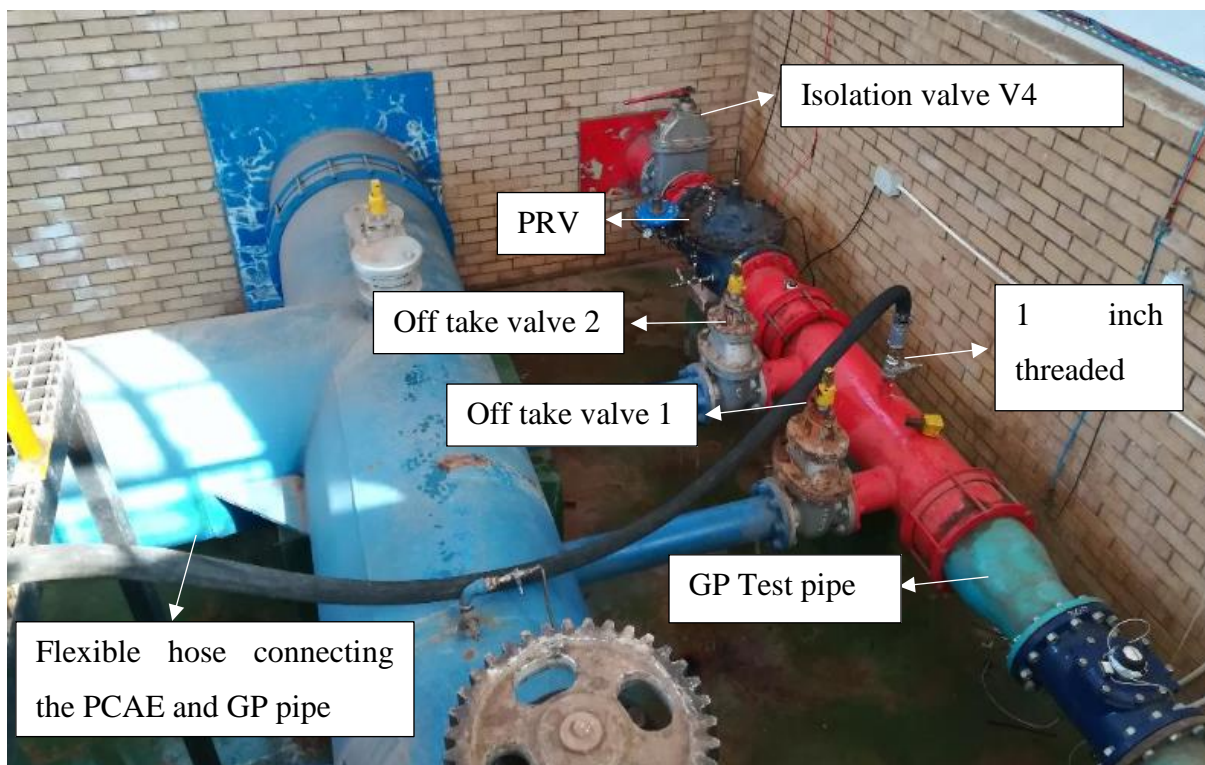


*Figure 5-18: Chamber housing valve V2, Valve V3, valve V4 and other apparatus installed on the GP pipeline*

## 5.5.2 Leak test procedure

The tests began at the Garsfontein reservoir, where the operator closed isolation valve AV1 (PRV). According to the operator, the PRV valve closed effectively and no sign of leakage through the valve was observed or heard.

The PCAE was connected to the GP pipeline via the 1 inch threaded connection installed on the main pipe, as shown in Figure 5-19. The PCAE water tank was then filled, and after filling the tank, isolation valve V4 (also shown in Figure 5-19) was closed. The two valves on the respective off-takes were already closed on arrival. These two off take valves were apparently never operated, and the operational team was certain that they did not leak.



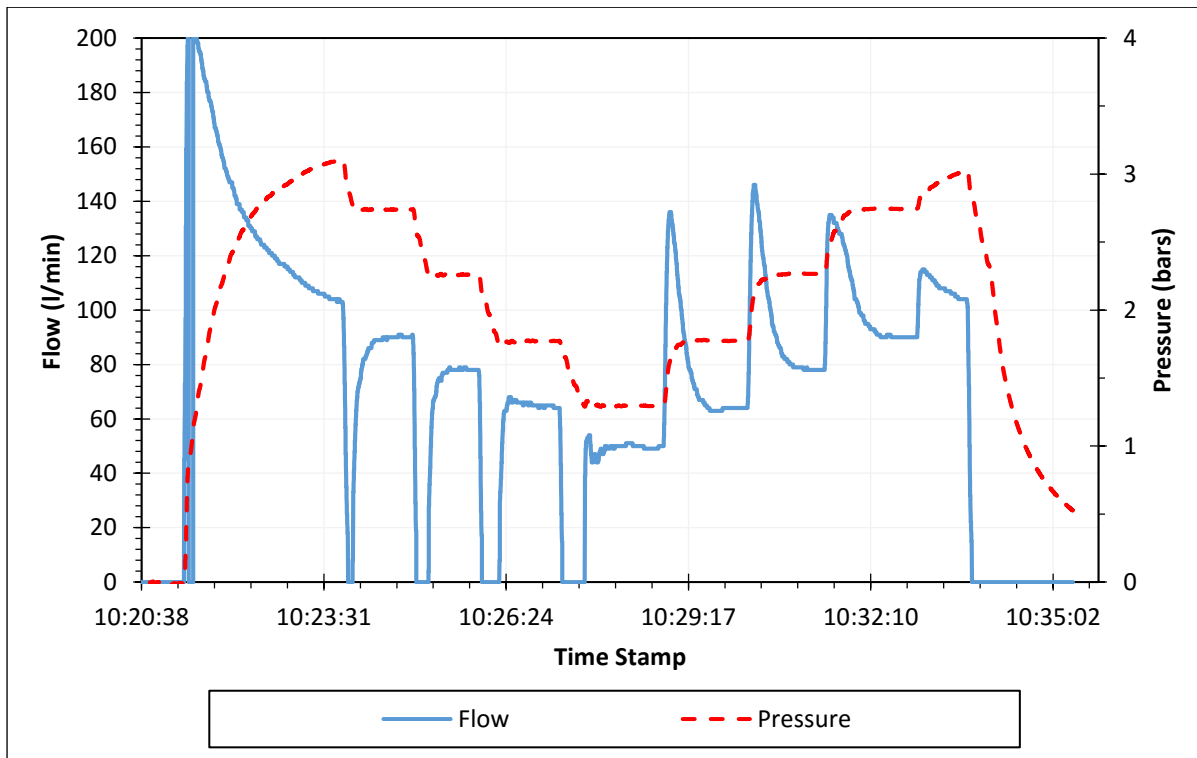
*Figure 5-19: Connection of testing equipment*

After isolating the GP pipeline, it appeared as if air was being sucked into the flexible hose, indicating that the GP pipeline was draining. Consequently, it was assumed that the isolation valves AV1 and V4 sealed the GP pipeline effectively.

The variable speed pump was then activated to pressurise the GP pipeline and commence the first leak test. The pump was set to the maximum pressure, which went up to of 3.1 bars, as

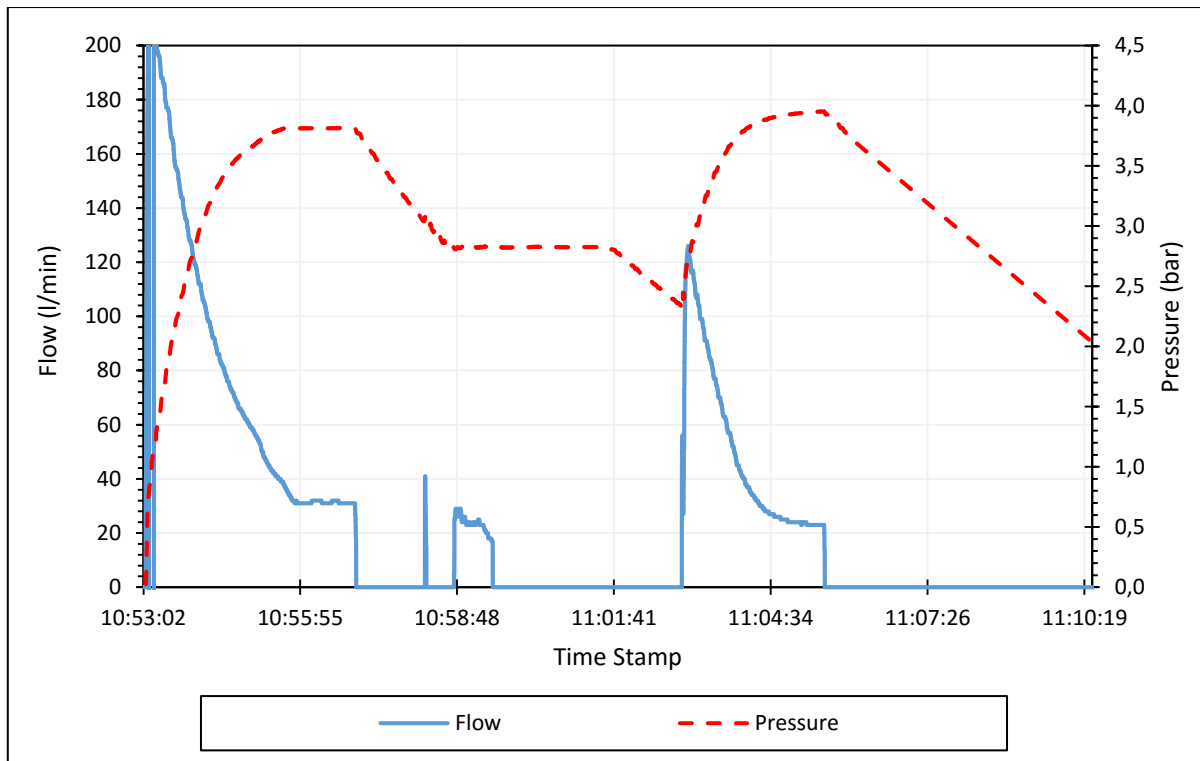
shown in Figure 5-20. Thereafter, the pressure was dropped at increments of 0.5 bars from 3.1 bars to 1.2 bars and then increased again incrementally by 0.5 bars.

A very clear leak was detected, and the leaked appeared to be pressure dependent, as the flow rate pattern was consistent with the pressure pattern. The PCAE water tank eventually emptied after about 15 minutes of testing.



*Figure 5-20: Flow and pressure raw data for the GP pipeline -first attempt*

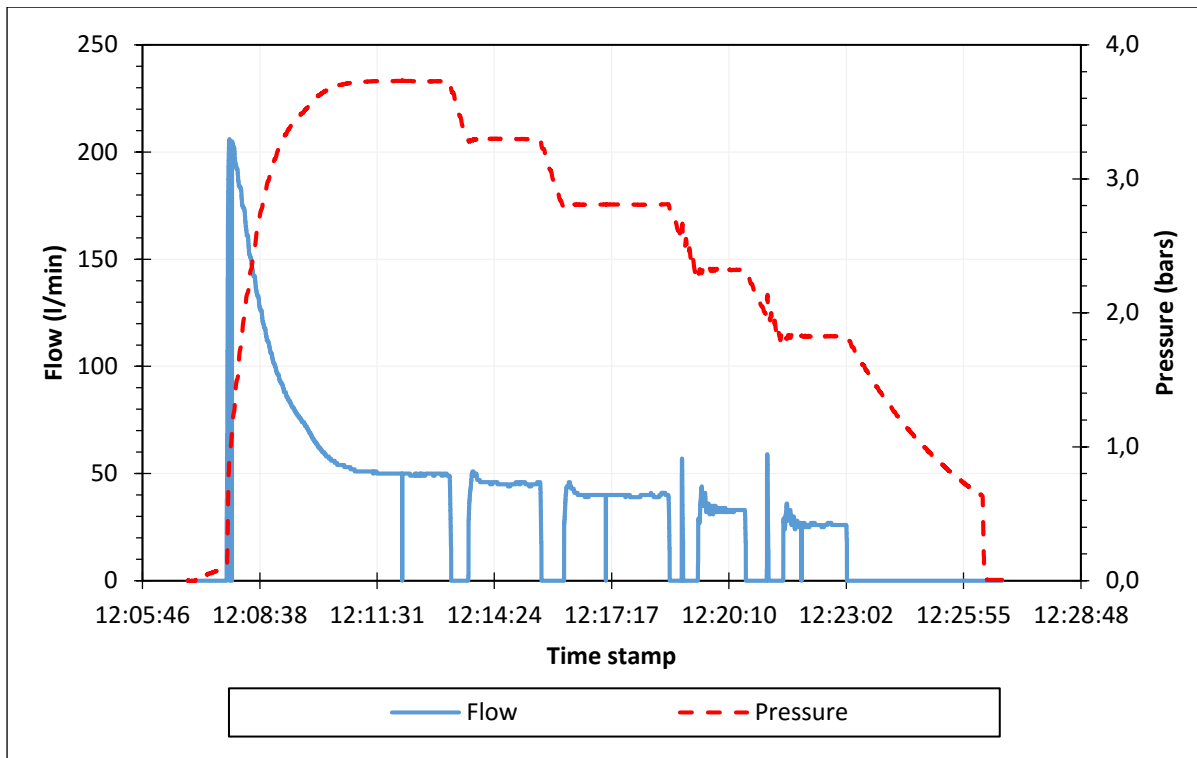
It was then decided to repeat the test. Valve V4 was then opened again in order to fill the PCAE water tank, and then closed again after the tank was full. The test was repeated, approximately 20 minutes later. It was immediately evident that the leakage drastically reduced with very different results from the first test, as shown by Figure 5-21. The flow and pressure did not stabilise very well.



*Figure 5-21: Flow and pressure raw data for the GP pipeline-second attempt*

The maximum pressure went up to 3.8 bars and was dropped by one bar, and the pressure was allowed to stabilise. It was also noted that the leakage was not very pressure dependant. It was unclear why the results were different because the pipe was isolated by closing valve AV1 and valve V4, as was done in the first attempt. It was also not clear where the leakage flow in the initial test (Figure 5-20) went to, as the pressure upstream and downstream of the GP pipeline was higher than 5 bar, meaning that, should any leak have occurred at the valves, the flow would have been into the GP pipeline and consequently the device would not be able to pressurise the pipeline.

Because of the inconsistency between the first two attempts, the test was repeated an hour later. An attempt was made to close the PRV (valve V3) as well, but due to the low flow and isolation of the pipe, it is not clear whether the PRV closed completely. The results of the third test attempt, illustrated in Figure 5-22, still did not match the first test.



*Figure 5-22: Flow and pressure raw data for the GP pipeline-third attempt*

It was still unclear why the test results were different because the only change between the initial two tests was the opening and closing of the control valve, and fidgeting of one of the two bypass valves that were already closed.

To investigate this inconsistency further, the hosepipe was disconnected in order to check whether there was any flow coming out of the test pipe via the connection point. A small inconsistent outflow was observed flowing out of the connection point. It appeared as if the flow was alternating between an outflow and inflow through the connection point.

A number of possibilities as to why the consistency occurred are discussed next:

- Possibility 1:

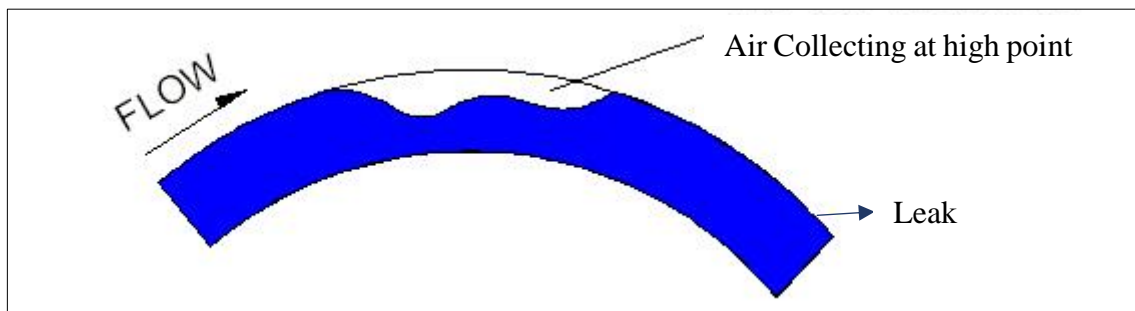
It was possible or likely that water was drawn off from the main pipeline, possibly by an illegal connection, but the operators believed this would be highly unlikely.

- Possibility 2:

As the pipe drains, after the isolation valve at Garsfontein and the supply from the reservoir was isolated, air was sucked into the pipe in order to compensate for the volume of water



leaving the pipe through a leak. When the supply to the reservoir was opened again, an air lock could have formed in the pipeline and collect at a high point as illustrated in Figure 5-23.



*Figure 5-23: Showing air pocket collecting at a high point in a pipe*

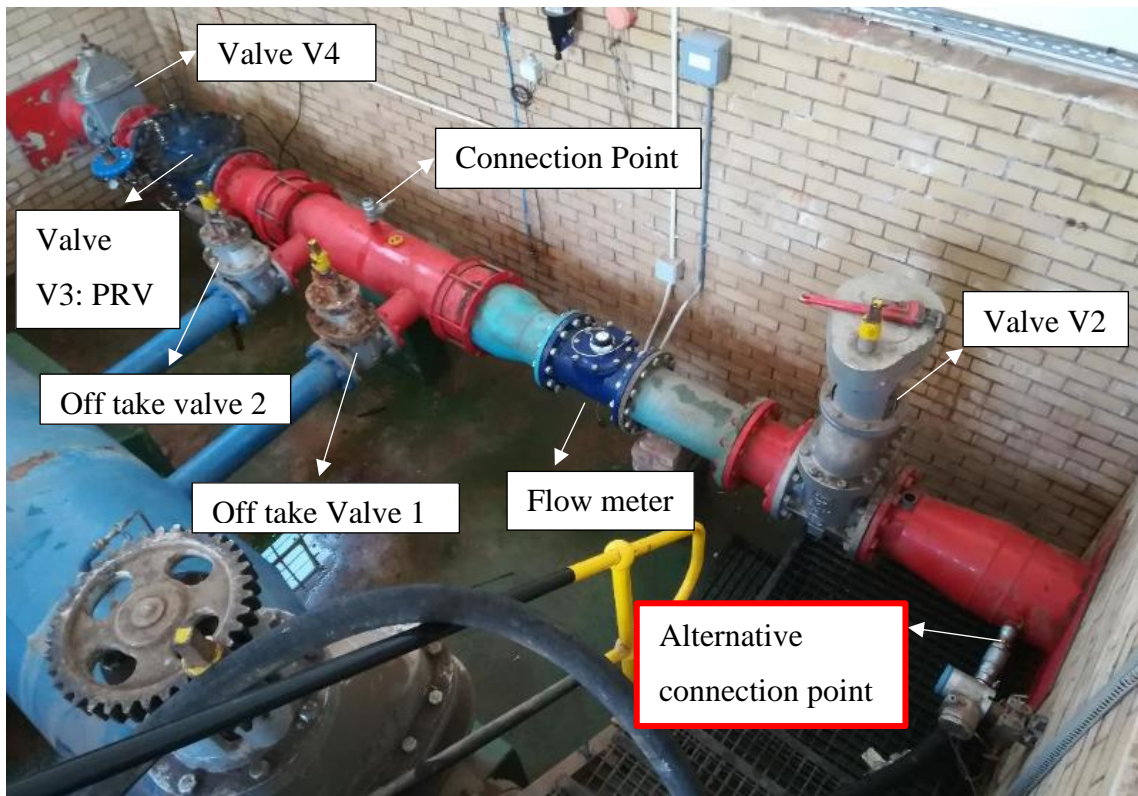
Note the associated reduced pipe diameter because of the air pocket in Figure 5-23. Water will trickle over the elbow and fill the pipe from the other side. If the leak is on the downstream side of the pipeline, then the water level on the other side will continue to drop due to the downstream leak.

As the pressure is increased, the level before the elbow rises due to the compression of the air. This possibly results in a higher flow rate over the bend. It would therefore appear as though water was lost through a leak, yet most of the flow is only filling the pipeline and compressing air.

- Possibility 3:

The third and final possibility explains why the first attempt experienced a high leakage rate, and then much lower leakage. This could have happened because air was sucked into the pipe through a small leak in order to replace the volume lost through the larger leak downstream. Then, as the pipe was pressurised, the air was forced back out through the same leak through which it entered. The flow rate of air through a leak was, however, much higher than water. Therefore, while the leaking of air contributed to the replacement of water pumped into the pipe, it appeared as if there was a huge leak. Once all the air was out, the rate reduced, as water will not leave the pipe at the same rate.

Due to the uncertainty about leaking valves, and the large number of valves on the tested pipe, it was decided to repeat the test by isolating the pipe with valve V2, rather than the PRV valve or valve V4. This effectively ensured that ineffective isolation of the off-take pipes would not influence the results.



*Figure 5-24: Alternative connection point – in red*

A close up image of the alternative connection point is shown in Figure 5-25. The alternative connection point was a 1.25-inch connection point. The tank was filled from this alternative connection point. Once the tank was full, isolation valve V2 was now closed, instead of v3 as was done previously.

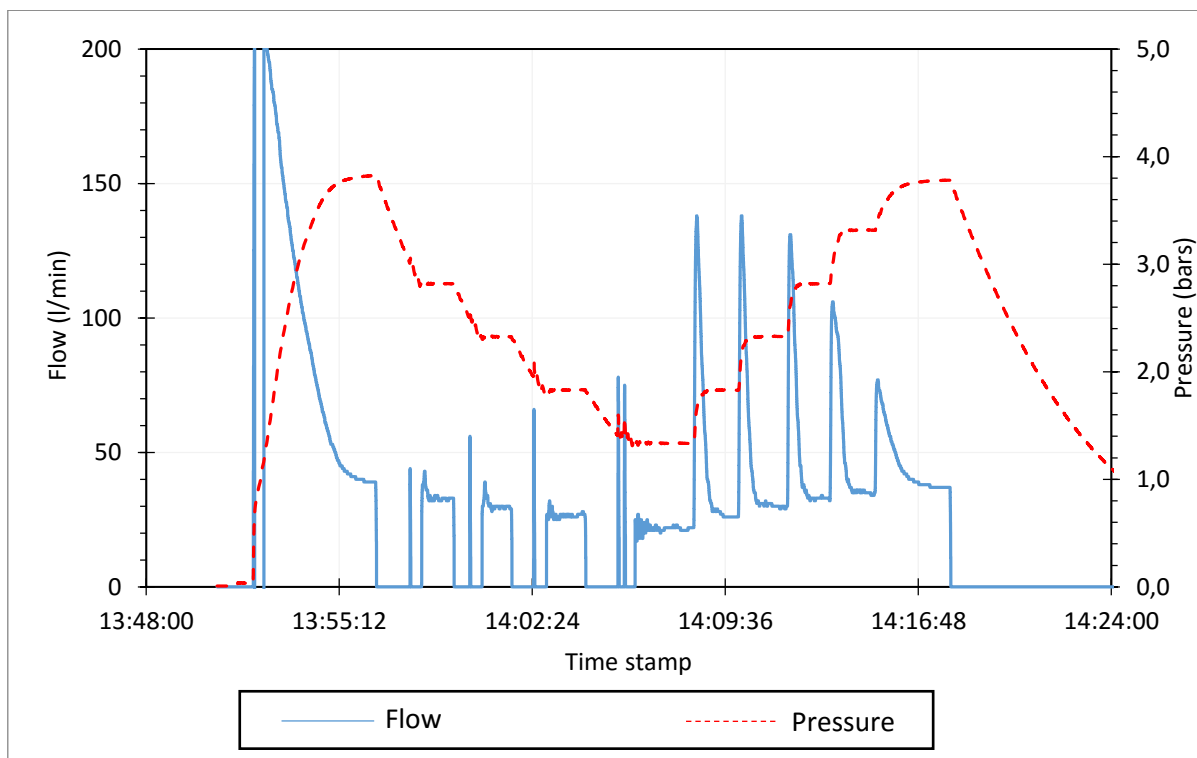


*Figure 5-25: Alternative connection point*

Unfortunately, even though effort was made to keep the pipe pressurised, air entered the pipe through the connection point during the disconnection and reconnection of the testing equipment, because the connection point could not be isolated.

To assess whether the valves AV1 and V2 closed effectively, the level of water in the tank was monitored over a period. The water level in tank appeared to drop, rather than rise, indicating that water was flowing back into the GP pipeline. If the valves were not sealing, the water level in the tank would be expected to rise since the pressures just downstream of valve AV1, and just upstream of valve V2, were higher than in the pipe and therefore would result in flow entering the GP pipeline, and subsequently filling the water tank, hence the water would rise. In addition, the operators were also confident that these valves did not leak.

Unfortunately, after connecting to the pipe, there was air in the pipeline, which could not be discarded. Nonetheless, the test was carried out and Figure 5-26 shows the flow and pressure results of the test.



*Figure 5-26: Flow and pressure raw data for the GP pipeline-fourth attempt*

There was much more confidence in this test, and a consensus that a leak was identified, although not as large as previously expected in the first attempt. The higher fluctuation in the

flow that can be seen when the pressure is incrementally increased could be due to the air pockets in the pipeline, which potentially dampened the effect of a pressure change.

### 5.5.3 Leak test results for the GP pipeline

#### 5.5.3.1 Data analysis procedure

Figure 5-27 shows the elevation profile section of the GP pipeline. The pipeline starts at valve AV1, then dips by 27 meters, to “Bottom Valley 1”, then rises by 13.96 meters to “Top of valley”, and thereafter dips again by 29.74 meters to “Bottom valley 2”, and then rises to the final isolation valves, valve V2, V3 and V4,

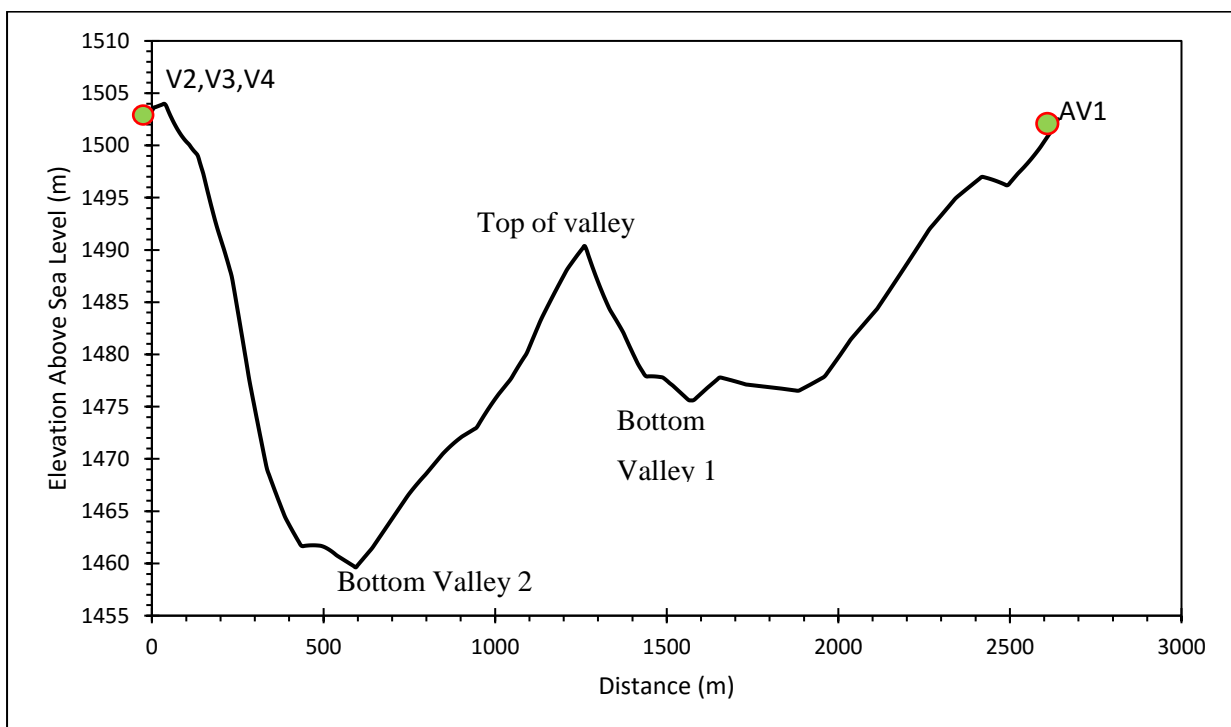


Figure 5-27: Elevation profile of the GP pipeline

Nodes were assigned at critical points on the pipeline as shown in Figure 5-28. The downstream valve 1, where the pipe starts, was assigned node 4. The lowest point of the pipe, “Bottom Valley 2” was assigned node 3. In addition, node 2 was the isolation valve at the end of the pipe. The connection point on the pipeline was assigned node 1, and finally the PCAE pressure sensor was assigned node 0.

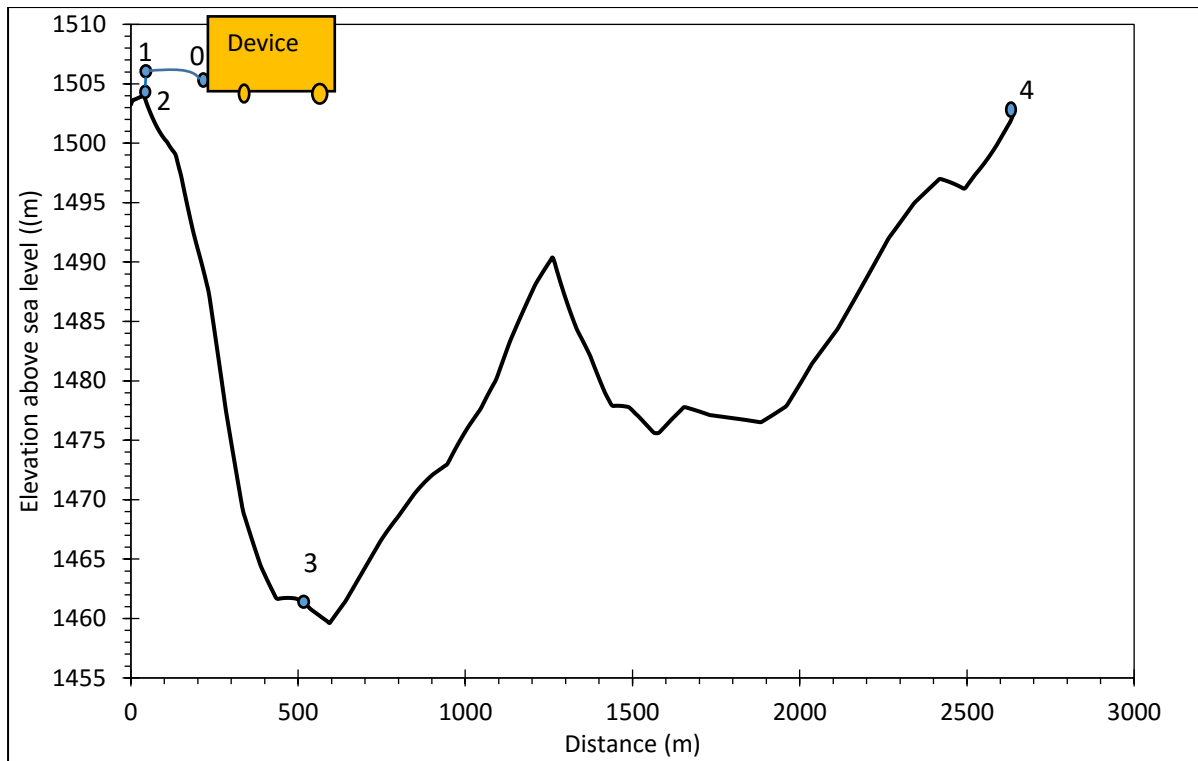


Figure 5-28: Elevation profile with nodes for the GP pipeline

A summary of the pipe properties between each node is given in Table 5-5. These pipe properties are used to calculate the head losses between each node and therefore adjust the pressure accordingly for each node. Since the pressure head at node zero is known (measured pressure head), the analysis starts from node 0, and ends at node 4. The minor loss coefficients,  $k$ , and absolute roughness,  $e$ , are obtained from Finnemore & Franzini, 2002.

Table 5-5: Pipe properties for each node

Pipe properties	0 - 1	1 - 2	2 - 3	3 - 4
Pipe Section Identity	Delivery hose pipe	Connection	Test pipe	Test pipe
Diameter, $d$ (mm)	50	25	500	500
Absolute roughness, $e$ (mm)	0.3	0.03	0.15	0.15
Minor loss coefficient, $k$	0.3	0.33	0.5	0
Elevation difference, $\Delta z$ (m)	1.85	0.8	56.92	-47
Length of pipe, $l$ (m)	10	0.8	600	2040
$e/d$	$6.0 \times 10^{-3}$	$1.80 \times 10^{-3}$	$3.0 \times 10^{-4}$	$3.0 \times 10^{-4}$
Pipe Area, $A$ (m <sup>2</sup> )	$1.96 \times 10^{-3}$	$4.91 \times 10^{-4}$	$1.96 \times 10^{-1}$	$1.96 \times 10^{-1}$

### 5.5.3.2 Data interpretation

The raw flow and pressure data obtained from the PCAE recorder is plotted against time in Figure 5-29. As can be seen from the figure, the pressure was varied at increments of 0.5 bars, and the flow rate was allowed to stabilise before another pressure increment was set. The flow rate detected suggests that a leak existed in the pipeline.

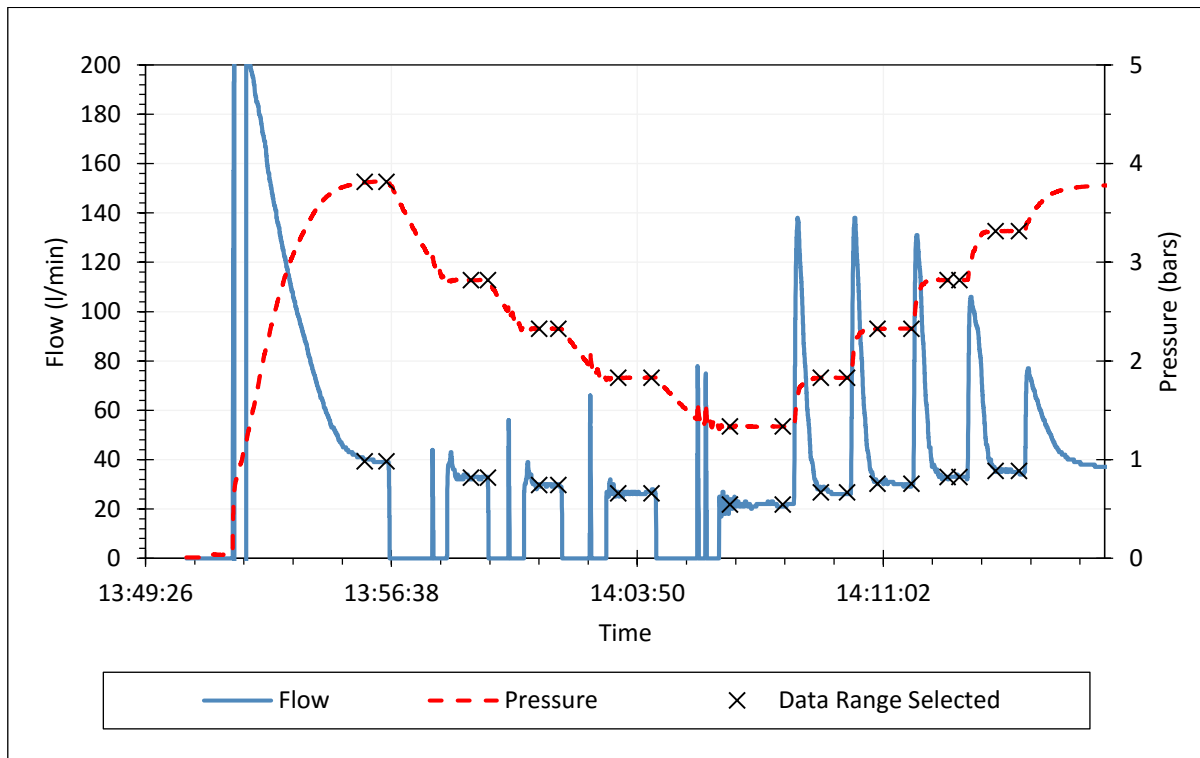


Figure 5-29: Flow and Pressure raw data showing the stabilised data range selected for the GP pipeline

While the pressure curve showed clear transitions between steps, the flow curve dropped below the stabilised value at the start of each downwards step, and above the stabilised value at the start of each upwards step. The reason for this behaviour is the contraction and expansion of the pipe diameter (and thus internal volume) because of the changes in pressure. The higher flow fluctuation, at the start of each upward step can be attributed to the potential air pockets in the pipeline. The air pockets may have caused a dampening effect as the pressure changes.

The x-markers on the graphs in Figure 5-29 indicate the periods of stable flow and pressure that were used for further analysis. The measured pressure values were adjusted for each node. This was done by taking into account the elevation difference, pipe friction and minor losses

between the pressure sensor and each node. Table 5-6 gives a summary of the pressure at each node. It is important to note that node 0 represents the device and thus the measured pressure.

*Table 5-6: Flow and adjusted pressure for each node on the GP pipeline*

Q (m <sup>3</sup> /s) Flow rate	h (m)at node 0	h (m) at node 1	h (m)at node 2	h (m) at node 3	h (m) at node 4
6.57x10 <sup>-04</sup>	38.9	40.7	41.45	94.7	47.7
5.45x10 <sup>-04</sup>	28.8	30.6	31.31	84.6	37.6
4.95x10 <sup>-04</sup>	23.7	25.6	26.30	79.6	32.6
4.40x10 <sup>-04</sup>	18.7	20.5	21.25	74.5	27.5
3.64x10 <sup>-04</sup>	13.6	15.5	16.23	69.5	22.5
4.45x10 <sup>-04</sup>	18.7	20.5	21.25	74.5	27.5
5.05x10 <sup>-04</sup>	23.7	25.6	26.31	79.6	32.6
5.50x10 <sup>-04</sup>	28.8	30.6	31.30	84.6	37.6
5.90x10 <sup>-04</sup>	33.8	35.6	36.36	89.6	42.6

It can be seen from Table 5-6 that the highest pressures were found to occur at node 3, the lowest point of the pipe (see Figure 5-28). The lowest pressures occurred at node 0, as expected because this was the highest point of the analysis. Due to the conservation of mass principal, the flow rate,  $Q$ , measured at node 0, was assumed the same for each node.

For the leakage modelling analyses (power equation and modified orifice equation), only the nodes located on the test pipe were used for analysis. These nodes included node 2, node 3 and node 4.

### ***5.5.3.3 Leakage parameters for the power equation***

The flow and adjusted pressure values for node 2, node 3 and node 4 in Table 5-6 are plotted in Figure 5-30. The reason why only node 2, 3 and 4 are plotted is because these nodes are located on the GP pipeline, and therefore, the leakage parameters obtained at these nodes provide an envelope of possible leakage parameters on the pipe.

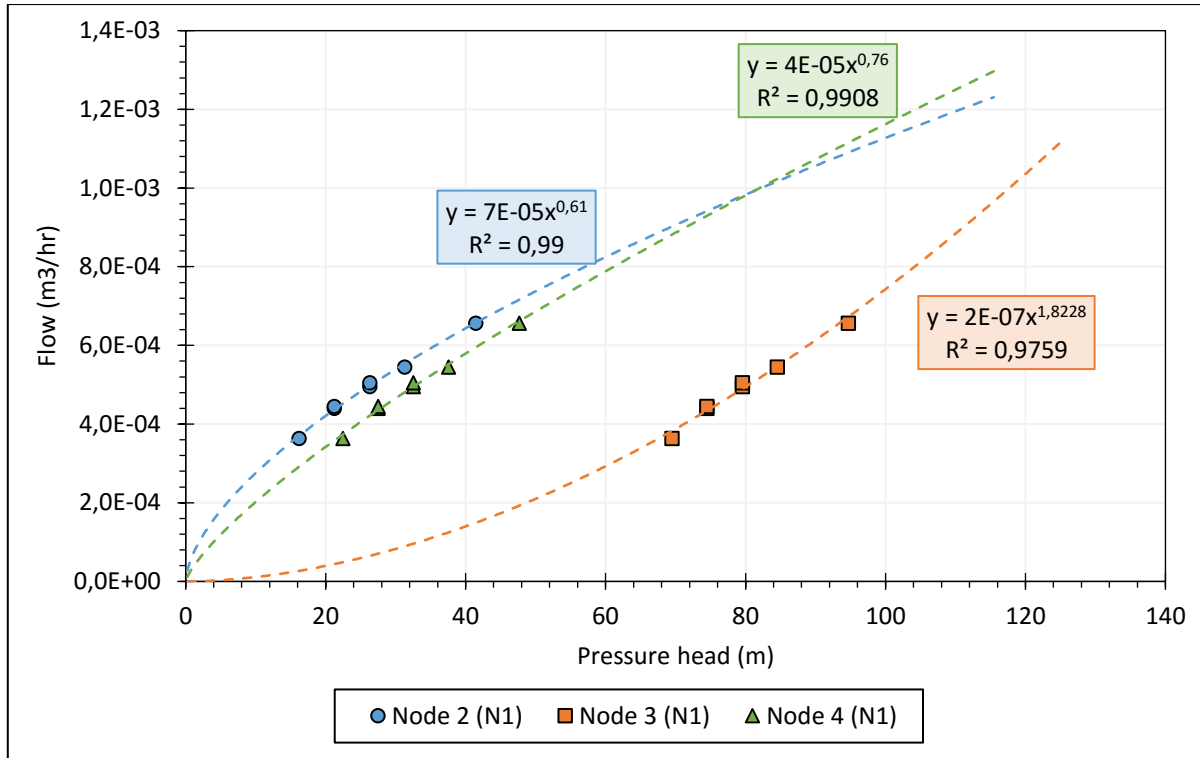


Figure 5-30: Flow against pressure data with power equation fitted for ode2, node 3 and node 4.

A power equation is fitted on the data points as indicated in Figure 5-30. From the power equation the leakage coefficient,  $C$ , and the leakage exponent,  $NI$ , were obtained for each node, and are given in Table 5-7.

Table 5-7: Summary of power equation leakage parameters for node 2, 3 and 4 on the GP pipeline

Node	Leakage Coefficient, $C$	Leakage Exponent, $NI$
2	$7 \times 10^{-5}$	0.61
3	$2 \times 10^{-7}$	1.82
4	$4 \times 10^{-5}$	0.76

It can be seen that the largest leakage exponent,  $NI = 1.82$ , was obtained at node 3, which had the highest pressures (see Table 5-6), followed by,  $NI = 0.76$ , at node 4, and finally  $NI = 0.61$ , which was obtained at node 2. Generally, it can be seen that the nodes with higher pressures also had the largest leakage exponents but lowest leakage coefficient.

Since the GP pipeline is a steel pipeline, it can be classified as a rigid pipe. Consequently, the  $NI$  exponent would be expected to be around 0.5. However, node 2, node 3 and node 4 all had



$Nl$  exponents greater than 0.5. These higher leakage exponents can occur in rigid pipes due to excessive corrosion. Therefore, the leakage exponent results could suggest that the pipeline has potentially undergone some excessive corrosion; particularly for the section of pipe between node 3 and node 4.

### 5.5.3.4 Leakage parameters for the modified orifice equation

If the leakage flow rates and pressure heads are known, then the effective leakage areas can be estimated by re-arranging the orifice equation as follows:

$$C_d A = A' = \frac{Q}{\sqrt{2gh}}$$

Equation 5-4

The effective leakage areas at each pressure was calculated for node 2, node 3 and node 4 using Equation 5-4 and the results are shown in Table 5-8. It can be seen from Table 5-8, that the largest leakage areas were found to occur at node 2, even though this node had the smallest averaged pressure heads. This is because, the flow rate is assumed to be the same at each node, and from Equation 5-4, it is clear that for the same flow rate, if the pressure head,  $h$  reduces, then the leakage area increases.

Table 5-8: Effective leak area and adjusted pressure for node2, 3 and 4 on the GP pipeline

Q, m <sup>3</sup> /hr	Node 2		Node 3		Node 4	
	h (m)	A' <sub>2</sub> (mm <sup>2</sup> )	h (m)	A' <sub>3</sub> (mm <sup>2</sup> )	h (m)	A' <sub>4</sub> (mm <sup>2</sup> )
6.57x10 <sup>-04</sup>	41.45	23.03	94.70	15.23	47.70	21.46
5.45x10 <sup>-04</sup>	31.31	21.99	84.56	13.38	37.56	20.07
4.95x10 <sup>-04</sup>	26.30	21.81	79.55	12.54	32.55	19.60
4.40x10 <sup>-04</sup>	21.25	21.55	74.50	11.51	27.50	18.94
3.64x10 <sup>-04</sup>	16.23	20.38	69.48	9.85	22.48	17.31
4.45x10 <sup>-04</sup>	21.25	21.80	74.50	11.64	27.50	19.16
5.05x10 <sup>-04</sup>	26.31	22.22	79.56	12.78	32.56	19.97

The effective leakage area  $A'$  against pressure head was plotted for node 2, node 3 and node 4, as shown in Figure 5-31. A linear function was fitted to the data points, the intercept of each

linear line with the area axis (y-axis) gave the effective initial leak area,  $A'_0$  and the slope of the line gave the effective head-area slope,  $m'$ .

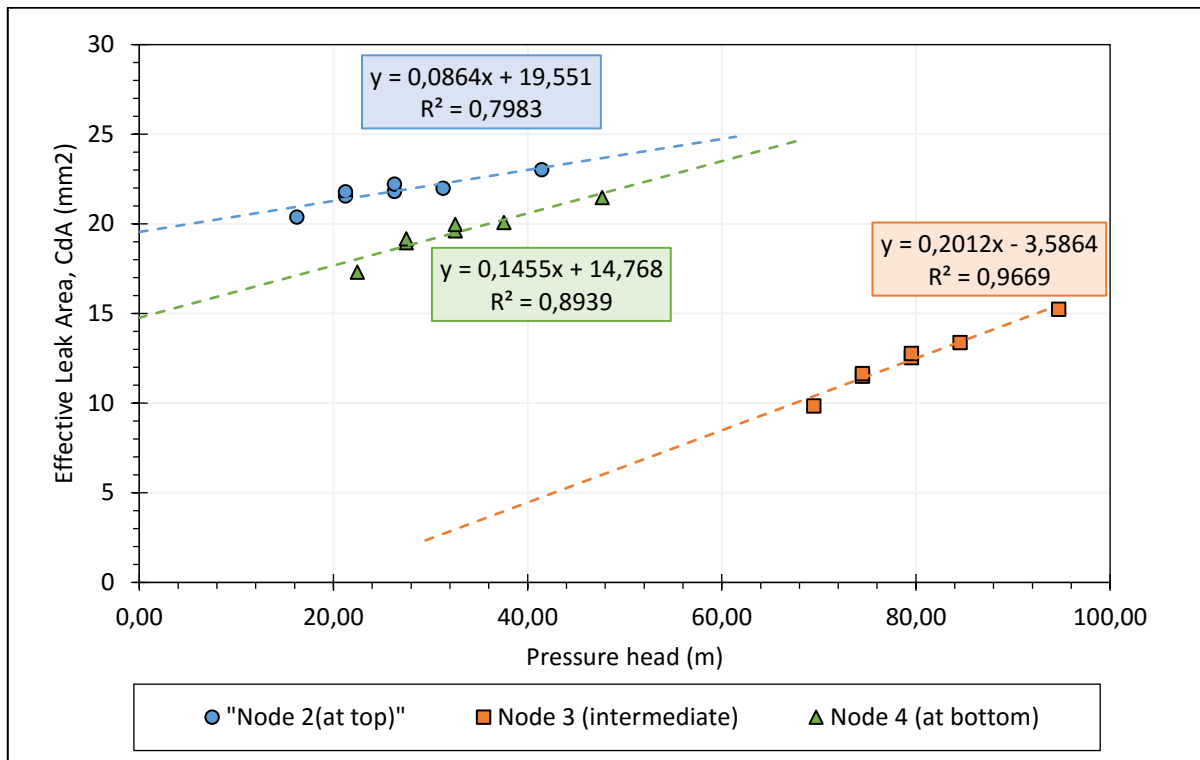


Figure 5-31: Effective leak area against pressure for node2,3 and 4 on the GP pipeline

The results shown in Figure 5-31 show that all nodes had leaks with positive head area slopes, but with varying magnitudes. Node 3, had the largest head-area slope of 0.20mm<sup>2</sup>/m, followed by node 4 with 0.15mm<sup>2</sup>/m, and finally node 2 with a head-area slope of 0.086mm<sup>2</sup>/m. A summary of the results is provided in Table 5-9.

Table 5-9: Summary of the modified orifice equation leakage parameters for node 2,3 and 4 on the GP pipeline

Node	Effective Initial leak area, $A'_0$ (mm <sup>2</sup> )	Effective head-area slope, $m'$ (mm <sup>2</sup> /m)	Leak Characteristic
2	19.55	0.086	Round hole
3	-3.59	0.20	Longitudinal crack
4	13.74	0.15	Longitudinal crack

The results in Table 5-9 show that if all the leakage occurred at node 2, then the leak could be characterised as a round hole. This is because of the small expansion rate of about 0.086 mm<sup>2</sup> per meter head, which is characteristic of a round hole. The initial leakage area of approximately 19.5 mm<sup>2</sup>, would then imply that the round hole has a diameter of approximately 5mm.

The results obtained for node 3, show that if the leakage occurs at node 3, then the expansion rate would be 0.20 mm<sup>2</sup> per meter of pressure applied. A negative initial leakage area was obtained, and while this is not physically possible, this result suggests that the leak remains closed and only starts to open up at a pressure head of about 18.2 meters (the x-axis intercept).

The result for node 4, shows that if all the leakage were located at node 4, then the leakage area would be expanding at 0.15 mm<sup>2</sup> per meter of pressure. This positive expansion rate is consistent with a longitudinal crack with an initial leakage area was approximately 14.77 mm<sup>2</sup>.

The leakage flow rate,  $Q$ , from the pipe at each node, can be predicted for different operating pressures in the pipeline using the modified orifice equations developed using the results in Table 5-9 as follows:

$$Q_{at\ node\ 2} = \sqrt{2g}(19.55h^{0.5} + 0.086h^{1.5}) \times 10^{-6}$$

*Equation 5-5*

$$Q_{at\ node\ 3} = \sqrt{2g}(-3.59h^{0.5} + 0.20h^{1.5}) \times 10^{-6}$$

*Equation 5-6*

$$Q_{at\ node\ 4} = \sqrt{2g}(14.77h^{0.5} + 0.15) \times 10^{-6}$$

*Equation 5-7*

## **5.6 Brickfields and Constantia Reservoir pipeline**

### **5.6.1 Introduction**

The examined steel bulk pipeline - hereafter referred to as the Brickfields to Constantia reservoir pipeline (BC pipeline) – was a rising main, fed by gravity. The main characteristics of the pipeline were: Length = +/- 5000m and a nominal diameter of = 450mm.

The layout of the BC pipeline is shown in Figure 5-32. The section of the pipeline that was tested starts from isolation valve AV1 (butterfly valve) and ends at isolation V2 (PRV). The

elevation difference between the operating system pressure upstream of valve AV1 was approximately 10 bars, and downstream of V2 was approximately 3 bars.

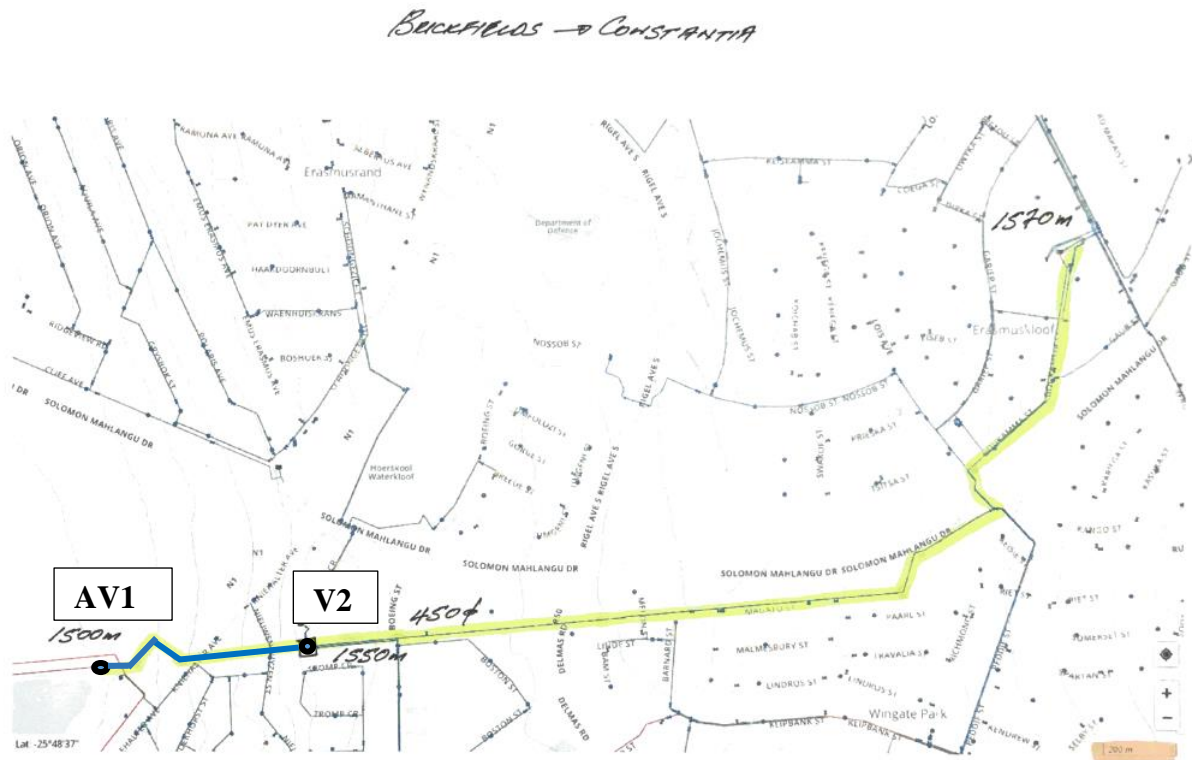


Figure 5-32: Layout of BC pipeline route starting at AV1 and ending at V2

### 5.6.2 Leak test procedure

The test began at isolation valve V2, where the PRV housed in an underground chamber was isolated by the operational team. It was observed that the pipes near this chamber were not in a good condition. Some of the pipes in this vicinity were corroded excessively, and it appeared as though a large area, just near the chamber, was recently excavated to fix a leak.

The operational team then drove to Brickfield to close isolation valve AV1 (butterfly valve). After 2 hours, the operational team returned to isolation valve V2, and explained that the valve AV1 did not seal at all. A large flow still passed the valve in its closed position. Based on this and the recommendation by operational team, it was decided that this test be abandoned.

### **5.6.3 Leak test results for the BC pipeline**

No results were obtained for this test because the butterfly valve, at isolation valve AV1, from which the pipeline is fed, did not seal. A large flow was heard passing through the butterfly valve in its closed position. Furthermore, this was a complex pipeline that required a number of isolation valves to be closed.

It became apparent that over longer periods, butterfly valves do not isolate effectively when compared to gate valves.

## **5.7 Fort Klapperkop reservoirs to Carina pipeline**

### **5.7.1 Introduction**

The examined steel bulk pipeline - hereafter referred to as the Fort Klapperkop Reservoir to Carina pipeline (FC pipeline) – is a gravity fed, rising pipeline. It is directly supplied from the national bulk water supplier, Rand Water.

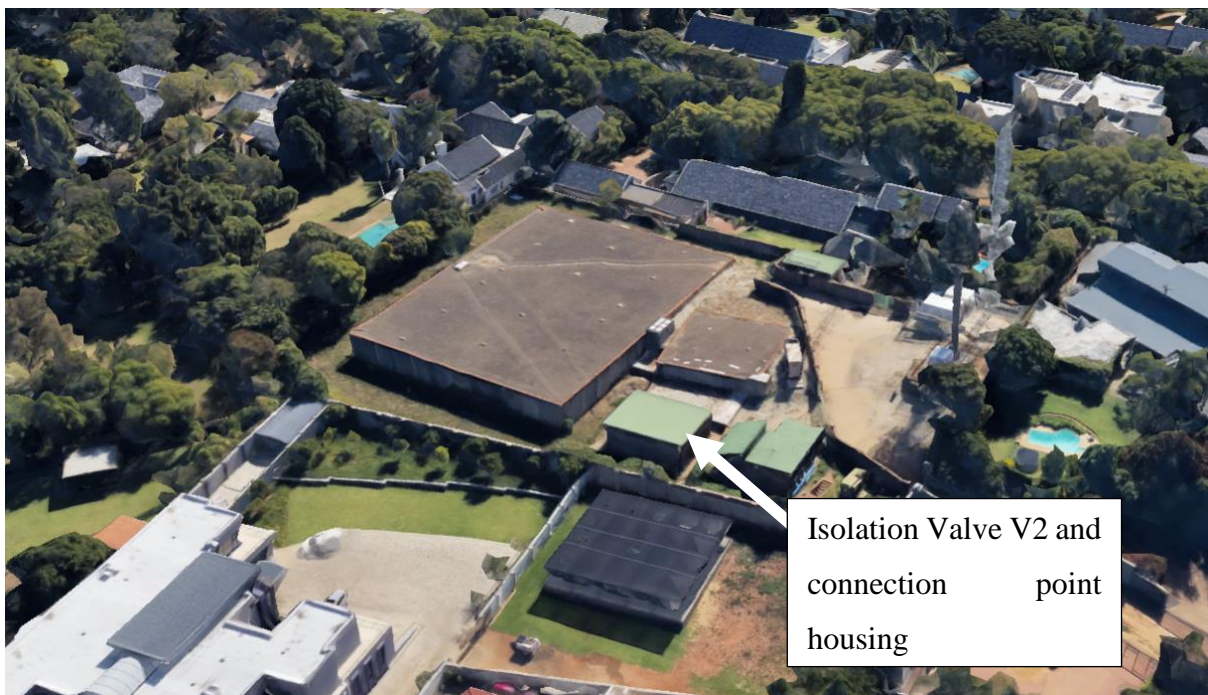
The main characteristics of the pipeline are: length = 2700 m, nominal diameter = 406mm and the pipe internal thickness = 3.15mm.

The layout of the FC pipeline is shown in Figure 5-33. The section of pipe tested starts at the isolation valve AV1 (gate valve), at the Fort Klapperkop reservoir, and then the pipeline rises to a maximum height after dropping down to the final isolation valve V2 (gate valve), at Carina Street, where it ends. Isolation valve AV1, at the bottom, was pressurised by a Rand water line, to a pressure of at least 5 bars, and the isolation valve V2, at the top, was pressurised to approximately 0.3bars.



*Figure 5-33: Map showing FC pipeline route starting at AV1 (5bar+) and ending at V2 0.3 bar+)*

A google earth image of the reservoir configuration at Carina Street is shown in Figure 5-34, with the location of the chamber that housed the gate valve that was used to isolate the pipe at V2.



*Figure 5-34: Google earth image of configuration at Carina street where isolation V2 was housed and the PCAE was connected*

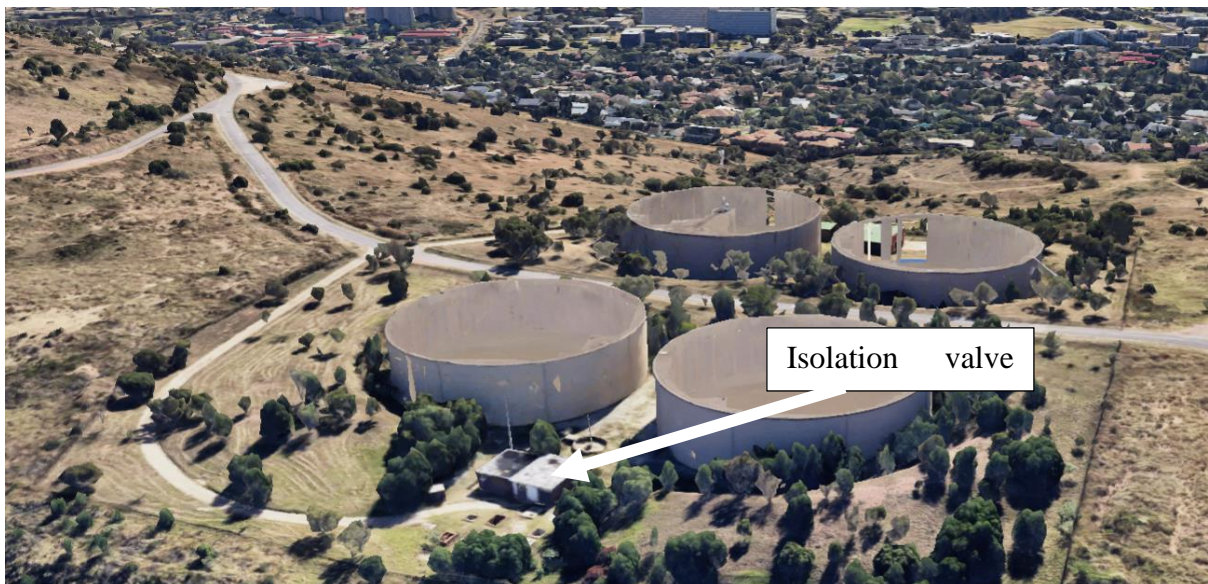
It was observed that the chamber housing isolation V2 had a number of PRVs on branches, as shown in Figure 5-35, all of which had to be closed in order to isolate the pipeline. It was also noted that a strainer on the tested pipe had a significant leak, resulting in a spray of water in

the room. The spray appeared to be pressure dependant, as it significantly reduced immediately after the pipe was isolated. The size of this leak is unfortunately unknown.



*Figure 5-35: Carina street inside chamber housing isolation valve V2*

A google earth image of the Fort Klapperkop Reservoir setup is shown in Figure 5-36. The FC pipeline is directly supplied from a Rand Water pipe and isolated on this site by a PRV. The pipeline is not related to the reservoirs in this figure.



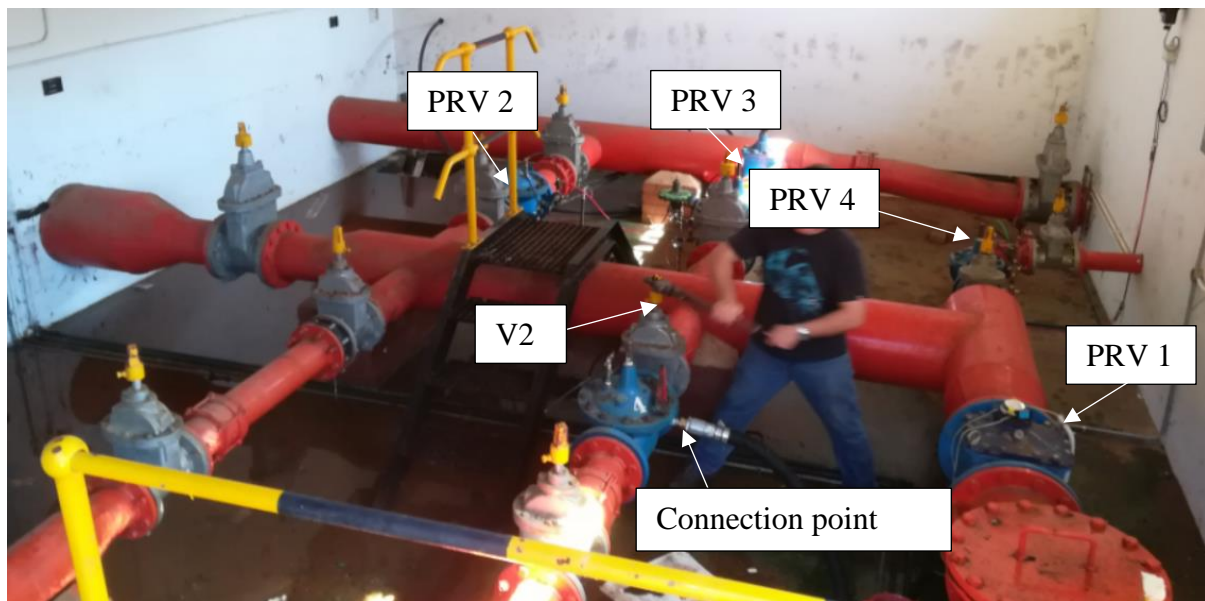
*Figure 5-36: Image of Fort Klapperkop reservoir setup.*

## 5.7.2 Leak Test Procedure

The test began at isolation valve AV1 at the Fort Klapperkop reservoirs (Figure 5-36), where the FC pipeline was supplied from a Rand Water pipe. An operator remained at the valve in order to operate the valve once the tests commence.

The rest of the team then drove to Carina street chamber that housed isolation valve V2, shown in Figure 5-37. This chamber was approximately 2.7 km from isolation valve AV1. Four PRVs in the chamber had to be closed in order to isolate the FC pipeline.

In addition, three gate valves also isolated this pipeline, but two of the three were already in a closed and sealed position. The third gate valve was downstream of the PRV onto which the testing equipment was connected to. This means, in total, 7 valves had to be closed in this chamber in order to isolate the pipe. The operator was very confident that all 7 valves closed 100%. The bottom valve feeding the pipe was definitely closed, because the pressure in the pipe dropped to much lower levels than would be expected if the valve were even slightly open.



*Figure 5-37: PRV's that were closed to isolate the FC pipeline*

A closer view of the connection point is shown in Figure 5-38. The connection point was a 3/4 Inch connection to a PRV valve, directly on the main pipe and just downstream of the isolation valve V2.





*Figure 5-38: PCAE connection point on the PRV*

The hose of the testing device was then connected. The operator who remained at valve AV1 Valve was instructed to open the valve in order to provide pressure to fill the tank. After filling the tank, the pipeline was isolated on both sides AV1 and V2.

Once the FC pipeline was fully isolated, the PCAE pump was activated at maximum pressure. The pressure could not be raised higher than 1.6 bar, indicating that there was a leak on the pipe. The pressure was then dropped at increments of 0.1 bar up to 0.73bars, and increased again at increments of 0.1 up to 0.9 bars, as shown in Figure 5-39. For each pressure step, the flow allowed to stabilise.

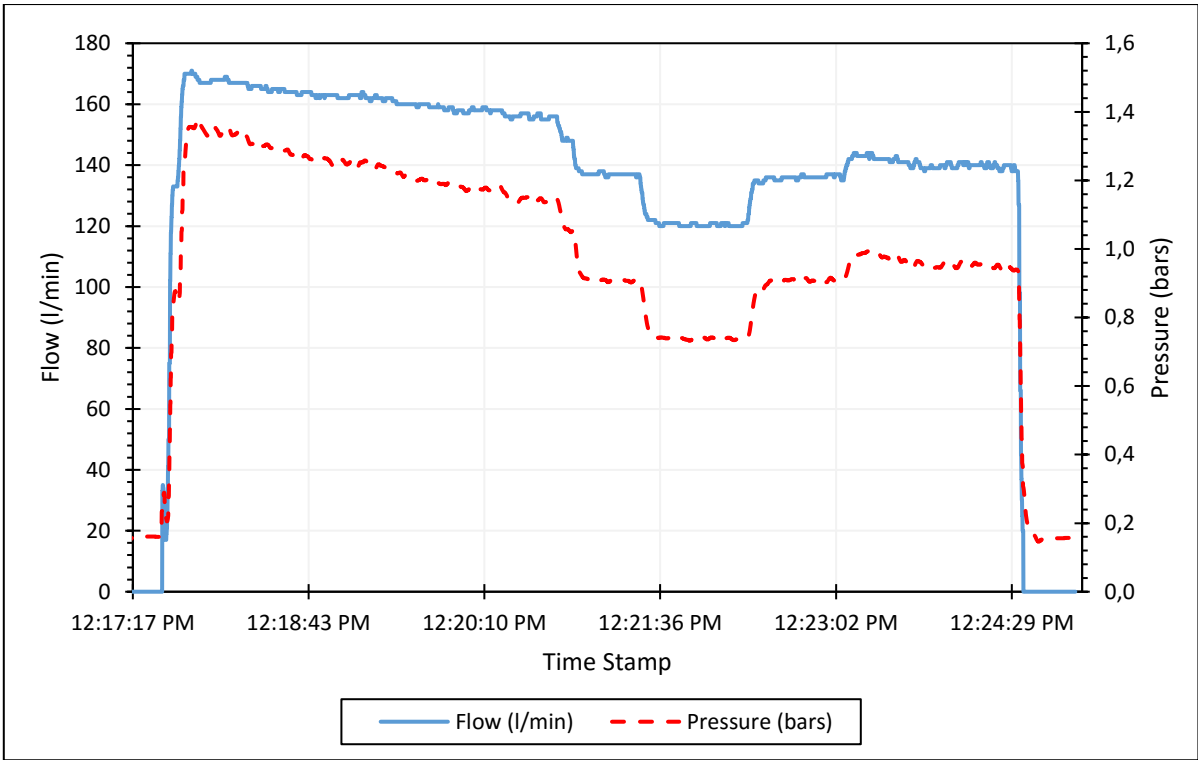
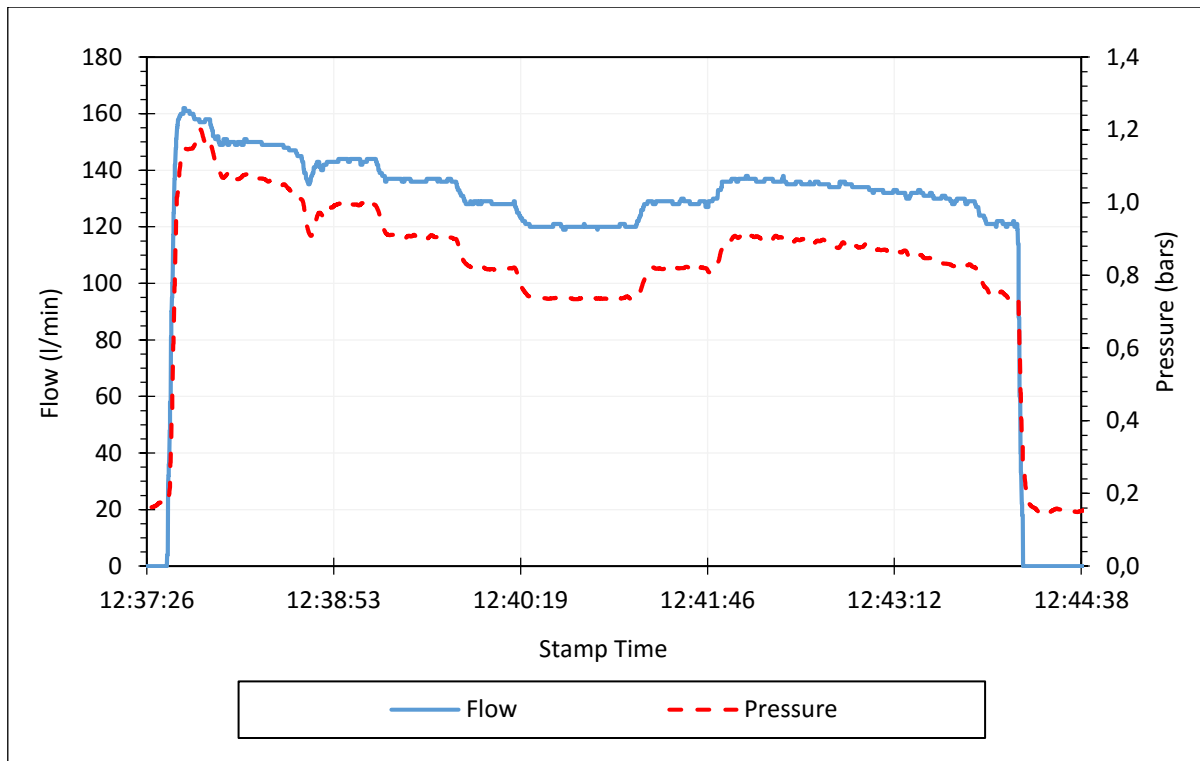


Figure 5-39: Flow and pressure raw data for the FC pipeline- attempt 1

A second attempt was done to check if the pressure and flow data would be similar to the first attempt. The PCAE tank was filled again by requesting the operator at valve AV1 to open the valve and pressurise the FC pipeline in order to fill the tank. Once the tank was filled, the pipeline was isolated again by closing the valves AV1 and V2. The test was repeated and the pressure and flow results for this second attempt are shown in Figure 5-40.



*Figure 5-40: Flow and pressure raw data for the FC pipeline- attempt 2*

The results obtained for the second attempt show similar results to the first attempt. A very clear leak was detected that was also pressure dependent. Furthermore, the leakage flow rate obtained for the second attempt was similar to the leakage flow rate obtained in the first attempt, with the lowest pressures giving a leakage flow rate of 120l/min. The data obtained in the second attempt was used for further analysis.

A very clear leak was detected, that was strongly pressure dependent. It must be investigated whether the leakage was through the valves, but it did not appear that way, because the pressure dropped to levels lower than what would be expected from the downstream reservoir. The upstream valve was definitely closed, as the pressure dropped to much lower levels than would be expected if that valve were even slightly open.

## 5.7.3 Leak test data analysis and results

### 5.7.3.1 Data Analysis Procedure

The elevation profile of the FC pipeline is shown in Figure 5-41. Nodes were assigned at critical points on the pipeline. The downstream isolation valve AV1, was assigned node 4. The pipeline consistently rises, and an intermediate point between Fort Klapperkop and Carina street reservoir was assigned node 3. The pipeline continues to rise until the Carina street reservoir where the connection point was assigned node 2, and the isolation valve V2 was assigned node 1. The location of the PCAE was assigned node 0.

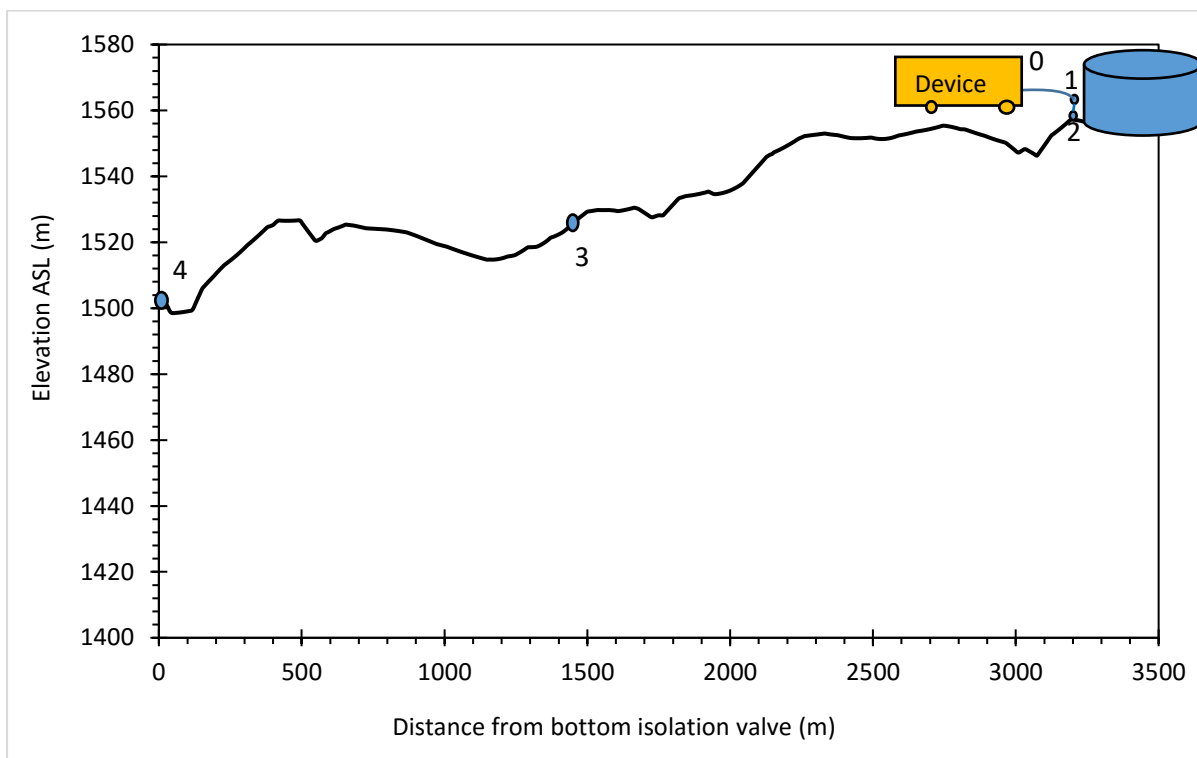


Figure 5-41: Elevation profile of the FC pipeline.

A summary of the pipe properties between each node is given in Table 5-10. These pipe properties are used to calculate the head losses between each node. The pressure head at node 0 (the device) is known because the pressure is measured by the pressure sensor, the analysis starts from node 0, and ends at node 4. The minor loss coefficients,  $k$ , and absolute roughness,  $e$ , are obtained from Finnemore and Franzini, 2002.

Table 5-10: Summary of pipe properties between nodes.

Pipe properties	0 - 1	1 - 2	2 - 3	3 - 4
Pipe Section Identity	Delivery hose pipe	Connection	Test pipe	Test pipe
Diameter, D (mm)	50	25	400	400
Absolute roughness, e (mm)	0.3	0.03	0.15	0.15
Minor loss coefficient, K	0.3	0.33	0.5	0
Elevation difference, $\Delta z$ (m)	1	0.08	27.00	27
Length of pipe, l (m)	10	0.08	1305.89	1305.89
e/D	$6.00 \times 10^{-3}$	$1.80 \times 10^{-3}$	$3.75 \times 10^{-4}$	$3.75 \times 10^{-4}$
Pipe Area, A (m <sup>2</sup> )	$1.96 \times 10^{-3}$	$4.91 \times 10^{-4}$	$1.26 \times 10^{-1}$	$1.26 \times 10^{-1}$

### 5.7.3.2 Data interpretation

The raw flow and pressure data obtained from the PCAE recorder is plotted against time in Figure 5-42. As can be seen from the figure, a clear leak was detected, that was pressure dependent. The pressure was dropped at increments of 0.1 bars, and a flow rate was detected, suggesting that a leak existed in the pipeline. The leakage flow rate was then allowed to stabilise before another pressure increment was set.

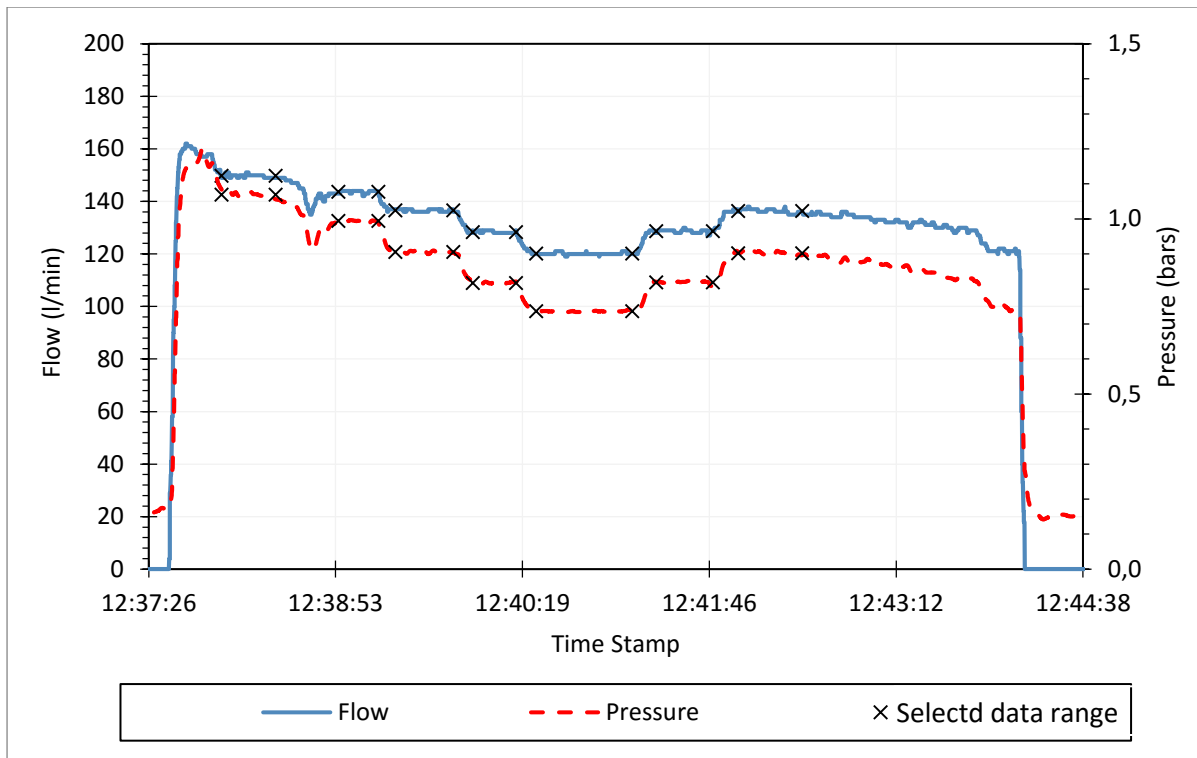


Figure 5-42: Flow and pressure raw data showing the stabilised data range selected

The graph clearly shows a step down and step up pattern repeated for both the pressure and flow data profile the stabilised data range of each pressure and flow step was used for further analysis. The selected stabilised range of the pressure and flow rate is shown by the cross markers in Figure 5-42.

While the measured flow rate represents the water flowing from the tank into the pipeline and out of the pipeline through leakage, the measured pressure represents the pressure at the sensor and is not necessarily the pressure at each node. In order to obtain the pressure at each nodes the measured pressure must be adjusted to take into account the elevation and other parameters that influence the pressure. The Bernoulli's principal was used to obtain the adjusted pressure at each node. A summary of the pressure at each node is given in Table 5-11.

*Table 5-11: Summary of the flow and adjusted pressures for each node on the FC pipeline*

Q (m <sup>3</sup> /s)	head at 0, h <sub>0</sub> (m)	head at 1, h <sub>1</sub> (m)	head at 2, h <sub>2</sub> (m)	head at 3, h <sub>3</sub> (m)	head at 4, h <sub>4</sub> (m)
2.50x10 <sup>-03</sup>	10.908	11.4	10.9	37.9	64.9
2.39x10 <sup>-03</sup>	10.145	10.6	10.2	37.2	64.2
2.28x10 <sup>-03</sup>	9.239	9.78	9.41	36.4	63.4
2.14x10 <sup>-03</sup>	8.337	8.93	8.62	35.6	62.6
2.00 x10 <sup>-03</sup>	7.511	8.16	7.89	34.9	61.9
2.14 x10 <sup>-03</sup>	8.355	8.95	8.64	35.6	62.6
2.27 x10 <sup>-03</sup>	9.205	9.75	9.39	36.4	63.4

From Table 5-11 it can be seen that the highest pressures occurred at node 4, followed by node 3 and finally the nodes at the top (node2, 1 and 0) had the lowest pressures. This was expected because the pipeline was pressurised from the top, and subsequently due to elevation difference (see Figure 5-41) the pressure will increase downstream of the pipeline.

For further analysis only the pressure at node2, node 3 and node 4 will be used because these nodes are located on the pipeline,

### ***5.7.3.3 Leakage parameters for the power equation***

The flow and pressure data for node 2, node 3 and node 4, from Table 5-11, are plotted in Figure 5-43. The reason only node 2, node 3 and node 4, were selected was because these nodes are located on the pipeline, and therefore, the leakage parameters obtained for each of these nodes provides an envelope of possible leakage behaviour at different location on the pipeline. Of which, the most realistic solution, would probably be a good indicator of the leakage behaviour and possibly location.

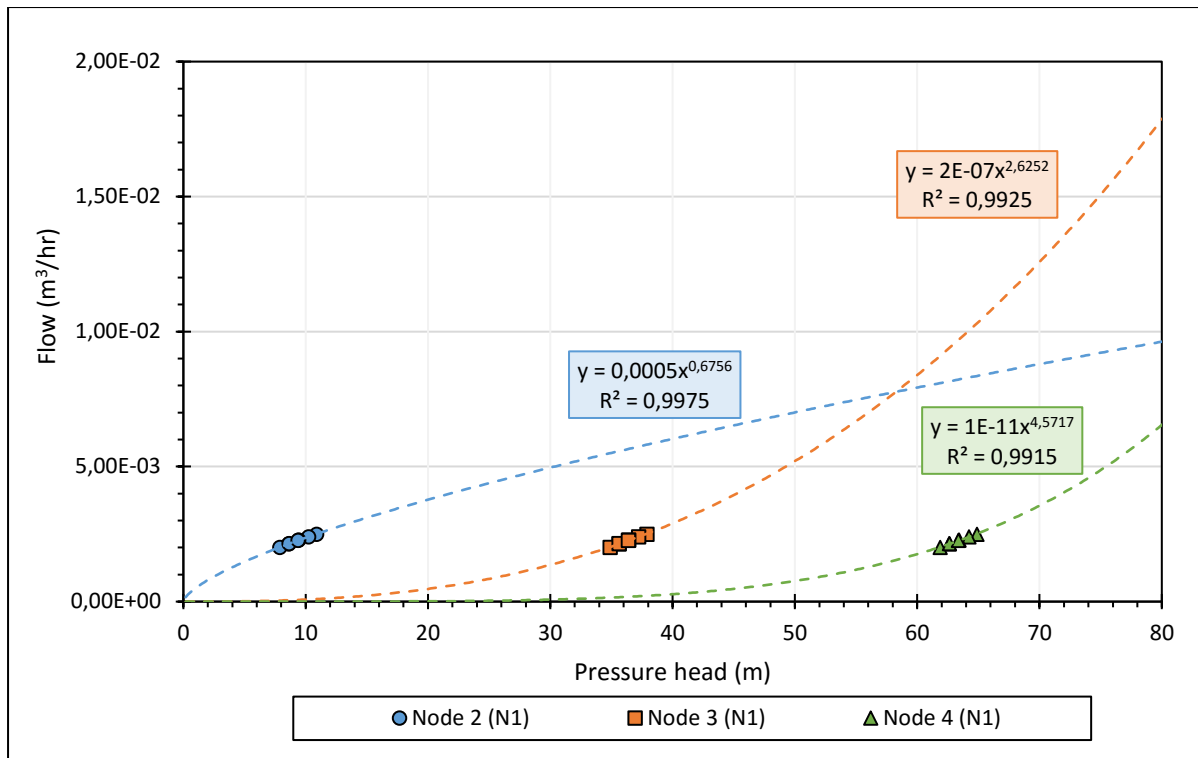


Figure 5-43: Flow against pressure with power equation fitted for node 2, node 3 and node 4 on the FC pipeline

From Figure 5-43, it can be seen that the result of node 2 had a leakage exponent of 0.67 which was the smallest, and perhaps the most realistic, when compared to node 3 and node 4 that had leakage exponents of 2.62 and 4.57, respectively. Furthermore, it can be seen that as the leakage exponent increases the leakage coefficient becomes smaller and smaller, seemingly approaching zero. A summary of the power equation leakage parameters is provided in Table 5-12.

Table 5-12: Summary of the power equation leakage parameters for node 2, 3 and 4 on the FC pipeline

Node	Leakage Coefficient, C	Leakage Exponent, N1
2	$5 \times 10^{-4}$	0.67
3	$2 \times 10^{-7}$	2.62
4	$1 \times 10^{-11}$	4.57



From Table 5-12, it can be seen, that if all the leakage occurs at node 2, then the leakage exponent is 0.67 and the leakage coefficient is  $5 \times 10^{-4}$ . This result is within the exponent range that can be explained by the modified orifice equation i.e.  $0.5 < N1 < 1.5$ . This result is synonymous with the leak that was observed on the strainer at node 2.

If all leakage occurred at node 3, then the leakage exponent would be 2.62 and the leakage coefficient would be  $2 \times 10^{-7}$ . A leakage exponent greater than 1.5 could occur due to an isolation valve bridge or data error, however for this test, it is known that the isolation valve sealed properly and the data obtained had no errors, and thus could be indicative of an unlikely.

If all leakage occurred at node 4, then the leakage exponent would be 4.57 and leakage coefficient would be  $1 \times 10^{-11}$ . This high leakage exponent is also unlikely to be due to an isolation valve bridge or errors in the data, and thus, could indicate that it is unlikely result.

### ***5.7.3.4 Leakage parameters for the modified orifice equation***

The effective leakage areas at each pressure was calculated for node 2, node 3 and node 4 and the results are shown in Table 5-13. It can be seen from Table 5-13, that the largest leakage areas were found to occur at node 2, followed by node 3 and finally node 4. This was expected because of the format of the effective leakage area equation in which the leakage flow rate is a numerator and the pressure is a denominator. Subsequently, if the leakage flow rate at each node is assumed the same, then the nodes with large pressures (node 4) will have a smaller effective leakage area whilst nodes with small pressures (node 2) will have larger leakage areas.

*Table 5-13: Summary of effective leak area and pressure for each node on the FC pipeline*

Q (m <sup>3</sup> /s)	head at 2, h <sub>2</sub> (m)	C <sub>d</sub> A <sub>2</sub> (mm <sup>2</sup> )	head at 3, h <sub>3</sub> (m)	C <sub>d</sub> A <sub>3</sub> (mm <sup>2</sup> )	head at 4, h <sub>4</sub> (m)	C <sub>d</sub> A <sub>4</sub> (mm <sup>2</sup> )
2.50x10 <sup>-3</sup>	10.9	171	37.9	91.5	64.90	69.9
2.39x10 <sup>-3</sup>	10.2	169.	37.2	88.6	64.22	67.5
2.28x10 <sup>-3</sup>	9.42	167	36.4	85.2	63.41	64.5
2.14x10 <sup>-3</sup>	8.62	165	35.6	80.9	62.62	61.0
2.00x10 <sup>-3</sup>	7.89	161	34.9	76.5	61.89	57.5
2.14x10 <sup>-3</sup>	8.64	165	35.6	81.1	62.63	61.2
2.27x10 <sup>-3</sup>	9.39	167	36.4	85.0	63.38	64.4

The effective leakage area  $A'$  against pressure head was plotted for node 2, node 3 and node 4 and a linear function was fitted to the data points, as shown in Figure 5-44. The intercept of each linear line with the area axis (y-axis) gave the effective initial leak area,  $A'_0$  and the slope of the line gave the effective head-area slope,  $m'$ .

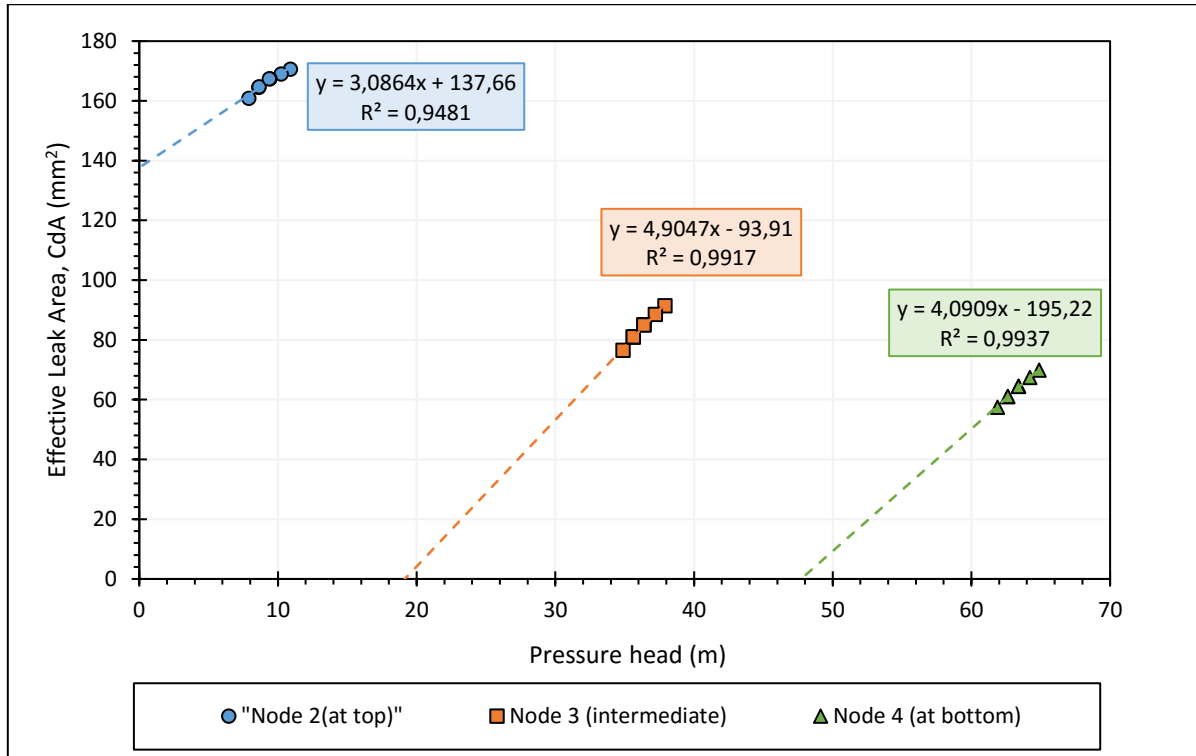


Figure 5-44: Effective leakage area against pressure head for node2 node 3 and node 4 on the FC pipeline

The results shown in Figure 5-44 show that all nodes had leaks with positive head area slopes, but with varying magnitudes. Node 3, had the largest head-area slope of  $4.9\text{mm}^2/\text{m}$ , followed by node 4 with  $4.09\text{mm}^2/\text{m}$ , and finally node 2 with a smallest head-area slope of  $3.08\text{mm}^2/\text{m}$ . A summary of the results is provided in Table 5-14.

Table 5-14: Summary of the modified orifice equation leakage parameters for node 2, 3 and 4 on the FC pipeline

Node	$A'_0$ (mm <sup>2</sup> )	$m'$ (mm <sup>2</sup> /m)	Leak Characteristic
2	138	3.1	Excessive Corrosion
3	-94	4.9	Longitudinal crack
4	-195	4.1	Longitudinal crack

Table 5-14 shows that the results obtained for node 2, suggest that if all the leakage occurred at node 2, then the effective head-area slope would be 3.1 mm<sup>2</sup>/m, implying that the leakage area would expand by 3.1 mm<sup>2</sup> for every meter of internal pressure the pipeline is subjected to. Furthermore, at zero internal pressure, the results obtained suggests that the size of the effective leakage area is approximately 138 mm<sup>2</sup>. This is a significant leak size and can be associate with the leak that was observed on the strainer on the tested pipeline at node 2.

The results obtained for node 3, suggest that if all the leakage occurred at node 3, then the effective head-area slope would be 4.9 mm<sup>2</sup>/m, implying that the leakage area expands by 4.9 mm<sup>2</sup> for every meter of internal pressure that the pipeline is subjected to. At zero internal pressure, a negative effective initial leakage area was obtained. While a negative effective initial leak area is not physically possible, this result implies that the leak remains closed until a certain pressure is reached, for node 3, the internal pressure required for the leakage area to open is approximately 19 meters.

The results obtained for node 4, suggest that if all the leakage occurred at node 4, then the effective head-area slope would be 4.1 mm<sup>2</sup>/m, implying that the leakage area expands by 4.1 mm<sup>2</sup> for every meter of internal pressure subjected to the pipeline. At zero pressure, a negative effective initial leak area was obtained. While a negative effective initially leakage area is not physically possible, this result implies that the leakage area remains closed at node 4, until a certain pressure is achieved, after which the leakage area starts opening. For node 4, the internal pressure required for the leakage area to start opening is about 48 m.

The results obtained for the effective initial leakage area at node 3 and node 4 suggest that the leakage is not corrosion because corrosion damage deteriorates the material and consequently results in a positive effective initial leak area, such as the case at node 2. For this reason, the

results for node 3 and node 4, perhaps indicates that leakage is unlikely to occur at these nodes and the most realistic result is the result obtained for node 2.

The leakage flow rate,  $Q$ , from the pipe at each node, can be predicted for different operating pressures in the pipeline using the modified orifice equations developed using the results in Table 5-14 as follows:

$$Q_{at\ node\ 2} = \sqrt{2g}(138 h^{0.5} + 3.1 h^{1.5}) \times 10^{-6}$$

*Equation 5-8*

$$Q_{at\ node\ 3} = \sqrt{2g}(-94 h^{0.5} + 4.9 h^{1.5}) \times 10^{-6}$$

*Equation 5-9*

$$Q_{at\ node\ 4} = \sqrt{2g}(-195 h^{0.5} + 4.1 h^{1.5}) \times 10^{-6}$$

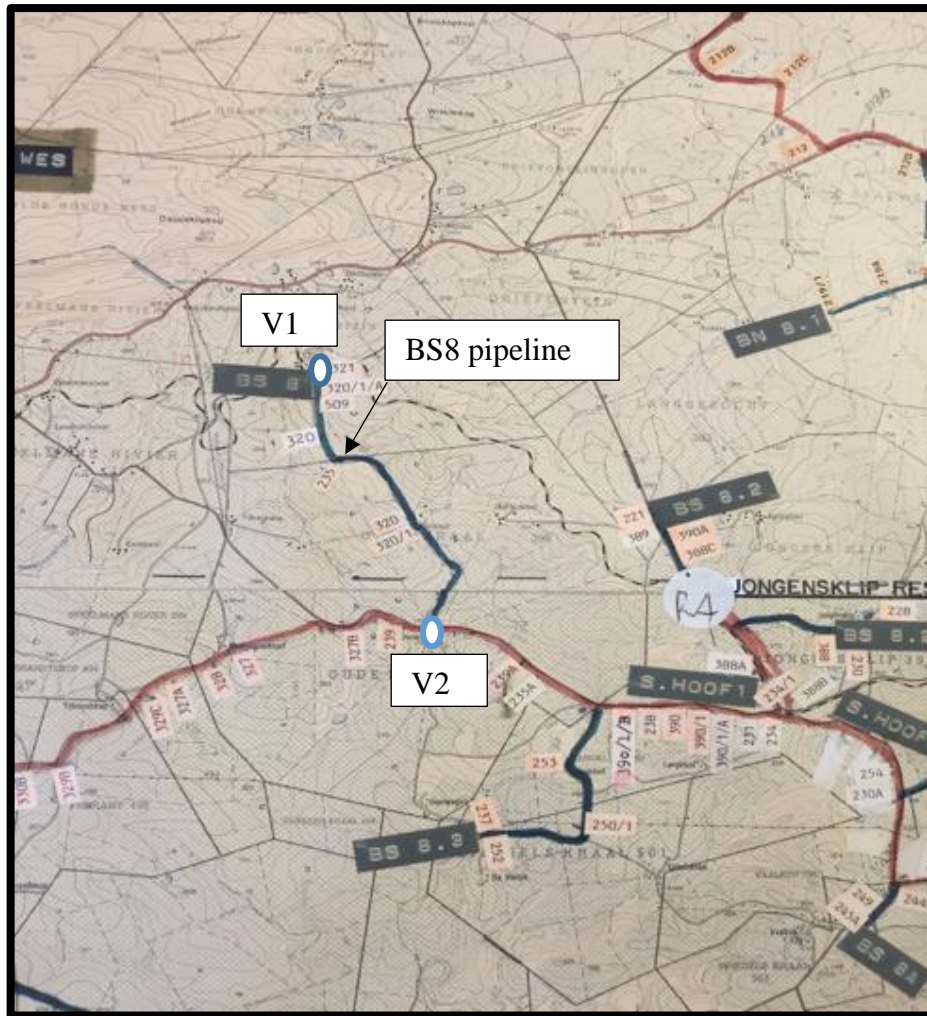
*Equation 5-10*

## **5.8 BS 8 Pipeline - Test 1**

### **5.8.1 Introduction**

The examined test pipeline – hereafter referred to as BS 8 pipeline – was a gravity pipeline, situated in the Caledon region, approximately 115km away from the Cape Town Central Business District. The pipeline was identified, in consultation with the Overberg Water Board (OWB), who suspected that there was a leak on the steel section of the pipe.

The OWB is responsible for the operation and maintenance of the entire Overberg Water Pipe Network. Figure 5-45 depicts a section of the Overberg Water Pipe Network of which the BS 8 pipeline is a part. As can be seen, the BS 8 pipeline is an off take pipeline that is charged from a main pipe labelled S.HOOF1 in Figure 5-45.



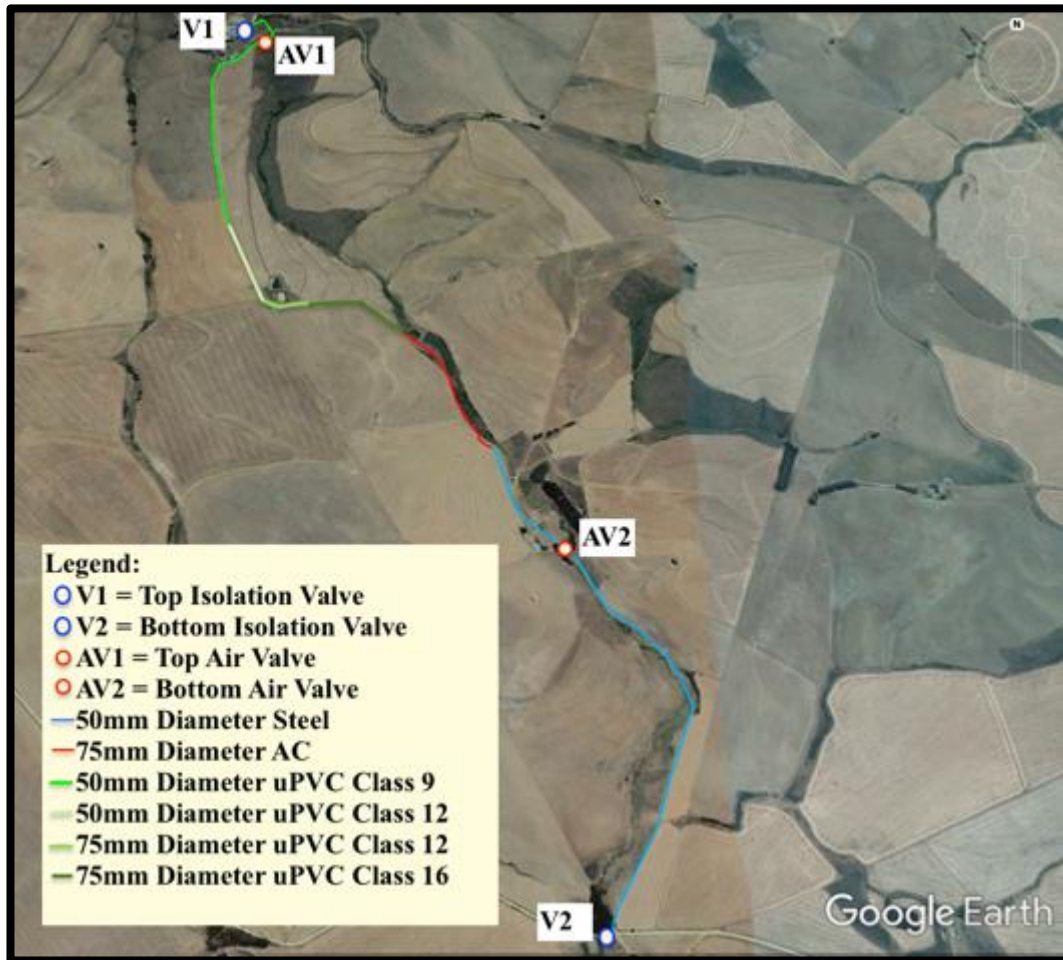
*Figure 5-45: Part of the Overberg water network that shows the BS 8 pipeline spanning from V1 to V2*

The BS 8 pipeline consisted of the following components: one isolation valve at the off take, a closed flange at the top of the pipe, six-user take offs (mainly farmers), seven air valves and seven scour valves along the pipeline. The total length of the BS 8 pipeline is approximately 5.4km, with nominal diameters (ND), ranging between 50 and 75mm, and has a burial depth of about 1.5m. The pipeline is made up of various pipe material, including Asbestos Cement (AC), Steel and uPVC pipe material.

The OWB indicated that, historically, the BS 8 pipeline has been a particularly problematic pipeline, with leakage being the major problem. In attempting to minimise the leaks, sections of the pipeline have been replaced with new uPVC plastic pipes and, hence, the mixed pipe materials that make up the BS 8 pipeline.

A data file, provided by OWB, with information about the BS 8 pipeline layout and components, was uploaded to Google Earth Software. Using the software, the BS 8 pipeline

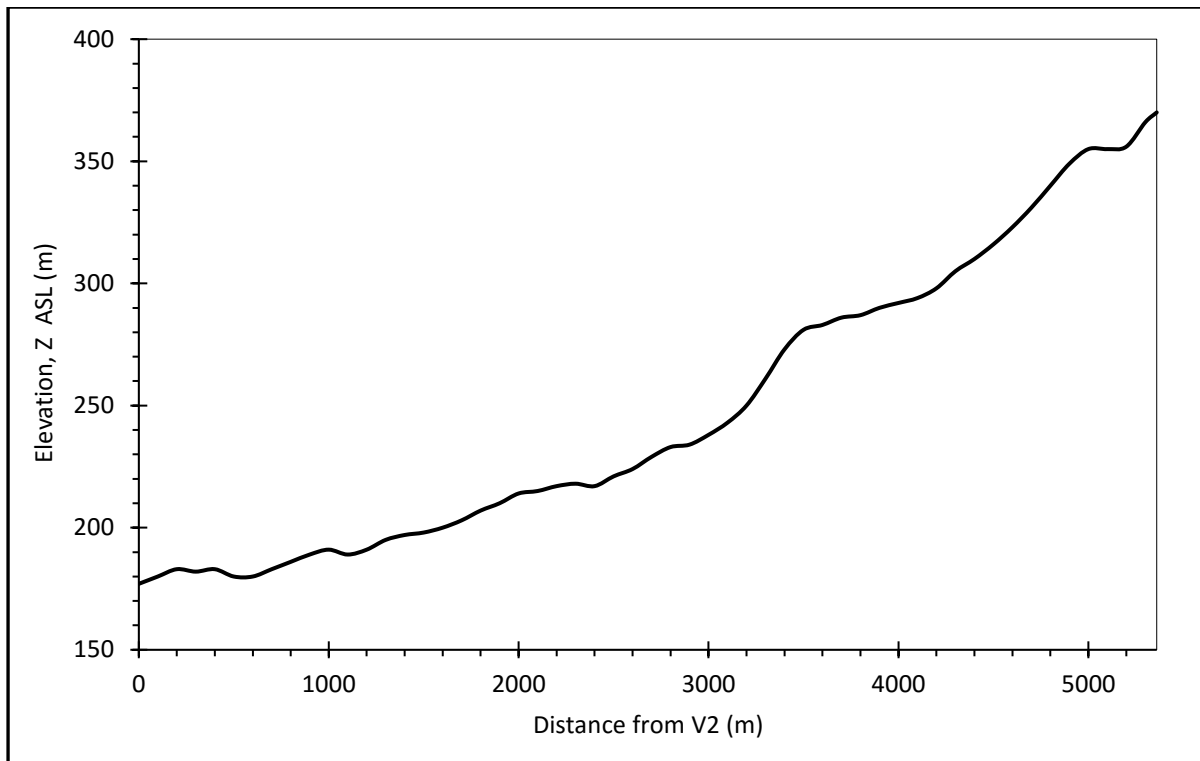
was plotted on to a satellite image of the area. Figure 5-46 depicts the satellite image layout of the BS 8 pipeline. It must be noted that the figure only shows the components necessary for the leak test done in this study.



*Figure 5-46: BS 8 pipeline layout with locations of the components used for the leak test*

The overall elevation profile of the BS 8 pipeline was extracted from the Google Earth Software.

Figure 5-47 shows the elevation profile from the bottom isolation valve (V2) to the top of the pipe. The overall elevation difference between the bottom and top of the BS 8 pipeline was found to be approximately 190 m.



*Figure 5-47: Showing the Overberg test pipeline elevation profile*

### **5.8.2 Leak test procedure**

The PCAE was connected to the BS 8 pipeline via an air valve. The air valve was the most convenient because of its ease of access. During the site visit, it was observed that all air valves on the BS 8 pipeline were housed in a small cylindrical concrete chamber, shown in Figure 5-48. Inside the concrete chamber the air valve, shown in Figure 5-49 (a) was connected to the BS 8 pipeline via a stop valve shown in Figure 5-49 (b). The air valve and stop valve were connected to each other via a threaded connection.



*Figure 5-48: Air valve concrete chamber*



*Figure 5-49: (a) Air valve (b) BS 8 Pipeline stop valve connection*

When selecting the most suitable air valve connection point to connect the PCAE, the main objective was to identify a connection point on the pipeline, such that, when the PCAE pump was activated from that connection point, the entire pipeline would be pressurised. This was important to consider since the line was a gravity line and the PCAE pump could only deliver a maximum pressure head of 43 meters, whilst the elevation head from the bottom to the top of the BS 8 pipeline was approximately 190m. For example, the PCAE pump would not be able to pressurise the entire pipeline if the PCAE was connected at the bottom of the BS 8 pipeline. Therefore, the most suitable connection point was at the top of the pipeline and, hence, the topmost air valve (AV1 in Figure 5-46) was identified as the most suitable point to connect the PCAE, and the PCAE was transported to its location along the BS 8 pipeline.

Prior to removing the air valve, the stop valve was closed to ensure that water does not flow from the BS 8 pipeline. The air valve was then removed, and replaced with a 25mm male threaded Gardena quick release coupling. The quick release coupling connected the PCAE hosepipe to the BS 8 pipeline, as shown in Figure 5-50.



*Figure 5-50: PCAE connected to the BS 8 pipeline*

The operational pressure at the AV1, where the PCAE was connected, was examined and it was found to be about 15 meters. This low pressure was expected as this connection point was



very close to the highest point on the BS 8 pipeline (see Figure 5-46). Because of this low pressure, the water tank was filling very slowly. In order to speed up the process of filling the tank, a connection point with a higher pressure was required.

In consultation with the OWB operations team, a bottom air valve, shown as AV2 in Figure 5-46, was identified as a suitable connection point with a higher pressure. Because of the higher pressure, the tank could be filled up quicker. The PCAE was transported to AV2. Upon arrival, the air valve chamber at AV2 was opened and the stop valve was closed. Thereafter, the air valve was removed and replaced with a Gardena fitting which was used to connect the hosepipe to the BS 8 pipeline.

Prior to filling the PCAE water tank, the stop valve on the pipeline was opened to flush the BS 8 pipeline. However, it should be noted that AV2 was located on the steel section of the BS 8 pipeline and, because the stop valve was initially opened too quickly, this stirred up sediments in the pipeline and made the colour of the water brown, as shown in Figure 5-51.



*Figure 5-51: Showing the colour of water during the flushing process of the BS8 pipeline test 1 pipeline*

After 5 minutes of flushing the BS 8 pipeline, it was observed that the water never changed colour and remained brown. This was brought to the attention of the Overberg Water operations team on site. They were not particularly concerned about the colour of the water, and granted permission to carry on with the test. The PCAE tank was then filled with the brown water from the BS 8 pipeline manually from the top, as shown by Figure 5-52.



*Figure 5-52: PCAE water tank being filled Up at AV2*

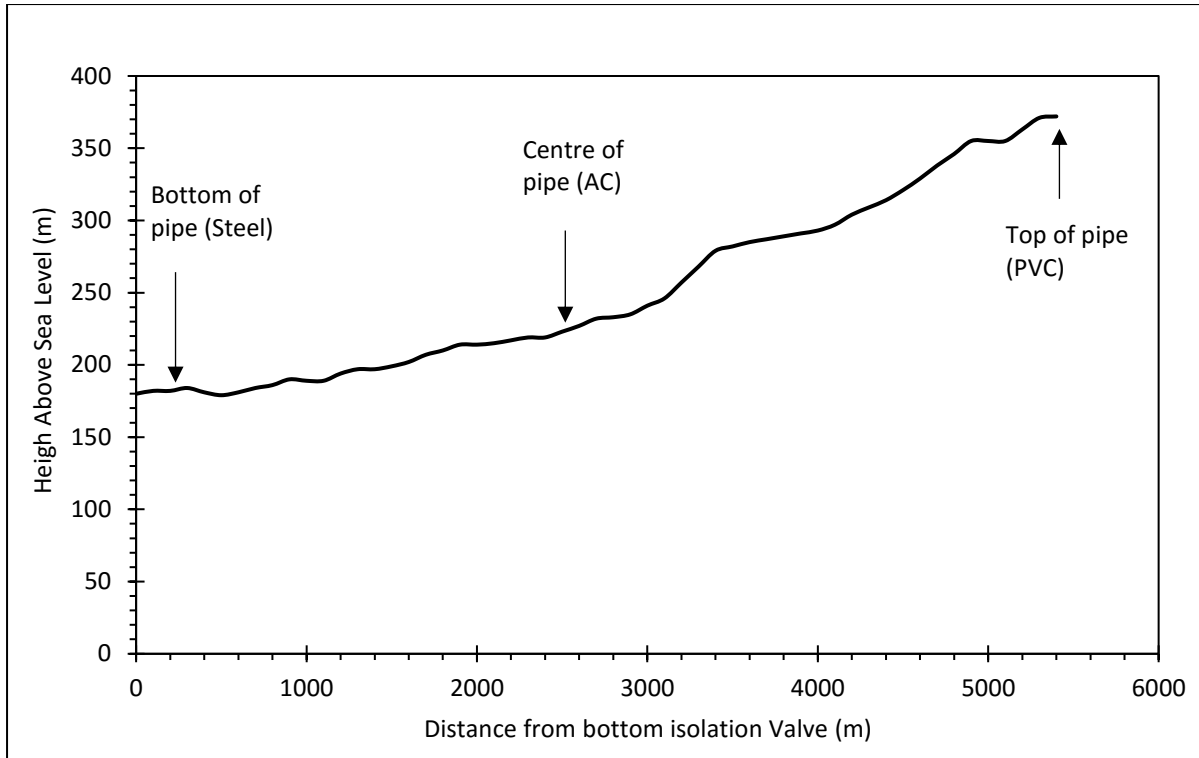
Once the tank was full, the PCAE was transported back to AV1, where the PCAE was reconnected to the BS 8 pipeline. The PCAE pump was switched on, and the leak test was executed.

### **5.8.3 Leak test data analysis and results**

#### ***5.8.3.1 Data analysis procedure***

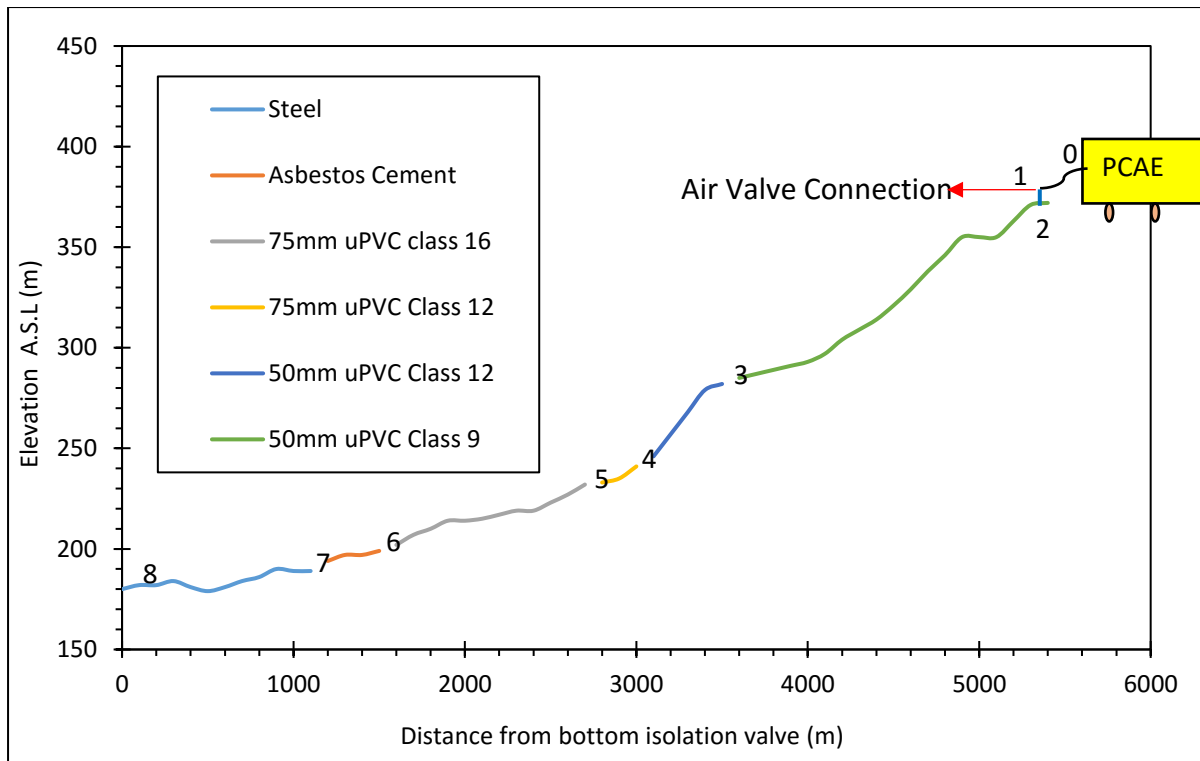
For this test, it was important to take into account the significant elevation difference, of about 190m, between the top and the bottom of the test pipeline. This was important because, depending on where the leakage occurred on the test pipeline, the pressure readings obtained by the PCAE need to be adjusted to reflect the pressure where the leak is anticipated on the pipeline, failing which, the results could be affected. Because the pipeline is a gravity line, the pressures along the pipeline can be determined by simply adding the static head pressure, due to the elevation difference to the pressure measured by the PCAE.

Since the PCAE was connected at the top of the BS8 pipeline, this implied that the measured pressure data represented only the pressure at the top of the pipeline. The measured pressure then had to be adjusted for the different points on the BS 8 pipeline, i.e. at the centre and bottom of the pipe, as shown in Figure 5-53.



*Figure 5-53: Elevation profile showing the different points analysed (top, centre and bottom) on the BS 8 pipeline.*

Since the BS 8 pipeline consisted of multiple pipelines, nodes were assigned at points where the pipeline changed either its pipe material or pipe diameter. Figure 5-28 shows the elevation profile with the various nodes depicting changes in pipe material and diameter along the BS 8 pipeline. The figure also shows where the PCAE was connected on the pipeline.



*Figure 5-54: Elevation profile of the BS 8 pipeline with various nodes depicting change in pipe material and diameter*

The pipe properties associated with each section of pipe, i.e. between nodes, are given in Table 5-15. The properties listed in this table are used for data analysis to calculate the head losses between each node and therefore adjust the pressure accordingly for each node.

Table 5-15: Summary of the various pipe sections properties of the BS8 pipeline used for analysis

Pipe properties	Delivery hose pipe	Connection pipe	uPVC class 9	uPVC Class 12	uPVC Class 12	uPVC Class 16	AC	Steel
Pipe Section Identity	0-1	1-2	2-3	3-4	4-5	5-6	6-7	7-8
Length (m)	10	1.5	1905	569	227	1165	483	1052
Diameter (mm)	50	25	50	50	75	75	75	50
Absolute roughness, e (mm)	0.3	0.045	$1.5 \times 10^{-3}$	$1.5 \times 10^{-3}$	$1.5 \times 10^{-3}$	$1.5 \times 10^{-3}$	3	0.045
Minor loss coefficient, K	0.3	0.33	0.5	0	0.51	0	0	0.22
Acceleration due to gravity, g (m/s <sup>2</sup> )	9.81	9.81	9.81	9.81	9.81	9.81	9.81	9.81
Fluid Density, $\rho$ (kg/m <sup>3</sup> )	1000	1000	1000	1000	1000	1000	1000	1000
Fluid Kinematic Viscosity, $\nu$ (kg/m.s)	$1.14 \times 10^{-6}$	$1.14 \times 10^{-6}$	$1.14 \times 10^{-6}$	$1.14 \times 10^{-6}$	$1.14 \times 10^{-6}$	$1.14 \times 10^{-6}$	$1.14 \times 10^{-6}$	$1.14 \times 10^{-6}$
Elevation difference, $\Delta z$ (m)	1.5	1.5	67	20	8	41	30	24
e/D	$6.00 \times 10^{-3}$	$1.80 \times 10^{-3}$	$3.00 \times 10^{-5}$	$3.00 \times 10^{-5}$	$2.00 \times 10^{-5}$	$2.00 \times 10^{-5}$	$4.00 \times 10^{-2}$	$9.00 \times 10^{-4}$
Pipe Area, A (m <sup>2</sup> )	$1.96 \times 10^{-3}$	$4.91 \times 10^{-4}$	$1.96 \times 10^{-3}$	$1.96 \times 10^{-3}$	$4.42 \times 10^{-3}$	$4.42 \times 10^{-3}$	$4.42 \times 10^{-3}$	$1.96 \times 10^{-3}$

### 5.8.3.2 Data interpretation

A graphical representation of the raw flow and pressure data, plotted against time, is shown in Figure 5-55. The flow rate represents the leakage flow rate, and the graph clearly shows that there was some significant leakage on the BS 8 pipeline.

It is typically expected that the pressure and flow rate profile, over the same period, would show similar profile patterns. For this test, for example, both data profiles were expected to show a clear step up and step down that is repeated for the duration of the test. However, Figure 5-55 suggests that only the pressure data showed a clear step up and step down pattern, whilst the flow rate data did not vary significantly throughout the period of the test. This was an unexpected result. However, this anomaly can be attributed to the elevation difference between the point the PCAE was connected to the BS 8 pipeline and the point on the pipeline where the leakage actually occurred.

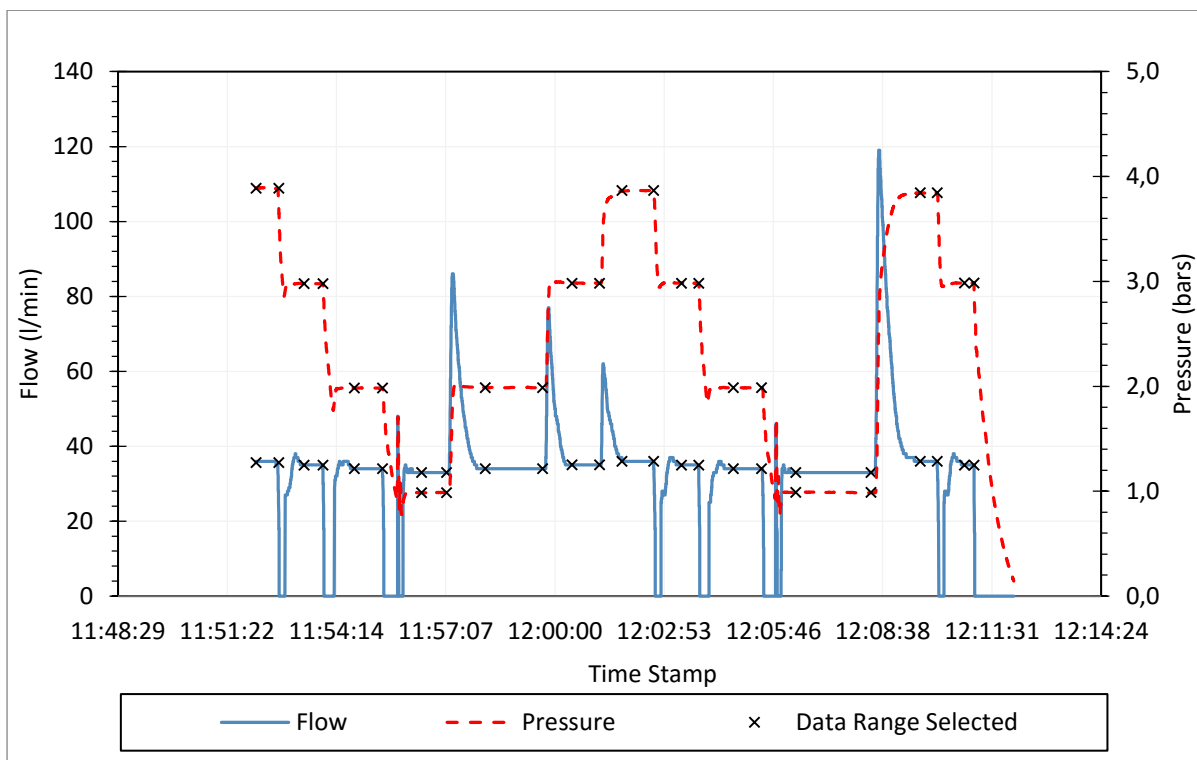


Figure 5-55: Showing the pressure and flow data for the BS8 pipeline test 1

In general, it was observed, from c, that the pressure steps were more stable compared to the flow steps. It was also observed that the largest fluctuations in the flow steps occurred at the

beginning of the step, typically when the pressure was changed or varied. For instance, when the pressure step increased, a sudden spike in the flow rate occurs before the flow rate stabilises; and when the pressure is decreased, the reverse happens. This was because a sudden increase in pressure increases the pipe diameter and, consequently, increases the volume of water entering the pipe. A decrease in pressure, on the other hand, reduces the volume of water entering the pipe and, thus, will result in a sudden reduction in flow rate.

The x-markers on the graphs indicate the periods of stable flow and pressure that were used in the analysis. Table 5-16 shows the averaged stabilised flow and pressure data for the BS 8 pipeline at the top, centre and bottom of the pipeline.

*Table 5-16: Averaged flow and pressure values for the BS 8 pipeline at the top centre and bottom.*

Average Flow (l/min)	Pressure at Top (m)	Adjusted Pressure at Centre (m)	Adjusted Pressure at Bottom (m)
36	37	127	217
35	27	117	207
34	17	107	197
33	7	97	187
34	17	107	197
35	27	117	207
36	36	126	216
35	27	117	207
34	17	107	197
33	7	97	187
36	36	126	216
35	27	117	207

### **5.8.3.3 Leakage parameters for the power equation**

The flow and pressure data points, from Table 5-16, were plotted on a graph for each case scenario, and a power equation was fitted to the data points, as shown in Figure 5-56. The power equation was used to determine the leakage exponent  $Nl$  and the leakage coefficient  $C$  for each scenario. It can be seen that the three power equations had an  $R^2$  greater than 0.9, suggesting the power equation was a good fit to the data points for all three cases.

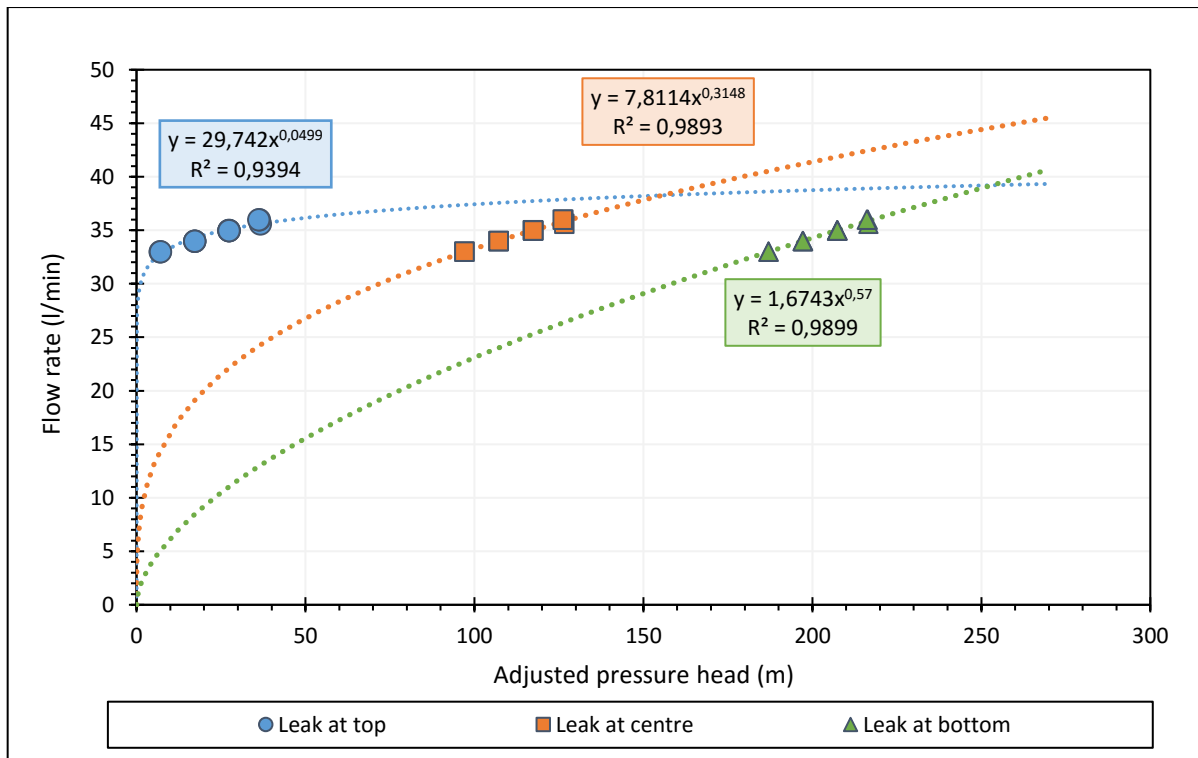


Figure 5-56: Flow Rate against Pressure for the Three Scenarios

From Figure 5-56 it can be seen that the data points with higher pressure simply shifted the flow rate data to the right hand side of the graph. Consequently, the three scenarios presented different power equations and, therefore, different *NI* leakage parameters. The results in Figure 5-56 show that if the leak were at the top or at the centre, the *NI* leakage exponent would be 0.0499 and 0.31, respectively, which is less than the theoretical value of 0.5. However, if the leak were at the bottom, the *NI* leakage exponent would be slightly greater than the theoretical value, at 0.57. Table 5-17 shows a summary of the *NI* leakage parameter results.

Table 5-17: Showing the *NI* Leakage Parameters Results

Scenario	<i>NI</i>	C	R <sup>2</sup>
Leak at the top of the pipe	0.049	29.7	0.94
Leak at the centre of the pipe	0.32	7.81	0.99
Leak at the bottom of the pipe	0.56	1.67	0.99

From Table 5-17, a comparison can be made between the leakage parameter results of the three case scenarios. For the leak at the top, where the pipe material was a uPVC section, the *NI* of



0.049 is highly unlikely, because this result suggests that the leak closes with pressure, which is not common in plastic pipes in the field (Greyvenstein & van Zyl, 2005; Malde & van Zyl, 2015). For the leak at the centre, where the BS 8 pipeline consists of an AC pipe section, the  $NI$  of 0.32 is also unlikely for such a rigid pipe. The  $NI$  of less than 0.5, for the leak at the centre, also suggests that the leak closes as the pipe pressure increases. For the leak at the bottom on the steel pipe section, the  $NI$  was slightly greater than 0.5, which is a typical  $NI$  result for steel pipes with round holes ( Ferrante et al., 2014; Greyvenstein & van Zyl, 2005). Based on this, the most likely result is the result found for the leak at the bottom.

#### **5.8.3.4 Leakage parameters for the modified orifice equation**

To determine the modified orifice equation leakage parameters, the effective initial leak area ( $C_d A_0$ ) and effective head-area slope ( $C_d m$ ) for each case scenario had to be determined. This was done by determining the effective leak areas ( $C_d A$ ) at each pressure step using the orifice equation. Table 5-18 shows the results of the effective leak areas for the BS 8 pipeline at the top, at the centre and at the bottom.

*Table 5-18: The Effective Area against pressure for the Three Scenarios*

Adjusted Pressure at Top (m)	Adjusted Pressure at Centre (m)	Adjusted Pressure at Bottom (m)	Effective Area at Top (mm <sup>2</sup> )	Effective Area at Centre (mm <sup>2</sup> )	Effective Area at Bottom (mm <sup>2</sup> )
37	127	217	22	12	9.10
27	117	207	25	12	9.14
17	107	197	31	12	9.11
7	97	187	47	13	9.08
17	107	197	31	12	9.11
27	117	207	25	12	9.15
36	126	216	22	12	9.21
27	117	207	25	12	9.14
17	107	197	31	12	9.11
7	97	187	47	13	9.08
36	126	216	23	12	9.21
27	117	207	25	12	9.14

The effective leak area and pressure data points, from Table 5-18, were plotted on a graph for each case scenario, and a linear equation was fitted to the data points, as can be seen in Figure 5-57.

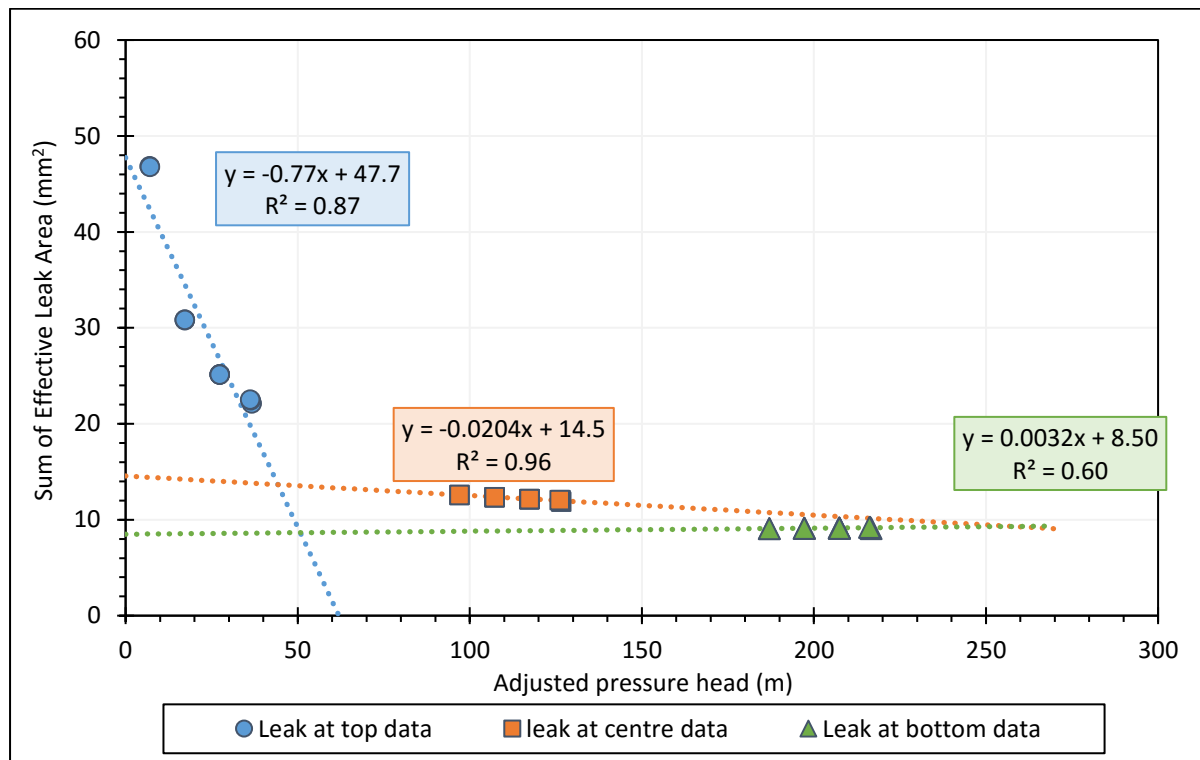


Figure 5-57: Showing the Modified Orifice Equation Leakage Parameters

Figure 5-57 shows how the effective leak area varies with the pressure head for the three scenarios: i.e. for leaks at the top, centre and bottom. The effective leak area changes differently for all three scenarios. The leak at the top and centre portrayed a negative head–area slope of  $-0.77\text{mm}^2/\text{m}$  and  $-0.02\text{mm}^2/\text{m}$ , respectively, suggesting that the leak areas contracted as pressure increases. The leak at the bottom, however, portrayed a small positive head-area slope of  $0.0032\text{mm}^2/\text{m}$  indicating that the leak area expanded ever so slightly with increasing pressure.

It was also clear that the initial leak areas ( $C_dA_0$ ), for all three scenarios, were different. The leak at the top had the largest initial leak area of  $47\text{mm}^2$ , followed by the leak at the centre, with a  $C_dA_0$  of  $14.5\text{mm}^2$ . The leak at the bottom had the smallest initial leak area of  $8.50\text{mm}^2$ .

Table 5-19 summarises the Modified Orifice Equation leakage parameter results for the three case scenarios.

Table 5-19: Shows a Summary of the Modified Orifice Equation Leakage Parameter Results

Scenario	Effective initial leak area, $A'_0$ (mm <sup>2</sup> )	Effective head-area slope, $m'$ (mm <sup>2</sup> /m)
Leak at the top of the pipe	47.7	-0.77
Leak at the centre of the pipe	14.5	-0.02
Leak at the bottom of the pipe	8.50	0.0032

Table 5-19 compares the modified orifice equation leakage parameters for the three case scenarios. For the leak at the top, the result obtained suggested that the uPVC section of the BS 8 pipeline consisted of a circumferential crack, which was highly unlikely to occur because the uPVC plastic pipes were relatively new installations.

For the leak at the centre, the results obtained suggested that the AC section of the BS 8 pipeline had a circumferential crack, which results in the negative head-area slope. This is inconsistent with typical failures reported to occur on AC pipes, which are commonly longitudinal cracks (Greyvenstein & van Zyl 2005).

Finally, for the leak at the bottom, the results obtained suggest that the steel section of the BS 8 pipeline consisted of small round holes. This is consistent with small corrosion holes, which have been reported to occur on metallic pipes, such as steel. The small positive head-area slope is also consistent with findings from experimental and modelling studies (Cassa and van Zyl, 2014; Malde & van Zyl, 2015; Nsanzubuhoro et al, 2016) that have investigated the leak behaviour of round holes.

### ***5.8.3.5 Linking power equation and the modified orifice equation to data***

The  $NI$  and modified orifice equation flow prediction, for each case scenario, was determined to compare the equations to the data.

Table 5-20 shows the power equations and the modified orifice equations for the three scenarios. The leakage parameters obtained in Sections 5.8.3.3 and 5.8.3.5 were used to formulate these equations.

Table 5-20: Power equation and modified orifice equations for the three case scenarios

Scenario	Power Equation (l/min)	Modified orifice equation ( $60 \times 10^{-3}$ l/min)
Leak at top	$Q = 29.7 h^{0.049}$	$Q = \sqrt{2g}(47.7h^{0.5} - 0.77h^{1.5})$
Leak at centre	$Q = 7.81 h^{0.36}$	$Q = \sqrt{2g}(14.5h^{0.5} - 0.02h^{1.5})$
Leak at bottom	$Q = 1.67 h^{0.56}$	$Q = \sqrt{2g}(8.50h^{0.5} + 0.0032h^{1.5})$

Using the equations in, the flow rates were generated for various pressure heads, ranging from 0 to 270m. The flow rates for the N1 and modified orifice equation were then plotted with the data in order to see how well the equations fit the data. Figure 5-58 shows the power equation and the modified orifice equation alongside the data points for the three scenarios.

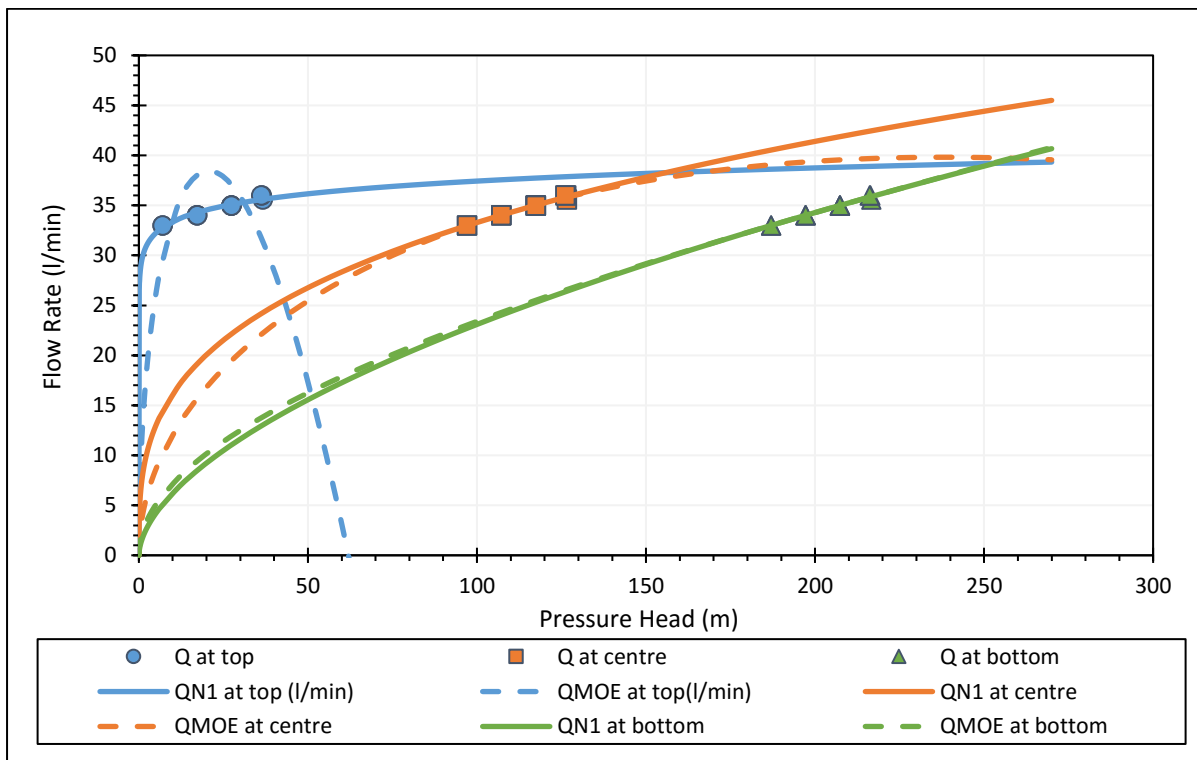


Figure 5-58: Shows the comparison of the power equation and the modified orifice equation to the data

From Figure 5-58, it can be seen that for each case scenario the N1 and the modified orifice equation predicted flows differently for the examined pressure range.

For the leak at the bottom, the *NI* and the modified orifice equation are almost identical and fit the data points well. This can be attributed to the nature of the leak: since it is a round hole with a very small head-area slope, it can be assumed that only the first term of the modified orifice equation contributes significantly. A close look at the first term of the modified orifice equation, for the leak at the bottom, shows it is clear that its form is very similar to the power equation obtained for the leak at the bottom, with a 12% difference in their leakage exponent.

For the leak at the centre, the *NI* and the modified orifice equation predicted the data points well. However, differences were seen, especially at lower and higher pressures of the measured data. The power equation predicts a higher flow rate at lower pressure (van Zyl et al., 2017). For the leak at the centre, it was observed that the *NI* and the modified orifice equation fit the data points well. However, at pressures below 90 meters and above 130 meters, the power equation predicts higher flows, compared to the modified orifice equation. It can also be seen that the flow, predicted by the modified orifice equation, reaches a peak and starts reducing with pressure. This can be attributed to the negative head-area slope that indicates that the leak closes with increasing pressure.

For the leak at the top, it was observed that the *NI* and the modified orifice equation showed the largest differences. For this scenario, only the power equation fitted the data points. The modified orifice equation showed a negative parabolic relationship between the predicted flow and pressure. This relationship can be attributed to the large negative head-area slope that resulted in the second term of the modified orifice equation that accounts for the varying leak area being dominant. This finding was consistent with the theoretical discussion about the behaviour of leak openings with negative head-area slopes and positive initial leak areas (van Zyl et al., 2017).

#### **5.8.4 Comparing the leak test results with field condition**

The OWB team had scheduled a pipe replacement for the steel pipe section of the BS 8 pipeline. This replacement was triggered by a stream that had emerged near this section of the BS 8 pipeline. This pipe replacement was due to take place two weeks after the condition assessment was done, using the PCAE. The total length of steel pipe that was replaced was approximately 100m.

Unfortunately, during the time that the work for removing the pipe took place, the author was not present. However, after consultation with the OWB, it was revealed that small round holes

were found on the top of the steel pipe. This finding was consistent with the results of the condition assessment leak test.

The detected leakage on the steel section of the BS 8 pipeline could, therefore, be characterised as follows:

*Table 5-21: Characteristics of the leakage detected on the steel section of the BS 8 Pipeline*

<b>Leakage Parameters</b>	<b>Values</b>
Initial Leak Area, $A'_0$ (mm <sup>2</sup> )	8.50
Head-Area Slope, $m'$ (mm <sup>2</sup> /m)	$3.2 \times 10^{-3}$
Leakage Exponent N1	0.56
Leakage Coefficient C	1.67

The total size of the leaks was 8.50 mm<sup>2</sup> and the leaks expanded by 3.2mm<sup>2</sup> per meter of pressure head – not very sensitive to pressure. The *NI* leakage exponent was 0.56, also suggesting that the leak was not very sensitive to pressure. The obtained leakage parameters were consistent with a round hole leak, potentially due to corrosion on the steel pipe.

Equation 5-11 and Equation 5-12 represent the N1 and Modified orifice equation that can be used to predict the leakage flow rate through the steel section of the BS8 pipeline.

$$Q = 1.67h^{0.56}$$

*Equation 5-11*

$$Q = \sqrt{2g}(8.50h^{0.5} + 0.0032h^{1.5})$$

*Equation 5-12*

The leakage number was also obtained to be:

$$L_N = 3.76 \times 10^{-4}h$$

*Equation 5-13*

## **5.9 BS 8 Pipeline - Test 2**

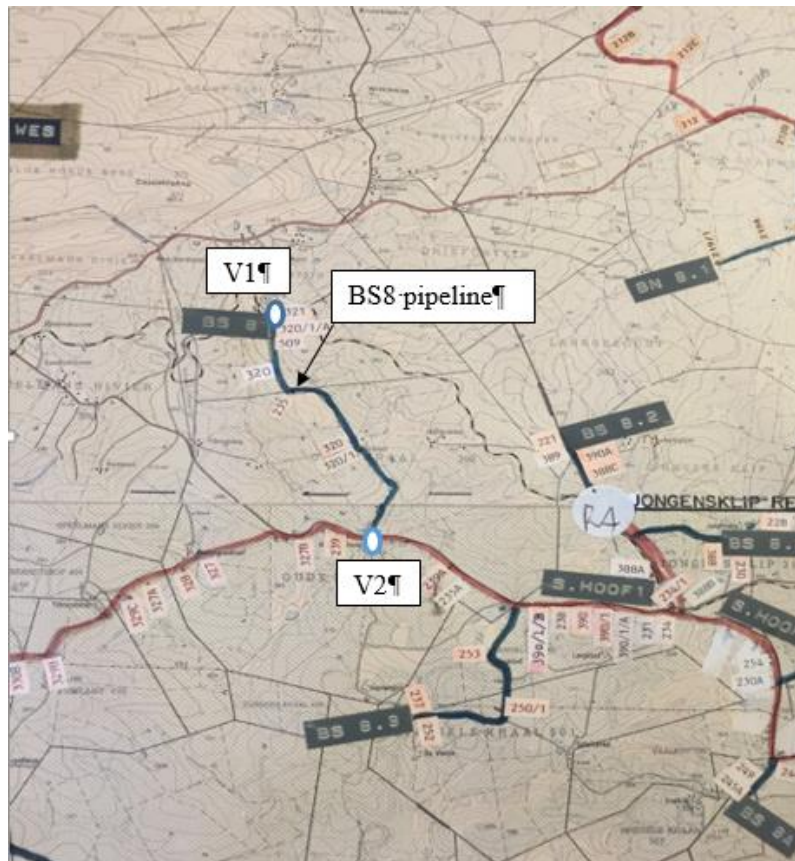
### **5.9.1 Introduction**

A second test was conducted on the same BS 8 pipeline in the Overberg region. The second test was done after a section of the leaking steel pipe was replaced. This section will discuss the the field-test results that were obtained for the second test. The results of the second tests

will be compared to the results obtained in the first test, to assess whether the extent of leakage improved or became worse after the steel section was replaced.

## 5.9.2 Leak test procedure

The first step was to fill the PCAE water tank. Unlike Test 1, where the tank was filled via a bottom air valve connection on the BS 8 pipeline, for Test 2, the tank was filled via a reservoir. Figure 5-59 shows the location of the reservoir in the Overberg network, labelled as R4 in the figure. This reservoir is called Jongensklip Reservoir and stores water from the main pipe (S. Hoof) – through which the BS 8 pipeline is charged. The stored water in the reservoir is then gravitated back to the main pipe via the BS 8.2 pipeline.



*Figure 5-59: Location of the Jongensklip reservoir*

Figure 5-60 shows the Jongensklip Reservoir on site. The reservoir had a tap connection. A hosepipe was connected to the tap, and the hosepipe was directed into the water tank, as depicted in Figure 5-61. The tap from the reservoir was opened until the tank was full.



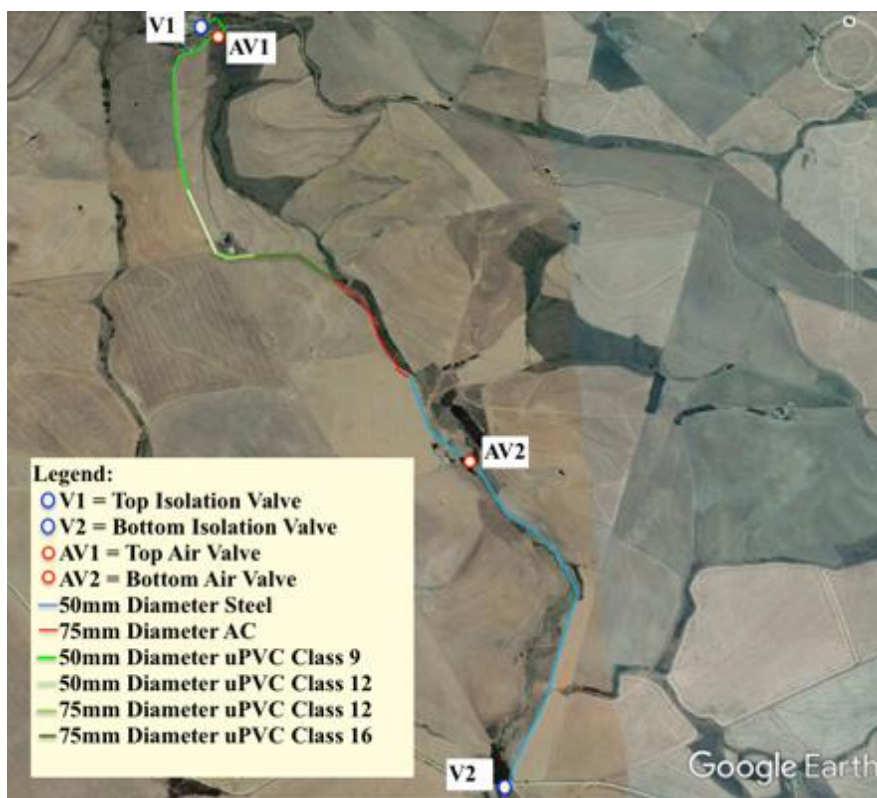
*Figure 5-60: Jongensklip Reservoir*



*Figure 5-61: Filling the PCAE Water Tank using a Hosepipe Connected to the Tap Reservoir*

Once the tank was full, the PCAE was transported to the point on the BS 8 pipeline where it would be connected for the condition assessment test. As in Test 1, the most suitable point of connection for Test 2 was also the topmost air valve - for similar reasons highlighted in Section 5.8.2. Figure 5-62 shows the location of the topmost air valve (AV1) on the BS 8 pipeline layout.





*Figure 5-62: AV1 the Topmost Air Valve where the PCAE was Connected for the Leak Test*

After removing the air valve at AV1 and connecting the 50mm delivery hosepipe, it was observed that there was no water flowing from the BS 8 pipeline. Water was expected to flow directly from the BS 8 pipeline once the shut off valve at the connection point was fully opened. However, this was not the case.

After investigating various possibilities as to why no water was flowing out of the BS 8 pipeline, it was discovered that the OWB operations team, assisting on site, had isolated the BS 8 pipeline about 20 minutes prior to our arrival. This prolonged pipe isolation period had some implication, because the water in the pipeline had started draining out. Subsequently, there was no water at the top of the pipe (AV1) where the PCAE was connected.

In order to resolve this problem, the bottom isolation valve (V2 in Figure 5-62) was opened to allow the BS 8 pipeline to be recharged. It was not known how long it would take to recharge the pipe. Therefore, the shut-off valve at the point of connection was left opened, while the pipeline recharged, to monitor when the pipeline was sufficiently charged.

After the BS 8 pipeline was sufficiently charged, the PCAE was connected to the connection point to carry out the leak test. Prior to carrying out the leak test, the BS 8 pipeline was isolated again, by closing the bottom isolation valve.

### 5.9.3 Leak test results

#### 5.9.3.1 Data interpretation

The isolated BS8 pipeline was analysed as one system with the PCAE connected to it, as depicted in Figure 5-63. In the figure, the BS 8 pipeline is shown with its various pipe materials. Nodes were assigned to every connection point as well as any change in pipe material and pipe diameter on the BS8 pipeline. An intermediate node *i* was introduced between node 2 and 3, as no leak was expected to occur beyond node 3.

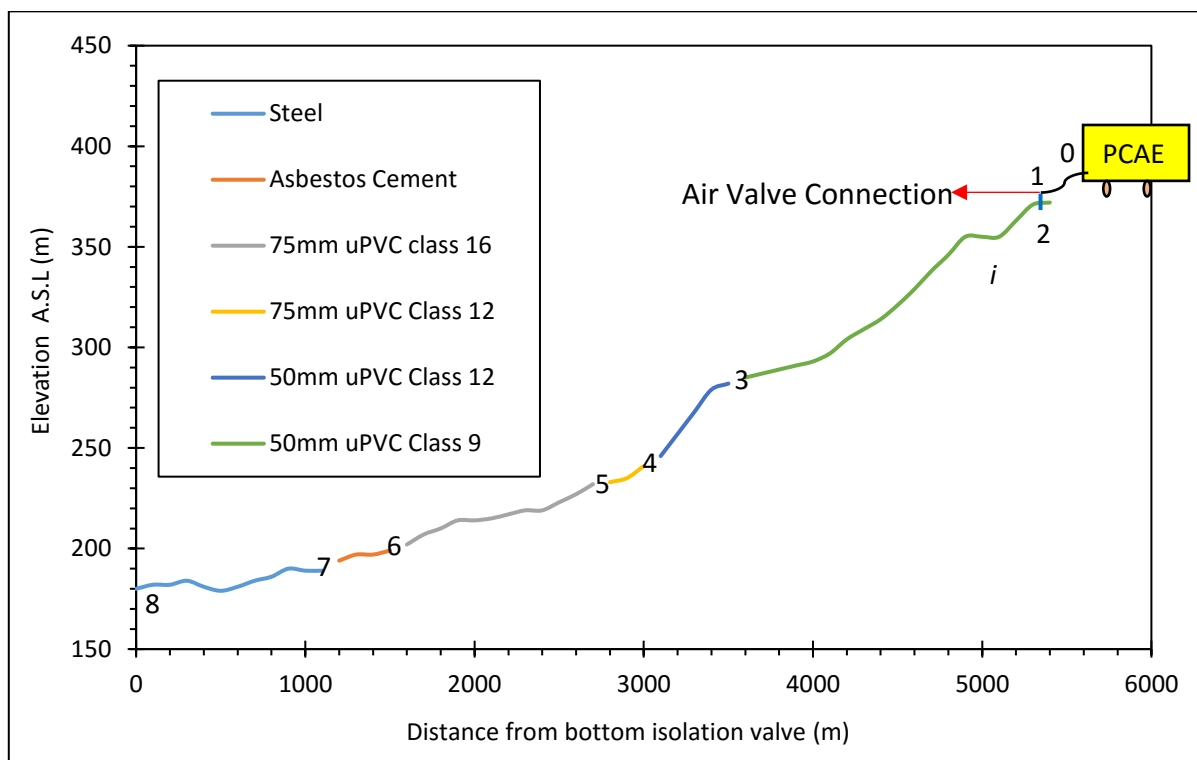


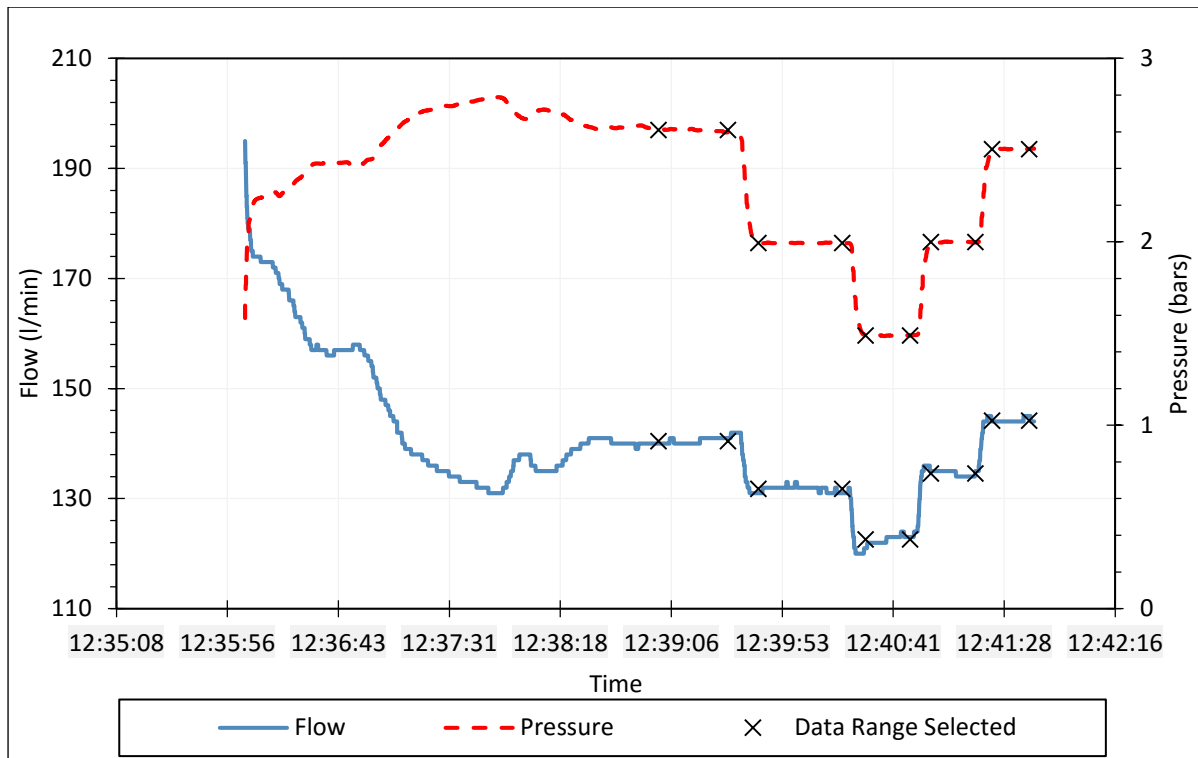
Figure 5-63: BS8 pipeline elevation profile with nodes from 0-8 showing its various pipe material and diameters

Table 5-22 shows a summary of the elevations for all the nodes.

Table 5-22: Node elevations

Node	Elevation (m)
0	373
1	371.5
2	370
3	303
4	283
5	275
6	234
7	204
8	180

Figure 5-64 shows a graphical representation of the flow and pressure raw data recorded using the PCAE at the connection point. It can be seen from the figure that, when the flow rate and pressure both stabilised, the pressure was reduced by two incremental steps and, thereafter, increased. The results show that a very large leak was present on the pipe with flow rate as high as 190 L/min (11.4 m<sup>3</sup>/h) at a pump pressure of only 2 bar. Due to the large leakage, only five stabilised steps were achieved before the water in the tank was emptied.



*Figure 5-64: Flow and Pressure Profile*

The graphical representation of the data was then used to identify stabilised levels of flow and pressure. The pressure and flow data range selected is indicated by the markers in Figure 5-64. The flow and pressure data for each node was determined.

The flow and pressure data obtained for node 1, node 2 and node i (See Figure 5-63) were the only data set used for this analysis. This was because the pressures at node 3 to node 8 were found to be negative. The negative pressures were because of the high friction head losses experienced on the pipe section between node 2 and node 3 - containing a 50mm diameter uPVC class 9 pipe. The negative pressures suggested that a leak could not physically occur at this point. For this reason, an intermediate point upstream of node 3 with positive pressures was required for the analysis. Hence, the introduction of node i, which was located about 200m just downstream of node 2. Table 5-23 shows the results of the flow and pressure at node 1, node 2 and node i.

Table 5-23: The averaged flow and pressure at Node 1, 2, and i

Q (m <sup>3</sup> /s)	h <sub>1</sub> (m)	h <sub>2</sub> (m)	h <sub>i</sub> (m)
2.34x10 <sup>-03</sup>	27.59	26.92	69.70
2.20x10 <sup>-03</sup>	21.36	20.94	64.40
2.04x10 <sup>-03</sup>	16.29	16.12	60.25
2.24x10 <sup>-03</sup>	21.40	20.90	64.15
2.40x10 <sup>-03</sup>	26.49	25.71	68.20

### 5.9.3.2 Leakage parameters for the power equation

Figure 5-65 shows the flow and pressure data plotted for the nodes 1, 2 and i. The  $N1$  values for node 1 and 2 were very similar, at 0.29 and 0.3 respectively. Even though these  $N1$ 's were unrealistic, it was clear from these results that the  $N1$  was increasing in the downstream direction. Considering that the node i was located downstream of node 2, the  $N1$  was expected to be higher as can be seen from Figure 5-65, which shows  $N1$  of 1 for node i. This result is consistent with plastic pipe behaviour and therefore could potentially present the most realistic leak on the pipeline.

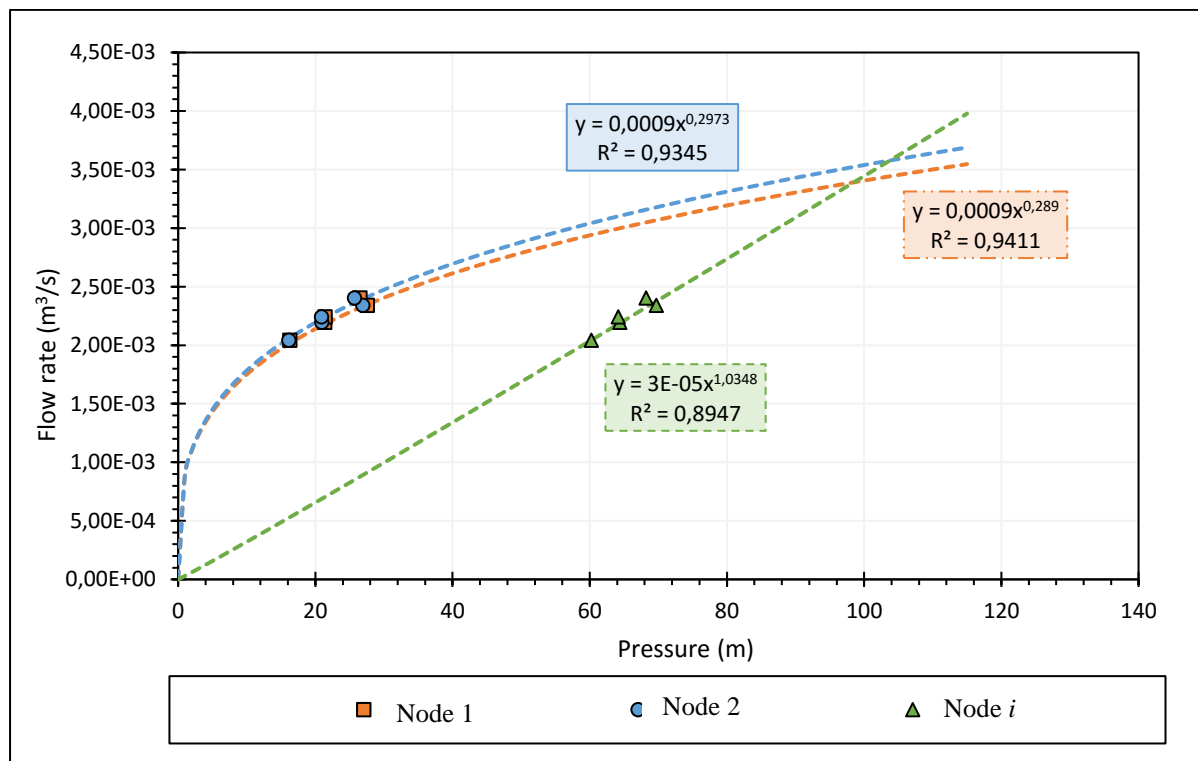


Figure 5-65: Flow and Pressure data with a power equation fitted for node 1, 2 and i

A summary of the power equation leakage parameters is provided in Table 5-24. The data in Table 5-24 shows that the N1 leakage exponent increased downstream of the pipeline, even though node 1 and 2 have similar results. The *N1* parameters for node 1 and 2 are less than 0.5, suggesting that the head – area slope is negative and thus associated with circumferential crack failure. This failure mechanism is not a common in uPVC pipes where node 1 and 2 were located.

*Table 5-24: Summary of the N1 leakage parameters found for BS8 pipeline Test 2*

Node	N1 leakage exponent	Leakage coefficient
1	0.29	$9 \times 10^{-4}$
2	0.3	$9 \times 10^{-4}$
i	1	$3 \times 10^{-5}$

### ***5.9.3.3 Leakage parameters for the modified orifice equation***

The effective area against the pressure head data for node 1, 2 and i are plotted in Figure 5-66. Node 1 and 2, had very similar results both portraying a negative head-area slope of  $-1.1\text{mm}^2/\text{m}$  and  $-1.0\text{mm}^2/\text{m}$ , respectively. These negative head-area slopes suggests that the leaks at these nodes were closing with increasing pressure. On the other hand, the leak at node i, had a positive head-area slope of  $0.5\text{mm}^2/\text{m}$ , suggesting that the leak increases with increasing pressure.

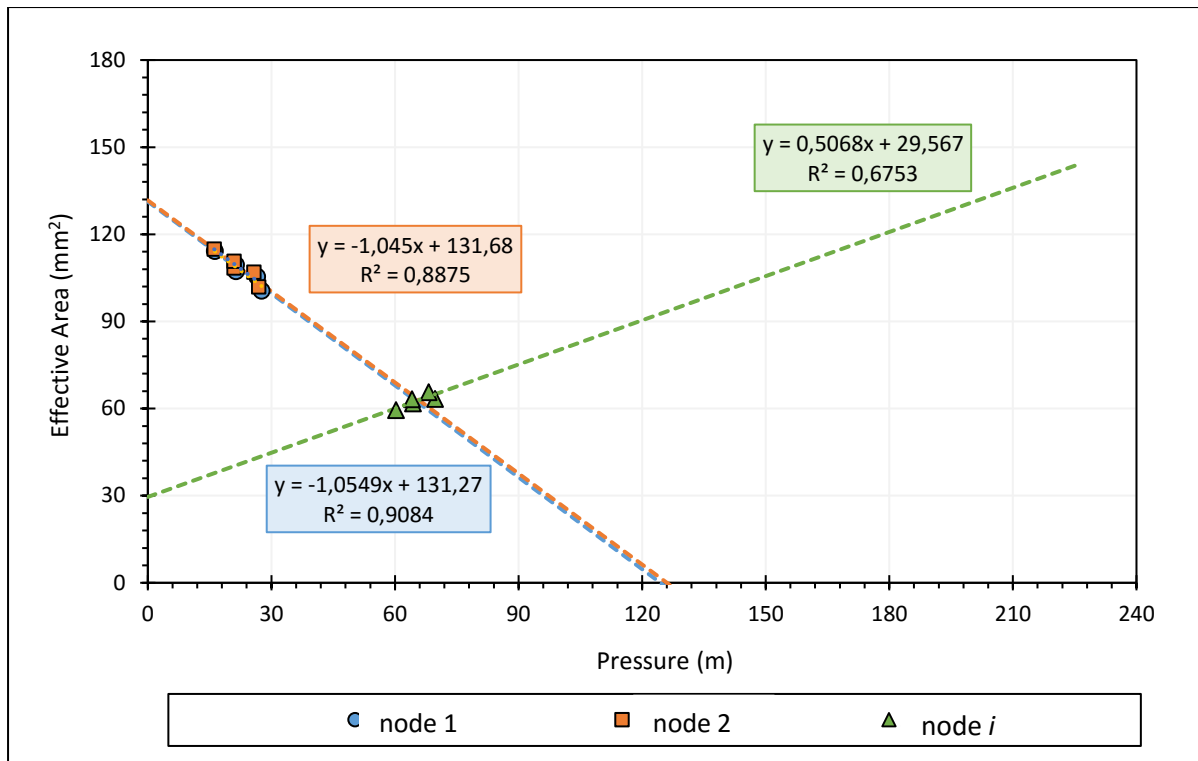


Figure 5-66: Effective area against the pressure head for node 1, node 2 and node i.

#### 5.9.4 Comparison of BS8-pipeline Test 1 and Test 2

Table 5-25 shows a summary of leak test 1 and leak test 2 carried out on the BS 8 pipeline. The table shows that leakage characteristics were different for the two tests. Test 1 results showed that the leak was a round hole on the 50mm diameter steel section of the BS8 pipeline. This was found to be correct. Test 2, which was done after a section of the steel pipe was replaced, showed that a large new longitudinal leak occurred on the pipe, most likely on the middle or upper parts of the uPVC pipe section.

This new longitudinal crack, which was found in test 2, could have occurred due to the increased pressure associated with fixing the previous leak. The leak found on the steel pipe (test 1) could have been releasing excess pressures in pipeline as water escapes through the leak. Therefore, when the leak was fixed, the pressure in the pipeline could have change significantly and thus lead to new leaks occurring elsewhere in the pipe, as it was found in test 2.

Table 5-25: Comparison of results from test 1 and test 2 of the BS8-Pipeline

Leak characteristics	Test 1	Test 2
Section on the pipe	Steel	uPVC
Effective initial leak area, $A'_0$ (mm <sup>2</sup> )	8.5	29.6
Effective head-area slope, $m'$ (mm <sup>2</sup> /m)	$3.2 \times 10^{-3}$	0.5
N1	0.56	1
Leak type	Round hole	Longitudinal crack

## 5.10 Wingfield Pipeline – Test 1

### 5.10.1 Introduction

The test pipeline examined at the Wingfield Military Base was a bulk Asbestos Cement Pipeline. Figure 5-67 shows the layout of the Wingfield pipeline, spanning from valve AV1 to valve V4. The main characteristics of the Wingfield pipeline are  $L = 1000\text{m}$ , DN300 (nominal diameter) and the pipeline depth below ground level was 1m.

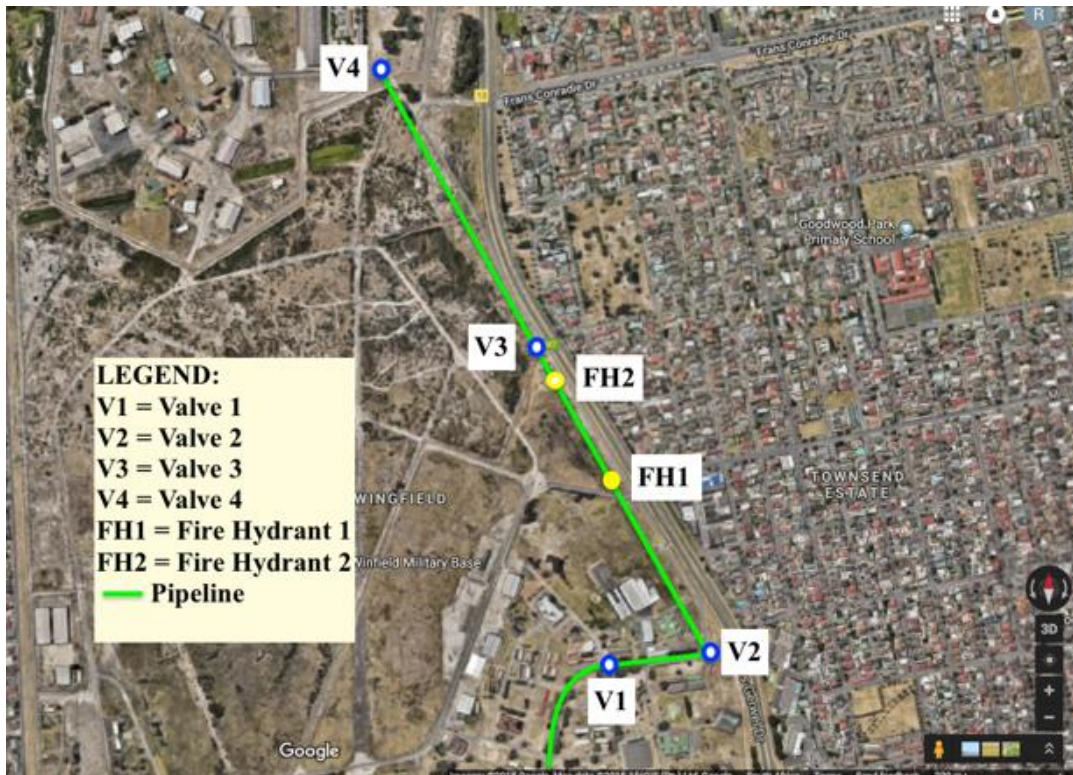
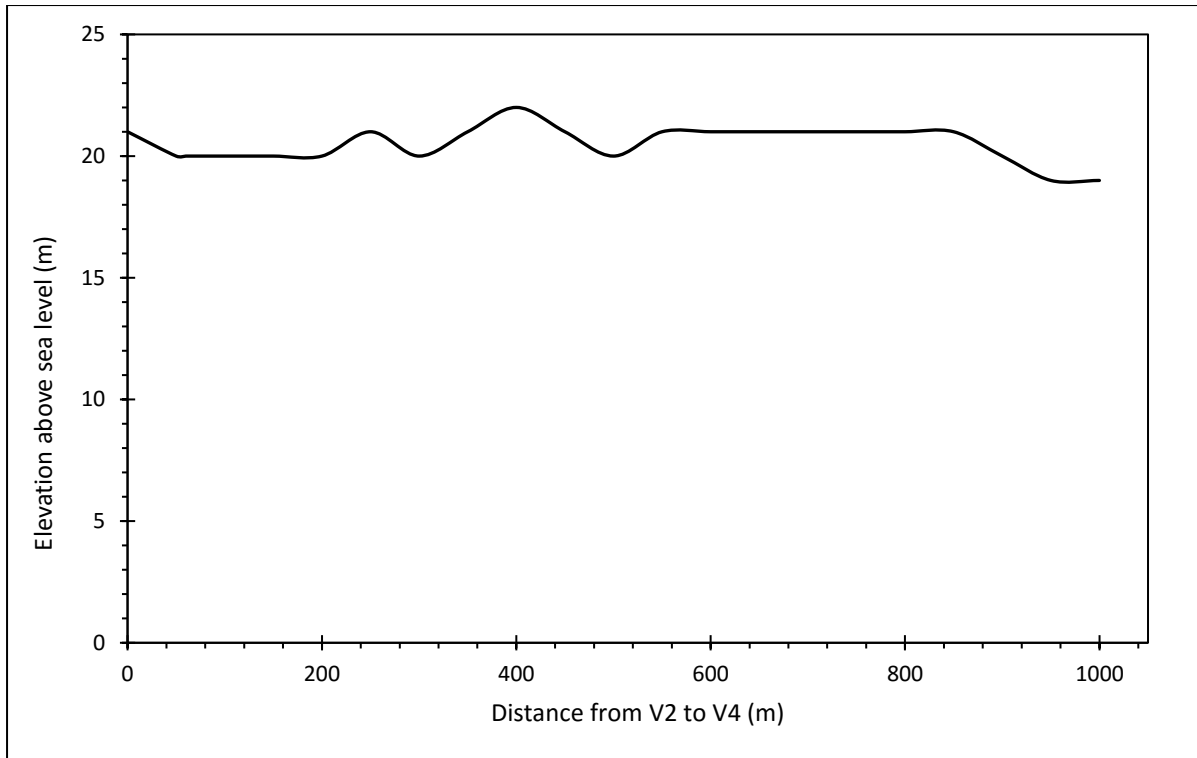


Figure 5-67: Wingfield pipeline layout



Figure 5-68 shows the elevation of the Wingfield test pipe from V2 to V4. It can be seen from the figure that the overall elevation did not vary much for the test pipe.



*Figure 5-68: Elevation profile from valve V2 to valve V4*

The test pipe was identified in consultation with a consulting company named Re-Solve which, at the time of the tests, were doing water demand and leakage management on several of the Department of Public Works' sites, Wingfield being one of them.

The identified Wingfield pipeline was empty because it was not in use at the time of the tests. Consequently, prior to commencing the tests, the test pipe had to be charged with water. This meant that valve AV1, in Figure 5-67, had to be open fully to allow water from the Wingfield pipe network to charge the entire test pipe. After about 10 minutes, the test pipe was fully charged with water.

### 5.10.2 Leak test procedure

The above ground fire hydrant, located between V2 and V4, was identified as the most convenient connection point of the test pipe. A 50mm reinforced hosepipe was connected to the fire hydrant, as shown by Figure 5-69.



*Figure 5-69: Shows the PCAE 50mm hosepipe being connected to the fire hydrant*

After successfully connecting to the fire hydrant, the hydrant was flushed briefly to clear sediments and any stagnant water in the hydrant pipe. The flushing process entailed briefly opening the fire hydrant and allowing water from the test pipe to flow through the hydrant and discharge through the hosepipe outlet, shown in Figure 5-70. The figure also shows the colour of the water immediately after the fire hydrant was flushed.



*Figure 5-70: Showing the colour of water during flushing*

The hydrant remained open until the water from the test pipe turned clear, as shown in Figure 5-71. Once the water was clear, the hosepipe outlet was connected to the PCAE tank and the tank was filled up with clear water.



*Figure 5-71: Shows the clear water after flushing*

Once the tank was filled, the tank valve was closed, and the hosepipe was disconnected from the tank to the testing connection of the PCAE. This meant that water was now flowing directly into the PCAE. However, due to the non-return valve in the inverter, water could not flow past the inverter and, thus, there was a pressure build up. This pressure build up was indicated on the display panel of the inverter. The pressure continued to increase until a maximum pressure, which stabilised, and was recorded as the operational pressure in the test pipe.

Once the operational pressure was logged by the PCAE recorder, the PCAE variable speed pump was then activated and set to suitable test pressures. Two tests were done:

- The first test involved isolating Valve V2 and Valve V3, in Figure 5-67.
- The second test involved isolating Valve V2 and V4, in Figure 5-67.

For each test, after the pipeline was isolated, the leak tests was executed.

### 5.10.3 Leak test results

#### 5.10.3.1 Data interpretation

The first test involved isolating the pipeline by closing valve V2 and V3 displayed no leak in the results. No leakage flow rate was detected, and the pressure profile was constant. Because of this, the second test was then carried out, where the pipeline was isolated between V2 and V4.

The raw flow and pressure data obtained from the second test is plotted in Figure 5-72. While the pressure curve is smooth, the flow curve displayed local scatter at the start of the step and then, eventually, stabilised. The stabilised data range, selected for analysis, is shown by the markers in Figure 5-72.

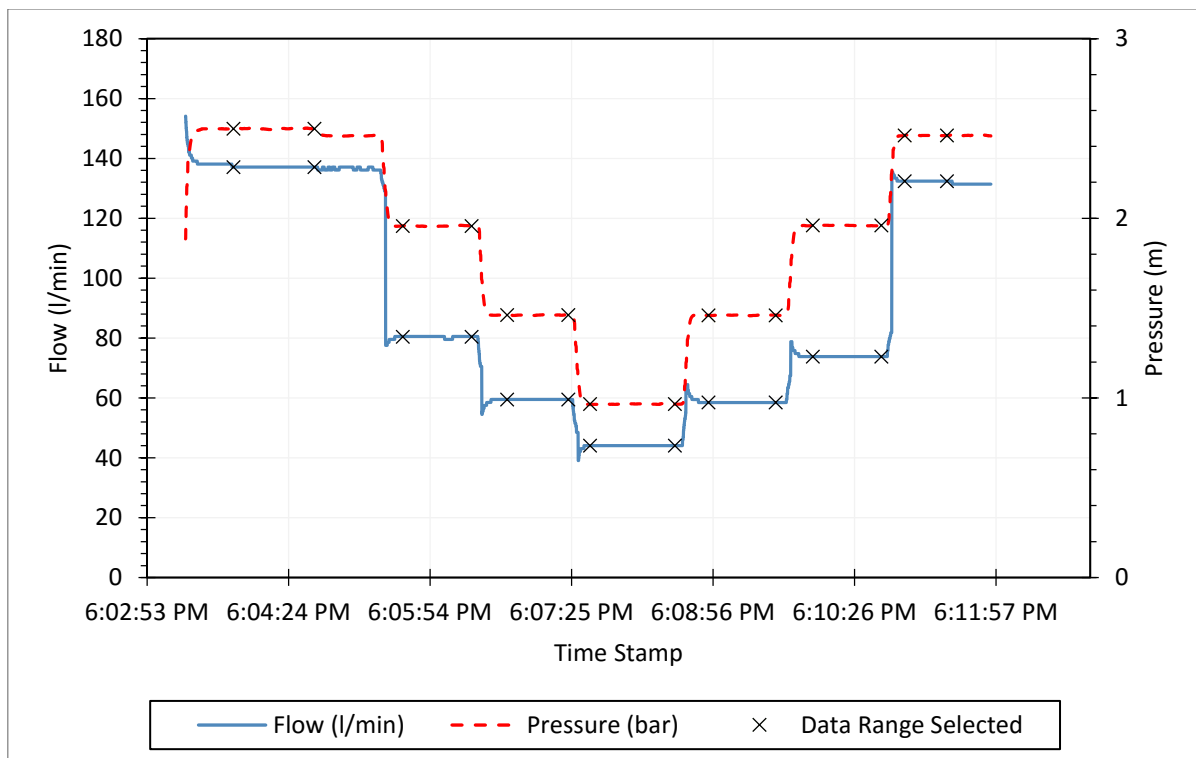


Figure 5-72: Shows the flow against pressure raw data for the Wingfield test pipe

Using the stabilised flow and pressure data points, the average flow and pressure for each step was calculated. Table 5-26 proceeds to show the average pressure and flow values obtained for each step. From Table 5-26, it can be seen that, for each step, the average measured pressure ( $h_{\text{measured}}$ ) and flow ( $Q_{\text{measured}}$ ) were converted to SI units, from bars and l/min, to meters (m) and cubic meters per second ( $\text{m}^3/\text{s}$ ), respectively. Additionally, the measured pressure head (h

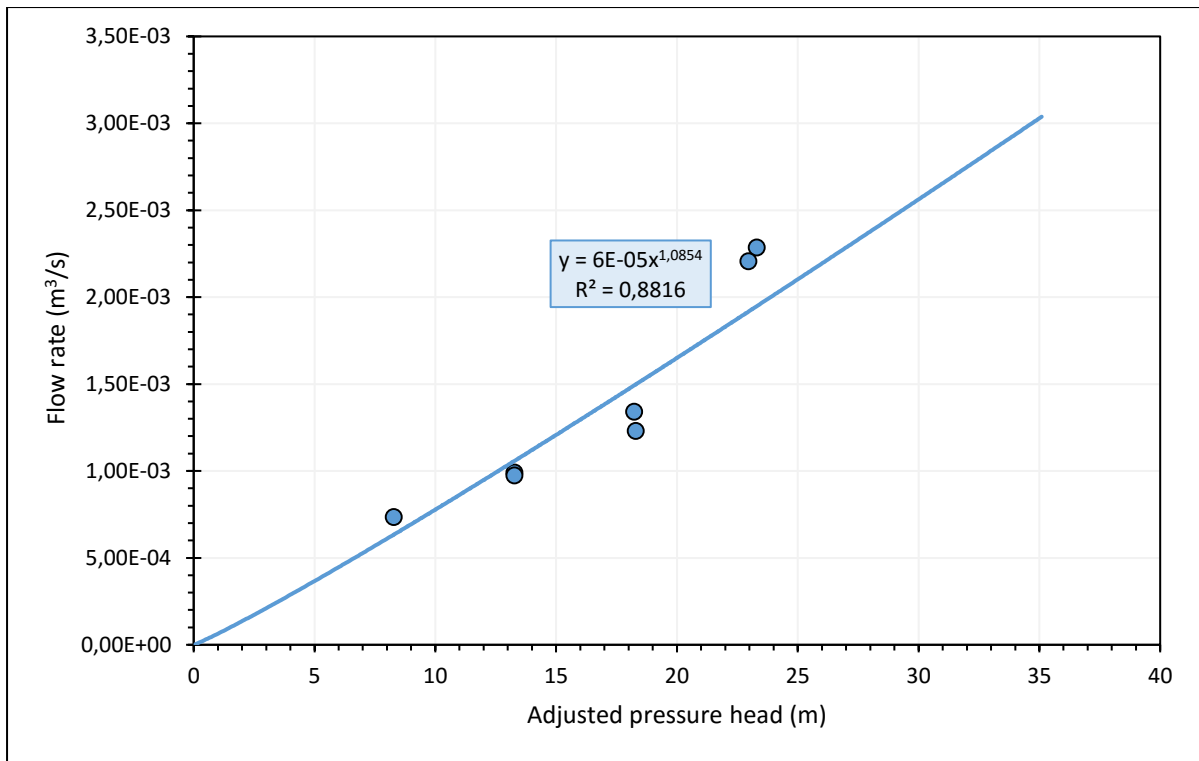
measured) has been adjusted to give the actual pressure in the test pipe ( $h_{\text{adjusted}}$ ) which takes into account the friction losses ( $h_f$ ) and the static head difference ( $h_s$ ) between the test pipe and the PCAE.

*Table 5-26: Shows the averaged stabilised flow and pressure for Each Step Test*

Step	$h_{\text{measured}}$ (bars)	$h_{\text{measured}}$ (m)	$h_f$ (m)	$h_s$ (m)	$h_{\text{adjusted}}$ (m)	$Q_{\text{measured}}$ (l/min)	$Q_{\text{measured}}$ ( $\text{m}^3/\text{s}$ )
1	2.5	25.50	$4.11 \times 10^{-01}$	1.3	23.79	136.6	$2.28 \times 10^{-03}$
2	2	20.40	$1.41 \times 10^{-01}$	1.3	18.96	80	$1.33 \times 10^{-03}$
3	1.5	15.30	$7.59 \times 10^{-02}$	1.3	13.92	58.71	$9.79 \times 10^{-04}$
4	1	10.20	$4.16 \times 10^{-02}$	1.3	8.86	43.44	$7.24 \times 10^{-04}$
5	1.5	15.30	$7.38 \times 10^{-02}$	1.3	13.93	57.87	$9.65 \times 10^{-04}$
6	2	20.40	$1.18 \times 10^{-01}$	1.3	18.98	73.3	$1.22 \times 10^{-03}$
7	2.5	25.50	$3.77 \times 10^{-01}$	1.3	23.82	130.8	$2.18 \times 10^{-03}$

### **5.10.3.2 Leakage parameters for the power equation**

The measured flow rate ( $Q_{\text{measured}}$ ) and the adjusted pressure head were plotted against one another, as shown in Figure 5-73. A power equation was then fitted through the data points to determine the  $N1$  leakage parameters, namely: the  $N1$  leakage exponent and the leakage coefficient ( $C$ ).



*Figure 5-73: Flow and pressure head for the varying pump speeds*

Figure 5-73 shows that there was an increase in flow with an increase in pressure head. When taking a closer look at the result in Figure 5-73, it was observed that the two steps at the high pressures did not fit well to the power equation fitted to the data. Because of this observation, two power equations were fitted to the data points: One power equation was fitted at the lower pressure data points, and the other was fitted to the higher-pressure data points. Figure 5-74 shows two power equations fitted to the pressure and flow data set and Figure 5-75 shows the net result of the two curves.

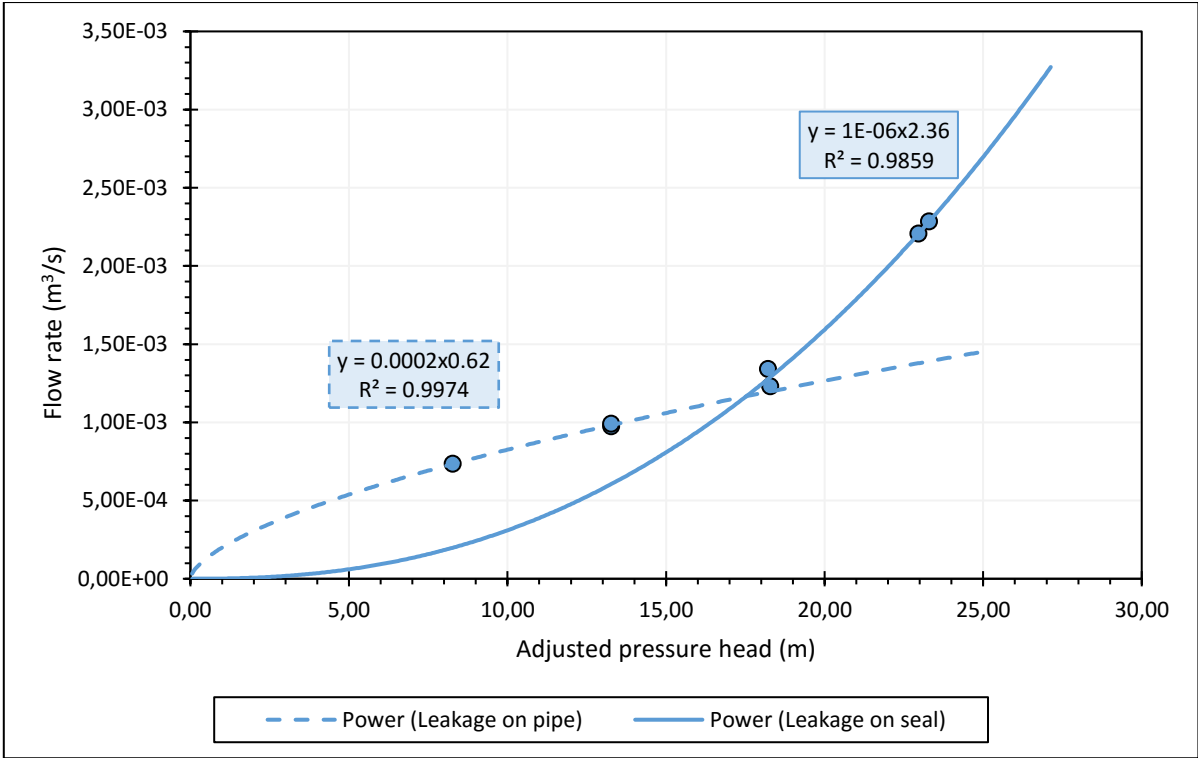


Figure 5-74: Flow against pressure data

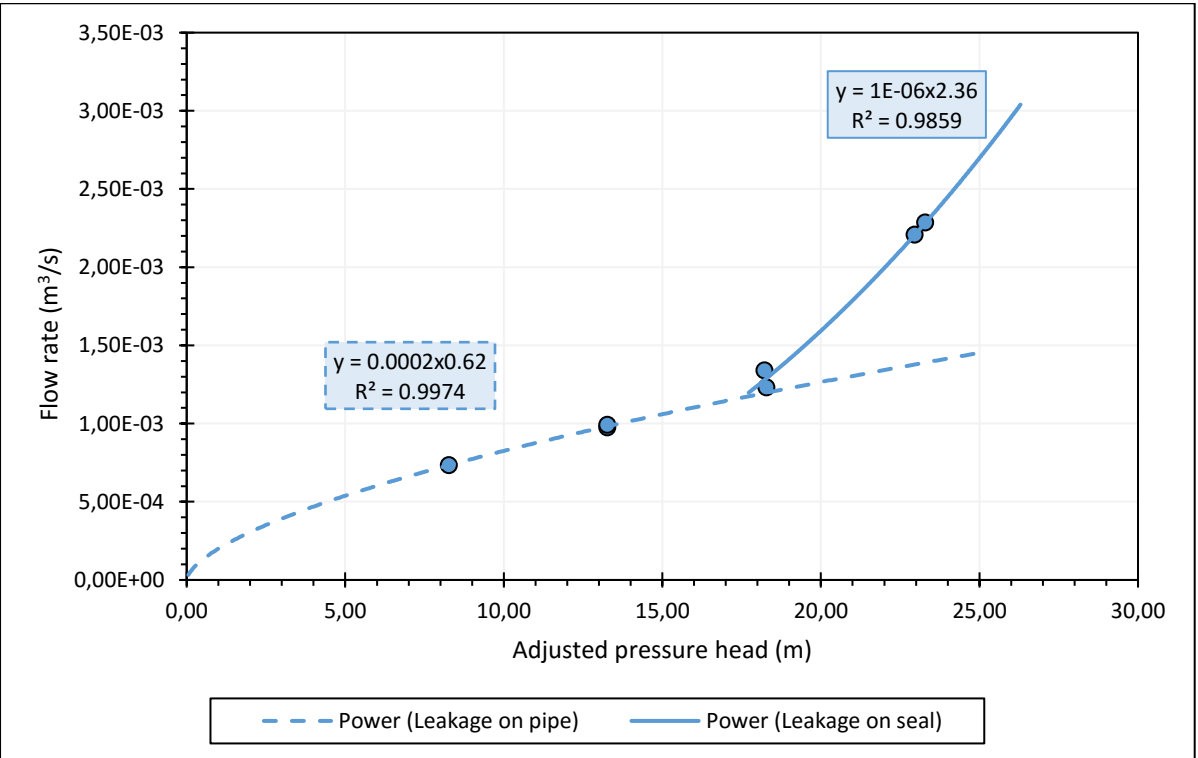


Figure 5-75: The nett result of flow against pressure curves

In Figure 5-75 the two curves fitted the data very well, with  $R^2$  greater than 0.9. This result suggested that two mechanisms could describe the overall leakage in the pipeline. The first

process begins to occur at the lower pressures (dotted curve), whilst the second process starts to occur at the higher pressures (solid curve).

The  $N1$  obtained for the process occurring at the lower pressures was 0.6, suggesting that this process occurred on a rigid section of the pipe system, such as the pipe itself. The  $N1$  obtained for the process that transpired at the higher pressures was 2.3, suggesting that this process was happening on a component of the pipe system that was very sensitive to pressure – e.g. a rubber seal. Figure 5-62 that follows shows a summary of the  $N1$  leakage parameters for the two processes.

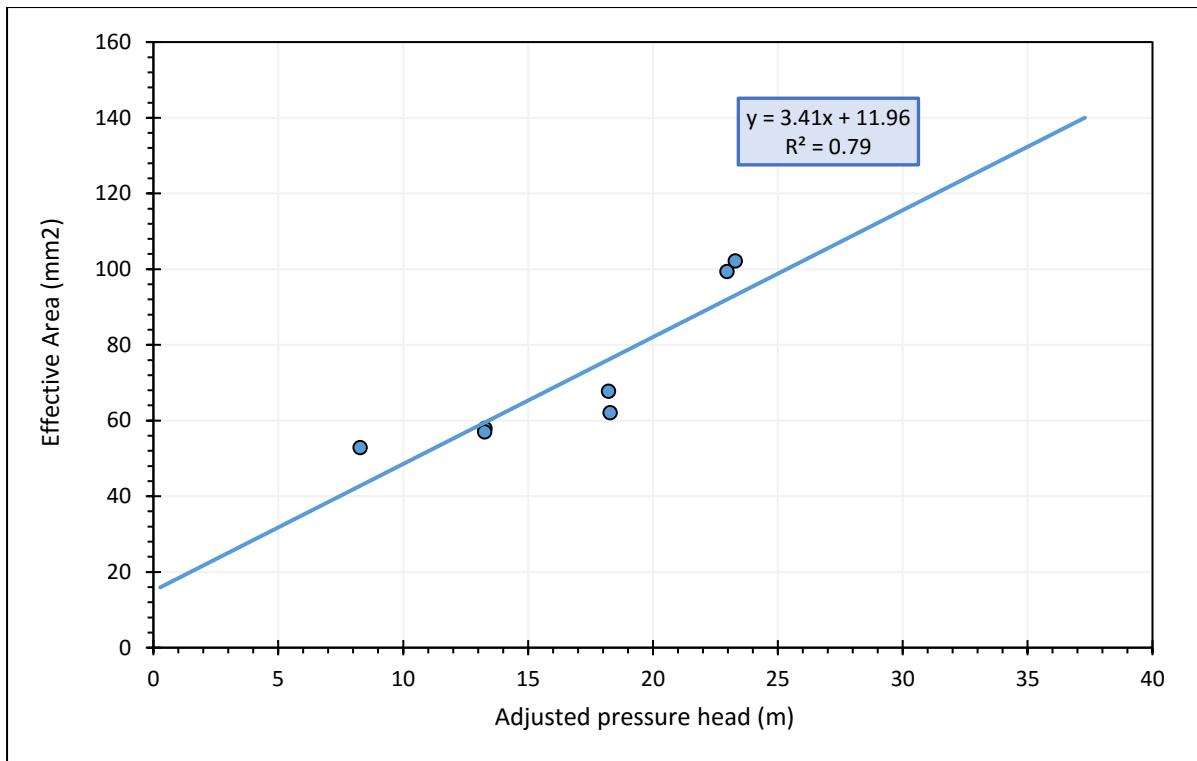
*Table 5-27: Summary of the  $N1$  leakage parameters*

<b>N1 Leakage Parameter</b>	<b>Leak on Pipe</b>	<b>Leak on Seal</b>
N1	0.6	2.36
C	$2 \times 10^{-4}$	$1 \times 10^{-6}$
R <sup>2</sup>	0.99	0.98

### **5.10.3.3      *Leakage parameters for the modified orifice equation***

To check the Modified Orifice Equation leakage parameters; the effective leak area ( $C_d A_0$ ) and the effective head – area slope ( $C_d m$ ) for the leak were determined. The effective leak area was then plotted against the pressure head in Figure 5-76.





*Figure 5-76: Effective area against pressure Head for the Wingfield Test 1*

A linear line was fitted to the data set and used to obtain the effective leak area ( $C_d A_0$ ) and the effective head –area slope ( $C_d m$ ). The effective initial leak area, which was given by the intercept of the line, was found to be 11.96mm. The effective head-area slope, which was given by the gradient of the line, was found to be  $3.41\text{mm}^2/\text{m}$ .

A closer look at Figure 5-76 revealed that the data points at the high pressure did not fit very well to the overall linearity of the other points. This observation warranted further investigation, as to whether two distinct mechanism played a role – with one mechanism already having an effect at the lower pressures, and other mechanisms being induced at the higher pressures.

To investigate this further, two linear lines were plotted as shown in Figure 5-77 and the net result of the two lines are shown in Figure 5-77. One line was plotted through the data set at the lower pressures representing the characteristics of the first mechanism and the other linear line was plotted at the higher pressures of the data set representing the characteristics of the second mechanism.

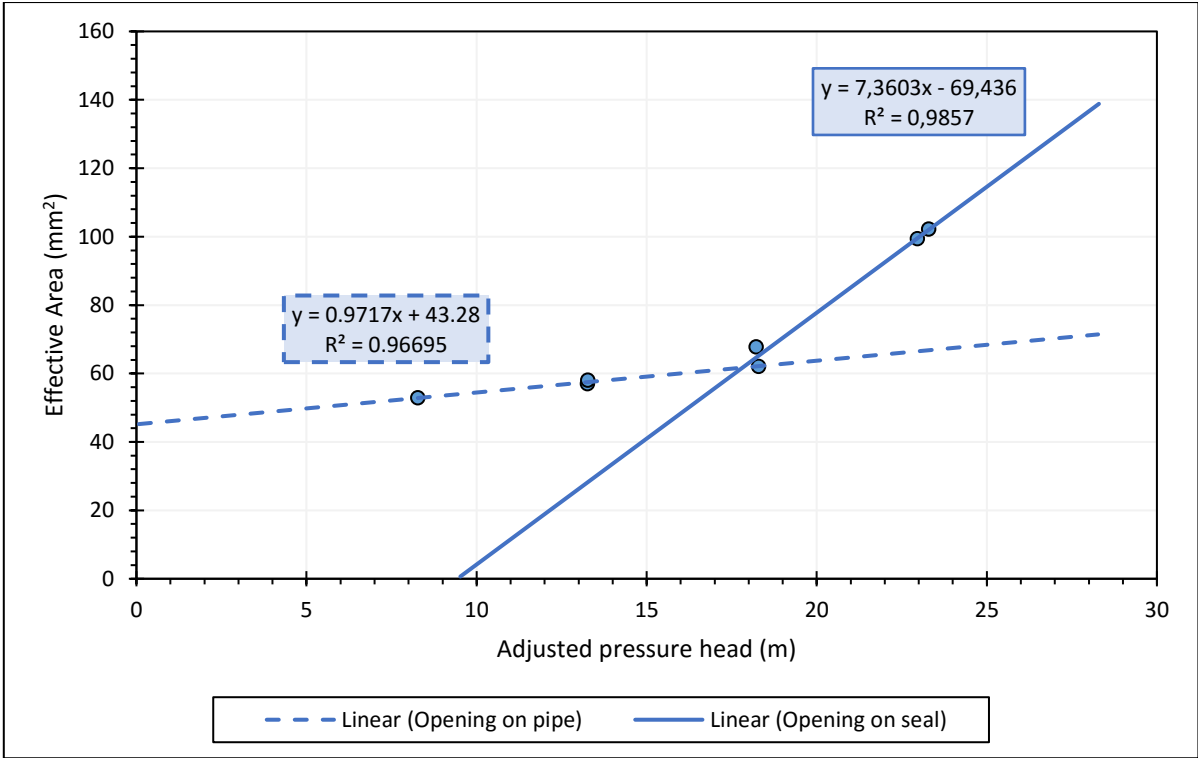


Figure 5-77: Effective Area against pressure for the Wingfield pipeline

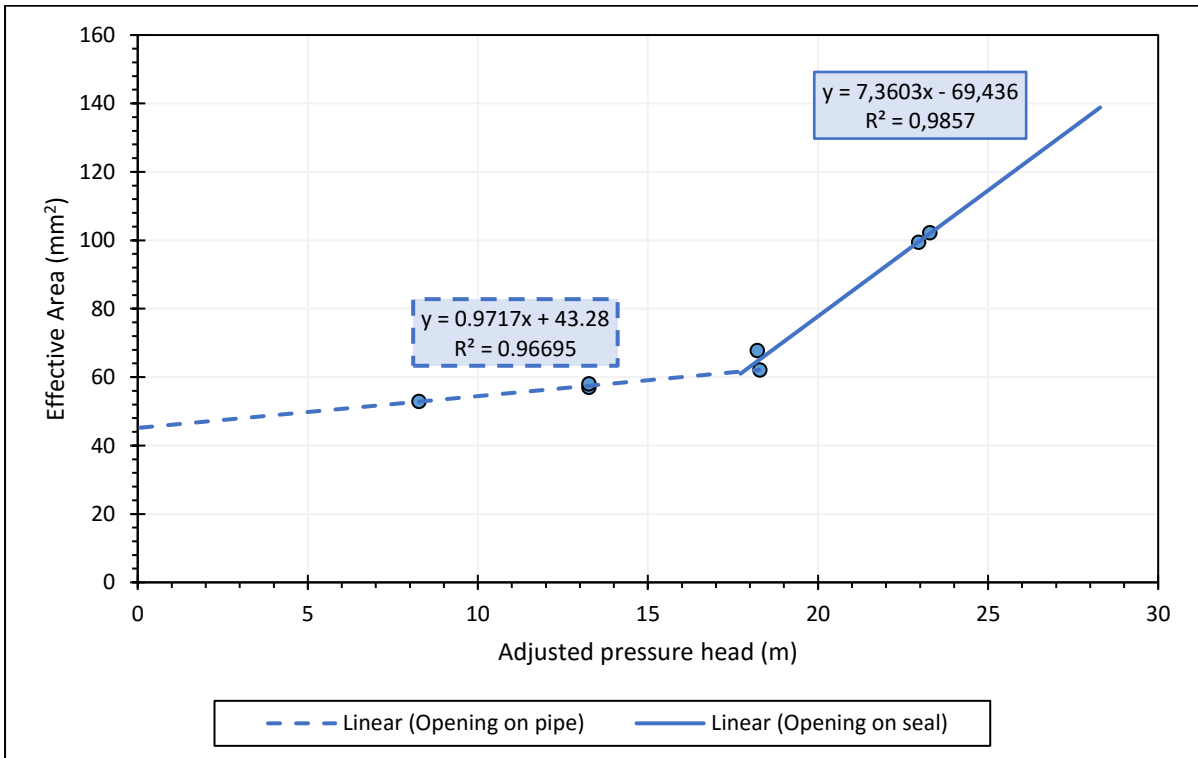


Figure 5-78: The nett result of the effective area against pressure for the Wingfield pipeline.

It can be seen, from Figure 5-77 that the first mechanism has an effective initial leak area of  $43\text{mm}^2$  and an effective head – area slope of  $0.97\text{mm}^2/\text{m}$ . This is consistent with a longitudinal crack, which is the typical failure mechanism of AC pipes, as shown in Figure 5-79.



*Figure 5-79: Typical failure mechanisms in AC pipes ( Greyvenstein & van Zyl, 2005)*

The second mechanism, which is a combination of the first mechanism and another mechanism resulted in an effective initial leak area of  $69.44\text{mm}^2$  and an effective head-area slope of  $7.36\text{mm}^2/\text{m}$ . The pressure head at the intercept of the two linear lines in Figure 5-77 could potentially indicate the pressure at which the second mechanism starts to play an effect on the behaviour of the leak. From the image shown in Figure 5-79, it is anticipated that the first process is a longitudinal crack, which opens up with pressure. When a certain pressure is reached, approximately 18 m, the crack opening interferes with the seal and hence the second mechanisms.

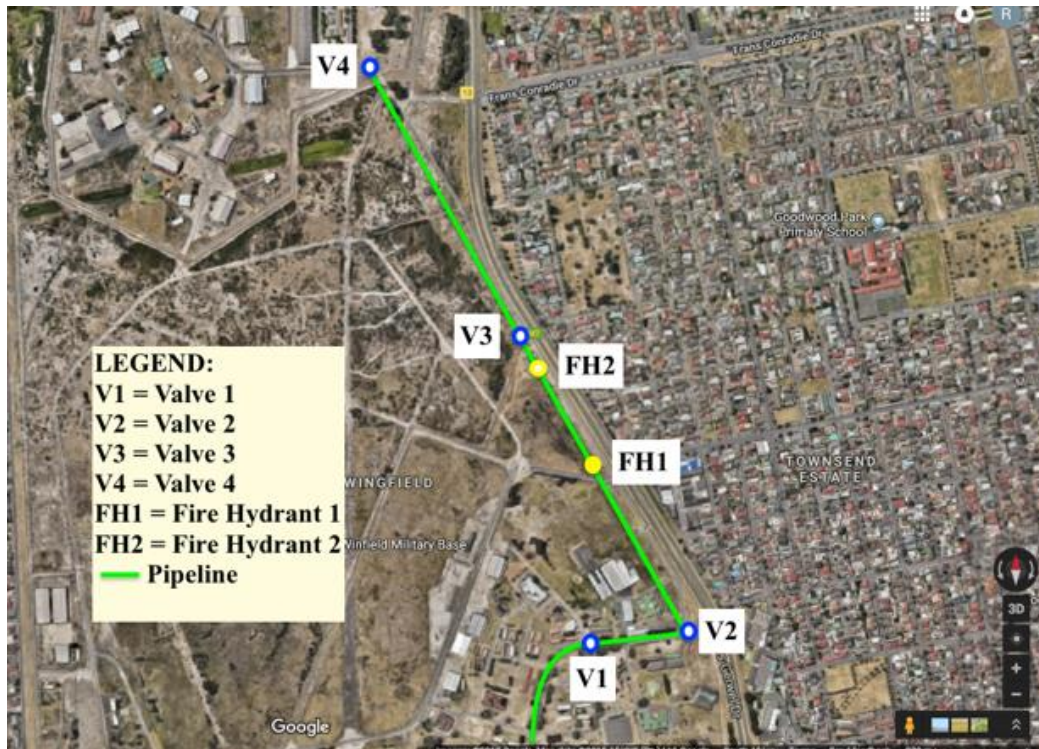
## **5.11 Wingfield Pipeline – Test 2**

### **5.11.1 Introduction**

A second test was conducted on the Wingfield AC pipeline exactly three months after the first leak test was done. According to the consultants in charge of the Wingfield pipeline on site, the pipeline was isolated and had never been in operation since the last leak test. Prior to carrying out Leak Test 2, it was requested that the pipeline be recharged overnight so that the pipe was full on the day of the test.

### 5.11.2 Leak test procedure

The PCAE was transported to the Wingfield site. The first step was to connect the PCAE by means of a 50mm rubber hosepipe. The hosepipe was connected to an above ground fire hydrant located at FH 1 in Figure 5-80.



*Figure 5-80: Wingfield pipeline layout*

Figure 5-81 shows the condition of the hydrant stand pipe that the PCAE was connected too. It can be seen from the figure that the hydrant pipe was severely corroded. Nonetheless, the test continued.



*Figure 5-81: Fire hydrant connection*

After connecting the hosepipe to the hydrant, the hydrant valve was then opened to flush out any sediments. Immediately after opening the hydrant, the hydrant pipe failed through a burst on the galvanised steel pipe feeding the hydrant. This failure may have occurred for two reasons: firstly, because the hydrant valve was opened too quickly, and the sudden shock induced in the system caused the failure and, secondly, because of the already severely corroded hydrant pipe, the integrity of the pipe wall was extremely compromised and any sudden pressure in the pipe caused the pipe to fail. Figure 5-82 shows the corroded hydrant after the burst. The hydrant head did not fail; however, the hydrant pipe wall disintegrated. For this reason, the test was discontinued, and another was scheduled after the hydrant pipe was replaced.



*Figure 5-82: Failed fire hydrant pipe*

## **5.12 Wingfield Pipeline – Test 3**

### **5.12.1 Introduction**

A third leak test was conducted on the Wingfield AC pipeline, after the hydrant pipe that burst during Leak Test 2 was replaced. Figure 5-83 shows the new hydrant pipe that was installed at FH1 in Figure 5-84.



Figure 5-83: Replaced fire hydrant pipe and head

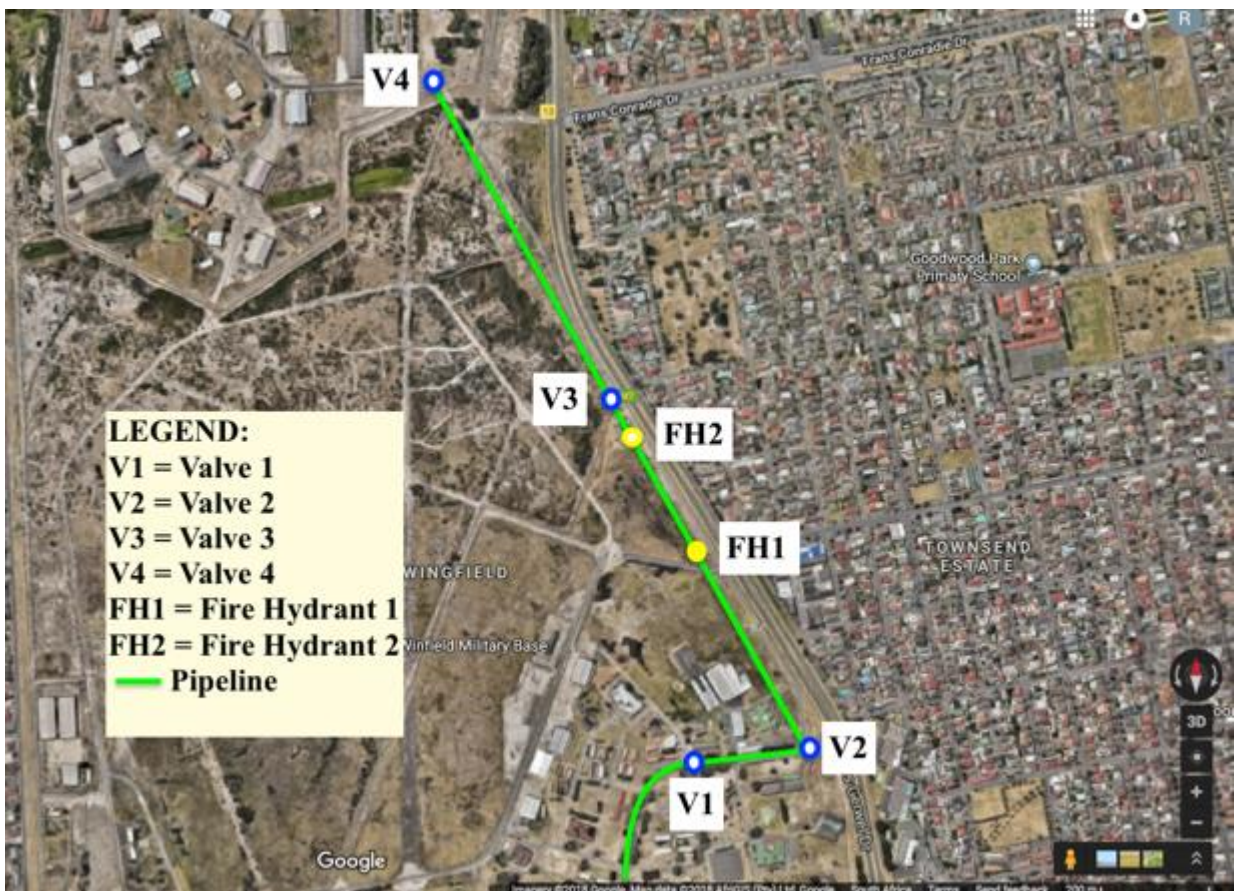


Figure 5-84: Wingfield pipeline layout

### 5.12.2 Leak Test Procedure

The first step was to connect the PCAE to the pipeline. The fire hydrant was identified as the most suitable connection point to the pipeline. The fire hydrant at FH1 in Figure 5-84 was selected because it was the same connection used to connect the PCAE and the pipeline during Leak Tests 1 and 2. However, it was discovered on site that the replaced fire hydrant head, installed at FH1, was not compatible with the PCAE rubber hosepipe connection fitting. Consequently, the PCAE could not be connected at this hydrant and, thus, an alternative connection point along the pipeline had to be identified.

The alternative connection point was the second fire hydrant on the pipeline, located at FH2 in Figure 5-84. The fire hydrant at FH2 had no hydrant head and was found covered, as shown in Figure 5-85. A spanner was used to remove the cover. The contractor organised a hydrant head, which matched the fire hydrant pipe, as well as the PCAE connection fitting.



*Figure 5-85: Covered fire hydrant*



*Figure 5-86: Installed fire hydrant head with the PCAE Connected*

After connecting the PCAE hosepipe to the fire hydrant, as depicted in Figure 5-86, the fire hydrant was opened to flush any sediments in the pipeline. After the water cleared, the PCAE water tank was filled with water from the pipeline until the water tank was full.

After filling the tank, the isolation of the pipeline was isolated by shutting off valve V2 and V4. After the pipeline was isolated, the PCAE variable speed pump was activated and the leak test was executed.

### **5.12.3 Leak Test Results**

The raw flow and pressure data obtained from this test is plotted against time, as shown in Figure 5-87. It is clear from the figure that the pipe has deteriorated substantially after the previous test and that it had a very large leak of around 190 L/min (11.4 m<sup>3</sup>/h). As the figure shows, it was not possible to stabilise the flow and pressure values. Consequently, to vary the pressure, the pressure steps were not held long enough to stabilise.

This leak could not be analysed any further due to the unstable flow and pressure results. Subsequently, the leakage characteristics were not determined. It was of the view that, should there have been a longer allowance for pressure to stabilise, at least two steps could have been achieved and the leakage could have been characterised.



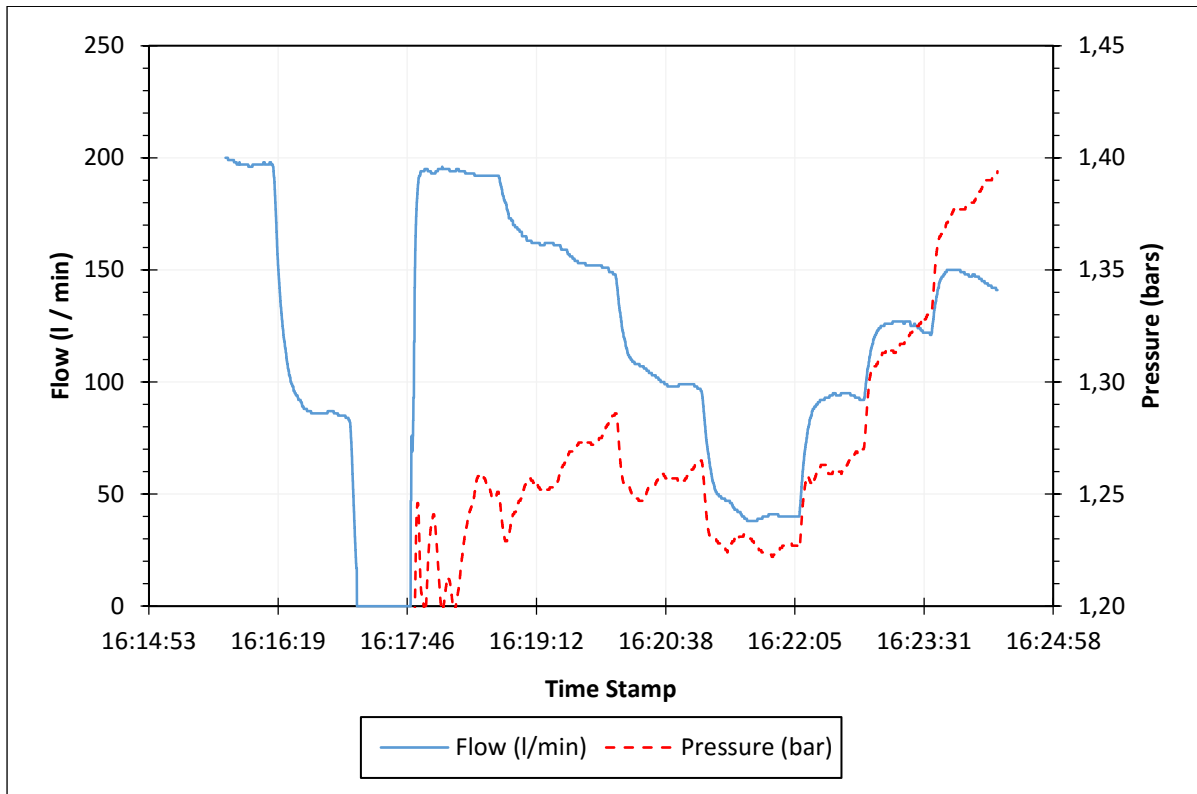


Figure 5-87: Flow and pressure raw data for Wingfield test 3

## 5.13 Conclusions

This chapter reports on the several bulk pipelines that were tested using the pipe condition assessment equipment. The field tests results demonstrated that pressure – based leakage characterisation is an effective and suitable testing technique for bulk pipelines.

To test a bulk pipeline, a section of the pipe was isolated and the PCAE was connected to an access point. Initial checks were performed to ensure that the section was isolated and no air present in the pipeline. The PCAE pump was used to induce a sequence of different pressures in the isolated bulk pipeline. At each pressure, the flow rate into the pipe, which represents the leakage rate, was measured.

The flow and pressure data was then analysed to determine the power equation and modified orifice equation leakage parameters. The modified orifice equation leakage parameters, i.e. initial leak area and head-area slope were further used to characterise the leak.

The initial leakage area represented the sum of all the areas of individual leaks on the pipe under zero pressure conditions, and thus the size of the leak can be determined. The head-area slope describes the rate at which leak areas vary as a function of the pressure in the pipe, and thus, was used to estimate the type of leaks (round holes, corrosion leaks, longitudinal or circumferential cracks) present on the pipe.

This chapter also highlights some challenges that were encountered that lead to the withdrawal of a test the main factors that contributed to the withdrawal of a test were: damaged connection points, large leaks and dysfunctional isolation valves. In any case, some useful information about the condition of the pipeline was inferred from the evidence observed on site. Table 5-28 shows a summary of the successful tests carried out.

Table 5-28: Summary of successful tests

Pipeline	Material	Diameter (mm)	Length (m)	Type	Connection Point	Average System Pressure (meters)	N1	C	A <sub>0</sub> ' (mm <sup>2</sup> )	m' (mm <sup>2</sup> /m)
Wingfield Test 1	AC	300	1000	Pump	Fire Hydrant	30	1.09	6.0 x 10 <sup>-5</sup>	12	3.4
BS 8 Pipeline Test 1	Mixed	55.21	5401	Gravity	Air Valve	50	0.56	1.7	8.5	3.2x10 <sup>-3</sup>
BS 8 Pipeline Test 2	Mixed	55.21	5401	Gravity	Air Valve	50	1.03	3.0 x 10 <sup>-5</sup>	30	0.51
UCT Pipeline	AC	300	160	Gravity	Fire Hydrant	57	1.033	1.3 x 10 <sup>-5</sup>	4.9	0.51
Lynnwood to Koedoesnek	Steel	500	850	Gravity	PRV connection	97	0.86	1.0 x 10 <sup>-4</sup>	23	0.13
Garsfontein to Parkmore High Level Reservoir	Steel	500	2500	Gravity	Stop Valve	50	0.69	5.5 x 10 <sup>-5</sup>	18	9.7 x 10 <sup>-2</sup>
Klapperkop to Carina Street Pipeline	Steel	406	2700	Gravity	PRV Connection	50	0.67	5.0 x 10 <sup>-4</sup>	138	3.1
Line to Florauna High Level Reservoir	Steel	300	1260	Gravity	1 inch threaded connection	85	0.86	9.0 x10 <sup>-5</sup>	40	0.94

# 6 Dynamic Pressure Tests

## 6.1 Introduction

When a pressurised pipe without any leakage is isolated from the rest of the system, its pressure will remain constant at the pre-isolation level. However, if the isolated pipe has a leak, the pressure in the pipe will drop with time due to the water leaving the pipe. This process will continue until the pressure inside the pipe equals the pressure outside the pipe.

The leakage characteristics of the pipe are estimated from the pressure vs time data: if the pressure remains constant, the pipe is without a leak. If the pressure drops, a novel mathematical model is fitted to the pressure vs time curve, using the known pipe properties to determine (a) the initial leak area, and (b) the head-area slope.

This chapter presents the derivation of the mathematical model used in the pressure drop analysis procedure. While stresses in pipe walls can vary greatly and are affected by numerous factors (such as internal fluid pressures and external soil loads), in this derivation only the wall stresses that are induced by the internal fluid pressure were considered.

## 6.2 Derivation methodology

This derivation seeks to develop a relationship between pressure and time, when a pressure drop occurs in a leaking isolated pipeline. It takes some or all the following factors into account:

- the variation of the internal pipe volume with changes in pressure due to pipe wall strain
- the compressibility of the fluid inside the pipe
- orifice hydraulics
- the variation in the leak(s) area as a function of pressure.

In order to obtain the relationship between pressure and time, the conservation of mass principal is used. According to the conservation of mass principal, the total change in volume of the pipe due to a change in pressure is equal to the change in volume due to the compressibility of the fluid, plus the change in volume due to the outflow from the leakage flow rate. The leakage flow rate through the leak is described by the modified orifice equation.

From the conservation of mass equation, a non-linear ordinary differential equation (ode) is generated. This is done by making the rate of change of pressure with respect to time ( $\partial h/\partial t$ ) the subject of the mass balance equation. The non-linear ode contains the modified orifice leakage parameters ( $C_d A_0$  and  $C_d m$ ) as unknown constants.

The non-linear ode is solved explicitly in terms of known integrals, and the function for pressure with respect to time,  $h(t)$ , is derived. The derived function contains a constant of integration which must be evaluated.

In order to evaluate the constant of integration, the modified orifice equation leakage parameters are initialised as random values in the derived function,  $h(t)$ . The constant of integration is then evaluated using the initial conditions obtained from field or experimental pressure time data, i.e. pressure at time = 0. It is worth noting that the constant of integration is set up as a function of the leakage parameters  $C(A'_0, m')$  and can be adjusted as the leakage parameters change.

When the function  $h(t)$  is used, the pressure at each time can be calculated and compared to the pressure values of the given data. The error between the measured and calculated pressure values is evaluated using the sum of least squares equation. Using an optimisation solver, the error between the measured and calculated values (the objective function) is minimised to zero by changing the leakage parameters ( $A'_0$  and  $m'$ ).

## **6.3 The derivation of an analytical solution for the dynamic pressure**

### **6.3.1 Conservation of mass**

Consider the fully charged isolated pipeline with a small leak  $Q$ , as is shown in *Figure 6-1*. According to the conservation of mass principle – when a change in pressure occurs in the pipeline, the total change in the volume,  $\delta V_{total}$ , due to circumferential and longitudinal expansion or contraction is equal to the change in volume due to the fluids compressibility,  $\delta V_c$ , plus the change in volume due to the leakage outflow  $\delta V_{out}$ . Subsequently, the conservation of mass equation can be expressed as follows:

$$\delta V_{total} = \delta V_C + \delta V_{out}$$

Equation 6-1

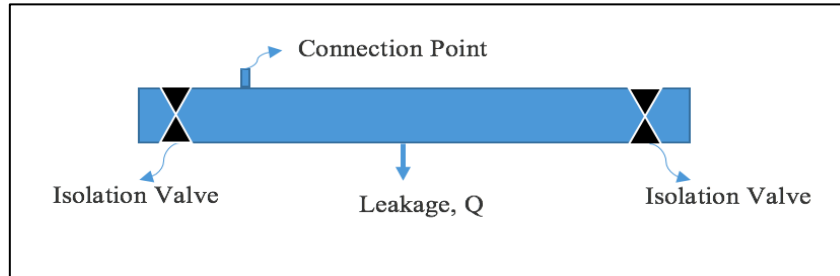


Figure 6-1: Isolated pipeline with leakage  $Q$

When the material behaviour of pressurised pipes as well as fluid mechanics principals are considered, each of the components in the conservation of mass equation (in Equation 6-1) can be evaluated.

### 6.3.2 Total change in volume

Any pressure change,  $\delta P$ , in a pipe, during time interval,  $\delta t$ , can be expressed by  $(\partial P / \partial t) \delta t$ . This pressure change causes the pipe walls to experience a change in circumferential stress,  $\delta \sigma_{circ}$ , and longitudinal stress,  $\delta \sigma_{long}$ . The circumferential stress changes due to the change in internal pressure acting uniformly on the internal wall of the pipeline, whilst the longitudinal stress changes due to the change in internal pressure pulling the pipe apart in an axial direction.

It is possible to derive the equations for the change in circumferential stresses,  $\delta \sigma_{circ}$ , and change in longitudinal stresses,  $\delta \sigma_{long}$ , induced in the pipe wall as a result of the pressure change,  $\delta P$ , as shown by Gere (2001).

$$\delta \sigma_{circ} = \frac{\delta P d_0}{2b}$$

Equation 6-2

$$\delta \sigma_{long} = \frac{\delta P d_0}{4b}$$

Equation 6-3

Where  $d_0$  is the initial pipe diameter and  $b$  is the pipe wall thickness. The associated change in circumferential strain,  $\varepsilon_{circ}$ , and longitudinal strain,  $\varepsilon_{long}$ , will occur in response to the change in circumferential and longitudinal stress, respectively. The circumferential strain,  $\delta\varepsilon_{circ}$ , may be defined as the change in the circumference,  $\delta C$ , divided by the initial circumference,  $C_0$ , and can be expressed as follows:

$$\delta\varepsilon_{circ} = \frac{\delta C}{C_0} = \frac{\pi(d_0 + \delta d) - \pi d_0}{\pi d_0} = \frac{\delta d}{d_0}$$

*Equation 6-4*

*Equation 6-4* shows that the change in circumferential strain,  $\delta\varepsilon_{circ}$ , is the same as the diametric strain, i.e. the strain based on diameters. The longitudinal strain,  $\varepsilon_{long}$ , on the other hand, may be defined as the change in length of the pipeline,  $\delta l$ , divided by the initial length,  $l_0$ , and can be expressed as follows:

$$\delta\varepsilon_{long} = \frac{\delta l}{l_0}$$

*Equation 6-5*

When the new diameter changes to  $d_1$ , then the change in diameter,  $\delta d$ , is given by:

$$\delta d = d_1 - d_0$$

*Equation 6-6*

And when the new length changes to  $l_1$ , then the change in length,  $\delta l$ , is given by:

$$\delta l = l_1 - l_0$$

*Equation 6-7*

When *Equation 6-6* is substituted into *Equation 6-4* and *Equation 6-7* into *Equation 6-5*, the new diameter,  $d_1$ , and new length,  $l_1$ , can be deduced using the following expression:

$$d_1 = d_0(\delta\varepsilon_{circ} + 1)$$

*Equation 6-8*

$$l_1 = l_0(\delta\varepsilon_{long} + 1)$$

*Equation 6-9*

When Hooke's Law is applied, the strain in the pipe can also be related to the stress in the pipe ( $\varepsilon = \sigma/E$ ). However, since both circumferential and longitudinal stresses develop, a positive strain (tensile) in one direction will also contribute a negative (compressive) strain in the other direction. In order to take this effect into account, the Poissons ratio,  $\nu$ , is introduced. When superposition is applied, the overall change in circumferential strain and longitudinal strain can be related to the change in respective stress as follows:

$$\delta\varepsilon_{circ} = \frac{1}{E} [\delta\sigma_{circ} - \nu\delta\sigma_{long}] = \frac{1}{E} \left[ \frac{\delta P d_0}{2b} - \nu \frac{\delta P d_0}{4b} \right]$$

*Equation 6-10*

$$\delta\varepsilon_{long} = \frac{1}{E} [\delta\sigma_{long} - \nu\delta\sigma_{circ}] = \frac{1}{E} \left[ \frac{\delta P d_0}{4b} - \nu \frac{\delta P d_0}{2b} \right]$$

*Equation 6-11*

In *Equation 6-10* and *Equation 6-11*  $E$  is the elastic modulus of the pipe material. Due to the change in pressure resulting in circumferential and longitudinal deformation, the new volume of the pipe,  $V_1$ , can be deduced using the following equation (*area*  $\times$  *length*):

$$V_1 = \frac{\pi d_1^2}{4} l_1$$

*Equation 6-12*

Substituting *Equation 6-8* and *Equation 6-9* into *Equation 6-12* gives the volume in terms of the change in circumferential and longitudinal strain:

$$V_1 = \frac{\pi}{4} (d_0(\delta\varepsilon_{circ} + 1))^2 (l_0(\delta\varepsilon_{long} + 1))$$

*Equation 6-13*

This can be evaluated as:

$$V_1 = \frac{\pi d_0^2}{4} l_0 [(\delta\varepsilon_{circ}^2 + 2\delta\varepsilon_{circ} + 1)(\delta\varepsilon_{long} + 1)]$$

*Equation 6-14*

Multiplying out the brackets and ignoring the product of small terms, such as  $\delta\varepsilon_{circ}^2 \delta\varepsilon_{long}$ ,  $\delta\varepsilon_{circ}^2$ , and  $\delta\varepsilon_{circ} \delta\varepsilon_{long}$ , this can be reduced to:



$$V_1 = \frac{\pi d_0^2}{4} l_0 [2\delta\varepsilon_{circ} + \delta\varepsilon_{long} + 1]$$

*Equation 6-15*

It should be noted that the initial volume of the pipe is given as:

$$V_0 = \frac{\pi d_0^2}{4} l_0$$

*Equation 6-16*

Then the new Volume,  $V_1$ , can be expressed in terms of the initial volume,  $V_0$ , as follows:

$$V_1 = V_0 [2\delta\varepsilon_{circ} + \delta\varepsilon_{long} + 1]$$

*Equation 6-17*

Now, the total change in volume of the pipe,  $\delta V_{total}$ , due to the change in pressure can be computed as:

$$\delta V_{total} = V_1 - V_0$$

*Equation 6-18*

Substituting  $V_1$  from *Equation 6-17* into *Equation 6-18* will yield the total change in volume,  $\delta V_{total}$ , as:

$$\delta V_{total} = V_0 [2\delta\varepsilon_{circ} + \delta\varepsilon_{long} + 1] - V_0$$

*Equation 6-19*

Multiplying out the brackets and substituting  $\delta\varepsilon_{circ}$  and  $\delta\varepsilon_{long}$  from *Equation 6-10* and *Equation 6-11* respectively, *Equation 6-19* becomes:

$$\delta V_{total} = \frac{\delta P d_0}{bE} V_0 - \frac{\delta P d_0 v}{2bE} V_0 + \frac{\delta P d_0}{4bE} V_0 - v \frac{\delta P d_0}{2bE} V_0 + V_0 - V_0$$

*Equation 6-20*

Which can be simplified to:

$$\delta V_{total} = \frac{\delta P d_0}{bE} V_0 \left( \frac{5}{4} - v \right)$$

*Equation 6-21*

And noting that  $\delta P = (\partial P / \partial t) \delta t$ , then

$$\delta V_{total} = \frac{\partial P d_0}{\partial t b E} V_0 \left( \frac{5}{4} - \nu \right) \delta t$$

*Equation 6-22*

### 6.3.3 Change in volume due to compressibility

In the conservation of mass equation (*Equation 6-1*), the expression for the change in volume due to the fluid compressibility,  $\delta V_c$ , can now be derived using the bulk modulus of elasticity of a fluid,  $K$ , which is defined as:

$$K = \frac{-\delta P}{\delta V_c / V_0}$$

*Equation 6-23*

Re-arranging *Equation 6-23* so that the change in volume due to compressibility,  $\delta V_c$ , is the subject of the formula, yields:

$$\delta V_c = -\frac{\delta P V_0}{K}$$

*Equation 6-24*

And noting that  $\delta P = (\partial P / \partial t) \delta t$ , *Equation 6-24* can be expressed as follows:

$$\delta V_c = \frac{-\partial P}{\partial t} \frac{V_0}{K} \delta t$$

*Equation 6-25*

### 6.3.4 Change in volume due to leakage

As the water leaks out of the pipe, there is a change in the volume of the fluid in the pipe. From the conservation of mass equation (*Equation 6-1*), the expression for the change in volume due to the leakage flow,  $\delta V_{out}$ , can be evaluated by multiplying the leakage flow rate,  $Q_{MOE}$ , by the time duration of the leak,  $\delta t$ , as follows:

$$\delta V_{out} = -Q_{MOE} \delta t$$

*Equation 6-26*

The leakage flow rate,  $Q_{MOE}$ , can be described by the modified orifice equation given here as:

$$Q_{MOE} = \sqrt{2g}(C_d A_0 h^{0.5} + C_d m h^{1.5})$$

Equation 6-27

It should be noted that while the discharge coefficient  $C_d$  is unknown in Equation 6-27, it can be eliminated by combining it with the initial area and head-area slope (van Zyl & Malde, 2017). In this arrangement,  $A'_0$  is called the effective initial leak area ( $A'_0 = C_d A_0$ ) and  $m$  is called the effective head-area slope ( $m' = C_d m$ ). Equation 6-27 now becomes:

$$Q_{MOE} = \sqrt{2g}(A'_0 h^{0.5} + m' h^{1.5})$$

Equation 6-28

Substituting  $Q_{MOE}$  from Equation 6-28 into Equation 6-26 yields  $\delta V_{out}$  as:

$$\delta V_{out} = -\sqrt{2g}(A'_0 h^{0.5} + m' h^{1.5})\delta t$$

Equation 6-29

### 6.3.5 Pressure and time relationship

To model how the pressure head,  $h$ , varies over time,  $t$ , the two variables are related to each other when a differential equation is used to arrive at a solution in the form  $h = h(t)$ . This ordinary differential equation is developed by first substituting  $\delta V_{total}$  (Equation 6-22),  $\delta V_c$  (Equation 6-25) and  $\delta V_{out}$  (Equation 6-29) into the conservation of mass equation (Equation 6-1), which yields:

$$\frac{\partial P}{\partial t} \left( \frac{d_0 V_0}{bE} \right) \left[ \frac{5}{4} - v \right] \delta t = -\frac{\partial P}{\partial t} \frac{V_0}{K} \delta t - \sqrt{2g}(A'_0 h^{0.5} + m' h^{1.5})\delta t$$

Equation 6-30

Note that  $P = \rho gh$  and dividing by  $\delta t$ , Equation 6-30 becomes:

$$\frac{\partial \rho gh}{\partial t} \left( \frac{d_0 V_0}{bE} \right) \left[ \frac{5}{4} - v \right] = -\frac{\partial \rho gh}{\partial t} \frac{V_0}{K} - \sqrt{2g}(A'_0 h^{0.5} + m' h^{1.5})$$

Equation 6-31

This can be simplified further to take on the following form:

$$\frac{\partial h}{\partial t} = \frac{-\sqrt{2g}}{\rho g V_0 \left[ \frac{d_0}{bE} \left( \frac{5}{4} - v \right) + \frac{1}{K} \right]} (A'_0 h^{0.5} + m' h^{1.5})$$

Equation 6-32

It can be seen that *Equation 6-32* is in the form of a set of separable non-linear ordinary differential equations. In these equations there is one independent variable,  $t$ , and one dependent variable,  $h$ . All other variables are known geometric and fluid constants, except  $m'$  and  $A'_0$  which are unknown constants which represent the parameters of the leak and are time invariant.

The ordinary differential equation represented by *Equation 6-32* can be solved by separating the equation as follows:

$$\frac{1}{(A'_0 h^{0.5} + m' h^{1.5})} \partial h = - \frac{-\sqrt{2g}}{\rho g \left[ \frac{d_0}{2bE} \left( \frac{5}{4} - \nu \right) + \frac{V_0}{K} \right]} \partial t$$

*Equation 6-33*

A closed form solution for this equation can be obtained by integrating both sides:

$$\int \frac{1}{(A'_0 h^{0.5} + m' h^{1.5})} \partial h = \int - \frac{-\sqrt{2g}}{\rho g \left[ \frac{d_0}{2bE} \left( \frac{5}{4} - \nu \right) + \frac{V_0}{K} \right]} \partial t$$

This yields:

$$\frac{2}{\sqrt{m'} \sqrt{A'_0}} \tan^{-1} \left( \frac{\sqrt{m'}}{\sqrt{A'_0}} h(t)^{0.5} \right) = - \left( \frac{\sqrt{2g}}{\rho g \left[ \frac{d_0}{bE} \left( \frac{5}{4} - \nu \right) + \frac{V_0}{K} \right]} \right) t + C(m', A'_0)$$

*Equation 6-34*

or

$$h(t) = \frac{A'_0}{m'} \tan^2 \left[ \frac{\sqrt{m'} \sqrt{A'_0}}{2} \left( - \left( \frac{\sqrt{2g}}{\rho g V_0 \left[ \frac{d_0}{bE} \left( \frac{5}{4} - \nu \right) + \frac{1}{K} \right]} \right) t + C(m', A'_0) \right) \right]$$

*Equation 6-35*

Where  $C(m', A'_0)$  is the constant of integration and can be solved using initial conditions,  $h(t_0) = h_0$ . It is set up as a function of the leakage parameters,  $m'$  and  $A'_0$ , because these parameters are initially unknowns and thus initialised as random values. An optimisation

process is used to find these parameters. For this reason,  $m'$  and  $A'_0$  are likely to change from the initialised random values, and in turn the integration constant will also change.

According to *Equation 6-35*, the effective head-area slope cannot be zero, i.e.  $m \neq 0$ . This is expected because the pipe material is elastic and will expand and contract somewhat when subjected to any form of pressure differential.

## 6.4 Discontinuities in the analytical solution

The effective leakage parameters,  $m'$  and  $A'_0$ , can either be positive or negative real numbers (van Zyl et al., 2017). However, the analytical solution derived (*Equation 6-35*) consists of a square root product of the leakage parameters  $\sqrt{m'} \times \sqrt{A'_0}$ , suggesting that as is, the solution is only defined for positive  $m'$  and positive  $A'_0$  and may be undefined for certain cases such as:

- Case 1: when the effective head-area slope is negative,  $-m'$ , and the effective initial leak area is positive,  $A'_0$
- Case 2: when the head-area slope is positive,  $m'$ , and the initial leak area is negative,  $-A'_0$ .
- Case 3: when the head-area slope is negative,  $-m'$ , and the initial leak area is negative,  $-A'_0$

To overcome this, imaginary numbers were used to evaluate the equation for each of the above cases.

### 6.4.1 Case 1: negative head-area slope and positive initial leak area

For the case where the effective head-area slope is negative ( $-m'$ ) but the effective initial leak is positive ( $A'_0$ ), *Equation 6-35* becomes:

$$h(t) = \frac{A'_0}{-m'} \tan^2 \left[ \frac{\sqrt{-m'} \sqrt{A'_0}}{2} \left( - \left( \frac{\sqrt{2g}}{\rho g V_0 \left[ \frac{d_0}{bE} \left( \frac{5}{4} - \nu \right) + \frac{1}{K} \right]} \right) t + C(m', A'_0) \right) \right]$$

*Equation 6-36*

In *Equation 6-36*, the solution for the square root of a negative number,  $\sqrt{-m'}$ , does not exist among any of the set of real numbers  $m'$  can take on. In an effort to address this problem, the imaginary number was introduced as shown in *Equation 6-37*:

$$h(t) = \frac{A'_0}{-m'} \tan^2 \left[ \frac{\sqrt{|m'|} \sqrt{A'_0}}{2} \left( - \left( \frac{\sqrt{2g}}{\rho g V_0 \left[ \frac{d_0}{bE} \left( \frac{5}{4} - v \right) + \frac{1}{K} \right]} \right) t + C(m', A'_0) \right) i \right]$$

*Equation 6-37*

As a result of the imaginary number, the trigonometric function of the form  $\tan^2(ix)$  is relatable to a hyperbolic function,  $-\tanh^2(x)$ , and thus *Equation 6-37* can be expressed mathematically as follows:

$$h(t) = -\frac{A'_0}{-m'} \tanh^2 \left[ \frac{\sqrt{|m'|} \sqrt{A'_0}}{2} \left( - \left( \frac{\sqrt{2g}}{\rho g V_0 \left[ \frac{d_0}{bE} \left( \frac{5}{4} - v \right) + \frac{1}{K} \right]} \right) t + C(-m', A'_0) \right) \right]$$

*Equation 6-38*

Or

$$h(t) = \frac{A'_0}{m'} \tanh^2 \left[ \frac{\sqrt{|m'|} \sqrt{A'_0}}{2} \left( - \left( \frac{\sqrt{2g}}{\rho g V_0 \left[ \frac{d_0}{bE} \left( \frac{5}{4} - v \right) + \frac{1}{K} \right]} \right) t + C(-m', A'_0) \right) \right]$$

*Equation 6-39*

*Equation 6-39* gives the analytical solution for the case where the effective head-area slope might be negative. It differs from *Equation 6-35* in that it is a hyperbolic function. For this case, the effective initial leak area,  $A'_0$ , was kept positive.

## 6.4.2 Case 2: positive head-area slopes and negative initial leak area

In this case where the effective head-area slope is positive ( $m'$ ) but the effective initial leak area is negative ( $-A'_0$ ), *Equation 6-35* becomes:

$$h(t) = \frac{-A'_0}{m'} \tan^2 \left[ \frac{\sqrt{m'} \sqrt{-A'_0}}{2} \left( - \left( \frac{\sqrt{2g}}{\rho g V_0 \left[ \frac{d_0}{bE} \left( \frac{5}{4} - v \right) + \frac{1}{K} \right]} \right) t + C(m', -A'_0) \right) \right]$$

Equation 6-40

It can be seen that Equation 6-40 consists of a square root of a negative number,  $\sqrt{-A'_0}$ , for which a solution does not exist among any of the set of real numbers  $A'_0$  can take on. The imaginary number,  $i$ , is introduced again to address this problem:

$$h(t) = \frac{-A'_0}{m'} \tan^2 \left[ \frac{\sqrt{m'} \sqrt{|A'_0|}}{2} \left( - \left( \frac{\sqrt{2g}}{\rho g V_0 \left[ \frac{d_0}{bE} \left( \frac{5}{4} - v \right) + \frac{1}{K} \right]} \right) t + C(m', -A'_0) \right) i \right]$$

Equation 6-41

Taking note of the relation between trigonometric and hyperbolic functions,  $\tan^2(ix) = -\tanh^2(x)$ , Equation 6-45 then becomes:

$$h(t) = -\frac{A'_0}{m'} \tanh^2 \left[ \frac{\sqrt{m'} \sqrt{|A'_0|}}{2} \left( - \left( \frac{\sqrt{2g}}{\rho g V_0 \left[ \frac{d_0}{bE} \left( \frac{5}{4} - v \right) + \frac{1}{K} \right]} \right) t + C(m', -A'_0) \right) \right]$$

Equation 6-42

Or

$$h(t) = \frac{A'_0}{m'} \tanh^2 \left[ \frac{\sqrt{m'} \sqrt{|A'_0|}}{2} \left( - \left( \frac{\sqrt{2g}}{\rho g V_0 \left[ \frac{d_0}{bE} \left( \frac{5}{4} - v \right) + \frac{1}{K} \right]} \right) t + C(m', -A'_0) \right) \right]$$

Equation 6-43

### 6.4.3 Case 3: negative head-area slopes and negative initial leak area

For the case where the effective head-area slope is negative ( $-m'$ ) and the effective initial leak area is also negative ( $-A'_0$ ), Equation 6-35 becomes:

$$h(t) = \frac{-A'_0}{-m'} \tan^2 \frac{\sqrt{-m'} \sqrt{-A'_0}}{2} \left[ - \left( \frac{\sqrt{2g}}{\rho g V_0 \left[ \frac{d_0}{bE} \left( \frac{5}{4} - v \right) + \frac{1}{K} \right]} \right) t + C(-m', -A'_0) \right]$$

Equation 6-44

It can be seen that Equation 6-48 consists of a product of two square roots with a negative number,  $\sqrt{-m'}$  and  $\sqrt{-A'_0}$ , and that solutions do not exist for any of the set of real numbers  $A'_0$  and  $m'$  can take on. Once again the imaginary number,  $i$ , is introduced to address this problem. For this case two imaginary numbers are introduced for the  $\sqrt{-m'}$  and  $\sqrt{-A'_0}$ , and thus Equation 6-48 becomes:

$$h(t) = \frac{-A'_0}{-m'} \tan^2 \frac{\sqrt{|m'|} \sqrt{|A'_0|}}{2} \left[ - \left( \frac{\sqrt{2g}}{\rho g V_0 \left[ \frac{d_0}{bE} \left( \frac{5}{4} - v \right) + \frac{1}{K} \right]} \right) t + C(-m', -A'_0) \right] i \times i$$

Equation 6-45

If the product of two imaginary number is negative 1, i.e  $i^2 = -1$ , then Equation 6-41 can be expressed as follows:

$$h(t) = \frac{-A'_0}{-m'} \tan^2 \left[ - \frac{\sqrt{|m'|} \sqrt{|A'_0|}}{2} \left( - \left( \frac{\sqrt{2g}}{\rho g V_0 \left[ \frac{d_0}{bE} \left( \frac{5}{4} - v \right) + \frac{1}{K} \right]} \right) t + C(-m', -A'_0) \right) \right]$$

Equation 6-46

Or

$$h(t) = \frac{A'_0}{m'} \tan^2 \frac{\sqrt{|m'|} \sqrt{|A'_0|}}{2} \left[ - \left( \frac{\sqrt{2g}}{\rho g V_0 \left[ \frac{d_0}{bE} \left( \frac{5}{4} - v \right) + \frac{1}{K} \right]} \right) t + C(-m', -A'_0) \right]$$

Equation 6-47



## 6.5 Optimisation process to determine the true leakage parameters

The true leakage parameters,  $A_0$  and  $m$ , are estimated by means of an optimisation solver. The solver is configured to minimise the error between the pressure head calculated,  $h_{calculated}$ , using the analytical equations, and the actual measured pressure head,  $h_{measured}$ , for the same time.

The optimisation solver uses an error function,  $E(A_0, m)$ , as the objective function, and is set up as the sum of least squares between the measured head and the calculated head, as follows:

$$E(A_0, m) = \sum_i^N [h_{measured,i} - h_{calculated,i}(A_0, m)]^2$$

*Equation 6-48*

The optimisation solver is then used to find values of  $A_0$  and  $m$  in such a way that the objective function is minimised to zero. This is tested for all cases, and the case whose equation fits the data best is used as the solution.

## 6.6 Numerical approximation for verifying the analytical solution

### 6.6.1 Introduction

A verification test was set up to verify the efficacy of the derived analytical pressure-time equation. The verification was in form of a numerical model. The numerical model solution was compared to the analytical solution. The numerical model was set up as a time-step procedure to obtain the behaviour of the pressure in the pipe over time and for each time step.

### 6.6.2 Developing the numerical model

The numerical model was based on a mass balance equation given by:

$$\dot{M}_{in} - \dot{M}_{out} = \frac{\delta M}{\delta t}$$

*Equation 6-49*

Where  $\dot{M}_{in}$  is the mass flow rate into the pipe,  $\dot{M}_{out}$  is the mass flow rate leaking out of the pipe, and  $\delta M / \delta t$  is the total rate of change of mass. Since the pipe is isolated, there is no inflow into the pipe, i.e.  $\dot{M}_{in} = 0$ , and thus *Equation 6-49* becomes:

$$-\dot{M}_{out} = \frac{\delta M}{\delta t}$$

*Equation 6-50*

According to *Equation 6-50*, the rate of change of mass is influenced only by the mass flow rate leaking out of the isolated pipe. Furthermore, the mass flow rate leaking out can be expressed in terms of volumetric flow rate,  $Q_{out}$ , as follows:

$$-Q_{out}\rho = \frac{\delta M}{\delta t}$$

*Equation 6-51*

Where  $Q_{out}$  is the leakage volumetric flow rate, given by the modified orifice equation ( $Q_{MOE} = \sqrt{2g}(A'_0 h^{0.5} + m' h^{1.5})$ ), and  $\rho$  is the density of water in the pipe. The effective leakage parameters,  $A'_0$  and  $m'$ , are unknown and can therefore be initialised as random values.

The change in mass,  $\delta M$ , for a given incremental change in the time period,  $\delta t$ , can be determined by re-arranging *Equation 6-51* as follows:

$$-Q_{out}\rho \delta t = \delta M$$

*Equation 6-52*

Now the initial mass,  $M_0$ , at the initial conditions,  $h(t_0) = h_0$ , must be determined. This is done by writing a mass equation in terms of the pressure head, and then evaluating the mass at the initial pressure head. Using the basic density equation, the mass in the pipe can be evaluated as follows:

$$M = \mathcal{V} \times \rho$$

*Equation 6-53*

The volume,  $\mathcal{V}$ , can be expressed as a function of pressure. *Equation 6-15*, repeated here, shows the equation of the pipe volume,  $\mathcal{V}$ , taking into account the expansion and contraction of the pipe as a result of an internal pressure:

$$\mathcal{V} = \frac{\pi d^2}{4} l [2\varepsilon_{circ} + \varepsilon_{long} + 1]$$

Substituting the circumferential strain,  $\varepsilon_{circ}$ , and the longitudinal strain,  $\varepsilon_{long}$ , by *Equation 6-10* and *Equation 6-11* respectively, the volume equation can be written in terms of the pressure, fluid properties as well as the pipe geometric properties, as follows:

$$\Psi = \frac{\pi d^2}{4} l \left[ \frac{2Pd}{2bE} - \nu \frac{2Pd}{4bE} + \frac{Pd}{4bE} - \nu \frac{Pd}{2bE} + 1 \right]$$

*Equation 6-54*

Taking note that the pressure  $P = \rho gh$ , *Equation 6-54* can be simplified further to become:

$$\Psi = \frac{\pi d^2}{4} l \left[ \frac{5\rho gh d}{4bE} - \nu \frac{\rho gh d}{2bE} + 1 \right]$$

*Equation 6-55*

Or

$$\Psi = \frac{\pi d^2}{4} l \left[ \left( \frac{5\rho gh d}{4bE} - \nu \frac{\rho gh d}{2bE} \right) h + 1 \right]$$

*Equation 6-56*

*Equation 6-56* shows that if the internal pressure head,  $h$ , is zero, then the volume simply becomes the cross-sectional area,  $\pi d^2/4$ , multiplied by the length of pipe,  $l$ . Substituting *Equation 6-56* into the mass equation (*Equation 6-53*) yields an equation for the mass,  $M$ , as a function of pressure head,  $h$ ,

$$M = \frac{\pi d^2}{4} l \left[ \left( \frac{5\rho gh d}{4bE} - \nu \frac{\rho gh d}{2bE} \right) h + 1 \right] \rho$$

*Equation 6-57*

The initial mass,  $M_0$ , at the initial conditions time,  $t_0$ , can be determined by substituting the initial pressure head,  $h_0$ , into *Equation 6-57*, which in turn becomes:

$$M_0 = \frac{\pi d^2}{4} l \left[ \left( \frac{5\rho gh_0 d}{4bE} - \nu \frac{\rho gh_0 d}{2bE} \right) h_0 + 1 \right] \rho$$

*Equation 6-58*

At time  $t_1 = t_0 + \delta t$ , the initial mass in the pipe will change as a consequence of the leak, and thus the new mass,  $M_1$ , can be evaluated by the mass balance equation in this form:

$$M_1 = M_0 + \delta M$$

*Equation 6-59*

Substituting *Equation 6-52* into *Equation 6-59*, the new mass,  $M_1$ , can be evaluated as follows:

$$M_1 = M_0 - (Q_{out})_0 \rho \delta t$$

*Equation 6-60*

*Equation 6-59* can be written in a more generalised form, such that the mass for each time step  $j$  can be represented as follows:

$$M_j = M_0 - \sum_{j=0}^n (Q_{out} \rho)_j \delta t$$

*Equation 6-61*

Where the subscript,  $j$ , represents the time steps for the duration of the test. The pressure head at each time step,  $h_j$ , can be calculated from the calculated mass,  $M_j$ . This is done by rearranging *Equation 6-57* such that  $h$  is the subject of the equation:

$$h(M_j) = \frac{4bE}{\rho g d_0 (5 - 4\nu)} \left[ \left( \frac{M_j}{\rho V_0} \right) - 1 \right] = h_j$$

*Equation 6-62*

The pressure head obtained for each time step is compared to the pressure head obtained from the analytical solution.

### 6.6.3 Comparing the numerical and analytical solutions

An isolated pipe section with given pipe, fluid and leak properties was used to compare the numerical model with the analytical solution derived for the dynamic pressure test. *Table 6-1* shows the known pipe, fluid and leak properties of an isolated pipeline.

Table 6-1: Pipe, fluid and leak properties

Property	Value	Units
Fluid density, $\rho$	1000	kg/m <sup>3</sup>
Pipe length, $L$	0.2	m
Nominal diameter, $D_0$	0.35	m
Gravity, $g$	9.81	m/s <sup>-2</sup>
Discharge coefficient, $C_d$	unknown	
Elastic modulus, $E$	$2.60 \times 10^7$	N/m <sup>2</sup>
Thickness, $b$	0.008	Mm
Poissons ratio, $\nu$	0.25	
Effective head-area slope, $m'$	1	mm <sup>2</sup> /m
Effective initial leak area, $A'_0$	$8 \times 10^{-2}$	mm <sup>2</sup>
Initial pressure at time = 0, $h_0$	27.7	m

#### 6.6.4 Analysis procedure

The following procedure was carried out to compare the numerical model with the analytical solution:

- **Step 1:** Using the derived analytical pressure-time equation described by Equation 6-35, the pressure,  $h_{analytical}$ , was calculated at time intervals of 0.1 seconds.
- **Step 2:** A graph of the  $h_{analytical}$  against time was plotted.
- **Step 3:** The initial mass,  $M_0$ , was determined at the initial pressure,  $h_0$ , using Equation 6-58.
- **Step 4:** The modified orifice leakage equations given in Table 6-1 was used to calculate the leakage flow rate,  $Q$ , as follows:

$$Q_{out} = \sqrt{2g}(8 \times 10^{-2}h^{0.5} + h^{1.5}) \times 10^{-6}$$

- **Step 5:** The rate of change of mass flow rate,  $\Delta\dot{M}$ , was calculated by multiplying the leakage flow rate,  $Q_{out}$ , by the fluid density,  $\rho$ , given in Table 6-1:

$$\Delta\dot{M} = -Q_{out} \times \rho$$

- **Step 6:** The total change in mass for a given time interval was calculated. This was done by multiplying the change in mass flow rate,  $\Delta\dot{M}$ , by a time interval,  $\Delta t$ .

$$\Delta M = \Delta\dot{M} \times \Delta t = -Q_{out} \times \rho$$

- **Step 7:** Using the mass balance equation, mass inside the pipe,  $M_{in}$ , was calculated. This was done by subtracting the current mass in the pipe by the mass leaking out:

$$M_{in} = M_0 + \Delta M$$

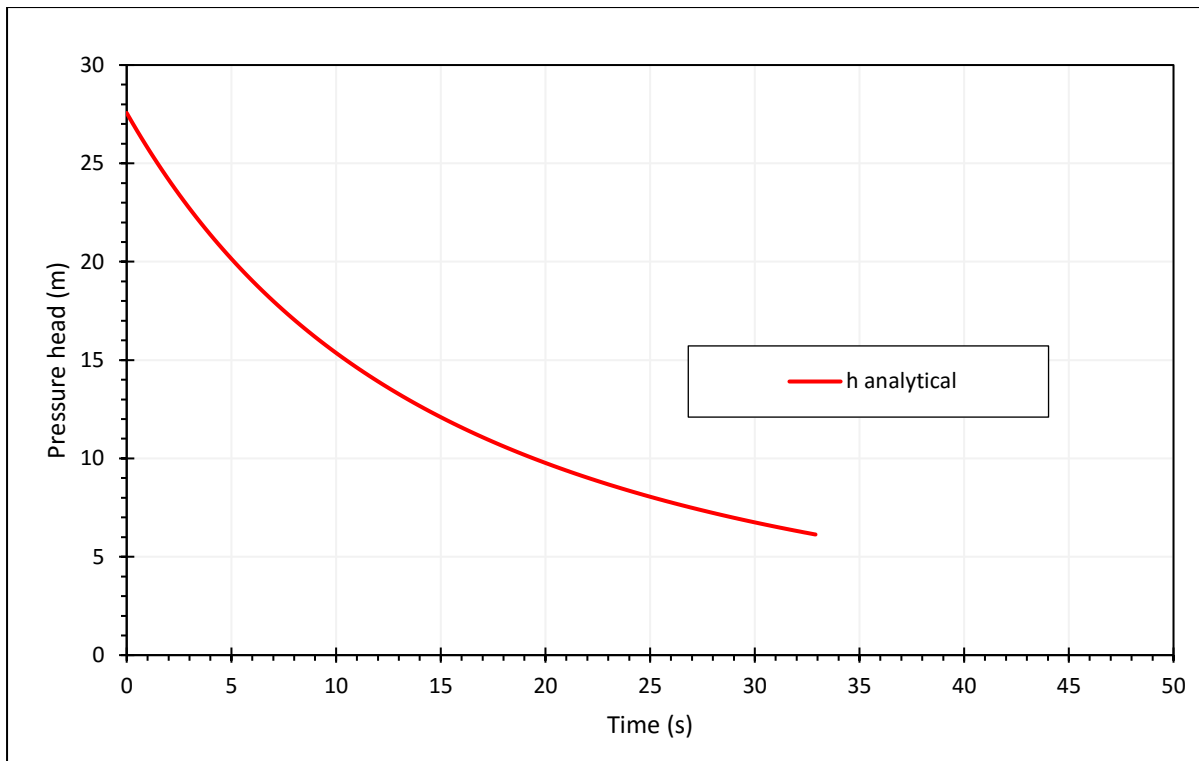
- **Step 8:** The mass numerical pressure head was calculated by substituting the mass in the pipe,  $M_{in}$ , into Equation 6-62:

$$h_{numerical} = \frac{4bE}{\rho g d_0 (5 - 4\nu)} \left[ \left( \frac{M_{in}}{\rho V_0} \right) - 1 \right]$$

- **Step 9:**  $h_{numerical}$  was plotted against the time.
- **Step 10:** Since the accuracy of the numerical model depends on the time interval used, the smaller the time interval the more accurate the model becomes in predicting the analytical solution. For this reason, three time intervals (15 sec, 10 sec, and 1 sec) are used to illustrate this.

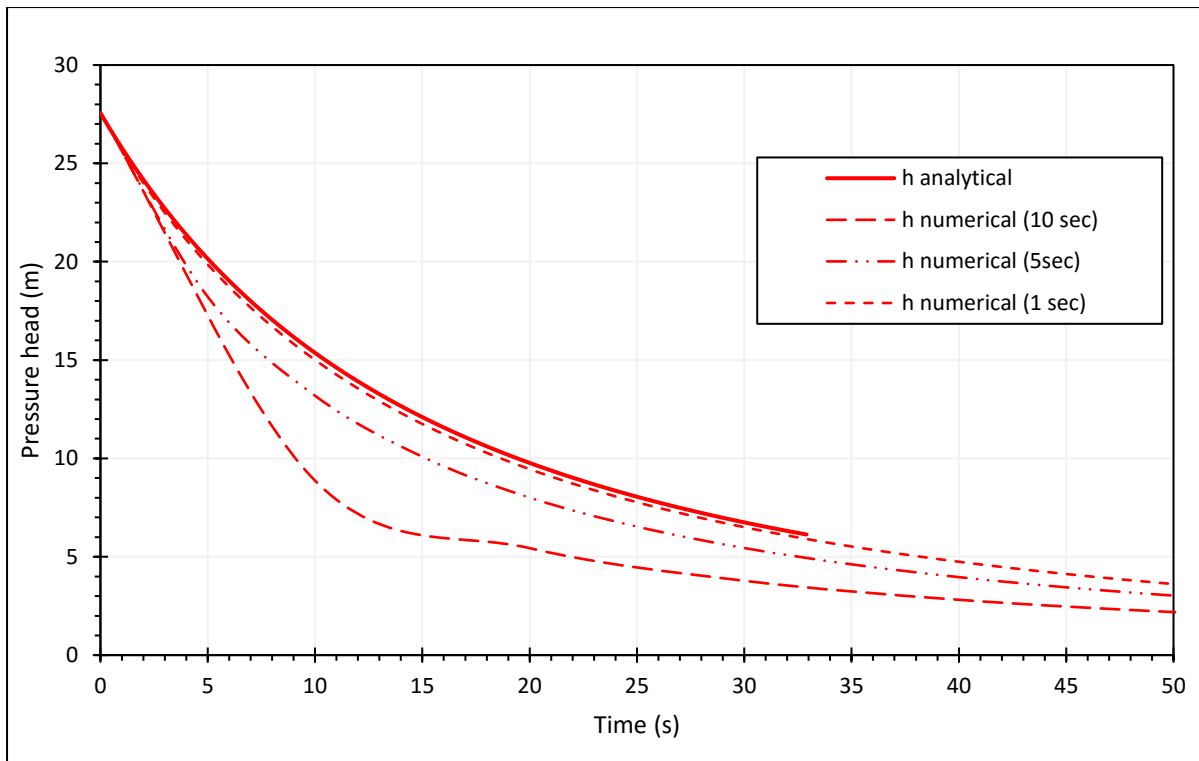
### 6.6.5 Results

Using the properties in *Table 6-1*, the analytical pressure head was calculated at time intervals of 0.1 seconds, from 0 to 33.0 seconds. The analytical pressure head was plotted against time as is shown in *Figure 6-2*. It can be seen from the figure that the pressure head dropped over time, reflecting a leak on the isolated pipe section.



*Figure 6-2: Analytical pressure head against time*

The numerical pressure head model was then evaluated to investigate how well the numerical model predicts the analytical solution. Various time intervals were used to evaluate the numerical model. This was done to illustrate the effect the time interval has on the accuracy of the numerical model. *Figure 6-3* shows the plot of the numerical pressure head against time for the various time intervals. In the figure, the continuous line represents the analytical pressure head calculated at 0.1 second time intervals.



*Figure 6-3: Numerical pressure head plotted against time for various time intervals*

Figure 6-3 shows that the accuracy of the numerical model improves as the time interval used in the numerical model gets smaller. The largest difference between the analytical and numerical pressure-time model occurred when the time interval for the numerical model was set to 10 seconds. Conversely, when the time interval of the numerical model was set to 0.1 second, the numerical pressure head plots very closely to the analytical pressure head.

These results confirmed and verified that the theoretical background of the numerical model is consistent with the analytical model theory which was developed for describing the relationship between the pressure head and time in an isolated pipe section. However, it was shown that the accuracy of the numerical model depends on the time interval used.



## 6.7 Laboratory tests: pressure drop tests

### 6.7.1 Introduction

Taylor (2018), a UCT student doing research on water distribution systems, conducted an experimental study that was used to verify the numerical model developed for the variation of pressure with time for an isolated pipe section.

The experimental study was limited to uPVC pipe sections that were drilled or cut in order to create sources of leakage. The uPVC pipe section properties that could be measured or calculated are presented in *Table 6-2*.

*Table 6-2: Measured properties of the test pipes*

Property	Symbol	Value	Unit
Diameter of pipe	$d$	0.113	$m$
Length of pipe	$L$	1.0	$m$
Pipe wall thickness	$V_0$	0.011	$m^3$
Initial pipe volume	$b$	0.005	$m$

The properties that were taken from literature and remained constants for each experiment are given in *Table 6-3*.

*Table 6-3: Constant properties taken from literature*

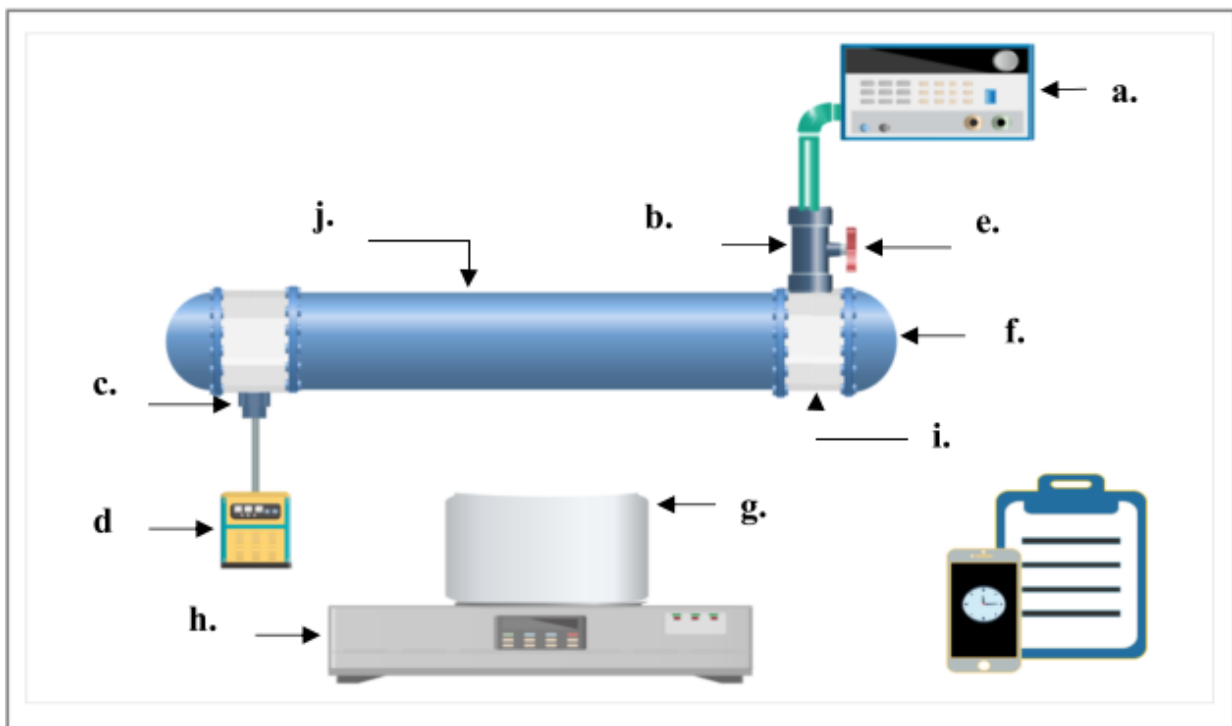
Property	Symbol	Value	Unit
Acceleration due to gravity	$g$	9.81	$m/s^2$
Fluid bulk modulus of elasticity	$K$	$2.17 \times 10^{12}$	$N/m^2$
Fluid density	$\rho$	997	$kg/m^3$
Pipe elastic modulus	$E$	$2.8 \times 10^9$	$N/m^2$
Poissons ratio	$\nu$	0.4	—

Various leak types were investigated, namely a round hole, a longitudinal crack and a circumferential crack. This section describes the experimental setup and procedure and discusses the verification results.

## 6.7.2 Experimental setup

A schematic layout of the main components of the experimental setup is shown in *Figure 6-4* and consisted of the following apparatus:

- a. Flowmeter
- b. Hose to saddle connection
- c. Pressure transducer to saddle connection
- d. Pressure transducer
- e. Shut-off valve
- f. Pipe and end caps
- g. Collection bucket
- h. Digital balance
- i. Clamped saddle
- j. 110mm uPVC pipe with fabricated leak



*Figure 6-4: Schematic layout of the main components (Taylor, 2018)*

The apparatus was carefully assembled, with each end of the uPVC test pipe fitted with a saddle and an end cap to ensure that water only escaped via the fabricated leak at the centre of the pipe. A photograph of the experimental setup is shown in *Figure 6-5*.

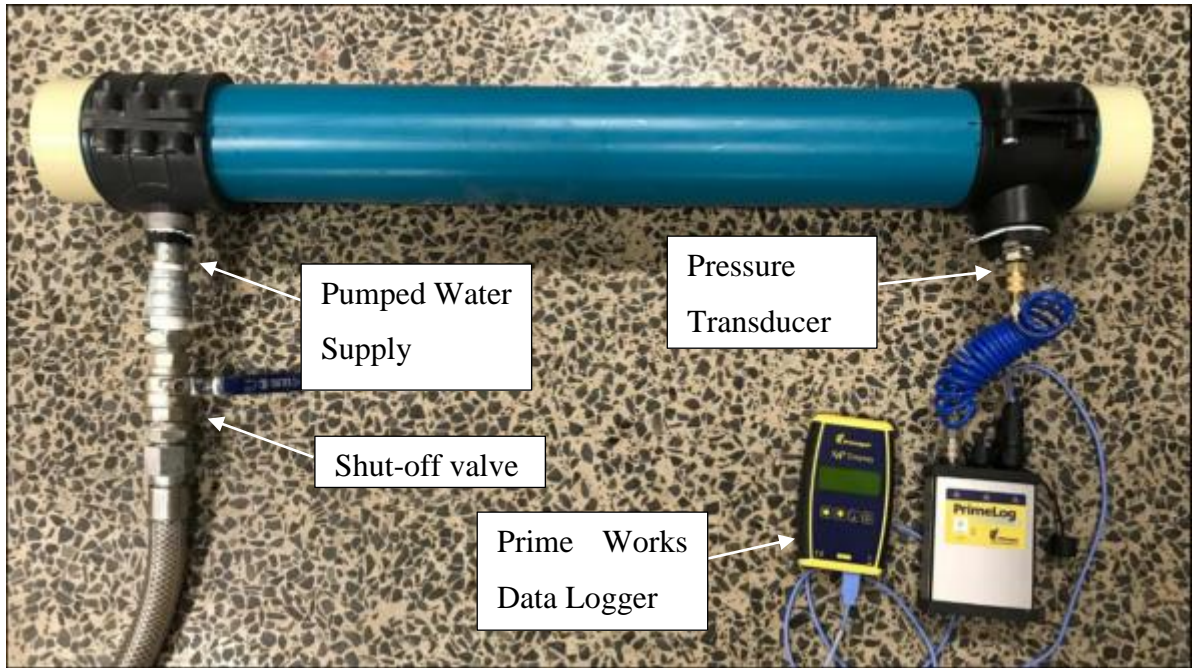


Figure 6-5: Photograph showing experimental setup

One end of the setup was connected to a pumped water supply from an underground sump through a 25mm calibrated magnetic flow meter. The other end of the setup was fitted with a calibrated pressure transducer.

### 6.7.3 Test pipe samples

#### 6.7.3.1 Pipe01: uPVC round hole

Pipe01 was drilled at the centre to create a round hole leak, as illustrated in Figure 6-6. The round hole had a diameter of 1mm.

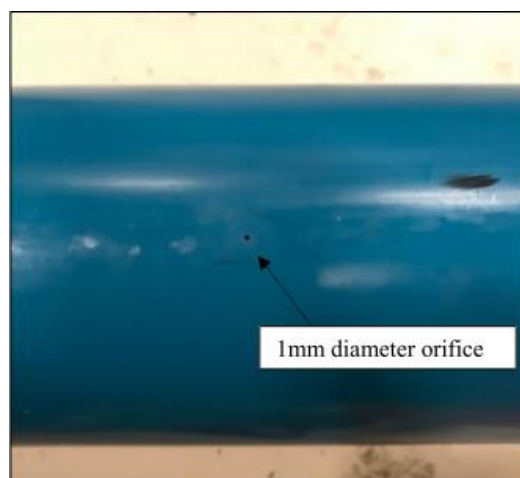


Figure 6-6: Pipe01 with round hole leak

#### 6.7.4 Experimental procedure

During the experiment, three variables were measured and recorded, namely the internal fluid pressure, the mass of water escaping through the leak, and the time. The internal fluid pressure was measured using a *Prime Works* data logger, while the mass of water escaping through the leak was measured using a digital scale and recorded by a continuous video of the balance screen. Finally, the time was measured using the stopwatch of the video recording device.

The experimental procedure carried out in Taylor's (2018) study was as follows:

- **Step 1:** The experimental setup shown in *Figure 6-5* was elevated between two tables to a height of about 1.5 meters, with the fabricated leak facing downwards for ease of collection.
- **Step 2:** A spirit level was used to ensure that the setup was horizontally level.
- **Step 3:** The collection bucket was placed in position (directly under the leak) and the digital balance scale was zeroed to ensure that the bucket weight was not accounted for.
- **Step 4:** The shut-off valve on the hose pipe was then opened (shown in *Figure 6-5*) to allow water to fill the test pipe.
- **Step 5:** Trapped air was removed from the test pipe by disconnecting the pressure transducer and allowing a small amount of water to flow through the pressure transducer connection.
- **Step 6:** Once the air was being expelled from the test pipe and the test pipe was full of water, the transducer was reconnected.
- **Step 7:** The pumped water supply was set to a desired pressure and the test pipe was pressurised. Water could leak into the collection bucket while the water from the pumped supply continued to fill and pressurise the test pipe. The pressure in the test pipe could build up until the desired pressure was reached, and then the shut-off valve was closed.
- **Step 8:** As soon as the shut-off valve was closed, the time on the recording device was split to note the time representing the start of the experimental results. Simultaneously, the video recording device was set to begin capturing the continuous stream of mass

results as displayed by the digital balance. After 10 minutes of recording, the data logger was disconnected and the video recording was stopped.

- **Step 9:** After recording, the pipe was then allowed to drain completely. The experiment was then reset and repeated three times to test repeatability.
- **Step 10:** After three attempts, the test pipe was disconnected from the saddles and thereafter replaced with the next pipe sample to be tested. The steps were repeated from step 1 to step 9.

## **6.7.5 Experimental test data analysis procedure**

### ***6.7.5.1 Data capturing***

The three variables (pressure, mass and time) that were measured during the experiment were sampled differently depending on the accuracy of the device used to measure the variable. The tests had a total duration of 10 minutes; however, due to the amount of data collected, a duration of 5 minutes of data was used in an attempt to minimise errors.

The pressure transducer had a sampling rate of 1 second and therefore the pressure signal inside the pipe was recorded at intervals of 1 second.

The digital scale used to measure the mass of water escaping through the leak was found to be sensitive to the movement of the water inside the collection bucket, consequently it was not possible to have a mass reading for every second. The mass was therefore sampled only at time stamps in which the scale registered a “balanced” signal.

The recording device that was used as a timer was capable of measuring a time stamp every second for the entire duration of the experiment.

### ***6.7.5.2 Experimental data analysis procedure***

The first part of the analysis deals with making sense of the experimental data. Various graphs were plotted to understand how the different variables (pressure head and mass) measured change over time. Additionally, the leakage flow rate was calculated directly from the experimental data and was also plotted against time. The steps of the analysis were as follows:

- **Step 1:** The measured pressure head ( $h_{measured}$ ) was plotted over a time of 5 minutes.

- **Step 2:** The mass readings recorded during the experiment, ( $M_{measured}$ ), were plotted against time. It is worth noting that the  $M_{measured}$  is also equal to the cumulative mass of water leaving the pipe into the bucket,  $M_{out}$ , over the test period of 5 minutes.
- **Step 3:** The measured mass ( $M_{measured}$ ) was converted into volume ( $V_{measured}$ ) by dividing the measured mass by the density value given in *Table 6-3*. This yields the cumulative volume,  $V_{out}$ .
- **Step 4:** From the cumulative volume of the leak,  $V_{out}$ , the incremental volume,  $\Delta V_{out}$ , could be determined by evaluating the difference between volumes at two time stamps, i.e.:

$$\Delta V_{out} = (V_{out})_{t+1} - (V_{out})_t$$

*Equation 6-63*

- **Step 5:** The measured flow rate,  $Q_{measured}$ , was determined by dividing the incremental volume,  $\Delta V_{out}$ , by the corresponding time interval,  $\Delta t$ , yields the measured

$$Q_{measured} = \frac{\Delta V_{out}}{\Delta t}$$

*Equation 6-64*

- **Step 6:** The measured flow rate,  $Q_{measured}$ , was plotted against time.

### ***6.7.5.3 Leakage modelling analysis***

The second part of the analysis deals with leakage modelling calculations. Using the experimental data, the modified orifice equation leakage parameters ( $C_d A$  and  $C_d m$ ) and the power equation leakage parameters ( $C$  and  $N1$ ) were determined.

- Step 1: A graph of the measured flow rate against the pressure was plotted using the experimental data values. A power equation was fitted to the graph to obtain the power equation leakage parameters: leakage exponent  $N1$  and the leakage coefficient  $C$ .
- Step 1: The effective leak area ( $C_d A$ ) at various measured pressures was calculated using the re-ordered orifice equation:

$$C_d A = \frac{Q_{measured}}{\sqrt{2gh_{measured}}}$$

Equation 6-65

- Step 2: The effective leak area, ( $C_d A$ ), was plotted against the measured pressure,  $h_{measured}$ , and a linear function fitted to the data points. The intercept of this line with the effective area axis gives the effective initial leak area, ( $C_d A_0$ ), and the slope of this line gives the effective head-area slope ( $C_d m$ ).
- Step 3: The modified orifice equation model was developed for predicting the leakage flow rate,  $Q_{Modified\ orifice\ equation}$ , at various measured pressures. The  $Q_{Modified\ orifice\ equation}$  can be derived by substituting ( $C_d A_0$ ) and ( $C_d m$ ), determined from step 2, into the Equation 6-66:

$$Q_{Modified\ orifice\ equation} = \sqrt{2g} [(C_d A_0)h_{measured}^{0.5} + (C_d m)h_{measured}^{1.5}]$$

Equation 6-66

- Step 4: The discharge coefficient,  $C_d$ , was determined by dividing the effective initial leakage area,  $C_d A_0$ , by the physically measured leak area,  $A_{measured}$ , of the round hole.

$$C_d = \frac{C_d A_0}{A_{measured}}$$

Equation 6-67

- Step 5: Using leakage flow rate of the modified orifice equation was obtained for the measured pressures.
- Step 6: The  $Q_{Modified\ orifice\ equation}$  and  $Q_{measured}$  were plotted against the measured pressure head,  $h_{measured}$ , on the same graph, and the two flow rates compared.

#### 6.7.5.4 Calibration of the numerical model using the experimental results

The third and final part of the analysis used the experimental data to calibrate the numerical model proposed in Section 6.6. The two main numerical model equations that were used for calibration are Equation 6-57 and Equation 6-62, repeated here, and respectively representing mass and pressure as a function of time:

$$M_{numerical} = \rho V_0 \left[ \left( \frac{5\rho ghd}{4bE} - v \frac{\rho ghd}{2bE} \right) h + 1 \right]$$

Equation 6-57

$$h_{numerical} = \frac{4bE}{\rho g d_0 (5 - 4v)} \left[ \left( \frac{M}{\rho V_0} \right) - 1 \right]$$

Equation 6-62

The only variable that could be used from *Equation 6-57* and *Equation 6-62* to calibrate the models was the initial volume of water,  $V_0$ . The reason is that, although the pipe appeared to initially be completely full of water at the start of the experiment, this is unknown as it was not visible. The other parameters such as the elastic modulus  $E$ , Poisson's ratio  $v$ , wall thickness  $b$ , and the pipe diameter at zero pressure  $d_0$  were kept as fixed variables in the model.

The steps carried out to calibrate the numerical model were as follows:

- **Step 1:** A graph of measured cumulative mass,  $V_{measured}$ , were plotted against the pressure head.
- **Step 2:** A best fit curve was fitted to the data points plotted in step 1. The intercept of the best fit curve to the cumulative volume,  $V_{measured}$ , axis represents the initial volume ( $V_0$ ).
- **Step 3:** The calibrated value for  $V_0$  was then used in the calculation for  $h_{numerical}$ , as described by *Equation 6-62*.
- **Step 4:** The instantaneous initial mass ( $M_0$ ) at the initial pressure ( $h_0$ ) was determined, using *Equation 6-57*.
- **Step 5:** Using the mass balance, the numerical mass at different pressures was calculated:

$$M(h)_i = \rho V_0 \left[ \left( \frac{5\rho ghd}{4bE} - v \frac{\rho ghd}{2bE} \right) h_i + 1 \right] - \sqrt{2g} [(C_d A_0) h_i^{0.5} + (C_d m) h_i^{1.5}] \Delta t$$

Equation 6-68

- **Step 6:** The change in mass between two pressures was determined. This is the amount of water in the bucket.



$$\Delta M_{numerical} = M(h)_i - M(h)_{i+1}$$

Equation 6-69

- **Step 7:** The cumulative mass of  $\Delta M_{numerical}$  was calculated.
- **Step 8:** The cumulative numerical mass,  $\Delta M_{numerical}$ , and the cumulative measured mass against the pressure head were plotted.
- **Step 10:** The total absolute relative error between the  $m_{numerical}$  and  $m_{measured}$  was determined by using the following equation:

$$\varepsilon_{relative\ error} = \sum_{i=0}^n \frac{|M_{(measured),i} - M_{(numerical)i}|}{M_{(measured)i}}$$

- **Step 11:** The numerical pressure head was determined using Equation 6-62:

$$h_{numerical} = \frac{4bE}{\rho g d_0 (5 - 4\nu)} \left[ \left( \frac{M}{\rho V_0} \right) - 1 \right]$$

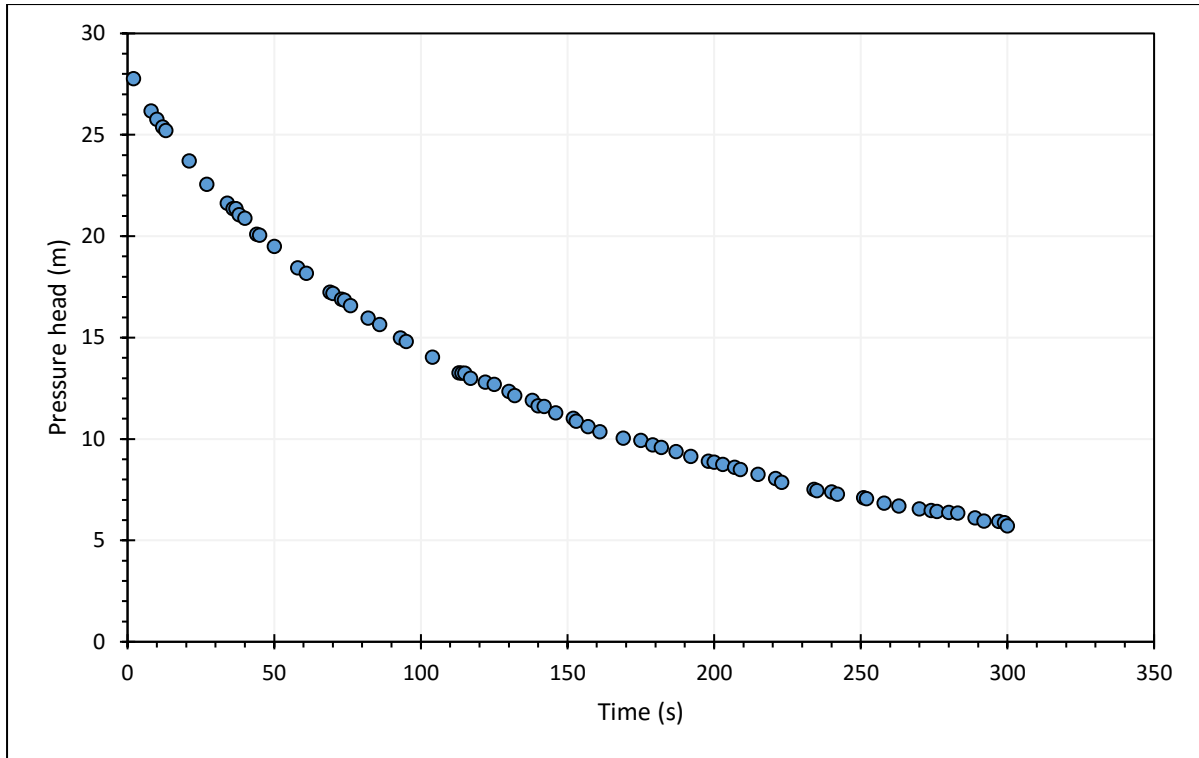
- **Step 12:**  $h_{numerical}$  and  $h_{measured}$  were plotted against time to check correlation.
- **Step 13:** The total absolute relative error between the  $h_{numerical}$  and  $h_{measured}$  were determined by using the following equation:

$$\varepsilon_{relative\ error} = \sum_{i=0}^n \frac{|h_{(measured),i} - h_{(numerical)i}|}{h_{(measured)i}}$$

## 6.7.6 Results of the pressure drop experiment

### 6.7.6.1 Experimental data results

The measured pressure head inside the test pipe was plotted against time as shown in Figure 6-7. The plot shows that the pressure head followed the expected trend. A gradual pressure drop signature was evident as time progressed. This pressure drop symbolises an existing leak in the isolated pipe which gradually depressurises a pipe that would have otherwise remained at a constant pressure.



*Figure 6-7: Measured pressure head against time*

The cumulative mass, collected in the bucket placed directly under the leak, is plotted against time in *Figure 6-8*. As expected, because of the leak, the cumulative mass leaving the pipe continues to increase as the pipe empties. In other words, as the conservation of mass states, the total mass of the system is equal to the sum of water leaving the pipe and the mass of water remaining in the pipe:

$$M_{system} = M_{inside\ pipe} + M_{leaving}$$

*Equation 6-70*

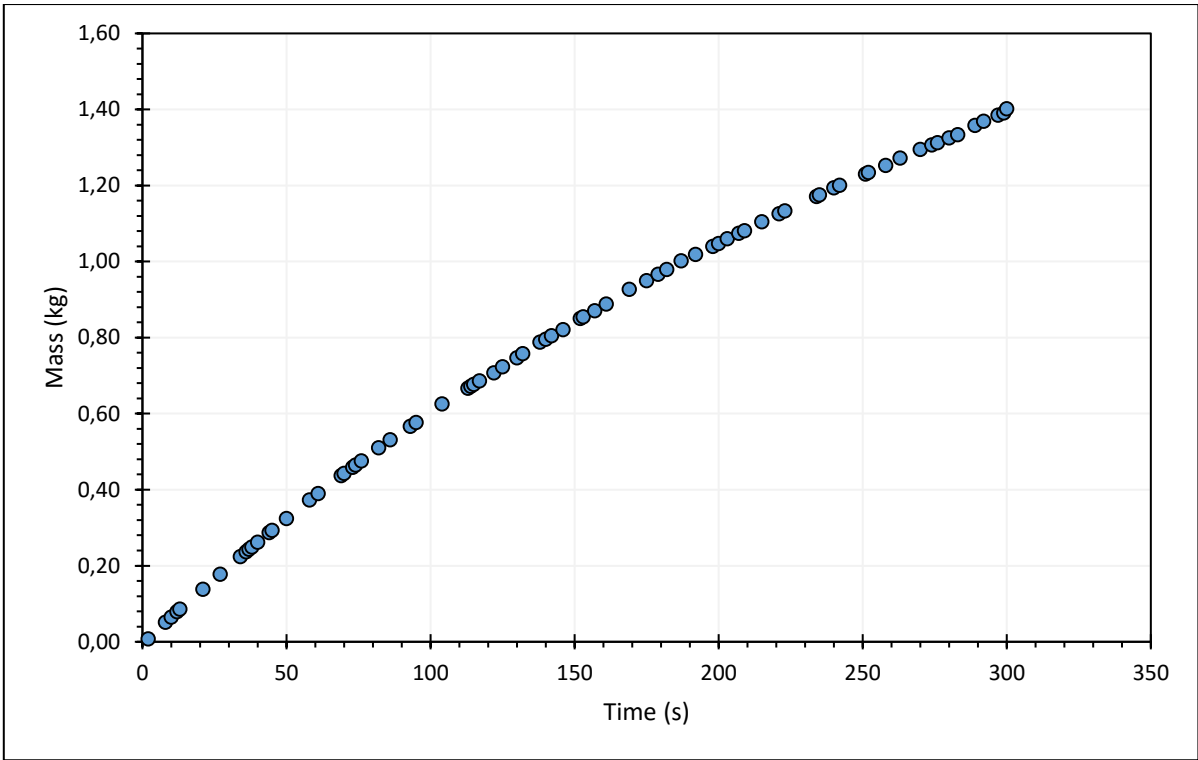
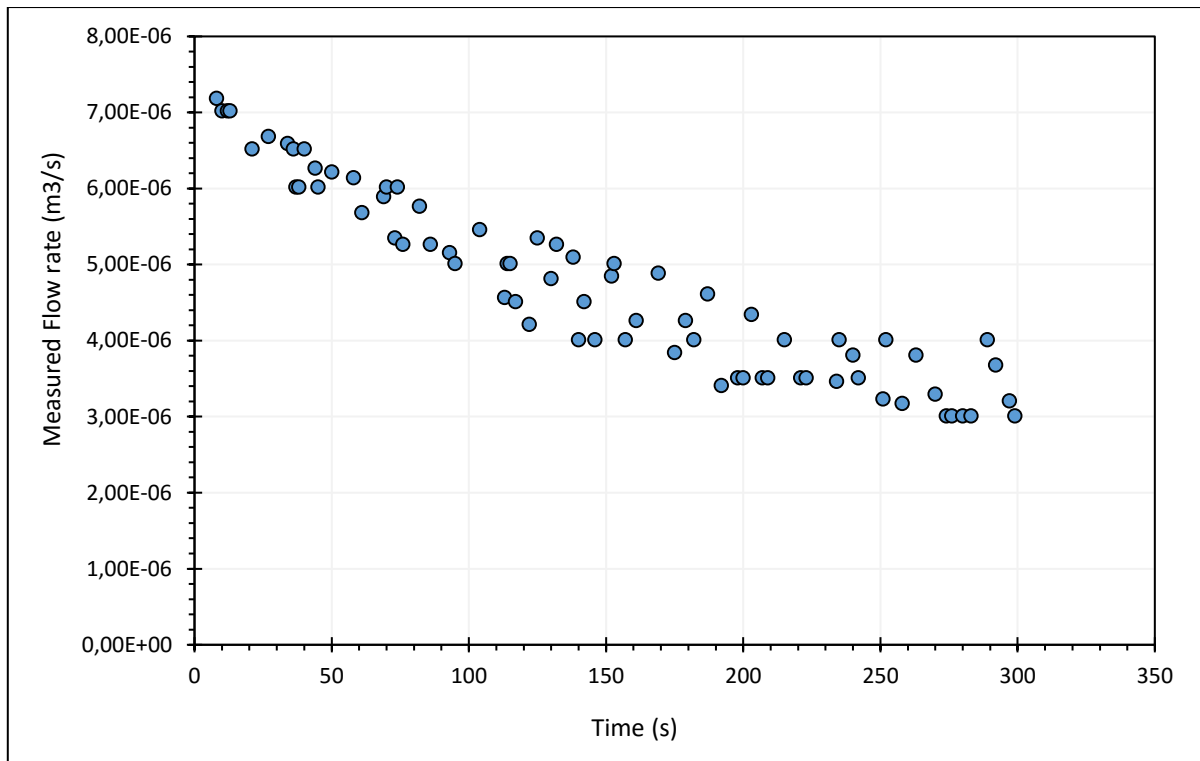


Figure 6-8: Cumulative mass measured in the bucket against time

The cumulative measured mass was converted to a cumulative volume by multiplying it by the density of water as provided in *Table 6-3*. From the cumulative volume, the incremental volume was determined. Dividing the incremental volume by the corresponding time interval yields the flow rate (representing the leakage flow rate). The measure leakage flow rate,  $Q_{measured}$ , against time is plotted in *Figure 6-9*:



*Figure 6-9: Measured leakage flow rate against time*

Figure 6-9 shows that while there was a scatter in the data, the overall trend suggests that the leakage flow rate decreased with time. This trend was expected since the pressure head is one of the main factors affecting leakage and with time. Subsequently, the leakage flow rate is also expected to decrease.

#### **6.7.6.2 Leakage parameters for the power equation**

The measured leakage flow rate and pressure head values were plotted as shown in *Figure 6-10*. A power equation was fitted to the data to obtain the leakage parameters for the power equation. From the power equation, the leakage exponent ( $N1$ ) and the leakage coefficient,  $C$ , are 0.54 and  $1 \times 10^{-6}$ , respectively.

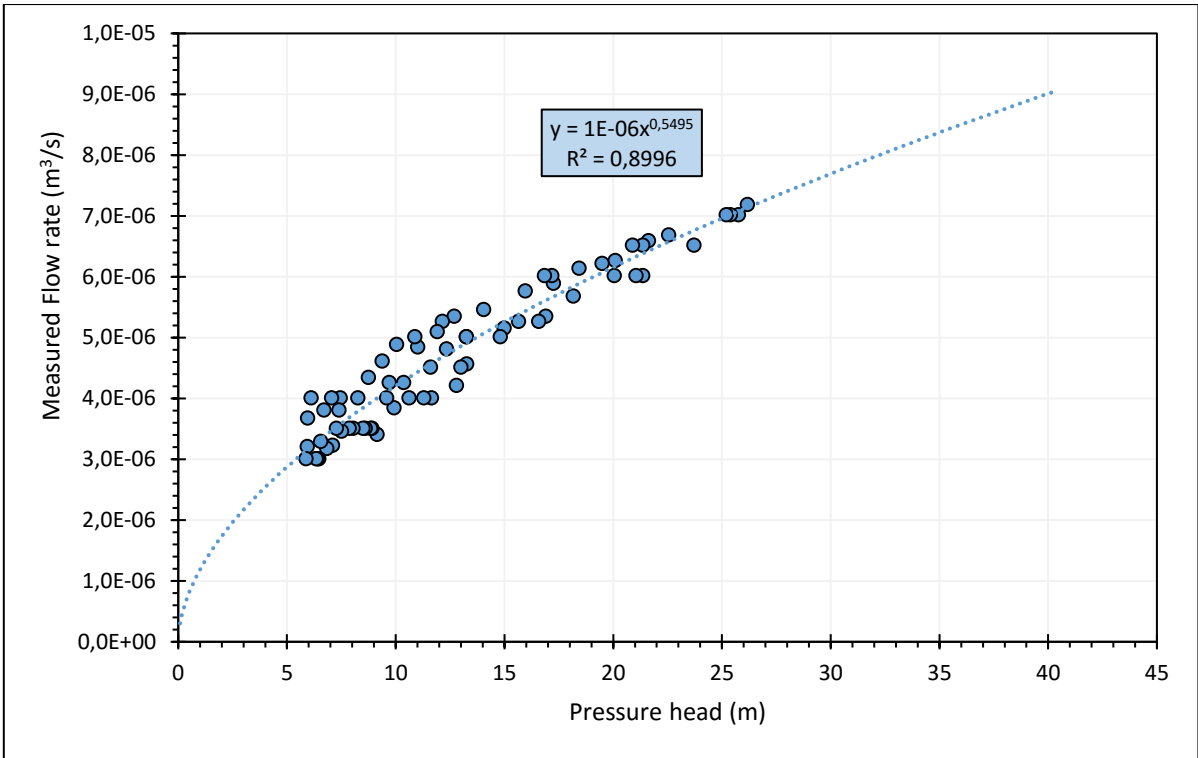


Figure 6-10: Measured flow rate against pressure

The results of the leakage parameters of the power equation are summarised in *Table 6-4*. The leakage exponent obtained was higher than the value of 0.5, typically expected for round hole leaks (Malde & van Zyl, 2015). This could be due to the accuracy in which the flow rate was measured; nonetheless, this result is still within a 10% error of the expected value.

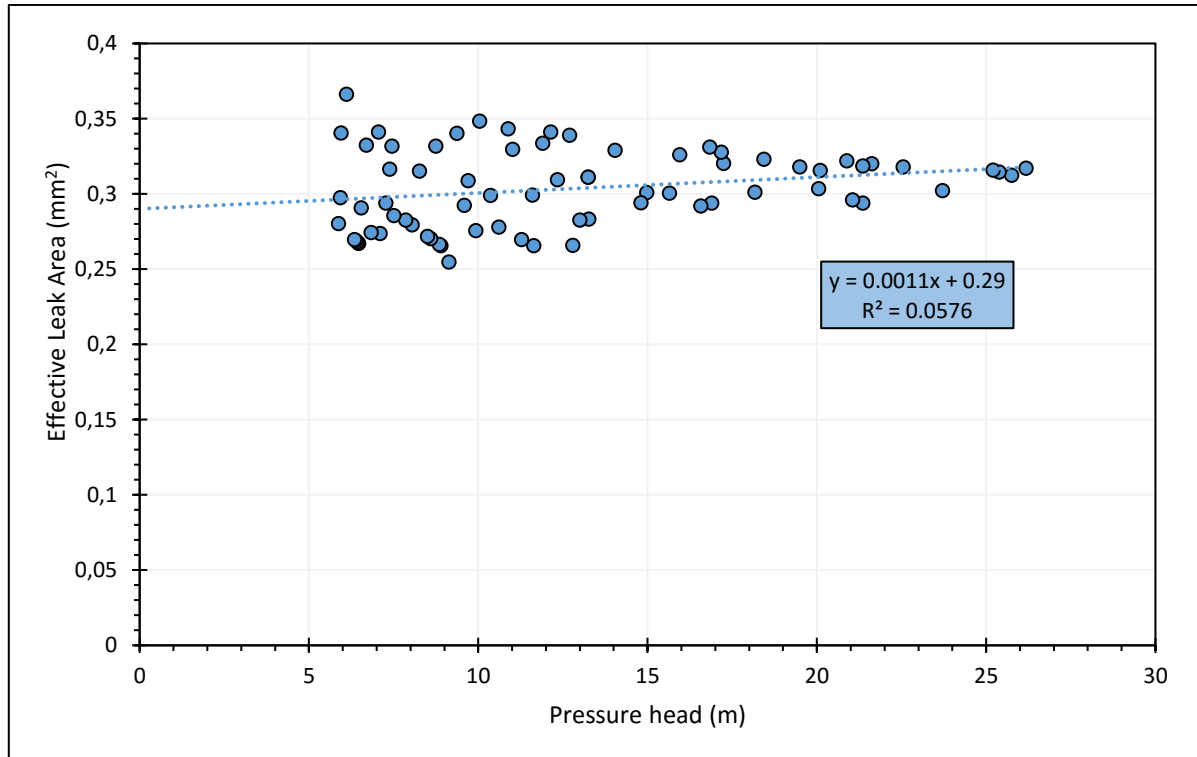
Table 6-4: Leakage parameters for the power equation

Leakage parameters of the power equation	Value
Leakage exponent, $N1$	0.55
Leakage coefficient, $C$	$1 \times 10^{-6}$

### 6.7.6.3 Leakage parameters for the modified orifice equation

The leakage parameters for the modified orifice equation include the head-area slope,  $m$ , and the initial leak area,  $A_0$ . It should be noted that because the discharge coefficient,  $C_d$ , is an unknown, it was eliminated by combining it with the initial leak area and the head-area slope, so that the leakage parameters become the effective initial leak area,  $(C_d A_0)$ , and the effective head-area slope  $(C_d m)$ .

In order to obtain the leakage parameters for the modified orifice equation, a graph of the effective leak area against the pressure head was plotted, as shown in *Figure 6-11*. The figure shows that the data points were scattered sporadically at the lower pressures but become more grouped together at the higher pressures.



*Figure 6-11: Effective leakage area against pressure head*

A linear line was plotted through the data points, and the overall trend shows that the effective leakage area increased with the pressure head. The intercept of the linear function represented the effective initial leak area, ( $C_d A_0$ ), and the slope of the linear function represented the effective head-area slope, ( $C_d m$ ).

The results of the leakage parameters for the modified orifice equation are summarised in *Table 6-5*. The table shows that the effective head-area slope was obtained as  $0.0011 \text{ mm}^2/\text{m}$  and the effective initial leak area was obtained as  $0.29 \text{ mm}^2$ . This result is consistent with a leak that is stable and does not expand very much with pressure; this is synonymous with round holes leaks.

Table 6-5: Results of the leakage parameters for the modified orifice equation

Leakage parameters	Values
Effective initial leak area, $A'_0$ (mm <sup>2</sup> )	0.29
Effective head-area slope, $m'$ (mm <sup>2</sup> /m)	0.0011

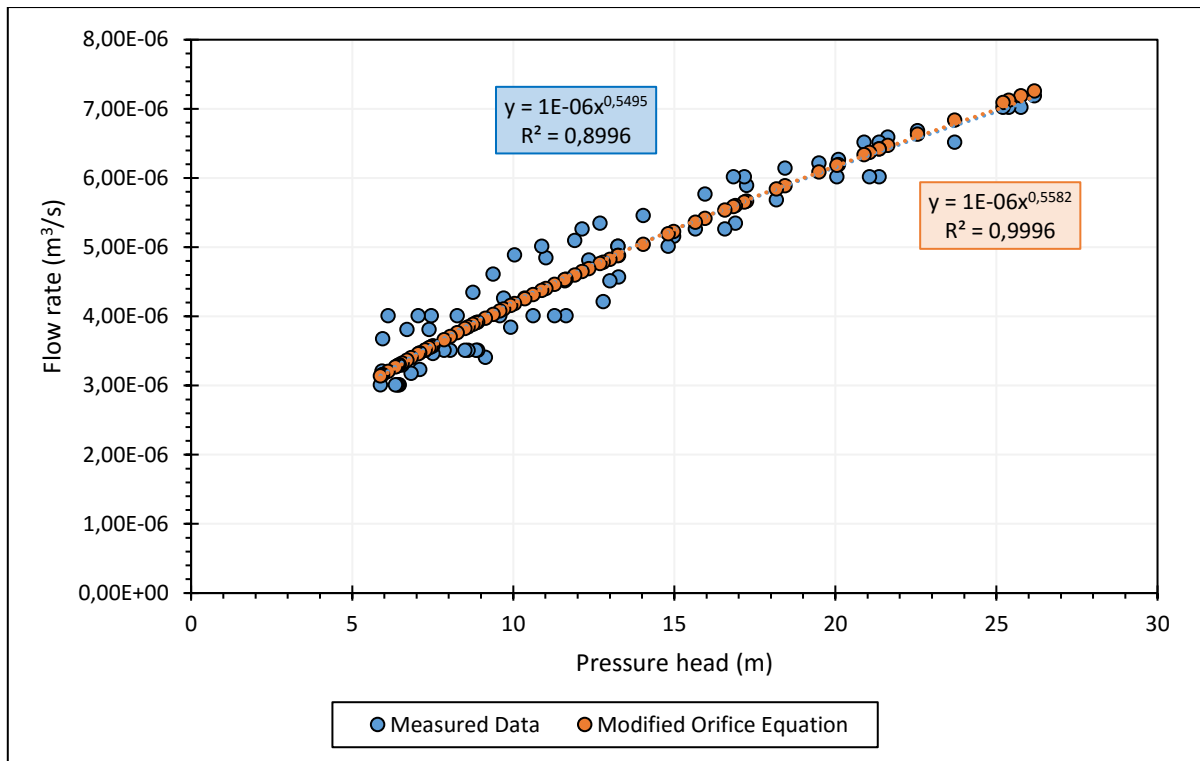
The discharge coefficient,  $C_d$ , was evaluated by dividing the obtained effective leak area of 0.29 mm<sup>2</sup> by the physically measured leak area of 0.78mm<sup>2</sup> (Equation 6-67). The  $C_d$  was calculated to be 0.36. This  $C_d$  was lower than the typical discharge coefficient of 0.65 as is suggested in the literature for a round hole in a uPVC pipe (Schwaller, 2012). This disparity could be caused by the fact that the actual leak opening was very small (1 mm diameter) in comparison to the distance of the leak hole from the inner surface of the pipe to the outer surface which was 5mm (thickness of pipe).

Based on the effective initial leak area and the effective head-area slope (given in Table 6-5), the leakage flow rate can be evaluated using the following equation:

$$Q_{\text{modified orifice equation}} = \sqrt{2g} [0.29h^{0.5} + 0.0011h^{1.5}] \times 10^{-6}$$

Equation 6-71

Using Equation 6-71, the leakage flow rate from the pipe can be determined at different pressures. Figure 6-12 shows a plot of the leakage flow rate determined from Equation 6-71,  $Q_{\text{modified orifice equation}}$ , against the measured pressure head. In the same figure, the measured flow rate was also plotted against the measured pressure for comparison.



*Figure 6-12: Plot of measured flow rate against pressure head*

Figure 6-12 shows that the data points of the measured flow rate plotted against the pressure head, and the leakage flow rate predicted by the modified orifice equation plotted against pressure head displayed similar trajectories. Both data sets displayed increasing flow rate with a power exponent of about 0.55.

#### **6.7.6.4 Calibration results for numerical modelling**

Since the initial volume of water,  $V_0$ , at the initial pressure,  $h_0$ , could not be determined during the experiment, the measured cumulative volume and pressure readings were used to calibrate the initial volume. This was done by first plotting the measured cumulative volume against the measured pressure head, as shown in Figure 6-13.



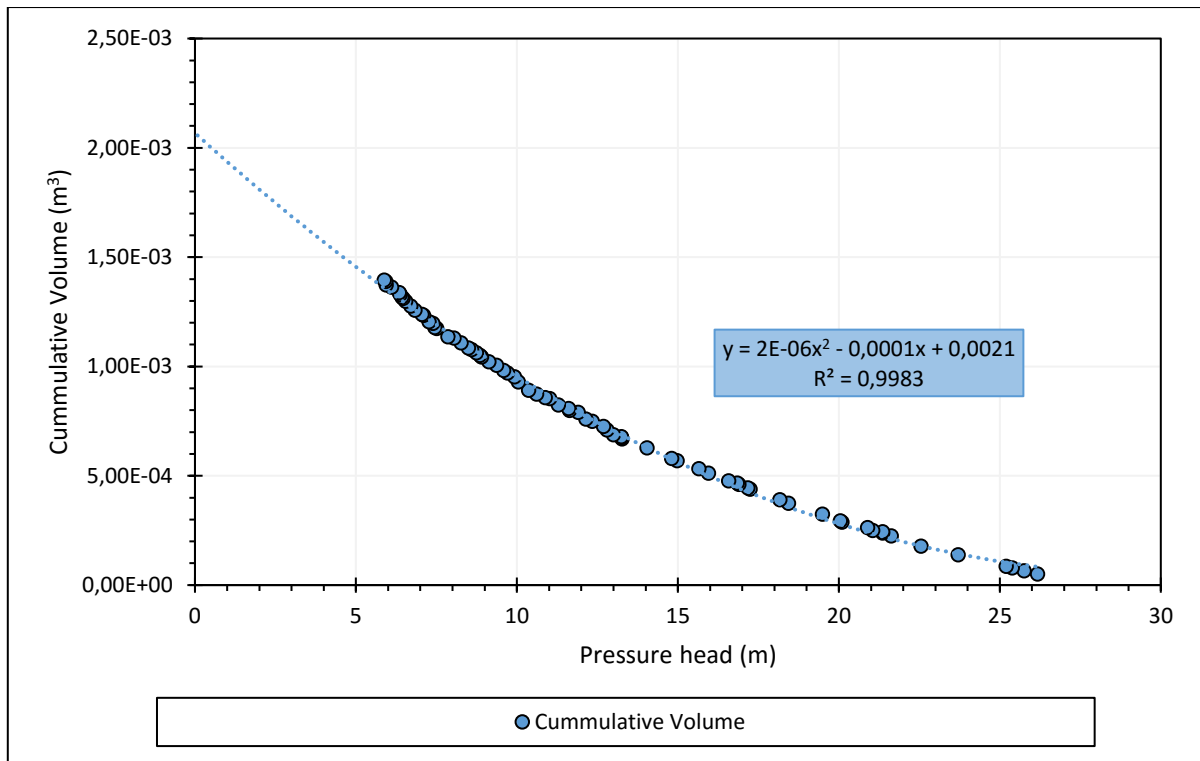


Figure 6-13: Measured cumulative volume against pressure head readings

A polynomial best fit line was fitted to the data points as shown in *Figure 6-13*. The correlation between the data points was approximately 0.99, suggesting that over 99% of the variation in the data can be explained by the polynomial equation. Subsequently, the equation was used to extrapolate and calibrate the initial volume. The intercept of the polynomial line with the cumulative volume axis gave the initial volume, which was determined as  $0.0021\text{m}^3$ .

The calibrated value,  $V_0$ , was then used to calculate the numerical mass in the pipe using *Equation 6-57*. It must be emphasized that the numerical equation derived for mass does not serve to calculate the variable mass at each pressure head, but rather the instantaneous initial mass at a given initial pressure head. The theoretical cumulative mass of water in the collection bucket was calculated using *Equation 6-68* and *Equation 6-69*.

A plot of the numerical cumulative mass collected in the bucket and the measured cumulative mass was plotted against the pressure head, as shown in *Figure 6-14*. It is evident that both masses have a similar trend line.

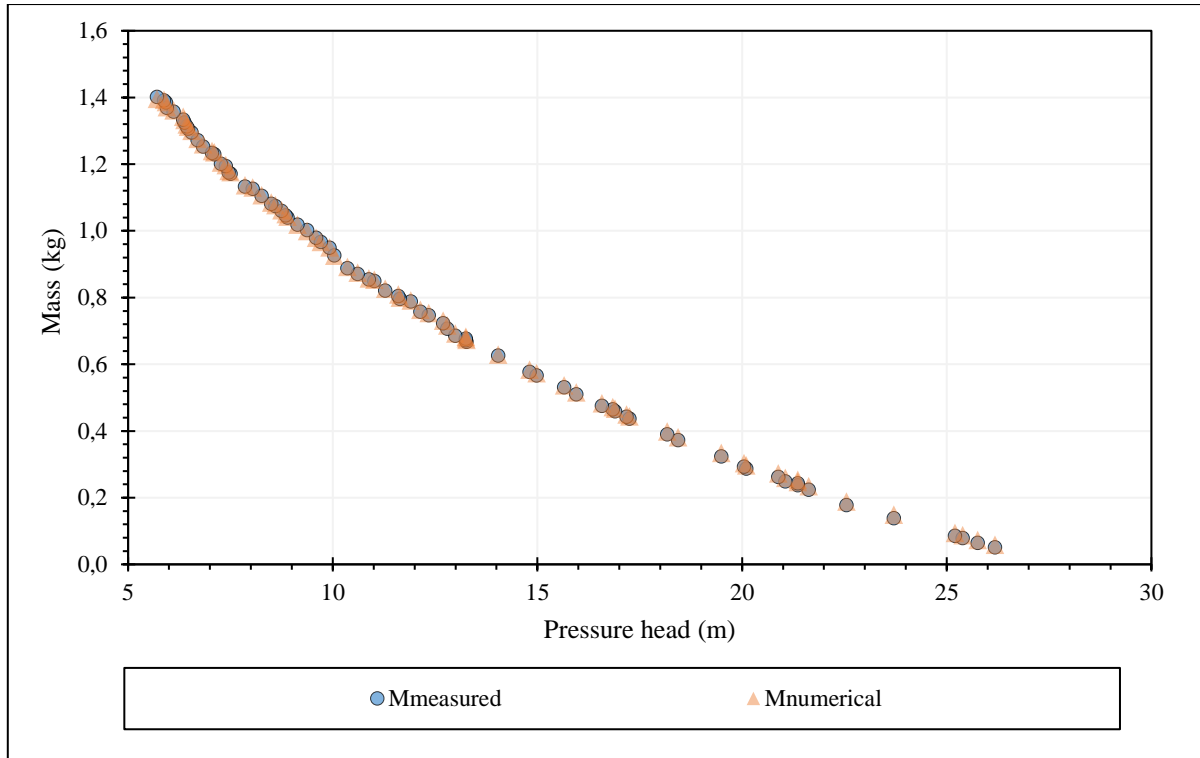


Figure 6-14: Correlation between  $m_{measured}$  and  $m_{numerical}$  against pressure head

The total absolute relative error of the measured mass and the numerical mass was determined to establish the similarity between the two mass results. The total absolute relative error was calculated to be 2.31. This error was considered sufficiently small to conclude that the model was calibrated to the experimental data, and that the model itself was mathematically sound.

Using the numerical mass, the numerical pressure was calculated using Equation 6-62. Figure 6-15 shows a plot of the measured pressure and the numerical pressure against time. The figure shows that both the measured and numerical pressures have a similar trend line.

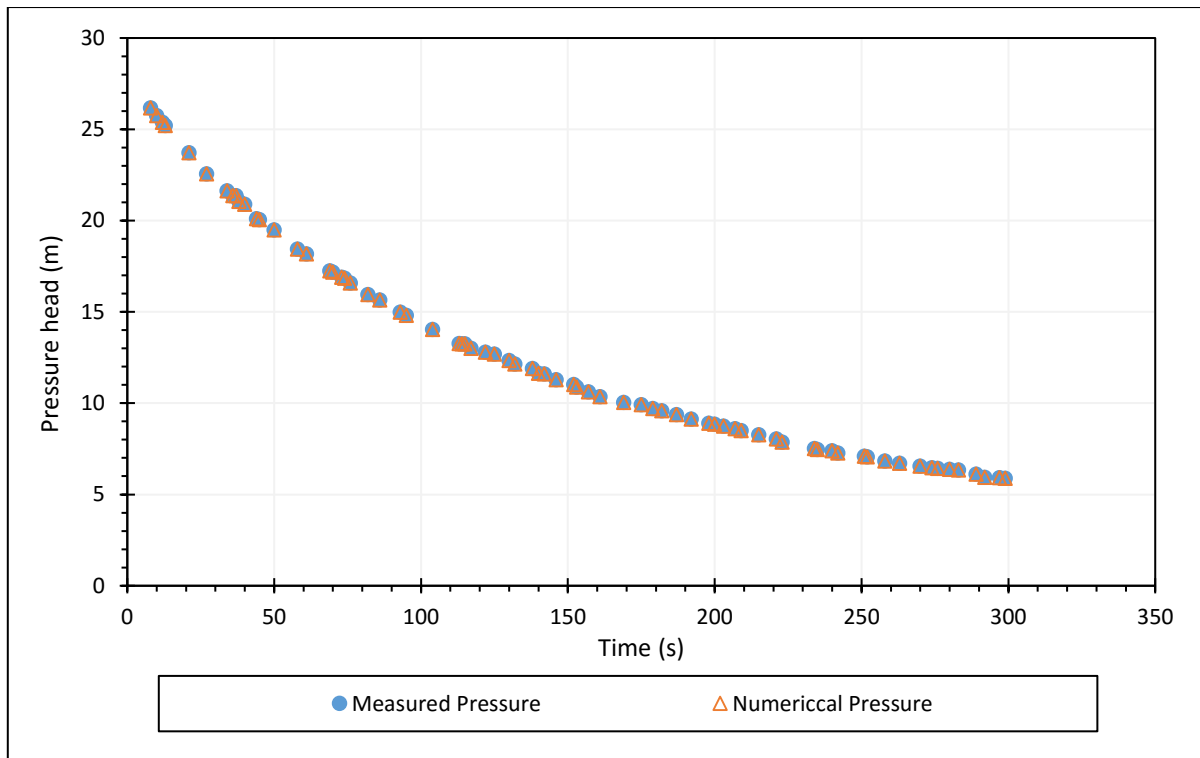


Figure 6-15: Comparison of  $h$  numerical and  $h$  measured

The total absolute relative error between the measured pressure and the numerical pressure was calculated to be  $4.7 \times 10^{-12}$ . This value was small, indicating that the calculated  $h_{numerical}$  was almost identical to the  $h_{measured}$ .

## 6.8 Field application of the pressure drop test

### 6.8.1 Introduction

The examined asbestos cement pipeline at the University of Cape Town (UCT) - hereafter referred to as the UCT test pipe - runs along the north western corner of Ring Road, as illustrated in Figure 6-16, where the blue line indicates its layout. The main characteristics of the UCT pipeline are:  $L = 160\text{m}$  (= length),  $DN200$  (= nominal diameter).

This UCT pipeline was identified in consultation with the university's maintenance team, which is tasked with managing and maintaining all pipelines within the campus area. This pipeline was selected as the most feasible option because it has the least interruptions from the supply.

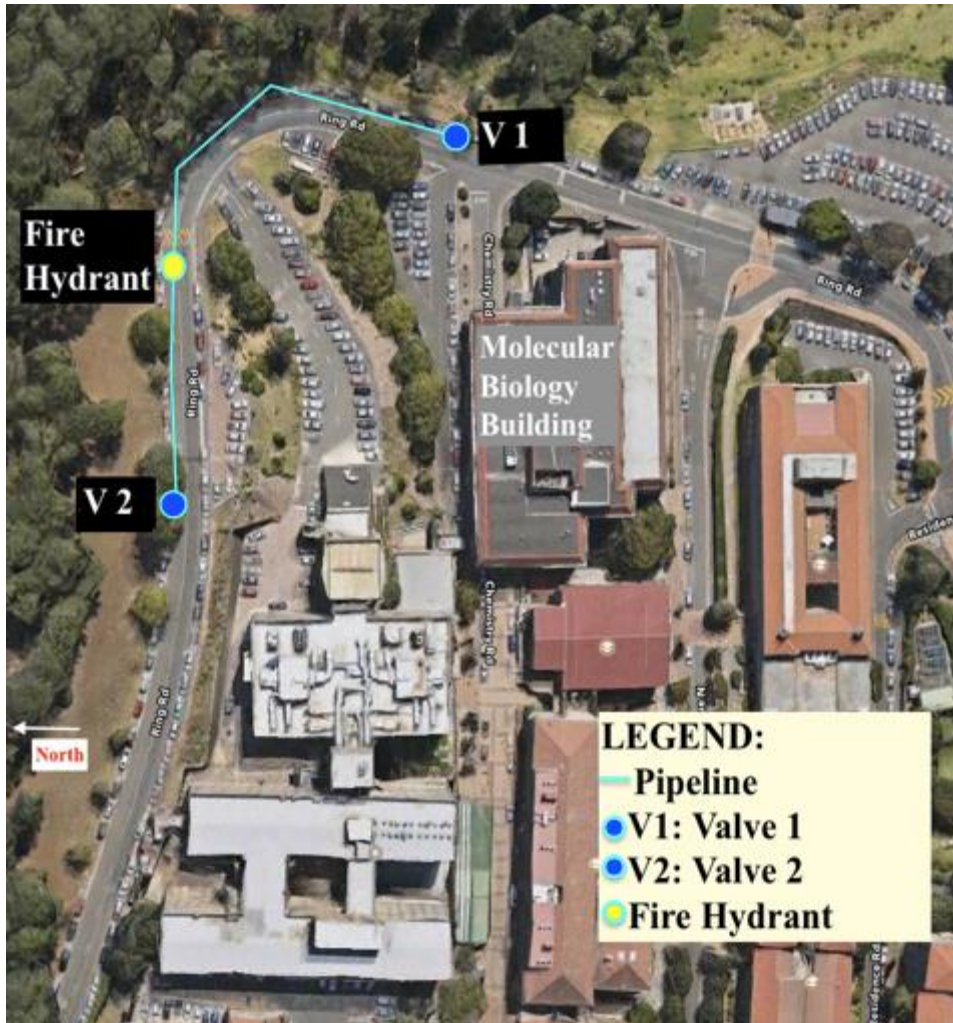


Figure 6-16: The pipeline layout at the University of Cape Town (the blue line indicates the route)

### 6.8.2 Leak test procedure

The UCT maintenance team assisted to connect the PCAE equipment to the connection point while the pipe was in operation. The connection point was an underground fire hydrant depicted in *Figure 6-17*.



*Figure 6-17: The underground fire hydrant connection*

After the hose pipe was successfully connected to the fire hydrant, the fire hydrant was briefly open to flush out any sediments in the test pipe. After the water cleared, the tank was filled with water from the test pipe. Then the hose was connected to the testing equipment so that the pressure in the pipeline could be observed.

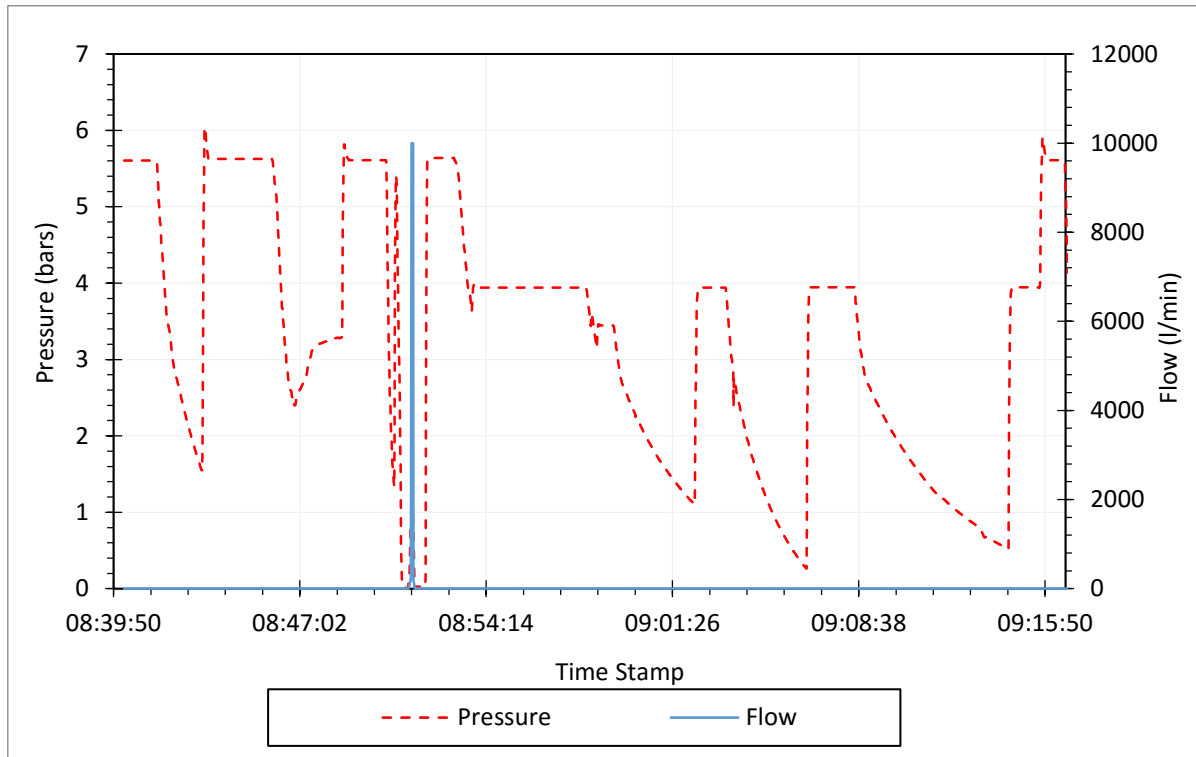
The downstream isolation valve, AV1, was then closed, thereafter the upstream isolation valve was closed as well. A pressure drop was observed but before zero pressure was reached, the pipe condition assessment equipment pump was activated. The test data are presented next.

### **6.8.3 Pressure drop test data**

*Figure 6-18* depicts the graph of the data recorded for the UCT test pipe. The graph shows that the starting pressure detected before isolation of the pipeline was 5.6 bars, approximately 56 m. The starting pressure represented the operational pressure in the test pipe. As soon as the test pipe was isolated, a sudden drop in pressure was observed. However, no flow rate was detected.

The isolation valve was opened again, and the pressure rose to about 5.6 bars - the operational pressure. The pipe was isolated again, and a drop in pressure was again observed. This was

repeated one more time and still no flow rate was detected. This result confirmed that a leak existed, resulting in the pressure drop during isolation; however, the leak on the AC pipe was too small to be measured with the testing equipment.



*Figure 6-18: The raw data output from the UCT pipeline test*

In a next step, a leak was simulated by disconnecting the hose pipe from the fire hydrant connection. This meant that the equipment pressurised water from the tank into the atmosphere via the hose pipe. As a result, a sudden large flow rate was detected and the pressure dropped significantly due to the large flow rate, as can be seen in *Figure 6-18*. This once again confirmed that the leak on the test pipeline was too small to be detected by the flow meter, i.e. less than 4 litre/min.

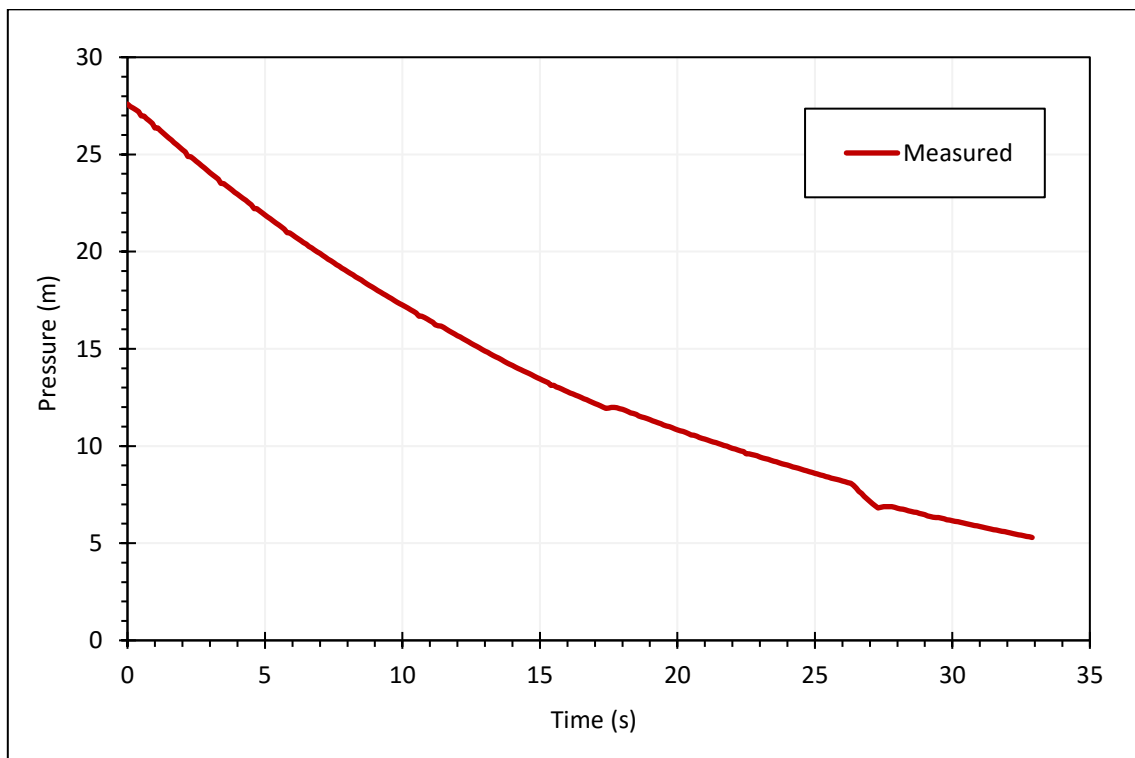
The hose pipe was then reconnected to the fire hydrant connection. The upstream isolation valve was opened again to fill the tank and ensure that the AC test pipe was full of water. The pressure in the test pipe rose to its normal operational pressure of 5.6 bars, indicating that the test pipe was fully charged. Before the upstream valve was closed, the PCAE pump was activated and set to the maximum pressure that could be supplied by the pump, which was about 4 bars. The upstream valve was then closed.

A pressure drop was observed, and when the pressure in the pipe reached 4 bars, the pump pressurised the AC test pipeline. A consistent 4 bar pressure was observed, but the flow rate was too low for the flow meter to provide a reading. The pump was then switched off and a gradual pressure drop signature was observed. The pressure drop test was repeated three times and each time the variable speed pump was set to 4 bars, thereafter the pump was switched off and a pressure drop signature was observed.

It can be observed that at the end of the test when the isolation valves were re-opened, the pressure returned to the operational pressure of about 5.6 bars.

#### 6.8.4 Analysis of the pressure drop data

The pressure-drop curves observed when the PCAE pump was switched off were analysed further. The most consistent pressure-drop curve signature with minimal disturbances and noises interrupting the pressure was chosen for analysis. *Figure 6-18* shows that the last curve on the pressure profile was the most consistent. *Figure 6-19* shows the pressure-drop curve that was chosen.



*Figure 6-19: Pressure against time data for the UCT pipeline test*

Figure 6-19 shows that the pressure in the AC test pipeline was dropping gradually with time as expected, indicating the existence of a leak. This pressure curve was analysed using the pressure drop theory developed in this chapter to assess the leakage parameters for the modified orifice equation of the leak. These leakage parameters were used to model the observed curve.

Table 6-6 shows the table with the AC test pipe properties and other constants used for the analysis:

Table 6-6: Table of constants

Constants	Value	Units
Fluid density, $\rho$	1000	kg/m <sup>3</sup>
Time, $\Delta t$	0.1	s
Pipe length, $L$	0.2	m
Nominal diameter, $D_0$	0.35	m
Gravity, $g$	9.81	m/s <sup>-2</sup>
Discharge coefficient, $C_d$	unknown	
Elastic modulus, $E$	$2.60 \times 10^7$	N/m <sup>2</sup>
Thickness, $b$	0.008	Mm
Poissons ratio, $\nu$	0.25	

The leakage parameters for the modified orifice equation were initialised as guessed values. The guessed values were 0.001mm<sup>2</sup> and 0.001mm<sup>2</sup>/m for the effective initial leak area ( $A'_0$ ) and the effective head-area slope ( $m'$ ) respectively. These values were selected because when they were inserted into the modified orifice equation at the maximum pump pressure of 40 meters, the resulting flow rate was less than the minimum flow rate detected by the flow meter.

$$Q = \sqrt{2g}(0.001h^{0.5} + 0.001h^{1.5})$$

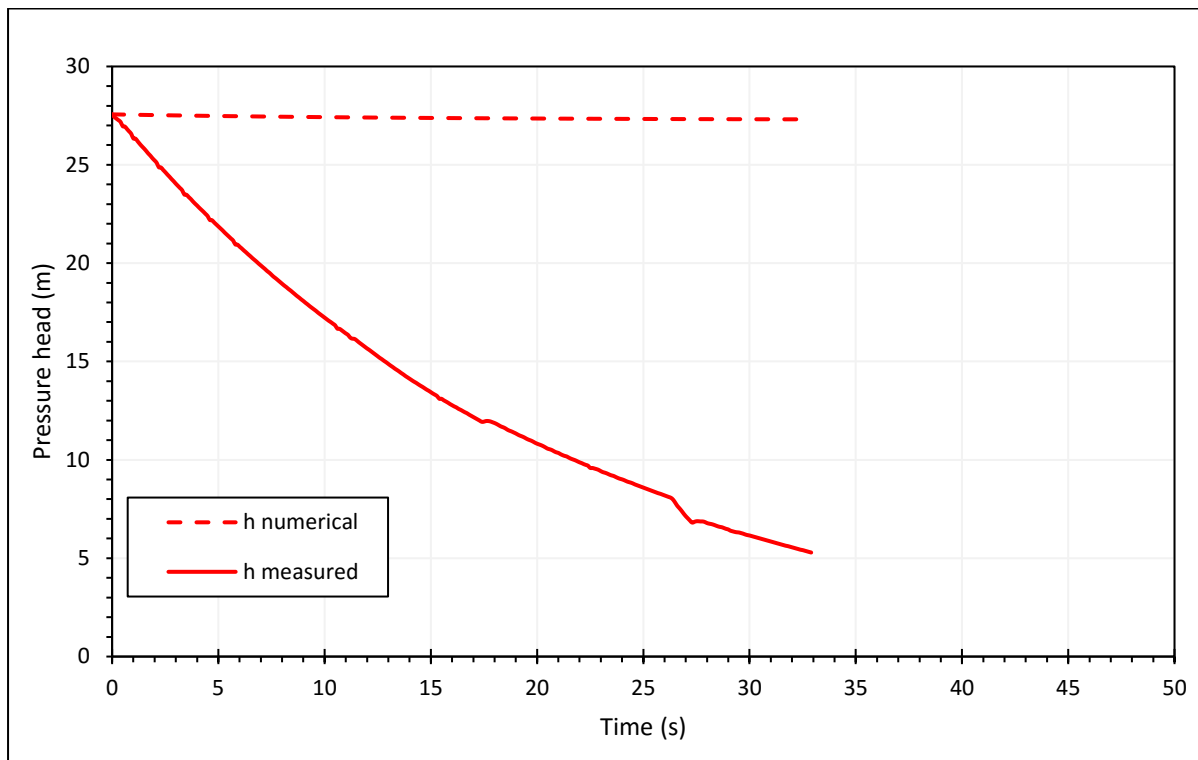
Equation 6-72

When the maximum pump pressure of 40 meters is substituted into Equation 6-72, the leakage flow rate is predicted to be about 0.71 litres per minute, which is less than the minimum detectable flow rate of the PCAE flow meter.



### 6.8.4.1 Numerical analysis

The numerical analysis used a mass balance model to determine the corresponding pressure head for the guessed leakage parameters ( $A'_0 = 0.001 \text{ mm}^2$  and  $m' = 0.001 \text{ mm}^2/\text{m}$ ). *Figure 6-20* shows a plot of the numerical pressure head against time. For purposes of comparison, the plot of the measured pressure data against time is also presented.



*Figure 6-20: Measured pressure and calculated pressure from guessed leakage parameters*

*Figure 6-20* shows that there was a large discrepancy between the numerical and measured pressure head curve. The total pressure drop for the numerical pressure was found to be 5 meters, while the total drop in pressure for the measured data was about 23 meters for the duration of the test. These findings suggest that the guessed leakage parameters did not predict the behaviour of the leak very well.

Using the optimisation solver, the objective function, describing the sum of errors between the numerical pressure and calculated pressures, was minimised by changing  $A'_0$  and  $m'$ . *Table 6-7* shows the leakage parameter results obtained after the objective function was minimised.

Table 6-7: Leakage parameters

Leakage Parameters	Value
Effective head-area slope, $m'$ ( $\text{mm}^2/\text{m}$ )	0.535
Effective initial leak area, $A'_0$ ( $\text{mm}^2$ )	5.89

The numerical pressure head for each time step was determined using the optimised leakage parameters and plotted in *Figure 6-21*. The figure shows the optimised numerical pressure head against time and the measured pressure head against time. It is evident that after the leakage parameters were optimised, there was a better correlation between the numerical pressure head and the measured pressure head.

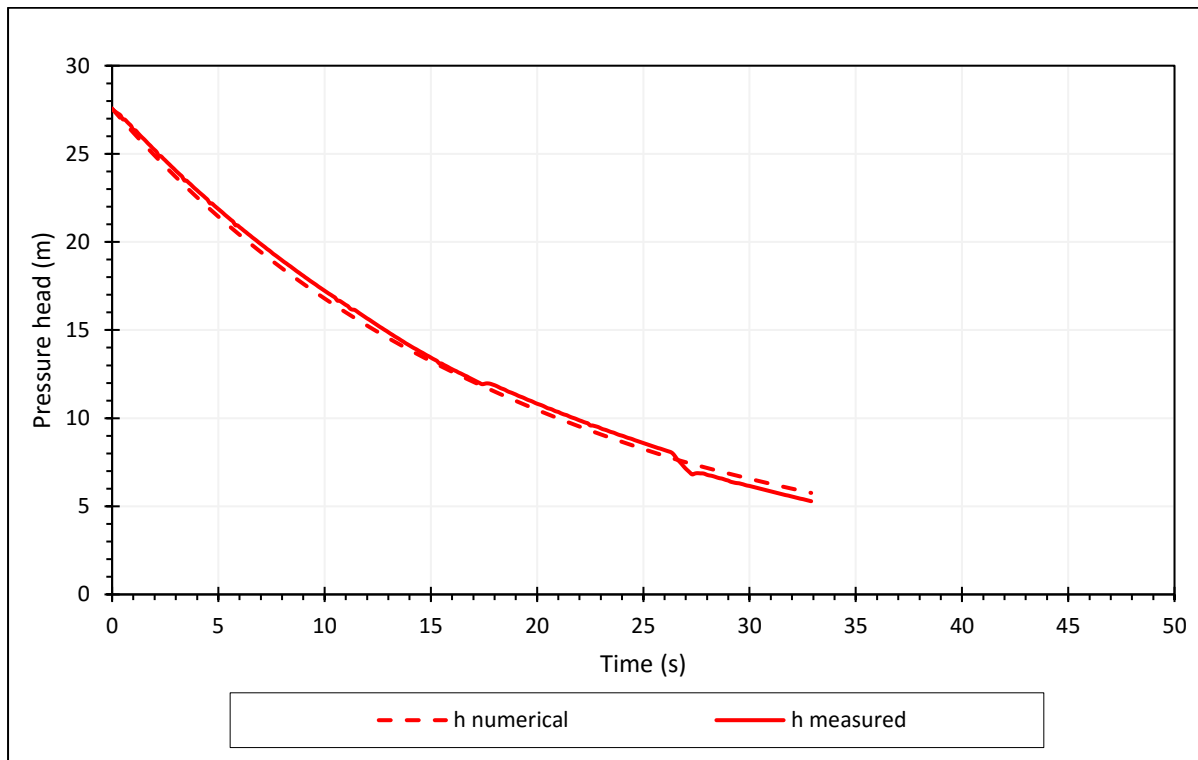


Figure 6-21: Measured pressure head and pressure calculated from the simulated leakage parameters

The sum of the absolute relative error between the measured and the numerical pressure head over the time period was calculated using the following equation:

$$\text{Relative numerical error} = \sum \frac{|h_{\text{measured}} - h_{\text{numerical}}|}{h_{\text{measured}}}$$

Equation 6-73

The total absolute error was calculated to be 10. This value could potentially be improved by using a better optimiser.

#### 6.8.4.2 Analytical solution

The analytical analysis used the derived analytical pressure-time equation, describing the relationship between the pressure head and time for an isolated pipeline with a leak. This analytical pressure-time equation is given here:

$$h(t) = \frac{A'_0}{m'} \tan^2 \left[ \frac{\sqrt{m'} \sqrt{A'_0}}{2} \left( - \left( \frac{C_d \sqrt{2g}}{\rho g V_0 \left[ \frac{d_0}{bE} \left( \frac{5}{4} - \nu \right) + \frac{1}{K} \right]} \right) t + C(m', A'_0) \right) \right]$$

The constants shown in *Table 6-6* were used to calculate the pressure. The leakage parameters for the modified orifice equation,  $A'_0$  and  $m'$ , were initialised as  $1 \times 10^{-8} \text{ mm}^2$  and  $1 \times 10^{-8} \text{ mm}^2/\text{m}$ , respectively.

*Figure 6-22* shows two pressure and time curves. The dotted curve represents the pressure head curve calculated from the derived equation using the guessed leakage parameters against time. The continuous line represents the measured pressure head against time. It is evident that there was a disparity between the two pressure head curves over time.

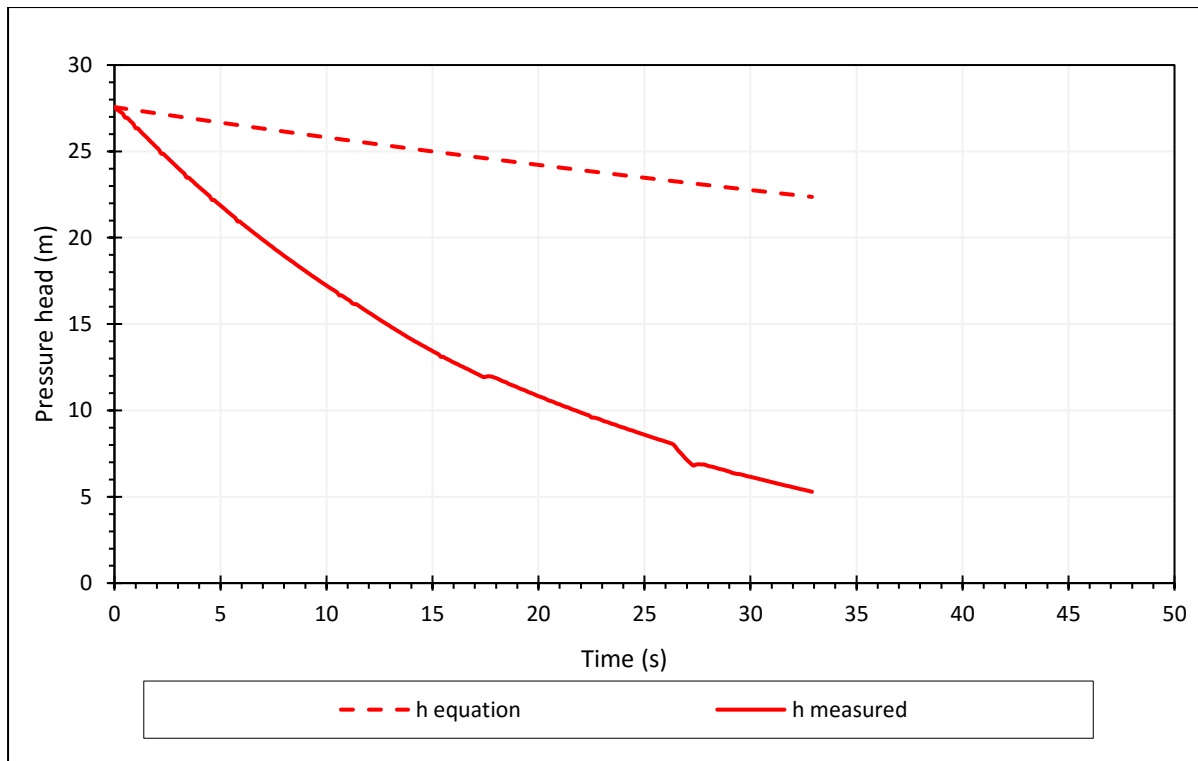


Figure 6-22: Plot of calculated pressure and measured pressured against time

In order to minimise the disparity between the two curves, the leakage parameters were optimised. Using the Microsoft Excel optimiser, the leakage parameters were optimised so as to minimise the error between the calculated pressure and the measured pressure. *Table 6-8* shows the results of the optimisation which were similar to the results of the numerical solution.

Table 6-8: Results of the leakage parameters for the analytical solution

Leakage Parameters	Value
Effective head-area slope, $m'$ ( $\text{mm}^2/\text{m}$ )	0.535
Effective initial leak area $A'_0$ ( $\text{mm}^2$ )	5.89

Using the optimised leakage parameter results, the pressure head was recalculated using the analytical pressure-time equation. *Figure 6-23* below shows the relationship between the calculated pressure head and time, using the optimised leakage parameter results, as well as the correlation between the calculated and measured pressure values.

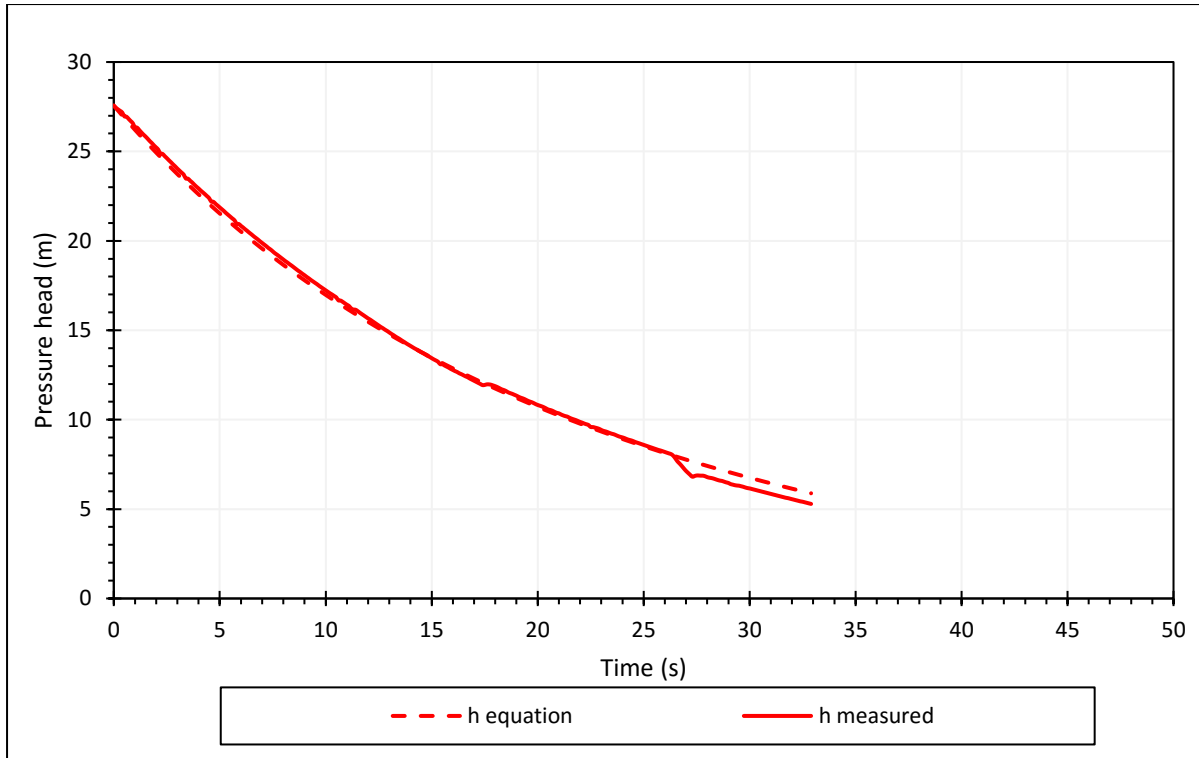


Figure 6-23: Calculated pressure head against time and measured pressure head against time

Figure 6-23 shows that the analytical pressure-time equation predicted the measured pressures reasonably well when the optimised leakage parameters were used. It can be noted that after 26s there is a slight lack of similarity. This anomaly could occur as a result of a temporary external noise that influenced the reading measurement. Mostly, however, the curve obtained from the equation predicts a similar trajectory to the measured curve.

The absolute relative error between the optimised calculated pressure and the measured pressure was calculated using the following equation:

$$Relative\ analytical\ error = \sum \frac{|h_{measured} - h_{equation}|}{h_{equation}}$$

Equation 6-74

The absolute relative error was calculated to be 8. This was a lower value compared to the value obtained for the numerical analysis, suggesting that the analytical solution provided a better correlation to the measured pressure curve.

### 6.8.5 Leakage characterisation

Since the obtained leakage parameters predicted the leak behaviour, these parameters were used to characterise the leakage in the pipeline. The obtained leakage parameters were consistent with a small longitudinal crack. According to Greyvenstein & van Zyl (2005), longitudinal crack failure is common in AC pipelines and could potentially be indicative of the beginning of a leak near a seal that will propagate further with time.

The ratio of the effective head area slope to the effective initial leak area, multiplied by the pressure head, gives the leakage number,  $L_N$ . The leakage number ( $L_N$ ) for the AC test pipe can therefore be obtained as follows:

$$L_N = \frac{m'h}{A'_0} = \frac{0.535}{5.89} h = 0.09h_{average}$$

*Equation 6-75*

If the pressure in the pipeline is known, then the leakage number can be obtained using *Equation 6-75*. Cassa and Zyl's (2014) equation that links the leakage number and the  $N1$  can be used to obtain the  $N1$  leakage exponent for the pipeline as follows:

$$N1 = \frac{1.5 L_N + 0.5}{L_N + 1} = \frac{1.5 (0.09h) + 0.5}{0.09h + 1}$$

*Equation 6-76*

## 6.9 Conclusion

In this chapter a novel mathematical model was derived to describe the dynamic pressure drop behaviour. The pressure drop behaviour occurs when an isolated pipe has a leak and the pressure in the pipe drops with time due to the water leaving the pipe.

The leakage characteristics of the pipe are estimated from the pressure vs time data. If the pressure remains constant, the pipe is without a leak. If the pressure drops, the mathematical model was fitted to the pressure vs time curve, using the known pipe properties, to determine the leakage parameters for the modified orifice equation ( $A_0$  and  $m$ ).

An experimental setup designed by Taylor (2018) was assembled to test the mathematical model. The setup consisted of the pipe sample, end sections to isolate the sample, a connection pipe to the water distribution network that can be controlled with a shut-off valve, and the appropriate measuring equipment. A uPVC pipe with a 1mm round hole leak was tested.

The test pipe was pressurised by allowing water to enter the pipe from the water distribution systems. Once the desired pressure was reached, the valve was closed and the pressure monitored while water escaped the leak. During this time, the mass of the outflowing water was measured. The values were recorded as a continuous stream of data captured by a video recording device. The film of each set of mass readings was then edited using software, allowing for the stream to be slowed and for the individual measurements to be manually recorded.

The data was then processed and analysed to determine the relevant relationships between the flow rate, pressure head and leak area. The experimental data was compared to theoretical values calculated using the equations proposed by the mathematical model. A method was employed to calibrate the theoretical models to the experimental data in an attempt to verify the adequacy and accuracy of the models.

The dynamic pressure drop test was also carried out in the field. Using the derived mathematical model, the leakage characteristic of the pipe was determined from the pressure and time data obtained using the PCAE.

# **7 Assessing water losses in bulk pipelines**

## **7.1 Introduction**

Performance indicators are measurements of the efficiency and effectiveness of the water utility with regards to specific aspects of the system's behaviour (IPART, 2018). When water losses are assessed in water distribution systems, various suitable performance indicators are available which take into account relevant network parameters. However, thus far there is no clear consensus as to the best performance indicator (Koelbl & Zipperer, 2018).

Past experiences and research show that water utilities often assess water losses on transmission mains in percentages of the system input volume. However, this indicator fails to take account any of the main local influences and is subsequently not considered to be an appropriate performance indicators for comparing transmission mains (Farley, 2003).

For real losses in distribution systems, a number of technical performance indicators have been developed (Farley, 2001), namely: Current Annual Real Losses (CARL), Unavoidable Annual Real Losses (UARL), and Infrastructure Leakage Index (ILI). These indicators are based on a statistical analysis of international data which include 27 diverse water supply systems in 19 countries. Such data sets do not exist for transmission mains.

This chapter aims to explore potential performance indicators for assessing water losses on bulk pipelines. The performance indicators are used to evaluate each bulk pipeline that was tested in the field, using the PCAE, and the performance indicator results are then compared. The chapter then elaborates on the challenges in comparing water losses of different bulk systems. In this chapter, the terms 'transmission mains' and 'bulk water pipelines' are used interchangeably.

## **7.2 Characteristics of non-revenue water (NRW)**

### **7.2.1 Introduction**

This section outlines some of the challenges encountered when volumes of real losses and apparent losses in bulk pipelines are assessed. The standard methodology for assessing these



losses is by conducting a water audit and evaluating the components of non-revenue water (NRW). The characteristics of NRW for bulk pipeline are explored.

### 7.2.2 Water balance

Table 7-1 shows the best practice water balance as published by the International Water Association (IWA). The IWA water balance is used as a standard methodology for identifying components that make up the total demand for water at the input of a water supply system. A key problem with the water balance is that most of the subcomponents of the water balance are not readily quantifiable (Bruinette & Claasens, 2016).

Table 7-1: IWA water balance (Farley, 2001)

System Input Volume	Authorised Consumption	Billed Authorised Consumption	Billed Metered Consumption	Revenue Water
			Billed Unmetered Consumption	
		Unbilled Authorised Consumption	Unbilled Metered Consumption	Non-Revenue Water
			Unbilled Unmetered Consumption	
	Water Losses	Apparent Losses	Unauthorised Consumption	
			Metering Inaccuracies and Data Handling Errors	
		Real Losses	Leakage on Raw Water Mains and Treatment Plants (if applicable)	
			Leakage on Transmission and/or Distribution Mains	
	Leakage and Overflows at Transmission and/or Distribution Storage Tanks			
			Leakage on Service Connections up to the Measurement Point	

The components of NRW for both transmission and distribution networks are also evaluated from the water balance. It is important to note that for transmission mains, the System Input Volume (SIV) is significantly greater than the NRW. Therefore, small metering inaccuracies in the SIV can lead to large error margins in NRW components.

The NRW components for transmission mains include: unbilled authorised consumption, apparent losses, and real losses. According to a study by Koelbl & Zipperer (2018), the characteristics of the NRW components on transmission mains vary between developed and developing countries.

In developed countries, unbilled authorised consumption is a small component of the NRW, while real and apparent losses are the largest components of NRW on transmission mains. Real losses occur during bursts, which typically have a short run-time as they are quickly detected and repaired. The apparent losses for developed countries mainly comprise of metering inaccuracies.

In developing countries, real and apparent losses on transmission mains are more extensive when compared to developed countries, and characteristics of the components are different. In developing countries, leaks that are difficult to repair can have run times of several years. Furthermore, apparent metering inaccuracies are also higher and illegal consumption at all kinds of accessible points is not uncommon, thus making apparent losses higher compared to those in developed countries.

In this study, only the real loss components of the NRW were evaluated to assess water losses on the transmission pipes that were tested, using the PCAE . The unbilled authorised consumption and apparent losses of the tested pipes were ignored due to lack of data.

### **7.2.3 Challenges in bulk water systems**

The preferred performance indicator for distribution systems is a non-dimensional index called the Infrastructure Leakage Index (ILI). This index is evaluated as the ratio of the actual current annual real losses (CARL) to the unavoidable annual real losses (UARL):

$$ILI = \frac{CARL}{UARL}$$

*Equation 7-1*

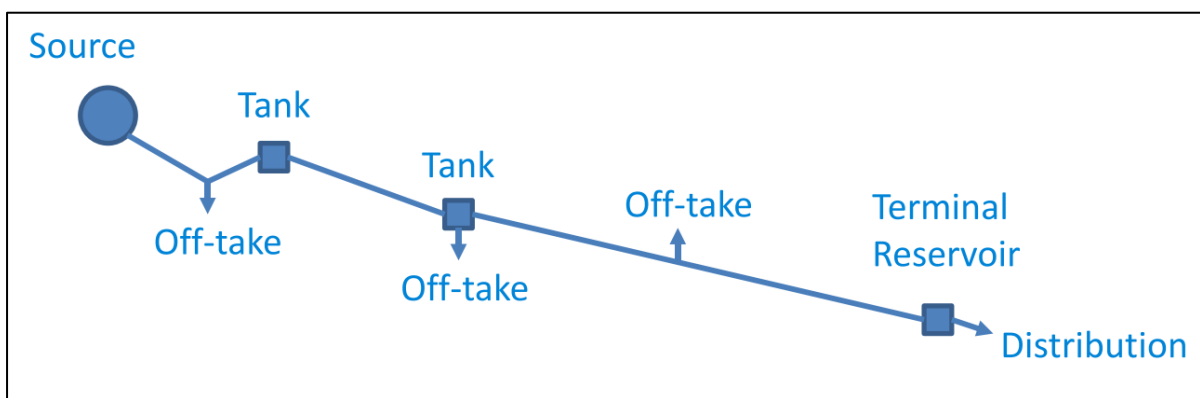
The ILI is based on a reference value, i.e. unavoidable annual real losses (UARL), which originates from a data set of numerous distribution networks with diverse pipe materials and diameters. The UARL of a network can be obtained using the following expression:

$$UARL (m^3/year) = (6.57 \times L_M + 0.256 \times N_c + 9.13 \times L_T) \times P$$

*Equation 7-2*

The UARL can be used to compare losses from different distribution pipes. However, for transmission pipes, the UARL is seen as an unsuitable reference for comparing the losses on bulk pipes, for the following reasons:

- Unlike distribution pipes, transmission pipes have homogeneous material and diameters, with little variations along the pipeline corridor. It is, for example, meaningless to compare water losses of a 1000mm reinforced concrete pipe with those of a 500mm cast iron pipe.
- Typically, transmission pipes will have very limited number of offtakes, as shown in *Figure 7-1*.
- Each transmission system has its own characteristic regarding pipe material, couplings and diameters.



*Figure 7-1: Illustrating a typical transmission main network*

There are currently no guidelines that provide suitable concepts for standardised assessments of losses on transmission pipes.

## **7.3 Performance indicators for transmission mains**

### **7.3.1 Introduction**

Several technical performance indicators are considered to analyse and compare the level of water loss among the bulk pipelines that were tested using the PCAE. First, the total real losses are evaluated for all the tested bulk pipes using the modified orifice equation. Thereafter, the real losses per mains length are evaluated to assess the variation of real losses per unit length of tested pipe. This is followed by the real losses per lateral surface area, and finally a dimensionless indicator of the effective initial leak area per lateral surface is considered.

### 7.3.2 Total real losses in bulk pipelines

The real (physical) losses referred to here are only the losses obtained from the condition assessment tests carried out on the pipelines using the PCAE. These losses were predominantly leakage and comprise of the physical losses from the test pipe as well as from joints and fittings on the test pipe. Overflows from service reservoirs are not included in the analysis because these were not detected or measured during testing.

In Chapter 5, the leakage parameters for the modified orifice equation, i.e. the effective initial leak area ( $C_d A_0$ ) and the effective head-area slope ( $C_d m$ ), were obtained from the pressure-leakage response of leaks on the tested bulk pipeline. A model predicting leakage flows from the pipelines was obtained using the modified orifice equation theory. The modified orifice equation model is given here and expressed in cubic meters per annum:

$$Q_{(leakage)} = \sqrt{2g}[(C_d A_0)h^{0.5} + (C_d m)h^{1.5}] \frac{m^3}{s} \times \frac{60s}{1 \text{ min}} \times \frac{60 \text{ mins}}{1 \text{ hr}} \times \frac{24 \text{ hrs}}{1 \text{ day}} \times \frac{365 \text{ days}}{1 \text{ year}}$$

*Equation 7-3*

According to the model, if the leakage parameters ( $C_d A_0$  and  $C_d m$ ) are known, then the leakage rate (total real losses) from the test pipeline can be determined at different operating pressures,  $h$ . For the analysis, an average operating pressure of 50 meters was assumed to determine the total leakage in the pipeline.

### 7.3.3 Real losses per mains length

In water distribution systems, real losses are either expressed to the number of service connections of the supply system or over the length of pipe. Given that leakage component analyses across the world have conveyed that the largest proportion of physical losses occurs at service connections, the denominator with the best range of applicability for real losses on distribution pipes is the number of service connections.

Because bulk pipes have fewer service connection or off-takes, it is unsuitable to express real losses to the number of service connections when assessing real losses. Subsequently, for bulk pipelines it is more suitable to express real losses to the mains length (Alegre et al, 2017). The real losses per mains length can be evaluated using the following expression:

$$\text{Real loss per mains length (m}^3\text{/annum/m)} = \frac{\text{Real losses (m}^3\text{/annum)}}{\text{Mains length (m)}} = \frac{Q_{leakage}}{L}$$

*Equation 7-4*

For the analysis described in this chapter, the real loss obtained for each pipeline,  $Q_{leakage}$ , is divided by the length of the pipeline. The length of pipe spanned the two isolation valves that were used to isolate and test the pipeline, using the PCAE. Any off-takes between the two valves isolating the bulk pipe are not considered in the analysis. It is assumed that they will not have a significant contribution to the physical losses as there were very few.

### 7.3.4 Real losses per lateral surface

The level of water loss on pipelines is affected by various important factors such as the length of mains, the pipe diameters and the network structure. Compared to distribution systems, transmission networks typically consist of longer pipelines that are larger in diameter (Koelbl & Zipperer, 2018). Therefore only the mains length and embedded diameters are considered here

In order to express water losses to the length of mains as well as the pipe diameter, the lateral surface area of the mains was considered as a denominator. The lateral surface area of the pipe can be expressed mathematically as the circumference multiplied by the length of pipe:

$$\text{Lateral surface} = C \times L = \pi \times D \times L$$

*Equation 7-5*

Where  $C$  is the circumference,  $L$  is the length of pipe, and  $D$  is the pipe diameter. The real losses per lateral surface can therefore be evaluated using the following expression:

$$\text{Real losses per lateral surface} = \frac{\text{Real losses}}{\text{Lateral surface}} = \frac{Q_{leakage}}{\pi \times D \times L}$$

*Equation 7-6*

The length indicator for real losses per mains only uses a longitudinal denominator. In contrast, this indicator provides some advantages for transmission systems because the real losses per lateral surface also incorporates a radial dimension given by the diameter, another important dimension of the pipe.

### 7.3.5 Effective initial leakage area per lateral surface

The power equation model and the modified orifice equation model are used as pressure-leakage models to predict the leakage behaviour of a pipe network or sections of pipe network. The power equation is used to determine the leakage parameters  $N1$  and  $C$ . The modified orifice equation is used to determine the leakage parameters  $A'_0$  and  $m'$ .

For this performance indicator the initial leakage area ( $A'_0$ ) is required. The initial leakage area represents the sum of all the areas of individual leaks on the pipe under zero pressure conditions.

Each pipeline that was tested using the PCAE was found to have some leakage. The leakage was analysed using the power equation and the modified orifice equation to determine the leak characteristics. Since the exact location of the leak on the test pipe was not known, the analysis was carried out at different nodes located on the test pipe. The nodes represented critical points on the pipe, namely the start point, end point, lowest point, highest point and intermediate point.

The leakage characteristics of each node on the pipeline were obtained. Based on the results, the node with the most realistic leakage parameters ( $N1, C, A'_0, m'$ ) was selected as the representative node. In other words, the leakage parameters of the representative node represented the leakage parameters of the entire test pipe.

In cases where more than one node on a test pipe showed realistic results, the leakage parameter results from all the nodes were averaged to get a mean value. *Equation 7-7* to *Equation 7-10* present the equations used to calculate the averaged leakage parameters, starting with the averaged leakage exponent,  $N1_{averaged}$ , followed by the leakage coefficient,  $C_{averaged}$ , then the effective initial leak area,  $A'_{0\ averaged}$ , and finally the effective head area slope,  $m'_{averaged}$ . Where  $n$  is the number of nodes.

$$N1_{averaged} = \frac{N1_{node\ 1} + N1_{node\ 2} + N1_{node\ 3} + \dots \dots + N1_{node\ n-1} + N1_{node\ n}}{n}$$

*Equation 7-7*

$$C_{averaged} = \frac{C_{node\ 1} + C_{node\ 2} + C_{node\ 3} + \dots \dots + C_{node\ n-1} + C_{node\ n}}{n}$$

*Equation 7-8*

$$A'_{0 \text{ average}} = \frac{A'_{0 \text{ node } 1} + A'_{0 \text{ node } 2} + A'_{0 \text{ node } 3} + \dots + A'_{0 \text{ node } n-1} + A'_{0 \text{ node } n}}{n}$$

*Equation 7-9*

$$m'_{\text{average}} = \frac{m'_{\text{node } 1} + m'_{\text{node } 2} + m'_{\text{node } 3} + \dots + m'_{\text{node } n-1} + m'_{\text{node } n}}{n}$$

*Equation 7-10*

The performance indicator of the effective initial leak area per lateral surface is a non-dimensional indicator which can be evaluated as follows:

$$\text{Leakage area per lateral surface} = \frac{\text{initial leakage area}}{\text{lateral surface}} = \frac{A'_{0 \text{ average}}}{\pi DL}$$

Where  $A'_0$  is the initial leakage area,  $D$  is the pipe diameter, and  $L$  is the pipe length. The results of this indicator give the ratio of the size of leakage area to the total surface area of the pipe. The ratios can be used to assess and compare the size of total leakage area in a bulk pipeline relative to the surface area of the pipeline.

An advantage of this indicator is that it does not require system pressure.

## **7.4 Results of data analyses from performance indicators**

### **7.4.1 Introduction**

In this section, the results obtained from the data analysis of the indicators described in Section 7.3 are discussed for the tested bulk pipelines. The indicators are used to compare the extent of real losses of the tested pipelines.

First, the results of the total real losses, based on a base point operating pressure of 50 meters, are obtained and compared. Thereafter, the results obtained for the real losses per mains length indicator are compared. And finally, the results obtained for the real losses per lateral surface indicator are compared.

## 7.4.2 Total real losses

The total real losses evaluated are the total volume of water lost through leakage per year for each pipe. Using the modified orifice equation model, the leakage flow rate was calculated at an average pressure of 50 meters for all pipelines. *Table 7-2* shows a summary of the results for real losses per annum for each pipeline that was tested.

*Table 7-2: Results of real losses calculated from the modified orifice equation*

Pipeline	Average System Pressure (m)	A <sub>0</sub> ' (mm <sup>2</sup> )	m' (mm <sup>2</sup> /m)	Real Losses (m <sup>3</sup> /s)	Real Losses (m <sup>3</sup> /annum)
Wingfield Test 1	50	12	3.4	5.7 x 10 <sup>-3</sup>	1.8 x 10 <sup>5</sup>
BS 8 Pipeline Test 1	50	8.5	3.2 x 10 <sup>-3</sup>	2.7 x 10 <sup>-4</sup>	8.6 x 10 <sup>3</sup>
BS 8 Pipeline Test 2	50	30	0.51	1.7 x 10 <sup>-3</sup>	5.4 x 10 <sup>4</sup>
UCT Pipeline	50	4.9	0.51	9.5 x 10 <sup>-4</sup>	3,0 x 10 <sup>4</sup>
Lynnwood to Koedoesnek	50	23	0.13	9.2 x 10 <sup>-4</sup>	2.9 x 10 <sup>4</sup>
Garsfontein to Parkmore High Level Reservoir	50	18	0.10	7.1 x 10 <sup>-4</sup>	2.2 x 10 <sup>4</sup>
Klapperkop to Carina Street Pipeline	50	140	3.1	9.2 x 10 <sup>-3</sup>	2.9 x 10 <sup>5</sup>
Line to Florauna High Level Reservoir	50	40	0.9	2.7 x 10 <sup>-3</sup>	8.6 x 10 <sup>4</sup>

The results of the real losses per annum in *Table 7-2* are presented graphically by *Figure 7-2*. It is evident that the Klapperkop to Carina Street pipeline had the highest real losses per annum when compared to the other pipelines. The Klapperkop to Carina Street pipeline was found to have a longitudinal crack with an effective initial leak area of 137.66mm<sup>2</sup>, which was the largest effective initial leak areas among all the tested pipes.



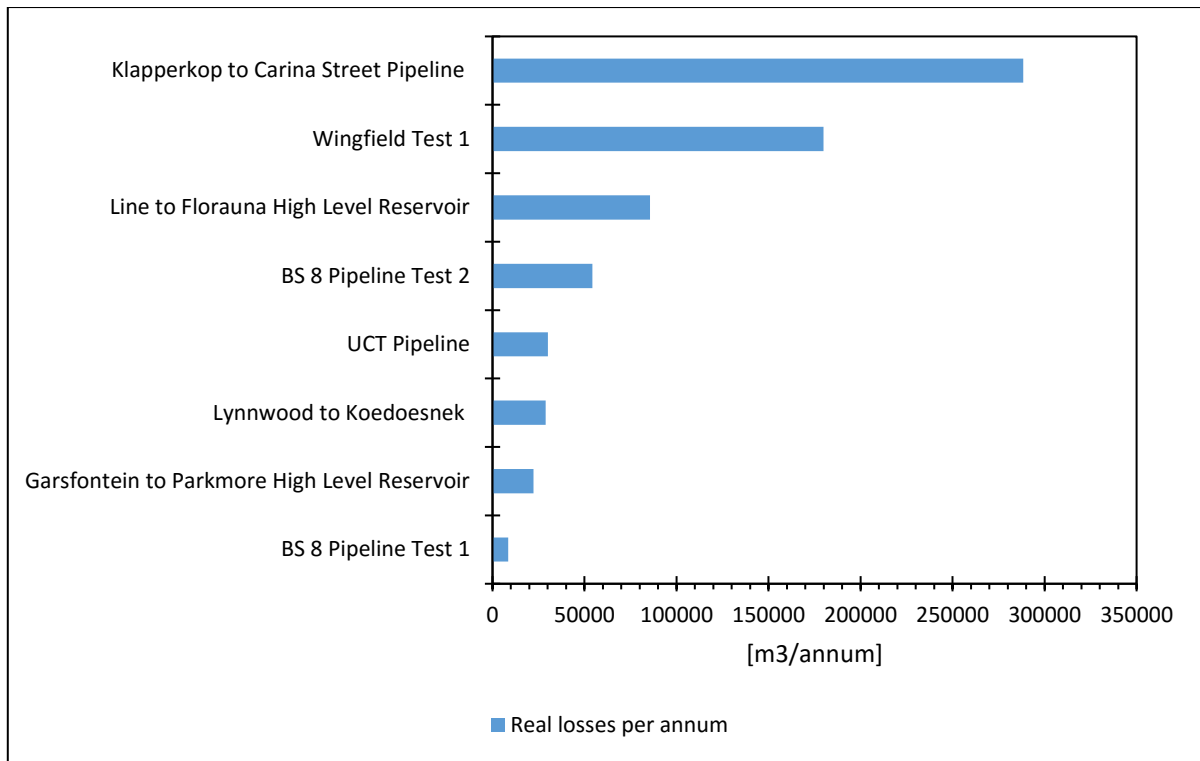


Figure 7-2: Real losses per annum for the tested pipelines

The BS 8 pipeline Test 1 had the lowest real losses per annum and was found to have round hole leaks. This is evident from the small head-area slope of  $0.0032\text{mm}^2/\text{m}$  which indicates round holes. The small head-area slope, coupled with a small effective initial leakage area of less than  $10\text{mm}^2$ , meant that the total flow leakage flow rate would not be as high as that of the other pipelines presented in the figure.

This indicator can be suitable for internal monitoring and comparison of water losses from one reference period to the next.

### 7.4.3 Real losses per mains length

The denominator of this indicator considers the mains length. *Table 7-3* shows the reference values from the German Water Loss Guidelines (DVGW-Guideline W 392, 2003) that were used as an evaluation scheme for pipe networks with fewer than 20 service connections per km.

Table 7-3: Water loss reference values

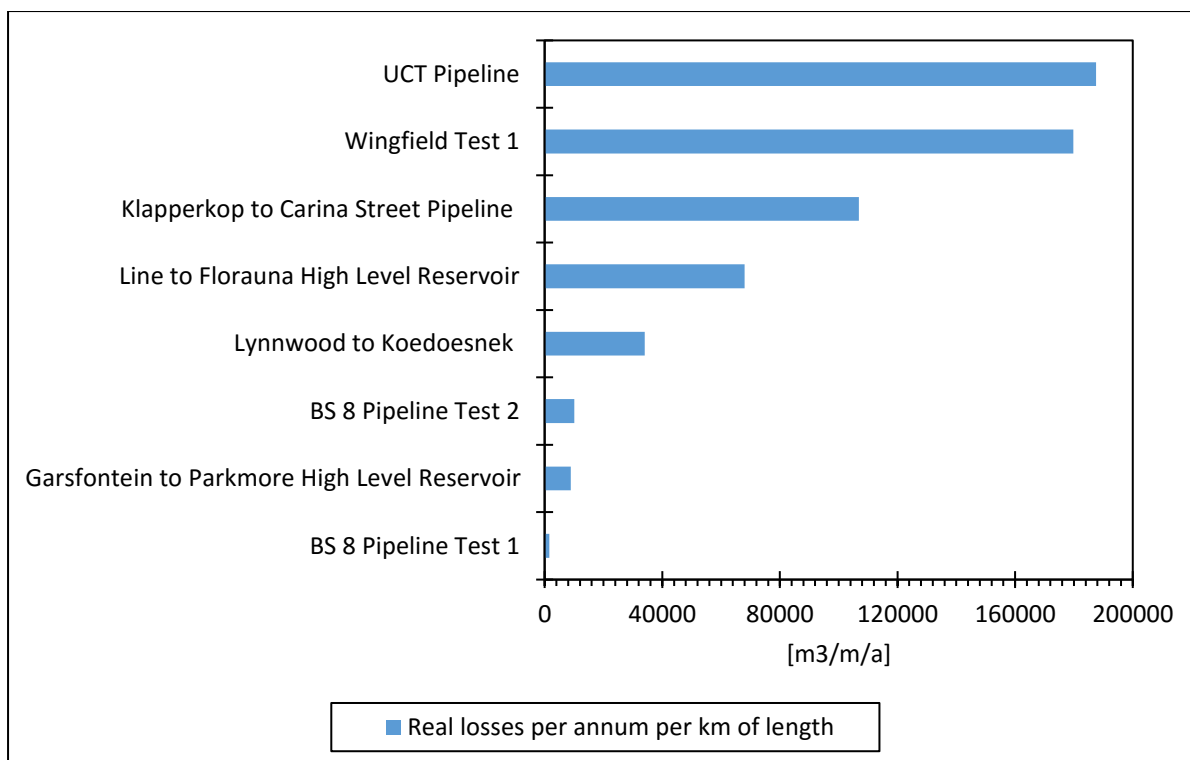
Levels of leakage	m <sup>3</sup> /km/h	m <sup>3</sup> /km/annum
Low	<0.05	<438
Medium	0.05-0.10	438 - 876
High	>0.10	>876

Although the German guidelines were updated in 2017 (DVGW- Guideline W 392, 2017) and the reference values given in *Table 7-3* are no longer included, it was considered interesting to compare them to the calculated values of real losses per mains length of the tested pipelines as shown in *Table 7-4*. However, it is important to note that the evaluation scheme was developed from distribution systems and was not meant to evaluate bulk pipelines. Nonetheless, the few off takes in bulk pipelines provides some synergy to the bulk pipeline characteristic.

Table 7-4: Results of the real losses per mains length

Pipeline	Real Losses (m <sup>3</sup> /annum)	Length (km)	m <sup>3</sup> /annum/m	m <sup>3</sup> /annum/km
Wingfield Test 1	1.8 x 10 <sup>5</sup>	1	180	1.8 x 10 <sup>5</sup>
BS 8 Pipeline Test 1	8.6 x 10 <sup>3</sup>	5.4	1.6	1.6 x 10 <sup>3</sup>
BS 8 Pipeline Test 2	5.4 x 10 <sup>4</sup>	5.4	10	1.0 x 10 <sup>4</sup>
UCT Pipeline	3.0 x 10 <sup>4</sup>	0.16	188	1.9 x 10 <sup>5</sup>
Lynnwood to Koedoesnek	2.9 x 10 <sup>4</sup>	0.85	34	3.4 x 10 <sup>4</sup>
Garsfontein to Parkmore High Level Reservoir	2.2 x 10 <sup>4</sup>	2.5	8.9	8.9 x 10 <sup>3</sup>
Klapperkop to Carina Street Pipeline	2.9 x 10 <sup>5</sup>	2.7	107	1.1 x 10 <sup>5</sup>
Line to Florauna High Level Reservoir	8.6 x 10 <sup>4</sup>	1.26	68	6.8 x 10 <sup>4</sup>

The calculated results of the real losses per mains length in *Table 7-4* are presented graphically in *Figure 7-3* for easier interpretation. Based on the reference values from the German Water Loss Guidelines presented in *Table 7-3* it is evident that all the pipelines in *Table 7-4* would fall within the category of high water losses.



*Figure 7-3: Real losses per mains length*

Interestingly, when the results in *Figure 7-3* are compared to those in *Figure 7-2*, it can be observed that the order of the pipelines has changed. Now the UCT pipeline was found to show the highest losses. Since the denominator is the length of mains, pipes with longer lengths are favoured. The UCT pipeline had the shortest length and hence is not favoured by this indicator.

The real losses per mains length indicator can be suitable when carrying out internal monitoring of water losses from one reference period to the next. However, it may not be a meaningful indicator when bulk pipelines are being compared, because other structural parameters such as diameters, materials and pressures are entirely different.

#### **7.4.4 Real losses per lateral surface**

The real losses per lateral surface indicator considers the mains length but at the same time also combines it with the pipe diameter to the unit area. This indicator was first proposed by Koelbl, Networks & Town (2018), but they did not find any evidence in their literature search that such an indicator was used to evaluate water losses. They could therefore not draw on documented evidence.

This indicator was used to evaluate and compare water losses on the pipelines that were tested using the PCAE . *Table 7-5* gives a summary of the calculated real losses per lateral surface and also shows the length and diameters of the various pipelines.

*Table 7-5: Results of real losses per lateral surface*

Pipeline	Real Losses (m <sup>3</sup> /annum)	Length (m)	Equivalent Diameter (mm)	Lateral Surface (m <sup>2</sup> )	Real losses/ lateral surface
Wingfield Test 1	1.8 x 10 <sup>5</sup>	1000	300	948	190
BS 8 Pipeline Test 1	8.6 x 10 <sup>3</sup>	5401	55	937	9.2
BS 8 Pipeline Test 2	5.4 x 10 <sup>4</sup>	5401	55	937	58
UCT Pipeline	3.0 x 10 <sup>4</sup>	160	300	151	199
Lynnwood to Koedoesnek	2.9 x 10 <sup>4</sup>	850	500	1335	22
Garsfontein to Parkmore High Level Reservoir	2.2 x 10 <sup>4</sup>	2500	500	3927	5.6
Klapperkop to Carina Street Pipeline	2.9 x 10 <sup>5</sup>	2700	406	3444	84
Line to Florauna High Level Reservoir	8.6 x 10 <sup>4</sup>	1260	300	1188	72

The calculated results of the real losses per lateral surface in *Table 7-5* are presented graphically in Figure 7-4 for easier interpretation.

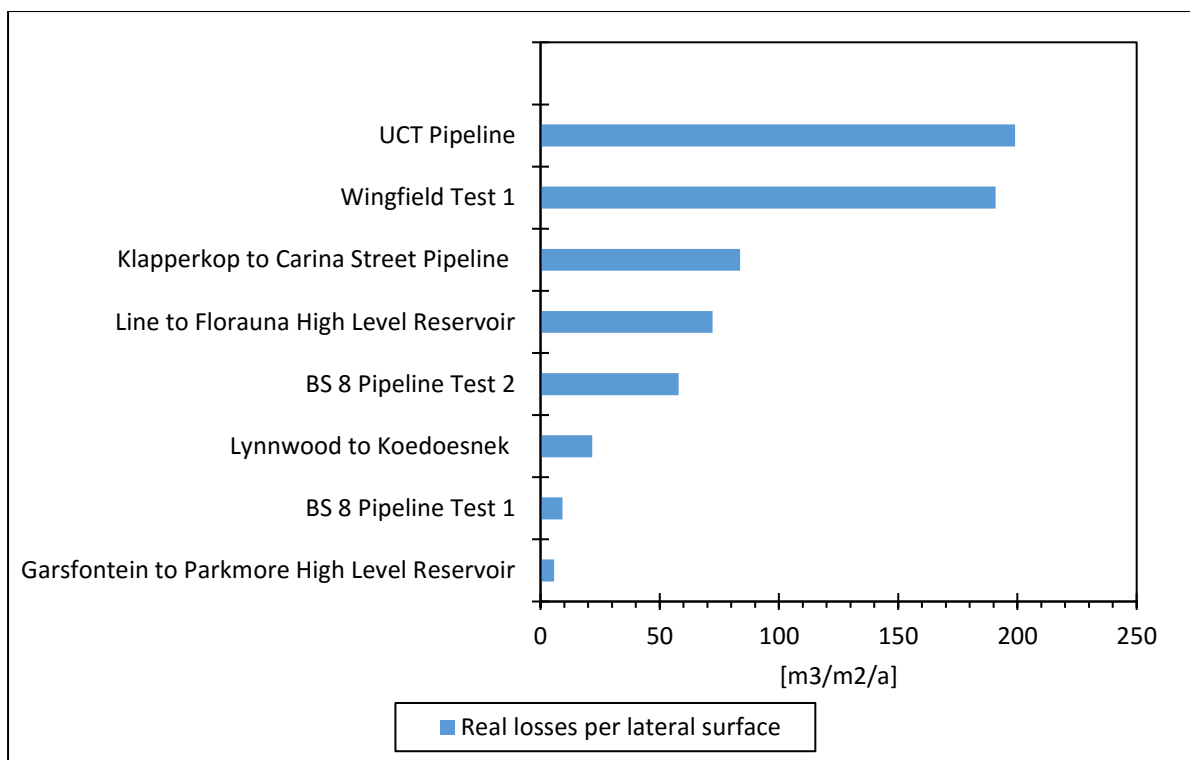


Figure 7-4: Real losses per lateral surface

It is immediately evident that the denominator favoured pipelines with a higher fraction of a larger pipe diameter and/or length, while it is less favourable for pipelines with a smaller diameter and/or length. *Figure 7-4* shows that for to this indicator the UCT pipelines appear to have the largest water losses because they have the smallest lateral surface.

When the results presented in *Figure 7-4* are compared to those in *Figure 7-3*, it is clear that the order of the pipelines changed slightly. Now, for to the real losses per lateral surface indicator, the lowest water losses were found to be in the line from Garsfontein to Parkmore High Level, and not the BS 8 pipeline Test 1 as for the real losses per length of main indicator.

Overall, this performance indicator appears suitable for comparisons of differently sized transmission mains because it incorporates both length and diameter. However, it does not consider other parameters such as the operational pressure, off-takes and pipe length.

#### 7.4.5 Effective initial leak area per lateral surface

The effective initial leak area per lateral surface indicator does not contain any volumetric parameters, unlike the other previously used indicators. This indicator is dimensionless and

simply indicates the ratio of the sum of all individual leak areas on the pipe under zero pressure conditions to the total surface area of the pipe.

Table 7-6 shows the effective initial leak areas for each tested pipeline, the lateral surface calculated for each tested pipeline, and (in the last column) the calculated effective initial leak area per lateral surface for the pipelines.

Table 7-6: Results of effective initial leak area per lateral surface indicator

Pipeline	A <sub>0</sub> (mm <sup>2</sup> )	Lateral surface (mm <sup>2</sup> )	A <sub>0</sub> / lateral surface
Wingfield Test 1	12	9.4 x 10 <sup>8</sup>	1.2 x 10 <sup>-8</sup>
BS 8 Pipeline Test 1	9	9.4 x 10 <sup>8</sup>	9.1 x 10 <sup>-9</sup>
BS 8 Pipeline Test 2	30	9.4 x 10 <sup>8</sup>	3.2 x 10 <sup>-8</sup>
UCT Pipeline	5	1.5 x 10 <sup>8</sup>	3.2 x 10 <sup>-8</sup>
Lynnwood to Koedoesnek	23	1.3 x 10 <sup>9</sup>	1.7 x 10 <sup>-8</sup>
Garsfontein to Parkmore High Level Reservoir	18	3.9 x 10 <sup>9</sup>	4.5 x 10 <sup>-9</sup>
Klapperkop to Carina Street Pipeline	138	3.4 x 10 <sup>9</sup>	4.0 x 10 <sup>-8</sup>
Line to Florauna High Level Reservoir	40	1.2 x 10 <sup>9</sup>	3.3 x 10 <sup>-8</sup>

First, the effective initial leak area was plotted to show, in hierarchical order, which pipeline had the largest effective initial leak area. The results in Figure 7-5 show that there is a factor of 28 between the largest and smallest effective initial leakage areas, which were the Klapperkop to Carina Street pipeline and the UCT pipeline, respectively.

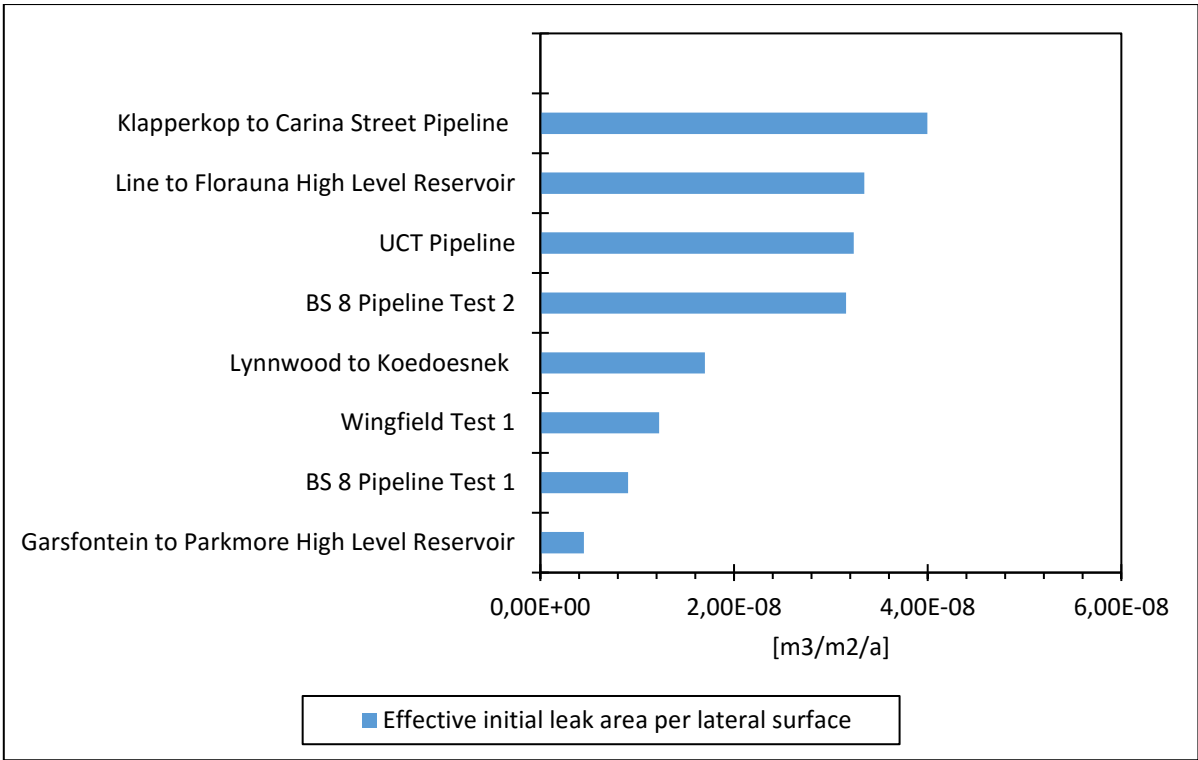
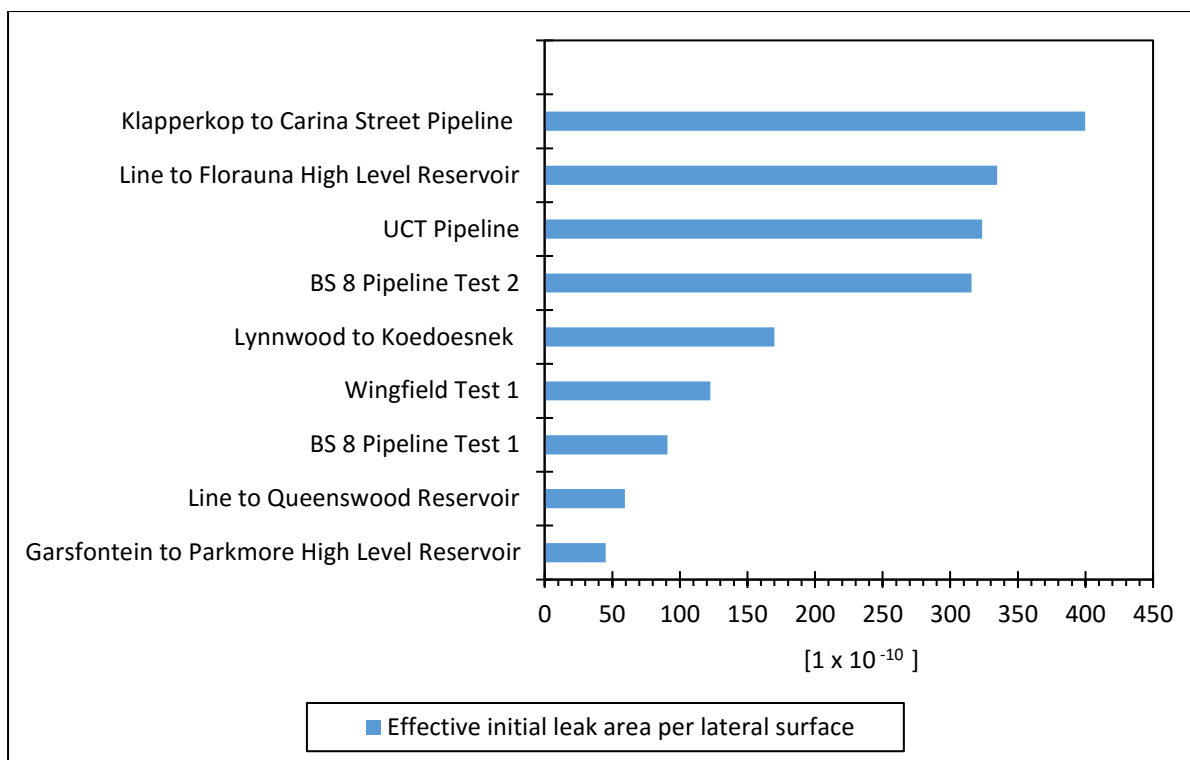


Figure 7-5: Results of the effective initial leak area for each pipeline.

As is the case with any other available water loss indicator, this indicator only partly considers the various factors that affect the level of water losses. It may, however, provide some advantages since it is dimensionless and gives a better physical interpretation of the size of the leak.

In addition, a dimensionless performance indicator, was explored. This dimensionless technical indicator takes into account the ratio of the effective initial leak area to the lateral surface area of the pipeline. *Figure 7-6* shows the results of the effective leak area per lateral surface indicator. In the *Figure*, the pipelines are sorted from the maximum to the minimum value.

While the pipeline with the maximum value was considered the worst case in the previous water loss indicators, in *Figure 7-6* the worst cast will be interpreted differently. The blue bars do not represent the water losses but a ratio, of the physical leak area to the lateral surface area of the pipe.



*Figure 7-6: Effective initial leak area per lateral surface*

For technical purposes, the effective initial leak area per lateral surface is a meaningful indicator since it compares a dimensionless ratio of the total leak size to the total surface area of the pipeline. It immediately gives an indication of the size of the leak and the severity of leak openings on the pipeline. However, this indicator still does not incorporate all the factors that influence leakage, e.g. operational pressure and number of off takes.

## 7.5 Conclusion

The assessment of water losses on transmission mains seems easier than that of distribution systems. However, the detail is more complicated, since every bulk pipeline has its unique characteristics regarding structural parameters such as diameter, pipe material, type of couplings and operating pressures, to name just a few factors.

Several performance indicators were used to analyse the bulk pipelines that were tested, using the PCAE. Based on the results, it can be concluded that the preferred performance indicators for assessing water losses on bulk pipelines depend on the purpose of the analysis:

- The real losses (m<sup>3</sup>/s or m<sup>3</sup>/day or m<sup>3</sup>/annum) indicator can be used to assess the volumetric leakage flow rate from one reference period to the next.



- The real losses per mains length ( $\text{m}^3/\text{km}/\text{h}$  or  $\text{m}^3/\text{km}/\text{annum}$ ) indicator can be used for internal monitoring of the water losses per meter of length from one reference period to the next. This indicator was found to favour very long pipelines.
- The real losses per lateral surface ( $\text{m}^3/\text{annum}/\text{m}^2$ ) indicator appears to be suitable for comparing differently sized bulk pipelines, because it incorporates differences in length and diameters of the pipelines.
- The effective initial leak area per lateral surface indicator is a dimensionless technical indicator which is suitable for comparing the relative sizes of the total leakage areas on the pipe with the pipe's surface area. There is no evidence that such an indicator has been used to evaluate water losses and there is no literature or experience to draw from. Nonetheless, this could be a meaningful indicator as it considers the current state of the pipe, the pipe diameter and the pipe length.

# 8 Conclusions

Bulk pipelines play a critical role in water supply systems as they connect water treatment plants to bulk reservoirs and distribute water from reservoirs to different towns or water supply zones. Bulk pipelines transport large quantities of water, often at very high pressures, and it is therefore critical that they are well maintained and that leaks are detected and repaired speedily when they occur. However, it is difficult to determine what the water losses in bulk pipelines are, because the high flow rates make measurement at both ends of bulk pipelines impractical. Cheap solutions such as ultrasonic flow meters or reservoir drop tests are prone to problems and do not have the required accuracy. There is therefore a need for a simple but accurate technique to perform a low-cost pipe condition assessment which can survey large sections of bulk pipe infrastructure in short periods of time with minimal disturbance to the operation of the infrastructure.

This research project aimed to develop such a low-cost pipe condition assessment technique. A summary of the research is presented in the sections below. The contributions made to the fields of leakage detection, leakage modelling and leakage characterisation are also described. Finally, some recommendations for further work are made, based on the results presented in this thesis.

## 8.1 Summary of this study

The primary objective of this study was to determine the characteristics and extent of water losses on bulk pipelines. This objective was achieved through the development of a device that uses pressure testing in combination with the latest models on the behaviour of leak areas with pressure.

### 8.1.1 The pipe condition assessment equipment (PCAE)

A novel device, named the pipe condition assessment equipment (PCAE), was designed and constructed for the purpose of detecting and characterising leakage. The main components and functions of this device are:

- Pump with variable speed to allow pressure variations and allows for control that holds pressure constant
- Flow measurement with accuracy of at least 2% with a minimum flow rate of 250 L/h

(the boundary between bursts and background leakage).

- Pressure measurement with accuracy of at least 2% with a pressure range of at least 1 to 9 bars
- Water storage with sufficient volume to test large leaks, but small enough to transport in the field
- Data recorder that records data automatically and provides field display with ease of extraction
- Hydraulic components that handle pressures of at least 12 bar, allow for air release
- The device was designed to be mobile but robust for field conditions and transport.

The efficacy of the device was verified through experimental tests in the laboratory. Three separate 800mm long class 9 uPVC test pipes were used. The pipes were each drilled to create a source of known leakage, namely a 12mm round hole, a 100mm by 1mm longitudinal crack, and a 100mm by 1mm circumferential crack.

The PCAE was used to determine the leakage parameters of the three test pipes. The leakage parameters obtained using the PCAE were compared to results from van Zyl & Malde's (2017) experimental study that also investigated similar leaks and pipes. It was found that the use of the PCAE provided results that are within the confidence intervals of the values obtained in van Zyl & Malde's (2017) study.

### **8.1.2 Bulk pipeline field tests using the device**

Several pipelines were tested around South Africa using the PCAE. A wide range of pipe diameters and lengths and materials were tested. Each pipe was selected in consultation with the asset manager responsible for maintenance and operations of the pipeline. Site surveys were done before the tests were carried out.

The field tests demonstrated that pressure-based leakage characterisation is an effective and suitable testing technique for bulk pipelines. It was shown that this method allows for simple, affordable and quick condition assessments that can be implemented with minimal disturbance to the operation of the pipeline. Not only did this method provide valuable information on the leakage characteristics of the pipeline, but it also provided clues on the most probable leak locations.

Although the success of this technique is directly dependent on the sealing capabilities of existing isolation valves on the tested pipe sections, it was found that most valves sealed sufficiently. Identifying problems with valves is an important finding in itself.

Out of a total of 11 pipelines that were scheduled to be tested, 2 pipelines could not be isolated and could therefore not undergo testing. Another reason that lead to withdrawing a test was poor or damaged components. For example, one pipeline which had an above-ground fire hydrant as the only point of connection could not be tested because the fire hydrant was damaged.

### **8.1.3 Dynamic pressure test for modelling and characterising small leaks**

A dynamic pressure test was developed to test pipelines that has leakage flow rates that were undetectable using PCAE. If an isolated pipeline had a leak, the pressure in the pipe would drop with time due to the water leaving the pipe. This process continued until the pressure inside the pipe equalised with the pressure outside the pipe.

The pressure and time data (from the pressure drop signature) was used in combination with a theoretically derived equation to estimate the leak area under zero pressure conditions and the slope of the leak area change with pressure.

If the pressure drops, a mathematical model was fitted to the pressure vs time curve, using the known pipe properties, to determine the following characteristics of the leak(s) present in the pipe:

- the initial leak area, which is the area of the leak under zero pressure conditions
- the head-area slope, which is the rate of expansion of the leak area as a function of pressure; this allows the type of leak (round hole, longitudinal crack or circumferential crack) as well as the dimensions of the leak (e.g. hole diameter or crack length) to be identified.

A mathematical model used in this procedure was developed and is novel. It takes some or all the following factors into account:

- the variation of the internal pipe volume with changes in pressure due to pipe wall strain
- the compressibility of the fluid inside the pipe

- orifice hydraulics
- the variation in the leak(s) area as a function of pressure.

The leakage parameters are determined by fitting the theoretical model to the test data.

### ***8.1.3.1 Experimental test***

An experimental setup designed by (Taylor, 2018) was used to verify the theoretical model. The experimental setup consisted of a uPVC pipe sample with a small round hole leak induced at the centre of the pipe.

The uPVC pipe was pressurised by allowing water to enter the pipe from the water network in the laboratory. Once the desired pressure was reached, the ball valve was closed and the pressure was monitored while water escaped through the leak. During this time, the mass of the outflowing water was captured in a bucket that was placed on a digital scale to measure the mass of water escaping the leak. The values were recorded as a continuous stream of data captured by a video recording device. The film of each set of mass readings was then edited using software, allowing for the stream to be slowed and for the individual measurements to be manually recorded.

The collected data was then processed and analysed to determine the relevant relationships between the flow rate, pressure head and leak area. The experimental data was compared to theoretical values, calculated using the equations proposed by the analytical derivation. A method was then employed to calibrate the theoretical models to the experimental data in an attempt to verify the adequacy and accuracy of the models.

### ***8.1.3.2 Field application***

The pressure drop test was also carried out on a real pipeline. The PCAE was used to record the variation of pressure over time. The device was connected and the water tank filled. Thereafter, the pipeline was isolated from the rest of the system by valves being closed, and the PCAE pump was activated. However, it was observed that no leakage flow rate was being detected by the PCAE. Consequently, the pump was deactivated and the pressure reading recorded over time.

The leakage characteristics of the pipe were estimated from the pressure vs time data: if the pressure remained constant, the pipe would not have a leak. When the pump was deactivated, it was immediately observed that the pressure in the pipe dropped with time, indicating that water was leaving the pipe. This process continued until the pump was re-activated. The pressure and time data along with the numerical model describing the pressure drop behaviour were used to characterise the leakage in the pipeline. The leakage flow rate was found to be smaller than the minimum flow rate that the PCAE's electromagnetic flow meter could detect.

#### **8.1.4 Performance indicators for assessing water losses in bulk pipelines**

A great deal of work has been done over the past two decades on distribution systems. Suitable performance indicators for assessing water losses in water distribution systems are therefore available. These performance indicators consider relevant structural network parameters and are based on data sets that include numerous distribution systems with miscellaneous pipe materials and diameters.

For bulk systems or transmission mains, however, so far there is no consensus as to the best performance indicators. In this thesis, several performance indicators were evaluated to assess water losses in the bulk pipelines that were tested. It was found that the preferred performance indicators for assessing water losses on bulk pipelines depend on the purpose of the analysis.

## **8.2 Contributions to the field**

### **8.2.1 Technology for leak detection and characterisation**

This study makes a number of contributions to the field of leak detection and characterisation in bulk pipelines as summarised here:

- A novel mobile device was designed and constructed for testing and characterising leakage in bulk pipelines. The device was capable of detecting leakage, quantifying the extent of leakage as well as identifying the characteristics of the leakage in bulk pipelines.
- The efficacy of the device was verified in the laboratory, and the pressure-based technique that the device uses to assess leakage was also verified by testing pipes with known leakage characteristics
- The device was used to test a range of bulk pipelines with different material, length and diameter. It was shown that the only two requirements for a successful test is that the

pipeline can be isolated from the network and that a convenient connection point on the pipeline can be accessed.

- This study also demonstrated the application of the pressure-based technique as a benchmarking tool to assist pipe owner with ranking pipes according to the severity of their condition, in order to allow for the optimal allocation of resources to maximise the impact of intervention efforts.
- The pressure and flow data was analysed using Microsoft Excel software that was developed. The software generated the leakage parameter results, i.e. the leakage parameters for the power equation and for the modified orifice equation respectively. The leakage parameters could provide information on the size of the actual leak and the type of leaks in the system.

### **8.2.2 Leakage modelling**

The presented work makes the following contributions to the field of leakage modelling:

- Previous studies have only applied the modified orifice equation in either a laboratory setting, a synthetic water distribution system or a hydraulic model. In this study, the modified orifice equation was applied to real bulk pipelines, which had not been done before.
- The modified orifice equation model was shown to provide a realistic model that can be used to determine the leakage flow rate from the bulk pipe at different pressures throughout the pipeline's operational range.
- A novel non-intrusive technique was developed, called the dynamic pressure drop method, which uses a pressure drop signature from an isolated pipe to detect and quantify leakage that is undetectable by the flow meter of the PCAE.
- The dynamic pressure drop analytical solution was derived, considering material behaviour, fluid mechanics, orifice behaviour and the variation of the leak area as a function of pressure. However, because of the composition of the derived analytical equation (comprising of square roots), this equation was only defined for positive initial leak areas and positive head-area slopes.

- The derived analytical equation was further developed to consider other characteristic leak cases, such as negative head-area slopes and negative initial leak areas. This was done by introducing complex numbers which allowed for other leak cases to be analysed.
- The dynamic pressure drop method was applied in a laboratory setting to demonstrate how the method can be applied.
- The dynamic pressure drop method was then applied to a real pipeline in the field to illustrate its efficacy on real-life systems.
- A new performance indicator for bulk systems was also developed that takes into account the size of the leak as well as the lateral surface of the pipeline.

### **8.2.3 Performance indicators for bulk systems**

The presented work makes the following contributions to the field of water loss assessment in bulk pipelines:

- The effective leak area per lateral surface performance indicator is a new dimensionless indicator that gives the ratio of the sum of all leak areas on the pipeline to the total surface area of the pipe.
- The tested bulk pipelines were compared using various performance indicators, illustrating how these indicators favour different characteristics of pipelines. The challenges in comparing water losses of different bulk systems were highlighted.

## **8.3 Recommendation for further work**

This study has identified a number of areas where further work can be undertaken.

### **8.3.1 Pipe condition assessment device**

The PCAE was designed for detecting, quantifying and characterising leakage in bulk pipelines. The device provides information on the nature of leaks (type of pipe crack or hole and amount of water lost through the leak) that may be present in a pipeline, but it does not indicate the location of the leak(s). One such technique that can be used for leak location is the transient test-based technique.



Further work can investigate the possibility of incorporating the inverse transient analysis (ITA) method for locating leakage. The ITA method takes pressure signals recorded in pipe systems, in which transients of known characteristics have been induced, and compares them to pressure traces generated by a numerical model simulating the same transients (Liggett & Chen, 1994).

Further work can be done to improve the PCAE by fitting it with processing and communication capabilities that will allow it to automatically transmit the results to a central control station.

### **8.3.2 Dynamic pressure test**

The experimental setup designed by Taylor (2018) was satisfactory and produced data suitable for the analysis. One improvement that could be made, however, is to use end caps with a higher wall thickness or even use longer sample test pipes. Because the pipe was only one metre in length, the effect of the water exerting pressure on the end caps could have had an effect on the readings taken by the pressure transducer. The end caps could also potentially affect the way the volume changes as a function of the pressure.

#### ***8.3.2.1 Improvements to testing***

As previously stated, the data collected for this experiment was accurate enough to provide a sufficient analysis. However, it is recommended that a more sensitive digital balance be used, as the one used in this setup does not measure anything to an accuracy higher than 1 gram.

It is also recommended that the digital balance be replaced by a setup which would involve a flowmeter on both the upstream and downstream end of the leak. This would improve the accuracy of the results as well as remove the tedious job of manually documenting the mass results. A flow meter would also allow more readings to be taken over a shorter period of time; this would improve the accuracy of the results.

To further improve the accuracy, it is recommended that the experiment be repeated at least three times in order to confirm the results of the test pipe.

#### ***8.3.2.2 Recommendations for further investigations***

It is recommended that the model be further calibrated by investigating and confirming the unusually low values for the initial volume and coefficient of discharge found during this

experiment. It was anticipated that the initial volume of water in the pipe would be consistent with that of a full pipe, and that it would therefore be easily calculated as a function of the pipe geometry. However, this was not the case, resulting in the need to calibrate the initial volume of water instead of using an assumed value. To improve on this model, it is suggested that an experiment be designed and conducted on a similar pipe as used for this study.

## 9 References

- ABB. 2017. ProcessMaster, HygienicMaster FEX300, FEX500. Rev. E. Available: [https://library.e.abb.com/public/2ddbfd9d23d54823860d29ff97918535/SM\\_FEX300\\_FEX500\\_FM\\_CSA\\_EN\\_E.pdf](https://library.e.abb.com/public/2ddbfd9d23d54823860d29ff97918535/SM_FEX300_FEX500_FM_CSA_EN_E.pdf) [2017, January 20].
- ABB. 2018a. 266 HART Pressure transmitters. Available: [https://library.e.abb.com/public/e86b2306c0c6425bb22b4348476f157f/OI\\_266HART-EN\\_M\\_11\\_2018.pdf](https://library.e.abb.com/public/e86b2306c0c6425bb22b4348476f157f/OI_266HART-EN_M_11_2018.pdf) [2018, January 12].
- ABB. 2018b. SM500F Field Mountable paperless recorder. DS/SM500F-EN Rev. AG. Available: [https://library.e.abb.com/public/6a3ca069d9f049fdb3f3ef19795b20b/DS\\_SM500F-EN\\_AG.pdf](https://library.e.abb.com/public/6a3ca069d9f049fdb3f3ef19795b20b/DS_SM500F-EN_AG.pdf) [2018, February 2018].
- Agrawal, C. & Sinha, S. 2015. *Infrastructure Asset Management: Risk Assessment*. Presentation, Virginia Tech.
- American Lifelines Alliance. 2005. *Seismic Guidelines for Water Pipelines*. G&E Report 80.01.01, Revision 0.
- American Water Works Service Company Inc. 2002. *Deteriorating Buried Infrastructure Management Challenges and Strategies*. United States Environmental Protection Agency.
- AVA .2010. *The metal casting industries: Ductile Iron pipe*. Available: <http://www.tpli.com.my/pipes.html> [2016, December 10]
- Bartlett, L. (2004). *Pressure Dependant Demands in Student Town Phase 3*. Final Year Project Report. Rand Afrikaans University (now University of Johannesburg), Auckland Park 2006, South Africa.
- Bennis, S., Fares, R., Guemouria, N., & Dubois, M. 2011. *Theoretical modeling and experimental validation of leakage in drinking water networks*. Journal American Water Works Association. 103(12): 61-72.
- Bruinette, K. & Claasens, T. 2016. *Managing the Water Balance*. Institute of Municipal Engineering of Southern Africa. 41(11): 17–20.

- Buckley, R.S. (2005). *Derivation of a leakage equation for round holes and investigation of cracks within pressurised pipes*. MEng Thesis. University of Johannesburg.
- Burn, S., Davis, P., Schiller, T., Tiganis, B., Tjandraatmadja, G., Cardy, M., Scott, G., Paul, Sadler., et al. 2004. *Long-term performance prediction for PVC pipes*. (Project #2879). Commonwealth Scientific and Industrial Research Organisation (CSIRO).
- Burstall Tim. 1997. *Bulk Water Pipelines*. London, United Kingdom: Thomas Telford.
- Carroll, M. 1985. *Polyvinylchloride pipe reliability and failure modes*. Reliability Engineering, 13(1): 11–21.
- Cassa, A.M., van Zyl, J. E., & Laubscher, R. F. 2010. *A numerical investigation into the effect of pressure on holes and cracks in water supply pipes*. Urban Water Journal. 7(2): 109–120. DOI:10.1080/15730620903447613.
- Cassa, A.M. & van Zyl, J.E. 2011. *Predicting the head-area slopes and leakage exponents of cracks in pipes*. Urban Water Management: Challenges and Opportunities, CCWI 2011: Computing and Control for the Water Industry. 2(337): 485–490.
- Cassa, A.M. & van Zyl, J.E. 2013. *Predicting the head-leakage slope of cracks in pipes subject to elastic deformations*. 62 (4): 214–223. DOI: 10.2166/aqua.2013.094
- Cassa, A.M. & van Zyl, J.E. 2014. *Predicting the leakage exponents of elastically deforming cracks in pipes*. Proceedings of the 12th International Conference on Computing and Control for the Water Industry. 2-4 September 2013. Perugia, Italy.
- Charalambous, B. 2005. *Experiences in DMA redesign at the Water Board of Lemesos, Cyprus*. Water Board of Lemesos.
- Clayton, C.R.I., & van Zyl, J. E. 2007. *The effect of pressure on leakage in water distribution systems*. Water Management. 160(2): 109–114. DOI: 10.1680/wama.2007.160.2.109
- Colombo, A.F. & Karney, B.W. 2002. *Energy and Costs of Leaky Pipes: Toward Comprehensive Picture*. Journal of Water Resources Planning and Management. 128(6):441-450. DOI: 10.1061/(ASCE)0733-9496(2002)128:6(441)
- Colombo, A.F., Lee, P., & Karney, B.W. (2009). *A selective literature review of transient-based leak detection methods*. Journal of Hydro-Environment Research. 2(4): 212–227. Doi:10.1016/j.jher.2009.02.003

DAB Water Technology. 2016. Active Driver Plus Instruction Manual. Available: <https://dabpumps.us/sites/dabpumps.us/files/2016-08/ACTIVE%20DRIVER%20Plus%20Instruction%20manual%20USA%202016.pdf> [2017, Feb 12].

de Miranda, S., Molari, L., Scalet, G., & Ubertini, F. 2014. *A physically-based analytical relationship for practical prediction of leakage in longitudinally cracked pressurized pipes*. Engineering Structures. 79: 142–148. <https://doi.org/10.1016/j.engstruct.2014.08.011>

De Rose, P.J., & Parkinson, R.W. 1985. *Corrosion of Ductile Iron Pipe*. Report TR241. WRc Engineering. Water Research Centre. Swindon, United Kingdom.

Deyi, M., van Zyl, J. & Shepherd, M. 2014. *Applying the FAVAD Concept and Leakage Number to Real Networks : a Case Study In Kwadabeka, South Africa*. Proceedings of the 16<sup>th</sup> Conference on Water Distribution System. 13-16 July 2014. Bari, Italy.1537–1544.

Dueck, R. 2010. Seminar: *PVC Failures*. Presentation. City of Calgary, water resources. Delivered: 8 September 2010.

DVGW-Guideline W 392. 2003. *Network inspection and water losses-activities, procedures and assessment*. DVGW, Bonn, Germany.

DVGW- Guideline W 392. 2017. *Water losses in distribution networks - Assessment, monitoring, classification, water balance, performance indicators*. DVGW, Bonn, Germany.

Echologics. 2017. *Large diameter water main leak detection*. Available: <https://www.echologics.com/services/large-diameter-leak-detection>. [2017, March 4].

Environmental Protection Agency [EPA]. 2010. *Control and mitigation of drinking water losses in distribution systems*. (EPA 816-R-10-019). Office of water.

Euroflow. 2016. *Horizontal multistage stainless-steel centrifugal pump manual*. Available: <http://seoca-pump.com/wp-content/uploads/2016/09/HMS-N.pdf> [2017, Feb 10].

Farley, M. 2001. *Leakage Management and Control : A Best Practice Training Manual*. World Health Organisation. Geneva: Switzerland

Farley, M. 2003. *Non-Revenue Water - International Best Practice for Assessment, Monitoring and Control*. Proceedings of the 12th Annual CWWA Water, Wastewater & Solid Waste Conference. 28 September – 3 October 2003. Atlantis, Paradise Island, Bahamas.

Farshad M. 2006. *Plastic pipe systems*. Great Britain: Elsevier.

Federation of Canadian Municipalities (FCM) & the National Research Council (NRC). 2003. *National Guide to Sustainable Municipal Infrastructure: Innovations and Best Practices*. Issue No. 1.1.

Ferrante, M., Massari, C., Brunone, B., & Meniconi, S. 2011. *Experimental evidence of hysteresis in the head-discharge relationship for a leak in a polyethylene pipe*. *Journal of Hydraulic Engineering*. 137(7): 775–780. DOI: 10.1061/(ASCE)HY.1943-7900.0000360.

Ferrante, M. 2012. *Experimental investigation of the effects of pipe material on the leak head-discharge relationship*. *Journal of Hydraulic Engineering*. 138 (8): 736-743. DOI:10.1061/(ASCE)HY.1943-7900.0000578.

Ferrante, M., Meniconi, S., & Brunone, B. 2014. *Local and global leak laws: The relationship between pressure and leakage for a single leak and for a district with leaks*. *Water Resources Management Journal*. 28(11): 3761–3782.

Ferrante, M., Brunone, B., Meniconi, S., Capponi, C. & Massari, C. 2014. *The leak law: From local to global scale*. Proceedings of the 12th International Conference on Computing and Control for the Water Industry. 2-4 September 2013. Perugia, Italy.

Finnemore, E.J. & Franzini, J.B. 2009. *Fluid Mechanics with Engineering Applications*. Rev. 10<sup>th</sup> ed. New York: McGraw-Hill.

Gere, J. 2001. *Mechanics of materials*. Rev. 5<sup>th</sup> ed. USA: CL Engineering.

Gerges, N.N., Issa, C.A. & Fawaz, S. 2016. *The effect of construction joints on the flexural bending capacity of singly reinforced beams*. *Case Studies in Construction Materials*. 5: 112-123. <https://doi.org/10.1016/j.cscm.2016.09.004>

GRANT. 2016. Civil Engineering Solutions. Available: <https://www.grantltd.co.uk/work-sectors/water-industry-civil-engineering/> [2016, November 15].

Greyvenstein, B. & van Zyl .2005. *An experimental investigation into the pressure leakage relationship of some failed water pipes*. Conference: Leakage 2005. August 2005. Halifax, Canada.

Herbst, P., & Raletjena, M. 2015. No Drop in the Context of Water Security. In the 5th Regional African Water Leakage Summit. 23-24 June 2015. 1–52. Available: [chrome-](#)

[extension://oemmndcbldboiebfnladdacbfmadadm/https://www.watersummit.co.za/assets/files/presentations\\_2015/23June2015\\_2a\\_Hebst\\_P.pdf](https://oemmndcbldboiebfnladdacbfmadadm/https://www.watersummit.co.za/assets/files/presentations_2015/23June2015_2a_Hebst_P.pdf) [2017, January 5]

Hiki, S. 1981. *Relationship between Leakage Quantity and Pressure*. Journal of Japan Waterworks Association. 51(5): 50–54.

Hunaidi, O. & Chu, W.T. 1999. *Acoustical characteristics of leak signals in plastic water distribution pipes*. Journal of Applied Acoustics. 58(3): 235-254.

Hunaidi, O., Wang, A., Bracken, M., Gambino, T. & Fricke, C. 2004. *Acoustic methods for locating leaks in municipal water pipe networks*. International Water Demand Management Conference. 30 May – 3 June 2004. Dead Sea, Jordan. 1-14.

Liggett A.J., and Li-Chung C. 1994. *Inverse Transient Analysis in Pipe Networks*. Journal of Hydraulic Engineering. 120(8): 934–955.

IPART (Independent Pricing and Regulatory Tribunal). 2018. Review of water utility performance indicators. New South Wales. Available: <https://www.ipart.nsw.gov.au/files/sharedassets/website/shared-files/licensing-administrative-water-performance-indicators-review-2018/working/final-report-water-utility-performance-indicators-review-2018---june-2018.pdf> [2018, March 12].

Karney, B., Khani, D. & Halfawy, M.R. 2008. *A Simulation Study on Using Inverse Transient Analysis for Leak Detection in Water Distribution Networks*. Stormwater and Urban Water Systems Modeling Conference. Toronto, Canada. DOI: 10.14796/JWMM.R235-23.

Kleiner, Y. & Rajani, B 2001. Comprehensive review of structural deterioration of water mains: Physically based models. Urban Water Journal. 3(3): 131–150.

Koelbl, J., & Zipperer, D. (2018). *Water Loss Assessment on Transmission Mains*. IWA Water Loss Conference 2018. 7-8 May. Cape Town, South Africa.

Kroon, D.H., Lindemuth, D., Sampson, S. & Vincenzo, T. 2005. Corrosion Protection of Ductile Iron Pipe. Journal of Materials Performance. 44(1): 1-15.

Lambert, A. 2002. *International report: Water losses management and techniques*. Water Science and Technology: water supply 2(4).

Lambert, A. & Hirner, W. 2000. *Losses from Water Supply Systems: Standard terminology and recommended performance measures*. London, UK: IWA: The Blue Pages.

Lambert, A. 2001. *What do we know about pressure: leakage relationships in distribution systems?* IWA Conference on Systems Approach to Leakage Control and Water Distribution Systems Management.

Lambert, A., Fantozzi, M. & Thornton, J. 2005. *Practical approaches to modeling leakage and pressure management in distribution systems – progress since 2005*. Proceedings of the 12th International Conference on Computing and Control for the Water Industry. 2-4 September. Perugia, Italy.

Laven, K. & Lambert, A. 2012. *What Do We Know About Real Losses On Transmission Mains?*. Water Loss Research and Analysis Ltd.

Ledochowski, W. 1956. *An analytic method of locating leaks in pressure pipelines*. The South African Institution of Civil Engineers. 6(12): 341 – 344.

Lee, J., Han, S., Kim, K., Kim, H. & Lee, U. 2013. *Failure analysis of carbon steel pipes used for underground condensate pipeline in the power station*. Engineering Failure Analysis. 34: 300–307. DOI: 10.1016/j.engfailanal.2013.08.005

Lee, P.J., Vítkovský, J.P., Lambert, M.F., Simpson, A.R., & Liggett, J.A. 2005. *Frequency domain analysis for detecting pipeline leaks*. Journal of Hydraulic Engineering. 13(7): 596. DOI: 10.1061/(ASCE)0733-9429(2005)131:7(596).

Liu, H . 2003. *Pipeline Engineering*. Boca Raton, Florida: CRC Press LLC. ISBN: 0-58716-140-0

Liu, Z., Kleiner, Y., Rajani, B., Condit, W. & Wang, L. 2012. *Condition Assessment Technologies for Water Transmission and Distribution Systems*. EPA/600/R-12/017. U.S. Environmental Protection Agency, Washington, DC.

Ma. C.H. 2011. *Internal Fluidisation due to Horizontal Seepage - A laboratory Study*. University of Southampton.

Makar,J.M., Desnoyers, R., & McDonald, S.E. 2001. *Failure modes and mechanisms in cast gray iron pipe*. Proceedings of underground infrastructure research: Municipal, Industrial and Environmental Applications. 10-13 June 2001. Kitchener, Ontario. 1-10.

Malde, R. & van Zyl, J.E. 2015. *An Analysis of Leakage Parameters of Individual Leaks on a Pressure Pipeline through the Development and Application of a Standard Procedure*. MSc.



Eng Thesis. University of Cape Town. Available: <https://open.uct.ac.za/handle/11427/13726> [2016, June 12].

May, J. (1994). *Pressure dependent leakage*. World Water & Environmental Engineer. 17 (8):10.

Mckenzie, R. & Seago, C.J. 2005. *Benchmarking of Leakage from Water Reticulation Systems in South Africa*. Report to the South African Water Research Commission. Report number TT 244/05. ISBN 1-77005-282-8.

Mckenzie, R., Siquelaba Z.N. & Wegelin W.A. 2012. *The State of Non-Revenue Water in South Africa*. (WRC report; no. TT 522/12). Gezina, South Africa: Water Research Commission.

Mora-Rodríguez, J., Delgado-Galván, X., Ramos, H.M. & López-Jiménez, P.A. 2013. *An overview of leaks and intrusion for different pipe materials and failures*. Urban Water Journal. 11(1): 1–10. DOI:10.1080/1573062X.2012.739630

Mordak, J. & Wheeler, J. 1988. *Deterioration of asbestos cement water mains*. Department of the Environment Contract Duration: PECD 7/7/117. Wilshire, UK: WRc Engineering.

Muhlbauer, W. K. 2004. *Pipeline risk management manual: Ideas, Techniques and Resources*. Rev. 3<sup>rd</sup> ed. Amsterdam, Boston, Heidelberg, London, New York, Oxford, Paris, Santiago, San Francisco, Singapore, Sydney, Tokyo: Gulf Professional Publishing.

Najafi, M., & Gokhale, S. 2005. *Trenchless technology: pipeline and utility design, construction, and renewal*. New York, Chicago, San Francisco, Athens, London, Madrid, Mexico City, Milan, New Delhi, Singapore, Sydney, Toronto: McGraw-Hill Education.

Nel, D. T. 2009. *Factors that may compromise bulk water distribution reliability*. Ph.D. Thesis. University of Johannesburg.

Nsanzubuhoro, R., van Zyl, J.E., & Zingoni, A. 2016. *Predicting the head-area slopes of round leaks in pipes subject to elastic deformations*. Proceedings of the 6th International Conference on Structural Engineering, Mechanics and Computation. 5-7 September. University of Cape Town, Cape Town, South Africa.

O'Connor, C. & Denton, G. 2012. *Polyethylene Pipeline Systems - Avoiding The Pitfalls of Fusion Welding*. Pipeline-Conference. Available: [http://www.pipeline-conference.com/sites/default/files/papers/ptc\\_2012\\_OConnor.pdf](http://www.pipeline-conference.com/sites/default/files/papers/ptc_2012_OConnor.pdf) [2017, August 15].

Ogura. 1979. Experiments on the relationship between leakage and pressure. Japan Water Works Association. 6(572):38-45 572 (in Japanese).

Ostapkowicz, P. 2016. Leak detection in liquid transmission pipelines using simplified pressure analysis techniques employing a minimum of standard and non-standard measuring devices. *Engineering Structures*. 113: 194–205. DOI:10.1016/j.engstruct.2016.01.040

Pike, S. 2015. *Experimental Investigation of Leakage-Induced Pipe Erosion Outside of Pipe Leaks*. M.Sc. Thesis. University of Cape Town. Available: <https://open.uct.ac.za/handle/11427/20518> [2017, January 26].

Pratt, C., Yang, H., Hodkiewicz, M. & Oldham, S. 2011. *Factors influencing pipe failures in the WA environment*. CEED Seminar Proceedings. Available: [https://ceed.wa.edu.au/wp-content/uploads/2017/02/Christopher.Pratt\\_.pdf](https://ceed.wa.edu.au/wp-content/uploads/2017/02/Christopher.Pratt_.pdf) [2016, November 10].

Prinsloo, K., Webb, M. & Wrigglesworth, M. 2011. Advancement of condition assessment techniques for large diameter pipelines. *South African Institute of Civil Engineers* 19(9): 20-25.

Pure Technologies. 2015. *SmartBall – Leak and Gas Pocket Detection*. Available: <https://puretechltd.com/technology/smartball-leak-detection/> [2016, January 26].

Puust, R., Kapelan, Z., Savic, D. & Koppel, T. 2010. *A review of methods for leakage management in pipe networks*. *Urban Water Journal*. 7(1): 25-45. DOI:10.1080/15730621003610878

Rajani, B. & Kleiner, Y. 2003. *Protection of ductile iron water mains against external corrosion: review of methods and case histories*. *Journal American Water Works Association*. 95(11): 110–125.

Rajani, B. & Abdel-Akher, A. 2013. Performance of cast-iron-pipe bell-spigot joints subjected to overburden pressure and ground movement. *Journal of Pipeline Systems Engineering and Practice*. 4(2): 98-114. DOI: DOI: 10.1061/(ASCE)PS.1949-1204.0000125.

Rajeev, P., Kodikara, J., Robert, D., Zeman, P. & Rajani, B. 2013. *Factors contributing to large diameter water pipe failure as evident from failure inspection*. LESAM IWA Leading-Edge Strategic Asset Management Conference. 10-12 September. Sydney Convention Centre., Australia.

Rand Water. 2007. Annual report 2007: Runs in your veins. Available: <http://www.randwater.co.za/Annual%20Reports/Annual%20Reports/2006-2007%20Annual%20Reports/RandWater%20AR2007.pdf> [2017, July 15].

Reed, C., Smart, D. & Robinson, A. 2006. Potential Techniques for the Assessment of Joints in Water Distribution Pipelines. (WRF report; no. 91126). Alexandria, USA: Water Research Foundation.

Rogers, D. 2014. Leaking water networks: an economic and environmental disaster. Proceedings of the 12<sup>th</sup> International Conference on Computing and Control for the Water Industry. 2-4 September. Perugia, Italy. 70: 1421-1429. [DOI:10.1016/j.proeng.2014.02.157](https://doi.org/10.1016/j.proeng.2014.02.157)

Robor Suppliers. 2015 Ductile iron pipe and fittings. Available: [http://www.robtor.co.za/FileBrowser/EditorFiles/catalogs/03\\_product\\_catalogs/03\\_conveyance/2376\\_Robor\\_Ductile\\_Iron\\_Brochure5.pdf](http://www.robtor.co.za/FileBrowser/EditorFiles/catalogs/03_product_catalogs/03_conveyance/2376_Robor_Ductile_Iron_Brochure5.pdf) [2016, December 10].

Roto Tank. 2016. Manufacturers of water, chemical, transport, septic tanks and silos. Available: <https://www.rototank.co.za/products/water-storage-tanks/> [2016, June 25].

Savić, D.A., Casey, R. & Kapelan, Z. 2011. *Water Distribution Systems*. UK: ICE publishing. 23–48. DOI:10.1680/wds.41127.023

Schwaller, J. & van Zyl, J.E. 2014. *Implications of the known pressure-response of individual leaks for whole distribution systems*. Proceedings of the 12<sup>th</sup> International Conference on Computing and Control for the Water Industry. 2-4 September. Perugia, Italy. 70: 1513–1517. DOI: 10.1016/j.proeng.2014.02.166

Schwaller, J., van Zyl, J. E. & Kabaasha, A.M. 2015. *Characterising the pressure-leakage response of pipe networks using the FAVAD equation*. Water Science and Technology: Water Supply. 15(6): 1373–1382. <https://doi.org/10.2166/ws.2015.101>.

Schwaller, J. & van Zyl, J.E. van. 2014. *Modeling the pressure-leakage response of water distribution systems based on individual leak behavior*. Journal of Hydraulic Engineering. 141(5): 1–8. [https://doi.org/10.1061/\(ASCE\)HY.1943-7900.0000984](https://doi.org/10.1061/(ASCE)HY.1943-7900.0000984).

Schwaller, J. 2012. *Modelling the effects of a large number of leaks in a water distribution network using the FAVAD*. Masters Thesis. University of Applied Sciences Karlsruhe.

Ssozi, E. N., Reddy, B.D., & van Zyl, J.E. 2015. *Numerical Investigation of the Influence of Viscoelastic Deformation on the Pressure-Leakage Behaviour of Plastic Pipes*. Journal of Hydraulic Engineering 142(3): 255-290.

Stephens, M.L., Dalius, M., Lambert, M.F., Simpson, A.R., Viykovsky, J.P. & Nixon, J. *Field verification of a continuous transient monitoring system for burst detection in water distribution systems*. Proceedings of the eighth International Conference on Computing and Control for the Water Industry. 5-7 September, 2005. Exeter, UK

Sun, H., Shi, B., Lytle, D. & Wang, D. 2014. *Formation and release behaviour of iron corrosion products under the influence of bacterial communities in a simulated water distribution system*. Environmental Science: Processes and Impacts. 16(3). DOI: 10.1039/c3em00544e.

Taylor, J. 2018. *Time-varying behaviour of an isolated pipe section with a small leak*. Final Year Project Report. University of Cape Town. South Africa.

The National Academies of Science and Engineering. 2011. *Corrosion - Its influence and control*. Available: <https://www.nap.edu/read/13032/chapter/3#35> [2016, November 18].

Thornton, J. & Lambert, A. 2005. *Progress in practical prediction of pressure: Leakage, pressure: Burst frequency and pressure: Consumption relationships*. Proceedings of IWA Special Conference 'Leakage 2005'. 12-14 September 2005. Halifax, Nova Scotia, Canada.

Thornton, J. & Lambert, A. 2007. *Pressure management extends infrastructure life and reduces unnecessary energy costs*. Conference proceedings of 2017 IWA Water Loss. 23 – 26 September 2007. Bucharest, Romania.

Turkowski, M., Bratek, A. & Stowikowski, M. 2007. *Methods and systems of leak detection in long range pipelines*. Journal of automation, mobile robotics & intelligent systems. 1(3): 39–46.

van Vuuren, L. 2014. *Water loss: are we wasting our way into a potential water crisis?* The Water Wheel. 18(4): 34–37.

van Zyl, J.E. & Cassa, A. 2011. *Linking the power and FAVAD equations for modeling*. Proceedings of the Eleventh International Conference on Computing and control for the water industry. 5-7 September 2011. Exeter: UK.

Van Zyl, J. E. & Malde, R. (2017). *Evaluating the pressure-leakage behaviour of leaks in water pipes*. *Journal of Water Supply and Technology*. Journal of Water Supply: Research and Technology- Aqua. 66(5):287-299. <https://doi.org/10.2166/aqua.2017.136>

Vítkovský, J.P., Simpson, A.R, Lambert M.F. & Wang, X.J. 2001. *An experimental verification of the inverse transient technique*. Proceedings of the 6th Conference on Hydraulics in Civil Engineering: "The State of Hydraulics". 28-30 November 2001. Hotel Grand Chancellor, Hobart, Tasmania.

Walski, T., Whitman, B., Baron, M. & Gerloff, F. 2009. *Pressure vs . Flow Relationship for Pipe Leaks*. World Environmental and Water Resources Congress. 17-21 May, 2009. Kansas City, Missouri, United States.

Water Services Association of Australia (2003). *Common failure modes in pressurised pipeline systems*. Water Services Association of Australia. 1–7.

Webb, M.C., Mergelas, B. & Laven, K. (2009). *Transmission Main Leak Detection in Sub-Saharan Africa*. The North American Society (NASTT) and the International Society for Trenchless Technology (IS TT). March 29- April 3, 2019. Paper B-4-04. 1-10.

Wolmarans, N. 2015. *Introduction to Fluid Mechanics*. [CIV1005W Lecture 6]. Department of Civil Engineering. University of Cape Town.

Ying, L. C. 2015. *Plug the leaks to curb non-revenue water*. Available: <https://www.star2.com/living/living-environment/2015/05/25/plug-the-leaks-to-curb-non-revenue-water/#OIzh1Copqe4sDAiE.99> [2015, September 25].

Ziegler, D., Trujillo, R., Oertle, E., Laures, C., Knobloch, A., Klingel, P., Hubschen, K., Fallis, P. et al. 2009. *Guidelines for water loss reduction*. Deutsche Gesellschaft für Internationale Zusammenarbeit (GIZ) GmbH.

van Zyl, J.E., Lambert, A. O. & Collins, R. 2017. Realistic modeling of leakage and intrusion flows through leak openings in pipes. *Journal of Water Resources Planning and Management*. 143(9): 3–9. DOI: 10.1061/(ASCE)HY.1943-7900.0001346.

# 10 Appendix

## 10.1 Calibration certificates for instrumentations

### Certificate of Calibration

Customer Name:	ABB South Africa (Pty) Ltd.	Certificate Number:	241746673X001_041212
Customer PO no.:	Randhart, Alberton, 1457	Accreditation Number:	-
Tag info:	-	Date of Calibration:	04.12.2012
Device no.:	8529812	Calibration Location:	Goettingen
Serial no.:	241746673X001	Test Rig:	Rig 0004
Meter Type:	Magnetic flowmeter ProcessMaster500	Fluid:	water
Model Number:	FEP511	Sensor Qmax:	200.0 l/min
Meter Size (mm):	DN 25	Calibration Range:	140.0 l/min
Process Connection:	Flanges DIN PN 40	Calibration Type:	Standard Accuracy 0,3%
Flange Material:	steel	Sensor Factor Sz:	1.2197 mm/s
Lining/Electrodes:	PTFE / Stainl. Steel 316Ti (1.4571)	Sensor Factor Ss:	175.9300 %
Excitation Frequency:	25 Hz	Accuracy Specification:	+/- (0.30 % rate + 0.02 % final)
Customer range:	0 - 200 l/min		-

No.	Fluid Temp. °C	Run time (s)	Ref. Lab Flow (l/min)	Test Meter Flow (l/min)	Calibrated Range %	Error %
1	21.4	50.0	28.1084	28.1480	20.08	0.14
2	21.4	50.0	28.1130	28.1387	20.08	0.09
3	21.4	50.0	126.6024	126.5173	90.43	-0.07
4	21.4	50.0	126.8495	126.7549	90.61	-0.07
5	-	-	-	-	-	-
6	-	-	-	-	-	-
7	-	-	-	-	-	-
8	-	-	-	-	-	-
9	-	-	-	-	-	-
10	-	-	-	-	-	-

All the above results reflect the fluid calibration at lab conditions.

The errors determined during the calibration are within the specified accuracy. This calibration certificate documents the traceability to national standards, which realize the units of measurement according to the International System of Units (SI). The user is obliged to have the object recalibrated at appropriate intervals.

Rev: 3.1.5
Certified by: D. Franke
Date: 04.12.2012

This certificate was generated automatically and is valid without signature.

---

ABB Automation Products Drahtfelder Str. 2 D-37070 Goettingen GERMANY	ABB Limited Oldenda Lane, Stonehouse Gloucestershire, GL 10 3JA ENGLAND	ABB Automation Inc. 125 East County Line Rd Warrimoor, PA 18974 USA	ABB Australia (Pty) Ltd. Seapeume Rd Moorebank NSW 2170 AUSTRALIA	ABB Canada 3450 Harvester Road Burlington, ON L7N 3W5 (JudongNewDistrict, Shanghai) 201319 CANADA	ABB Engineering Ltd. No. 4528, Kangxin Highway CHINA
--	--	--	--	--	--

Our ref: 689067  
Date: 2018-12-06



**LETTER OF CONFORMITY**

Customer: ABB South Africa  
Measurement and Analytics  
ABB Campus, 2 Lake Road, Longmeadow Business Estate (North)  
1609, Modderfontein, Gauteng, ZA  
South Africa

Customer Ref: 4400058617  
Tag Ref: -----

<u>Item</u>	<u>Qty</u>	<u>Description</u>	<u>Serial No</u>
1	1	SM50BFC/B3ET021E/STD Field Mount Videographic Recorder	3K210000070878

Deviations from standard: - NIL

Certified that the whole of the supplies detailed hereon have been inspected, tested, and unless stated above, conform in all respects to the published specification.

Signed \_\_\_\_\_ A. Kastenhofer  
Position \_\_\_\_\_ Calibration Standards Engineer



Please reply to:

Registered Office:

# 2600T Pressure Transmitters

Calibration record  
Kalibrationsprotokoll  
Rapporto di calibratura  
Rapport de calibration

Customer/Kunde/Client/Client

abcdefghijklmnp

Order - Auftrag - Ordine - Commande  
1234567890

ABB Instrumentation Inc  
East County Line Road  
WARMINSTER PA  
USA

Ref. Bestellung - Ref. Référence  
ABB1234567890

Factory  
ABB SpA Sace Division  
Factory Order Ack - Auftragsbest. - Conf. Ordine Intesa - @Commande reçue  
1234567890  
Internal OIA pos / s.pos  
00030 / 000001

## Transmitter Information

Product Code  
266DRH1234567890123456

Diaphragm seal S1 side  
S26RAH12345678901234567

Diaphragm seal S2 side  
S26RAL12345678901234567

Serial version nr.  
SR08123 SR08124 SR08125

Tag no. - Messstelle - Sigla - Repère  
123456789012345678901234567890

Communication Tag no. - Messstelle - Sigla - Repère  
DPT12345

Message  
PROJ. FU1  
Descriptor  
AIR FLOW TO BURNER 1

Serial Number - Serien-Nr. - Nr. Di serie - No. De série  
123456789012345678901234567890

Mean Range-Meßbereich-Campo-Cintenda de  
- 400 to + 400 mbar  
Adjusted to- Eingest. Auf-Tarato a: - Ajustado a:

0 to 250 mbar  
Output  
Linear

## Transducer information

Serial Number - Serien-Nr. - Nr. Di serie - No. De série  
2605401165

## Communication board information

Serial Number - Serien-Nr. - Nr. Di serie - No. De série  
34489  
Software revision  
1  
Hardware revision  
8

## Calibration Result - Ergebnis - Risultato -

Range Messpunkt Campo Echelle	Applied pressure Erwünschter Druck Press. Applicata	Digital Output Digital Profiling Uscita Digitale Sortie Numérique	Deviation Abweichung Deviazione Ecart	Output current Ausgangsstrom Corr. Uscita Sortie analogique	Deviation Abweichung Deviazione Ecart
%	bar	bar	% of span	mA	% of span
0	0,01	0,009	-0,01%	4,014	-0,01%
50	4,999	4,997	-0,02%	11,994	-0,02%
100	10,001	10	-0,01%	19,998	-0,01%
50	4,998	4,999	0,01%	12	0,02%
0	0,001	0,003	0,02%	4,005	0,02%

Max. deviation from characteristic [%]  
Max. Kennlinienabweichung [%]  
Massimo errore della caratteristica [%]  
Déviation max. de la caractéristique [%]  
**0,06**

Ambient temperature [°C]  
Umgebungstemperatur [°C]  
Temperatura ambiente [°C]  
**22°C**

## Test equipment information

Test equipment ID  
Tool nr.  
Operative mode  
Multimeter type  
Pressure controller (1)

DIPROCS: Calibration M30  
1  
Automatic configuration  
Fluke 45 Serial nr. 6025075 (1.7 D1.0)  
RUSKA 7000 040 kPa G.N. Serial nr. 40

## Calibration Location/ Date

LENNO - 21/03/2008

ABB S.p.A.  
22016 Lenno (CO)  
ITALY  
phone: +39 0344 58111  
fax: +39 0344 56728  
www.abb.com

Power and productivity  
for a better world™



# 10.2 Spreadsheet design for analysing PCAE data



## 1. Workbook Contents

**Click on tabs to access the following:**

[Tab 1. Contents \(current tab\)](#)

[Tab 2. Equipment Information](#)

[Tab 3. Test Site Information](#)

[Tab 4. Test Pipe Elevation Profile](#)

[Tab 5. Leak Test Data](#)

[Tab 6. Head Loss Analysis](#)

[Tab 7. Leakage Parameters](#)

**NB: All inputs in blue values and all  
output/calculation in red**

## 2. EQUIPMENT INFORMATION

Flow meter	
Make	ABB
Model	FEX500
Signal type	4-20mA
Signal parameters	Flow rate
Flow Range(l/min)	0-200
Flow direction	Forward flow
Measuring accuracy of rate	0,20%
Type	Electromagnetic
Min. flow range (l/min)	4
Max. flow range (l/min)	200

Pressure Transducer	
Make	ABB
Model	2600T
Pressure Range (bar)	0-10
Signal type	4-20mA
Signal parameters	Pressure
Last calibrated date	01/10/2017

Recorder	
Make	ABB
Model	SM500F
Time step (seconds)	0,1
Channel Tags	Pressure and Flow
Password	N/A

Delivery line from equipment to test pipe connection	
Material	Rubber
Rigid/Flexible	Flexible
Class	10
Nominal diameter (mm)	50
ID (mm)	45,2
Length (m)	10
Roughness coefficient (source:Finnemore Franzinin)	0,03
<b>Components on delivery line</b>	<b>Minor Loss Coefficient</b>
1 x 50mm Ball Valve	0,1
1 x 50mm Straight Connector	0,2
Total minor loss coefficient	0,3

Water Source	
Type	Water Tank on trailer
Size (l)	1000

Pump	
Make	Euroflow
Model	HS18-40N-1
Maximum h (m)	42
Maximum Flow rate at 17m pressure (m3/hr)	16
Minimum flow rate at 41m pressure (m3/hr)	4

Inverter	
Make	Active Driver Plus
Model	M/M 1.1
Pressure regulating Range (bar)	1-9
Maximum Pressure (bar)	13
Q max (l/min)	300
Non Return Valve flow direction	Forward

Generator	
Make	RYOBI
Model	RG-2700
Power output (kW)	2,7
Fuel type	Unleaded Petrol
Fuel Tank capacity (l)	12

### 3. SITE INFORMATION

Test Site information		Comment
Pipeline Name	Lynnwood Road to Koedoesnek Reservoir	
Owner	Tshwane Municipality	
Date	06-Jun-18	
Address	Pretoria East, Lynnwood/Faerie Glen	

Test Pipe		Comment
Name	Lynnwood Road to Koedoesnek Reservoir	
Empty/Full	Full	
Material	Steel	From Google Earth data file
Class		From Google Earth data file
Elastic Modulus (Mpa)		Based on the class
Year Installed	unknown	
Nominal Diameter (mm)	500	
Internal Diameter (mm)	unknown	
Wall Thickness	unknown	
Length (m)	707	Based on Googl Earth data file
Burial Depth (m)	1,5	Guessed
Soil Description	Sandy	Guessed from site visit

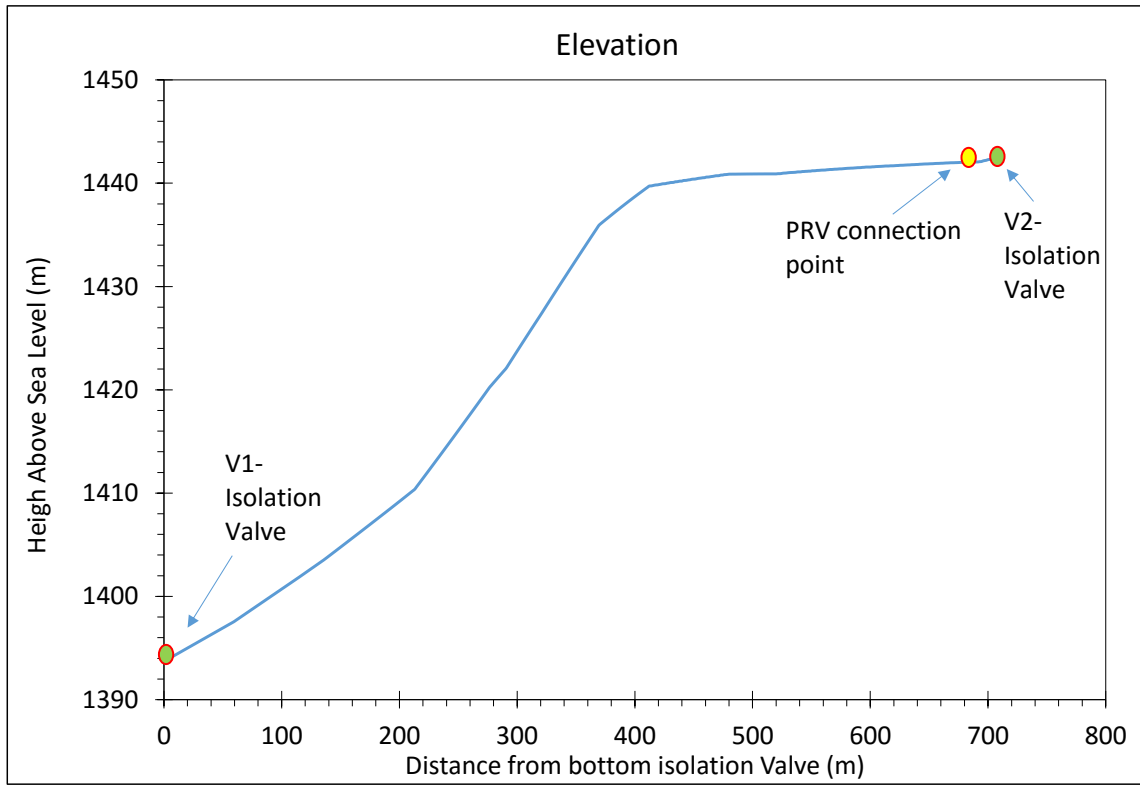
Test Pipe Connection Point		Comment
Type	Connection on PRV	
Size (mm)	50	Female thread
Location on test pipe	Highest point on pipeline	

V1 - Isolation valve		Comment
Type	Butterfly Vlve	
Size (mm)	500	Guessed based on pipe size
Opening Direction	anti-clockwise	Opened with THE assistance of technicians
Upstream/downstream pressure (bar)	> 10	Approximate
Functional/Not functional	Functional	

V2 - Isolation valve		Comment
Type	PRV	
Size (mm)	500	Guessed based on pipe size
Opening Direction	anti-clockwise	Opened with the assistance of technicians
Pressure (bar)	<1	Approximate
Functional/Not functional	Functional	



## 4. Elevation Profile Data



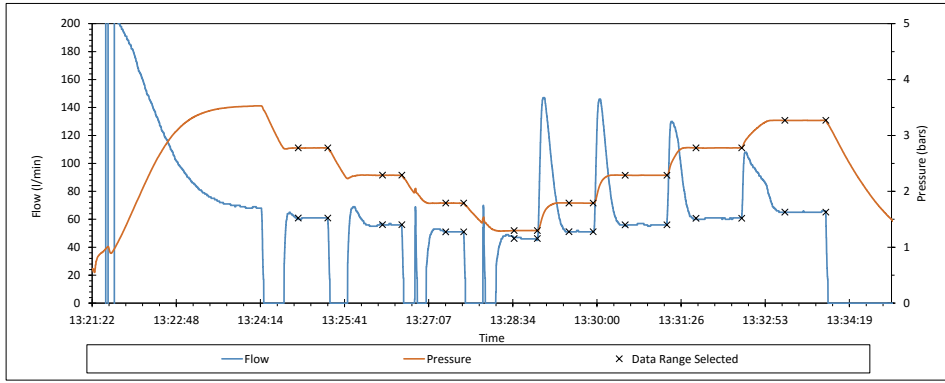
Distance from bottom (m)	Height Above Sea Level (m)
0,00	1393,70
1,38	1393,79
2,77	1393,88
4,15	1393,97
5,53	1394,06
6,92	1394,15
8,30	1394,24
9,68	1394,33
11,07	1394,42
12,45	1394,51
13,83	1394,60
15,22	1394,69
16,60	1394,78
17,98	1394,87
19,37	1394,96
20,75	1395,05
22,13	1395,13
23,52	1395,22
24,90	1395,31
26,28	1395,40
27,67	1395,49
29,05	1395,58
30,43	1395,67
31,82	1395,76
33,20	1395,85
34,58	1395,94
35,97	1396,03
37,35	1396,12
38,73	1396,21

40,12  
41,50  
42,88  
44,27  
45,65  
47,03  
48,42  
49,80  
51,18  
52,57  
53,95  
55,33

1396,30  
1396,39  
1396,48  
1396,57  
1396,66  
1396,75  
1396,84  
1396,93  
1397,02  
1397,10  
1397,19  
1397,28

Data omitted here

## 5. LEAK TEST DATA

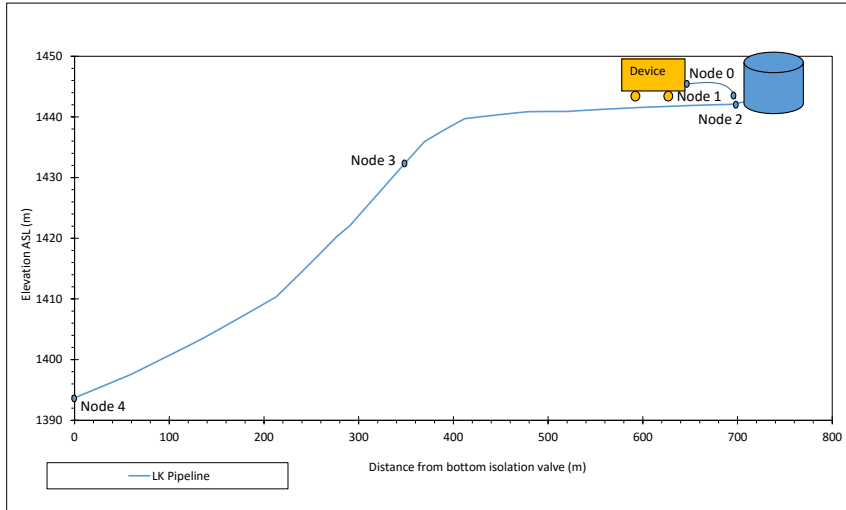


Step No.	Start time	End Time	Start Row Index	End Row Index	Average Leakage (l/min)	Average Pressure (bar)	Average Flow (m3/s)	Average Pressure (m)
1	2018/06/06 13:24:53,2	2018/06/06 13:25:23,6	4203	4507	60,88	2,78	1,01E-03	28,31
2	2018/06/06 13:26:19,7	2018/06/06 13:26:39,5	5067	5265	56,08	2,29	9,35E-04	23,34
3	2018/06/06 13:27:24,6	2018/06/06 13:27:43,1	5716	5901	50,99	1,79	8,50E-04	18,24
4	2018/06/06 13:28:34,9	2018/06/06 13:28:58,7	6419	6657	46,24	1,30	7,71E-04	13,24
5	2018/06/06 13:29:31,1	2018/06/06 13:29:56,0	6981	7230	51,08	1,79	8,51E-04	18,26
6	2018/06/06 13:30:28,9	2018/06/06 13:31:11,7	7559	7986	56,04	2,29	9,34E-04	23,33
7	2018/06/06 13:31:41,6	2018/06/06 13:32:28,5	8285	8754	60,65	2,78	1,01E-03	28,32
8	2018/06/06 13:33:12,8	2018/06/06 13:33:55,0	9197	9619	65,10	3,27	1,09E-03	33,35

Date/Time	Flow (l/min)	Pressure (bar)
2018/06/06 13:17:56,8	0	0,103
2018/06/06 13:17:56,9	0	0,103
2018/06/06 13:17:57,0	0	0,103
2018/06/06 13:17:57,1	0	0,103
2018/06/06 13:17:57,2	0	0,103
2018/06/06 13:17:57,3	0	0,103
2018/06/06 13:17:57,4	0	0,103
2018/06/06 13:17:57,5	0	0,103
2018/06/06 13:17:57,6	0	0,103
2018/06/06 13:17:57,7	0	0,103
2018/06/06 13:17:57,8	0	0,103
2018/06/06 13:17:57,9	0	0,103
2018/06/06 13:17:58,0	0	0,103
2018/06/06 13:17:58,1	0	0,103
2018/06/06 13:17:58,2	0	0,103
2018/06/06 13:17:58,3	0	0,103
2018/06/06 13:17:58,4	0	0,103
2018/06/06 13:17:58,5	0	0,103
2018/06/06 13:17:58,6	0	0,103
2018/06/06 13:17:58,7	0	0,103
2018/06/06 13:17:58,8	0	0,103
2018/06/06 13:17:58,9	0	0,103
2018/06/06 13:17:59,0	0	0,103
2018/06/06 13:17:59,1	0	0,103
2018/06/06 13:17:59,2	0	0,103
2018/06/06 13:17:59,3	0	0,103
2018/06/06 13:17:59,4	0	0,103
2018/06/06 13:17:59,5	0	0,103
2018/06/06 13:17:59,6	0	0,103
2018/06/06 13:17:59,7	0	0,103
2018/06/06 13:17:59,8	0	0,103
2018/06/06 13:17:59,9	0	0,103
2018/06/06 13:18:00,0	0	0,103
2018/06/06 13:18:00,1	0	0,103
2018/06/06 13:18:00,2	0	0,103
2018/06/06 13:18:00,3	0	0,103
2018/06/06 13:18:00,4	0	0,103
2018/06/06 13:18:00,5	0	0,103
2018/06/06 13:18:00,6	0	0,103
2018/06/06 13:18:00,7	0	0,103
2018/06/06 13:18:00,8	0	0,103
2018/06/06 13:18:00,9	0	0,103
2018/06/06 13:18:01,0	0	0,103
2018/06/06 13:18:01,1	0	0,103
2018/06/06 13:18:01,2	0	0,103
2018/06/06 13:18:01,3	0	0,103
2018/06/06 13:18:01,4	0	0,103
2018/06/06 13:18:01,5	0	0,103
2018/06/06 13:18:01,6	0	0,103
2018/06/06 13:18:01,7	0	0,103
2018/06/06 13:18:01,8	0	0,103
2018/06/06 13:18:01,9	0	0,104
2018/06/06 13:18:02,0	0	0,104
2018/06/06 13:18:02,1	0	0,104
2018/06/06 13:18:02,2	0	0,104
2018/06/06 13:18:02,3	0	0,104
2018/06/06 13:18:02,4	0	0,104
2018/06/06 13:18:02,5	0	0,104
2018/06/06 13:18:02,6	0	0,104
2018/06/06 13:18:02,7	0	0,104
2018/06/06 13:18:02,8	0	0,104
2018/06/06 13:18:02,9	0	0,104
2018/06/06 13:18:03,0	0	0,104
2018/06/06 13:18:03,1	0	0,104
2018/06/06 13:18:03,2	0	0,104
2018/06/06 13:18:03,3	0	0,104
2018/06/06 13:18:03,4	0	0,104
2018/06/06 13:18:03,5	0	0,104
2018/06/06 13:18:03,6	0	0,104
2018/06/06 13:18:03,7	0	0,104
2018/06/06 13:18:03,8	0	0,104
2018/06/06 13:18:03,9	0	0,104
2018/06/06 13:18:04,0	0	0,104

Data omitted here

## 6. HEAD LOSS ANALYSIS



### 1. Check constant variables required for analysis

Fluid Constant variables	Values
Acceleration due to gravity, $g$ (m/s <sup>2</sup> )	9,81
Fluid Density, $\rho$ (kg/m <sup>3</sup> )	1000
Fluid Kinematic Viscosity, $\nu$ (kg/m.s)	1,14E-06

Test pipe Constant variables	Values
Measure horizontal distance (m)	850
Static height difference (A)	1,85
Actual length of test pipe	707,00
Static height difference (B)	0,80

Laminar Flow:  $f = \frac{64}{Re}$

Smooth Pipe Turbulent Flow:  $f = \frac{0,316}{Re^{1/4}}$

Completely Turbulent Flow:  $f = [1,14 + 2 \log_{10}(\frac{D}{\epsilon})]^{-2}$

Transition Region:  $f = \left\{ -2 \log_{10} \left[ \frac{(\epsilon/D)}{3,7} + \frac{2,51}{Re (f^{1/2})} \right] \right\}^{-2}$

Fitting	K
Well rounded inlet	0.05
90° elbow, threaded	
Regular	1.4
Long radius	0.75
90° elbow, flanged	
Regular	0.31
Long radius	0.22
45° elbow, threaded, regular	0.35
45° elbow, flanged, regular	0.17
Return bend, threaded, regular	1.5
Return bend, flanged	
Regular	0.3
Long radius	0.2
T-joint, threaded	
Through flow	0.9
Branch flow	1.9
T-joint, flanged	
Through flow	0.14
Branch flow	0.69
Sudden expansion	
$d_1/d_2 = 0.5$	0.75
$d_1/d_2 = 0.7$	0.51
$d_1/d_2 = 0.9$	0.19
Sudden contraction	
$d_2/d_1 = 0.5$	0.3
$d_2/d_1 = 0.7$	0.2
$d_2/d_1 = 0.9$	0.1

### 2. From the figure determine the elevation at each node

Node	Elevation (m)
0	1440,5
1	1438,65
2	1437,85
3	1433,04
4	1393,7

### 2. Determine the pipe and fluid properties for each section. (Each section has a start node and end node)

Pipe properties	Delivery hose pipe	Connection point	Test Pipe	Test Pipe
Pipe Section Identity	0-1	1-2	2-3	3-4
Diameter (mm)	50	25	500	500
Absolute roughness, $\epsilon$ (mm)	0,3	0,03	0,15	0,15
Minor loss coefficient, K	0,3	0,33	0,5	0
Acceleration due to gravity, $g$ (m/s <sup>2</sup> )	9,81	9,81	9,81	9,81
Fluid Density, $\rho$ (kg/m <sup>3</sup> )	1000	1000	1000	1000
Fluid Kinematic Viscosity, $\nu$ (kg/m.s)	1,14E-06	0,00001139	1,14E-06	1,14E-06
Elevation difference, $\Delta z$ (m)	1,85	0,80	4,81	39,34
Length of pipe (m)	10	0,80	353,50	353,50
$\epsilon/D$	6,00E-03	1,80E-03	3,00E-04	3,00E-04
Pipe Area, $A$ (m <sup>2</sup> )	1,96E-03	4,91E-04	1,96E-01	1,96E-01

### 3. For each section first check the flow regime. Then Calculate the friction factor. Then calculate the friction head loss and minor head loss. Finally Calculate pressure at

Section 0-1							
Q (m <sup>3</sup> /s)	head at 0, $h_0$ (m)	Reynolds Number, $Re$	Flow Regime	Friction factor, $f$	Friction head loss, $hf_{0-1}$ (m)	Minor head loss, $hm_{0-1}$ (m)	head at 1, $h_1$ (m)
1,01E-03	28,31	22665,89	Turbulent	0,0321	0,087	4,08E-03	30,07
9,35E-04	23,34	20878,30	Turbulent	0,0321	0,074	3,46E-03	25,11
8,50E-04	18,24	18982,90	Turbulent	0,0321	0,061	2,86E-03	20,03
7,71E-04	13,24	17214,23	Turbulent	0,0321	0,050	2,36E-03	15,04
8,51E-04	18,26	19016,69	Turbulent	0,0321	0,061	2,87E-03	20,04
9,34E-04	23,33	20862,28	Turbulent	0,0321	0,074	3,46E-03	25,10
1,01E-03	28,32	22578,34	Turbulent	0,0321	0,087	4,05E-03	30,08
1,09E-03	33,35	24236,84	Turbulent	0,0321	0,100	4,67E-03	35,09

Section 1-2							
Q (m <sup>3</sup> /s)	head at 1, $h_1$ (m)	Reynolds Number, $Re$	Flow Regime	Friction factor, $f$	Friction head loss, $hf_{1-2}$ (m)	Minor head loss, $hm_{1-2}$ (m)	head at 2, $h_2$ (m)
1,01E-03	30,07	45331,77	Turbulent	0,023	0,159	7,19E-02	30,64
9,35E-04	25,11	41756,60	Turbulent	0,023	0,135	6,10E-02	25,71
8,50E-04	20,03	37965,80	Turbulent	0,023	0,111	5,04E-02	20,67
7,71E-04	15,04	34428,47	Turbulent	0,023	0,091	4,15E-02	15,70
8,51E-04	20,04	38033,38	Turbulent	0,023	0,112	5,06E-02	20,68
9,34E-04	25,10	41724,57	Turbulent	0,023	0,134	6,09E-02	25,71
1,01E-03	30,08	45156,68	Turbulent	0,023	0,157	7,13E-02	30,65
1,09E-03	35,09	48473,69	Turbulent	0,023	0,181	8,22E-02	35,63

Section 2-3							
Q (m <sup>3</sup> /s)	head at 2, h <sub>2</sub> (m)	Reynolds Number, Re	Flow Regime	Friction factor, f	Friction hed loss, hf <sub>2-1</sub> (m)	Minor head loss, hm <sub>2-1</sub> (m)	head at 3, h <sub>3</sub> (m)
1,01E-03	30,64	2266,59	Transitional	0,0149	2,87E-05	6,81E-07	35,45
9,35E-04	25,71	2087,83	Transitional	0,0149	2,44E-05	5,77E-07	30,52
8,50E-04	20,67	1898,29	Laminar	0,0149	2,01E-05	4,77E-07	25,48
7,71E-04	15,70	1721,42	Laminar	0,0149	1,66E-05	3,93E-07	20,51
8,51E-04	20,68	1901,67	Laminar	0,0149	2,02E-05	4,79E-07	25,49
9,34E-04	25,71	2086,23	Transitional	0,0149	2,43E-05	5,77E-07	30,52
1,01E-03	30,65	2257,83	Transitional	0,0149	2,85E-05	6,75E-07	35,46
1,09E-03	35,63	2423,68	Transitional	0,0149	3,28E-05	7,78E-07	40,44

Section 3-4							
Q (m <sup>3</sup> /s)	head at 3, h <sub>3</sub> (m)	Reynolds Number, Re	Flow Regime	Friction factor, f	Friction hed loss, hf <sub>3-1</sub> (m)	Minor head loss, hm <sub>3-1</sub> (m)	head at 4, h <sub>4</sub> (m)
1,01E-03	35,45	2266,59	Transitional	0,0149	2,87E-05	0,00E+00	74,79
9,35E-04	30,52	2087,83	Transitional	0,0149	2,44E-05	0,00E+00	69,86
8,50E-04	25,48	1898,29	Laminar	0,0149	2,01E-05	0,00E+00	64,82
7,71E-04	20,51	1721,42	Laminar	0,0149	1,66E-05	0,00E+00	59,85
8,51E-04	25,49	1901,67	Laminar	0,0149	2,02E-05	0,00E+00	64,83
9,34E-04	30,52	2086,23	Transitional	0,0149	2,43E-05	0,00E+00	69,86
1,01E-03	35,46	2257,83	Transitional	0,0149	2,85E-05	0,00E+00	74,80
1,09E-03	40,44	2423,68	Transitional	0,0149	3,28E-05	0,00E+00	79,78

Summary Results:

Flow rate, Q	h at node 0	h at node 1	h at node 2	h at node 3	h at node 4	H4 - H0
1,01E-03	28,31	30,07	30,64	35,45	74,79	46,48
9,35E-04	23,34	25,11	25,71	30,52	69,86	46,53
8,50E-04	18,24	20,03	20,67	25,48	64,82	46,57
7,71E-04	13,24	15,04	15,70	20,51	59,85	46,61
8,51E-04	18,26	20,04	20,68	25,49	64,83	46,57
9,34E-04	23,33	25,10	25,71	30,52	69,86	46,53
1,01E-03	28,32	30,08	30,65	35,46	74,80	46,48
1,09E-03	33,35	35,09	35,63	40,44	79,78	46,43



## 7. LEAKAGE PARAMETERS

1. Determine the N1 and FAVAD Leakage parameters at each node

Node	Leakage Coefficient, C	Leakage Exponent, N1	Effective Initial Leak Area, $C_0A_0$ (mm <sup>2</sup> )	Effective head-area slope, $C_{0m}$ (mm <sup>2</sup> /m)
0	0,00029	0,38	49,87	-0,24
1	0,00028	0,38	48,96	-0,22
2	0,00024	0,42	45,16	-0,13
3	0,00016	0,51	37,80	-0,22
4	0,00001	1,20	7,55	0,25

Flow, Pressure and Leakage Parameters at node 0									
Flow Rate, Q (m <sup>3</sup> /s)	head at 0, h0 (m)	Log Q	Log h0	Effective Leak Area, $C_0A_0$ (mm <sup>2</sup> )	Leakage Coefficient, C	Leakage Exponent, N1	Effective Initial Leak Area, $C_0A_0$ (mm <sup>2</sup> )	Effective head-area slope, $C_{0m}$ (mm <sup>2</sup> /m)	
1,01E-03	2,83E+01	-2,99E+00		1,45E+00	4,31E+01	2,88E-04	3,75E-01	4,99E+01	-2,45E-01
9,35E-04	2,33E+01	-3,03E+00		1,37E+00	4,37E+01				
8,50E-04	1,82E+01	-3,07E+00		1,26E+00	4,49E+01				
7,71E-04	1,32E+01	-3,11E+00		1,12E+00	4,78E+01				
8,51E-04	1,83E+01	-3,07E+00		1,26E+00	4,50E+01				
9,34E-04	2,33E+01	-3,03E+00		1,37E+00	4,37E+01				
1,01E-03	2,83E+01	-3,00E+00		1,45E+00	4,29E+01				
1,09E-03	3,33E+01	-2,96E+00		1,52E+00	4,24E+01				

Flow, Pressure and Leakage Parameters at node 1									
Flow Rate, Q (m <sup>3</sup> /s)	head at 1, h1 (m)	Log Q	Log h1	Effective Leak Area, $C_0A_0$ (mm <sup>2</sup> )	Leakage Coefficient, C	Leakage Exponent, N1	Effective Initial Leak Area, $C_0A_0$ (mm <sup>2</sup> )	Effective head-area slope, $C_{0m}$ (mm <sup>2</sup> /m)	
1,01E-03	2,87E+01	-2,99E+00		1,46E+00	4,27E+01	2,78E-04	3,84E-01	4,90E+01	-2,20E-01
9,35E-04	2,38E+01	-3,03E+00		1,38E+00	4,33E+01				
8,50E-04	1,87E+01	-3,07E+00		1,27E+00	4,44E+01				
7,71E-04	1,37E+01	-3,11E+00		1,14E+00	4,70E+01				
8,51E-04	1,87E+01	-3,07E+00		1,27E+00	4,45E+01				
9,34E-04	2,38E+01	-3,03E+00		1,38E+00	4,33E+01				
1,01E-03	2,87E+01	-3,00E+00		1,46E+00	4,26E+01				
1,09E-03	3,37E+01	-2,96E+00		1,53E+00	4,22E+01				

Flow, Pressure and Leakage Parameters at node 2									
Flow Rate, Q (m <sup>3</sup> /s)	head at 2, h2 (m)	Log Q	Log h2	Effective Leak Area, $C_0A_0$ (mm <sup>2</sup> )	Leakage Coefficient, C	Leakage Exponent, N1	Effective Initial Leak Area, $C_0A_0$ (mm <sup>2</sup> )	Effective head-area slope, $C_{0m}$ (mm <sup>2</sup> /m)	
1,01E-03	3,06E+01	-2,99E+00		1,49E+00	4,14E+01	2,38E-04	4,23E-01	4,52E+01	-1,27E-01
9,35E-04	2,57E+01	-3,03E+00		1,41E+00	4,16E+01				
8,50E-04	2,07E+01	-3,07E+00		1,32E+00	4,22E+01				
7,71E-04	1,57E+01	-3,11E+00		1,20E+00	4,39E+01				
8,51E-04	2,07E+01	-3,07E+00		1,32E+00	4,23E+01				
9,34E-04	2,57E+01	-3,03E+00		1,41E+00	4,16E+01				
1,01E-03	3,07E+01	-3,00E+00		1,49E+00	4,12E+01				
1,09E-03	3,56E+01	-2,96E+00		1,55E+00	4,10E+01				

Flow, Pressure and Leakage Parameters at node 3									
Flow Rate, Q (m <sup>3</sup> /s)	head at 3, h3 (m)	Log Q	Log h3	Effective Leak Area, $C_0A_0$ (mm <sup>2</sup> )	Leakage Coefficient, C	Leakage Exponent, N1	Effective Initial Leak Area, $C_0A_0$ (mm <sup>2</sup> )	Effective head-area slope, $C_{0m}$ (mm <sup>2</sup> /m)	
1,01E-03	3,55E+01	-2,99E+00		1,55E+00	3,85E+01	1,64E-04	5,10E-01	3,78E+01	1,56E-02
9,35E-04	3,05E+01	-3,03E+00		1,48E+00	3,82E+01				
8,50E-04	2,55E+01	-3,07E+00		1,41E+00	3,80E+01				
7,71E-04	2,05E+01	-3,11E+00		1,31E+00	3,84E+01				
8,51E-04	2,55E+01	-3,07E+00		1,41E+00	3,81E+01				
9,34E-04	3,05E+01	-3,03E+00		1,48E+00	3,82E+01				
1,01E-03	3,55E+01	-3,00E+00		1,55E+00	3,83E+01				
1,09E-03	4,04E+01	-2,96E+00		1,61E+00	3,85E+01				

Flow, Pressure and Leakage Parameters at node 4									
Flow Rate, Q (m <sup>3</sup> /s)	head at 4, h4 (m)	Log Q	Log h4	Effective Leak Area, $C_0A_0$ (mm <sup>2</sup> )	Leakage Coefficient, C	Leakage Exponent, N1	Effective Initial Leak Area, $C_0A_0$ (mm <sup>2</sup> )	Effective head-area slope, $C_{0m}$ (mm <sup>2</sup> /m)	
1,01E-03	7,48E+01	-2,99E+00		1,87E+00	2,65E+01	5,66E-06	1,20E+00	7,55E+00	2,52E-01
9,35E-04	6,99E+01	-3,03E+00		1,84E+00	2,52E+01				
8,50E-04	6,48E+01	-3,07E+00		1,81E+00	2,38E+01				
7,71E-04	5,99E+01	-3,11E+00		1,78E+00	2,25E+01				
8,51E-04	6,48E+01	-3,07E+00		1,81E+00	2,39E+01				
9,34E-04	6,99E+01	-3,03E+00		1,84E+00	2,52E+01				
1,01E-03	7,48E+01	-3,00E+00		1,87E+00	2,64E+01				
1,09E-03	7,98E+01	-2,96E+00		1,90E+00	2,74E+01				

